U.PORTO
FACULDADE DE CIÊNCIAS
UNIVERSIDADE DO PORTO

Discovery of target directed drugs for neurodegenerative diseases based on benzopyrone scaffold

André Manuel Ferreira Fonseca
Tese de Doutoramento apresentada à
Faculdade de Ciências da Universidade do Porto
Química
2017

O caos é uma ordem por decifrar.

José Saramago

The financial support was provided by “Fundação para a Ciência e a Tecnologia” (FCT) (SFRH/BD/80831/2011), under the POPH – QREN – Type 4.1 – Advanced Training, funded by the European Social Fund and by National funds from the “Ministério da Educação e Ciência”, and FEDER/COMPETE (Grants UID/QUI/00081/2015, POCI-01-0145-FEDER-006980).

Acknowledgements

It is hard for me to conceive how four and so years of my life can be condensed in such a short amount of words. The fact is that it isn't, but as my parents taught me, always try your best. However, in my tangled state of mind, I might overlook some of you. But, freight not! I got you covered: If you are reading this, thank you, you are indeed really special to me! Let's do this:

I'd like to thank Foundation for Science and Technology for the PhD grant SFRH/BD/80831/2011 and FEDER/COMPETE (Grants UID/QUI/00081/2015, POCI-01-0145-FEDER-006980) for their financial support.

First things first, Prof. Fernanda Borges, thank you! Since 2009, you have been behind me and my work, and I know that everything that I accomplish professionally will be always thanks to you. Just for that you would have a special place in my heart, but you always take the extra mile and I can confidently say that I'm also a better person because of you.

Prof. Eugenio Uriarte, I really don't know how you manage to always stay in excellent mood and see the good in everyone and everything. It was a pleasure to work these years with you and I also could not thank you enough. I will definitely try to take your approach in life whenever possible.

Prof. Lourdes Santana, thank you for all your help, my first years would not be the same without all the bibliographic data you so generously gave me. Also, nobody made me care for lab safety and proper conduct than you. I grew as a chemist also under your wing, thank you.

Alexandra, your wit and quick comebacks always astonish me. My first contact with a proper lab setting was under your scrupulous rule and as you can see I didn't turn out so bad, did I? Work is important, but life is more. More than a NMR consultant, you are a true friend. Thank you!

Maria, this work has so much of you in it, how can I ever repay you? Thank you for showing what it takes to be a good chemist and for all the knowledge you conveyed. Our friendship, started by the remarkable coumarin scaffold, was blessed with all Galician coffee liquor possible and will undoubtedly never end.

To all my colleagues and friends of the Santiago and Porto labs, all my gratitude. It was not easy to put up with all my jokes and questions, work related or not, so really really

thank you: Javi, Elias, Dolo, Maria, Jacobo, Niccolo, Francesco, Giulio, Andrea, Xosé, from across the border, and closer to home: Carlos, Sofia and Sofia, Joana, Tiago, Catarina, Fernando, Daniel “the father” and Daniel.

A broad acknowledgement is nice and all but Carlos, you were the uber before Uber. Thank you and Sofia for all the dinner parties and for your true friendship! Tiago, wow guys, who knew you would turn out to be such an important piece in this written testament of my work? Thank you for your insight. Joana, my go-to-girl in biological assays, thank you for all the nice moments, without you Ara Batúr would not have such a powerful meaning. Daniel “the father”, ten years have gone by and always you challenge me and open my mind to something new, I’ll always be grateful for that.

Pedro e Hugo, Santiago would not have been the same without some Portuguese guys trying to convince folks that Portugal is more than towels and cod fish. Thank you for everything.

To my beer veterans, Manu, Carlos, Fon, Gabry, Carbón, Victor and Suizo, all the moments we shared were really special to me. More than handball magicians, you were, and still are, awesome friends. Thank you all from the bottom of my heart for making Santiago incredible.

To Anahí, thank you for your support throughout the beginning of my work. You, your friends and your family have forever a place in my heart. I am grateful for the time we spent together and for making me feel at home in a foreign place.

Handball was always a great part of my life, and I am in debt to all the people in F.C. Infesta, my team for twenty years and until my dying days. Thanks to this institution I have made many friends: Marinho, my best friend since god knows when, Ferreira, o captain my captain, Farelo, because what happens in Resende stays in Resende, Cesário, the beach handball master and president… And all the people I shared a locker room with, since, truth be told, I probably spent more time with you guys playing than at home. Paulo, my coach and friend since I was fifteen, thank you for all the advice in and out of the court.

To my all-time friends Ricardo, Calvão, Fábio and Daniel, because even though time passes without us being together, it’s like it never does.

To all my family who accompanied me throughout this entire time, you guys are the greatest. Without you and your laughs, love and support I could never got where I am today. When I grow up, I wish I could be just like you.

To my parents, I owe you everything. Everything I am and will be it’s because of you. Thank you for showing me what unconditional love is like. You must know that if all people were like you, the world would be a better place.

To Saleta, my love, how did it come to this? This last year and a half was undoubtedly the best of my entire life. You and your family opened your hearts and your house to me and that is something that I will never be able to fully repay. There was not a moment with you that I didn’t feel so overwhelmed by how much I love you. I am looking forward for whatever life reserved for us. My genuine hope is that what we share together keeps growing. All I know is, Home is wherever you are. Thank you for showing me the world and believing in me.

Life is a road not meant for walking in a straight line. Detours and bumps along the way will always happen and the people around you will determine how difficult the curves are and how strong the bumps hit. Thank you all for making my journey softer!

“Yes, there are two paths you can go by, but in the long run there’s still time to change the road you’re on.”

Abstract

According to epidemiological studies, Parkinson's and Alzheimer's diseases are the most prevalent neurodegenerative disorders, representing a heavy burden on the patient, family, caregivers and society. Unfortunately, the available therapies are only palliative, which makes the design and development of new disease-modifying drugs an unmet clinical need for millions of patients worldwide.

Coumarins and chromones have been validated as privileged structures and are remarkable frameworks for the design and development of monoamine oxidase B and acetylcholinesterase inhibitors, and adenosine receptors ligands. Accordingly, benzopyrone libraries were designed to interact with multiple targets linked to neurodegeneration. The work developed in this project enabled the establishment of structure-activity relationships and hit/lead identification for the aforementioned targets.

The results gathered from *in vitro* assays showed that the most potent and selective monoamine oxidase B inhibitors were compound **29** (IC_{50} = 4.66 nM), and compound **125** (IC_{50} = 3.94 nM). These two derivatives were non-competitive and reversible monoamine oxidase B inhibitors. Additionally, screening of 3-arylcoumarins showed affinity towards adenosine receptors, especially for the A3 subtype. The derivatization of the C-6 position of the coumarin scaffold was of particular importance to modulate adenosine receptor selectivity and monoamine oxidase B inhibition. Compound **44** (IC_{50} MAO-B = 228 nM, K_i A_1AR = 41.0 µM, K_i A_3AR = 22.0 µM) was then identified as a monoamine oxidase B inhibitor/adenosine receptors ligand hit. Furthermore, preliminary acetylcholinesterase *in vitro* assays revealed low efficacy of the tested compounds (IC_{50} ≥ 186 µM). However, compound **24** was identified as a monoamine oxidase B/acetylcholinesterase inhibitor hit (IC_{50} MAO-B = 11.4 nM, IC_{50} AChE = 359 µM).

Additionally, docking studies were performed to assess the interaction of the most promising compounds with monoamine oxidase B, acetylcholinesterase and adenosine receptors. These studies' results confirmed the strong monoamine oxidase B inhibitory activity of compound **30**, and highlighted the fact that coumarin derivatives seem to be able to interact with the enzyme active center in two equally valid poses. Moreover, chromone derivatives may establish an additional hydrogen bond with Cys172. This interaction is of particular significance, since it leads to decreased plasticity of chromones over their coumarin counterparts, without compromising bioactivity.

Similarly, docking studies with adenosine receptors and acetylcholinesterase provided significant information regarding the ligand/receptor or ligand/enzyme complexes, namely potency and selectivity differences between derivatives. For instance, a glutamine residue existent only in the A3 adenosine receptor has a key role in modulating selectivity towards this target, as shown by the docking poses of compounds **5** and **11**.

Moreover, the drug-like properties of all the synthesized compounds were also calculated. The theoretical parameters considered (molecular weight, lipophilicity, number of hydrogen bond donors and acceptors, topological polar surface area and blood-brain partitioning multiparameter score) showed that the majority of derivatives might be able to cross the blood-brain barrier and have good oral bioavailability.

Altogether, the benzopyrone scaffold was further validated as a relevant framework for the development of target directed drugs for neurodegenerative diseases. The gathered data provided a solid understanding of the bioactivity of the developed benzopyrone libraries. Additionally, it also provided a base for further exploration of this scaffold towards other targets associated with neurodegeneration.

Keywords: Neurodegenerative diseases, Parkinson’s disease, Alzheimer’s disease, Monoamine oxidase, Acetylcholinesterase, Adenosine receptors, Benzopyrone, Coumarins, Chromones, *in vitro* assays, Docking studies, Drug-like properties.

Resumo

De acordo com estudos epidemiológicos, as doenças de Parkinson e Alzheimer são as doenças neurodegenerativas mais prevalentes, representando um pesado encargo para o paciente, família, cuidadores e a sociedade. No entanto, as terapias disponíveis são apenas paliativas, o que torna urgente o desenvolvimento de novos fármacos que alterem a progressão da doença.

Os núcleos das cumarinas e cromonas foram previamente validados como estruturas privilegiadas, sendo considerados úteis para o desenvolvimento de inibidores da monoamino oxidase B e acetilcolinesterase, bem como ligandos de recetores da adenosina. Deste modo, foram delineadas e sintetizadas diferentes séries de derivados da benzopirona como potenciais compostos dirigidos a múltiplos alvos intrinsecamente conectados com neurodegeneração. O trabalho desenvolvido neste projeto permitiu a determinação de relações estrutura-atividade e a identificação de *hits* e *leads* para os alvos previamente mencionados.

Os resultados *in vitro* mostraram que o composto **29** (IC_{50} = 4.66 nM) e o composto **125** (IC_{50} = 3.94 nM) foram os mais potentes e seletivos inibidores da monoamino oxidase B, apresentando um mecanismo de inibição não-competitivo e reversível. Adicionalmente, a série de 3-arilcumarinas exibiu afinidade para os recetores da adenosina, especialmente para o subtipo A3. A modificação da posição 6 do esqueleto cumarínico é de particular importância para modular a seletividade dos recetores da adenosina e inibição da monoamino oxidase B. Foi ainda possível identificar o composto **44** (IC_{50} MAO-B = 228 nM, K_i A_1AR = 41.0 µM, K_i A_3AR = 22.0 µM) como um *hit* inibidor da monoamino oxidase B/ligando de recetores da adenosina. Além disso, ensaios preliminares *in vitro* de determinação de inibição da acetilcolinesterase revelaram que os compostos testados apresentam baixa eficácia (IC_{50} ≥ 186 µM). No entanto, o composto **24** foi identificado como um *hit* para o desenvolvimento de inibidores monoamino oxidase B/acetilcolinesterase (IC_{50} MAO-B = 11.4 nM, IC_{50} AChE = 359 µM).

Finalmente, foram efetuados estudos de *docking* dos compostos mais promissores por forma a analisar a sua interação com os alvos terapêuticos pretendidos. Estes estudos corroboraram a atividade do composto **30** em relação à monoamino oxidase B. Para além disso, as cumarinas estudadas podem interagir com o centro ativo adotando duas conformações, ambas igualmente válidas e sem detrimento da atividade farmacológica. Por outro lado, as cromonas estudadas estabelecem uma ligação de hidrogénio adicional com o resíduo de cisteína 172, conferindo a estes derivados uma conformação mais rígida dentro do centro ativo, igualmente sem comprometer a sua atividade.

Os estudos computacionais efetuados com os recetores da adenosina e a acetilcolinesterase geraram parâmetros e dados fundamentais para o futuro desenvolvimento de novos compostos mais potentes e seletivos. Com estes estudos foi possível identificar interações conducentes à modulação de afinidade e/ou seletividade em alguns compostos. Por exemplo, um resíduo de glutamina existente apenas no recetor A3 de adenosina tem um papel fundamental na determinação da seletividade, conforme observado para os compostos **5** e **11**.

De forma a estabelecer uma caracterização mais detalhada dos compostos sintetizados e de avaliar a sua potencial utilização como fármacos, foram calculadas algumas propriedades físico-químicas de interesse para fármacos com ação central. Os parâmetros teóricos considerados (peso molecular, lipofilia, número de dadores ou aceitadores de pontes de hidrogénio e área topológica polar superficial), juntamente com o cálculo teórico de um parâmetro que descreve a probabilidade de passagem da barreira hemato-encefálica, permitem concluir que a maioria dos derivados sintetizados se enquadram nos requisitos gerais previamente estabelecidos na literatura, e podem efetivamente alcançar o sistema nervoso central.

Em suma, os dados obtidos neste trabalho sustentam a validação do núcleo da benzopirona como uma estrutura relevante para o desenvolvimento de novas entidades químicas dirigidas a alvos diretamente conectados com a neurodegeneração. Da mesma forma, estes resultados cimentaram a base para o futuro desenvolvimento de novos derivados baseados nos *hits* encontrados neste trabalho.

Palavras-chave: Doenças neurodegenerativas; Doença de Parkinson; Doença de Alzheimer; monoamino oxidase; acetilcolinesterase; recetores da adenosina; Benzopirona; Cumarinas; Cromonas; ensaios *in vitro*; Estudos de *docking*;

Thesis summary

This thesis is organized in four chapters:

- Chapter 1. Introduction. Chapter 1 includes a literature review on epidemiological, pathophysiological and pharmacological aspects of neurodegenerative diseases, namely Parkinson’s disease and Alzheimer’s disease. It also encloses a brief review of the synthesis, biological activity of the benzopyrone scaffold, focusing on neurodegenerative diseases. Finally, the main goals of this thesis are also outlined in this chapter.
- Chapter 2. Experimental section. Chapter 2 comprises the scientific articles prepared within the scope of the thesis.
- Chapter 3. Discussion, conclusions and future perspectives. Chapter 3 encloses the general discussion and conclusions of the experimental results obtained. The most relevant findings and future undertakings are also addressed in this section.
- Chapter 4. References. Chapter 4 lists all the bibliographic references used in the previous chapters.
- Annexes. Additional unpublished information and results of this thesis are included in this section.

Table of Contents

Acknowledgements v

Abstract ix

Resumo xi

Thesis summary xiii

Table of Contents xv

Figure Index xix

Table Index xxiii

Abbreviations Index xxv

CHAPTER 1 1

1.1. Introduction 3

1.2. Neurodegenerative diseases 4

1.2.1. Parkinson’s disease 5

1.2.1.1. Dopaminergic therapy of Parkinson’s disease 6

1.2.1.1.1. Dopamine 6

1.2.1.1.2. Dopamine receptor agonists 7

1.2.1.1.3. Catechol-O-methyltransferase inhibitors 7

1.2.1.1.4. Monoamine oxidase inhibitors 10

1.2.1.2. Non-dopaminergic approaches in PD therapy 11

1.2.1.2.1. Adenosine and adenosine receptors 11

1.2.2. Alzheimer’s disease 14

1.2.2.1. Acetylcholinesterase inhibitors 15

1.2.2.2. *N*-Methyl-D-aspartate receptor antagonists 17

1.2.2.3. Other targets in Alzheimer’s disease 18

1.3. One target versus multi target drugs 22

1.3.1. Multi target drugs for Parkinson’s disease 23

1.3.2. Multi target drugs for Alzheimer’s disease 24

1.4. Benzopyrones 26

1.4.1. Coumarins........27
1.4.1.1. Biological activities........27
1.4.1.2. Coumarins in neurodegenerative diseases........30
1.4.1.3. Synthesis of coumarins........31
1.4.2. Chromones........34
1.4.2.1. Biological activities........35
1.4.2.2. Chromones in neurodegenerative diseases........37
1.4.2.3. Synthesis of chromones........38
1.5. Objectives........43
CHAPTER 2........45
Manuscript I........47
Manuscript II........59
Manuscript III........73
Manuscript IV........85
Manuscript V........125
Manuscript VI........133
Manuscript VII........155
Manuscript VIII........167
CHAPTER 3........193
3.1. Discussion........195
3.1.1. Design and development of benzopyrone-based libraries........195
3.1.1.1. Synthesis of 3-carboxamidocoumarin library........196
3.1.1.2. Synthesis of 3-arylcoumarin based library........202
3.1.1.3. Synthesis of nitrooxy-coumarin based library........205
3.1.1.4. Synthesis of 3-carboxamidochromone-based library........206
3.1.2. Structural characterization of the benzopyrone derivatives........208
3.1.3. Looking for target directed drugs for neurodegenerative diseases based on the benzopyrone scaffold........211
3.1.3.1. Evaluation of drug-like properties........212

3.1.3.2. Benzopyrones as monoamine oxidase B inhibitors 213

3.1.3.3. Benzopyrones as adenosine receptors ligands 216

3.1.3.4. Benzopyrones as AChE inhibitors 219

3.2. Conclusions and future perspectives 222

CHAPTER 4 225

4.1. References 227

ANNEXES 243

Annex I 245

Annex II 255

Figure Index

Figure 1 – Global life expectancy for both genders since 1950. From the United Nations Population Division and Human Mortality Database.[4] 4
Figure 2 – Dopamine metabolism. 6
Figure 3 – Structures of carbidopa and benserazide. 7
Figure 4 – Structures of ergoline, and ergot and non-ergot dopamine receptor agonists. 8
Figure 5 – L-DOPA, dopamine and norepinephrine metabolism by COMT. 9
Figure 6 – Structure of second generation COMT inhibitors. 9
Figure 7 – MAOs catalysed reactions. 10
Figure 8 – Structures of selegiline, rasagiline and safinamide. 11
Figure 9 – Adenosine receptors. 12
Figure 10 – Structure of A_{2A} AR antagonists. 13
Figure 11 – AChE catalysis of ACh. 15
Figure 12 – Active site of AChE. 16
Figure 13 – Structures of tacrine, in red, and rivastigmine, donepezil and galanthamine. 17
Figure 14 – Structure of memantine. 18
Figure 15 – Representation of the transmembrane protein APP and its degradation by different secretases. 19
Figure 16 – Structure of BACE inhibitors presently on clinical trials. 20
Figure 17 – Caspase activation by β-amyloid fragments. 20
Figure 18 – Structures of caspase inhibitors. 21
Figure 19 – Structures of ladostigil and its major metabolite. 23
Figure 20 – Structures of MAO-B inhibitors and A_{2A}AR antagonists. 24
Figure 21 – Structures of memoquin, lipocrine and carbacrine. 25
Figure 22 – Structures of recognised privileged scaffolds. 26
Figure 23 – Biosynthesis of coumarin and related hydroxylated derivatives. 27
Figure 24 – Structures of: dicoumarol, warfarin, acenocoumarol and carbochromen. . 28
Figure 25 – Structure of novobiocin, clorobiocin and coumermycin A1. 28
Figure 26 – Structure of suksdorfin. 29
Figure 27 – Structures of geiparvarin (A) and novobiocin-inspired compounds (B). 29
Figure 28 – Structures of dual-target inhibitors. 30
Figure 29 – Condensation reactions used for coumarin synthesis. 31
Figure 30 – Perkin reaction. 32

Figure 31 – Pechmann reaction. 33
Figure 32 – Wittig (at the top) and Reformatsky reactions (at the bottom). 33
Figure 33 – Knoevenagel condensation. 34
Figure 34 – Structures of khellin, cromoglycate and pranlukast. 36
Figure 35 – Structure of stellatin. 36
Figure 36 – Structure of chromone derivatives with anti-microbial activities. 37
Figure 37 – Structures of 3-phenylcarboxamidochromones with picomolar MAO-B activity. 38
Figure 38 – Structures of chromone-based AR ligands. 38
Figure 39 – Simonis (left) and Ruhemann reactions (right). 39
Figure 40 – Synthesis of coumarins and chromones depending on MA structure. 39
Figure 41 – Chromones synthesised using salicylic acids as building blocks. 40
Figure 42 – Tautomerism between 2-hydroxychromones and 4-hydroxycoumarins 40
Figure 43 – Synthesis of 2-ethylchromone from 4-hydroxy-3-propionylcoumarin. 41
Figure 44 – Proposed conversion mechanism of 4-hydroxycoumarin (A) into 2,3-disubstituted chromones (B). 41
Figure 45 – Claisen condensation and lactonization. 42
Figure 46 – Chromone synthesis via Baker-Venkataraman rearrangement. 43
Figure 47 – Synthesis of 3-substituted chromones. 43
Figure 48 – Benzopyrone-based libraries developed in the thesis. 195
Figure 49 – Methodologies followed for the synthesis of 3-carboxamidocoumarin-based libraries. 196
Figure 50 – Methodology followed for the synthesis of 3-arylcoumarin-based library. 202
Figure 51 – Methodology followed for the synthesis of compounds **90**-**102**. 202
Figure 52 – Methodology followed for the synthesis of compounds **103**-**108**. 205
Figure 53 – Methodology followed for the synthesis of compounds **109**-**115**. 205
Figure 54 – Methodologies followed for the synthesis of 3-carboxamidochromone-based library. 207
Figure 55 – HMBC spectrum of compound **22**. 209
Figure 56 – X-ray structure of compound **33**. 209
Figure 57 – X-ray structure of compound **58**. 210
Figure 58 – X-ray structure of compound **27**. 210
Figure 59 – MAO-B activity of compounds **29** and **33**. 213
Figure 60 – Kinetic and reversibility profiles of compound **29**. 214
Figure 61 – MAO-B activity of coumarin and chromone derivatives. 215
Figure 62 - Kinetic and reversibility profiles of compounds **30** and **118**. 215
Figure 63 – MAO-B docking poses of compounds **30** and **118**. 216

Figure 64 – AR affinity of compounds **96**, **100** and **101**. 217
Figure 65 – AR selectivity and affinity of ocmpounds **5**, **22** and **39**. 217
Figure 66 – AR affinity and MAO-B activity of compounds **11** and **44**. 218
Figure 67 - A_3AR docking poses of compounds **5** and **11**. 218
Figure 68 - A_3AR and A_{2A}AR docking poses of compound **39**. 219
Figure 69 – Structures and AChE and MAO-B inhibitory activities of compounds **12**, **14** and **24**. 220
Figure 70 – Rational design of coumarin-quinoline hybrids. 220
Figure 71 – Docking pose of compound **81**, in yellow, in AChE active site. 221
Figure 72 – Lead compounds for MAO-B inhibitors. 223
Figure 73 – Multi target hits: compound **24** and **44**. 224

Table Index

Table 1 – Benzopyrone library based on aryl-3-carboxamidocoumarins. 197
Table 2 - Benzopyrone library based on quinolinyl-3-carboxamidocoumarins. 199
Table 3 - Benzopyrone library based on 3-arylcoumarins derivatives. 203
Table 4 - Benzopyrone library based on nitrooxy coumarin derivatives. 206
Table 5 - Benzopyrone library based on 3-carboxamidochromone........................... 208
Table 6 – Drug-like properties of several compounds of the benzopyrone library...... 212

Abbreviations Index

ACh – Acetylcholine

AChE – Acetylcholinesterase

AD – Alzheimer's disease.

AIBN – Azobisisobutyronitrile

AMP – Adenosine monophosphate

AR – Adenosine receptors

APP – Amyloid protein precursor

BACE – β-secretase

BBB – Blood-brain barrier

CAS - Catalytic anionic site

CNS – Central nervous system

COMT – Catechol *O*-methyl transferase

COSY – Correlation spectroscopy

DA – Dopamine

DCC – *N*,*N*'-diciclohexylcarbodiimide

DCM – Dichloromethane

DEPT – Distortionless enhancement by polarization transfer

DMAP – 4-Dimethylaminopyridine

DMF – Dimethylformamide

DMSO – Dimethyl sulfoxide

EDC – 1-Ethyl-3-(3-dimethylaminopropyl)carbodiimide

EI/MS – Electronic impact mass spectrometry

EOAD – Early onset Alzheimer's disease

ES – Esteratic site

FAD – Flavin adenine dinucleotide

FDA – Food and Drug Administration

GABA – γ-aminobutyric acid

HBA – Hydrogen bond acceptors

HBD – Hydrogen bond donors

HBMC – Heteronuclear multiple bond connectivity

HIV – Human immunodeficiency virus

HSQC - Heteronuclear single quantum coherence

HTS - High throughput screening

IUPAC – Internation Union of Pure and Applied Chemistry

L-DOPA – Levodopa

LOAD – Late onset Alzheimer’s disease

MA – Meldrum’s acids

MAO – Monoamine oxidase

MRSA - Methicillin-resistant *Staphylococcus aureus*

MW – Molecular weight

NBS – *N*-bromosuccinimide

NCE – New chemical entities.

ND – Neurodegenerative diseases

NFT – Neurofibrillary tangles

NMDA – *N*-methyl-D-aspartate

NMR – Nuclear magnetic resonance

*N*rotb – Number of rotatable bonds

PAS – Peripheral anionic site

PD – Parkinson’s disease.

ROS – Reactive oxygen species

SAR – Structure-activity relationship

SI – Selectivity index

SNP – Senile neuritic plaques

TBMDSCL – *tert*-butyldimethylsilyl chloride

TFA – Trifluoroacetic acid

TPSA – Topological polar surface area

CHAPTER 1

1.1. Introduction

Chemistry has been defined and redefined throughout the years, most recently by Dr. Raymond Chang, who gave the broadest definition of all stating that "*Chemistry is the study of matter and the changes it undergoes*".[1] Indeed, a broad definition is probably the best, given that so many fields of study are intrinsically connected to Chemistry, even the study of life itself, Biology. From the smallest to the largest, every living organism is dependent on organic molecules and the changes, or reactions, they undergo. In this sense, it is not surprising that many areas of study encompass these two subjects and, in this symbiosis, the study of Medicinal Chemistry grew.

This discipline deals with the design and discovery of new compounds and their development into useful medicines.[2] Even though its definition is fairly recent, for several thousands of years mankind has been practising Medicinal Chemistry by searching cures for ailments using diverse natural sources, like plants, roots, and berries. Initially, the search and use of medicines based on natural sources was based on empiric knowledge, and neither the chemical nature of the pharmacologically active compounds nor their exact mechanism of action was understood. Since then, our understanding of the chemistry and biology of the human organism grew exponentially. The development of new chemical entities (NCE) inspired in natural products drove drug discovery and development into its golden age.[3]

Nevertheless, there is still a long road to travel when it comes to neurodegenerative diseases (ND), since the pace of drug development has not accompanied the shift in demographics in industrialized countries. According to the latest data from the United Nations development report,[4] the majority of developed countries faces a demographic shift towards an elderly age group (Fig. 1). This implies that the number of patients with age-associated illnesses, like Alzheimer's disease (AD) and Parkinson's disease (PD), is increasing. In fact, in a 2015 report the Alzheimer's Disease International estimated that over 46 million people worldwide had AD and forecasted that number to increase up to 131 million by 2050.[5] Aside from the obvious health concerns and the progressive loss of cognitive function for the affected population, this also represents an important strain on the global economy, since the cost of AD is expected to reach 1 trillion US dollars by 2018.[5]

The same applies to PD, with an estimated prevalence of 1% of the worldwide population over 60 years old, potentially reaching 4% in oldest demographics.[6] Unfortunately, no shift in this paradigm is foreseeable, as it is projected that the population affected with

PD will double by 2030.[7] The economic burden of PD is also significant;[8] for instance, it estimated that in Europe, the yearly PD-associated costs will sum up to approximately 14 billion euros.[8]

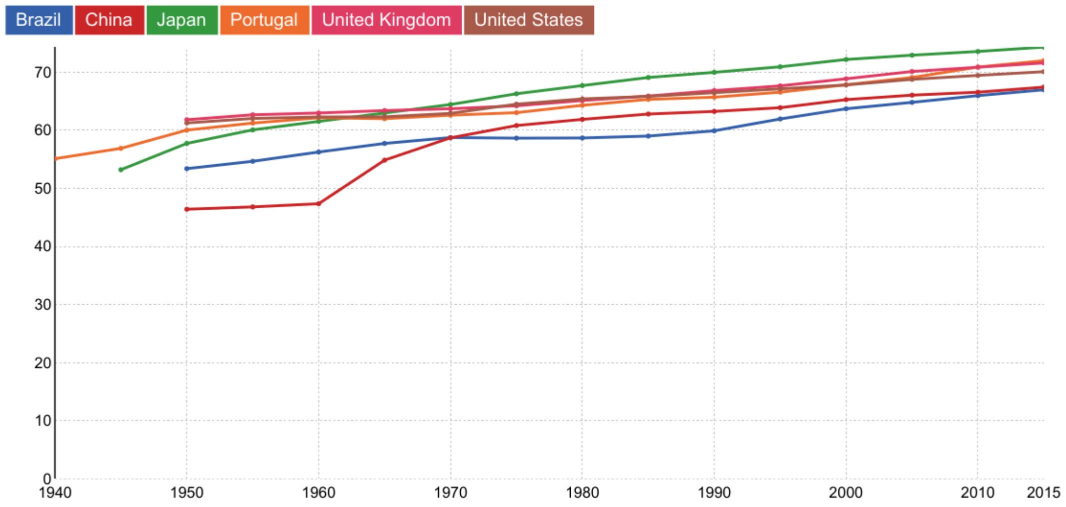

Figure 1 – Global life expectancy for both genders since 1950. From the United Nations Population Division and Human Mortality Database.[4]

Although these matters spark great interest and effort from pharmaceutical companies, no new and effective drugs have been released in the market. As it stands today, drug discovery is a fairly complex and time consuming endeavour. Moreover, the classic «one drug-one target» strategy, albeit successful in many cases, is slowly being replaced by a multi target approach, especially in multifactorial diseases like AD and PD.[9–11] Nevertheless, there is still a pressing and unmet clinical demand for NCE that can effectively overcome the challenges posed by these diseases.

1.2. Neurodegenerative diseases

Adding to their heterogeneous clinical expression, ND are broadly characterized by progressive degeneration of the structure and function of neuronal networks. According to epidemiological studies, AD and PD are the most prevalent ND, representing a heavy burden on the patient, family, caregivers and society.[5] Still, there is no cure available and, in spite of several different hypothesis being explored and studied in detail, no exact causes have yet been identified. However, it is consensual that these diseases are multifactorial and that symptoms arise as a result of impaired neuronal networks. Moreover, the available therapies are only palliative and are unable to halt or reverse disease progression. As such, the design and development of new disease modifying drugs is a priority and an unmet clinical need for millions of patients worldwide.

1.2.1. Parkinson's disease

The english surgeon James Parkinson, first described PD as an "*Involuntary tremulous motion, with lessened muscular power, in parts not in action and even when supported; with a propensity to bend the trunk forwards, and to pass from a walking to a running pace: the senses and intellects being uninjured*."[12] Nowadays, PD affects up to 10 million people worldwide, which makes it the second most prevalent ND.[6] Its main symptoms are tremors, hypokinesia, postural instability and mobility problems in the later stage, sometimes accompanied with psychological disorders such as anxiety and depression.[13] The pathophysiology of PD is mainly characterized by the loss of dopaminergic neurons in the *substantia nigra pars compacta* region of the midbrain, which leads to widespread dopamine (DA) depletion.[14]

In spite of being a high impact and extensively studied disorder, PD is still incurable and its aetiology remains unknown. Nevertheless, there are clues that point out that the loss of the dopaminergic neurons is associated with several different pathological mechanisms, such as impaired calcium homeostasis, inflammation, protein aggregation and inefficient metabolism.[15,16] In addition, several studies have shown that oxidative stress is a key factor in neuronal death, since mitochondrial dysfunction was observed in patients with PD.[17,18] Other risk factors have also been associated with PD, like genetics and environmental toxins.[19–21]

The motor symptoms of PD may derive mainly from DA reduction in the basal ganglia.[22] Several pathological features have been identified in PD, such as functional and anatomical alterations in the basal ganglia, thalamus and cortex, as well as DA depletion in these areas.[22] Moreover, the motor impairments and psychiatric manifestations are associated not only with DA deficiency in the brain, but also with its role in the modulation of other neurotransmitters, such as serotonin, acetylcholine (ACh), γ-aminobutyric acid (GABA), glutamate or norepinephrine.[14]

1.2.1.1. Dopaminergic therapy of Parkinson's disease

1.2.1.1.1. Dopamine

Given the establishment of dopaminergic loss as a pathological hallmark of PD, the therapeutic strategies until now have been focused on boosting the levels of DA in the brain. Since the results published by Yahr *et al.*[23] in the late 60's, levodopa (L-DOPA) is the gold standard drug for the clinical management of PD.[24] L-DOPA is a biosynthetic DA precursor which is decarboxylated by DOPA decarboxylase to yield DA in the brain (Fig. 2). The administration of L-DOPA is a therapeutic strategy to indirectly enhance DA levels within the central nervous system (CNS).

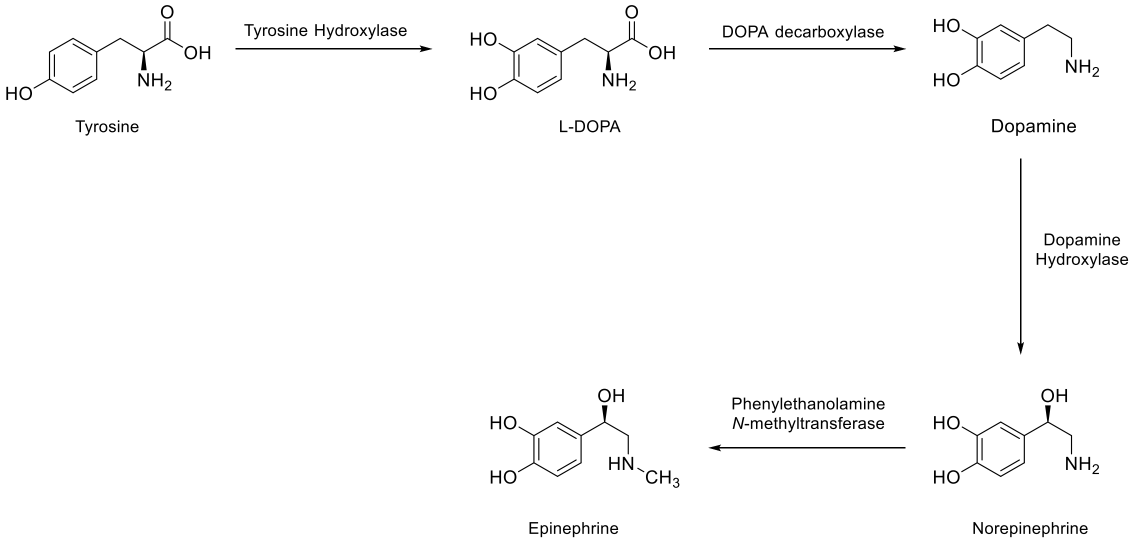
Tyrosine
Tyrosine Hydroxylase
L-DOPA
DOPA decarboxylase
Dopamine
Dopamine Hydroxylase
Norepinephrine
Phenylethanolamine *N*-methyltransferase
Epinephrine

Figure 2 – Dopamine metabolism.

However, long-term treatment with L-DOPA often induces serious adverse effects like nausea, vomiting, psychosis and diskinesias.[25] Moreover, its biological half-life is very reduced (60-90 min), which requires multiple daily administrations.[26] Furthermore, L-DOPA sustained treatment in PD patients induces "on-off" phenomenon.[27] The "on-off" phenomenon comprises profound diurnal fluctuations in the psychomotor state, where phases of dyskinesia and incapacity associated with depression alternate with jubilant periods.[27] In order to improve L-DOPA bioavailability, the use of enzyme inhibitors that prevent L-DOPA peripheral catabolism (e.g. carbidopa or benserazide) has been introduced (Fig. 3).

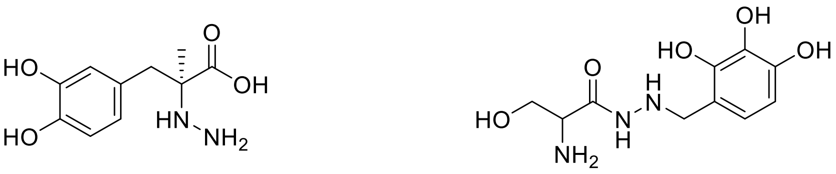

Carbidopa Benserazide

Figure 3 – Structures of carbidopa and benserazide.

Notwithstanding, L-DOPA remains the most effective treatment for the archetypal motor symptoms of PD. In addition to stimulating DA receptors, L-DOPA-derived DA might also activate adrenoceptors (a class of G protein-coupled proteins), DA transporters and trace amine receptors, all of which might contribute to the superior effect of L-DOPA in PD.[28]

1.2.1.1.2. Dopamine receptor agonists

In general, DA receptor agonists are divided into two main classes: ergot or non-ergot agonists. These two classes are defined according to a particular structural parameter, which is the presence or absence of an ergoline-like structure (Fig. 4). As an example, ergot agonists include bromocriptine, pergolide, and cabergoline, while non-ergot agonists include pramipexole, ropinirole, apomorphine and piribedil (Fig. 4).[29]

Generally, DA receptor agonists are effective in reducing the incidence of motor complications arising from long-term L-DOPA therapy.[29–31] There is increasing evidence that DA receptor agonists are not only beneficial to postpone L-DOPA therapy in early PD, but also have a neuroprotective effect.[32] The mechanism of DA receptor agonist-induced neuroprotection is mainly associated with their radical scavenging properties.[32] Also, DA receptor agonists were reported to have an important role in the CNS as neurogenesis promotors.[33]

However, many side effects to DA receptor agonists have been reported, mainly impulse control disorders such as hyper sexuality or binge eating. In order to diminish these effects, this therapy is initiated with low dosages and is slowly increased throughout an extended period of time to improve tolerance.[34]

1.2.1.1.3. Catechol-O-methyltransferase inhibitors

Catechol-*O*-methyltransferase (COMT) was first discovered by biochemist Julius Axelrod in 1957 and since then its function has been extensively studied.[35,36] Due to its role in DA metabolism (Fig. 5), COMT is a pharmacological target for the treatment of PD.

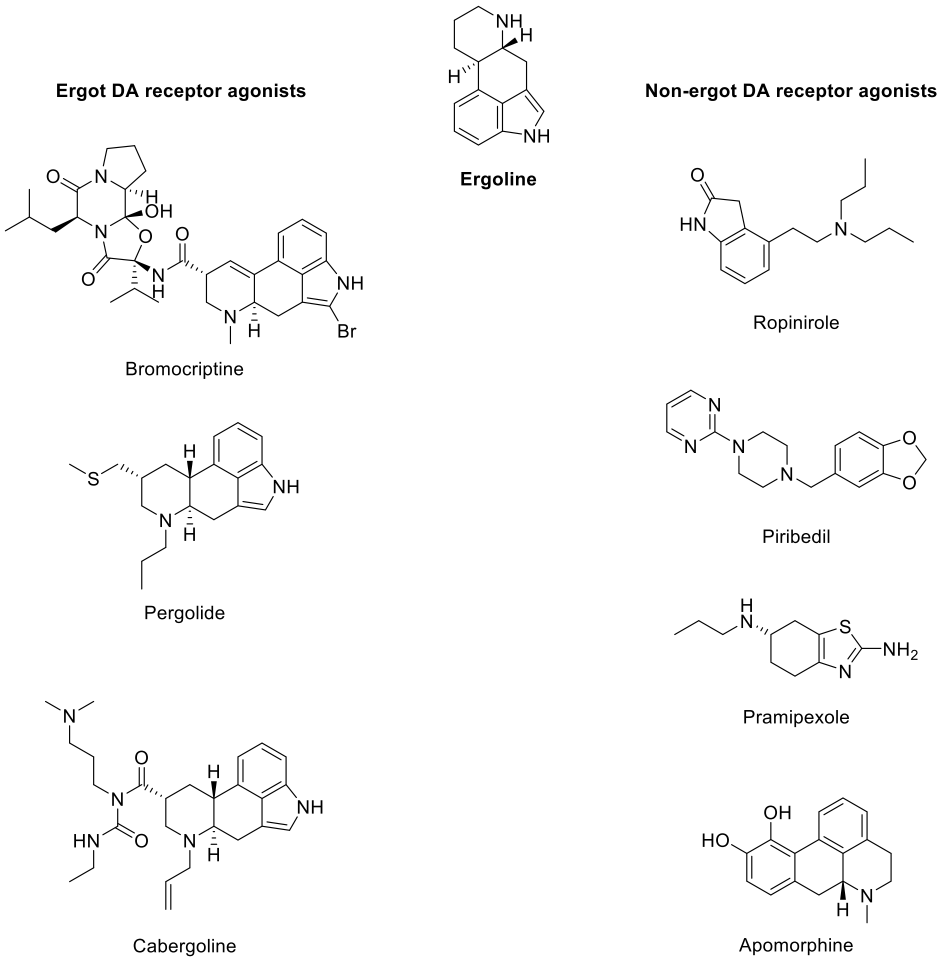
Ergot DA receptor agonists
Ergoline
Non-ergot DA receptor agonists
Bromocriptine
Ropinirole
Piribedil
Pergolide
Pramipexole
Cabergoline
Apomorphine

Figure 4 – Structures of ergoline, and ergot and non-ergot dopamine receptor agonists.

Peripherally, COMT can be found in large quantities in the liver and kidneys, where it promotes the *meta* oriented methylation of catecholamines.[36] Specifically, L-DOPA is extensively inactivated by peripheral COMT.[37] The pharmacological blockade of the degradation of L-DOPA by COMT inhibitors prevents its peripheral degradation and increases its plasma half-life, allowing orally administered L-DOPA to cross the blood-brain barrier (BBB) into the brain, where it is locally decarboxylated to DA.[38,39] This pharmacological approach indirectly compensates the extensive dopaminergic loss observed in PD patients.

Early catechol-based competitive COMT inhibitors lacked *in vivo* efficacy and had low plasmatic half-lives, showing poor selectivity and toxicological constrains.[36]

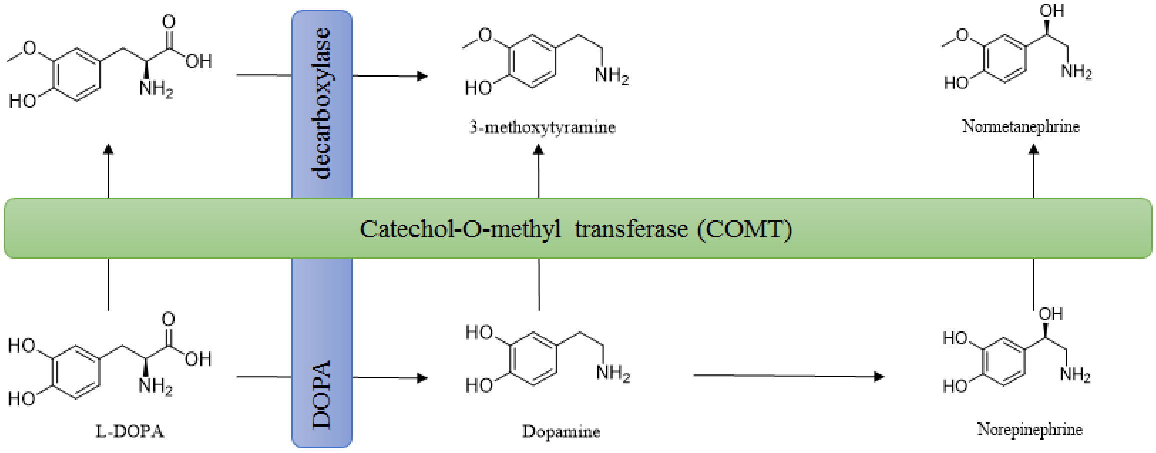
decarboxylase
DOPA
Catechol-O-methyl transferase (COMT)
3-methoxytyramine
Normetanephrine
L-DOPA
Dopamine
Norepinephrine

Figure 5 – L-DOPA, dopamine and norepinephrine metabolism by COMT.

Later on, second generation inhibitors were developed and, due to their increased efficacy over first generation inhibitors,[40] were introduced in the market for PD adjuvant therapy.[41] These selective and orally active COMT inhibitors bear a nitrocatechol scaffold, which is the pharmacophore for second generation tight-binding COMT inhibitors (Fig. 6).

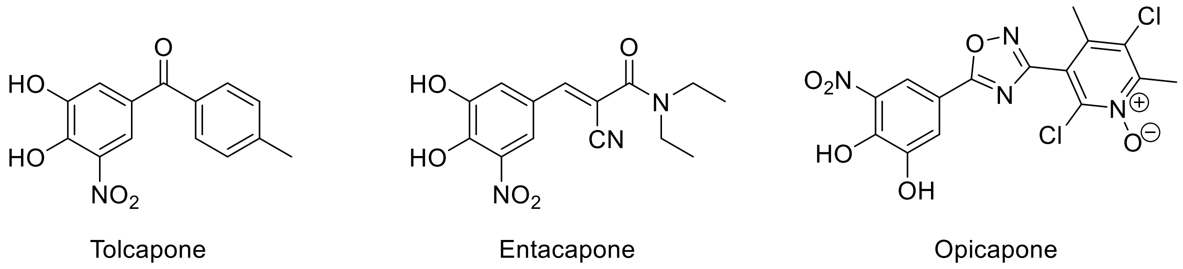
Tolcapone
Entacapone
Opicapone

Figure 6 – Structure of second generation COMT inhibitors.

Tolcapone and entacapone (Fig. 6) are highly selective and potent COMT inhibitors. The main difference between these two drugs relies on pharmacokinetics, particularly in brain bioavailability. Entacapone is a peripheral COMT inhibitor, while tolcapone is able to cross the BBB into the CNS, where it can locally prevent L-DOPA degradation catalysed by COMT.[42] Nevertheless, tolcapone has a high risk of hepatotoxicity,[43] and is currently used under very strict conditions and controlled medical supervision. Although entacapone has not been linked to hepatotoxicity risk, it has been associated with adverse effects, including nausea, vomiting and dyskinesia.[44] Accordingly, a third generation inhibitors was designed and tested for adjunctive therapy for PD. A new drug called opicapone (Fig. 6) successfully passed clinical trials, with 9 out of 600 patients experiencing severe adverse effects in phase III trials.[45] Also, it reduced off-times in PD patients by 2 hours compared to entacapone.[45] Under the brand name Ongentys®, opicapone was recently introduced in the United Kingdom and it is expected to be launched in the rest of European market in 2017.[46]

1.2.1.1.4. Monoamine oxidase inhibitors

Monoamine oxidases (MAOs) are flavin adenine dinucleotide (FAD)-containing enzymes mainly found in the outer mitochondrial membrane and are responsible for the metabolism of endogenous amines.[47] MAOs have two known isoforms, MAO-A and MAO-B, which catalyse the oxidation of different biogenic amines. The main MAO substrates are neurotransmitters such as adrenaline, noradrenaline, DA, serotonin and *β*-phenylethylamine. Under physiological conditions, noradrenaline and serotonin are substrates of MAO-A, while DA and β-phenylethylamine have a greater affinity for MAO-B.[48] MAOs metabolise neurotransmitters by oxidizing the amine function to an aldehyde, in a process where the FAD cofactor is reduced (Fig. 7). The FAD cofactor is then oxidized again by molecular oxygen, in a reaction where hydrogen peroxide (H_2O_2) is generated (Fig. 7).

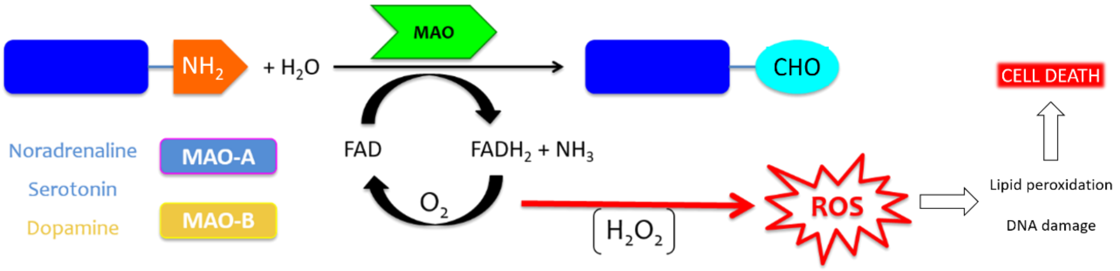

Figure 7 – MAOs catalysed reactions.

Although glutathione peroxidases can reduce hydrogen peroxide into water, the highly reactive hydroxyl radical can still be generated by a Fenton and Haber-Weiss reaction.[49,50] In this sense, MAO-B is a pharmacological target for the treatment of PD, since its inhibition enhances DA levels. Selective MAO-B inhibitors are generally a valid asset in early PD therapy in combination with L-DOPA. In fact, MAO-B inhibitors are administered in patients with mild motor symptoms before other pharmacological alternatives.[47] Moreover, MAO-B inhibitors may reduce the rate of motor fluctuations compared to initial L-DOPA therapy, with fewer adverse effects than DA receptor agonists.[51]

The first selective and irreversible MAO-B inhibitors introduced in the market were selegiline (L-deprenyl) and rasagiline (Fig. 8). However, some authors suggest that selegiline metabolism can lead to amphetamine-like metabolites, which can be neurotoxic.[52] On the other hand, the metabolism of rasagiline does not produce toxic metabolites.[53] In fact (*R*)-1-aminoindan, the major metabolite of rasagiline, exerts neuroprotective effects in PD animal models.[54] Similarly to selegiline, rasagiline improves the symptoms of PD patients, but it is more efficient if administered on the early stages of the disease.[55]

Recently, safinamide (Fig. 8), commercialized under the name of Xadago® was approved in Europe and United States.[56] Contrarily to selegiline and rasagiline, safinamide is a reversible MAO-B inhibitor.[57] In Europe, safinamide is approved for the treatment of mid- to late-stage fluctuating PD as add-on therapy to a stable dose of levodopa alone or in combination with other PD medications.[56] In 24-week, placebo-controlled clinical trials, safinamide increased daily on-time without dyskinesia in patients with mid- to late-stage PD with motor fluctuations.[58]

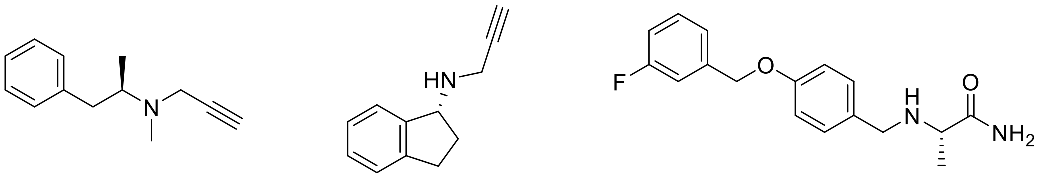

Selegiline Rasagiline Safinamide

Figure 8 – Structures of selegiline, rasagiline and safinamide.

1.2.1.2. Non-dopaminergic approaches in PD therapy

1.2.1.2.1. Adenosine and adenosine receptors

Current therapies for PD are mainly focused on targets of the dopaminergic system. However, it was found that this approach is not innocuous and could lead to severe complications, as previously discussed in item 1.2.1.1..[57,59] The drawbacks of dopaminergic therapies provided a driving force for the study of non-dopaminergic targets, such as adenosine receptors (AR). Adenosine is a purine nucleoside which regulates a plethora of CNS processes, such as learning and memory.[60] The responses triggered by adenosine are mediated by AR, which are G protein-coupled receptors embedded in cell membranes. Four different subtypes of AR are known, namely A_1, A_{2A}, A_{2B} and A_3.[61] Mechanistically, they differ on their action towards adenylate cyclase; A_1AR and A_3AR inhibit downstream adenylate cyclase, while the A_{2A}AR and A_{2B}AR subtypes have the opposite outcome (Fig. 9).[62]

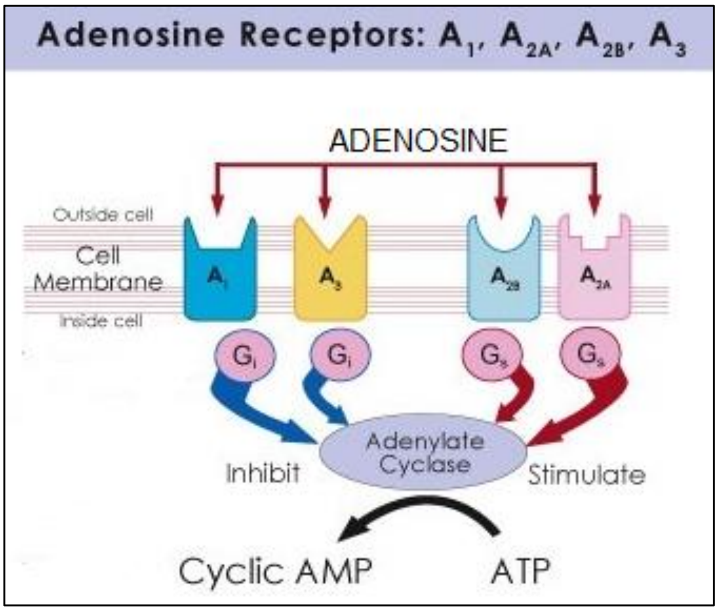

Figure 9 – Adenosine receptors.

While adenosine signalling is important in several CNS functions,[60] the most important within the context of PD are neuroprotection, locomotor effects and the control of DA levels.[63] The crosstalk between adenosine and DA has been extensively studied.[64] Besides DA, adenosine modulates the production and transmission of other neurotransmitters such as glutamate and, more importantly, GABA.[60,65] Stimulation of A_{2A}AR resulted in an increased release of GABA, while the activation of A_1AR inhibits its production.[60]

The A_{2A}AR is currently considered an important target for PD, due to its location and physical association with DA receptors.[66] In spite of their physical proximity and a tight interplay, they may have antagonic effects on specific signaling mechanisms, for instance in cyclic adenosine monophosphate (cAMP) production.[67,68] Moreover, it is known that A_{2A}AR activation reduces affinity of DA receptors in the striatum for its agonists and that its blockade increases DA receptors activity.[65] Aside from reducing the effects of DA depletion in the brain, A_{2A}AR antagonists showed potential neuroprotection and anti-inflammatory activity.[69] Preclinical studies in animal models of PD have shown that $A_{2A}AR$ antagonists in monotherapy can alleviate PD symptoms.[70,71] Moreover, the combination of $A_{2A}AR$ antagonists with L-DOPA can successfully reduce the effective dosage of the latter and, consequently, its side effects.[72,73]

Chemically, $A_{2A}AR$ antagonists can be classified in two categories: xanthine derivatives (*e.g.*: caffeine), and non-xanthine derivatives (*e.g.*: pyrimidines) (Fig. 10). Several compounds were found to act as $A_{2A}AR$ antagonists (Fig. 10), but clinical data regarding their effects in PD is scarce. Albeit several $A_{2A}AR$ antagonists have been described, only istradefylline, preladenant and vipadenant (Fig. 10) were studied in detail in preclinical and clinical settings for PD.

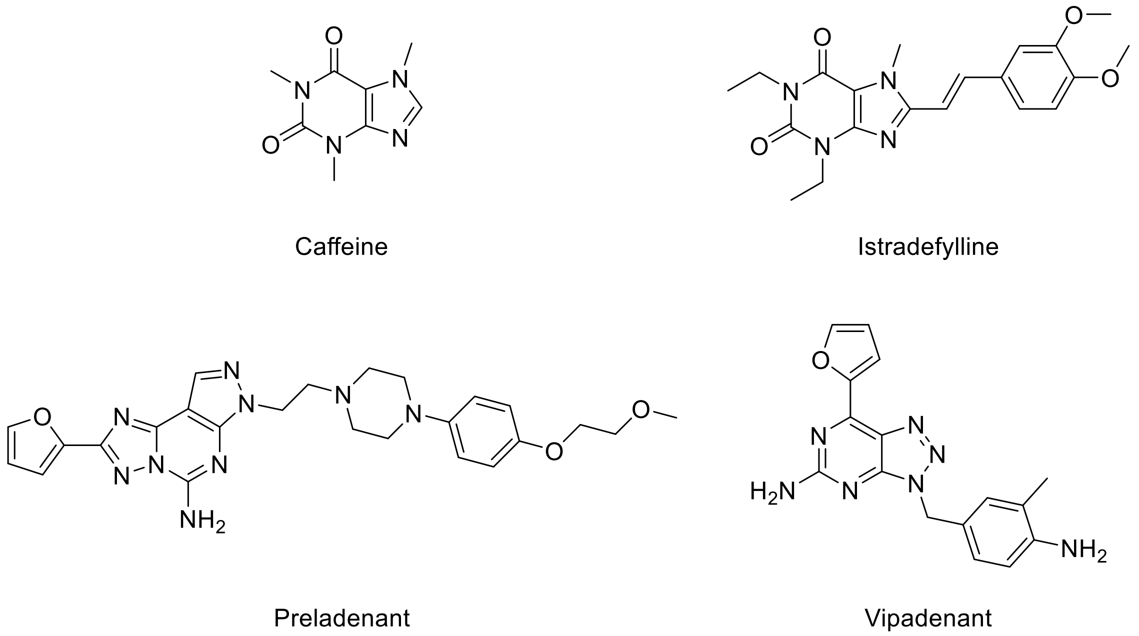
Caffeine
Istradefylline
Preladenant
Vipadenant

Figure 10 – Structure of A_{2A} AR antagonists.

Istradefylline (Fig. 10) was well tolerated in phase I clinical trials,[74] and offered a clinically meaningful reduction in off-time without increased troublesome dyskinesia.[75] However, the Food and Drug Administration (FDA) issued a non-approvable letter in 2008 demanding more follow-up data as part of phase IV evaluation commitments.[74] Thereafter, istradefylline has been approved for the treatment of PD in Japan.[74] Preladenant had positive results in phase II clinical trials in humans, although it did not prove to be more effective than placebo in phase III studies and, as a result, was discontinued in May 2013.[76,77] Finally, vipadenant studies were suspended due to safety concerns.[78,79] Nevertheless, vipadenant served as a scaffold for new generation compounds, one of which is in phase I clinical trials, still with undisclosed results.[80]

1.2.2. Alzheimer's disease

AD was first described in 1906, when a German neuropathologist named Alois Alzheimer gave a lecture on a case of a 51 year old woman suffering of severe dementia. At that time, her case was a curiosity, but it is now evident that she was suffering from a rare early onset form of AD. Nowadays, this progressive and degenerative disease is the most common cause of senile dementia.[81]

Chronologically, AD can be divided into three stages. In the initial stage, symptoms usually start with manifestations of cognitive deficit, such as the inability to produce new memories and skills.[82] In the intermediate stage, patients begin to show problems with speech and not being able to handle simple everyday tasks, such as dressing themselves and attending to their personal hygiene.[83] In the most advanced phase, AD is characterised by a state of full incapacity, confusion and disorientation.[84] In this phase, patients have major difficulties in mobility and frequently suffer from hallucinations and deliriums.[85] The most common form of this disease is the late-onset AD (LOAD) form, which accounts for approximately 95% of AD cases.[86] The specific cause of AD is still unknown, although some risk factors have been pointed out, such as advanced age or family history.[87] On the contrary, early onset AD (EOAD) is inherited by an autosomal dominant disorder, with four genes associated with disease onset and progression: the amyloid protein precursor (APP), preselinin 1 and 2, and the *ε*4 allele of the apolipoprotein E gene.[88]

The classic features in AD patients brains are: a) neuronal loss in regions linked with memory and cognition, mainly in the cholinergic neurons; b) low neurotransmitter levels, mainly acetylcholine (ACh) and c) synaptic dysfunction.[86,89] The histopathology of the disease is well studied, and AD brains often present abnormal protein deposits like senile neuritic plaques (SNP) and neurofibrillary tangles (NFT). Physiological *β*-amyloid protein has short beta sheets in solution in the cell, but when misfolded into tertiary structures, it can form SNP and abnormal extracellular deposits.[90] On the other hand, NFT are formed intracellularly, and are a product of an abnormal protein aggregation. Although tau protein is normally responsible for stabilizing the cytoskeleton, in AD it is aberrantly phosphorylated, which leads to protein aggregation and, ultimately, to an insoluble mass inside the cell.[91]

The formation of SNP and/or NFT leads to atrophy in the affected areas, usually the temporal and parietal lobes and in certain parts of the frontal cortex,[92] leading to reduced ACh levels. These effects may contribute to more death of cholinergic neurons resulting in a positive feedback loop.[93] Along this process, the levels of serotonin and norepinephrine levels are low while glutamate levels are usually high.[94,95]

Even though the histological hallmarks of the disease are well known, the primary cause of AD remains unknown. There are several hypothesis pointed out by different research groups in order to explain the disease onset and progression. The first hypothesis to be suggested was the cholinergic hypothesis,[96–98] but other have been proposed such as the amyloid hypothesis,[99–101] the glutamatergic hypothesis,[98,102,103] the oxidative stress hypothesis,[104–106] metal hypothesis,[107–109] and the inflammatory hypothesis.[87,110,111]

Current AD therapies are based on the cholinergic and glutamatergic hypothesis, and include acetylcholinesterase (AChE) inhibitors and *N*-methyl-D-aspartate (NMDA) receptor antagonists.[112] Nonetheless, none of the currently approved drugs is able to slow down disease progression, and provide only symptomatic relief. Thus, there is a pressing and unmet clinical need for new and potent anti-Alzheimer drugs.

1.2.2.1. Acetylcholinesterase inhibitors

The contractions of smooth muscle in several organ systems, including gastrointestinal and urinary tract, and eye movement is mediated by ACh.[113] This neurotransmitter is also responsible for decreasing heart rate and vasodilation.[114] Moreover, the cholinergic transmission has a vital role in the modulation of cerebral blood flow, memory and cognition.[115] According to the cholinergic hypothesis, the cholinergic system is the most affected in the early AD development.[93] As a consequence, there is a loss of enzymatic function for ACh synthesis, leading to memory loss and deterioration of cognitive and non-cognitive functions which sometimes culminates in psychiatric symptoms.[116]

The levels of ACh in the synaptic cleft are tightly regulated by AChE (Fig. 11), which can also be found in neuromuscular junctions and plasma.[87]

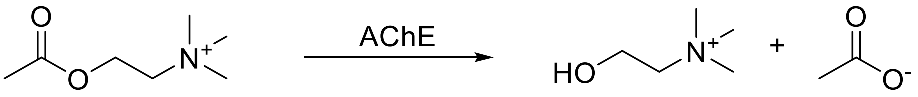

Figure 11 – AChE catalysis of ACh.

According to Sussman *et al.*[117], the active site of AChE is located at the bottom of a narrow gap, in which the catalytic anionic site (CAS) encloses four subsites: a) the anionic site, where the positively charged ACh interacts, b) the esteratic site (ES), which contains the three residues of the catalytic triad, c) the oxyanion hole and d) the acyl pocket, which is responsible for substrate selectivity. Another different sub-unit in the enzyme's active site is known as the peripheral anionic site (PAS) and it is located roughly 15 Å above the CAS (Fig. 12).

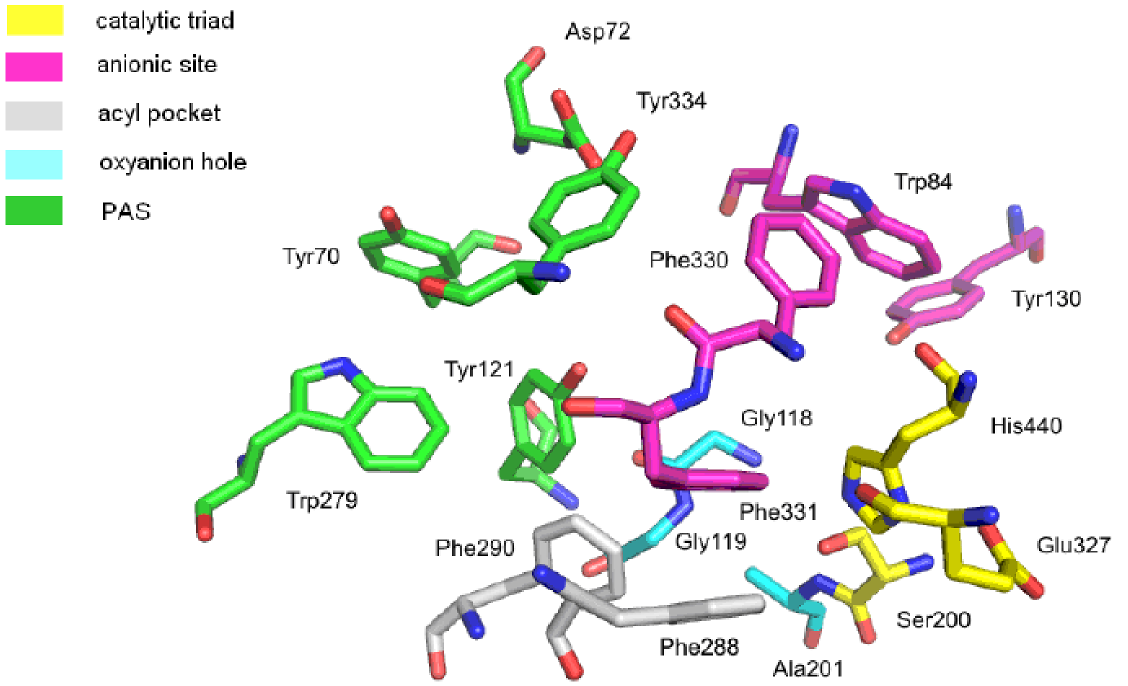

Figure 12 – Active site of AChE.

It is generally accepted that AChE acts not only as a key regulator of cholinergic transmission, but can also display a non-cholinergic function, attributed to the active site's PAS, namely promoting *β*-amyloid deposition.[118] This interaction promotes conformational changes in β-amyloid fibrils and induces the formation of SNP.[119] All these findings deepen the overly simplistic cholinergic hypothesis, and validate the use of AChE inhibitors as a valid approach to manage AD.[87]

The first AChE inhibitor approved as a drug was tacrine (Fig. 13), but its use has been discontinued due to its severe hepatotoxicity.[120] In spite of not being used anymore, tacrine is still used as scaffold for the design and development of novel AChE inhibitors.[87]

Currently, only three AChE inhibitors (Fig. 13) were approved by the FDA for the clinical management of AD, namely donepezil, rivastigmine and galantamine.[121] All compounds are known for their clinical benefits to patients' cognitive functions, leading to an improvement of the day-to-day activities and global functions.[122,123] However, donepezil is the only compound approved in the USA for patients with severe AD.[124] Although this type of inhibitors proved to delay cognitive decline for periods of up to 12 months, they exhibit several adverse effects, such as nausea, vomiting and diarrhoea.[122] Moreover, their use is also associated with higher rates of bradycardia and syncope, outlining a feeble risk-benefit relationship that requires careful consideration on later disease stages.[125]

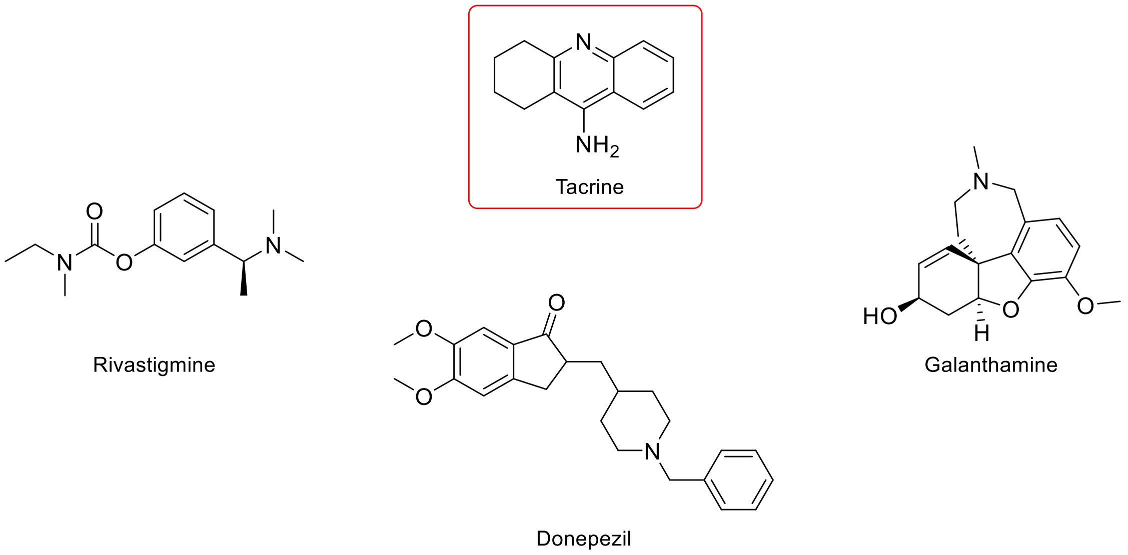

Figure 13 – Structures of tacrine, in red, and rivastigmine, donepezil and galanthamine.

Even though all these compounds enabled a noteworthy advance in the clinical management of AD, the research and development of new potent AChE inhibitors having disease-modifying properties is still an ongoing effort.[126]

1.2.2.2. *N*-Methyl-D-aspartate receptor antagonists

Glutamate is the most abundant neurotransmitter and it has an important role in neuronal differentiation, migration and survival in the developing brain.[127] It is also of particular interest due to its putative participation in the neurodegenerative processes.[128,129] Glutamate, endogenous and exogenous, can initiate cell death processes in AD, by causing excitotoxicity.[130] Excitotoxicity is a condition where neuronal damage is promoted by glutamatergic overstimulation, especially through an agonist effect on *N*-methyl-D-aspartate (NMDA) receptors, ultimately leading to calcium overload.[131,132] The role of NMDA in the neurodegenerative cascade is still elusive, but the subsequent selective neuronal death appears to be dependent on NMDA receptor activation.[130]

To this effect, NMDA receptor antagonists are an important therapeutic option for moderate to severe AD. Currently, only one NMDA receptor antagonist is marketed for the clinical management of AD.[131] Memantine (Fig. 14) is a NMDA receptor antagonist that protects neurons from excitotoxicity. McShane *et al*.[133] conducted a study in patients with moderate to severe AD showed a significant improvement in cognition, activities of daily living and behaviour following a 6 months treatment with memantine. Another study confirmed the previous findings and added that, under the treatment with memantine, patients reduced psychological symptoms of dementia.[134]

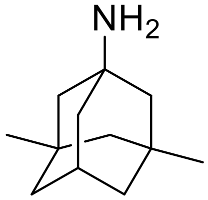

Figure 14 – Structure of memantine.

Nevertheless, patients undergoing memantine therapy frequently report side effects such as dizziness, headaches, confusion and agitation.[135] The combined therapy with memantine and donepezil (Fig. 13) in patients with severe AD showed a significant improvement in cognitive function, language and daily life activities when compared to memantine monotherapy.[136–138] The same outcome was not observed in patients with mild AD, therefore memantine is preferably administered in later stages of the disease, when patients have been already treated with donepezil.[139]

1.2.2.3. Other targets in Alzheimer's disease

The neurodegenerative cascade in AD has a wide range of pathologic features, which unveiled a large set of putative therapeutic targets. These targets are mostly enzymes involved in key physiological processes connected to neurodegeneration, such as MAO-B, secretases and caspases, among others.[87,140]

MAO-B inhibitors are more often used in PD therapy, as described in item 1.2.1.1.4. However, their neuroprotective effects may be useful in therapy of other ND including AD.[47,141] The metabolism of MAO-B leads to the formation of ROS and to an amplification of neuronal oxidative stress, as depicted in Fig. 7. Neurons are particularly susceptible to oxidative stress as a consequence of: a) their low pool in endogenous antioxidants, such as glutathione, b) high content on polyunsaturated fatty acids c) the great oxygen brain consumption and also d) a high content in iron.[142–144]

Secretases are enzymes that modulate the cleavage of the transmembrane APP (Fig. 15A) and are expressed in three isoforms: α-, *β*- and *γ*-secretase.[145] Briefly, the sequential cleavage by *β*-secretase (BACE) and *γ*-secretase leads to the *β*-amyloid fragment, which aggregates into SNP in AD patients (Fig. 15B). Contrarily, the processing of APP by α-secretase is non-amyloidogenic and yields a protective outcome, preventing the production of SNP (Fig. 15B).[145] Thus, owing to its amyloidogenic role, BACE is now considered a therapeutic target for AD.[145]

First generation BACE inhibitors were based on peptides, similar to the BACE cleavage site,[146] but several high affinity inhibitors with non-peptide backbones have thenceforth been developed.[147,148]

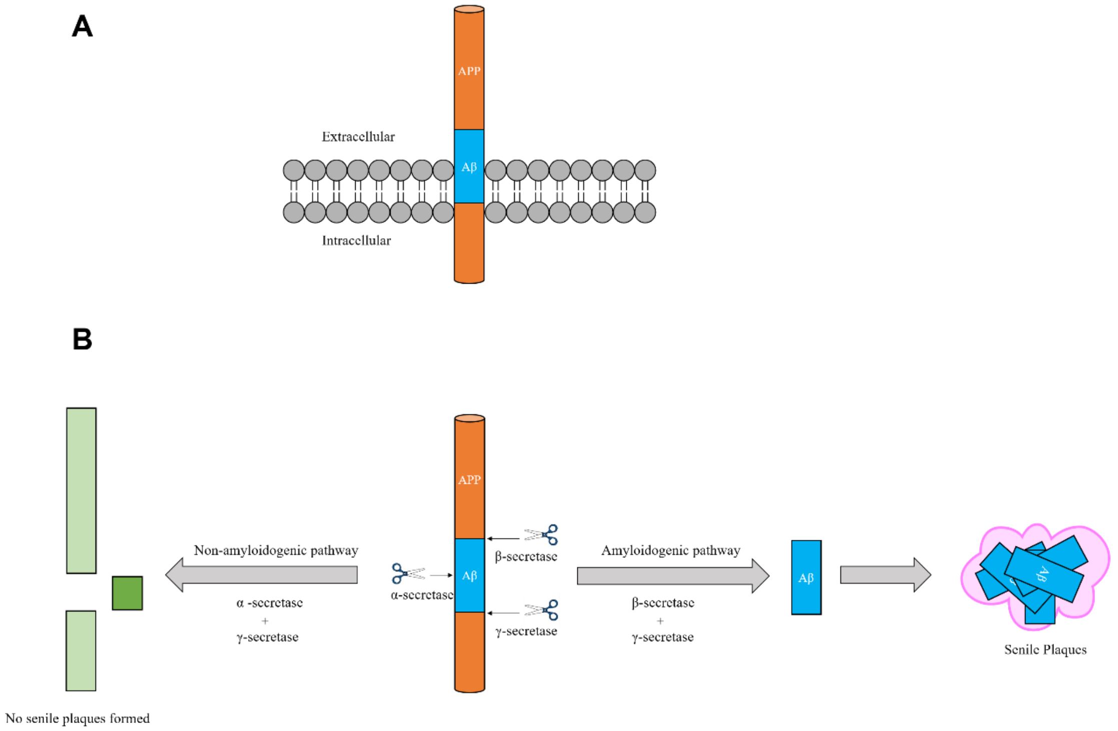
A
APP
Extracellular
Aβ
Intracellular
B
Non-amyloidogenic pathway
α -secretase
+
γ-secretase
APP
Aβ
α-secretase
β-secretase
γ-secretase
Amyloidogenic pathway
β-secretase
+
γ-secretase
Aβ
Aβ
Senile Plaques
No senile plaques formed

Figure 15 – Representation of the transmembrane protein APP and its degradation by different secretases.

Currently, the pharmaceutical company CoMentis has completed the first phase I clinical trial for a BACE inhibitor. However, the structure of the compound and trial results are undisclosed.[145,149] Additionally, two other inhibitors (AZD3293 and MK-8931, Fig. 16) finished Phase I clinical trials and are expected to end Phase II/III studies in 2019. Although the development of BACE inhibitors is in early stages, and information regarding their safety and toxicity is scarce, these preliminary findings of new BACE inhibitors are encouraging and may have a favourable outcome in LOAD.[149]

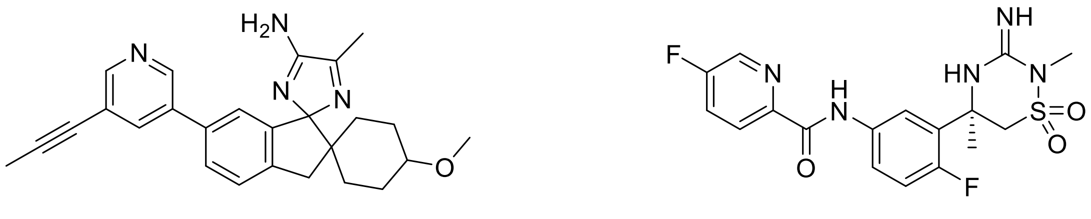

AZD3293 MK8931

Figure 16 – Structure of BACE inhibitors presently on clinical trials.

Caspases (cysteine-aspartic proteases) are a family of proteases are linked in cell regulatory networks, controlling inflammation and cell death.[150] Deregulated apoptosis caused by caspases have been linked to neurodegeneration processes and promotion of the biological cascade leading to AD.[151] Since the first caspase was identified by Horvitz *et al.*[152] several others have been discovered and categorised into two sub-families based on their biological function. Briefly, they were classified either as inflammatory caspases (caspase-1, -4, -5, -11 and -12) or apoptopic caspases (caspase-2. -3, -6, -7, -8, -9 and -10).[153,154]

Rohn *et al.*[151] hypothesized that *β*-amyloid fragments trigger the activation of caspases, leading to the proteolysis of tau and consequent NFT formation (Fig. 17). Along the biological cascade the over activation of caspases can lead to cytoskeletal disruption and tau protein hyperphosphorilation, ultimately ending in neuronal death (Fig. 17). Other studies have confirmed the hypothesis supporting the link between deregulated caspases and NFT production,[91,155,156] mainly caspase-2.[157]

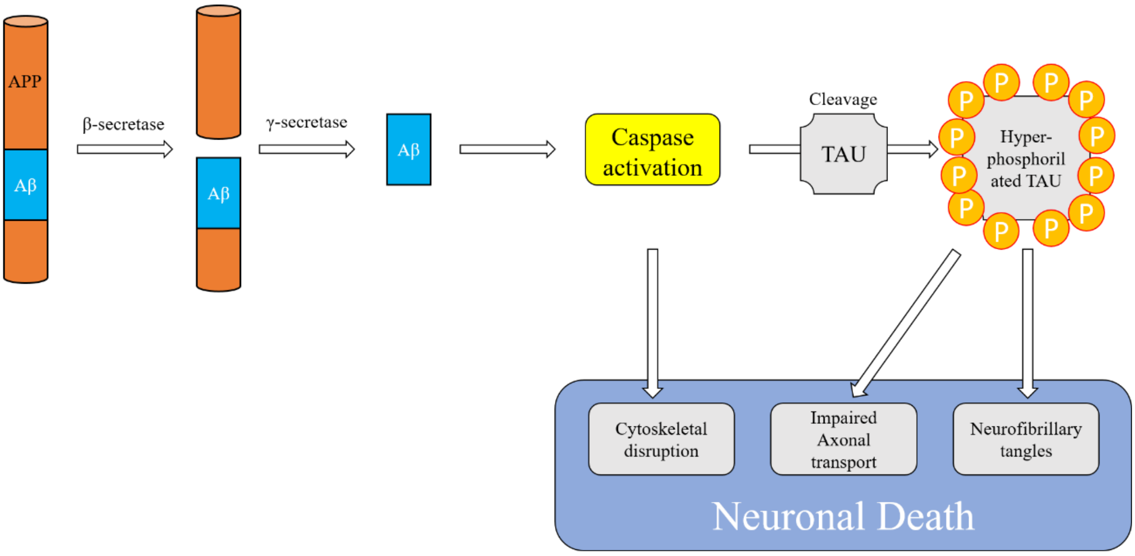
APP
Aβ
β-secretase
Aβ
γ-secretase
Aβ
Caspase activation
Cleavage
TAU
Hyper-phosphorilated TAU
P
Cytoskeletal disruption
Impaired Axonal transport
Neurofibrillary tangles
Neuronal Death

Figure 17 – Caspase activation by β-amyloid fragments.

Although caspase inhibitors could be beneficial in AD therapy, no drug has been researched and developed with that goal. Nevertheless, there are caspase inhibitors that could in a near future serve as inspiration for new drugs focusing on AD therapy.

In Fig. 18 examples of caspase inhibitors are shown. Pralnacasan, first developed to treat ischemia, is a selective and reversible caspase-1 inhibitor, withdrawn from clinical trials due to hepatotoxicity.[158] VX765 is also a reversible capase-1 inhibitor currently in Phase II trials for the treatment of inflammatory diseases.[159] Also developed as an anti-inflammatory drug, emricasan was withdrawn from clinical studies for undisclosed reasons in spite of promising results.[160] NCX1000 is a steroid-based, nitric oxide releasing and non-selective caspase inhibitor developed to treat portal hypertension.[161] It was deemed safe however the study was terminated in Phase II for unmet efficacy requirements.

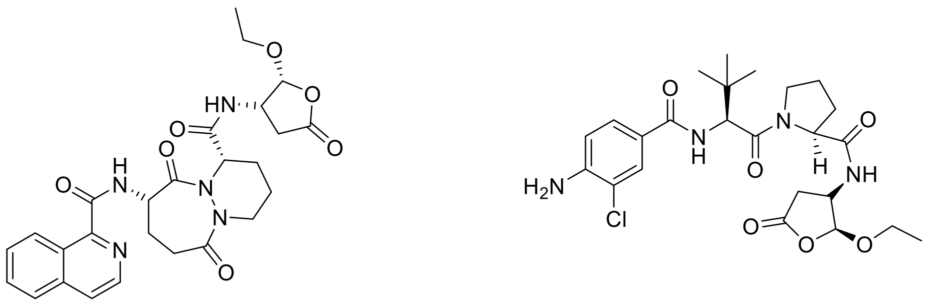

Pralnacasan VX765

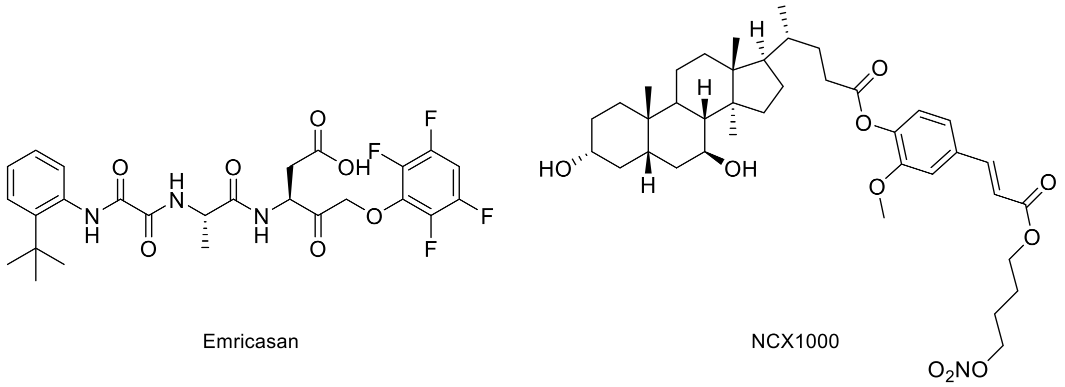

Emricasan NCX1000

Figure 18 – Structures of caspase inhibitors.

1.3. One target versus multi target drugs

Since the introduction of the “magic bullet” concept by Ehrlich, drug discovery efforts have been focusing on identifying single target drugs that interact with a specific target with a defined disease mechanism.[162] Generally, this approach has been successful, however it was unable to effectively tackle multifactorial diseases with high socioeconomic impact. Additionally, the single target approach is oblivious to processes connected by complex networks in biological systems. In these complex systems, cells may display a redundant effect since they have several mechanisms that yield the same outcome, such as gene expression, receptor response or protein degradation.[163] Therefore, this redundancy nulls the expected effect of single target drugs in a primary mechanism. Indeed, a clinical effect of a drug is sometimes owed to the interaction with multiple targets.[164]

In this context, the development of multi target drugs has gathered increased interest from academia and industry.[165] Nevertheless, the rational design of multi target drugs is still in its infancy and further development is critical. From a medicinal chemistry standpoint the rational design and multi target hit identification is very challenging. Moreover, lead optimization and comprehensive SAR studies for several different targets is extremely complex. To this end, different approaches were used, such as fragment-based design, molecular hybridization of active scaffolds or combination of compounds with known bioactivity.[166] Moreover, the analysis of approved drugs and recurrent bioactive compounds showed multi target binding affinity.[167]

The multi target approach is specifically relevant for ND, by definition multifactorial diseases with a complex network of pathological events. As mentioned in items 1.2.1. and 1.2.2., currently available single target treatments for PD and AD are only palliative and unable to alter disease progression. As such, the development of multi target directed drugs for different pharmacological ND targets is increasingly enticing attention.[168]

A significant advance in the progress of multi target directed drugs for ND was the development ladostigil, a drug designed to act as an AChE/MAO-B inhibitor.[169] Ladostigil (Fig. 19A) bears the propargyl moiety of MAO-B inhibitor rasagiline (Fig. 8) and the carbamate pharmacophore of AChE inhibitor rivastigmine (Fig. 13). As expected, the resulting molecule is a dual AChE/MAO-B inhibitor, developed for AD therapy and currently enrolled in phase II clinical trials.[169] Moreover, ladostigil major metabolite exhibits potent AChE inhibitory activity *in vivo*, in addition of neuroprotective effects (Fig. 19B).[170,171]

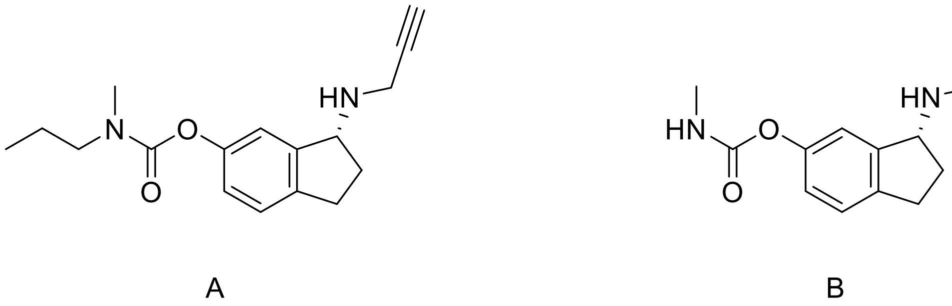

Figure 19 – Structures of ladostigil and its major metabolite.

1.3.1. Multi target drugs for Parkinson’s disease

The majority of PD multi target directed drugs developed so far combine MAO-B inhibition with other relevant targets. As discussed in item 1.2.1.1.4., MAO-B catalysis is one of the main sources of H_2O_2, a byproduct of selective oxidative monoamine deamination. This H_2O_2 may react with iron and copper and generate harmful ROS, namely $^{\cdot}OH$. Thus, iron chelation combined with MAO-B inhibition is considered a valid multi target approach. Zheng *et al.*[172] combined the iron chelating hydroxyquinoline scaffold with the propargylamine moiety and developed non-selective MAO-B inhibitors that exhibited potent inhibition of iron-dependent lipoperoxidation in rat brain homogenates. Moreover, due to the non-selectivity profile of these derivatives, they also showed potential adjunctive antidepressant activity.[173]

As previously discussed in item 1.2.1.2.1., A_{2A}AR antagonists effectively protected against neurodegeneration in different disease models, and were hypothesized to provide symptomatic relief of PD motor symptoms.[70] Petzer *et al.*[174] developed selective and potent nanomolar MAO-B inhibitors, which also exerted neuroprotective effects by means of A_{2A}AR antagonism (Fig. 20A). More recently, Pretorius *et al.*[175] found that 8-(4-phenylbutadien-1-yl)caffeine analogues were potent reversible MAO-B inhibitors with remarkable nanomolar A_{2A}AR affinity and antagonism (Fig. 20B).

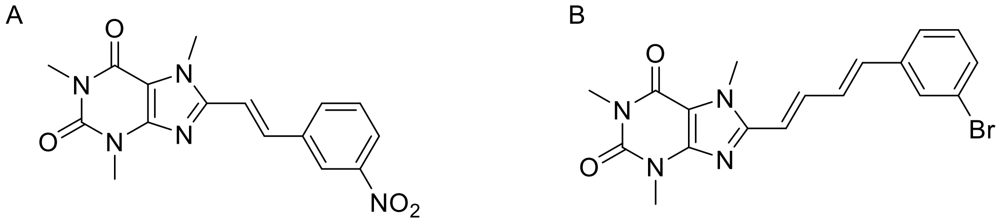

IC_{50} MAO-B = 160 nM
K_i $A_{2A}AR$ = 195 nM

IC_{50} MAO-B = 38 nM
K_i $A_{2A}AR$ = 59 nM

Figure 20 – Structures of MAO-B inhibitors and $A_{2A}AR$ antagonists.

1.3.2. Multi target drugs for Alzheimer’s disease

The discovery of AChE non-cholinergic actions, mainly their implication in the development of SNP, provided the driving force for the development of multi target drugs for AD. This strategy represents a new area of research based on both cholinergic and amyloid hypothesis. Furthermore, crystallographic studies of AChE provided additional insight of the enzyme’s structure, and triggered the development of dual binding AChE inhibitors, which interact with the catalytic site and the PAS.[176] Adding to ACh degradation inhibition, these dual-binding inhibitors also target the PAS and decrease the aggregation rate of β-amyloid.

Early dual-binding AChE inhibitors were based on the structural elucidation provided by Sussman *et al.*[117] and the reported X-ray structure of the donepezil-AChE complex.[177] Since then, a study by Tumiatti *et al.*[178] unraveled the potential of less flexible or rigid moieties (*e. g.* dipiperidines), as PAS-binding scaffolds. Moreover, the authors found that the synthesized compounds were able to inhibit self- and AChE-induced β-amyloid aggregation within the low micromolar range. In fact, a dual binding AChE inhibitor reached Phase II clinical trials for AD, however no structure is available and studies results are undisclosed.[176]

The development of dual-binding AChE inhibitors evolved to incorporate other bioactivities, such BACE inhibition. Since both enzymes are involved in protein aggregation, this constitutes a valid strategy for the development of new AD therapies. Within this class of compounds, memoquin (Fig. 21) is a potent AChE and BACE inhibitor, while retaining micromolar inhibition of β-amyloid aggregation.[179] Furthermore, memoquine was shown to improve cognitive impairment, and short and long-term memory in scopolamine-induced amnesia models.[180]

On the other hand, AChE inhibitors with antioxidant activity were also developed as a therapeutic strategy to tackle both cognitive deficit and the harmful effects associated with neuronal redox deregulation and ROS-induced damage observed in AD. To this effect, lipocrine (Fig. 21), a tacrine/lipoic acid heterodimer was developed as a potent AChE inhibitor able to interact with the enzyme's PAS and inhibit AChE-induced β-amyloid aggregation.[181] Moreover, lipocrine decreased by half the production of ROS at 10 µM and demonstrated improved neuroprotection against oxidative stress.[168,181]

Glutamate-related excitotocicity contributes to AD and occurs in part because of NMDA overactivation.[130] Moreover, oxidative stress and increased intracellular Ca^{2+} have been reported to enhance glutamate mediated neurotoxicity *in vitro*.[182] In this context, carbacrine (Fig. 21) was successfully developed as: a) AChE inhibitor within the nanomolar range, b) β-amyloid self- and AChE-induced aggregation inhibitor, c) NMDA antagonist, and d) antioxidant agent.[183]

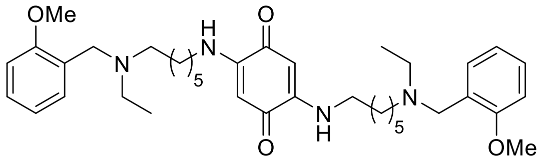

Memoquin

IC_{50} AChE = 1.55 nM

IC_{50} BACE = 108 nM

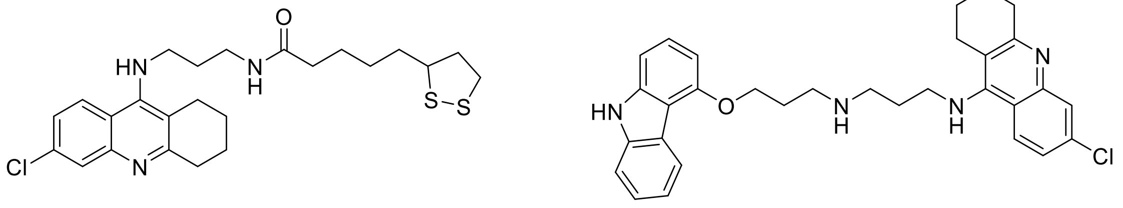

Lipocrine

IC_{50} AChE = 0.25 nM

%Inh. ROS 51 % at 10 µM

Carbacrine

IC_{50} AChE = 2.15 nM

K_i NMDAr = 740 nM

Figure 21 – Structures of memoquin, lipocrine and carbacrine.

1.4. Benzopyrones

Chemically, benzopyrones are composed of a pyrone fused with a benzene ring, and can be divided into benzo-α-pyrones and benzo-γ-pyrones, commonly designated as coumarins and chromones, respectively (Fig. 22A).[184]

In 1988, Evans *et al.*[185] struggled to explain the range of multiple activities towards a large class of G protein-coupled receptors of derivatives synthesised by his research group. At that time, the authors noticed that some structures were "privileged" and, as such, were seemingly capable of serving as ligands for an array of different receptors.[186] Accordingly, some of these structures could be used in drug discovery programs for the development of concise and diverse libraries.

Since then, the research performed over the past decades has unveiled other structural fragments which were categorised as privileged (Fig. 22B), many of them are present in currently marketed drugs.[186–188] Within this framework, benzopyrone-based systems, like chromones and coumarins (Fig. 22A), were also recognised as privileged structures and thus used in several drug discovery programs.[186,189–191]

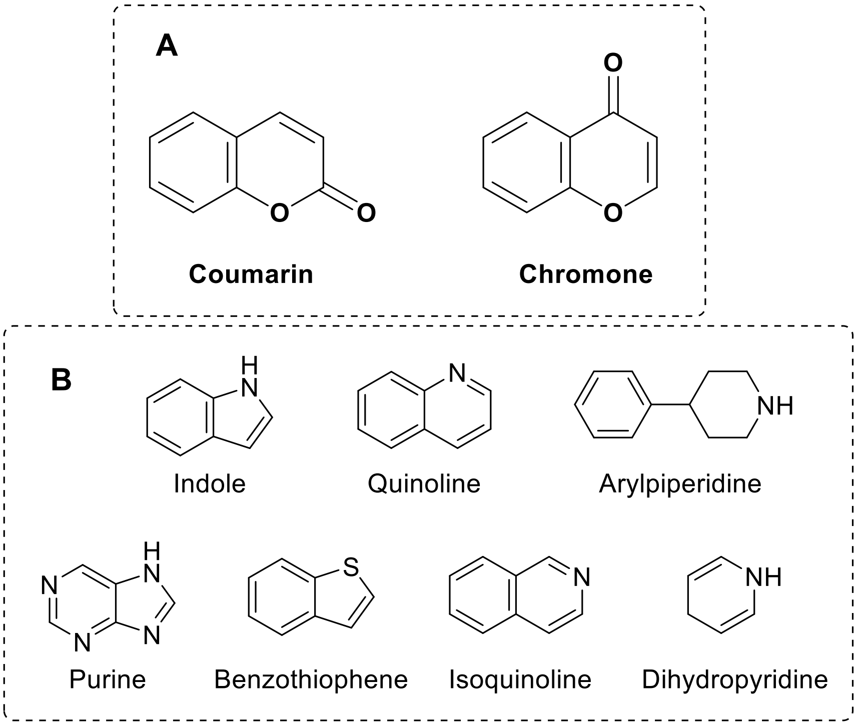

Figure 22 – Structures of recognised privileged scaffolds.

1.4.1. Coumarins

Coumarins are a large class of lactones that have been roughly classified in the following categories: simple coumarins, furanocoumarins, pyranocoumarins, bis and triscoumarins, and coumarinolignans.[192] Coumarin (Fig. 22A), or according to the International Union of Pure and Applied Chemistry (IUPAC) 2*H*-chromen-2-one, was discovered in 1820 by Vogel, isolating it from the tonka bean.[193]

Coumarins are widely distributed in nature, and can be found not only in plants but also in microorganisms and animals.[194] Simple coumarins are biosynthetically obtained by lactonization of *o*-hydroxycinnamic acids (Fig. 23), which can have diverse aromatic substituents.[195] These organic acids are glycosylated in a first step and posteriorly undergo isomerization, to *cis* derivatives, by enzymatic mediation or ultra-violet radiation.[196] From this process, after lactonization, multiple coumarins can be attained, namely 7-hydroxycoumarin (*umbelliferone,* Fig. 23). *Umbelliferone* can be further oxidized into derivatives like aesculetin, which in turn can undergo O-methylation yielding scopoletin.[195]

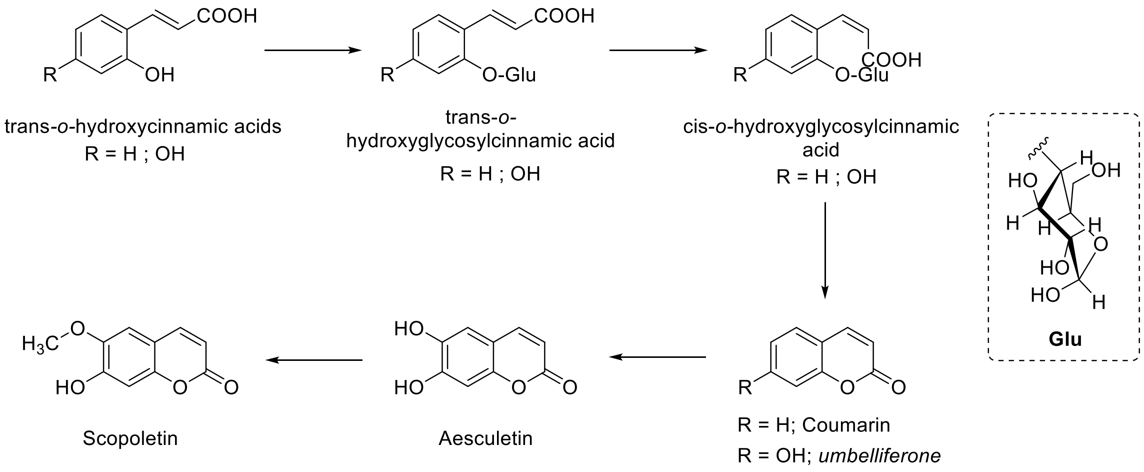
COOH
R
OH
trans-o-hydroxycinnamic acids
R = H ; OH
COOH
R
O-Glu
trans-o-hydroxyglycosylcinnamic acid
R = H ; OH
COOH
R
O-Glu
cis-o-hydroxyglycosylcinnamic acid
R = H ; OH
HO
H
OH
H
H
H
O
HO
HO
H
Glu
H3C
O
HO
O
O
Scopoletin
HO
HO
O
O
Aesculetin
R
O
O
R = H; Coumarin
R = OH; umbelliferone

Figure 23 – Biosynthesis of coumarin and related hydroxylated derivatives.

1.4.1.1. Biological activities

Coumarins are ubiquitously widespread in nature and have been associated with a wide range of pharmacological activities.[192] Indeed, coumarin derivatives can be found as drugs in several therapeutic categories,[197] namely in cardioprotection, due to their anticoagulant and/or vasorelaxant activities.[198] One of the well-known examples of a coumarin with anticoagulant properties is dicoumarol (Fig. 24), a naturally occurring compound found in mouldy hay.[199] Moreover, other coumarin-based drugs are currently marketed as anticoagulants, like warfarin and acenocoumarol (Fig. 24), which also share a 4-hydroxycoumarin fragment in their chemical structure.[200] Carbochromen, marketed under the name of Chromonar, is also a cardioprotective coumarin-based drug that displays vasorelaxant activity and platelet aggregation inhibition (Fig. 24).[201]

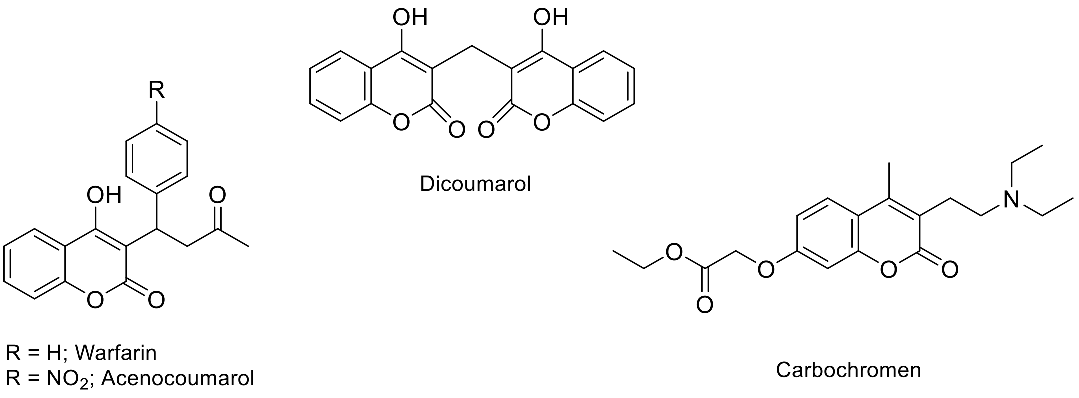
OH
OH
O
O
O
O
Dicoumarol
R
OH
O
O
O
R = H; Warfarin
R = NO_2; Acenocoumarol
N
O
O
O
O
O
Carbochromen

Figure 24 – Structures of: dicoumarol, warfarin, acenocoumarol and carbochromen.

Coumarin-based derivatives have also been marketed as antibiotics, showing effectiveness against gram-positive and/or gram-negative bacteria.[202] It is important to highlight the case of novobiocin (Fig. 25), a drug used to treat the problematic methicillin-resistant *Staphylococcus aureus* (MRSA).[203] Although it is a remarkable antibiotic, it has to be administered intravenously due to its poor water solubility,[204] and as such its hydrophilic analogues clorobiocin and coumermycin A_1 (Fig. 25) are sometimes preferred in therapy.[205]

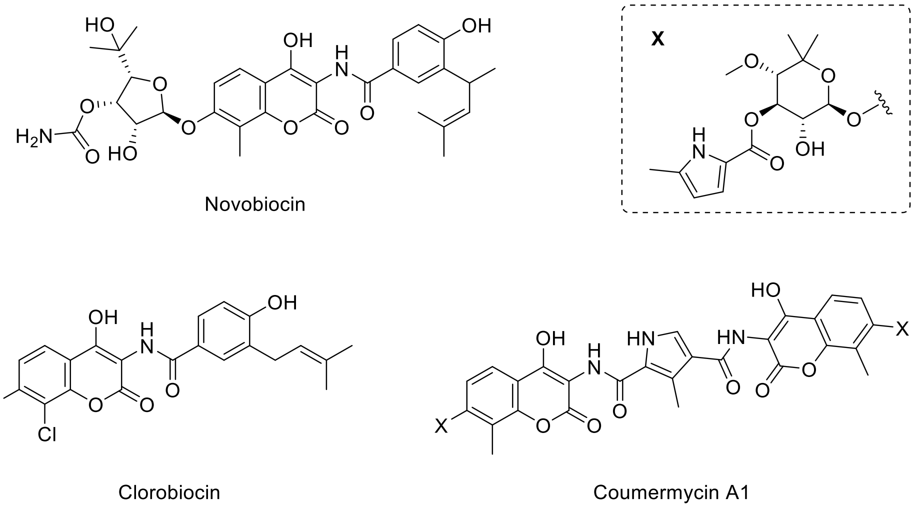
HO
OH
OH
H
N
O
O
H_2N
O
HO
O
O
O
O
Novobiocin
X
O
O
O
H
N
O
OH
O
OH
OH
H
N
O
X
Cl
O
O
Clorobiocin
HO
OH
H
N
HN
HN
X
X
O
O
O
O
O
O
Coumermycin A1

Figure 25 – Structure of novobiocin, clorobiocin and coumermycin A1.

Aside from antibacterial activity, coumarin-based compounds have also been reported as antifungal and antiparasitic agents.[197,206–209] Furthermore, naturally-occurring suksdorfin (Fig. 26) and its derivatives have been associated with anti-human immunodeficiency virus (HIV) activity.[210,211]

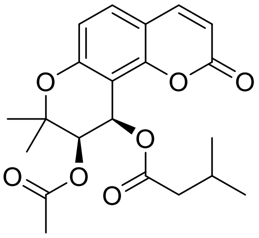

Figure 26 – Structure of suksdorfin.

The naturally occurring coumarin geiparvarin (Fig. 27A), isolated from *Geijera parviflora*,[212] exhibited potent *in vitro* anti-cancer activity in several cancer cell lines.[213,214] Likewise, novobiocin (Fig. 25) has also been used as a template for the development of anti-proliferative agents. (Fig. 27B).[215]

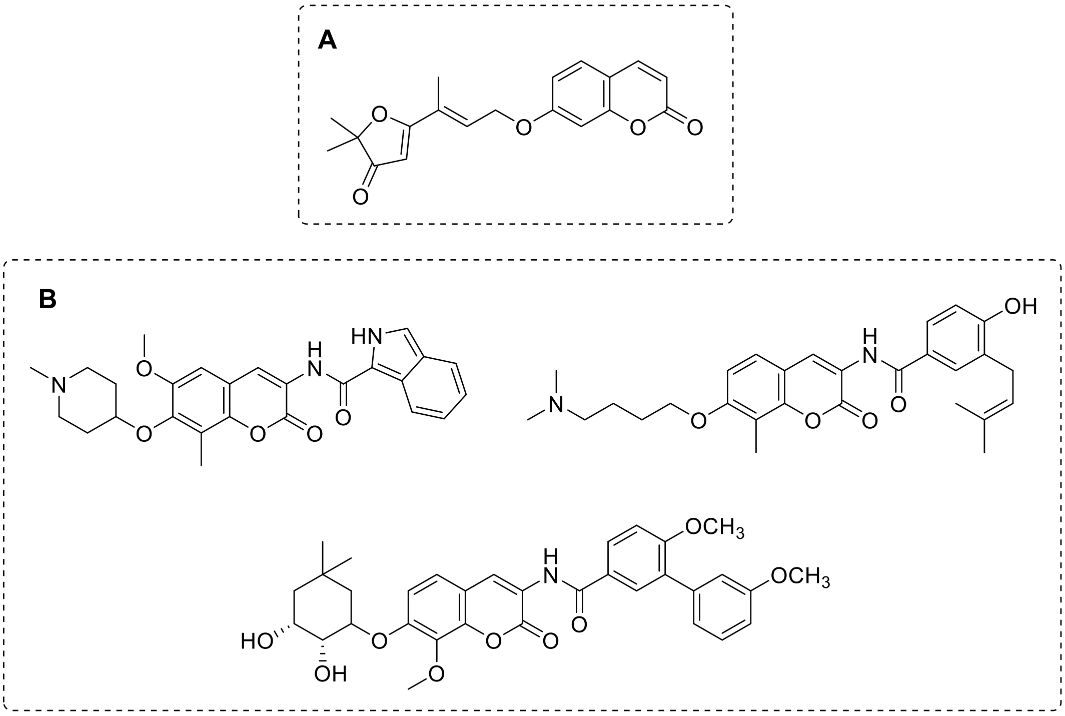

Figure 27 – Structures of geiparvarin (A) and novobiocin-inspired compounds (B).

The modification of the coumarin skeleton yielded a wide range of derivatives of compounds with remarkable anti-inflammatory and/or antioxidant activities.[216–221] Furthermore, hydroxylated derivatives of coumarins, such as the aforementioned *umbelliferone* (Fig. 23), have also been described as tyrosinase inhibitors.[222,223]

1.4.1.2. Coumarins in neurodegenerative diseases

Coumarin-based derivatives have long been studied for their ability to interact with enzymatic and non-enzymatic systems involved in the development of ND.[197] In particular, coumarins are remarkable MAO-B inhibitors.[140,197,224] Moreover, coumarin-based derivatives were active on other targets relevant for ND, such as AChE,[225–228] AR[229] and BACE.[230–232] However, the compounds evaluated in these studies are still in preliminary phases of research and development and so far none have been enrolled in clinical trials.

Throughout the last decade, coumarins were extensively studied as MAO-B inhibitors.[233–235] Adding to its potent MAO-B inhibitory activity, Viña *et al.*[236] modulated the coumarin scaffold to develop dual MAO-B/AChE inhibitors. The synthesised derivatives had AChE inihibition within low micromolar range, while maintaining or slightly decreasing MAO-B inhibition.

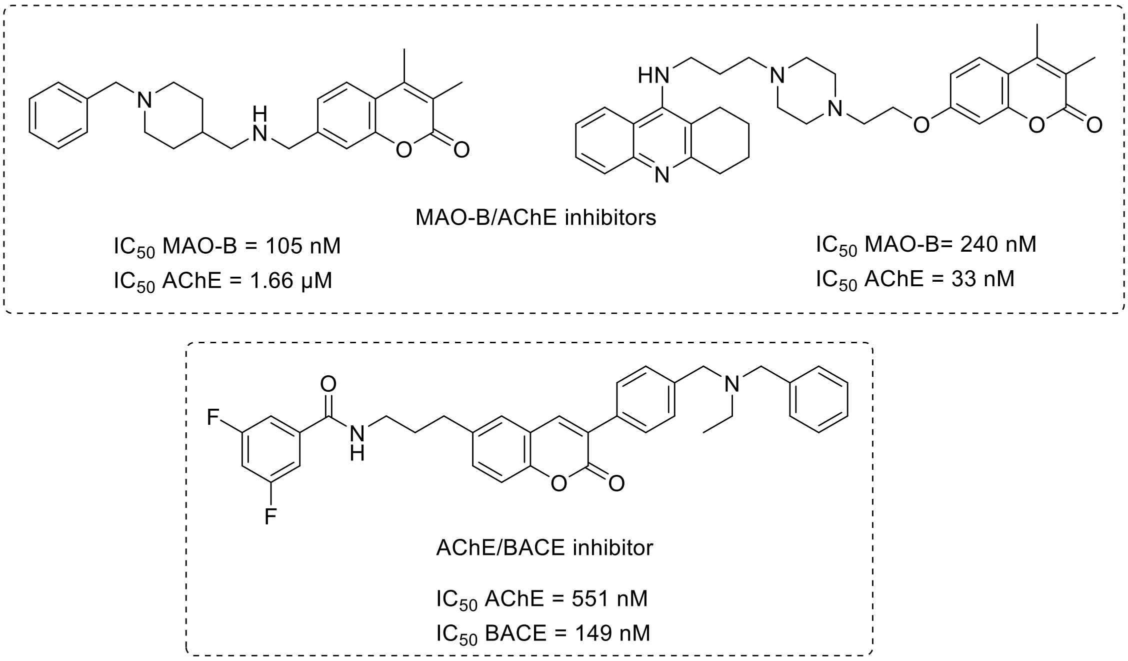
N
H
N
O
O
HN
N
N
N
O
O
O
MAO-B/AChE inhibitors
IC50 MAO-B = 105 nM
IC50 AChE = 1.66 μM
IC50 MAO-B= 240 nM
IC50 AChE = 33 nM
O
F
N
H
F
N
O
O
AChE/BACE inhibitor
IC50 AChE = 551 nM
IC50 BACE = 149 nM

Figure 28 – Structures of dual-target inhibitors.

More recently, efforts have been made to further develop coumarin-based dual MAO-B/AChE inhibitors. Indeed, in two different studies, Xie *et al*.[237,238] reported IC_{50} values within the nanomolar range for both enzymes by combining differently substituted coumarins with moieties of known AChE inhibitors (Fig. 13). These compounds were able to cross the BBB by passive diffusion and presented low cytotoxicity. In another study, Pisani *et al.*[239] developed coumarin derivatives with similar biological performance and enhanced aqueous solubility, by linking a piperidine moiety to the coumarin scaffold (Fig. 28).

Interestingly, Piazzi *et al*.[240] reported for the first time coumarin-based dual AChE/BACE inhibitors, which displayed a remarkable nanomolar affinity for both targets. (Fig. 28).

1.4.1.3. Synthesis of coumarins

Coumarins have a vast number of pharmacological activities, which makes them a useful scaffold in Medicinal Chemistry.[197] Throughout the years, chemists have tried to discover and improve synthetic methodologies to obtain different coumarins, as it would be impracticable to rely solely on natural sources. Within this endeavour, several synthetic processes were developed. However, many of them encompass multi-step reactions with poor overall yields.[241,242] Nowadays, the majority of coumarins are synthesised by the condensation reactions depicted in Fig. 29, such as Perkin, Pechmann, Wittig, Reformatsky, Kostanecki-Robinson or Knoevenagel.

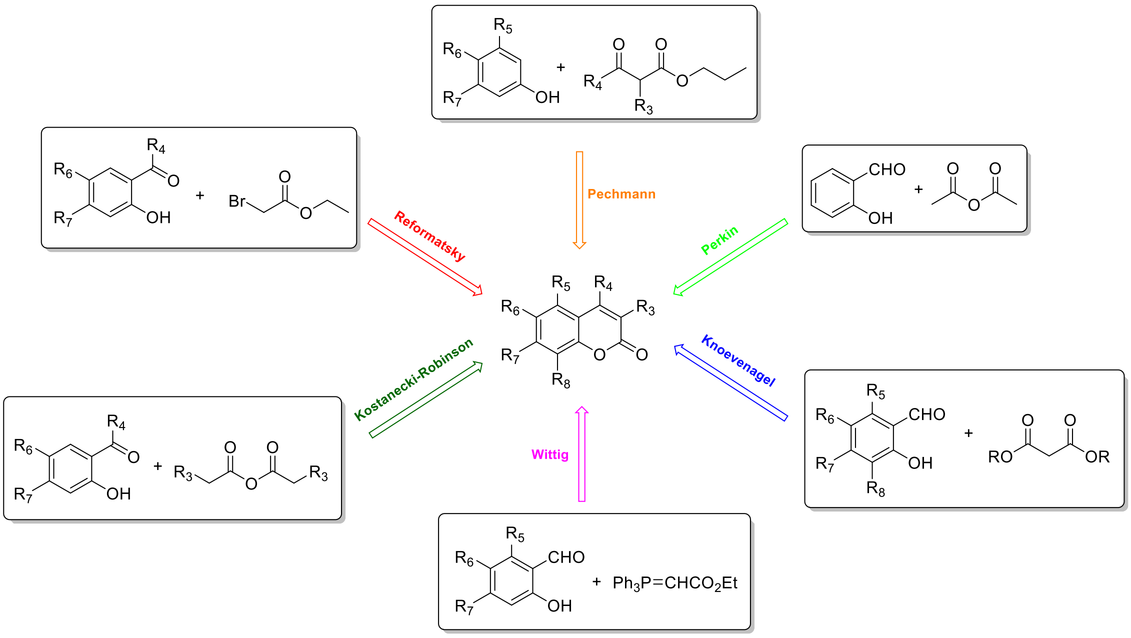

Figure 29 – Condensation reactions used for coumarin synthesis.

In 1868, Bristish chemist William Perkin, while working on new strategies to obtain dyes and perfumes, discovered a synthetic methodology to obtain coumarins by heating a sodium salt of salicylaldehyde with acetic anhydride (Fig. 30).[243] Perkin reaction involved the condensation of an anhydride and an aldehyde in presence of a weak base, often potassium or sodium acetate or even triethylamine, to yield unsaturated carboxylic acids.[244] Although often used, it has several drawbacks, such as relatively low yields and difficulty in preparing the needed salicylaldehydes. Throughout the years, this reaction has been continuously improved, by increasing reaction times and/or temperature, or by adding catalysts like *N*,*N*'-diciclohexylcarbodiimide (DCC),[245] iodine[246] or sodium fluoride.[247] Some studies have revealed the importance of the nature of the base: for instance, the use of sodium succinate, instead of sodium acetate yields 3-biscoumarins that were bound at position 3.[248] In this context, several variations have been made namely the Perkin-Oglialoro reaction, which consists in the exchange of the original sodium acetate by sodium or potassium phenylacetate.[249]

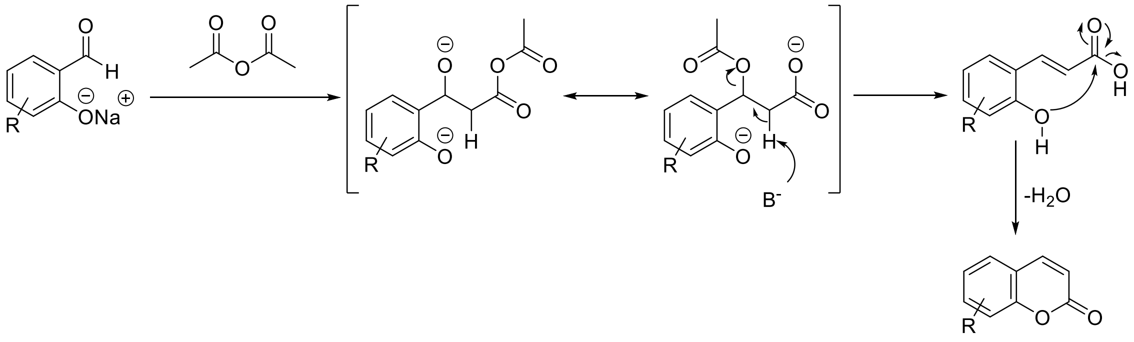

Figure 30 – Perkin reaction.

Although the mentioned modifications prove the versatility of Perkin's reaction, it is not the most widely used synthetic methodology for the synthesis of coumarins. Actually, the most common is the Pechmann reaction (Fig. 31),[250] which enables the synthesis of coumarins by the condensation of phenols with β-ketoesters, in the presence of strong Brønsted or Lewis acids.[251–253] Although the reaction mechanism is still unknown, a theoretical study by Daru and Stirling[254] suggested that *trans*-esterification, water elimination and an electrophilic attack can occur almost simultaneously. This important synthetic pathway was used to obtain umbelliferone (Fig. 23) and derivatives thereof.[255]

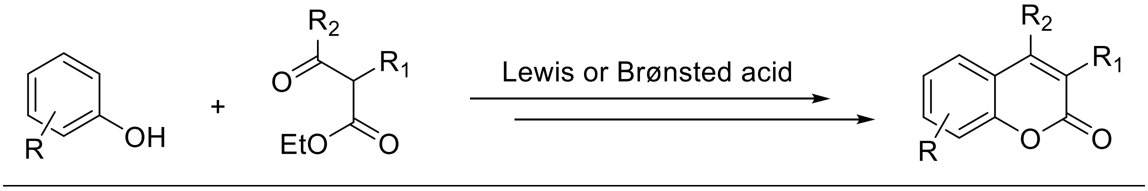

Figure 31 – Pechmann reaction.

As the coumarin skeleton is a cyclic ester of *o*-hydroxycinnamic acid (Fig. 23) some reactions to prepare coumarins use a cinnamic acid derivative as an intermediate, and a cyclization process as the last step. This cinnamic intermediate can be obtained by Wittig or Reformatski reactions (Fig. 32), using an ylide and diethylphenylamine, and zinc as a catalyst, respectively.

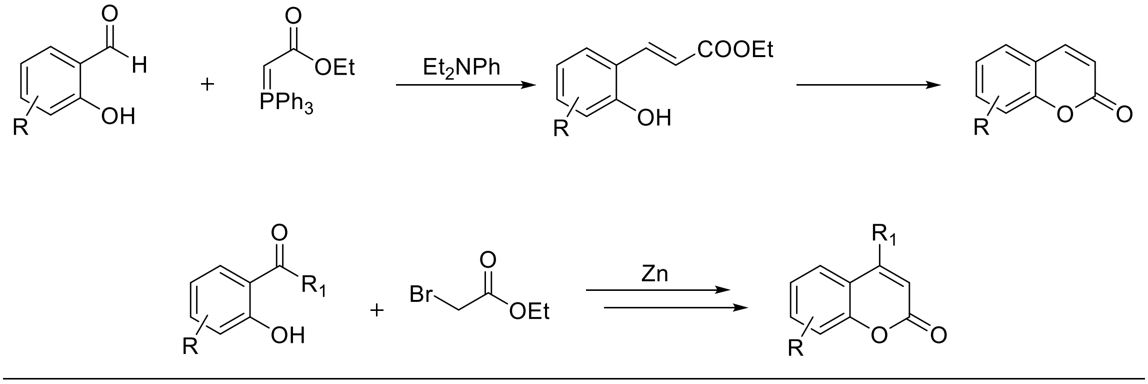

Figure 32 – Wittig (at the top) and Reformatsky reactions (at the bottom).

In general, the majority of the C3-substituted coumarin derivatives described in this thesis have been obtained by Knoevenagel condensation reaction (Fig. 33). Chemically, it can be described as a catalysed condensation between salicylaldehydes and activated methylenes, in order to afford α,β-unsaturated derivatives.[256] Briefly, an organic base, frequently piperidine, is initially used to form an enolate (Fig. 33A) which then reacts with salicyaldehyde undergoing a base-induced elimination (Fig. 33B). However, an alternative mechanism has been proposed that suggests that piperidine can also be used as an organocatalyst, with the formation of an iminium intermediate that acts as an acceptor.[257] Furthermore, the Knoevenagel reaction was modified by Doebner. This modification allows the presence of carboxylic acid groups and includes a pyridine-induced decarboxylation.[258] Classically, these type of reactions are performed in homogeneous medium with a variety of solvents and temperatures. Nevertheless, in recent years, there has been a push towards a “greener” Chemistry approach, that involves the use of less toxic solvents, microwave irradiation,[259,260] and an array of different catalysts like ionic liquids.[261,262]

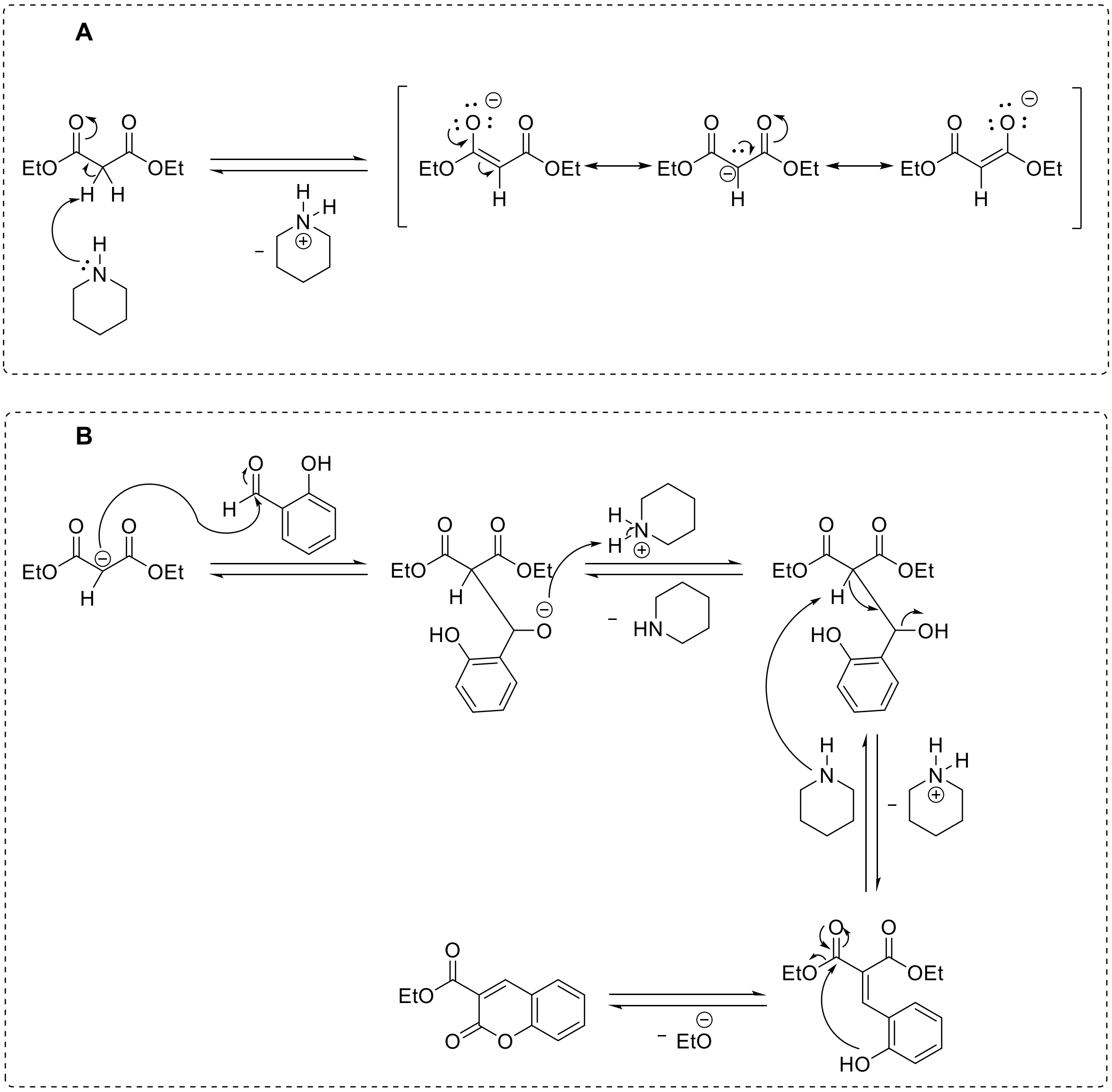

Figure 33 – Knoevenagel condensation.

1.4.2. Chromones

The term chromone was first coined in a 1900 study by Bloch and Kostanecki.[263] Interestingly, in this study they did not synthesise the unsubstituted chromone, but rather some of its derivatives.[263] Chromone (Fig. 22A) was only synthesised later on by Ruhemann, through decarboxylation of chromone-2-carboxylic acid derivative.[264]

Like coumarins, chromones are widely distributed in nature, mainly in plants and berries.[191] Equally, they are also divided into different categories, according to their structural backbone, in simple chromones, bichromones and bischromones, and fused-ring chromones, such as pyrano- and furanochromones.

From a biosynthetic standpoint, chromones and coumarins share a common route, using cinnamic acid or *p*-coumaric acid as building blocks of the chromones present in nature.[265–267]

1.4.2.1. Biological activities

Given their ubiquitous presence in nature, chromones have been used unknowingly as drugs for a very long time. For instance, the use of herbal medicines containing khellin (Fig. 34) and its derivatives dates back to ancient Egypt.[268] The extract of *Ammi visnaga*, from which khellin was isolated, has a cardioprotective effect, due to its vasorelaxant activity.[268] As such, this compound was studied for the treatment of angina pectoris and also for bronchial asthma.[269] However, the side effects associated with khellin, such as nausea and vomiting, have limited its application to topical use in the treatment of vitiligo.[270] Approaches based on molecular simplification successfully led to khellin-based derivatives lacking the furan ring. However, these derivatives showed poor vasorelaxant activity.[271] Cox *et al*.[272] continued the study of khellin derivatives, attaining compounds with vasorelaxant activity and with improved side effects. Along these studies chromone-2-carboxylic acid was synthesised as an attempt to improve water solubility.[273] However its biological half-life was proven too short to be effective. Further studies on the derivatization of chromone-2-carboxylic acid led to the discovery of disodium cromoglycate (Fig. 34), a drug for the treatment of bronchial asthma.[269] Although the current asthma treatment is mainly based on corticosteroids, cromoglycate is still used due to its increased safety and anti-inflammatory effect.[274]

The development of NCE based on the chromone scaffold in this field has been a continuous process, leading to pranlukast (Fig. 34), which was approved for asthma management and allergic rhinitis.[275,276]

Several other compounds bearing the chromone backbone have been described to have anti-inflammatory activity.[277,278] This is still a hot research topic as new selective anti-inflammatory drugs are still needed, without the side effects associated with currently available drugs. It is also important to stress that inflammatory processes play a key role in AD, PD and in cancer.[279–281] Accordingly, several research groups have been focusing on cyclooxygenases (COX) as a target related to these types of disease.[282,283]

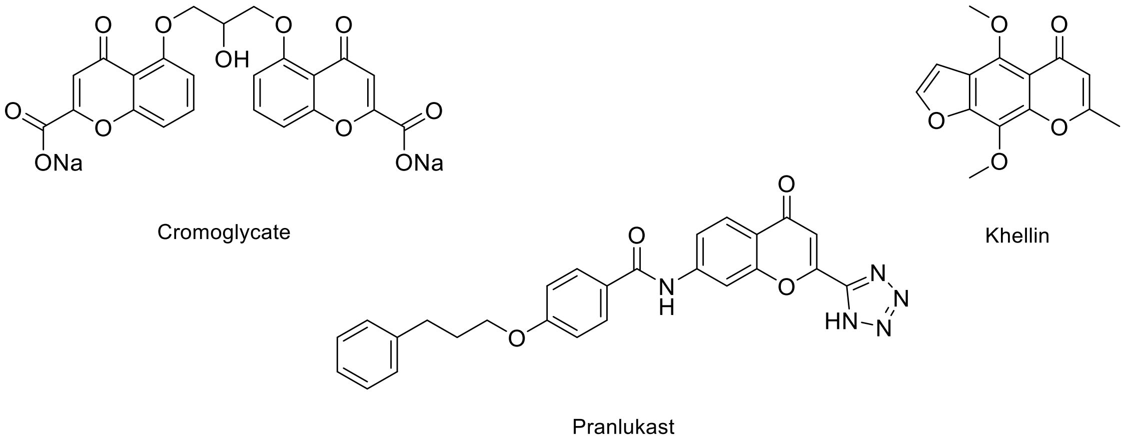

Figure 34 – Structures of khellin, cromoglycate and pranlukast.

Within this framework, stellatin (Fig. 35), a natural chromone isolated from *Dysophylla stellatais*,[284] showed relevant COX-1 and COX-2 inhibition, and thus several derivatives thereof were synthesised and screened for anti-inflammatory activity.[285] Some derivatives showed higher COX inhibition than stellatin, and significantly improved anti-inflammatory activity in *in vivo* studies.[285]

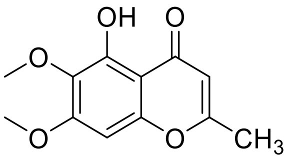

IC_{50} COX-1 = 22 μM
IC_{50} COX-2 = 20 μM

Figure 35 – Structure of stellatin.

Chromones have been also found to harbour the potential for antimicrobial activity.[191] Sulphonamide derivatives (Fig. 36A) showed relevant antibacterial activity against both Gram-negative and Gram-positive bacteria.[286] Interestingly, the same type of compounds also demonstrated activity against several fungi, including *Candida sp.*. Regarding anti-viral activity, chromone-styrene hybrids were proven active against norovirus (Fig. 36B).[287,288] Moreover, 5,6-dihydroxychromones showed selective antiviral activity against anti-hepatitis C virus (Fig. 36C).[289] Finally, the discovery of chromone-based reverse transcriptase and protease inhibitors is highlighted as they exhibit potent anti-HIV activity (Fig. 36D).[290–293]

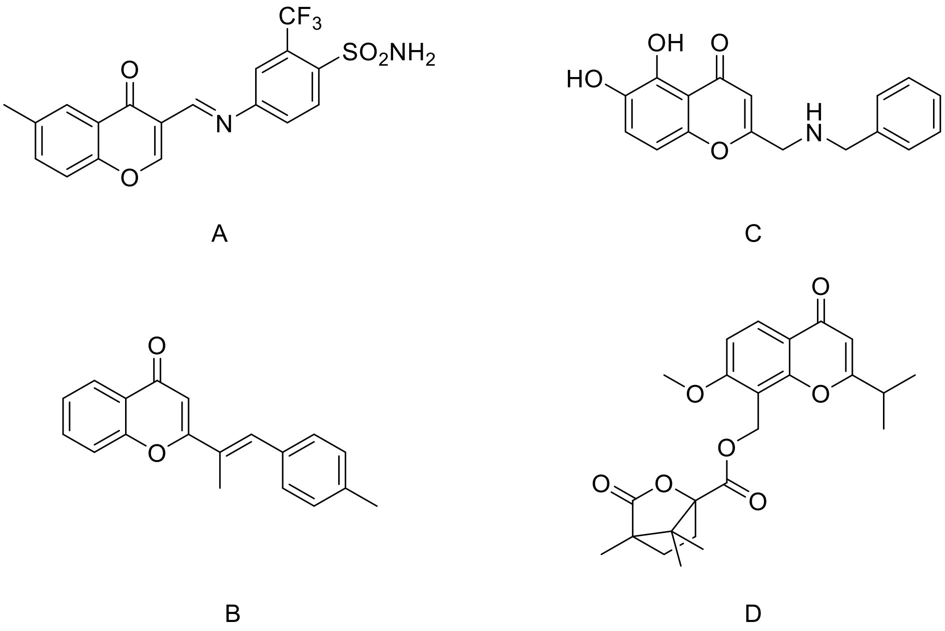

Figure 36 – Structure of chromone derivatives with anti-microbial activities.

In recent years, similarly to coumarins, there has been a breakthrough in the discovery of chromone derivatives for the potential application in anticancer therapy.[294,295] In terms of enzymatic targets connected with carcinogenesis and tumour growth, chromone analogues have been found to inhibit tyrosine phosphatases,[296] thymine phosphorylases,[295] aromatases,[297] and several kinases.[298–300]

1.4.2.2. Chromones in neurodegenerative diseases

Considering the many areas in which chromones are relevant, it is not surprising that this scaffold has been extensively used for the development of NCE acting upon pharmacological targets involved in ND. As discussed previously, the quest for selective and reversible MAO-B inhibitors remains of high interest for the inclusion in PD and AD therapy. Within this framework, 3-phenylcarboxamidochromones were extensively studied as MAO-B inhibitors.[301–303] In fact, in a comprehensive SAR study, Reis *et al.*[303] successfully attained selective and reversible MAO-B chromone-based inhibitors, some of which within the picomolar range (Fig. 37).

In a study by Parveen *et al.*[304], chromones have also been identified as potent AChE inhibitors, namely 3-formylchromone derivatives. Moreover, in a study conducted by Liu *et al.*[305], chromone derivatives also possessed moderate anti-oxidant activity and chelating properties. The authors also concluded that these derivatives had significant β-amyloid aggregation inhibitory activities.

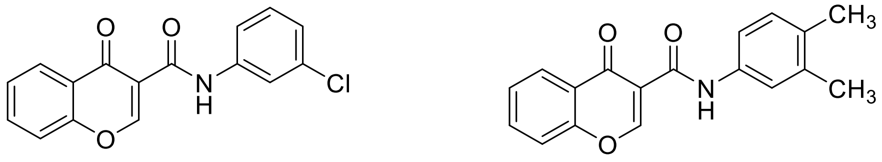

IC_{50} MAO-B = 400 pM

IC_{50} MAO-B = 670 pM

Figure 37 – Structures of 3-phenylcarboxamidochromones with picomolar MAO-B activity.

In a recent report, Razzaghi-Asl *et al.*[306] found that chromone-based derivatives were promising scaffolds for the discovery of novel BACE-1 inhibitors for the clinical management of AD. Moreover, flavone derivatives isolated from natural sources displayed promising BACE inhibitory activity.[307–309]

Additionally, compounds containing the chromone scaffold were recently recognised as ligands of AR, expanding their prevalence in ND targets. In fact, Cagide *et al.*[310] unveiled the first chromone-based A_1AR ligand (Fig. 38). Also, in a different study the same authors reported the discovery of A_3AR antagonist based on the same scaffold (Fig. 38).[311]

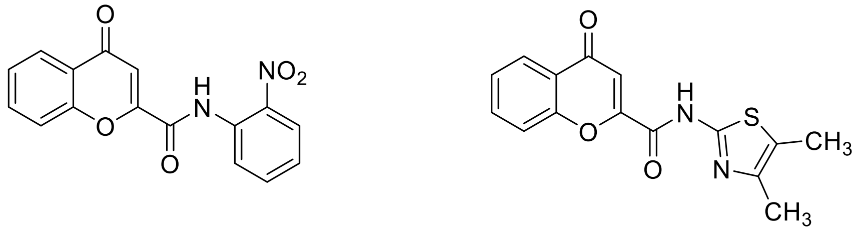

K_i A_1AR = 219 nM

K_i A_3AR = 167nM

Figure 38 – Structures of chromone-based AR ligands.

1.4.2.3. Synthesis of chromones

To obtain a wide variety of chromones chemists make use of different building blocks such as phenols, hydroxyarylalkyl ketones and salicylic acids, depending on the intended final compound. Simonis described a variation of the Pechmann reaction suitable for the synthesis of chromones. Simonis' reaction is based on a condensation of *β*-ketoesters with phenols, but it makes use of phosphorus pentoxide as a catalyst instead of aluminium trichloride generally used in the Pechmann's reaction. This change allows the activation of the ketone function in the *β*-ketoester, which react with the hydroxyl group of the phenol. Only afterwards the ester group is activated and prepared for the electrophilic attack of the aryl group (Fig. 39-left). Since then, several modifications and improvements of this reaction have been introduced. For instance, Ruhemann *et al.*[264] used chlorofumaric acid and other dicarboxylic acids in presence of metallic sodium or potassium carbonate in order to obtain chromone-2-carboxylic acid (Fig. 39-right). Additionally, other types of 2-substituted chromones, namely flavones and styrylchromones, can be obtained by minor modifications of Ruhemann's reaction, proving its versatility.[312]

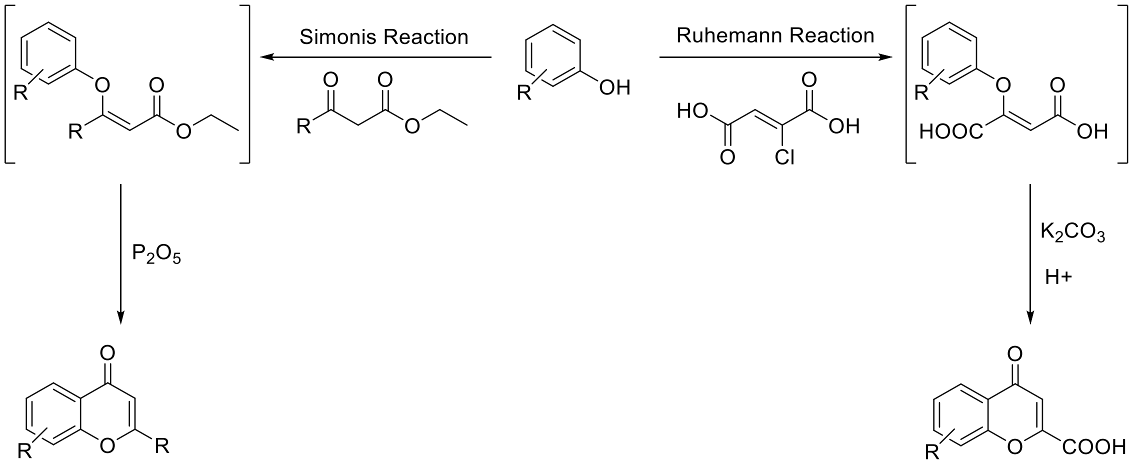

Figure 39 – Simonis (left) and Ruhemann reactions (right).

More recently, a study showed that the condensation of phenols with differently substituted Meldrum's acids (MA) in presence of a Lewis acid led to the synthesis of coumarins and chromones. The process is dependent on the nature of the substituents of the MA (Fig. 40).[313]

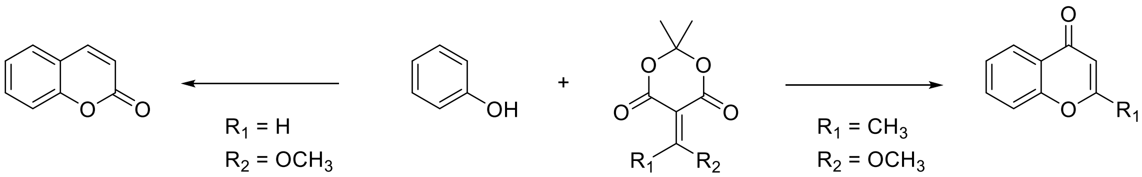

Figure 40 – Synthesis of coumarins and chromones depending on MA structure.

Chromones can also be synthesised from salicylic acids and its derivatives. Firstly, salicylic acid reacts with an anhydride to yield acyl or aryl ester analogues (Fig. 41). Then, chromone derivatives can be effectively attained by activating the aromatic carboxylic acid with *tert*-butyldimethylsilyl chloride (TBMDSCl) and adding (trimethylsilyl)-methylenetriphenylphosphorane (Fig. 41).[314] The novelty of this reaction is based on the existence of an intramolecular olefination, which consists in a modified approach of the previously described Wittig reaction (Fig. 32).

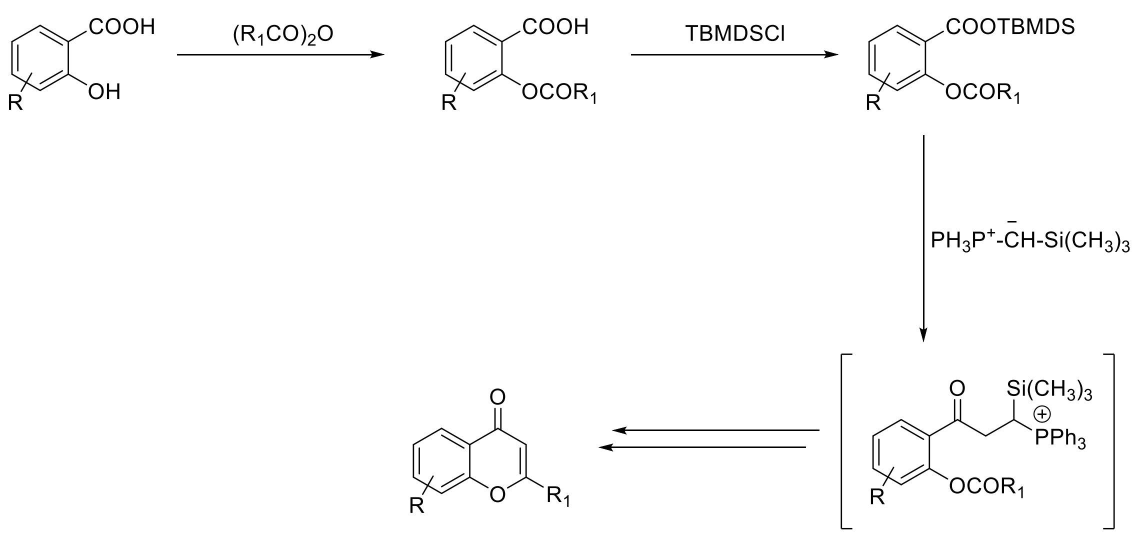

Figure 41 – Chromones synthesised using salicylic acids as building blocks.

Chromones can also be obtained from coumarins, closing even more the gap between these two scaffolds. Indeed, 4-hydroxycoumarins are tautomers of 2-hydroxychromones (Fig. 42), although its equilibrium is significantly shifted towards the coumarinic scaffold.[315]

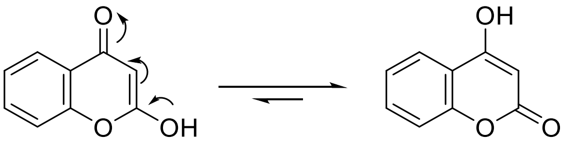

Figure 42 – Tautomerism between 2-hydroxychromones and 4-hydroxycoumarins

Nevertheless, it is achievable to synthesize chromones starting from coumarin derivatives. The first account of such transformation was in a study by Mentzer *et al*,[316] where the authors performed a heat-assisted acid hydrolysis of the lactone ring of 4-

hydroxy-3-propionylcoumarin. This reaction was followed by decarboxylation and ring closure, obtaining 2-ethylchromone in relatively good yields (Fig. 43).

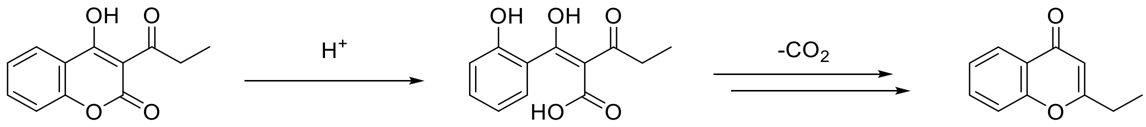
OH
O
O
O
H+
OH
OH
O
HO
O
-CO2
O
O

Figure 43 – Synthesis of 2-ethylchromone from 4-hydroxy-3-propionylcoumarin.

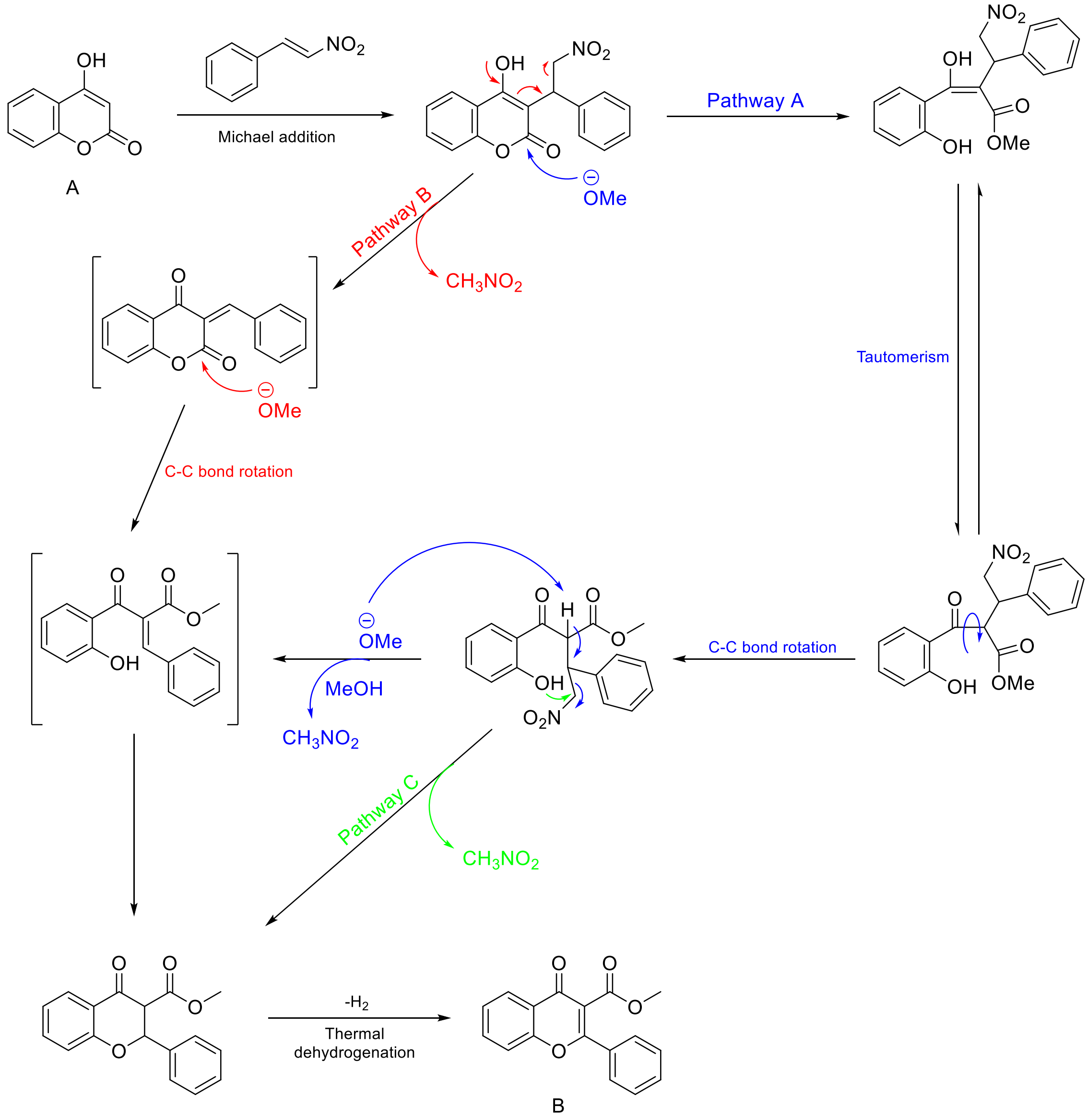
OH
O
O
A
NO2
Michael addition
OH
NO2
O
O
OMe
Pathway A
NO2
OH
O
OH
OMe
Pathway B
CH3NO2
O
O
O
OMe
Tautomerism
C-C bond rotation
O
O
O
OH
OMe
MeOH
CH3NO2
O
H
O
O
OH
O2N
C-C bond rotation
NO2
O
O
OH
OMe
Pathway C
CH3NO2
O
O
O
O
-H2
Thermal dehydrogenation
O
O
O
O
B

Figure 44 – Proposed conversion mechanism of 4-hydroxycoumarin (A) into 2,3-disubstituted chromones (B).

Following the same approach, 4-hydroxy-3-nitrocoumarin can be converted into 2-methyl-3-nitrochromone by a base induced lactone opening followed by the addition of acetic anhydride and pyridine.[317] Recently, the formation of 2,3-disubstituted chromones from 4-hydroxycoumarins, in the presence of alcohol and *β*-nitroalkenes was also reported (Fig. 44).[318] The reaction mechanism is not established, however it was proposed that the first step involves the *in situ* formation of a Michael adduct.

Chromones can also be synthesised from 2-hydroxyarylketones by means of a Claisen reaction. This reaction involves a condensation of an enolizable ketone and one nonenolizable ester in presence of a strong base. In order to obtain chromone derivatives, the lactonization process generally occurs in acidic conditions under reflux. (Fig. 45).[319]

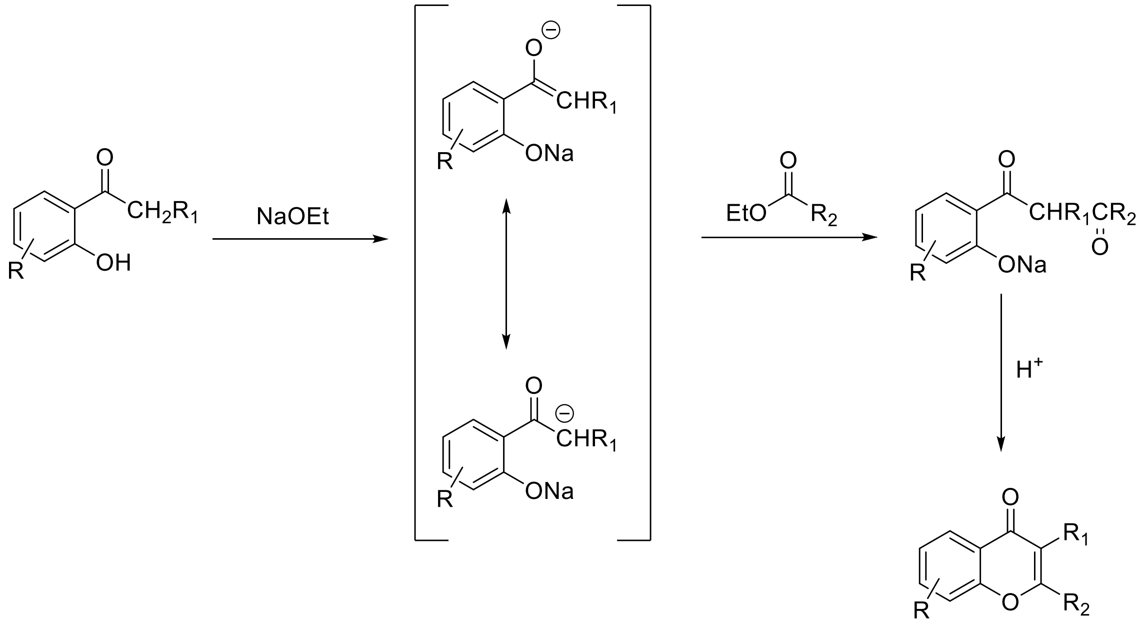

Figure 45 – Claisen condensation and lactonization.

Based on this reaction, Kostanecki *et al* [263] obtained chromone-2-carboxylic acids using diethyl oxalate and metallic sodium. A shortcoming of the Claisen reaction lies on the small range of variations of R_1 possible (Fig. 45) apart from hydrogen, alkyl or alkoxyl groups. Additionally, it is important to notice that if R_1 = COOEt (Fig. 45), the final product is a coumarin instead.[320]

Chromone derivatives can be also synthesised from *o*-acyloxyacylbenzenes by the Baker-Venkataraman rearrangement (Fig. 46).[321] In 1933, Baker [322] demonstrated that there was a base-induced transfer of the ester acyl group in an *o*-acylated phenol ester, which lead to a 1,3-diketone through the formation of an enolate, followed by an intramolecular acyl transfer (Fig. 46). The subsequent condensation can then occur, albeit under harsh conditions, usually concentrated sulphuric acid under reflux.

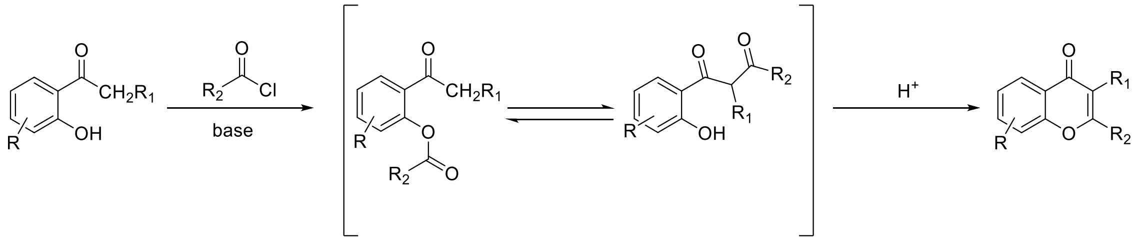

Figure 46 – Chromone synthesis via Baker-Venkataraman rearrangement.

The synthesis of 3-substituted chromones can be accomplished *via* a Vilsmeier-Haack condensation of *o*-hydroxyketones with formaldehydes or formic acid (Fig. 47).[191] Either dimethylformamide (DMF) or its corresponding acetal provide C-3 substituted chromones in an efficient one-pot reaction.[323] In fact, some of the derivatives described in this work have been prepared using this reaction (Fig. 47). This method does not require an acidification step, which is an advantage compared to the classic Claisen condensation.

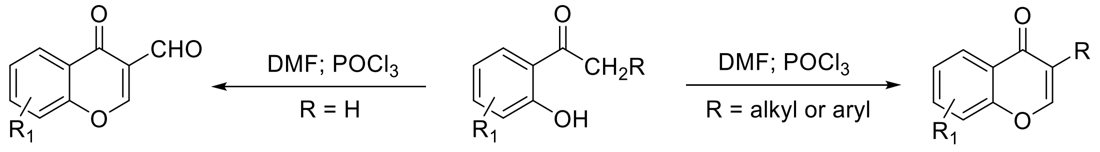

Figure 47 – Synthesis of 3-substituted chromones.

1.5. Objectives

The global aim of this work was to deepen our understanding of the benzopyrone nucleus as a privileged scaffold for the development of NCE with potential therapeutic application in ND. Originally, this thesis focused on the development of new MAO-B inhibitors and AR ligands, however the interaction with other ND-associated targets were also studied.

Accordingly, the specific aims set for the present study were the following:

- The rational design of NCE based on benzopyrone scaffold. Synthesis of such derivatives will be carried out by effective and versatile one-pot reactions, allowing their production in high yields.

- The *in vitro* screening of ND-associated targets. The benzopyrone-based libraries' activity towards MAO-B, AChE and AR will be screened and compared to standard inhibitors/ligands.
- Study of enzyme kinetics. Reversibility and kinetic assays will be performed in a small set of promising derivatives.
- Study of the binding mode of benzopyrone derivatives. Molecular modeling and docking studies will be performed to evaluate the interactions of the synthesized derivatives and their targets.
- Evaluation of drug-like properties. The assessment of drug-like properties will be utilized to establish criteria for a lead selection.
- Proposal of a lead multi target candidate. The derivatives with the most promising profile will be highlighted as possible lead candidates for further development.

CHAPTER 2

Manuscript I

Exploring coumarin potentialities: development of new enzymatic inhibitors based on the 6-methyl-3- carboxamidocoumarin scaffold.

RSC Advances, Volume 6, **2016**, Pages 49764-49768

RSC Advances

COMMUNICATION

Cite this: *RSC Adv.*, 2016, **6**, 49764

Received 28th February 2016
Accepted 11th May 2016

DOI: 10.1039/c6ra05262b

www.rsc.org/advances

Exploring coumarin potentialities: development of new enzymatic inhibitors based on the 6-methyl-3-carboxamidocoumarin scaffold†

A. Fonseca,[ab] M. J. Matos,[a] J. Reis,[a] Y. Duarte,[c] M. Gutiérrez,[c] L. Santana,[b] E. Uriarte[b] and F. Borges*[a]

Novel 6-methyl-3-carboxamidocoumarins (compounds **4–15**) were synthesized by an effective three step synthetic strategy and screened towards MAO, AChE and BuChE enzymes. In general, the compounds act as selective MAO-B inhibitors. Compound **11** is highlighted as a potent (IC_{50} *h*MAO-B = 4.66 nM), reversible and non-competitive MAO-B inhibitor.

The increase in average life expectancy in developed countries has led to a rise in diagnosed cases of neurodegenerative diseases (ND's), namely Parkinson's (PD) and Alzheimer's (AD) diseases,[1,2] and dementia. Currently none of these illnesses have an effective treatment to modify or stop their progress. The drugs currently available are only useful in delaying the progress of the diseases by controlling their symptoms.[2,3] Monoamine oxidases (MAOs) are enzymes present in the outer mitochondrial membrane, which have two isoforms named MAO-A and MAO-B, that catalyze the oxidation of biogenic amines.[4] Neurotransmitters, such as adrenaline, noradrenaline, dopamine, serotonin and β-phenylethylamine, are the main MAO substrates. Under normal conditions noradrenaline and serotonin are substrates of MAO-A while dopamine, a neurotransmitter present in low concentrations in the PD patient's brain, has a greater affinity for MAO-B.[5] Activity of MAO-B is also linked to the production of reactive oxygen species (ROS) that cause oxidative stress and neuronal damage. Expression levels of MAO-B in neuronal tissue augment 4-fold with aging, resulting in an increase of dopamine metabolism and, therefore, higher production of hydrogen peroxide (H_2O_2).[6] Thus, MAO-B inhibitors play an important role not only in dopamine metabolism but also in the reduction of brain oxidative damage. The involvement of MAO-B in AD is supported by the fact that neurons are extremely sensitive to oxidative stress as a consequence of: (a) their low content in endogenous antioxidants, such as glutathione, (b) the high proportion of an easily oxidized membrane covered by polyunsaturated fatty acids (c) the great oxygen brain consumption and also (d) a high content in iron.[7–9] In addition, concerning AD, MAO-B activity and the coproduction of H_2O_2 and other type of ROS are also increased, leading to an amplification of the neuron oxidative stress damage process. The current therapy for PD is only palliative and is focused in curtailing the motor symptoms by restoring the dopamine levels, namely by the administration of L-dopa, a dopamine precursor, alongside with other drug co-adjuvants, such as dopamine agonists, catechol-*o*-methyltransferase (COMT) and MAO-B inhibitors, such as selegiline. For AD, the therapy is only focused on the administration of acetylcholinesterase (AChE) inhibitors that target the cholinergic system, considering that the disease is characterized by a cholinergic neuronal loss, and consequently acetylcholine (ACh) depletion.[10] In brain synapses, ACh is hydrolyzed by AChE into choline and acetate.[11] At present butyrylcholinesterase (BuChE) was also proposed as a druggable target and as a result both enzymes represent putative therapeutic targets for improving the cholinergic deficit responsible for the decline in cognitive, behavioral and global functioning characteristic of AD.[12,13] Like in PD, none of the current drugs in therapy are able to modify disease progression, a condition that is well thought-out to be a driving force behind the ongoing research related to the discovery of new and potent inhibitors based on different types of scaffolds.[14]

Coumarins are heterocycles widely found in plants and other natural products that have synthetic accessibility and display remarkable biological properties, such as anticancer, antiviral, anti-inflammatory, antimicrobial and antioxidant agents.[15–29] Previous studies have shown that coumarin is a noteworthy scaffold for the discovery and development of new potent and selective MAO-B and AChE inhibitors.[25]

---

[a] *CIQUP/Departamento de Química e Bioquímica, Faculdade de Ciências, Universidade do Porto, 4169-007, Porto, Portugal*

[b] *Departamento de Química Orgánica, Facultade de Farmacia, Universidade de Santiago de Compostela, 15782, Santiago de Compostela, Spain*

[c] *Laboratorio de Síntesis Orgánica, Instituto de Química de Recursos Naturales Universidad de Talca, Casilla 747, 3460000, Talca, Chile*

† Electronic supplementary information (ESI) available. See DOI: 10.1039/c6ra05262b

Coumarins previously developed by our group (Fig. 1, structure A) have shown to display a remarkable potency and selectivity towards MAO-B activity. Till now our best-in-class IMAO-B coumarin was 3-(3-bromophenyl)-6-methylcoumarin (IC_{50} *h*MAO-B = 134 pM).[30] The data attained so far stimulate the progress of the project and in accordance a lead optimization process was implemented in which the effect of a linker, located between the coumarin core and the exocyclic aromatic ring, was studied regarding IMAO activity. In addition, and taking advantage of the expenditure of the project it was also decided to move on from one-target to a dual-target drug design approach. So, other targets of interest in neurodegenerative diseases, like AChE, have been involved. The first studies were focused on the role of carbonylamine type linker (Fig. 1, structure B). From the study, potent and selective IMAO-B were attained which were also able to inhibit AChE in the range from 12 μM to 69 μM.[29] The best dual candidate of the series was 3-(4′-chlorobenzamide)coumarin (IC_{50} *h*MAO-B = 1.95 μM and IC_{50} AChE = 18.71 μM). The best IMAO-B of the series was 3-(4′-methylbenzamide)-6-methylcoumarin (IC_{50} *h*MAO-B = 170 nM), which did not have relevant AChE inhibitory activity.

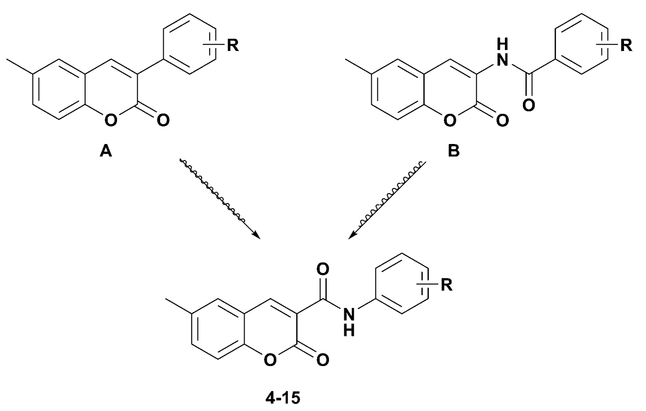

Fig. 1 Rational design followed in the present study to obtain the 3-substituted coumarins 4–15.

So, additional studies focused in the effect of a carboxamide linker, located between coumarin and the exocyclic aromatic substituent, were accomplished. Within this framework new 6-methyl-3-carboxamidocoumarins (compounds **4–15**, Fig. 1) were designed, synthesized and studied as MAO enzymatic inhibitors.

Coumarin derivatives (**4–15**) have been obtained efficiently by a three step synthetic strategy described in Scheme 1 and explained in detail in ESI.† Briefly, in the first step the coumarin used as starting material (compound **2**) was synthesized by a Knoevenagel condensation, in which 5-methylsalicylaldehyde (**1**) was refluxed with diethyl malonate in ethanol, in presence of catalytic amounts of piperidine. After subsequent hydrolysis, compound **3** was obtained with an overall yield of 89%.[31] Then, compounds **4–15** were synthesized by an amidation reaction in which the carboxylic acid **3** was activated with a coupling agent 1-ethyl-3-(3-dimethylaminopropyl)carbodiimide (EDC) in the presence of a nucleophilic catalyst 4-dimethylaminopyridine (DMAP).[32] After adding the primary aromatic amine with the desired substitution pattern, 6-methyl-3-carboxamidocoumarin derivatives (**4–15**) have been obtained with yields ranging from 56% to 83%. Structural characterization of the compounds was performed by ^1H and ^{13}C NMR spectroscopy, mass spectrometry (EI-MS) and elemental analysis and is included in ESI.† The biological evaluation of the compounds **4–15** towards *h*MAO-A and *h*MAO-B was investigated by measuring their effects on the production of H_2O_2 from *p*-tyramine (a MAO substrate), using the Amplex Red MAO assay kit and recombinant *h*MAO with selegiline as reference compound.[33] In addition, the inhibitory activities of the compounds **4–15** were evaluated towards *Electrophorus electricus* AChE and bovine serum BuChE using Ellman spectrophotometric method and galantamine as reference compound.[34] The biological activity results expressed as IC_{50} values are listed in Table 1.

In general, compounds **4–15** display a remarkable selectivity towards *h*MAO-B, as they were inactive against *h*MAO-A at the highest concentration tested, and an interesting structure-dependent inhibitory potency. The methyl (**4–6**) and bromine

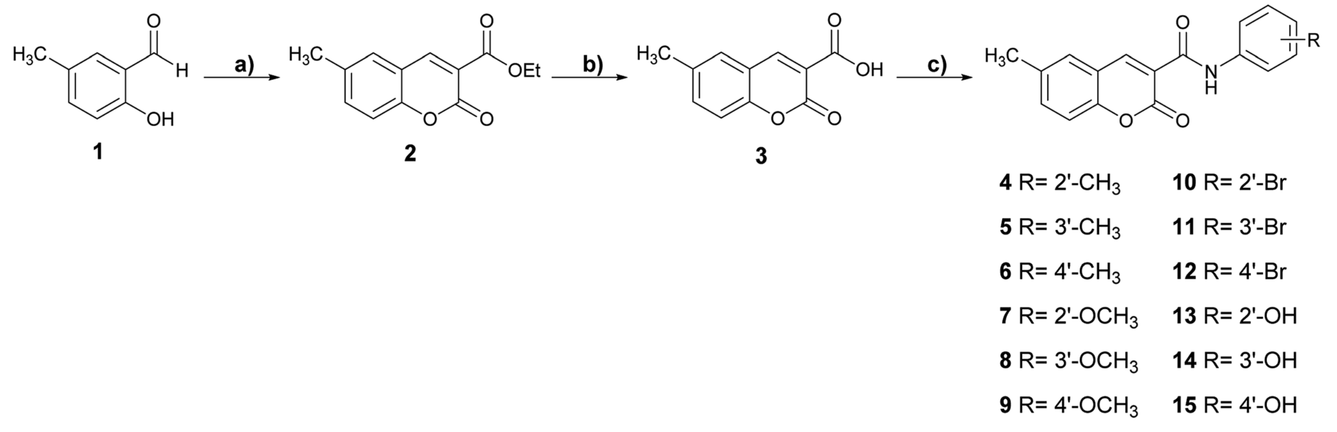

Scheme 1 Synthesis of coumarins 4–15. Reagents and conditions: (a) diethyl malonate, EtOH, piperidine, reflux, overnight. (b) NaOH (0.5% aq./EtOH), reflux, 4 h. (c) EDC, DMAP, DCM, corresponding amine, 0 °C to r.t., 4 h.

Table 1 *In vitro h*MAO-A, *h*MAO-B and AChE inhibitory activities of 6-methyl-3-carboxamidocoumarin derivatives (**4–15**) and reference compounds

Compound	IC_{50} (nM) *h*MAO-A	IC_{50} (nM) *h*MAO-B	SI	IC_{50} (μM) AChE
4	[a]	11.80 ± 1.10	>847.4[b]	[c]
5	[a]	7.52 ± 1.05	>1329.8[b]	535.24 ± 0.01
6	[a]	13.90 ± 1.30	>719.4[b]	657.22 ± 0.01
7	[a]	160.60 ± 1.10	>62.3[b]	494.45 ± 0.03
8	[a]	10.10 ± 1.20	>990.0[b]	470.52 ± 0.18
9	[a]	296.90 ± 5.90	>33.7[b]	[c]
10	[a]	13.50 ± 1.10	>740.7[b]	621.23 ± 0.07
11	[a]	4.66 ± 1.13	>2145.9[b]	591.44 ± 0.02
12	[a]	11.40 ± 1.20	>877.2[b]	358.88 ± 0.05
13	[a]	18.30 ± 1.60	>546.4[b]	666.37 ± 0.11
14	[a]	45.40 ± 1.30	>220.3[b]	[c]
15	[a]	621.70 ± 1.80	>16.1[b]	[c]
Selegiline	68 730 ± 420	17.00 ± 1.90 (ref. 3)	4042.9	[d]
Galantamine	[d]	[d]	[d]	0.54 ± 0.50

[a] Inactive at 10 μM (highest concentration tested). [b] Values obtained under the assumption that the corresponding IC_{50} against MAO-A is the highest concentration tested (10 μM). [c] Inactive at 1000 μM (highest concentration tested). [d] Not determined.

(**10–12**) derivatives, bearing substituents located at *ortho*, *meta* and *para* positions of the exocyclic aromatic ring, exhibit MAO-B activity in the low nanomolar range. In the case of the methoxy substituted coumarins (compounds **7–9**), only the *meta*-substituted derivative display potency in the same range. For the hydroxy coumarin derivatives (compounds **13–15**), it can be concluded that the MAO-B inhibitory activity is strongly dependent on the substituent location, being enhanced when they are located at *ortho* and *meta* positions. In summary, it was observed that the presence of electron donor substituents in the *para* position of the aryl ring attached to the amide group lead to a potency decrease, whereas derivatives bearing weak electron donors or acceptors do not change IMAO-B potency independently of their position. The 6-methyl-3-carboxamidocoumarins substituted in the *meta* position (compounds **5**, **8** and **11**) have a superior activity towards MAO-B than their *ortho* (compounds **4**, **7** and **10**) and *para* (compounds **6**, **9** and **12**) counterparts. In particular, compounds **5** (IC_{50} *h*MAO-B = 7.52 nM) and **11** (IC_{50} *h*MAO-B = 4.66 nM) showed *h*MAO-B inhibition at a low nanomolar range, slightly better than selegiline, and also benefiting from an excellent selective profile.

To examine the type of inhibition mechanism of the most promising *h*MAO-B inhibitor (compound **11**) kinetic experiments were performed. For this purpose, the initial rates of the MAO-B-catalyzed oxidation of *p*-tyramine at five different substrate concentrations, in the absence or presence of the selected coumarin inhibitor, at different concentrations, were measured. The results are depicted in Fig. 2.

Graphical analyses of the reciprocal Lineweaver–Burk plots allow the determination of Michaelis–Menten reaction kinetic parameters (Michaelis constant, K_m and maximum velocity, V_{max}). Concerning compound **11**, it was found that the K_m remained almost constant at different concentrations of the inhibitor whereas V_{max} decreased. The Lineweaver–Burk plots obtained for different concentrations of compound **11** (Fig. 2) displayed a series of converging lines on the same point of the *x*-axis (1/[S]) profiling a non-competitive inhibition mechanism. From the Dixon plots, obtained from the replots of the slopes of the Lineweaver–Burk plots *vs.* inhibitor concentrations (upper right corner), the *h*MAO-B inhibition binding affinities, determined as inhibition constants (K_i), were calculated. As a result, compound **11** (Fig. 2) displayed a K_i value of 2.70 nM. The

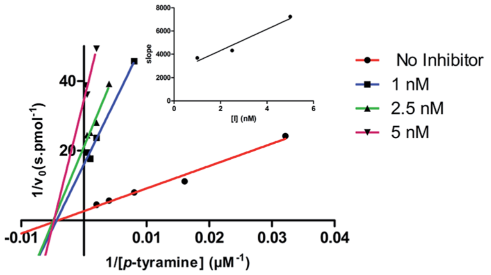

Fig. 2 Kinetic study on the mechanism of *h*MAO-B inhibition by compound **11**. The effect of the inhibitors on the enzyme was determined from the double reciprocal plot of 1/rate (1/*V*) *versus* 1/substrate concentration in presence of varying concentrations of the inhibitors. The K_i value was calculated by the intersection of the curves obtained by plotting 1/*V versus* the inhibitor concentration for each substrate concentration (Dixon plots insets on the top right).

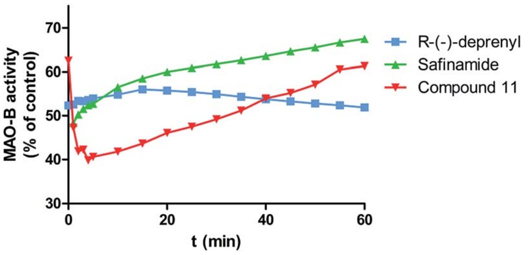

Fig. 3 Time-dependent inhibition of recombinant human MAO-B by standard compounds (*R*)-(−)-deprenyl (50 nM), safinamide (40 nM) and test compound **11** (15 nM), the remaining activity was expressed as % of activity. Data are the mean ± S.D. of three different experiments.

Table 2 Drug-like properties of 6-methyl-3-carboxamidocoumarin derivatives (**4–15**) and reference compounds

Compound	Molecular weight	clog *P*	TPSA ($Å^2$)	H-bond donor	H-bond acceptor	Volume ($Å^3$)
4/5/6	293.3	3.66/3.68/3.71	59.31	4	1	264.5
7/8/9	309.3	3.27/3.29/3.31	68.54	5	1	273.5
10/11/12	358.2	4.02/4.04/4.07	59.31	4	1	265.8
13/14/15	295.3	2.99/2.75/2.78	79.54	5	2	256.0
Selegiline	187.3	2.64	3.24	1	0	202.6
Galantamine	287.4	1.54	41.93	4	1	268.2

estimated K_i value correlated well with the inhibition mechanism suggested by the kinetic experiments, with the compound displaying IC_{50} and K_i values slightly different but within the low nanomolar range.

The reversibility of MAO-B inhibition by the test compound **11** was then assessed by time-dependent inhibition studies. The behavior of standard irreversible (*R*-(−)-deprenyl) and reversible (safinamide) inhibitors was also evaluated under the same experimental conditions. MAO-B activity (% of control) was measured along 60 minutes incubation with the enzyme inhibitors (Fig. 3). The analysis of time-dependent enzyme inhibition studies performed with the irreversible inhibitor (*R*-(−)-deprenyl, Fig. 3) showed that the enzyme residual activity decayed continuously after the first 15 minutes of incubation, which is consistent with irreversible enzymatic inhibition. In case of the reversible inhibitor safinamide (Fig. 3), an enhancement on enzymatic activity was observed along the analysis time. A similar behavior was observed for compound **11**, which shows the gradual link to the allosteric binding site (non-competitive inhibitor) in the first 15 minutes, proceeded by the enhancement of enzymatic activity along the last 60 minutes, as its expectable of a MAO-B reversible inhibition profile.

Finally, the drug-like properties of the compounds **4–15**, namely the lipophilicity (expressed as the octanol/water partition coefficient, and herein called clog *P*) and other properties (molecular weight, number of hydrogen acceptors and donors and volume) were calculated using the Molinspiration calculation software. Topological polar surface area (TPSA) that has been shown to be a very good descriptor of drug absorption, including intestinal absorption, bioavailability, Caco-2 permeability and blood–brain barrier penetration was also calculated. The data are presented in Table 2. Complete procedures of *in vitro* biological studies, statistical analysis and drug-like properties calculations are listed in the ESI.†

Analyzing the results for the inhibitory activity towards human AChE depicted in Table 1, one can conclude that all compounds presented a moderate inhibitory activity (micromolar range) towards the enzyme. None of the tested compounds displayed a noticeable activity towards BuChE at the highest concentration tested (10 mM) (data not shown). Compound **12**, the *para*-bromine coumarin derivative, was found to be the most active compound towards AChE ($IC_{50} = 358.88\ \mu M$). Analysing the overall data, one can conclude that the 6-methyl-3-carboxamidocoumarins substituted with a hydroxyl substituent (compounds **13–15**) are the less potent compounds of the series. However, when a methyl or methoxy substituent (compounds **5** and **8**) is located at *meta* position of the aromatic exocyclic ring a slight increment of inhibitory activity is observed, when compared with their *ortho* (compounds **4** and **7**) and *para* (compounds **6** and **9**) counterparts.

In our previous study, compound **6** analogue (compound **4** in ref. 29), which also have a methyl substituent, in *para* position, had displayed a IC_{50} *h*MAO-B = 170 nM, which is ten times lower. Nevertheless, it showed a superior affinity to AChE than the compounds presented here.[29] Thus, it can be concluded that the carboxamide spacer, and specially the location of the carbonyl group, is a key feature for MAO-B and AChE inhibitory activities.

Additionally, from the prediction drug-like properties of compounds **4–15** (Table 2) it can be observed that no violations of Lipinski's rule (molecular weight, log *P*, number of hydrogen donors and acceptors) were found and that the TPSA, described as a predictive indicator of the drug capacity of membrane penetration, is favorable. Therefore, the data provided a preliminary indication that this type of compounds can cross membranes and act in the central nervous system.

The remarkable results found for compounds **5** and **11** (*h*MAO-B IC_{50} of 7.52 and 4.66 nM respectively) encourage us to continue our research based on the coumarin scaffold. Compound **11** acts as a potent, selective, reversible and non-competitive MAO-B inhibitor. In addition, compound **12** (*h*MAO-B IC_{50} of 11.40 nM and AChE IC_{50} of 358.88 μM) can be looked as a stimulating framework to develop dual target MAO-B/AChE inhibitors. Further examination of the cytotoxic and pharmacokinetic properties of compounds **11** and **12** is important to define which one will be a candidate for *in vivo* studies. In summary, the data attained so far is a noteworthy contribution for the development of new drug candidates for PD and AD based on 6-methylcoumarin scaffold.

Acknowledgements

The authors would like to thank Fundação para a Ciência e Tecnologia (FCT) – QUI/UI0081/2015-POCI-01-0145-FEDER-006980 for the financial support. Thanks are due to FCT, POPH and QREN for the post-doctoral and doctoral grants: A. Fonseca (SFRH/BD/80831/2011) and J. Reis (SFRH/BD/96033/2013) and M. J. Matos (SFRH/BPD/95345/2013).

Notes and references

1 R. J. Castellani, R. K. Rolston and M. a. Smith, *Dis.-Mon.*, 2010, **56**, 484–546.

2 L. M. L. de Lau and M. M. B. Breteler, *Lancet Neurol.*, 2006, **5**, 525–535.

3 M. R. Farlow and J. L. Cummings, *Am. J. Med.*, 2007, **120**, 388–397.

4 J. P. Johnson, *Biochem. Pharmacol.*, 1968, **17**, 1285–1297.

5 M. B. Youdim, D. Edmondson and K. F. Tipton, *Nat. Rev. Neurosci.*, 2006, **7**, 295–309.

6 A. Gaspar, N. Milhazes, L. Santana, E. Uriarte, F. Borges and M. J. Matos, *Curr. Top. Med. Chem.*, 2015, **15**, 432–445.

7 P. Riederer, *Neurotoxicology*, 2004, **25**, 271–277.

8 V. Jain, M. C. Langham and F. W. Wehrli, *J. Cereb. Blood Flow Metab.*, 2010, **30**, 1598–1607.

9 T. A. Rouault, *Nat. Rev. Neurosci.*, 2013, **14**, 551–564.

10 M. Itakura, H. Nakajima, T. Kubo, Y. Semi, S. Kume, S. Higashida, A. Kaneshige, M. Kuwamura, N. Harada, A. Kita, Y.-T. Azuma, R. Yamaji, T. Inui and T. Takeuchi, *J. Biol. Chem.*, 2015, **290**, 26072–26087.

11 V. N. Talesa, *Mech. Ageing Dev.*, 2001, **122**, 1961–1969.

12 M. Khoobi, M. Alipour, A. Moradi, A. Sakhteman, H. Nadri, S. F. Razavi, M. Ghandi, A. Foroumadi and A. Shafiee, *Eur. J. Med. Chem.*, 2013, **68**, 291–300.

13 R. M. Lane, S. G. Potkin and A. Enz, *Int. J. Neuropsychopharmacol.*, 2006, **9**, 101–124.

14 M. Singh, M. Kaur, H. Kukreja, R. Chugh, O. Silakari and D. Singh, *Eur. J. Med. Chem.*, 2013, **70**, 165–188.

15 F. Borges, F. Roleira, N. Milhazes, L. Santana and E. Uriarte, *Curr. Med. Chem.*, 2005, **12**, 887–916.

16 F. Borges, F. M. F. Roleira, N. Milhazes, E. Uriarte and L. Santana, *Front. Med. Chem.*, 2009, **4**, 23–85.

17 M. Riveiro, N. De Kimpe, A. Moglioni, R. Vazquez, F. Monczor, C. Shayo and C. Davio, *Curr. Med. Chem.*, 2010, **17**, 1325–1338.

18 M. J. Matos, S. Vazquez-Rodriguez, L. Santana, E. Uriarte, C. Fuentes-Edfuf, Y. Santos and A. Munoz-Crego, *Med. Chem.*, 2012, **8**, 1140–1145.

19 D. Viña, M. J. Matos, G. Ferino, E. Cadoni, R. Laguna, F. Borges, E. Uriarte and L. Santana, *ChemMedChem*, 2012, **7**, 464–470.

20 M. J. Matos, S. Vazquez-Rodriguez, E. Uriarte, L. Santana and D. Viña, *Bioorg. Med. Chem. Lett.*, 2011, **21**, 4224–4227.

21 D. Secci, S. Carradori, A. Bolasco, P. Chimenti, M. Yáñez, F. Ortuso and S. Alcaro, *Eur. J. Med. Chem.*, 2011, **46**, 4846–4852.

22 S. Vazquez-Rodriguez, M. J. Matos, L. Santana, E. Uriarte, F. Borges, S. Kachler and K. N. Klotz, *J. Pharm. Pharmacol.*, 2013, **65**, 697–703.

23 I. Kostova, S. Bhatia, P. Grigorov, S. Balkansky, V. S. Parmar, A. K. Prasad and L. Saso, *Curr. Med. Chem.*, 2011, **18**, 3929–3951.

24 M. J. Matos, P. Janeiro, R. M. González Franco, S. Vilar, N. P. Tatonetti, L. Santana, E. Uriarte, F. Borges, J. A. Fontenla and D. Viña, *Future Med. Chem.*, 2014, **6**, 371–383.

25 M. J. Matos, D. Viña, E. Quezada, C. Picciau, G. Delogu, F. Orallo, L. Santana and E. Uriarte, *Bioorg. Med. Chem. Lett.*, 2009, **19**, 3268–3270.

26 M. J. Matos, D. Viña, C. Picciau, F. Orallo, L. Santana and E. Uriarte, *Bioorg. Med. Chem. Lett.*, 2009, **19**, 5053–5055.

27 M. J. Matos, S. Vazquez-Rodriguez, L. Santana, E. Uriarte, C. Fuentes-Edfuf, Y. Santos and A. Muñoz-Crego, *Molecules*, 2013, **18**, 1394–1404.

28 M. J. Matos, C. Terán, Y. Pérez-Castillo, E. Uriarte, L. Santana and D. Viña, *J. Med. Chem.*, 2011, **54**, 7127–7137.

29 D. Viña, M. J. Matos, M. Yáñez, L. Santana and E. Uriarte, *Med. Chem. Commun.*, 2012, **3**, 213–218.

30 M. J. Matos, S. Vilar, V. Garcia-Morales, N. P. Tatonetti, E. Uriarte, L. Santana and D. Viña, *ChemMedChem*, 2014, **9**, 1488–1500.

31 F. Chimenti, B. Bizzarri, A. Bolasco, D. Secci, P. Chimenti, A. Granese, S. Carradori, D. Rivanera, A. Zicari, M. Scaltrito and F. Sisto, *Bioorg. Med. Chem. Lett.*, 2010, **20**, 4922–4926.

32 C. Murata, T. Masuda, Y. Kamochi, K. Todoroki, H. Yoshida, H. Nohta, M. Yamaguchi and A. Takadate, *Chem. Pharm. Bull.*, 2005, **53**, 750–758.

33 M. Yáñez, N. Fraiz, E. Cano and F. Orallo, *Biochem. Biophys. Res. Commun.*, 2006, **344**, 688–695.

34 P. Torre, L. Saavedra, J. Caballero, J. Quiroga, J. Alzate-Morales, M. Cabrera and J. Trilleras, *Molecules*, 2012, **17**, 12072–12085.

Supporting Information for

Exploring coumarin potentialities: development of new enzymatic inhibitors based on the 6-methyl-3-carboxamidocoumarin scaffold

A. Fonseca[a, b], M. J. Matos[a], J. Reis[a], Y. Duarte[c], M. Gutiérrez[c], L. Santana[b], E. Uriarte[b], and F. Borges[a, *]

[a] *CIQUP/Departamento de Química e Bioquímica, Faculdade de Ciências, Universidade do Porto, 4169-007, Porto, Portugal*

[b] *Departamento de Química Orgánica, Faculdade de Farmacia, Universidade de Santiago de Compostela, 15782, Santiago de Compostela, España*

[c] Laboratorio de Síntesis Orgánica, Instituto de Química de Recursos Naturales Universidad de Talca, Casilla 747, 3460000, Talca, Chile

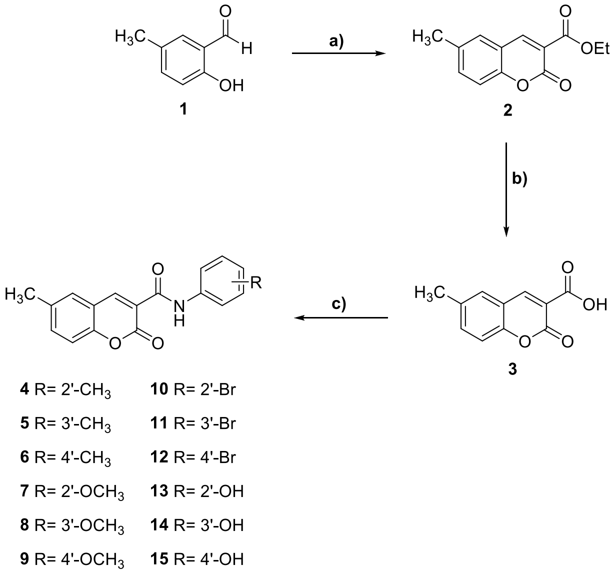

Scheme 1 – Synthesis of coumarins **4-15.** Reagents and conditions: a) diethyl malonate, EtOH, piperidine, reflux, overnight. b) NaOH (0.5% aq./EtOH), reflux, 4h. c) EDC, DMAP, DCM, corresponding amine, 0 ºC to r.t., 4h.

Reagents and materials.

All starting materials and reagents were obtained from commercial suppliers and were used without further purification (Sigma–Aldrich). Melting points (mp) were determined using a Reichert Kofler thermopan or in capillary tubes on a Büchi 510 apparatus and were not corrected. ^{1}H (250 MHz) and ^{13}C (63 MHz) NMR spectra were recorded on a Bruker AMX spectrometer, using DMSO-d6 or $CDCl_3$ as solvents. Chemical shifts (δ) and coupling constants (*J*) were expressed in ppm and in Hz, respectively, using TMS as internal standard. The notations used for spin multiplicities were: s (singlet), d (doublet),

---

Corresponding author. Tel.:+351220402560
E-mail adress: fborges@fc.up.pt

dd (double doublet), t (triplet), dt (double triplet) and m (multiplet). Mass spectrometry data was acquired with a Hewlett- Packard-5972-MSD spectrometer. Elemental analyses were performed with a PerkinElmer 240B microanalyzer and are within 0.4% of calculated values in all cases. Silica gel (Merck 60, 230–400 mesh) was used for flash chromatography (FC). Analytical thin layer chromatography (TLC) was performed on plates precoated with silica gel (Merck 60 F254, 0.25 mm). Organic solutions were dried over anhydrous Na_2SO_4. The solvents were evaporated on a rotary evaporator (Büchi Rotavapor). The purity of all the compounds was higher than 95%.

***Synthesis of 6-methylcoumarin-3-carboxylic acid* (3).**

Firstly, 5-methylsalicylaldehyde (**1**) (1 mmol), diethyl malonate (1 mmol) and catalytic amounts of piperidine were refluxed in ethanol (10 mL) overnight. After cooling to room temperature, the suspension was filtered off and ethyl 6-methylcoumarin-3-carboxylate (**2**) was attained. Afterwards, compound **2** was hydrolyzed in 20 mL of an ethanolic solution with 0.5% NaOH (aq.) at reflux for 1h. After reaction 10% HCl (aq.) was added and the desired carboxylic acid (**3**) was then filtered off and washed with water to yield 89%.[1]

General procedure for the synthesis of compounds* 4-15*.

To a solution of 6-methylcoumarin-3-carboxylic acid (**3**) (1 mmol) in dichloromethane (DCM) (5 mL) 1-ethyl-3-(3-dimethylaminopropyl)carbodiimide (EDC) (1.10 mmol) and 4-dimethylaminopyridine (DMAP) (1.10 mmol) were added. The mixture was kept in a round bottom flask with a flux of argon at 0 ºC for five minutes. Shortly after, the aromatic amine (1 mmol) with the pretended substitution pattern was added in small portions. The reaction mixture was stirred for 4 h at room temperature. The obtained precipitate was filtered and purified by column chromatography (hexane/ethyl acetate 9:1) or by recrystallization with ethanol to give the desired product.[2]

Determination of h*MAO-A *and h*MAO-B *inhibitory activity.

The effect of synthesized coumarins (compounds **4-15**) on *h*MAO isoforms was evaluated by a fluorimetric assay, following a previously described method, by measuring their outcome on the production of hydrogen peroxide (H_2O_2) from p-tyramine. In the assays the Amplex Red MAO assay kit (Molecular Probes, Inc., Eugene, OR, U.S.) and microsomal MAO isoforms prepared from insect cells (BTI-TN-5B1-4) infected with recombinant baculovirus containing cDNA inserts for *h*MAO-A or *h*MAO-B (Sigma-Aldrich Química S.A) have been used. The production of H_2O_2 catalyzed by MAO isoforms was detected using 10-acetyl-3,7-dihydroxyphenoxazine (Amplex Red reagent), a nonfluorescent and highly sensitive probe that reacts with H_2O_2 in the presence of horseradish peroxidase to produce resorufin, a fluorescent product. Briefly, 100 µL of sodium phosphate buffer (0.05 M, pH 7.4) containing various concentrations of the coumarins, or reference inhibitors with DMSO as co-solvent, and adequate amounts of recombinant *h*MAO-A or *h*MAO-B were incubated for 15 min at 37˚C in a flat-black-bottom 96-well microplate (BRANDplates®, pureGradeTM, BRAND GMBH, Wertheim, Germany) placed in a dark multimode microplate reader chamber. After the incubation period, the reaction was started by adding (final concentrations) 200 µM Amplex Red reagent, 1 U/mL horseradish peroxidase, and 1 mM tyramine. The production of H_2O_2 and consequently of resorufin was quantified at 37˚C in a multimode microplate reader (Biotek Synergy HT), based on the fluorescence generated (excitation, 545 nm, emission, 590 nm) over a 15 min period, along which the fluorescence increased linearly. Control experiments were carried out simultaneously by replacing the test drugs (new compounds and reference inhibitors) with appropriate dilutions. Additionally, assays have been performed to check the interference of the compounds with the fluorescence generated in the reaction due to a non-enzymatic inhibition (*e.g.,* for a direct reaction with Amplex Red reagent) by adding them to solutions containing only the Amplex Red reagent in a sodium phosphate buffer. To determine the kinetic parameters of *h*MAO-A and *h*MAO-B (Km and Vmax), their enzymatic activity was evaluated (under the experimental conditions above described) in the presence of different p-tyramine concentrations. The specific fluorescence emission, used to obtain the final results, was calculated after subtraction of the background activity, which was determined from wells containing all components except the MAO isoforms (replaced by a sodium phosphate buffer solution). The final results of the *h*MAO inhibitory activity were then expressed as IC_{50}, the concentration of each drug required to yield a 50% decrease on control value concentrations. Each assay was run in triplicate and each reaction was repeated at least three independent times being the highest concentration tested 10 µM. For the reference compound selegiline was used.[3]

Determination of AChE and BuChE inhibitory activity.

The AChE and BuChE inhibitory activities of the synthesized coumarins were determined in the following assays conditions. Briefly, the samples were dissolved in phosphate buffer (8 mM K_2HPO_4, 2.3 mM NaH_2PO_4, 150 mM NaCl, and 0.05% Tween 20 at pH 7.6) and AChE or BuChE solutions (50 µL, 0.25 unit/mL) from Electroporus electricus and equine serum, respectively, in the same phosphate buffer, were added. The assay solutions were pre-incubated with the enzyme for 30 min at room temperature in a 96-well microplate. After pre-incubation, a solution containing the enzyme subtract consisting of acetylthiocholine or butyrylthiocholine (0.24 mM) and 5,5′-dithio-bis-(2-nitrobenzoic acid) (0.2 mM, DTNB, Ellman's reagent) in Na_2HPO_4 (40 mM) was added. Then, the final absorbance was measured on a microtiter plate reader (Multiskan EX, Thermo,Vantaa, Finland) at 405 nm for 5 min. The background activity was given by a well with only sodium phosphate buffer solution. The final results were calculated by means of regression analysis and then expressed as IC_{50}. The alkaloid galantamine was used as the reference compound. Each assay was run in triplicate and each reaction was repeated at least three independent times.[4]

Data analysis and statistics.

The biological results were expressed as mean ± standard deviation of at least three different experiments. Statistical comparisons between control and test groups were carried by one-way analysis of variance (ANOVA-1) followed by Dunnett comparison post-test ($\alpha = 0.05$, 95% confidence intervals). Differences were considered to be significant for *p* values lower than 0.05. Plots and statistical analysis were performed using GraphPad Software, Inc. La Jolla, CA 92937, USA.

Theoretical evaluation of drug-like properties.

The ADME properties of the compounds under study were calculated using the Molinspiration property program. LogP and topological polar surface area (TPSA) were calculated as a sum of fragment-based contributions and correction factors. The method for the calculation of molecule volume developed at Molinspiration have been obtained by fitting the sum of fragment contributions to ‘real’ three dimensional (3D) volume for a training set of about 12 000, mostly drug-like molecules. 3D molecular geometries for a training set were fully optimized by the semi-empirical AM1 method.[5, 6]

Evaluation of hMAO-B-inhibitor kinetics.

To evaluate the mechanism of *h*MAO-B inhibition of compound **11**, substrate-dependent kinetic experiments were performed. The catalytic rates of *h*MAO-B were measured at five different concentrations of p-tyramine substrate (0.031 – 3 mM) in the absence or presence of the selected inhibitor (compound **11**), at concentrations between 1.0 and 5.0 nM. The results are presented as double reciprocal Lineweaver-Burk plots (1/V vs. 1/[S]) and the kinetic data, namely Michaelis-Menten constant (K_m) and maximum reaction rate (V_{max}), was acquired employing Michaelis-Menten equation. The Ki value was estimated using Dixon plots, by replotting the slope of each Lineweaver-Burk plot versus the inhibitor concentration. In the Dixon plots, the Ki value was obtained from the x-axis intercept ($-K_i$). The enzymatic reactions and measurements were performed using the same *h*MAO-B assay conditions as described above (n=3). Linear regression analysis was performed using Prism 5.

Evaluation of hMAO-B-inhibitior type of binding affinity.

The analysis of the type of binding of compound **11** and the standard inhibitors with *h*MAO-B was performed by a time-dependent inhibition assay. The enzyme was incubated for a 60 minute period with the coumarin based inhibitor as well as the standard inhibitors at their IC_{80} values. The final well concentrations were: compound **11** (15 nM), (R)-(−)-deprenyl (50 nM), safinamide (40 nM) and MAO-B (6.4 µg/mL). Control experiments without inhibitors were run simultaneously. The enzymatic activity was determined as described above (see determination of *h*MAO isoform activity). The percentage of enzyme activity was plotted against the incubation time to determine time-dependent enzyme-inhibition. Data are the mean ± SD of three independent experiments.

References:

1. Chimenti, F.; Bizzarri, B.; Bolasco, A.; Secci, D.; Chimenti, P.; Granese, A.; Carradori, S.; Rivanera, D.; Zicari, A.; Scaltrito, M. M.; Sisto, F. *Bioorg. Med. Chem. Lett.* **2010**, *20*, 4922–4926.

2. Murata, C.; Masuda, T.; Kamochi, Y.; Todoroki, K.; Yoshida, H.; Nohta, H.; Yamaguchi, M.; Takadate, A. *Chem. Pharm. Bull. (Tokyo).* **2005**, *53*, 750–758.

3. Yáñez, M.; Fraiz, N.; Cano, E.; Orallo, F. *Biochem. Biophys. Res. Commun.* **2006**, *344*, 688–695.

4. Torre, P.; Saavedra, L.; Caballero, J.; Quiroga, J.; Alzate-Morales, J.; Cabrera, M.; Trilleras, J. *Molecules* **2012**, *17*, 12072–12085.

5. Lipinski, C. a.; Lombardo, F.; Dominy, B. W.; Feeney, P. J. Adv. Drug Deliv. Rev. **2012**, 64, 4–17.

6. Molinspiration Cheminformatics, Bratislava University, Slovak Republic, 2009, http://www.molinspiration.com/services/properties.html (accessed January 2015).

Manuscript II

Coumarin-quinoline hybrids as cholinesterase inhibitors: synthesis, biological evaluation and molecular docking.

Submitted to ChemMedChem

WILEY-VCH

Coumarin-quinoline Hybrids as Cholinesterase Inhibitors: Synthesis, Biological Evaluation and Molecular Docking

Yorley Duarte,*[a] André Fonseca,[b] Maria João Matos,[b] Francisco Adasme-Carreño,[c] Camila Muñoz-Gutierrez,[c] Margarita Gutiérrez,[a] Lourdes Santana,[b] Eugenio Uriarte,[b] and Jans Alzate-Morales[c]

Abstract: The inhibition of the degradation of acetylcholine by cholinesterases (ChE) is one of the main targets for the treatment of Alzheimer disease (AD). In the present work, a new series of coumarin-quinoline hybrids were efficiently synthesized and evaluated as inhibitors against acetylcholinesterase (AChE) and butyrylcholinesterase (BuChE), using the colorimetric Ellman's method. Small structural variations allowed us to obtain compounds with dual AChE/BuChE activity, or selectivity towards AChE or BuChE. In addition, molecular docking studies were performed to better understand the structure-activity relationships. Most stable binding conformations for studied compounds within the binding site of AChE were determined by this methodology.

Introduction

Neurodegenerative diseases are the leading cause of morbidity and disability in the elderly population. Alzheimer disease (AD) is the most prevalent one, causing partially behavioural disturbances related with cholinergic deficiency. AD is the most common cause of dementia in older adults. This disease is characterized by a progressive loss of cognitive functions and behavioural disturbances.[1] This pathology includes symptomatological alterations caused by several factors such as the presence of extracellular *β*-amyloid plaques and neurofibrillary tangles in the brain.[2] Furthermore, it was proved that acetylcholine (ACh) deficit, which is related to the cholinergic hypothesis, it is involved in this pathology.[3] The decrease of ACh levels is directly connected with AD, and the increasing of cognitive functions improved because of the restoring of the cholinergic neurotransmission.[3,4] The enzyme responsible for the hydrolysis of ACh into choline and acetic acid is acetylcholinesterase (AChE). This enzyme is also implicated in the amyloid fibril formation.[5,6] In addition, another cholinesterase (ChE), butyrylcholinesterase (BuChE), is also involved in the cholinergic neurotransmission, but differs from AChE in the kinetics, selectivity and sensitivity to the inhibitors.[7] Unfortunately, the treatment for AD is still inexistent. However, several cholinergic drugs are used for the treatment of non-severe states of AD, such as tacrine [8], galantamine,[9] donepezil,[10] rivastigmine,[11] phenserine and, more recently, ensaculin (figure 1). The last, a coumarin derivative, proved to be helpful to prevent the progressive neurodegeneration. It allowed the increase of ACh levels, helping in the behavioural disturbances and finally, delaying the worsening of symptoms.[12,13] However, one of the major problems caused by the consumption of these drugs is a severe damage at the liver or hepatotoxicity, which leads to find drugs with fewer adverse effects to human health.

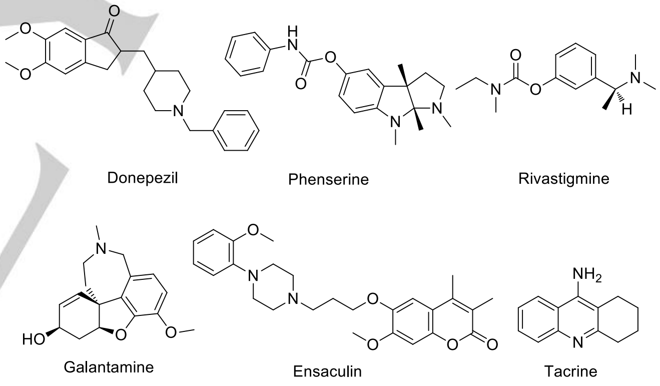

Figure 1. Chemical structures of some AChE inhibitors.

Structurally, AChE and BuChE enzymes have a high degree of similarity, although their biological roles are characteristic for each of them. The X-ray crystallography has revealed the three-dimensional structure for both enzymes, showing in detail their active sites.[14,15] Among the structural aspects of the AChE and BuChE enzymes, there are some important differences, as the residues laying their binding pockets show some key variations. For instance, residues Phe288 and Phe290 in AChE enzyme has been substituted by aliphatic residues, such Leu 286 and Val 288 in BuChE, which allows the access of some bulkier molecules to the catalytic centre.[16,17]

According to that evidence, and the premise of the existence of X-ray crystallography data for both enzymes, many researchers have tried to find selective AChE inhibitors, by synthesizing derivatives with binding moieties strategically placed to efficiently interact with both binding sites.[18–23]

---

[a] Y. Duarte, Dr. M. Gutiérrez.
Laboratory of Organic Synthesis, Institute of Chemistry of Natural Resources.
University of Talca
Mailbox 747, 3460000 Talca, (Chile)
E-mail: yorandre53@utlca.cl
[b] A. Fonseca, Dr. M. J. Matos, Prof. E. Uriarte, Prof. L. Santana
Department of Organic Chemistry, Faculty of Pharmacy
University of Santiago de Compostela
15782 Santiago de Compostela (Spain)
[c] F. Adasme-Carreño, C. Muñoz-Gutierrez, Dr. J. Alzate-Morales
Centre for Bioinformatics and Molecular Simulations (CBSM)
University of Talca
Mailbox 721, 3460000 Talca, (Chile)

In the course of our research, we have synthesized and evaluated series of molecules with very promising activity against some enzymes involved in neurodegenerative diseases.[24–26] Some of the studied coumarins, presenting amide groups at position 3, proved to be potent monoamineoxidase (MAO) and/or AChE inhibitors (Figure 2 – A and B).[26,27]

On the other hand, the quinoline scaffold also proved to display many biological properties, some of them related to neurodegenerative diseases. These molecules proved to act as γ-secretase inhibitors for the treatment of AD, and have also demonstrated to be very good ChE inhibitors (i.e. tacrine – Figure 1 or 2).[20,28–33]

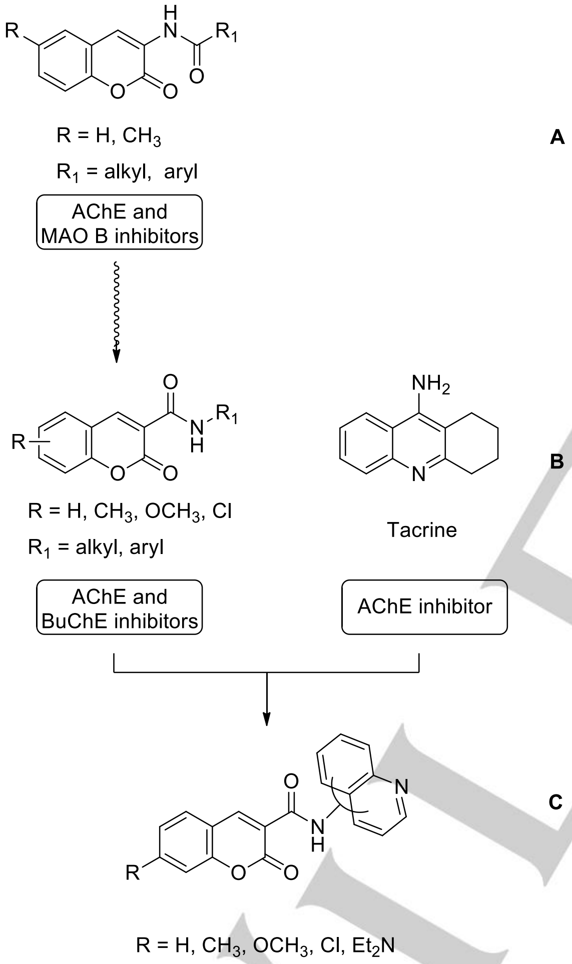
R
H
N
R$_1$
O
O
O
R = H, CH$_3$
R$_1$ = alkyl, aryl
AChE and MAO B inhibitors
A
O
N
R$_1$
H
R
O
O
R = H, CH$_3$, OCH$_3$, Cl
R$_1$ = alkyl, aryl
AChE and BuChE inhibitors
NH$_2$
N
Tacrine
AChE inhibitor
B
O
N
N
H
R
O
O
C
R = H, CH$_3$, OCH$_3$, Cl, Et$_2$N

Figure 2. Chemical structures of some dual MAO/AChE inhibitors (A), some AChE and BuChE inhibitors (B), and chemical strategy for the studied hybrid compounds (C).

Inspired by the aforementioned biological significance of both scaffolds, and in order to find more potent and selective compounds against ChE enzymes, we decided to combine the coumarin and quinoline structures in one single structural skeleton, connected by a carboxamide group (Figure 2 – C).

Therefore, we synthesized a new series of coumarin-quinoline hybrids, taking into account some structural features present in the main AChE inhibitors, such as the coumarin scaffold of ensaculin (Figure 1), our own results, the amine-quinoline fragment of tacrine (Figure 1) and the carboxamide linker of several potent ChE inhibitors. Taking into account previous studies about inhibitory capacity of some heterocyclic compounds against AChE, and also the features of those compounds analogous to our molecules,[26] we proposed the enzymatic evaluation of compounds **5**$_{a-d}$-**9**$_{a-d}$ against AChE and BuChE, with the aim of exploring the importance of the substituent at positions 3 and 7 of the coumarin scaffold, and the joint position of the quinolone. All computational studies were performed based on the reported X-ray data for the binding site of the enzymes and their possible interactions with the new synthesized compounds were predicted by means of molecular docking.

Results and Discussion

Chemistry

The ester derivatives, compounds **1**-**4**, were obtained by a Knoevenagel condensation reaction between different substituted *ortho*-hydroxybenzaldehydes and diethylmalonate, with piperidine as catalyst, in ethanol (Scheme 1 - a). Compound **5** was commercially available. The functionalized coumarins **6**-**9** required for the synthesis of coumarin-quinoline hybrids **6**$_{a-d}$-**9**$_{a-d}$ were synthesized by hydrolysis of the esters **1**-**4**, in NaOH and HCl, leading to the corresponding carboxylic acids **6-9**, respectively (Scheme 1 - b).[34] Coumarin-3-carboxylic acids **5**-**9** reacted with different aminoquinolines (3-aminoquinoline, 5-aminoquinoline, 6-aminoquinoline or 8-aminoquinoline), in anhydrous dichloromethane, 1-ethyl-3-(3-dimethylaminopropyl)carbodiimide hydrochloride (EDC·HCl) and *N*,*N*-dimethylaminopyridine (DMAP) under argon atmosphere, at 0 ºC, to give the desired differently substituted 3-amidocoumarin-quinolines **5**$_{a-d}$-**9**$_{a-d}$, respectively (Scheme 1 - c). All the compounds were obtained in good yields after the purification of the reaction mixture by flash chromatography, using mixtures of hexane/ethyl acetate as eluent. Structural elucidation of all the synthesized compounds was provided performing ^{1}H and ^{13}C NMR, mass spectroscopy, and melting points.

The new synthesized hybrids contain different substituents at position 7 of the coumarin moiety, likewise different amidoquinolines at position 3, in order to attest their relevance to modulate AChE/BuChE biological activities. Some previous studies have been reported regarding the substitution of the coumarin nucleus at position 3 with ethers, esters and amides, but scarce information is available concerning the presence of a quinoline ring in this position (coumarin-quinoline hybrids).[26,35–37]

WILEY-VCH

WILEY-VCH

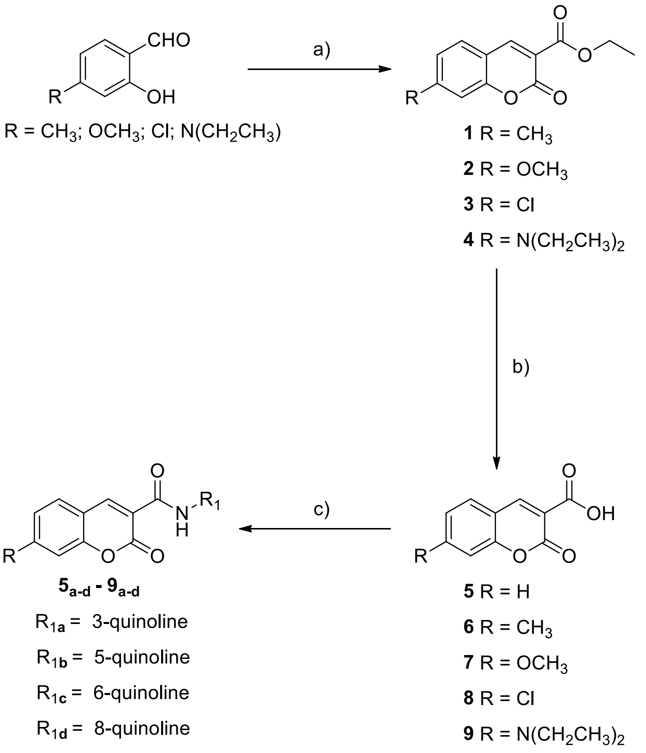

Scheme 1. General synthetic route to obtain compounds 1-9a-d. a) Diethylmalonate, piperidine, EtOH, 78 ºC; b) NaOH, reflux to r.t., HCl; c) Aminoquinoline derivative, EDC, DMAP, DCM, 0 ºC to r.t..

Biological Activities

The inhibitory activities of **5$_{a\text{-}d}$**-**9$_{a\text{-}d}$** were tested against *Electrophorus electricus* AChE and *bovine serum* BuChE, and they were measured using the spectrophotometric method of Ellman[38] with donepezil and galantamine as reference compounds. The biological activity results as IC$_{50}$ values are listed in Table 1.

The data presented in Table 1 shows that some of the new compounds exhibited moderate inhibitory activity against either one or both ChE. The most relevant information obtained from the structure-activity relationships study of these derivatives is related to the activity and selectivity of compounds **7$_a$**, **7$_b$**, **8$_b$** and **9$_c$**. Compound **7$_a$**, which contains a strong electron-donating group (methoxy group) at position 7, proved to be active against both studied enzymes (AChE IC$_{50}$ = 194 µM and BuChE IC$_{50}$ = 255 µM). This was the only dual compound of the entire series. However, compound **7$_b$**, which has the same substitution pattern at position 7 but a different amidoquinolone at position 3, showed to be selective for AChE enzyme (AChE IC$_{50}$ = 181 µM). Compound **8$_b$**, with the same amidoquinolone as compound **7$_b$** at position 3 but with an electron-withdrawing atom (chloride atom) at position 7 of the coumarin scaffold, proved to be the only selective BuChE inhibitor of the entire series (BuChE IC$_{50}$ = 146 µM). A slight tendency could be observed in these results, and this could be important for further studies with these kinds of derivatives.

Compound **9$_c$**, with an electron-donating group (diethylamine group) at position 7 and a 6-quinoline derivative at position 3, turned out to be the most active and selective AChE compound of the entire series. This is interesting because the presence of other electron-donating groups at position 7 (methyl and methoxy groups, compounds **6$_c$** and **7$_c$** respectively) is opposite to this tendency, showing the partial importance of the diethylamine substituents at position 7 for the binding affinity against this ChE.

Table 1. AChE and BuChE inhibitory activity of compounds **5$_{a\text{-}d}$**-**9$_{a\text{-}d}$**.

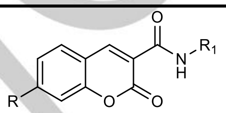

Compound	R	R$_1$	AChE (IC$_{50}$) µM	BuChE (IC$_{50}$) µM
5a	H	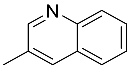 N	324.88 ± 0.01	>500
5b	H	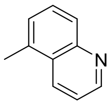 N	>500	>500
5c	H	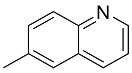 N	237.36 ± 0.02	>500
5d	H	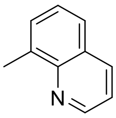 N	269.91 ± 0.03	>500
6a	CH$_3$	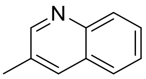 N	>500	>500
6b	CH$_3$	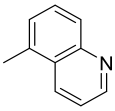 N	422.70 ± 0.16	>500
6c	CH$_3$	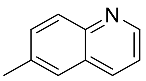 N	>500	>500
6d	CH$_3$	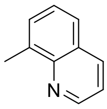 N	324.69 ± 0.05	>500
7a	OCH$_3$	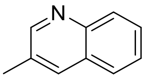 N	194.23 ± 0.04	255.60 ± 0.05

7b	OCH_3	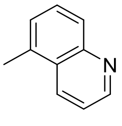	181.72 ± 0.01	>500
7c	OCH_3	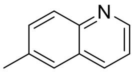	>500	>500
7d	OCH_3	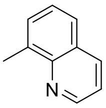	>500	>500
8a	Cl	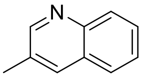	497.55 ± 0.24	>500
8b	Cl	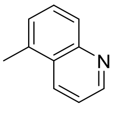	>500	146.74 ± 0.06
8c	Cl	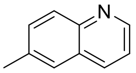	477.66 ± 0.49	>500
8d	Cl	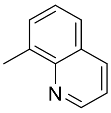	>500	>500
9a	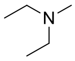	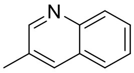	276.14 ± 0.01	>500
9b	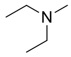	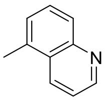	>500	>500
9c	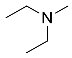	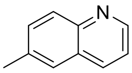	159.53 ± 0.01	>500
9d	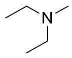	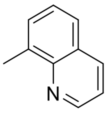	>500	>500
Galantamine	-	-	0.54 ± 0.5	8.80 ± 0.7
Donepezil	-	-	0.04 ± 0.8	0.38 ± 0.5

Each IC_{50} value is the mean ± SEM of three independent measurements. 500 µM was the highest tested concentration. At higher concentrations the compounds precipitated.

Molecular Docking and Binding Affinity Calculations

Regarding the results presented before, and the structural similarity between all molecules, molecular docking calculations against both ChE were carried out to elucidate the molecular basis of this outcome.

Almost all molecules adopted approximately the same position and orientation within the AChE binding site (Figure 3), displaying a good overlap of the coumarin ring that was predicted to stack against the peripheral anionic site (PAS) amino acids, namely Tyr70, Tyr121, Trp279 and Tyr334, which are located at the entry to the active cavity. In particular, it was observed that this moiety established a rather strong π-stacking interaction with Trp279, which it is known to be an anchor point for potent inhibitors, thus being responsible for extra activities.[16] Furthermore, most molecules established hydrogen bonds with either Phe288 or Arg289 main chain, or even both, through the carbonyl group of the coumarin ring. Whereas both residues rarely take part in the binding affinity, it has been reported that Phe288 do establish a hydrogen bond with donepezil-tacrine hybrid derivatives.[19] On the other hand, the head groups at the coumarin ring were completely exposed to the solvent, therefore not establishing interactions with the enzyme that may have contributed positively to the overall binding affinity.

Additionally, several molecules were capable of establishing a hydrogen bond with the side chain of the residue Tyr121, through either the oxygen atom at the linker (3- and 6-substituted quinoline, Figure 3a and 3b) or the nitrogen atom at the quinoline ring (8-substituted quinoline, Figure 3d). In both cases, this hydrogen bond exhibited a very similar geometry indicating that it may not be a decisive factor in the binding affinity. Finally, the quinoline ring was surrounded by aromatic amino acids at the anionic site (known to be responsible for binding the ACh quaternary ammonium group through cation-π interactions), establishing some weak aromatic contacts. Nonetheless, for the 3- and 6-substituted-quinoline ligands, the quinoline ring was capable to be placed in a parallel conformation with respect to Phe330 side chain, thus forming a well-defined π stacking interaction (Figure 3a and 3b). In this regard, it can be noticed that the spatial arrangement of the docking binding poses mainly depended on the relative location of the substitution at the quinoline ring, where 3- and 6-substituted-quinoline derivatives showed a similar orientation, and likewise, the 5- and 8-substituted-quinoline ligands (Figure 3c and 3d) presented an alike positioning within the AChE active site.

It is worthy to note that compound $\mathbf{9_b}$, a close analogue to the most active compound reported in this work ($\mathbf{9_c}$), showed almost no inhibition against AChE with an IC_{50} value higher than 500 µM. This outcome was unexpected since the only difference between those compounds is the substitution at the quinoline ring. While this difference was not observed with other compounds, like 8c and 5c, the latter presented some, but low, activity; hence we explored in more detail the molecular basis of this result. A closer look into the docking binding modes (Figure 4) showed that $\mathbf{9_b}$ lacked some key intermolecular interactions that are established by $\mathbf{9_c}$, which could explain its very low activity. For instance, $\mathbf{9_b}$ was incapable to form a hydrogen bond with either Tyr121 or Phe288 through its amide linker. Resembling the docking poses showed by its counterparts (5-substituted quinoline), the quinoline ring in $\mathbf{9_b}$ was pointing towards the Phe330 backbone rather than its side chain, diminishing or even preventing the formation of an aromatic contact with this residue. Taking all these considerations together, it was possible to infer that a minor change in the relative position of the nitrogen atom with respect to the coumarin ring accounted for the great difference in activity between $\mathbf{9_b}$ and $\mathbf{9_c}$ close analogues, since it modulates the quinoline ring placement relative to the Phe330 residue as stated above.

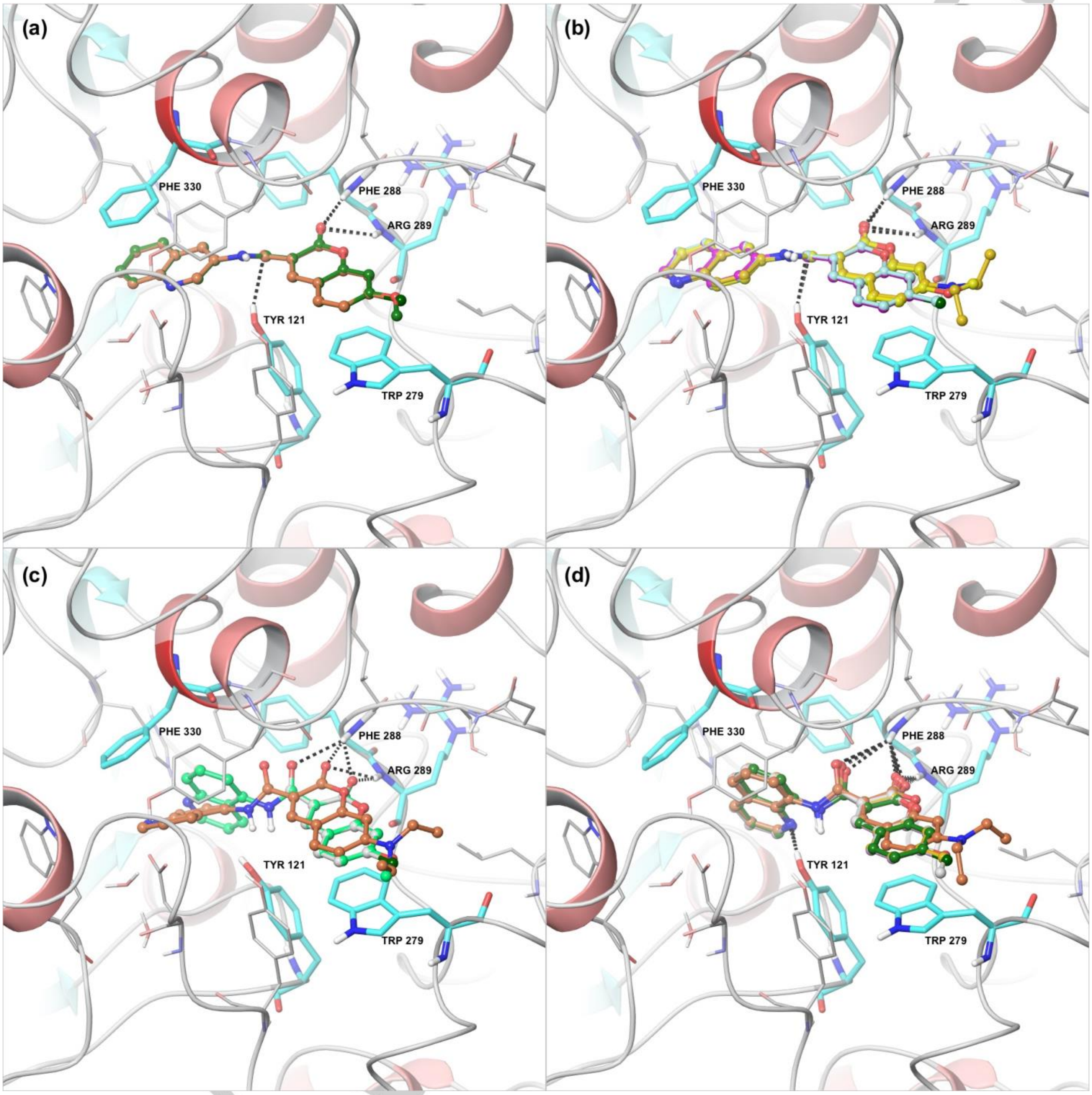
(a)
PHE 330
PHE 288
ARG 289
TYR 121
TRP 279
(b)
PHE 330
PHE 288
ARG 289
TYR 121
TRP 279
(c)
PHE 330
PHE 288
ARG 289
TYR 121
TRP 279
(d)
PHE 330
PHE 288
ARG 289
TYR 121
TRP 279

Figure 3. Predicted docking binding modes of the synthesized compounds within the active site of AChE. Docking poses are grouped by its substitution at the linker: (a) 3-substituted-quinoline, $\mathbf{6_a}$-$\mathbf{7_a}$, (b) 5-substituted-quinoline, $\mathbf{5_b}$-$\mathbf{9_b}$, (c) 6-substituted-quinoline, $\mathbf{5_c}$-$\mathbf{9_c}$, and (d) 8-substituted-quinoline, $\mathbf{5_d}$-$\mathbf{9_d}$. Molecules are displayed in ball & stick representation, where carbon atoms colouring identify each bounded ligand. Amino acids that directly interact with one or more ligands are shown in cyan tube, while side chain of nearby residues are displayed in grey thin tubes. Black dashed lines indicate identified inter-molecular hydrogen bonds.

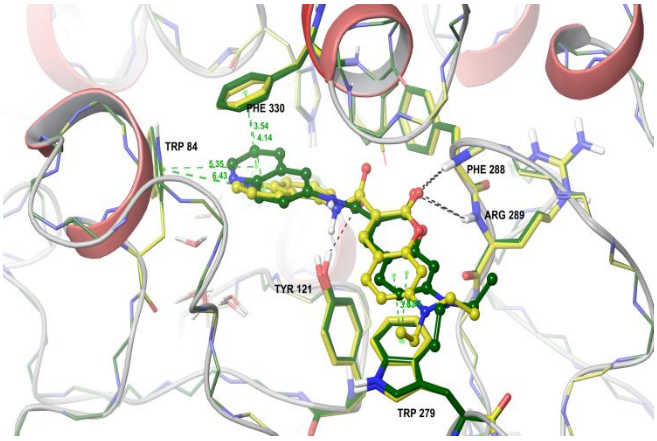

Figure 4. Superimposed and optimized protein-ligand complexes between AChE and compounds $\mathbf{9_b}$ (in yellow) and $\mathbf{9_c}$ (in green). Important amino acids are labelled and highlighted in tube representation, while side chains of nearby residues are displayed in thin tubes. Green dashed lines represent π-stacking contacts (connecting aromatic ring centroids) while black dashed lines indicate identified inter-molecular hydrogen bonds.

In Table 2 are presented the predicted Glide SP score values obtained from molecular docking for compounds $\mathbf{9_c}$ and $\mathbf{9_b}$. E$_{model}$ energy values are roughly in agreement with the measured inhibitory activities: compound $\mathbf{9_c}$ binds more strongly to AChE than compound $\mathbf{9_b}$ (-67.379 and -57.921 kcal mol^{-1}, respectively). The inspection of the Glide SP scoring terms revealed that both energy terms, the vdW interaction energy and the intramolecular hydrogen bond reward, are higher for compound $\mathbf{9_c}$ than $\mathbf{9_b}$, which is in accordance with the stronger interactions established by the quinolinic ring in the active compound.

Table 2. Comparison of experimental biological data *versus* docking binding energy (in kcal/mol) for selected compounds presenting activity against AChE.

Molecules	AChE activity IC50 (µM)	E$_{model}$†	E$_{vdW}$††	E$_{coul}$††	E$_{hbond}$†††
9b	N.A.	-57.921	-41.169	-2.514	-0.060
9c	159.2	-67.379	-44.489	-3.198	-0.256

N.A. – No active against the highest tested concentration (500 µM).
†E$_{model}$ is a specific combination of Docking Score, CvdW (CvdW = Coul + vdW is the non-bonded interaction energy between the ligand and the receptor) and the internal torsional energy of the ligand conformer.
††E$_{vdw}$ and Ecoul are the vdW and electrostatic interaction energies, respectively, between ligand and receptor calculated using Glide SP.
†††E$_{hbond}$ corresponds to the reward of intermolecular hydrogen bonds estimated by Glide SP.

Unlike the AChE case, and with the purpose to explore possible binding modes for the only two active compounds toward BuChE ($\mathbf{7_a}$ and $\mathbf{8_b}$), we docked and studied their molecular behaviour against this enzyme. As same as before, we performed docking calculations with Glide SP, obtaining some minor variations in their binding modes that could explain the slight difference in activity. Both molecules are oriented within the BuChE active site in a similar direction (Figure 5), where the quinolone ring is placed in the vicinity of the anionic site forming π-stacking interactions with Phe329 and Trp231 residues, as well as it is at the proximity of the catalytic triad, namely His438, Ser198 and Glu325 residues. A key difference is that the amide-linker of compound $\mathbf{8_b}$ forms a hydrogen bond with the carbonyl group of Pro285 backbone, while the compound $\mathbf{7_a}$ did not present this kind of interaction; perhaps this hydrogen bond could dictate the slight increase in the biological activity of the former (146.7µM vs. 255.6 µM, respectively). Finally, the coumarin ring and the substituents at this scaffold were directed toward the outside of the enzyme cavity, being completely exposed to the solvent and so they didn't interact with the enzyme.

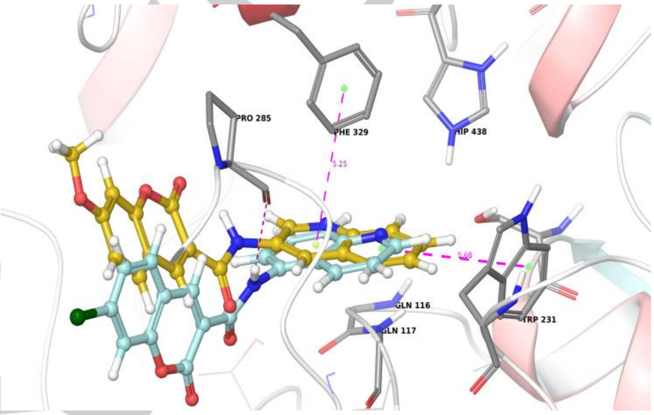

Figure 5. Protein-ligand complexes between BuChE and compounds **7a** (in yellow) and **8b** (in blue). Important amino acids are labelled and highlighted in tube representation, while side chains of nearby residues are displayed in thin tubes. Black dashed lines indicate identified inter-molecular hydrogen bonds.

In turn, the docking energies are more favourable for the most active compound $\mathbf{8_b}$ in about 10 kcal/mol (Table 3), probably due to the additional hydrogen bond established by this molecule. Moreover, the substitution of the coumarin ring with an electron-drawing group such as the chlorine atom in compound $\mathbf{8_b}$ could also lead to an increase of the inhibitory activity of enzyme, in contrast to the electron-donating (methoxy group) presented in compound $\mathbf{7_a}$.

Table 3. Comparison of experimental biological data *versus* docking binding energy (in kcal/mol) for selected compounds presenting activity against BuChE.

Molecules	**AChE activity IC50 (µM)**	**E$_{model}$†**	**E$_{vdW}$††**	**E$_{coul}$††**	**E$_{hbond}$†††**
7a	255.6	-53.609	-39.112	-1.187	-0.00
8b	146.7	-64.999	-42.885	-3.654	-0.181

N.A. – No active against the highest tested concentration (500 µM).
†E$_{model}$ is a specific combination of Docking Score, CvdW (CvdW = Coul + vdW is the non-bonded interaction energy between the ligand and the receptor) and the internal torsional energy of the ligand conformer.
††E$_{vdw}$ and Ecoul are the vdW and electrostatic interaction energies, respectively, between ligand and receptor calculated using Glide SP.
†††E$_{hbond}$ corresponds to the reward of intermolecular hydrogen bonds estimated by Glide SP.

Despite that this molecular docking protocol did not aim to establish an accurate model to estimate binding affinities for the new synthesized series, it permitted us to get a rough estimation of the structural and energetic differences observed in the predicted binding modes for those analysed compounds. In this way, this allowed us to estimate the effect of such a subtle structural differences in a series of newly synthesized coumarin-quinoline analogues and therefore, to establish new synthetic hypothesis in the future.

Theoretical evaluation of ADME properties

The prediction of ADME properties of the coumarin-quinoline hybrids compounds was determined. The lipophilicity (expressed as the octanol/water partition coefficient and herein called logP), number of hydrogen bond donor (n-OHNH) and acceptors (n-OH) and total polar surface area (TPSA) were calculated using the Molinspiration property programme.[39] The predicted data are summarized in Table 4. None of the compounds synthesized break any point of the Lipinski's parameters and these compounds had logP values compatible with those required to cross membranes. From the results, we can conclude that evaluated compounds ($\mathbf{7_a}$, $\mathbf{8_b}$, $\mathbf{9_b}$ and $\mathbf{9_c}$) possess property of drug-likeness.

Table 4. Theoretical ADME properties of the coumarin-quinoline hybrids.

Hybrid compound	Log P	Molecular Weight	TPSA	n-ON acceptors	n-OHNH donors	Volume
7a	3.02	346.34	81.44	6	1	296.76
8b	3.75	350.76	72.20	5	1	284.75
9b	3.92	387.44	75.44	6	1	350.73
9c	3.64	387.44	75.44	6	1	350.73

log P octanol/water partition coefficient; TPSA topological polar surface area; n-ON, number of hydrogen acceptors; n-OHNH, number of hydrogen bond donors. The data was determined with Molinspiration calculation software.

Conclusions

In this study, a series of coumarin-quinoline derivatives were synthesized using an amidation reaction between the coumarin-3-carboxilic acids and the aminoquinolines as key step, obtaining a new series of compounds with good yields. These compounds were evaluated as AChE and BuChE inhibitors, enzymes implicated in AD. In general, the substitution pattern in the seventh position of the coumarin, and the pattern of quinolone ring substitution slightly modulate the activity. Small structural variations allow obtaining inactive compounds, compounds with dual AChE/BuChE activity, as compound $\mathbf{7_a}$, or selective AChE compounds, as compounds $\mathbf{7_b}$ and $\mathbf{9_c}$, or selective BuChE compounds, as compound $\mathbf{8_b}$. In this last case, the difference being the substitution at position 7 of the coumarin (a methoxy group by a chlorine atom, respectively). Moreover, through molecular docking computations, we could analyse the main interactions presented between ligands and AChE/BuChE enzymes. The molecular docking results for compound with better inhibitory AChE potency (compound $\mathbf{9_c}$), indicated a strong and well-defined π-stacking interaction with residue Phe330. Moreover, this compound was capable of forming a hydrogen bond with Tyr121, while the inactive compounds could not establish these above-mentioned interactions. Regarding the BuChE enzyme, the molecular docking results are in good agreement with experimental values for $\mathbf{7_a}$ and $\mathbf{8_b}$ compounds.

Experimental Section

Chemistry

Melting points were measured using a Büchi apparatus and are uncorrected. The purity of compounds was checked by means of analytical TLC (Thin Layer Chromatography) on silica gel plates (Merck 60 F254) and they were purified by column chromatography, when necessary. Chemicals were bought from Aldrich and used without further purification. ^{1}H NMR (300 MHz) and ^{13}C NMR (75MHz) or ^{1}H NMR (400 MHz) and ^{13}C NMR (100 MHz) spectra were recorded in $CDCl_3$ or DMSO-*d*$_6$, with a Bruker AMX or a Bruker AM-400 spectrometers. High-resolution mass spectrometry ESI-MS and ESI-MS/MS analyses were conducted in a high-resolution hybrid quadrupole (Q) and orthogonal time-of-flight (TOF) mass spectrometer (Waters/Micromass Q-TOF micro, Manchester, UK) with a constant nebulizer temperature of 100 °C. The samples were directly infused into the ESI source, via a syringe pump, at flow rates of 5 µL min^{-1}, via the instrument's injection valve.

General procedure for the synthesis of 3-carboxicoumarins 6-9. The suitable salicylaldehyde (1.0 mmol) in ethanol (30 mL) was refluxed under magnetic stirring with diethylmalonate and catalytic amounts of piperidine for 24 h. After cooling to room temperature, the suspension was filtered to give the desired ethyl ester of 3-coumarin carboxylic acid (1-4). Hydrolysis with 10% NaOH (100 mL) and addition of HCl 3 N, for 2-6 h, led to the desired products 6-9.[34]

Ethyl 7-methylcoumarin-3-carboxylate (1): Yield 92%. Mp 101-103 °C. ^{1}H NMR (DMSO-*d*$_6$) δ (ppm): 8.77 (s, 1H, H-4), 7.85 (d, *J* = 7.9 Hz, 1H, H-5), 7.28-7.33 (m, 2H, H-6, H-8), 4.35 (q, *J* = 7.1 Hz, 2H, CH_2), 2.44 (s, 3H, CH_3), 1.36 (t, *J* = 7.1 Hz, 3H, CH_3). ^{13}C NMR (DMSO-*d*$_6$) δ (ppm): 162.8, 154.8, 148.9, 148.0, 146.1, 130.0, 126.1, 116.2, 115.6, 115.5, 61.2, 21.5, 14.1. MS (ESI, *m/z*): 233.41 ([M+H])$^+$, 254.85 ([M+Na])$^+$, 270.00 ([M+K])$^+$.

Ethyl 7-methoxycoumarin-3-carboxylate (2): Yield 94%. Mp 136-138 °C. ^{1}H NMR (DMSO-*d*$_6$) δ (ppm): 8.72 (s, 1H, H-4), 7.84 (d, *J* = 8.5 Hz, 1H, H-5), 7.01 (dd, *J* = 8.5, 2.3 Hz, 2H, H-6, H-8), 4.27 (q, *J* = 7.1 Hz, 2H, CH_2), 3,89 (s, 3H, CH_3), 1.30 (t, *J* = 7.1 Hz, 3H, CH_3). ^{13}C NMR (DMSO-*d*$_6$) δ (ppm): 165.7, 164.9, 162.9, 157.1, 149.4, 131.8, 113.4, 113.3, 111.5, 100.3, 61.0, 56.3, 14.2. MS (ESI, *m/z*): 249.07 ([M+H])$^+$, 271.03 ([M+Na])$^+$.

Ethyl 7-chlorocoumarin-3-carboxylate (3): Yield 97%. Mp 171-172 °C. ^{1}H NMR (DMSO-*d*$_6$) δ (ppm): 8.71 (s, 1H, H-4), 8.05 (d, *J* = 2.4 Hz, 1H, H-8), 7.77 (dd, *J* = 8.9, 2.4 Hz, 1H, H-6), 7.48 (d, *J* = 8.9 Hz, 1H, H-5), 4.31 (q, *J* = 7.1 Hz, 2H, CH_2), 1.31 (t, *J* = 7.1 Hz, 3H, CH_3). ^{13}C NMR (DMSO-*d*$_6$) δ (ppm): 162.5, 155.7, 153.3, 147.6, 134.0, 129.2, 128.6, 119.3, 118.9, 118.3, 61.6, 14.2. MS (ESI, *m/z*): 253.04 ([M+H])$^+$, 275.61 ([M+Na])$^+$, 291.51 ([M+K])$^+$.

Ethyl 7-diethylaminocoumarin-3-carboxylate (4): Yield 98%. Mp 143-145 °C. ^{1}H NMR (CDCl$_3$) δ (ppm): 8.65 (s,1H, H-4), 7.45 (d, *J* = 9.0 Hz, 1H, H-5), 6.71 (dd, *J* = 9.0, 2.2 Hz, 1H, H-6), 6.53 (d, *J* = 2.1 Hz, 1H, H-8), 4.34 (q, *J* = 7.1 Hz, 2H, CH$_2$), 3.53 (q, *J* = 7.1 Hz, 4H, 2(CH$_2$)), 1.31 (t, *J* = 7.1 Hz, 3H, CH$_3$) 1.26 (t, *J* = 7.1 Hz, 6H, 2(CH$_3$)). ^{13}C NMR (CDCl$_3$) δ (ppm): 163.8, 161.9, 158.0, 153.2, 132.8, 130.3, 115.1, 114.2, 101.9, 97.0, 61.2, 45.5, 14.1, 12.9. MS (ESI, *m/z*): 290.12 ([M+H])$^+$, 312.19 ([M+Na])$^+$.

7-Methylcoumarin-3-carboxylic acid (6): Yield 86%. Mp 156-157 °C. ^{1}H NMR (DMSO-*d$_6$*) δ (ppm): 12.80 (s, 1H, COOH), 8.67 (s, 1H, H-4), 7.74 (d, *J* = 7.9 Hz, 1H, H-5), 7.32-7.06 (m, 2H, H-6, H-8), 2.40 (s, 3H, CH$_3$). ^{13}C NMR (DMSO-*d$_6$*) δ (ppm): 164.2, 157.0, 154.8, 148.7, 145.9, 142.0, 130.0, 126.1, 116.3, 115.7, 21.6. MS (ESI, *m/z*): 205.13 ([M+H])$^+$, 227.15 ([M+Na])$^+$.

7-Methoxycoumarin-3-carboxylic acid (7): Yield 90%. Mp 195-196 °C. ^{1}H NMR (DMSO-*d$_6$*) δ (ppm): 12.80 (s, 1H, COOH), 8.70 (s, 1H, H-4), 7.82 (d, *J* = 8.4 Hz, 1H, H-5), 7.02-6.98 (m, 2H, H-6, H-8), 3.90 (s, 3H, CH$_3$). ^{13}C NMR (DMSO-*d$_6$*) δ (ppm): 164.8, 164.3, 157.3, 157.1, 149.2, 131.7, 113.9, 113.4, 111.7, 100.4, 56.4. MS (ESI, *m/z*): 221.43 ([M+H])$^+$, 243.07 ([M+Na])$^+$.

7-Chlorocoumarin-3-carboxylic acid (8): Yield 76%. Mp 265-266 °C. ^{1}H NMR (DMSO-*d$_6$*) δ (ppm): 12.70 (s, 1H, COOH), 8.68 (s, 1H, H-4), 8.03 (d, *J* = 2.4 Hz, 1H, H-8), 7.75 (dd, *J* = 9.2, 2.4 Hz, 1H, H-6), 7.47 (d, *J* = 9.2 Hz, 1H, H-5). ^{13}C NMR (DMSO-*d$_6$*) δ (ppm): 181.6, 172.6, 161.0, 158.8, 146.9, 133.7, 129.1, 121.8, 121.1, 118.3,. MS (ESI, *m/z*): 225.44 ([M+H])$^+$, 247.43 ([M+Na])$^+$.

7-Diethylaminocoumarin-3-carboxylic acid (9): Yield 95%. Mp 224-225 °C. ^{1}H NMR (CDCl$_3$) δ (ppm): 12.35 (s, 1H, COOH), 8.65 (s, 1H, H-4), 7.45 (d, *J* = 9.0 Hz, 1H, H-5), 6.71 (dd, *J* = 9.0, 2.3 Hz, 1H, H-6), 6.53 (d, *J* = 2.1 Hz, 1H, H-8), 3.50 (q, *J* = 7.1 Hz, 4H, 2(CH$_2$)), 1.27 (t, *J* = 7.1 Hz, 6H, 2(CH$_3$)). ^{13}C NMR (CDCl$_3$) δ (ppm): 164.9, 154.5, 150.8, 150.6, 139.9, 132.6, 132.4, 111.7, 111.6, 97.5, 46.1, 13.1. MS (ESI, *m/z*): 262.13 ([M+H])$^+$, 285.16 ([M+Na])$^+$.

General procedure for the synthesis of compounds $5_{a\text{-}d}$-$9_{a\text{-}d}$. The appropriate quinolinoamines were added, dropwise with stirring, into an ice cold suspension of coumarin-3-carboxylic acid (1.0 mmol), 1-ethyl-3-(3-dimethylaminopropyl)carbodiimide hydrochloride (EDC·HCl) (1.1 mmol) and *N,N*-dimethylaminopyridine (DMAP) (1.1 mmol) in dichloromethane (20 mL). The reaction mixture was stirred for 1 h at room temperature, and then the mixture was washed with saturated aqueous NaHCO$_3$ and water. The organic layer was dried over anhydrous Na$_2$SO$_4$ and the solvent was evaporated. The residue was purified by column chromatography on silica gel eluted with hexane/ethyl acetate (9:1). Recrystallization from ethanol gave some derivatives as pale yellow needles in 53-81% yield.

***N*-(Quinolin-3-yl)coumarin-3-carboxamide** (**5_a**): Yield 81%. Mp 281-283 °C. ^{1}H NMR (DMSO-*d$_6$*) δ (ppm): 10.95 (s, 1H, NH), 9.04 (s, 1H), 8.93 (s, 1H), 8.80 (s, 1H), 8.01-7.94 (m, 3H), 7.79-7.50 (m, 5H). ^{13}C NMR (DMSO-*d$_6$*) δ (ppm): 163.4, 159.5, 158.6, 156.4, 155.2, 153.0, 148.0, 144.6, 141.8, 137.2, 136.3, 131.4, 126.5, 122.5, 119.4, 113.6, 108.0, 104.7, 100.7. MS (ESI, *m/z*): 317.27 ([M+H])$^+$, 339.22 ([M+Na])$^+$, 355.18 ([M+K])$^+$.

***N*-(Quinolin-5-yl)coumarin-3-carboxamide** (**5_b**): Yield 76%. Mp 280-283 °C. ^{1}H NMR (CDCl$_3$) δ (ppm): 11.46 (s, 1H, NH), 9.07 (s, 1H, H-4), 8.95-8.90 (m, 1H), 8.48 (d, *J*= 8.3 Hz, 1H), 8.42 (d, *J* = 7.6 Hz, 1H), 7.95 (d, *J* = 8.3 Hz, 1H, H-5), 7.77-7.60 (m, 3H), 7.56-7.42 (m, 3H). ^{13}C NMR (CDCl$_3$) δ (ppm): 161.9, 155.5, 154.4, 150.3, 149.4, 146.4, 134.6, 132.5, 130.0, 129.5, 129.4, 126.8, 125.6, 122.2, 121.1, 119.3, 116.7, 108.5, 106.7. MS (ESI, *m/z*): ([M+H])$^+$, 339.26 ([M+Na])$^+$, 355.15 ([M+K])$^+$.

***N*-(Quinolin-6-yl)coumarin-3-carboxamide** (**5_c**): Yield 68%. Mp 250-251 °C. ^{1}H NMR (CDCl$_3$) δ (ppm): 11.10 (s, 1H, NH), 9.03 (s, 1H, H-4), 8.82 (m, 1H), 8.50 (d, *J* = 2.3 Hz, 1H), 8.15 (d, *J* = 8.5 Hz, 1H, H-5), 8.08 (d, *J* = 9.1 Hz, 1H), 7.80 (dd, *J* = 9.1, 2.4 Hz, 1H), 7.76-7.66 (m, 2H), 7.46-7.35 (m, 3H). ^{13}C NMR (CDCl$_3$) δ (ppm): 160.4, 154.0, 153.9, 149.7, 147.6, 145.2, 136.0, 135.8, 134.5, 130.5, 129.9, 128.4, 125.4, 125.3, 123.8, 122.1, 118.6, 116.4, 116.3. MS (ESI, *m/z*): 317.27 ([M+H])$^+$, 339.22 ([M+Na])$^+$, 355.18 ([M+K])$^+$.

***N*-(Quinolin-8-yl)coumarin-3-carboxamide** (**5_d**): Yield 68%. Mp 275-276 °C. ^{1}H NMR (DMSO-*d$_6$*) δ (ppm): 12.55 (s, 1H, NH), 9.10 (s, 1H, H-4), 8.99-8.96 (m, 1H), 8.91 (d, *J* = 7.6 Hz, 1H), 8.42 (d, *J* = 8.2 Hz, 1H), 8.05 (d, *J* = 7.8 Hz, 1H), 7.82-7.43 (m, 6H). ^{13}C NMR (DMSO-*d$_6$*) δ (ppm): 164.0, 159.8, 156.7, 149.5, 148.9, 136.7, 134.7, 134.6, 130.7, 128.0, 127.2, 126.4, 125.4, 122.9, 122.5, 122.4, 118.8, 117.3, 116.4. MS (ESI, *m/z*): 317.32 ([M+H])$^+$, 339.34 ([M+Na])$^+$, 355.25 ([M+K])$^+$.

7-Methyl-*N*-(quinolin-3-yl)coumarin-3-carboxamide (**6_a**): Yield 74%. Mp 285-287 °C. ^{1}H NMR (DMSO-*d$_6$*) δ (ppm): 10.94 (s, 1H, NH), 9.00 (s, 1H), 8.86 (s, 1H), 8.74 (s, 1H), 7.95-7.00 (m, 7H), 2.35 (s, 3H, CH$_3$). ^{13}C NMR (DMSO-*d$_6$*) δ (ppm): 163.3, 160.2, 160.0, 154.0, 143.5, 141.5, 137.6, 134.1, 130.4, 129.9, 129.1, 128.0, 127.3, 126.1, 125.2, 124.9, 119.3, 110.41, 100.9, 21.9. MS (ESI, *m/z*): 331.43 ([M+H])$^+$, 353.43 ([M+Na])$^+$, 369.41 ([M+K])$^+$.

7-Methyl-*N*-(quinolin-5-yl)coumarin-3-carboxamide (**6_b**): Yield 67%. Mp 293-294 °C. ^{1}H NMR (DMSO-*d$_6$*) δ (ppm): 11.18 (s, 1H, NH), 8.98-8.94 (m, 2H), 8.48-8.43 (m, 1H), 8.25-8.22 (m, 1H), 7.97-7.10 (m, 6H), 2.36 (s, 3H, CH$_3$). ^{13}C NMR (DMSO-*d$_6$*) δ (ppm): 176.7, 165.6, 160.9, 156.0, 154.9, 145.2, 141.9, 140.1, 137.2, 131.6, 128.6, 121.5, 119.8, 117.2, 116.4, 116.0, 111.3, 106.8, 102.2, 24.4. MS (ESI, *m/z*): 331.44 ([M+H])$^+$, 353.43 ([M+Na])$^+$, 369.41 ([M+K])$^+$.

7-Methyl-*N*-(quinolin-6-yl)coumarin-3-carboxamide (**6_c**): Yield 53%. Mp 272-273 °C. ^{1}H NMR (DMSO-*d$_6$*) δ (ppm): 10.91 (s, 1H, NH), 8.89 (s, 1H, H-4), 8.80-8.77 (m, 1H), 8.43 (s, 1H), 8.31 (d, *J* = 8.7 Hz, 1H), 8.02-7.85 (m, 3H), 7.48-7.25 (m, 3H), 2.45 (s, 3H, CH$_3$). ^{13}C NMR (DMSO-*d$_6$*) δ (ppm): 173.5, 168.2, 160.0, 155.5, 153.8, 152.8, 150.7, 149.5, 146.3, 140.0, 136.0, 128.8, 124.0, 123.0, 122.6, 116.4, 107.4, 106.5, 102.6, 21.2. MS (ESI, *m/z*): 331.38 ([M+H])$^+$, 353.41 ([M+Na])$^+$, 369.38 ([M+K])$^+$.

7-Methyl-*N*-(quinolin-8-yl)coumarin-3-carboxamide (**6_d**): Yield 61%. Mp 274-275 °C. ^{1}H NMR (DMSO-*d$_6$*) δ (ppm): 10.94 (s, 1H, NH), 9.06 (s, 1H, H-4), 9.00-8.79 (m, 2H), 8.46-8.31 (m, 2H), 7.98-7.87 (m, 2H), 7.69-7.27 (m, 3H), 2.94 (s, 3H, CH$_3$). ^{13}C NMR (DMSO-*d$_6$*) δ (ppm): 165.6, 161.2, 160.8, 156.1, 147.6, 143.9, 141.2, 138.5, 133.8, 132.7, 132.2, 130.7, 129.4, 128.3, 126.8, 120.0, 118.3, 111.4, 98.8, 20.3. MS (ESI, *m/z*): 331.25 ([M+H])$^+$, 353.23 ([M+Na])$^+$, 369.21 ([M+K])$^+$.

7-Methoxy-*N*-(quinolin-3-yl)coumarin-3-carboxamide (**7_a**): Yield 58%. Mp 287-289 °C. ^{1}H NMR (DMSO-*d$_6$*) δ (ppm): 10.94 (s, 1H, NH), 9.04 (d, *J* = 2.3 Hz, 1H), 8.93 (s, 1H, H-4), 8.82-8.79 (m, 1H), 7.99-7.92 (m, 2H), 7.75-7.48 (m, 2H), 7.23-7.02 (m, 2H), 6.86 (s, 1H, H-8), 3.90 (s, 3H, CH$_3$). ^{13}C NMR (DMSO-*d$_6$*) δ (ppm): 176.3, 171.5, 165.7, 156.8, 156.3, 151.8, 150.7, 150.4, 150.2, 140.3, 139.7, 139.2, 137.3, 134.7, 133.3, 126.5, 126.1, 118.8, 98.5, 63.8. MS (ESI, *m/z*): 347.59 ([M+H])$^+$, 369.54 ([M+Na])$^+$.

7-Methoxy-*N*-(quinolin-5-yl)coumarin-3-carboxamide (**7**$_b$): Yield 67%. Mp 261-262 °C.^{1}H NMR (DMSO-d_6) δ (ppm): 11.22 (s, 1H, NH), 8.99-8.90 (m, 2H), 8.45-8.39 (m, 1H), 8.28-8.22 (m, 1H), 7.95-7.50 (m, 4H), 7.17-7.00 (m, 2H), 3.89 (s, 3H, CH_3). ^{13}C NMR (DMSO-d_6) δ (ppm): 171.3, 164.4, 162.2, 161.1, 158.9, 155.7, 154.8, 154.2, 143.1, 137.8, 133.8, 132.9, 129.8, 129.4, 128.5, 127.0, 115.2, 115.1, 97.6, 59.2. MS (ESI, *m/z*): 347.58 ([M+H])$^+$, 369.54 ([M+Na])$^+$.

7-Methoxy-*N*-(quinolin-6-yl)coumarin-3-carboxamide (**7**$_c$): Yield 57%. Mp 252-253. °C. ^{1}H NMR (DMSO-d_6) δ (ppm): 11.25 (s, 1H, NH), 9.10-8.90 (m, 2H), 8.58-8.25 (m, 3H), 8.06-7.66 (m, 3H), 7.25-7.08 (m, 2H), 3.90 (s, 3H, CH_3). ^{13}C NMR (DMSO-d_6) δ (ppm): 169.8, 162.2, 156.4, 153.0, 146.2, 146.1, 137.4, 129.7, 127.3, 126.6, 126.2, 125.0, 121.5, 121.1, 119.6, 116.8, 114.2, 110.3, 99.0, 63.9. MS (ESI, *m/z*): 347.52 ([M+H])$^+$, 369.51 ([M+Na])$^+$.

7-Methoxy-*N*-(quinolin-8-yl)coumarin-3-carboxamide (**7**$_d$): Yield 65%. Mp 277-279 °C. ^{1}H NMR (DMSO-d_6) δ (ppm): 12.46 (s, 1H, NH), 8.98-8.84 (m, 3H), 8.40-8.35 (m, 1H), 7.95-7.87 (m, 1H), 7.72-7.55 (m, 3H), 7.09-6.95 (m, 2H), 3.88 (s, 3H, CH_3). ^{13}C NMR (DMSO-d_6) δ (ppm): 174.0, 169.4, 165.2, 160.4, 153.0, 151.7, 151.2, 147.4, 136.6, 134.5, 134.2, 132.4, 129.2, 127.2, 120.5, 114.4, 110.5, 100.2, 97.5, 63.7. MS (ESI, *m/z*): 347.55 ([M+H])$^+$, 369.56 ([M+Na])$^+$.

7-Chloro-*N*-(quinolin-3-yl)coumarin-3-carboxamide (**8**$_a$): Yield 73%. Mp 292-294 °C. ^{1}H NMR (DMSO-d_6) δ (ppm): 10.93 (s, 1H, NH), 9.05-9.02 (m, 1H), 8.90-8.75 (m, 2H), 8.20-8.05 (m, 1H), 8.03-7.86 (m, 2H), 7.78 (s, 1H), 7.66-7.48 (m, 3H). ^{13}C NMR (DMSO-d_6) δ (ppm): 177.5, 170.7, 166.0, 158.9, 146.5, 143.9, 139.5, 135.8, 132.2, 131.9, 130.5, 126.1, 119.4, 119.0, 109.4, 104.5, 100.5, 98.3, 97.2. MS (ESI, *m/z*): 351.36 ([M+H])$^+$, 374.54 ([M+Na])$^+$.

7-Chloro-*N*-(quinolin-5-yl)coumarin-3-carboxamide (**8**$_b$): Yield 69%. Mp 245-247 °C. ^{1}H NMR (DMSO-d_6) δ (ppm): 11.09 (m, 1H, NH), 8.96-8.93 (m, 2H), 8.45 (d, *J* = 8.5 Hz, 1H), 8.20-8.17 (m, 2H), 7.91-7.75 (m, 3H), 7.65-7.59 (m, 2H). ^{13}C NMR (DMSO-d_6) δ (ppm): 169.8, 164.2, 158.0, 155.6, 148.8, 146.5, 143.1, 141.1, 136.6, 135.2, 132.0, 123.2, 120.0, 117.5, 117.0, 114.8, 114.2, 108.2, 97.6. MS (ESI, *m/z*): 351.36 ([M+H])$^+$, 374.54 ([M+Na])$^+$.

7-Chloro-*N*-(quinolin-6-yl)coumarin-3-carboxamide (**8**$_c$): Yield 53%. Mp 286-288 °C. ^{1}H NMR (DMSO-d_6) δ (ppm): 10.90 (s, 1H, NH), 8.86-8.74 (m, 2H), 8.49-8.22 (m, 2H), 8.14-7.40 (m, 6H). ^{13}C NMR (DMSO-d_6) δ (ppm): 171.0, 164.8, 160.9, 153.1, 151.7, 149.6, 146.3, 141.0, 136.7, 136.0, 130.1, 129.4, 128.4, 124.0, 122.3, 118.5, 114.4, 100.2, 99.2. MS (ESI, *m/z*): 351.39 ([M+H])$^+$, 373.54 ([M+Na])$^+$.

7-Chloro-*N*-(quinolin-8-yl)coumarin-3-carboxamide (**8**$_d$): Yield 62%. Mp 254-256 °C. ^{1}H NMR (DMSO-d_6) δ (ppm): 12.53 (s, 1H, NH), 9.06 (s, 1H, H-4), 8.96-8.87 (m, 2H), 8.47-8.38 (m, 1H), 8.20 (d, *J* = 1.6 Hz, 1H), 7.81-7-57 (m, 5H). ^{13}C NMR (DMSO-d_6) δ (ppm): 169.4, 163.6, 161.4, 156.7, 155.5, 147.8, 146.6, 142.3, 137.7, 132.5, 130.3, 127.2, 122.7, 119.8, 115.2, 114.0, 106.8, 103.7, 96.3. MS (ESI, *m/z*): 351.39 ([M+H])$^+$, 373.56 ([M+Na])$^+$.

7-(Diethylamino)-*N*-(quinolin-3-yl)coumarin-3-carboxamide (**9**$_a$): Yield 68%. Mp 282-283 °C. ^{1}H NMR ($CDCl_3$) δ (ppm): 11.24 (s, 1H, NH), 8.98 (d, *J* = 1.9 Hz, 1H), 8.93 (s, 1H), 8.83 (s, 1H), 8.08 (d, *J* = 8.6 Hz, 1H), 7.86 (d, *J* = 8.0 Hz, 1H), 7.65 (t, *J* = 7.6 Hz, 1H), 7.60-7.47 (m, 2H), 6.70 (d, *J* = 8.6 Hz, 1H), 6.57 (s, 1H, H-8), 3.49 (q, *J* = 7.1 Hz, 4H, 2(CH_2)), 1.28 (t, *J* = 7.1 Hz, 6H, 2(CH_3)). ^{13}C NMR ($CDCl_3$) δ (ppm): 163.6, 162.3, 161.0, 158.3, 153.5, 149.1, 145.6, 145.3, 132.4, 131.9, 129.5, 128.8, 128.4, 128.2, 127.4, 124.3, 110.8, 110.0, 109.0, 45.6, 12.8. MS (ESI, *m/z*): 388.58 ([M+H])$^+$, 410.58 ([M+Na])$^+$, 426.58 ([M+K])$^+$.

7-(Diethylamino)-*N*-(quinolin-5-yl)coumarin-3-carboxamide (**9**$_b$): Yield 64%. Mp 236-237 °C. ^{1}H NMR ($CDCl_3$) δ (ppm): 11.59 (s, 1H, NH), 8.99-8.94 (m, 1H), 8.88 (s, 1H, H-4), 8.58 (d, *J* = 8.5 Hz, 1H), 8.49 (d, *J* = 7.6 Hz, 1H), 7.95 (d, *J* = 8.5 Hz, 1H, H-5), 7.77 (t, *J* = 8.1 Hz, 1H), 7.55-7.49 (m, 2H), 6.71 (d, *J* = 8.5 Hz, 1H), 6.58 (s, 1H, H-8), 3.50 (q, *J* = 7.1 Hz, 4H, 2(CH_2)), 1.29 (t, *J* = 7.0 Hz, 6H, 2(CH_3)). ^{13}C NMR ($CDCl_3$) δ (ppm): 164.0, 161.9, 158.3, 153.4, 150.6, 149.2, 149.1, 133.9, 131.8, 130.3, 130.0, 126.4, 122.0, 121.4, 119.3, 110.8, 110.4, 109.1, 97.1, 45.6, 12.8. MS (ESI, *m/z*): 388.57 ([M+H])$^+$, 410.58 ([M+Na])$^+$, 426.57 ([M+K])$^+$.

7-(Diethylamino)-*N*-(quinolin-6-yl)coumarin-3-carboxamide (**9**$_c$): Yield 71%. Mp 252-253 °C. ^{1}H NMR ($CDCl_3$) δ (ppm): 11.20 (s, 1H, NH), 8.85 (m, 2H), 8.57 (s, 1H), 8.18 (d, *J* = 9.0 Hz, 1H), 8.10 (d, *J* = 9.0 Hz, 1H), 7.84 (d, *J* = 9.0 Hz, 1H), 7.51 (d, *J* = 9.0 Hz, 1H), 7.42-7.38 (m, 1H), 6.71 (d, *J* = 8.9 Hz, 1H), 6.57 (s, 1H, H-8), 3.50 (q, *J* = 7.1 Hz, 4H, 2(CH_2)), 1.28 (t, *J* = 7.0 Hz, 6H, 2(CH_3)). ^{13}C NMR ($CDCl_3$) δ (ppm): 163.5, 161.9, 158.4, 158.3, 153.4, 149.0, 141.9, 140.1, 136.8, 131.8, 126.8, 124.6, 121.9, 116.8, 110.7, 110.3, 109.0, 102.4, 97.1, 45.6, 12.8. MS (ESI, *m/z*): 388.56 ([M+H])$^+$, 410.52 ([M+Na])$^+$, 426.61 ([M+K])$^+$.

7-(Diethylamino)-*N*-(quinolin-8-yl)coumarin-3-carboxamide (**9**$_d$): Yield 59%. Mp 223-224 °C. ^{1}H NMR ($CDCl_3$) δ (ppm): 12.74 (s, 1H, NH), 9.01-8.93 (m, 2H), 8.82 (s, 1H, H-4), 8.13 (dd, *J* = 8.3, 1.7 Hz, 1H), 7.58-7.40 (m, 4H), 6.64 (dd, *J* = 9.0, 2.5 Hz, 1H, H-6), 6.52 (d, *J* = 2.4 Hz, 1H, H-8), 3.44 (q, *J* = 7.1 Hz, 4H, 2(CH_2)), 1.23 (t, *J* = 7.1 Hz, 6H, 2(CH_3)). ^{13}C NMR ($CDCl_3$) δ (ppm): 162.2, 160.9, 159.3, 148.7, 148.4, 148.2, 136.1, 135.9, 135.5, 131.1, 128.0, 127.1, 121.7, 121.3, 118.3, 117.5, 109.8, 108.5, 96.6, 44.9, 12.3. MS (ESI, *m/z*): 388.59 ([M+H])$^+$, 410.58 ([M+Na])$^+$, 426.58 ([M+K])$^+$.

Pharmacological assays: AChE/BuChE inhibitory assay

This assay was performed in 96-well plates, where 50 µL of sample were dissolved in phosphate buffer (it contain: 8 mM K_2HPO_4, 2.3 mM NaH_2PO_4, 150 mM NaCl, and 0.05% Tween 20 at pH7.6) and a solution of 50 µL of AChE/BuChE (0.25 unit/mL) from *Electroporus electricus* and bovine serum, respectively, in the same phosphate buffer, was added. The assay solutions, without substrate, were incubated with the enzyme for 30 min at room temperature. After incubation, the substrate was added. The substrate solution consisted of Na_2HPO_4 (40 mM), acetylthiocholine/butyrylthiocholine (0.24 mM) and 5,5′-dithio-bis-(2-nitrobenzoic acid) (0.2 mM, DTNB, Ellman's reagent). Absorbance of the yellow anion product, due to the spontaneous hydrolysis of substrate, was measured at 405 nm for 5 min on a Microtiter plate reader (Multiskan EX, Thermo, Vanta, Finland). The AChE/BuChE inhibition was determined for each compound. The enzyme activity was calculated as a percentage compared to a control sample using only the buffer and enzyme solution. The compounds were assayed in the dilution interval of 500 to 15 µg/mL, and the alkaloid galantamine and donepezil were used as the reference compounds. Each assay was run in triplicate and each reaction was repeated at least three independent times. The IC_{50} values were calculated by means of regression analysis.

Docking calculations

All computational calculations were performed using the Schrödinger's Small-Molecule Drug Discovery Suite. Protein and ligand preparation was carried out following the recommended protocol by Schrödinger, which is detailed elsewhere.[40] Briefly, three-dimensional coordinates were generated for all twenty compounds with LigPrep,[41] where ionization/tautomeric states were predicted at physiological pH conditions using Epik,[42] followed by an energy minimization in gas phase using Macromodel[43] with the OPLS_2005 force field.[44]

The crystal structures of AChE and BuChE, complexed with the commercially available inhibitor Donepezil and with benzoic acid (PDB codes 1EVE[45] and 3O9M, respectively), were used for docking experiments. The abovementioned AChE x-ray structure was selected since Donepezil is the most alike AChE ligand to the compounds reported here which has an available structure. The Protein Preparation Wizard[46] of Schrödinger was employed for preparing the protein in order to assign bond orders, add hydrogens, and generate rotamers and protonation states for all amino acids. The hydrogen bonding network was optimized using the 'exhaustive sampling' option at neutral pH in the presence of conserved X-ray waters, which are almost always present at the same position, regardless of the selected X-ray complex structure[16] Finally, the resulting structure was subject to a restrained molecular minimization using the Impref module of impact[47] with a termination criteria of a heavy atom RMSD of 0.18 Å relative to the initial X-ray crystal structure coordinates.

The docking calculations were performed with Glide[48] v6.2 using the Single Precision (SP) mode. Docking grids were generated with the default settings in Glide using the co-crystallized ligand to define the centre of the grid box. Top-ranked poses were then visually clustered to ensure a good overlap of the coumarin ring for the series, thus retaining only the best binding mode for each ligand satisfying this restriction.

Finally, an optimization of the resulting protein-ligand complexes was conducted using the Refinement module in Prime[49] We employed the variable dielectric solvent model VSGB 2.0,[50] which includes empirical corrections for modelling directionality of hydrogen bonding interactions and π stacking interactions, and it has been successfully applied to study protein-ligand complexes,[51] Residues within 5.0 Å of the ligand were allowed to move while minimizing the complex in order to relieve minor steric clashes in the modelled complexes.

Acknowledgements

This research work was partially supported by project FONDECYT Nº 1100481 and PIEI-Quim-Bio, UTALCA. Spanish researchers personal funds and University of Santiago de Compostela. Y.D. thanks a PhD fellowship granted by Universidad de Talca through the Applied Sciences doctoral program. M.J.M. thanks Fundação para a Ciência e Tecnologia for her postdoctoral grant (SFRH/BPD/95345/2013).

Keywords: Coumarin-quinoline hybrids • Synthesis • Biological evaluation • Cholinesterase inhibitors • Molecular docking.

[1] P. T. Francis, A. M. Palmer, M. Snape, G. K. Wilcock, *J. Neurol. Neurosurg. Psychiatry* **1999**, *66*, 137–147.
[2] M. P. Mattson, *Nature* **2004**, *430*, 631–639.
[3] M. Goedert, M. G. Spillantini, *Science* **2006**, *314*, 777–81.
[4] A. Basiri, V. Murugaiyah, H. Osman, R. S. Kumar, Y. Kia, A. Hooda, R. B. Parsons, *Bioorg. Med. Chem.* **2014**, *22*, 906–16.
[5] W. Xie, J. A. Stribley, A. Chatonnet, P. J. Wilder, A. Rizzino, R. D. Mccomb, P. Taylor, S. H. Hinrichs, O. Lockridge, *J. Pharm. Exp. Ther.* **2000**, *293*, 896–902.
[6] N. C. Inestrosa, A. Alvarez, R. D. Moreno, M. Vicente, C. Linker, O. I. Casanueva, C. Soto, J. Garrido, *Neuron* **1996**, *16*, 881–891.
[7] A. Andreani, S. Burnelli, M. Granaiola, M. Guardigli, A. Leoni, A. Locatelli, R. Morigi, M. Rambaldi, M. Rizzoli, L. Varoli, et al., *Eur. J. Med. Chem.* **2008**, *43*, 657–61.
[8] P. P. Davis Kenneth, *Lancet* **1995**, *345*, 625–630.
[9] C. Bartolucci, E. Perola, C. Pilger, G. Fels, D. Lamba, *Proteins* **2001**, *42*, 182–91.
[10] H. Sugimoto, Y. Yamanishi, Y. Iimura, Y. Kawakami, *Curr. Med. Chem.* **2000**, *7*, 303–39.
[11] M. L. Onor, M. Trevisiol, E. Aguglia, *Clin Interv A ging* **2007**, *2*, 17–32.
[12] S. F. Razavi, M. Khoobi, H. Nadri, A. Sakhteman, A. Moradi, S. Emami, A. Foroumadi, A. Shafiee, *Eur. J. Med. Chem.* **2013**, *64*, 252–9.
[13] R. Hoerr, M. Noeldner, *CNS Drug Rev.* **2002**, *8*, 143–58.
[14] Y. Nicolet, O. Lockridge, P. Masson, J. C. Fontecilla-Camps, F. Nachon, *J. Biol. Chem.* **2003**, *278*, 41141–7.
[15] H. Dvir, H. L. Jiang, D. M. Wong, M. Harel, M. Chetrit, X. C. He, G. Y. Jin, G. L. Yu, X. C. Tang, I. Silman, et al., *Biochemistry* **2002**, *41*, 10810–8.
[16] M. Bajda, A. Więckowska, M. Hebda, N. Guzior, C. a Sotriffer, B. Malawska, *Int. J. Mol. Sci.* **2013**, *14*, 5608–32.
[17] F. Leonetti, M. Catto, O. Nicolotti, L. Pisani, A. Cappa, A. Stefanachi, A. Carotti, *Bioorg. Med. Chem.* **2008**, *16*, 7450–6.
[18] M. T. M. Kenna, G. R. Proctor, L. C. Young, A. L. Harvey, *J. Med. Chem.* **1997**, *40*, 3516–3523.
[19] D. Alonso, I. Dorronsoro, L. Rubio, P. Muñoz, E. García-Palomero, M. Del Monte, a Bidon-Chanal, M. Orozco, F. J. Luque, a Castro, et al., *Bioorg. Med. Chem.* **2005**, *13*, 6588–97.
[20] Y. Duarte, M. Gutiérrez, L. Astudillo, J. Alzate-Morales, N. Valdés, *Molecules* **2013**, *18*, 12951–65.
[21] M. I. Fernández-Bachiller, C. Pérez, G. C. González-Muñoz, S. Conde, M. G. López, M. Villarroya, A. G. García, M. I. Rodríguez-Franco, *J. Med. Chem.* **2010**, *53*, 4927–37.
[22] L. Pisani, M. Catto, I. Giangreco, F. Leonetti, O. Nicolotti, A. Stefanachi, S. Cellamare, A. Carotti, *ChemMedChem* **2010**, *5*, 1616–30.
[23] S.-S. Xie, X.-B. Wang, J.-Y. Li, L. Yang, L.-Y. Kong, *Eur. J. Med. Chem.* **2013**, *64*, 540–53.
[24] G. Ferino, S. Vilar, M. J. Matos, E. Uriarte, E. Cadoni, *Curr. Top. Med. Chem.* **2012**, *12*, 2145–62.
[25] M. J. Matos, C. Terán, Y. Pérez-Castillo, E. Uriarte, L. Santana, D. Viña, *J. Med. Chem.* **2011**, *54*, 7127–37.
[26] D. Viña, M. J. Matos, M. Yáñez, L. Santana, E. Uriarte, *Medchemcomm* **2012**, *3*, 213.
[27] M. J. Matos, D. Viña, S. Vazquez-Rodriguez, E. Uriarte, L. Santana, *Curr. Top. Med. Chem.* **2012**, *12*, 2210–39.
[28] A. Marella, O. P. Tanwar, R. Saha, M. R. Ali, S. Srivastava, M. Akhter, M. Shaquiquzzaman, *SAUDI Pharm. J.* **2012**, 1-12.
[29] K.-H. Lam, K. K.-H. Lee, R. Gambari, R. S.-M. Wong, G. Y.-M. Cheng, S.-W. Tong, K.-W. Chan, F.-Y. Lau, P. B.-S. Lai, W.-Y. Wong, et al., *Phytomedicine* **2013**, *20*, 166–71.
[30] M. T. Fodero-Tavoletti, N. Okamura, S. Furumoto, R. S. Mulligan, A. R. Connor, C. a McLean, D. Cao, A. Rigopoulos, G. a Cartwright, G. O'Keefe, et al., *Brain* **2011**, *134*, 1089–100.
[31] N. Okamura, T. Suemoto, S. Furumoto, M. Suzuki, H. Shimadzu, H. Akatsu, T. Yamamoto, H. Fujiwara, M. Nemoto, M. Maruyama, et al., *J. Neurosci.* **2005**, *25*, 10857–62.
[32] V. Sridharan, P. a Suryavanshi, J. C. Menéndez, *Chem. Rev.* **2011**, *111*, 7157–259.

[33] P. Camps, X. Formosa, C. Galdeano, D. Muñoz-Torrero, L. Ramírez, E. Gómez, N. Isambert, R. Lavilla, A. Badia, M. V. Clos, et al., *J. Med. Chem.* **2009**, *52*, 5365–79.

[34] F. Chimenti, B. Bizzarri, A. Bolasco, D. Secci, P. Chimenti, A. Granese, S. Carradori, D. Rivanera, A. Zicari, M. M. Scaltrito, et al., *Bioorg. Med. Chem. Lett.* **2010**, *20*, 4922–6.

[35] M. Alipour, M. Khoobi, A. Foroumadi, H. Nadri, A. Moradi, A. Sakhteman, M. Ghandi, A. Shafiee, *Bioorg. Med. Chem.* **2012**, *20*, 7214–22.

[36] X. Zhou, X. Wang, T. Wang, L. Kong, *Bioorg. Med. Chem.* **2008**, *16*, 8011–8021.

[37] M. Catto, L. Pisani, F. Leonetti, O. Nicolotti, P. Pesce, A. Stefanachi, S. Cellamare, A. Carotti, *Bioorg. Med. Chem.* **2013**, *21*, 146–52.

[38] R. M. F. George L. Ellman, K.Diane Courtney, Valentino Andres jr., *Biochem. Pharmacol.* **1961**, *7*, 88–95.

[39] M Cheminformatics, Bratislava, SlovakRepublic, http://www.molinspiration.com/services/properties.html(accessed Jan 2015).

[40] W. Sastry, G Madhavi · Adzhigirey, Matvey · Day, Tyler ·Annabhimoju, Ramakrishna · Sherman, *J. Comput. Mol. Des.* **2013**, *27*, 221–234.

[41] LigPrep, version 2. 9. Schrödinger, LLC. New York, 2014.

[42] Epik, version 2. 2. Schrödinger, LLC. New York, 2011.

[43] Schrödinger, LLC, version 10. 3. MacroModel, *New York, NY,* **2014**.

[44] A. G. Kaminski and R. A. Friesner, *J. Phys. Chem. B* **2001**, *105*, 6474–6487.

[45] G. Kryger, I. Silman, J. Sussman, *Structure* **1999**, *7*, 297–307.

[46] Schrödinger Suite 2011 Protein Preparation Wizard; Epik version 2.2, Schrödinger, LLC, New York, NY, 2011; Impact version 5.7, Schrödinger, LLC, New York, NY, 2011; Prime version 3.0, Schrödinger, LLC, New York, NY, 2011.

[47] J. L. Banks, H. S. Beard, Y. Cao, A. E. Cho, W. Damm, R. Farid, A. K. Felts, T. a Halgren, D. T. Mainz, J. R. Maple, et al., *J. Comput. Chem.* **2005**, *26*, 1752–80.

[48] Glide, version 6.2, Schrödinger, LLC, New York, 2014.

[49] Prime, version 3.5, Schrödinger, LLC, New York, 2014.

[50] J. Li, R. Abel, K. Zhu, Y. Cao, S. Zhao, R.A. Friesner, *Proteins Struct. Funct. Bioinforma.* **2011**, *79*, 2794–2812.

[51] C. Mulakala, V.N. Viswanadhan, *J. Mol. Graph. Model.* **2013**, *46*, 41–51.

WILEY-VCH

Manuscript III

Insight into the Interactions between Novel Coumarin Derivatives and Human A3 Adenosine Receptors

ChemMedChem, Volume 9, **2014**, Pages 2245-2253

CHEMMEDCHEM
FULL PAPERS

ChemPubSoc Europe

DOI: 10.1002/cmdc.201402205

Insight into the Interactions between Novel Coumarin Derivatives and Human A_3 Adenosine Receptors

Maria João Matos,*[a, b] Santiago Vilar,[a, c] Sonja Kachler,[d] André Fonseca,[a, b] Lourdes Santana,[a] Eugenio Uriarte,[a] Fernanda Borges,[b] Nicholas P. Tatonetti,[c] and Karl-Norbert Klotz[d]

A study focused on the discovery of new chemical entities based on the 3-arylcoumarin scaffold was performed with the aim of finding new adenosine receptor (AR) ligands. Thirteen synthesized compounds were evaluated by radioligand binding (A_1, A_{2A}, and A_3) and adenylyl cyclase activity (A_{2B}) assays in order to study their affinity for the four human AR (hAR) subtypes. Seven of the studied compounds proved to be selective A_3AR ligands, with 3-(4′-methylphenyl)-8-(2-oxopropoxy)coumarin (**12**) being the most potent ($K_i = 634$ nM). None of the compounds showed affinity for the A_{2B} receptor, while four compounds were found to be nonselective AR ligands for the other three subtypes. Docking simulations were carried out to identify the hypothetical binding mode and to rationalize the interaction of these types of coumarin derivatives with the binding site of the three ARs to which binding was observed. The results allowed us to conclude that the 3-arylcoumarin scaffold composes a novel and promising class of A_3AR ligands. ADME properties were also calculated, with the results suggesting that these compounds are promising leads for the identification of new drug candidates.

Introduction

Extracellular adenosine has been shown to be modulator of a vast range of physiological functions through activation of one or more of the four known cell surface receptor subtypes: A_1, A_{2A}, A_{2B}, and A_3.[1] Adenosine receptors (ARs) are included in the family of G protein-coupled receptors (GPCRs) and consist of a single polypeptide chain that transverses the membrane from the extracellular side.[2] Human A_1 and A_3 ARs share the highest sequence identity, being 49% identical.[3] In general, the activation effects of ARs by selective ligands generally have a protective role (i.e., decreasing energy demand and increasing energy supply) in different organs and tissues under a wide variety of physiological conditions. Extracellular adenosine levels substantially rise in response to stress, such as hypoxic stress, and the resultant activation of ARs acts to adapt to the stress.[4]

In particular, A_3AR, the most recently identified AR subtype, was found in human lungs, liver, heart, kidneys, and neutrophils, macrophages, and glial cells.[2,5] Due to the relation of the A_3AR to apoptosis, it was suggested that A_3AR ligands might play an important role in the treatment of diseases in which either cytotoxicity is undesirable (e.g., neurodegeneration) or desirable (e.g., cancer and inflammation). Therefore, progress in the development of A_3AR ligands is significant for the treatment of inflammatory and neurodegenerative diseases, asthma, and the protective effects in cardiac ischemia.[6] In addition, in the heart, both A_1 and A_3ARs ligands appear to protect cardiac myocytes.[7] Therefore, dual activity in both ARs could be an interesting therapeutic strategy.

Of the large number of compounds discovered so far as potent and selective toward ARs,[4] one should mention the xanthine and adenine derivatives that are known as classical AR antagonists. In the search for non-classical AR ligands, novel structures have recently been proposed, namely with quinolinone (Figure 1, structures **I** and **II**)[8] and chromone (structure **III**) scaffolds.[9–11] These compounds are particularly interesting, as they are analogues of another well-known family of heterocyclic compounds, the coumarins.

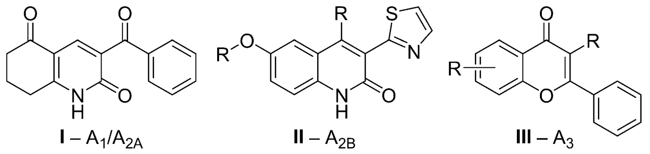

Figure 1. Examples of non-classical AR ligands: quinolinone derivatives **I** and **II** and chromone derivatives **III**.

---

[a] Dr. M. J. Matos, Dr. S. Vilar, A. Fonseca, Prof. L. Santana, Prof. E. Uriarte
Department of Organic Chemistry
Faculty of Pharmacy, University of Santiago de Compostela
Avda. das Ciencias, 15782 Santiago de Compostela (Spain)
E-mail: mariacmatos@gmail.com

[b] Dr. M. J. Matos, A. Fonseca, Prof. F. Borges
CIQUP, Department of Chemistry & Biochemistry
Faculty of Science, University of Porto
Rua do Campo Alegre 687, 4169-007 Porto (Portugal)

[c] Dr. S. Vilar, Dr. N. P. Tatonetti
Department of Biomedical Informatics
Columbia University Medical Center
622 West 168th Street VC5, New York, NY 10032 (USA)

[d] Dr. S. Kachler, Prof. K.-N. Klotz
Institite of Pharmacology & Toxicology
University of Würzburg, Versbacher Str. 9, 97078 Würzburg (Germany)

Coumarins represent an important family of naturally occurring and/or synthetic oxygen-containing heterocycles. A wide range of biological properties has been ascribed to this scaffold, namely as anticoagulant, vasorelaxant, anti-inflammatory, anticancer, antioxidant, antimicrobial, antiviral, and enzymatic inhibitors.[12,15]

In previous studies, our groups found that the coumarin scaffold is also a valid scaffold to develop novel ARs ligands.[16–18] Based on these findings, it seemed relevant to thoroughly explore this fused heterocyclic framework in the design of potent and selective AR ligands. Recent data acquired for the 3-arylcoumarin skeleton[18] encouraged us to perform its decoration and the synthesis of derivatives suitable to improve the understanding of structure–activity relationships (SAR). In the present work, we report the synthesis, pharmacological evaluation, docking, and SAR studies, as well as the theoretical assessment of ADME properties of a series of 3-arylcoumarins (compounds **1**–**13**) that were designed to attain a potent and selective AR ligand and to reinforce the significance of coumarin as a privileged structure in medicinal chemistry programs.

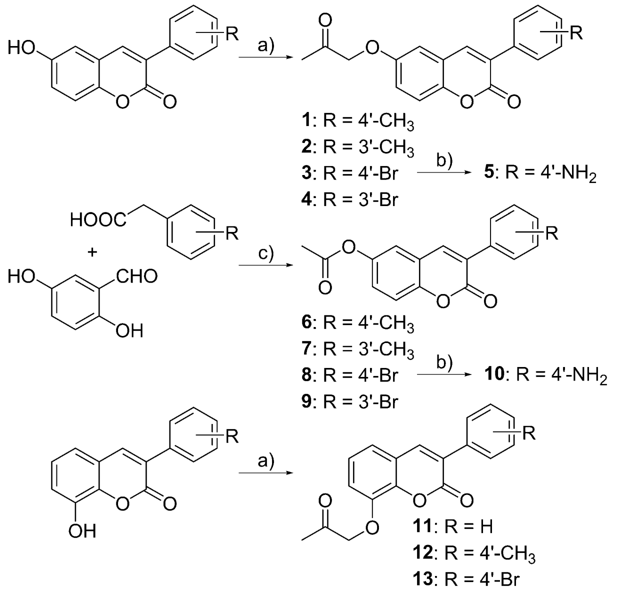

Scheme 1. *Reagents and conditions:* a) chloroacetone, K_2CO_3, acetone, reflux, 16 h; b) 1. CuI, K_2CO_3, molecular sieves, trifluoroacetamide, DMEDA, dioxane, 75 °C, 24 h, 2. $MeOH/H_2O$, RT, 5 h; c) CH_3CO_2K, Ac_2O, reflux, 20 h.

Chemistry

Coumarin derivatives **1**–**13** were efficiently synthesized according to the protocol outlined in Scheme 1. The general reaction conditions and structural characterization of the new compounds were described in the Experimental Section. The Williamson reaction of the 3-aryl-6-hydroxycoumarins or 3-aryl-8-hydroxycoumarins with chloroacetone, under reflux with acetone for 16 h, gave the corresponding ethers **1**–**4** and **11**–**13**, respectively, with good yields.[15,18,19]

Compounds **6**–**9** were obtained starting from the 2,5-dihydroxybenzaldehyde and the corresponding phenylacetic acids using potassium acetate in acetic anhydride, under reflux, for 20 h. Acetylation of the hydroxy groups and pyrone ring closure occurred simultaneously under Perkin–Oglialoro conditions.[20] The CuI/DMEDA (*N*,*N*′-dimethylethylenediamine) catalytic system was used to promote the amination of compounds **3** and **8** with TFA and potassium carbonate in dioxane at 70 °C to give amino derivatives **5** and **10**, respectively.[21]

Pharmacology

In the present work, 3-arylcoumarin ether and ester derivatives decorated with methyl, amino, or bromine substituents located in the 3-aryl ring (compounds **1**–**13**, Figure 1) were synthesized, characterized, and evaluated for their affinity toward ARs (Table 1). Based on the experimental results, we identified interesting SAR.

Theoretical evaluation of ADME-related physicochemical/structural parameters

One of the important requirements for a molecule to be a good drug candidate is the ability to cross membranes. Associated with this characteristic, a molecule must possess the appropriate ADME properties. To better understand the overall properties of the synthesized 3-arylcoumarins, the preliminary data for an ADME profile analysis was calculated using the Mo-

Table 1. Binding affinity values of coumarins **1**–**13** for human A_1, A_{2A}, and A_3 ARs expressed in CHO cells, evaluated by radioligand binding assays.[22–24]

Compd	K_i [μM][a] hA$_1$	hA$_{2A}$	hA$_3$	Selectivity hA$_1$/hA$_3$	hA$_{2A}$/hA$_3$
1	> 30.0	> 30.0	4.68 (3.87–5.66)	> 6.4	> 6.4
2	15.40 (9.93–23.80)	> 30.0	25.50 (27.00–27.10)	0.6	> 1.2
3	> 100.0	> 100.0	> 30.0	–	–
4	> 100.0	> 100.0	> 30.0	–	–
5	17.40 (10.00–30.00)	> 100.0	8.03 (7.00-9.22)	2.2	> 12
6	> 30.0	> 30.0	7.28 (4.13-12.80)	> 4.1	> 4.1
7	> 30.0	> 100.0	14.60 (7.78-27.30)	> 2.0	> 6.8
8	> 100.0	> 100.0	2.78 (1.92–4.01)	> 36	> 36
9	> 30.0	> 100.0	9.40 (9.09-9.72)	> 3.2	> 11
10	6.78 (5.09-9.03)	19.20 (13.90–26.40)	2.46 (2.10–2.88)	2.8	7.8
11	10.40 (9.38–11.60)	16.10 (12.80–20.20)	7.06 (6.18–8.06)	1.5	2.3
12	> 100.0	> 100.0	0.63 (0.41–0.97)	> 159	> 159
13	> 100.0	> 100.0	> 30.0	–	–
theophylline	6.77 (4.07–11.30)	–	86.40 (73.60–101.30)	0.08	> 1.2

[a] Data represent the mean of three independent experiments performed in duplicate; values in parentheses are 95 % confidence intervals.

linspiration property calculation program.[25] Lipophilicity, expressed as the octanol/water partition coefficient (represented as log *P*), was also calculated.[25] The theoretical prediction of ADME properties of all compounds is described by the different parameters detailed in Table 2.[26,27]

Table 2. Calculated structural properties of coumarin derivatives **1**–**13**.[a]

Compd	log *P*[b]	M_r [Da]	TPSA [Å^2][c]	*n*OH[d]	*n*OHNH[d]	*V* [Å^3][e]
1	3.76	308.33	56.52	4	0	277.89
2	3.74	308.33	56.52	4	0	277.89
3	4.12	373.20	56.52	4	0	279.21
4	4.10	373.20	56.52	4	0	279.21
5	2.39	309.32	82.54	5	2	272.62
6	3.71	294.31	56.52	4	0	261.09
7	3.69	294.31	56.52	4	0	261.09
8	4.07	359.18	56.52	4	0	262.41
9	4.05	359.18	56.52	4	0	262.41
10	2.34	295.29	82.54	5	2	255.81
11	3.29	294.31	56.52	4	0	261.33
12	3.74	308.33	56.52	4	0	277.89
13	4.10	373.20	56.52	4	0	279.21

[a] Data were calculated with Molinspiration calculation software.[25] [b] Calculated octanol/water partition coefficient. [c] Topological polar surface area. [e] Number of hydrogen bond acceptors (*n*OH) and donors (*n*OHNH). [f] Molecular volume.

Molecular docking studies

Using the hA_{2A} crystal structure (PDB: 3EML) as a template,[28] homology models were constructed for the hA_1 and hA_3 ARs (see Experimental Section for more details). A set of homology models was selected to test their ability to distinguish between ligands and decoys and between subtype-selective compounds. In the first test, 200 decoys in the ZINC database were randomly selected.[29] The decoys were mixed with 22 known high-affinity compounds for both the hA_1 and hA_3 ARs, extracted from a previous publication.[30] The database was docked against the hA_1 and hA_3 homology models using Glide-SP mode.[31] In this test, 22 hA_1 or 22 hA_3 ligands were deemed true positives (TP), 200 decoys were deemed false positives (FP), and the area under the receiver operating characteristic (ROC) curve was calculated (Table 3). In a similar way as described by Katritch et al.,[30] a second, more exhaustive, test was carried out, docking 22 hA_1-, 22 hA_{2A}-, and 22 hA_3-selective compounds to each model. In the hA_1 system, 22 hA_1-selective compounds were termed TP and 22 $hA_{2A}+22$ hA_3 compounds termed FP. In the hA_3 test, 22 hA_3 compounds were deemed TP and 22 $hA_{2A}+22$ hA_1 FP. Table 3 shows the results extracted from both tests for the best homology models using ROC curves. Similar results were found previously.[30]

Table 3. Area under the receiver operating characteristic (ROC) curve (AUROC) for the best homology models.[a]

	hA_1	hA_3
AUROC test 1	0.91	0.95
AUROC test 2	0.86	0.82

[a] Test 1 differentiates ligands from decoys; test 2 discriminates subtype-selective compounds.

The hA_{2A} crystal structure (3EML) and the best hA_1 and hA_3 homology models were selected to run Glide-SP molecular docking simulations using our newly synthesized compounds. The extracted poses were optimized using Prime MM-GBSA.[32] As reported previously,[10] the calculations showed great variability in the extracted binding modes, particularly in the homology models. The proposed binding modes were selected by considering the number of similar poses extracted from the calculations and geometrical resemblance to co-crystallized compounds in the hA_{2A} AR (Figure 2 a). To calibrate the docking protocol, the RMSD between the calculated and the crystallographic poses of the ligands in 3EML and 3UZC (RMSD values of 0.69 and 1.90, respectively) was measured.[28,33]

The hypothetical binding modes for the compounds in the three ARs oriented the oxygen atoms of the coumarin ring toward residues Asn 254, Asn 253, or Asn 250 in the hA_1, hA_{2A}, or hA_3 ARs, respectively (Asn$^{6.55}$ in Ballesteros-Weinstein superscript numbers). The compounds established hydrogen bond interactions with the amide moiety of the residue (Figure 2). On the other hand, the 3-aryl fragment of the compounds is oriented to the bottom of the protein pocket. This hypothetical binding mode agrees reasonably well with the co-crystallized ligands in the 3EML and 3UZC protein structures (Figure 2 a).[28,34] Previous results also showed the importance of residue Asn$^{6.55}$ in ligand recognition.[10,35]

Compound **10**, with good affinity for hA_1, hA_{2A}, and hA_3 ARs, displayed the described binding mode in all the three ARs (Figure 2 b–d). However, the pose retrieved for the hA_{2A} AR was slightly shifted and did not yield hydrogen bonds with the residue Asn 253. Other compounds in the series showed binding modes in the hA_{2A} AR that interact with residue Asn 253 through hydrogen bonds (data not shown). The 6-acetoxy group seems to play an important role in ligand stabilization through possible hydrogen bonds with different residues in the second extracellular loop (EL2; residues Phe 171, Glu 169, and Gln 167 of hA_1, hA_{2A}, and hA_3 ARs, respectively). On the other hand, the 4′-amino group in the 3-aryl ring may establish hydrogen bonds with residues Ile 80 and Ala 59 in the hA_{2A} AR and with residue Thr 87 in the hA_3AR.

The interaction energy contribution of the different pocket residues in the case of compound **10** (Figure 3) were calculated. To increase the robustness of the analysis, the average contribution, taking into account all of the similar poses extracted from the calculations, is shown. Interaction energies for each residue were calculated as the sum of Coulomb, van der Waals, and hydrogen bonding scores. The results showed a high contribution of residues Phe 168 and Glu 169 in hA_{2A} and corresponding residues in hA_1 and hA_3 in stabilization of the ligand (Figure 3). As was previously described, residue Asn 254 in the hA_1 AR and the corresponding Asn 250 in the hA_3 AR are also important in the interaction with compound **10**. However, as shown in Figure 2, compound **10** in the hA_{2A} AR is shifted away from residue Asn 253, causing a decrease in the energy contribution. Residue Glu 258 in EL3 of the hA_3 AR shows high

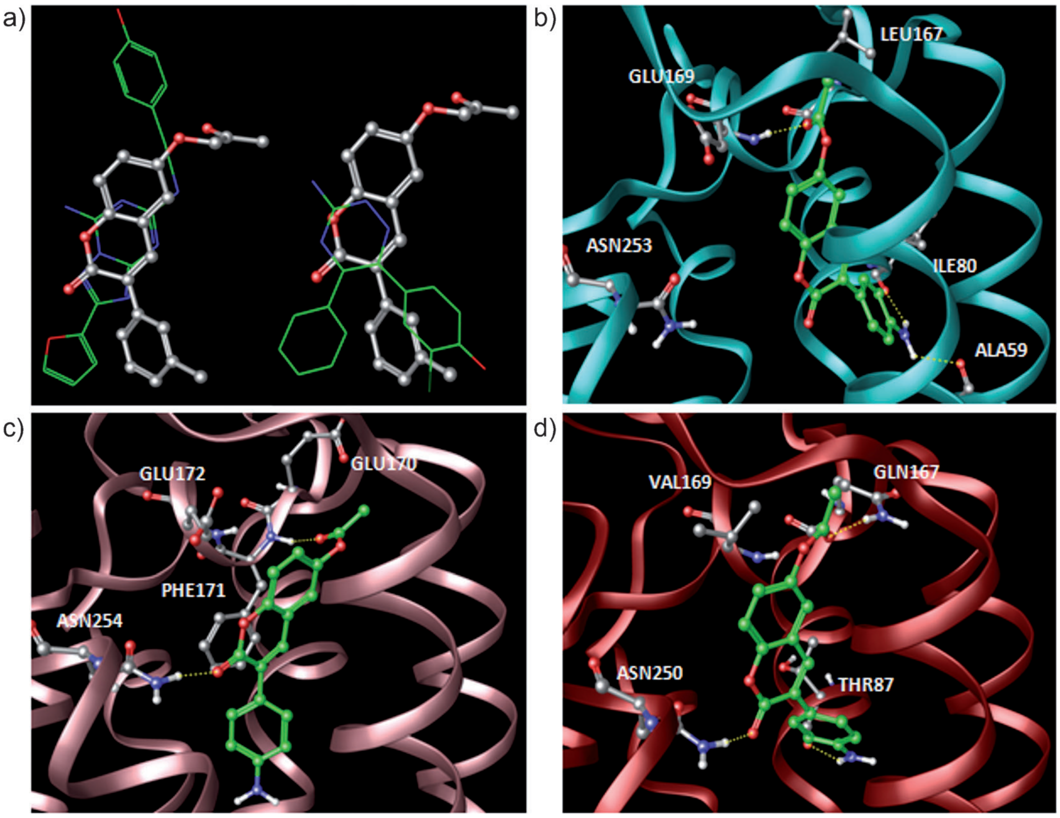

Figure 2. a) Comparison of the binding mode of compound **2** extracted from the $hA_{2A}AR$ docking calculations (grey carbon atoms) with the co-crystallized ligands (green) in the $hA_{2A}AR$ [3EML (left) and 3UZC (right)]. b) Pose calculated with docking for compound **10** inside the $hA_{2A}AR$. c) Hypothetical binding mode for compound **10** in the hA_1AR protein pocket. d) Pose obtained through docking simulations for compound **10** in the hA_3AR. Hydrogen bond interactions are represented in yellow in all panels.

energy contribution. This increased contribution could be due to Coulomb attraction between the negative charge of the side chain carboxylic acid of Glu 258 and the partial positive charge of the carbonyl carbon of the acetoxy group. The nature of the substituent at position 6 of compounds **1**–**10** seems to be important for interaction with the extracellular area of the AR and may modulate selectivity.

According to docking results for compounds **11**–**13**, oxopropoxy substitution at position 8 of the coumarin ring caused a different hypothetical binding mode in the hA_3 AR. Although ligand recognition occurs in the same area of the TM bundle, and compounds **11**–**13** also oriented the oxygen atoms of the coumarin toward residue Asn 250, the 3-aryl ring points toward the upper region of the cavity. Hydrogen bonds between residue Asn 250 and the oxygen atoms in the coumarin ring and the oxopropoxy chain were detected (Figure 4 b and c). This stronger interaction between the ligand and residue Asn 250 in the hA_3 AR is captured in Figure 3 b and could contribute to the highest affinity shown by compound **12**. Another residue with higher contribution to the hA_3 binding affinity could be Met 177, due to an increase in van der Waals interactions with the coumarin rings of the compounds. However, contributions of residues 167–169 are lower in the hA_3 AR, which could indicate that other forces, such as hydrophobic interactions, play a key role in ligand stabilization. The three ARs differ by some residues, with different physicochemical nature in the extracellular area. In fact, the hA_3 AR has some hydrophobic residues, such as Val 169 and Leu 264 (not present in hA_1 and A_{2A}), which could favor hydrophobic interactions with substituents like the 4′-methyl group, present in compound **12**, the most active compound in the series. Previous results also indicated that lipophilicity and steric hindrance contribute to hA_3 selectivity.[18,35] Moreover, this difference in some residues could also influence the entrance of the ligands to the TM region of the ARs. Lenzi et al.[35] showed the presence of hydrophobic residues in the binding access site of the hA_3 AR, whereas in the binding pocket gate of the hA_{2A} AR, there are some ionic residues.[36]

On the other hand, the hypothetical binding mode for compounds **11**–**13** in the hA_1 AR is more similar to the pose previously reported for compounds **1**–**10**. The oxopropoxy group is located in the upper region, whereas the aryl ring is located in the bottom of the pocket in a similar region as the furan ring of the co-crystallized ligand ZM241385 in the 3EML hA_{2A} AR crystal structure (Figure 4 a). In the hA_{2A} crystal structure, docking calculations yielded both conformations in the pocket.

Results and Discussion

All the described coumarins in this report (compounds **1**–**13**) were efficiently synthesized and evaluated for their ability to interact with AR. The corresponding K_i values and selectivity

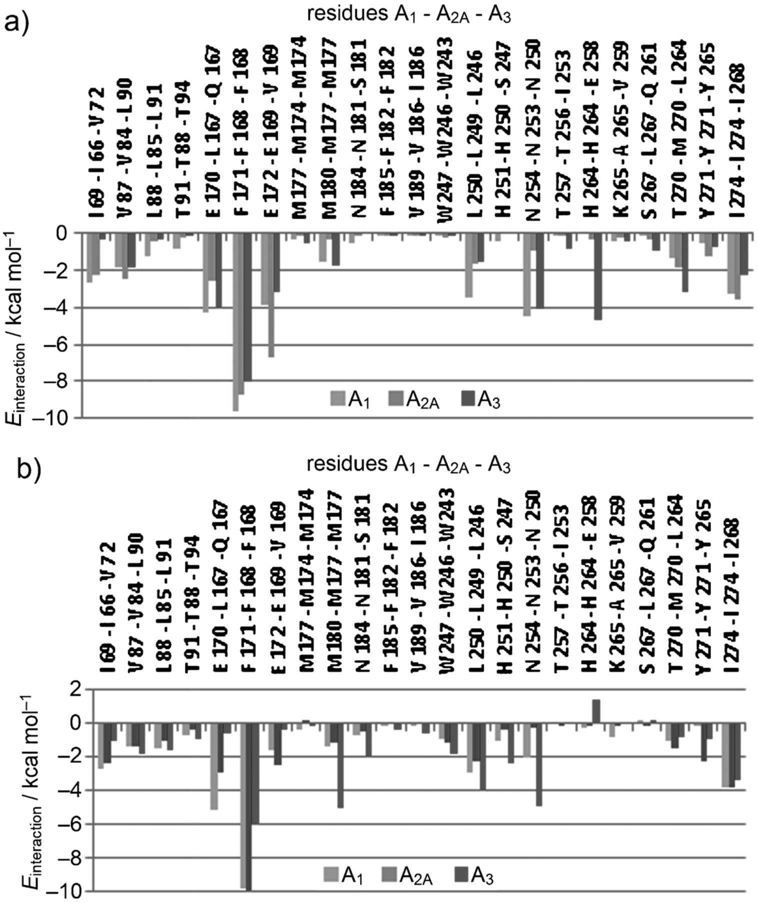

Figure 3. a) Interaction energy between compound **10** and residues in the pockets of hA_1, hA_{2A}, and hA_3 ARs. b) Residue interaction scores for compounds **11**–**13** in the three ARs. Interaction energies for each residue in both panels are represented as the sum of Coulomb, van der Waals, and hydrogen bonding scores.

ratios are shown in Table 1. The chemical structures of the newly designed compounds, as well as the biological and docking results, can help us with an interesting SAR study. A theoretical prediction of the ADME parameters, based on in silico-derived physicochemical descriptors, was carried out, and the results encouraged us to explore the potential of this chemical family as drug candidates.

Firstly, the effect of the presence of ether (compounds **1**–**5**) or ester (compounds **6**–**10**) substituents at position 6 of 3-arylcoumarin scaffold was studied. The selection of this particular aromatic position to be explored was supported by previously published data that correlate the presence of hydrophobic substituents with hA_3AR ligand selectivity.[18] In fact, the present data corroborate the previous assumption as the presence of hydrophobic substituents at position 6 (oxopropoxy or acetoxy groups) enhanced hA_3AR ligand affinity. Docking studies also showed that residues in EL2 can be very important in the ligand recognition and selectivity. The substituents in the 3-aryl exocyclic ring of these compounds displayed different activity profiles. The first series of compounds under study was the group of 6-(2-oxopropoxy) derivatives (compounds **1**–**5**). Compound **1**, with a *p*-methyl group in the 3-aryl ring (4′-CH_3), turned out to be a selective A_3AR ligand with a K_i value of 4.68 μM. Moving the methyl group to the *meta* position (3′-CH_3, compound **2**) led to a loss of selectivity, reducing A_3 affinity by a factor of five (A_3 $K_i = 25.50$ μM) (Table 1). This observation suggests that the position of the methyl substituent is critical for affinity toward A_3AR. Replacing the methyl group (4′- or 3′-CH_3) with a bromine (4′- or 3′-Br), as in compounds **3** and **4**, caused a complete loss of measurable binding affinity. Finally, when the *p*-bromine substituent was replaced by an amino group, the resulting compound **5** exhibited dual A_1A_3 AR affinity (K_i $A_1 = 17.40$ μM and K_i $A_3 = 8.03$ μM; Table 1). From these preliminary results, one can conclude that compound **1**, the *p*-methyl derivative, was the most interesting candidate in the series, with a 6-ether substituent as a potential hA_3AR ligand. The type and position of the substituent on the aromatic exocyclic system of the 3-arylcoumarin scaffold seems to be an important variable to modulate potency and selectivity toward AR.

As was reported previously,[18] electron-withdrawing substituents in the 3-aryl ring, such as nitro groups (or a bromine atom, as in the current study), decrease adenosine activity. Accordingly, compounds **3** and **4** did not show detectable affinity for ARs.

The second series of compounds under study were the 6-acetoxy derivatives (compounds **6**–**10**). These compounds differ from the previous ones by the lack of a methylene bridge on the substituent located at position 6 of the coumarin ring. This slight modification endorsed important changes in their AR activities. The *para* and *meta* methyl and bromine derivatives (compounds **6**–**9**) proved to be A_3AR-selective ligands (Table 1). The best compound of the series was compound **8**, with a *p*-bromine substituent on the aromatic exocyclic ring ($K_i = 2.78$ μM). Transformation of the *p*-bromine into a *p*-amino derivative (compound **10**) was accompanied by an improvement of the affinity for all three receptor subtypes. Compound **10** presents as a nonselective ligand with affinity toward A_1 ($K_i = 6.78$ μM), A_{2A} ($K_i = 19.20$ μM) and A_3 ($K_i = 2.46$ μM) ARs (Table 1).

The introduction of polar substituents in the 3-aryl exocyclic ring, such as the amino group, seems to assist the interaction with all receptor subtypes. In fact, compound **10**, with an amino substituent in the aryl ring, displayed activity toward A_1 and A_{2A} ARs, whereas the derivatives with methyl and bromine substituents do not bind to these subtypes. This can be explained, for instance, by the presence of some water molecules at the bottom of the pocket in the hA_{2A} AR crystal structure (3EML) that can stabilize the interaction of the ligands with the receptor. In fact, the aryl exocyclic ring of the studied derivatives is oriented toward this area. Polar substituents in the 3-aryl ring probably are better accommodated in the pocket, rather than hydrophobic or electron-withdrawing substituents such as halogens. Moreover, position and displacement of water molecules inside ARs could play an important thermodynamic role that could help to explain the SAR obtained thus far.

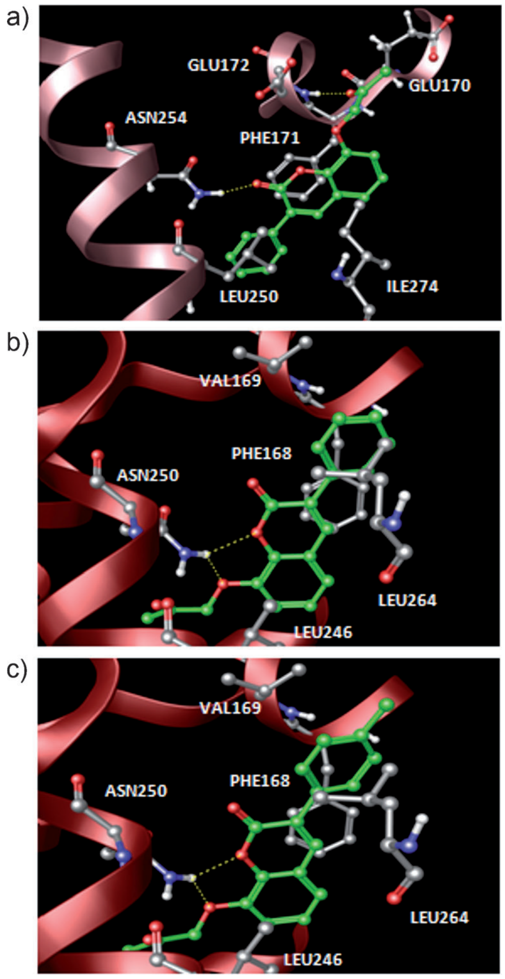

Figure 4. a) Hypothetical binding mode of compound **11** (green carbon atoms) in the hA_1AR. The compound establishes hydrogen bonds with Glu 172 and Asn 254 (yellow). b) Pose calculated with docking for compound **11** inside the hA_3AR. Hydrogen bonds are represented in yellow. c) Hypothetical binding mode for compound **12** in the hA_3 protein pocket.

Compounds **1** and **5**–**12** present better hA_3 affinity than theophylline, which was used as a reference compound. In addition, compounds **1**, **6**–**9**, and **12** are hA_3-selective ligands, with compound **12** being 137-fold more active against hA_3 than the reference compound. Regarding hA_1 AR affinity, compounds **2**, **5**, **10**, **11**, and **13** presented similar K_i values to theophylline.

Finally, a series presenting an ether substituent at position 8 of the 3-arylcoumarin scaffold was also synthesized and explored (compounds **11**–**13**). Compound **11**, having a non-substituted 3-aryl ring, proved to be nonselective, with affinity for A_1 (K_i = 10.40 μM), A_{2A} (K_i = 16.10 μM) and A_3 (K_i = 7.06 μM) ARs (Table 1). Compound **13**, the *p*-bromine derivative, did not bind to any of the ARs. On the other hand, compound **12**, the *p*-methyl derivative, was the best compound of the entire series. This derivative presented an interesting profile, with a K_i value of 0.634 μM at the A_3AR and no affinity for the other AR subtypes. This compound will be a valuable lead for further SAR studies. Docking studies reveal a different binding mode for compounds **11**–**13** to the hA_3AR, allowing us to conclude that residue Asn 250 could be an important determinant for hA_3AR recognition by this type of derivatives. Moreover, in the case of compound **12**, the hydrophobic substituent in the 3-aryl exocyclic ring can interact with hydrophobic residues like Val 169 and Leu 264 (not present in the hA_{2A} and hA_1 ARs) and favor affinity and selectivity toward hA_3AR.

Finally, the obtained theoretical ADME results (Table 2) show that no violations of Lipinski's rule (molecular weight, log *P*, number of hydrogen donors and acceptors) were found for the described 3-arylcoumarins. Therefore, the most potent and selective compounds have the desired properties to be good leads for novel drug candidates.

Conclusions

Evidence was acquired in this study to demonstrate that 3-arylcoumarin is a valid scaffold for the design of novel A_3-selective or A_1A_3 dual AR ligands. In particular, compounds **1**, **6**–**9**, and **12** were the coumarins presenting the best affinities and selectivity for A_3AR, with compound **12** being the most promising of the whole series. Docking experiments clarified some of the interactions of this compound with the receptors. Hydrogen bonds between the residue Asn 250 and the oxygen atoms in the coumarin ring and the oxopropoxy chain at position 8 were detected. This stronger interaction between the ligand and residue Asn 250 in the hA_3AR could contribute to the highest affinity shown by compound **12**. Compound **5** can be considered a promising A_1A_3 dual AR ligand. The results obtained so far point out an important role of the presence of a methyl group in *para* position of the 3-aryl exocyclic ring (compounds **1**, **6**, and **12**). The affinity could be improved by the presence of a substituent at position 8 of the 3-arylcoumarin scaffold. These two inferences can serve as the base for the lead optimization step and will be the basis for future studies. Active but nonselective compounds like **10** and **11** may aid in learning more about the common structural determinants of the binding pockets of the AR subtypes. Analyzing the theoretical ADME properties, these compounds could be considered promising leads that, after optimization, could afford new drug candidates. Finally, progress in the development of A_3AR ligands is significant for the treatment of inflammatory and neurodegenerative diseases. As the 3-arylcoumarins have already proven to be very good inhibitors of some enzymes involved in these pathologies, the proposed approach supports the concept of multi-target recognition. These could be promising results for further studies.

Experimental Section

Chemistry

General methods: Starting materials and reagents were obtained from Sigma–Aldrich and were used without further purification. Melting points (mp) are uncorrected and were determined with a Reichert Kofler thermopan or in capillary tubes in a Büchi 510 apparatus. ^1H NMR (300 MHz) and ^{13}C NMR (75.4 MHz) spectra were recorder with a Bruker AMX spectrometer using $CDCl_3$ as solvent. Chemical shifts (δ) are expressed in parts per million (ppm) using TMS as an internal standard. Coupling constants (*J*) are expressed in hertz (Hz). Spin multiplicities are given as s (singlet), d (doublet), dd (doublet of doublets), and m (multiplet). Mass spectrometry was carried out with a Hewlett–Packard 5988A spectrometer. Elemental analyses were performed using a PerkinElmer 240B microanalyzer and were within ±0.4% of calculated values in all cases. The analytical results are ≥98% purity for all compounds. Flash chromatography (FC) was performed on silica gel (Merck 60, 230–400 mesh); analytical TLC was performed on precoated silica gel plates (Merck 60 F254). Organic solutions were dried over anhydrous sodium sulfate. Concentration and evaporation of the solvent after reaction or extraction was carried out on a rotary evaporator (Büchi Rotavapor) operating under reduced pressure.

General procedure for the preparation of 3-aryl-6-(2-oxopropoxy)coumarins (1–4): The chloroketone (0.25 mmol) was added to a suspension of anhydrous K_2CO_3 (0.25 mmol) and the corresponding 3-aryl-6-hydroxycoumarin (0.13 mmol) in anhydrous acetone (3 mL). The suspension was held at reflux for 16 h. The mixture was cooled, and the precipitate was recovered by filtration and washed with anhydrous acetone (3×40 mL). The dry residue was purified by FC (hexane/EtOAc, 85:15), to afford the desired compound.

3-(4′-Methylphenyl)-6-(2-oxopropoxy)coumarin (1): White solid (70 mg, yield: 74%): mp: 128–129 °C.[15]

3-(3′-Methylphenyl)-6-(2-oxopropoxy)coumarin (2): White solid (50 mg, yield: 79%): mp: 138–139 °C; ^{1}H NMR (300 MHz; $CDCl_3$): $\delta = 2.38$ (s, 3H, CH_3), 2.49 (s, 3H, CH_3), 4.69 (s, 2H, CH_2), 7.02 (d, 1H, $J = 2.9$, H-5), 7.20 (dd, 1H, $J = 9.0$, $J = 2.9$, H-4′), 7.29–7.45 (m, 3H, H-2′, H-3′, H-7), 7.55 (s, 1H, H-6), 7.58 (s, 1H, H-8), 7.80 ppm (s, 1H, H-4); ^{13}C NMR (75 MHz; $CDCl_3$): $\delta = 21.5$, 26.6, 73.5, 111.0, 117.8, 119.4, 120.2, 125.6, 128.4, 129.2, 129.8, 134.5, 138.1, 139.2, 148.5, 154.2, 160.5, 204.7 ppm; DEPT (75 MHz; $CDCl_3$): $\delta = 21.5$, 26.6, 73.5, 111.0, 117.8, 119.4, 125.7, 128.4, 129.2, 129.8, 139.2 ppm; MS (EI, 70 eV): m/z (%): 309 (14) $[M+H]^+$, 308 (85) $[M]^+$, 294 (33), 265 (10), 252 (25), 224 (33), 207 (11), 165 (11), 152 (15); Anal. calcd for $C_{19}H_{16}O_4$: C 74.01, H 5.23; found: C 73.98, H 5.20.

3-(4′-Bromophenyl)-6-(2-oxopropoxy)coumarin (3): White solid (80 mg, yield: 81%): mp: 157–158 °C.[19]

3-(3′-Bromophenyl)-6-(2-oxopropoxy)coumarin (4): White solid (80 mg, yield: 83%): mp: 167–168 °C.[19]

General procedure for the synthesis of 6-acetoxy-3-arylcoumarins (6–9): Compounds **6**–**9** were synthesized under anhydrous conditions, using material previously dried at 60 °C for at least 12 h and at 300 °C during the few minutes immediately prior to use. A solution containing anhydrous CH_3CO_2K (2.94 mmol), the phenylacetic acid derivative (1.67 mmol), and the 2,5-dihydroxybenzaldehyde (1.67 mmol) in Ac_2O (1.2 mL) was held at reflux for 20 h. The reaction mixture was cooled, neutralized with 10% aqueous $NaHCO_3$, and extracted (3×30 mL) with EtOAc. The organic layers were combined, washed with distilled water, dried (anhydrous Na_2SO_4), and evaporated under reduced pressure. The product was purified by recrystallization in EtOH and dried to afford the desired compound.

6-Acetoxy-3-(4′-methylphenyl)coumarin (6): White solid (300 mg, yield: 61%): mp: 146–147 °C.[18]

6-Acetoxy-3-(3′-methylphenyl)coumarin (7): White solid (450 mg, yield: 75%): mp: 124–125 °C; ^{1}H NMR (300 MHz; $CDCl_3$): $\delta = 2.35$ (s, 3H, CH_3), 2.43 (s, 3H, CH_3), 7.11–7.13 (m, 1H, H-4′), 7.25 (dd, 2H, $J = 8.8$, $J = 2.6$, H-5, H7), 7.31 (d, 2H, $J = 2.7$, H-5′, H-6′), 7.37 (d, 1H, $J = 8.9$, H-8), 7.49 (d, 2H, $J = 8.0$, H-2′, H-5′), 7.74 ppm (s, 1H, H-4); ^{13}C NMR (75 MHz; $CDCl_3$): $\delta = 21.0$, 40.9, 117.3, 119.9, 124.7, 125.6, 126.2, 128.3, 129.0, 129.7, 130.0, 134.2, 138.0, 138.9, 146.6, 150.8, 160.2, 169.2 ppm; DEPT (75 MHz; $CDCl_3$): $\delta = 21.0$, 40.9, 117.3, 119.9, 124.7, 125.6, 128.3, 129.7, 130.0, 138.9 ppm; MS (EI, 70 eV): m/z (%): 295 (13) $[M+H]^+$, 294 (76) $[M]^+$, 253 (13), 252 (55), 224 (41), 165 (13), 152 (15); Anal. calcd for $C_{18}H_{14}O_4$: C 73.46, H 4.79; found: C 73.44, H 4.76.

6-Acetoxy-3-(4′-bromophenyl)coumarin (8): White solid (440 mg, yield: 82%): mp: 181–182 °C; ^{1}H NMR (300 MHz; $CDCl_3$): $\delta = 2.34$ (s, 3H, CH_3), 7.25–7.39 (m, 3H, H-2′, H-6′, H-7), 7.50–7.60 (m, 4H, H-3′, H-5′, H-5, H-8), 7.76 ppm (s, 1H, H-4); ^{13}C NMR (75 MHz; $CDCl_3$): $\delta =$ 21.1, 117.5, 119.8, 120.1, 123.5, 125.2, 126.7, 130.1, 131.7, 133.2, 139.1, 146.8, 151.0, 159.9, 169.3 ppm; DEPT (75 MHz; $CDCl_3$): $\delta =$ 21.1, 117.5, 120.1, 125.2, 130.1, 131.7, 139.1 ppm; MS (EI, 70 eV): m/z (%): 361 (9), 360 (18), 359 (10) $[M+H]^+$, 358 (23) $[M]^+$, 317 (100), 289 (53), 288 (49), 181 (20), 152 (60), 138 (12), 126 (23); Anal. calcd for $C_{17}H_{11}BrO_4$: C 56.85, H 3.09; found: C 56.88, H 3.10.

6-Acetoxy-3-(3′-bromophenyl)coumarin (9): White solid (200 mg, yield: 84%): mp: 104–105 °C; ^{1}H NMR (300 MHz; $CDCl_3$): $\delta = 2.33$ (s, 3H, CH_3), 7.21–7.37 (m, 4H, H-5′, H-6′, H-5, H-7), 7.52 (d, 1H, $J = 8.1$, H-8), 7.63 (dt, 1H, $J = 8.8$, $J = 1.7$, H-4′), 7.74 (s, 1H, H-4), 7.82 ppm (t, 1H, $J = 1.8$, H-2′); ^{13}C NMR (75 MHz; $CDCl_3$): $\delta = 21.1$, 117.5, 119.8, 120.3, 122.5, 125.4, 127.3, 127.5, 130.0, 131.4, 132.0, 136.4, 139.8, 146.8, 151.0, 159.8, 169.3 ppm; DEPT (75 MHz; $CDCl_3$): $\delta = 21.1$, 117.5, 120.3, 125.4, 127.3, 130.0, 131.4, 132.0, 139.8 ppm; MS (EI, 70 eV): m/z (%): 361 (10), 360 (20), 359 (10) $[M+H]^+$, 358 (21) $[M]^+$, 318 (30), 317 (11), 316 (33), 290 (23), 288 (24), 181 (10), 152 (100), 151 (58), 150 (22); Anal. calcd for $C_{17}H_{11}BrO_4$: C 56.85, H 3.09; found: C 56.83, H 3.06.

General procedure for the preparation of 3-aminophenylcoumarins (5 and 10): A catalytic amount of CuI (5 mol%), K_2CO_3 (2.0 mmol), and molecular sieves (4 AMS, 0.500 g) were added to a dry 20 mL two-neck round-bottom flask. The two-neck round-bottom flask was evacuated and back-filled with argon. Then compounds **3** or **8** (1.0 mmol), 2,2,2-trifluoroacetamide (1.5 mmol), DMEDA (10 mol%), and dioxane (2 mL) were added, and the mixture was stirred for 24 h at 75 °C. The mixture was then cooled to room temperature, and a mixture of MeOH/H_2O, 1:1 (6 mL total) was added. The suspension was stirred for 5 h and then extracted with EtOAc (3×20 mL). The residue obtained after evaporation of the solvent was purified by column chromatography (hexane/EtOAc, 9:1) to give the desired 3-aminophenylcoumarin (**5** or **10**).

3-(4′-Aminophenyl)-6-(2-oxopropoxy)coumarin (5): White solid (44 mg, yield: 90%): mp: 99–100 °C; ^{1}H NMR (300 MHz; $CDCl_3$): $\delta =$ 2.31 (s, 3H, CH_3), 3.49 (s, 2H, CH_2), 4.60 (s, 2H, NH_2), 6.95 (d, 1H, $J = 2.9$, H-5), 7.12–7.17 (m, 1H, H-7), 7.30 (t, 2H, $J = 9.4$, H-3′, H-5′), 7.58 (s, 3H, H-2′, H-6′, H-8), 7.75 ppm (s, 1H, H-4); ^{13}C NMR (75 MHz; $CDCl_3$): $\delta = 27.6$, 80.1, 111.8, 115.0, 118.1, 118.4, 122.7, 125.5, 128.3, 132.1, 145.4, 150.0, 153.9, 158.2, 163.1, 203.2 ppm.; DEPT (75 MHz; $CDCl_3$): $\delta = 27.6$, 80.1, 111.8, 115.0, 118.1, 118.4, 132.1, 145.4 ppm; MS (EI, 70 eV): m/z (%): 310 (23) $[M+H]^+$, 309 (100) $[M]^+$, 214 (16), 170 (51), 126 (22), 98 (17), 91 (13), 89 (18), 83 (32), 71 (15), 69 (13), 56 (26); Anal. calcd for $C_{18}H_{15}O_4$: C 69.89, H 4.89; found: C 69.91, H 4.92.

6-Acetoxy-3-(4′-aminophenyl)coumarin (10): White solid (51 mg, yield: 69%): mp: 206–207 °C; ^{1}H NMR (300 MHz; $CDCl_3$): $\delta = 2.43$ (s, 3H, CH_3), 3.99 (s, 2H, NH_2), 7.09–7.12 (m, 1H, H-3′), 7.28–7.33 (m, 2H, H-4′, H-5′), 7.35–7.81 (m, 2H, H-7, H-8), 7.57–7.60 (m, 1H, H-6′), 7.65–7.69 (m, 1H, H-5), 7.80 ppm (s, 1H, H-4); ^{13}C NMR (75 MHz; $CDCl_3$): $\delta = 25.1$, 113.4, 116.4, 119.4, 124.5, 127.4, 127.9, 130.1, 131.4, 131.6, 132.9, 133.1, 134.1, 140.0, 142.6, 147.0 ppm; DEPT (75 MHz;

$CDCl_3$): $\delta = 25.1$, 119.4, 124.5, 127.4, 130.1, 131.6, 133.1, 140.0, 142.6 ppm; MS (EI, 70 eV): m/z (%): 252 (20) $[M+H]^+$, 251 (89) $[M]^+$, 236 (29), 235 (80), 178 (23), 152 (33), 76 (13); Anal. calcd for $C_{16}H_{13}NO_2$: C 76.48, H 5.21; found: C 76.46, H 5.18.

General procedure for the preparation of 3-aryl-8-(2-oxopropoxy)coumarins (11–13): The chloroketone (0.25 mmol) was added to a suspension of anhydrous K_2CO_3 (0.25 mmol) and the corresponding 3-aryl-8-hydroxycoumarin (0.13 mmol) in anhydrous acetone (3 mL). The suspension was held at reflux for 16 h. The mixture was cooled, and the precipitate was recovered by filtration and washed with anhydrous acetone (3×40 mL). The dry residue was purified by FC (hexane/EtOAc, 85:15) to afford the desired compounds.

8-(2-Oxopropoxy)-3-phenylcoumarin (11): White solid (328 mg, yield: 76%): mp: 145–146 °C; ^1H NMR (300 MHz; $CDCl_3$): $\delta = 2.37$ (s, 3H, CH_3), 4.74 (s, 3H, CH_2), 6.98 (dd, 1H, $J = 5.6$, $J = 3.8$, H-7), 7.20–7.22 (m, 2H, H-5, H-6), 7.44–7.47 (m, 3H, H-3′, H-4′, H-5′), 7.72 (dd, 2H, $J = 7.6$, $J = 1.5$, H-2′, H-6′), 7.81 ppm (s, 1H, H-4); ^{13}C NMR (75 MHz; $CDCl_3$): $\delta = 26.6$, 74.2, 115.5, 120.8, 124.3, 128.5, 128.8, 129.0, 129.1, 129.4, 134.5, 139.8, 145.1, 159.7, 205.2 ppm; DEPT (75 MHz; $CDCl_3$): $\delta = 26.6$, 74.2, 115.5, 120.8, 124.3, 128.5, 129.0, 139.8 ppm; MS (EI, 70 eV): m/z (%): 295 (13) $[M+H]^+$, 294 (60) $[M]^+$, 252 (39), 251 (100), 223 (21) 222 (31), 193 (15), 167 (11), 165 (45), 152 (18), 43 (18); Anal. calcd for $C_{18}H_{14}O_4$: C 73.46, H 4.79; found: C 73.48, H 4.78.

3-(4′-Methylphenyl)-8-(2-oxopropoxy)coumarin (12): White solid (80 mg, yield: 80%): mp: 144–145 °C; ^1H NMR (300 MHz; $CDCl_3$): $\delta = 2.36$ (s, 3H, CH_3), 2.40 (s, 3H, CH_3), 4.73 (s, 2H, CH_2), 6.96 (dd, 1H, $J = 5.8$, $J = 3.7$, H-7), 7.14–7.20 (m, 2H, H-5, H-6), 7.22–7.29 (m, 2H, H-3′, H-5′), 7.62 ppm (d, 2H, $J = 8.1$, H-2′, H-6′); ^{13}C NMR (75 MHz; $CDCl_3$): $\delta = 21.3$, 26.6, 74.2, 115.3, 120.8, 120.9, 124.3, 128.4, 128.7, 129.2, 131.6, 139.0, 139.1, 143.3, 145.1, 159.8, 205.2 ppm; DEPT (75 MHz; $CDCl_3$): $\delta = 21.3$, 26.6, 74.2, 115.3, 120.8, 124.3, 128.4, 129.2, 139.1 ppm; MS (EI, 70 eV): m/z (%):309 (14) $[M+H]^+$, 308 (65) $[M]^+$, 266 (33), 265 (100), 237 (23), 236 (33), 207 (18), 179 (19), 178 (14), 165 (12), 152 (13), 43 (12); Anal. calcd for $C_{19}H_{16}O_4$: C 74.01, H 5.23; found: C 73.99, H 5.20.

3-(4′-Bromophenyl)-8-(2-oxopropoxy)coumarin (13): White solid (70 mg, yield: 78%): mp: 185–186 °C; ^1H NMR (300 MHz; $CDCl_3$): $\delta = 2.36$ (s, 3H, CH_3), 4.74 (s, 2H, CH_2), 6.95–7.06 (m, 1H, H-7), 7.15–7.24 (m, 2H, H-5, H-6), 7.59 (s, 4H, H-2′, H-3′, H-5′, H-6′), 7.81 ppm (s, 1H, H-4); ^{13}C NMR (75 MHz; $CDCl_3$): $\delta = 26.6$, 74.2, 115.7, 120.6, 120.9, 123.3, 124.5, 127.7, 130.1, 131.7, 133.3, 139.8, 143.3, 145.1, 159.5, 205.0 ppm; DEPT (75 MHz; $CDCl_3$): $\delta = 26.6$, 74.2, 115.7, 120.6, 124.5, 130.1, 131.7, 139.8 ppm; MS (EI, 70 eV): m/z (%): 375 (11), 374 (56), 373 (11) $[M+H]^+$, 372 (56) $[M]^+$, 332 (39), 331 (100), 330 (40), 329 (98), 303 (16), 302 (25), 301 (16), 300 (23), 273 (15), 271 (12), 245 (15), 243 (12), 165 (17), 164 (20), 163 (22), 152 (26), 43 (32); Anal. calcd for $C_{18}H_{13}BrO_4$: C 57.93, H 3.51; found: C 57.91, H 3.48.

Pharmacology

Adenosine receptor binding assays: The affinities of compounds **1–13** for the human AR subtypes hA_1, hA_{2A}, and hA_3 were determined by radioligand competition experiments in Chinese hamster ovary (CHO) cells that were stably transfected with the individual receptor subtypes.[22–24] The radioligands used were 1 nM (2*R*,3*R*,4*S*,5*R*)-2-(2-chloro-6-cyclopentylamino-purin-9-yl)-5-hydroxymethyl-tetrahydro-3,4-diol ([^{3}H]CCPA) for hA_1, 10 nM (1-(6-amino-9*H*-purin-9-yl)-1-deoxy-*N*-ethyl-β-dribofuronamide) ([^{3}H]NECA) for hA_{2A}, and 1 nM [^{3}H]2-(1-hexynyl)-N^6-methyladenosine ([^{3}H]HEMADO) for hA_3 ARs. The highest concentrations tested were different depending on the solubility of compounds and assay conditions for the respective receptor subtype. K_i values (Table 1) were calculated with the program SCTFIT[24] and are reported as geometric means (95% confidence intervals in parentheses) of three independent experiments with each tested concentration of compound measured in duplicate. The potency of antagonists at the $hA_{2B}AR$ (expressed in CHO cells) was determined by inhibition of NECA-stimulated adenylyl cyclase activity.[22] As none of the compounds showed measurable affinity for the $A_{2B}AR$, no data are reported in Table 1 for this subtype. Details for pharmacological experiments are described in previous work.[22,23]

Molecular modeling

Homology models were constructed using MOE (molecular operating environment) software.[37] Molecular docking calculations were performed using the Schrödinger package.[31,32]

Homology modeling: hA_1 and hA_3 ARs: For construction of the hA_1 and hA_3 models, we used the crystal structure of the $hA_{2A}AR$ (PDB: 3EML).[28] The protein sequence between the three receptors was aligned as previously described by Katritch et al.,[30] taking into account highly conserved residues in the TM helices. Geometry of the protein models was also assessed (Phi–Psi plots, bond lengths, bond angles, dihedrals, rotamers, atom clashes, and contact energies). The protein pockets in the developed models were optimized through Induced Fit Docking[38] using high-affinity compounds (compounds coll_11 and jaco_mre3008_f20, described by Katritch et al.).[30] Induced Fit workflow included Glide-SP docking of the ligands, protein pocket optimization using Prime, and Glide-XP docking in the refined pocket. We tested the different models extracted from Induced Fit Docking according to their ability to differentiate: 1) ligands from decoys and 2) subtype-selective compounds. The best models were selected to further study our newly synthesized series of compounds using molecular docking simulations.

Molecular docking of adenosine receptors: The dataset for coumarin derivatives was prepared with the LigPrep module using the Schrödinger package.[39] Different protonation states at pH 7.0 ± 2.0 and tautomers were generated through this process. Protein structures were pre-processed using the Protein Preparation Workflow.[39] No water molecules were included in the pocket. We performed molecular docking simulations in the $hA_{2A}AR$ using the crystal structure 3EML and in the hA_1 and hA_3 homology models. We docked the compounds in the Schrödinger package using the standard precision mode (Glide-SP).[31] Ten poses were collected by each compound and optimized along with the protein pocket (5 Å from the ligand) using the Prime module.[32] We selected the final binding modes considering the number of similar poses extracted by each compound along with geometric similarity with co-crystallized ligands in the $hA_{2A}AR$.

Acknowledgements

This project was partially supported by personal funds of Spanish researchers and the University of Santiago de Compostela (Spain). M.J.M. thanks the Fundação para a Ciência e Tecnologia (FCT) for the fellowship (SFRH/BPD/95345/2013). S.V. thanks the Angeles Alvariño program from the Xunta de Galicia (Spain).

Keywords: 3-arylcoumarin scaffold · adenosine receptor ligands · ADME properties · docking studies · radioligand binding

[1] B. B. Fredholm, A. P. IJzerman, K. A. Jacobson, K.-N. Klotz, J. Linden, *Pharmacol. Rev.* **2001**, *53*, 527 – 552.

[2] B. B. Fredholm, A. P. IJzerman, K. A. Jacobson, J. Linden, C. E. Müller, *Pharmacol. Rev.* **2011**, *63*, 1 – 34.

[3] P. A. Borea in *A_3 Adenosine Receptors: From Cell Biology to Pharmacology and Therapeutics*, Springer, Dordrecht, **2010**.

[4] C. E. Müller, K. A. Jacobson, *Biochim. Biophys. Acta Biomembr.* **2011**, *1808*, 1290 – 1308.

[5] S. Gessi, S. Merighi, K. Varani, E. Leung, S. M. Lennan, P. A. Borea, *Pharmacol. Ther.* **2008**, *117*, 123 – 140.

[6] F. Luan, A. Melo, F. Borges, M. N. Cordeiro, *Bioorg. Med. Chem.* **2011**, *19*, 6853 – 6859.

[7] V. J. McIntosh, R. D. Lasley, *J. Cardiovasc. Pharmacol. Ther.* **2012**, *17*, 21 – 33.

[8] R. Bansal, G. Kumar, D. Gandhi, L. C. Young, A. L. Harvey, *Chem. Biodiversity* **2011**, *8*, 1290 – 1300.

[9] C. J. Langmead, S. P. Andrews, S. M. Congreve, J. C. Errey, E. Hurrell, F. H. Marshall, J. S. Mason, C. M. Richardson, N. Robertson, A. Zhukov, M. Weir, *J. Med. Chem.* **2012**, *55*, 1904 – 1909.

[10] A. Gaspar, J. Reis, S. Kachler, S. Paoletta, E. Uriarte, K.-N. Klotz, S. Moro, F. Borges, *Biochem. Pharmacol.* **2012**, *84*, 21 – 29.

[11] A. Gaspar, J. Reis, M. J. Matos, E. Uriarte, F. Borges, *Eur. J. Med. Chem.* **2012**, *54*, 914 – 918.

[12] F. Belluti, G. Fontana, L. Bo, N. Carenini, C. Giommarelli, F. Zunino, *Bioorg. Med. Chem.* **2010**, *18*, 3543 – 3550.

[13] K. C. Fylaktakidou, D. J. Hadjipavlou-Litina, K. E. Litinas, D. N. Nicolaides, *Curr. Pharm. Des.* **2004**, *10*, 3813 – 3833.

[14] I. Kostova, *Curr. HIV Res.* **2006**, *4*, 347 – 363.

[15] M. J. Matos, C. Terán, Y. Pérez-Castillo, E. Uriarte, L. Santana, D. Viña, *J. Med. Chem.* **2011**, *54*, 7127 – 7137.

[16] S. Vazquez-Rodriguez, M. J. Matos, L. Santana, E. Uriarte, F. Borges, S. Kachler, K.-N. Klotz, *J. Pharm. Pharmacol.* **2013**, *65*, 697 – 703.

[17] M. J. Matos, A. Gaspar, S. Kachler, K.-N. Klotz, F. Borges, L. Santana, E. Uriarte, *J. Pharm. Pharmacol.* **2013**, *65*, 30 – 34.

[18] M. J. Matos, V. Hogger, A. Gaspar, S. Kachler, F. Borges, E. Uriarte, L. Santana, K.-N. Klotz, *J. Pharm. Pharmacol.* **2013**, *65*, 1590 – 1597.

[19] M. J. Matos, S. Vilar, V. García-Morales, N. P. Tatonetti, E. Uriarte, L. Santana, D. Viña, *ChemMedChem* **2014**, *9*, 1488 – 1500.

[20] L. M. Kabeya, A. A. Marchi, A. Kanashiro, N. P. Lopes, C. H. T. P. Silva, M. T. Pupo, Y. M. Lucisano-Valim, *Bioorg. Med. Chem.* **2007**, *15*, 1516 – 1524.

[21] M. J. Matos, A. Gaspar, F. Borges, E. Uriarte, L. Santana, *Org. Prep. Proced. Int.* **2012**, *44*, 522 – 526.

[22] K.-N. Klotz, J. Hessling, J. Hegler, C. Owman, B. Kull, B. B. Fredholm, M. J. Lohse, *Naunyn-Schmiedeberg's Arch. Pharmacol.* **1997**, *357*, 1 – 9.

[23] K.-N. Klotz, N. Falgner, S. Kachler, C. Lambertucci, S. Vittori, R. Volpini, G. Cristalli, *Eur. J. Pharmacol.* **2007**, *556*, 14 – 18.

[24] A. De Lean, A. A. Hancock, R. J. Lefkowitz, *Mol. Pharmacol.* **1982**, *21*, 5 – 16.

[25] *Molinspiration Cheminformatics*, Bratislava University, Slovak Republic, **2009**, http://www.molinspiration.com/services/properties.html (accessed July 2014).

[26] C. A. Lipinski, F. Lombardo, B. W. Dominy, P. J. Feeney, *Adv. Drug Delivery Rev.* **1997**, *23*, 3 – 25.

[27] P. Ertl, B. Rohde, P. Selzer, *J. Med. Chem.* **2000**, *43*, 3714 – 3717.

[28] V. P. Jaakola, M. T. Griffith, M. A. Hanson, V. Cherezov, E. Y. Chien, J. R. Lane, A. P. IJzerman, R. C. Stevens, *Science* **2008**, *322*, 1211 – 1217.

[29] J. J. Irwin, B. K. Shoichet, *J. Chem. Inf. Model.* **2005**, *45*, 177 – 182.

[30] V. Katritch, I. Kufareva, R. Abagyan, *Neuropharmacology* **2011**, *60*, 108 – 115.

[31] Small-Molecule Drug Discovery Suite 2011: Glide, version 5.7, Schrödinger LLC, New York, NY (USA), **2011**.

[32] Schrödinger Release 2011: Prime, version 3.0, Schrödinger LLC, New York, NY (USA), **2011**.

[33] M. Congreve, S. P. Andrews, A. S. Doré, K. Hollenstein, E. Hurrell, C. J. Langmead, J. S. Mason, I. W. Ng, B. Tehan, A. Zhukov, M. Weir, F. H. Marshall, *J. Med. Chem.* **2012**, *55*, 1898 – 1903.

[34] G. S. Inamdar, A. N. Pandya, H. M. Thakar, V. Sudarsanam, S. Kachler, D. Sabbadin, S. Moro, K.-N. Klotz, K. K. Vasu, *Eur. J. Med. Chem.* **2013**, *63*, 924 – 934.

[35] O. Lenzi, V. Colotta, D. Catarzi, F. Varano, D. Poli, G. Filacchioni, K. Varani, F. Vincenzi, P. A. Borea, S. Paoletta, E. Morizzo, S. Moro, *J. Med. Chem.* **2009**, *52*, 7640 – 7652.

[36] C. Higgs, T. Beuming, W. Sherman, *ACS Med. Chem. Lett.* **2010**, *1*, 160 – 164.

[37] Molecular Operating Environment (MOE), version 2011.10, Chemical Computing Group Inc., 1010 Sherbooke St. West, Suite #910, Montreal, QC, H3A 2R7, (Canada), **2011** http://www.chemcomp.com.

[38] W. Sherman, T. Day, M. P. Jacobson, R. A. Friesner, R. Farid, *J. Med. Chem.* **2006**, *49*, 534 – 553.

[39] Schrödinger Suite, Schrödinger LLC, New York, NY (USA), **2011**.

Received: May 20, 2014
Published online on July 18, 2014

Manuscript IV

Coumarin *versus* chromone monoamine oxidase B inhibitors: Quo vadis?

To be submitted to Journal of Medicinal Chemistry

Coumarin *versus* chromone monoamine oxidase B inhibitors: Quo vadis?

André Fonseca,[a,b] Joana Reis,[a] Maria Matos,[a,b] Donatella Bagetta,[c] Francesco Ortuso[c] Stefano Alcaro,[c] Eugenio Uriarte,[b] Fernanda Borges.[a]

[a] CIQUP/Department of Chemistry and Biochemistry, Faculty of Sciences, University of Porto, 4169-007, Porto, Portugal.
[b] Department of Organic Chemistry, Faculty of Pharmacy, University of Santiago de Compostela, 15782, Santiago de Compostela, Spain
[c] Department of "Scienze della Salute", University "Magna Græcia" of Catanzaro, Campus "Salvatore Venuta", Viale Europa, 88100, Catanzaro, Italy

Abstract

The last years' research has focused on the validation of benzopyrone as a privileged structure; in particular, our group has recently shown that the coumarin and chromone cores are outstanding frameworks for the design and development of monoamine oxidase (MAO) isoform B inhibitors. Thus, as coumarin and chromone are structural isomers, a comparative study between both scaffolds was performed. As a result, a small library of coumarin (**8a-21a**) and chromone (**8b-21b**) derivatives was synthesized and screened towards MAO-A and -B isoforms. Coumarin **10a** (IC_{50} = 5.07 nM) and chromones **10b** (IC_{50} = 4.2 nM) and **17b** (IC_{50} = 3.94 nM) were found to be the most potent IMAO-B. Compounds **10a** and **10b** have also presented drug-like properties and are potent reversible and non-competitive inhibitors. Theoretical studies firstly performed with the non-substituted coumarin (**1a**) and chromone (**1b**)-3-phenylcarboxamides show that both isomers have the ability to recognize MAOs with preference for isoform B. The data of the molecular modelling studies highlight the existence of a Cys172 hydrogen bonding involving the carboxamide spacer located at position 3 of the pyrone ring, a feature that validate the experimental *h*MAO-B selectivity data.

Introduction

There is nowadays a surge of diagnosed cases of neurodegenerative diseases (ND), mainly Parkinson (PD) and Alzheimer (AD) diseases.[1,2] Unfortunately, neither of these disorders has an effective treatment, with the drugs that are available being only used to delay the progress of neurodegeneration by controlling their symptoms.[2,3] Monoamine oxidases (MAOs) are FAD-containing enzymes present in the outer mitochondrial membrane, in neuronal, glial as well as other mammalian cells.[4] MAOs have two known isoforms, MAO-A and MAO-B, that catalyse the oxidation of different biogenic amines.[5] The isoform MAO-A has greater affinity for serotonin and noradrenaline while MAO-B favours the deamination of benzylamines and phenylethylamines, such as dopamine,[6] an important neurotransmitter that is present in very low concentrations in the brain of PD patients.[7] Additionally, a side effect of the normal activity of MAO-B is the production of reactive oxygen species (ROS) and consequent neuronal damage.[8] Indeed, considering that the levels of MAO-B in the brain increase with aging,[9] this means that not only dopamine levels will drop but also a rise of ROS will occur. This way, MAO-B is also linked to AD as neurons are especially sensitive to oxidative stress.[10–12] Generally, therapy for both diseases is only palliative so there is a continued effort for finding new potent enzymatic inhibitors.

Heterocycles play a key role in the discovery of new pharmacologically active compounds.[13] In the late 1980’s Evans *et al.* coined the term privileged structures,[14] under which the benzopyrone family fall into.[15,16] Benzopyrones, namely coumarin (α-benzopyrone) and chromone (γ-benzopyrone) (Figure 1a), are currently considered as valid templates for the design and development of new chemical entities.[8]

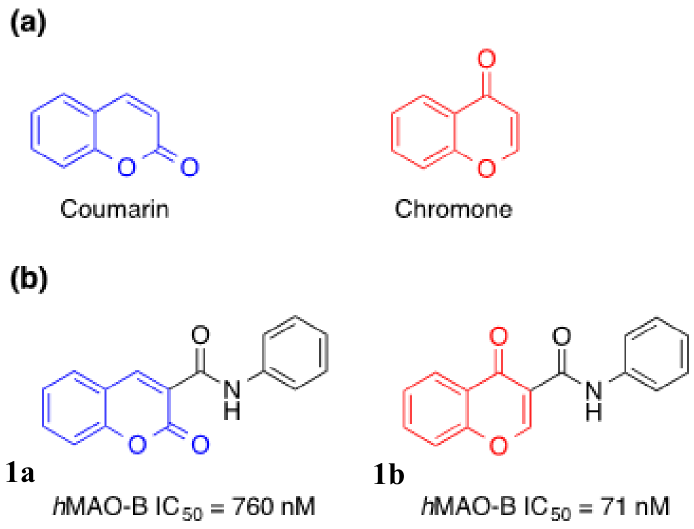

Figure 1. (a) Coumarin (2H-benzopyran-2-one) and chromone (4H-benzopyran-4-one) scaffolds; (b) Coumarin-3-phenylcarboxamide (**1a**) and chromone-3-phenylcarboxamide (**1b**) MAO-B inhibitors.[17,18]

Coumarins are a huge family of both natural and synthetic compounds existing in significant amounts in nature,[19] reporting some relevant pharmacological activities such as anti-inflammatory, antioxidant, cardioprotective, antimicrobial and enzyme inhibitors properties.[19–21] Chromones are also widely found in nature, being the central nucleus of several flavonoids, such as flavones and isoflavones.[22] Due to their synthetic availability and remarkable pharmacological activities, chromones play a key role in drug discovery programs. For instance, they have been described as potent antioxidants, anti-inflammatory, antitumor, anti-HIV and enzyme inhibitors.[22–26]

The last years' research has been focused in validating benzopyrone as a privileged structure, in particular our group has recently shown that benzopyrone, namely coumarin-3-phenylcarboxamide (**1a**) and chromone-3-phenylcarboxamide (**1b**), are an outstanding framework for the design and development of MAO-B inhibitors.[17,18]

As coumarin and chromone are structural isomers, the present study was conducted to compare their biological performance as MAO-A and/or MAO-B inhibitors. As a result, a small library of coumarin (**8a-21a**) and chromone (**8b-21b**) derivatives was synthetized and their MAO activity was evaluated *in vitro*. Targets recognition has been investigated at molecular level by means of docking simulation. To the best of our knowledge, this is the first time that a comprehensive structure-activity relationship (SAR) study is performed between these two structural isomers.

Results and Discussion

Chemistry. Coumarin-3-phenylcarboxamide and chromone-3-phenylcarboxamide derivatives were synthesized and evaluated as MAO inhibitors.

The coumarin derivatives were synthesized starting from the 5-methylsalicylaldehyde (**2a**) or 5-methoxysalicylaldehyde (**3a**) to yield the correspondent coumarin-3-carboxylates (**4a** or **5a**) using diethyl malonate and catalytic amounts of piperidine in ethanol under reflux. After hydrolysis with ethanolic solution with 0.5% NaOH (aq.) at reflux, the corresponding coumarin carboxylic acids **6a** and **7a** were obtained.[27] Finally, the coumarin-3-carboxamide derivatives **8a-21a** were synthesized through a coupling reaction involving ethyl-3-(3-dimethylaminopropyl)carbodiimide (EDC) and 4-dimethylaminopyridine (DMAP) in dichloromethane (DCM) and subsequent addition of the appropriate arylamine.[28]

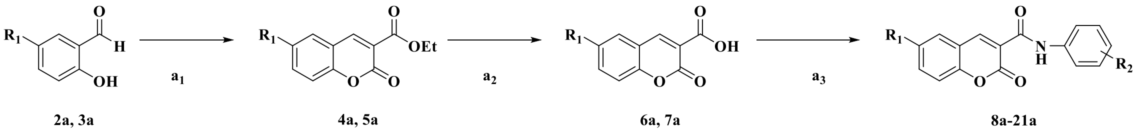

2a, 4a, 6a R_1=CH_3

3a, 5a, 7a R_1=OCH_3

8a	R_1=CH_3; R_2=H	**15a**	R_1=OCH_3; R_2=H
9a	R_1=CH_3; R_2=3'-CH_3	**16a**	R_1=OCH_3; R_2=3'-CH_3
10a	R_1=CH_3; R_2=3'-Cl	**17a**	R_1=OCH_3; R_2=3'-Cl
11a	R_1=CH_3; R_2=3'-OH	**18a**	R_1=OCH_3; R_2=3'-OH
12a	R_1=CH_3; R_2=4'-CH_3	**19a**	R_1=OCH_3; R_2=4'-CH_3
13a	R_1=CH_3; R_2=4'-Cl	**20a**	R_1=OCH_3; R_2=4'-Cl
14a	R_1=CH_3; R_2=4'-OH	**21a**	R_1=OCH_3; R_2=4'-OH

Scheme 1. Synthetic strategy followed for the synthesis of the coumarin derivatives **8a-21a** Reagents and conditions: (a_1) diethyl malonate, EtOH, piperidine, reflux, overnight; (a_2) NaOH (0.5% aq./EtOH), reflux, 4h (a_3) EDC, DMAP, DCM, appropriate arylamine, 0° to r.t., 4h.

The chromone-based compounds were synthesized starting from the 2-hydroxy-5-methylacetophenone (**2b**) or 2-hydroxy-5-methoxyacetophenone (**3b**) to yield their correspondent chromon-3-carbaldehyde (**4b** or **5b**) using a phosphoryl chloride ($POCl_3$) in *N,N*-dimethylformamide (DMF) at a low temperature.[29] Then, and after the oxidation of the formyl group with sodium chlorite, the chromone carboxylic acids **6b** and **7b** were obtained.[30] Finally, the chromone-3-carboxamide derivatives **8b-21b** were obtained through a reaction that encompass the *in situ* generation of an acyl chloride intermediate, using $POCl_3$ in DMF, and the subsequent addition of the appropriate arylamine.[26]

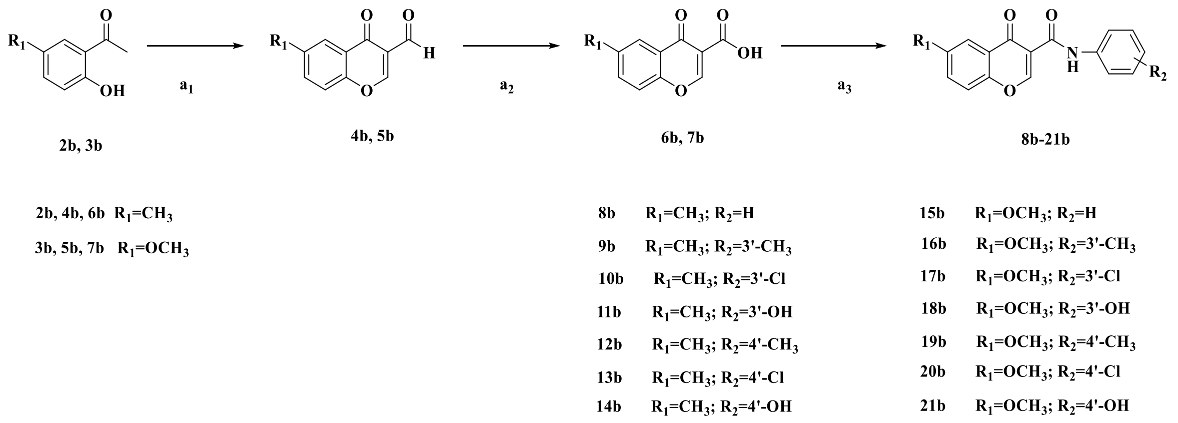
R1
O
OH
a1
2b, 3b
R1
O
O
H
O
4b, 5b
a2
R1
O
O
OH
O
6b, 7b
a3
R1
O
O
N
H
R2
O
8b-21b
2b, 4b, 6b R1=CH3
3b, 5b, 7b R1=OCH3
8b R1=CH3; R2=H
9b R1=CH3; R2=3'-CH3
10b R1=CH3; R2=3'-Cl
11b R1=CH3; R2=3'-OH
12b R1=CH3; R2=4'-CH3
13b R1=CH3; R2=4'-Cl
14b R1=CH3; R2=4'-OH
15b R1=OCH3; R2=H
16b R1=OCH3; R2=3'-CH3
17b R1=OCH3; R2=3'-Cl
18b R1=OCH3; R2=3'-OH
19b R1=OCH3; R2=4'-CH3
20b R1=OCH3; R2=4'-Cl
21b R1=OCH3; R2=4'-OH

Scheme 2. Synthetic strategy followed for the synthesis of chromone-3-phenylcarboxamide **8b-21b**. Reagents and conditions: (a_1) $POCl_3$, DMF, -10ºC, 15h; (a_2) H_3NSO_3, $NaClO_2$, 0ºC, 12h (a_3) $POCl_3$, DMF, appropriate arylamine, r.t., 1-5h.

Monoamine oxidase inhibition studies. The evaluation of MAO inhibitory activity was performed, on human isozymes (*h*), using the Amplex Red MAO assay kit and microsomal MAO isoforms from insect cells (BTI-TN-5B1-4) infected with recombinant baculovirus containing *h*MAO-A or *h*MAO-B cDNA inserts.[31] The production of H_2O_2 by MAO isoforms was detected using 10-acetyl-3,7-dihydroxyphenoxazine (Amplex Red reagent), a non-fluorescent and highly sensitive probe that reacts with H_2O_2 in the presence of horseradish peroxidase to produce a fluorescent product (resorufin). The benzopyrone derivatives under study and standard inhibitors did not react directly with the Amplex Red reagent, which indicated that they did not interfere with the measurements.

The *h*MAO-A and -B *in vitro* inhibition (IC$_{50}$) and selectivity, expressed as SI ([IC$_{50}$ (MAO-A)]/[IC$_{50}$ (MAO-B)]), of compounds under study and known antagonists (clorgyline for MAO-A and (R)-(−)-deprenyl, rasagiline, safinamide for MAO-B), are shown in Table **1.**

Table 1. MAO inhibitory activities of benzopyrone derivatives **8a**-**21a** and **8b**-**21b** and standard inhibitors.

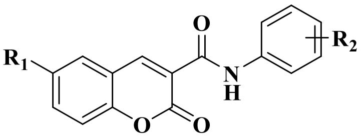

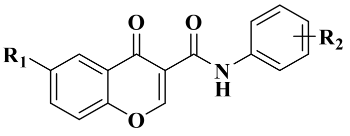

	R$_1$	R$_2$	IC$_{50}$ (nM)		SI		R$_1$	R$_2$	IC$_{50}$ (nM)		SI
			***h*MAO-B**	***h*MAO-A**					***h*MAO-B**	***h*MAO-A**	
8a	CH$_3$	H	15.32 ± 1.02	*	>653^{a}	**8b**	CH$_3$	H	21.35 ± 1.10	*	>468^{a}
9a	CH$_3$	*m*-CH$_3$	7.52 ± 1.05	*	>1330^{a}	**9b**	CH$_3$	*m*-CH$_3$	17.10 ± 1.17	*	>585^{a}
10a	CH$_3$	*m*-Cl	5.07 ± 1.25	*	>1972^{a}	**10b**	CH$_3$	*m*-Cl	4.20 ± 1.08	*	>238^{a}
11a	CH$_3$	*m*-OH	45.40 ± 1.30	*	>220^{a}	**11b**	CH$_3$	*m*-OH	78.22 ± 1.30	*	>128^{a}
12a	CH$_3$	*p*-CH$_3$	13.90 ± 1.30	*	>719^{a}	**12b**	CH$_3$	*p*-CH$_3$	151.6 ± 5.14	*	>66^{a}
13a	CH$_3$	*p*-Cl	11.08 ± 1.20	*	>903^{a}	**13b**	CH$_3$	*p*-Cl	45.42 ± 2.32	*	>220^{a}
14a	CH$_3$	*p*-OH	621.70 ± 1.8	*	>16^{a}	**14b**	CH$_3$	*p*-OH	512.6 ± 2.81	*	>20^{a}
15a	OCH$_3$	H	5.95 ± 1.28	*	>1681^{a}	**15b**	OCH$_3$	H	41.8 ± 2.2	*	>239^{a}
16a	OCH$_3$	*m*-CH$_3$	47.24 ± 1.12	*	>212^{a}	**16b**	OCH$_3$	*m*-CH$_3$	21.80 ± 1.21	*	>459^{a}
17a	OCH$_3$	*m*-Cl	9.03 ± 1.07	*	>111^{a}	**17b**	OCH$_3$	*m*-Cl	3.94 ± 1.08	*	>2538^{a}
18a	OCH$_3$	*m*-OH	228.6 ± 1.26	*	>44^{a}	**18b**	OCH$_3$	*m*-OH	113.5 ± 1.10	*	>88^{a}
19a	OCH$_3$	*p*-CH$_3$	19.43 ± 1.19	*	>515^{a}	**19b**	OCH$_3$	*p*-CH$_3$	210.8 ± 8.1	*	>47^{a}
20a	OCH$_3$	*p*-Cl	18.90 ± 1.01	*	>530^{a}	**20b**	OCH$_3$	*p*-Cl	10.31 ± 1.55	*	>970^{a}
21a	OCH$_3$	*p*-OH	*	*	n.a.	**21b**	OCH$_3$	*p*-OH	674.2 ± 1.72	*	>15^{a}
R-(-)-Deprenyl			16.73 ± 1.48	68730 ± 421	4108						
Rasagiline			49.66 ± 2.26	52974 ± 742	1067						
Safinamide			23.07 ± 2.07	**	>4335^{b}						

(*) Inactive at 10 µM; (**) Inactive at 100 µM (highest concentration tested); n.a. non applicable; SI: hMAO-B selectivity index = IC$_{50}$(*h*MAO-A)/IC$_{50}$(*h*MAO-B). ^{a} Values obtained under the assumption that the corresponding IC$_{50}$ against MAO-A is 10 µM. ^{b} Values obtained under the assumption that the corresponding IC$_{50}$ against MAO-A is the highest concentration tested (100 µM).

Structure-activity relationship studies. Following the previous studies on coumarin-[32] and chromone-based[26] compounds as MAO inhibitors, and to understand the effect of substituents located at similar positions on the isomeric scaffolds, an innovative SAR study was performed. The rational design strategy described in Figure 2 was mainly focused on the study of a) the effect of different substituents (R$_1$ = CH$_3$; OCH$_3$) on the benzopyrone ring; b) the effect of different electron donating or withdrawing substituents (R$_2$ = H, CH$_3$, Cl, OH) located at *meta* and *para* positions (the most relevant positions found in previous chromone-based studies[26]) on the exocyclic aromatic ring, and on c) the assessment of the influence of the position of the carbonyl group on the benzopyrone isomeric structures (coumarin vs chromone) on MAO activity. Both systems have in common a carboxamide spacer located at 3-position of the pyrone ring (Figure 2).

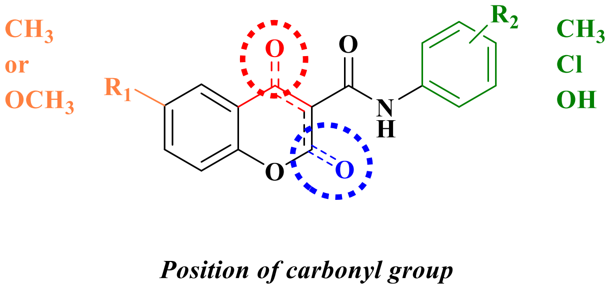

Figure 2. Rational design strategy followed in the present work.

Effect of coumarin substituents on MAO inhibitory activity

From the data it is observed that the introduction of methyl or methoxy substituents at position 6 of the coumarin scaffold resulted in potent and selective MAO-B inhibitors. In general, 6-methylcoumarin derivatives (compounds **8a**-**14a**) displayed a higher potency than the 6-methoxy analogues (**15a**-**21a**): for compounds **8a**-**14a** the activities ranged from 5.07 nM (compound **10a**, *m*-chloro) to 621.70 nM (compound **14a**, *p*-

hydroxyl) while for 6-methoxycoumarin derivatives (compounds **15a-21a**) from 19.43 nM (compound **20a**, *p*-chloro) to >10 µM (compound **21a**, *p*-hydroxyl). Compounds **15a** (without substituents in the exocyclic ring) and **17a**, with a *m*-chloro substituent, showed an MAO-B IC_{50} of 5.95 and 9.03 nM, respectively.

The analysis of the influence of the substituents located at the exocyclic aromatic ring demonstrated that for both 6-methyl and 6-methoxycoumarins, a higher potency was observed for derivatives bearing substituents at *meta* position. Compound **10a** was found to be the most potent IMAO-B coumarin-based ligand (IC_{50} = 5.07 nM). The introduction of *para*-substituents resulted in a decrease of activity, with the exception of compound **19a**, bearing a *p*-methyl group, (IC_{50} = 19.43 nM) when compared to compound **16a** with a *m*-methyl group (IC_{50} = 47.24 nM). Finally, considering the overall data, one can conclude that the presence of a hydroxyl group either in *meta* or *para* position was not favourable.

All coumarins under study were selective towards MAO-B as no significant activity (cut-off 100 µM) was found towards MAO-A (Table 1).

Effect of chromone substituents on MAO inhibitory activity

The data have demonstrated that the introduction of methyl or methoxy substituents at position 6 of the chromone scaffold led to IMAO-B working in a low nanomolar range: For 6-methylchromone derivatives (compounds **8b-14b**), the activities ranged from 4.20 nM (compound **10b**, *m*-chloro) to 512.60 nM (compound **14b**, *p*-hydroxyl), while for 6-methoxychromone derivatives (compounds **15b-21b**), from 3.94 nM (compound **17b**, *m*-chloro) to 674.2 µM (compound **21b**, *p*-hydroxyl). In general, the introduction of methyl or methoxyl substituents at the position 6 of the chromone scaffold had no noteworthy influence on MAO-B activity, with exception of compound **8b** (no substituents on the chromone exocyclic ring) which exhibited a higher MAO-B activity (IC_{50} = 21.35 nM) than the corresponding methoxy-substituted one (compound **15b**, IC_{50} = 41.8 nM).

Considering the effect of the substituents located at the chromone exocyclic ring, generally, it was observed a higher MAO-B inhibitory activity when they were located at *meta* position. Remarkably, the most active compounds of the series were **10b** (6-methyl; *m*-chloro IC_{50} = 4.2 nM) and **17b** (6-methoxy; *m*-chloro IC_{50} = 3.94 nM). Additionally, the presence of a hydroxyl group at *meta* or *para* position led to a significant decrease of MAO-B inhibition: compounds **11b** and **14b** displayed an IC_{50} =78.22 nM and IC_{50} = 512.6 nM, respectively in the 6-methyl chromone series; as for the 6-methoxychromone series, compounds **18b** and **19b** exhibited an IC_{50} = 113.5 nM and IC_{50} = 674.2 nM, respectively.

All chromones under study were selective towards MAO-B as no significant activity (cut-off 100 µM) was found towards MAO-A (Table 1).

Chromone vs. Coumarin

Considering that the currently studied coumarin- and chromone-based MAO-B inhibitors have showed similar activity and selectivity, the next step consisted in the comprehensive study of coumarins **10a** (6-methyl, *m*-chloro IC_{50} = 5.07 nM) and **17a** (6-methoxy, *m*-chloro IC_{50} = 9.03 nM), and chromones **10b** (6-methyl; *m*-chloro IC_{50} = 4.2 nM) and **17b** (6-methoxy; *m*-chloro IC_{50} = 3.94 nM). As a result, it was observed that in both series the presence of a chlorine substituent at *meta*-position was favourable for the enhancement of MAO-B inhibitory activity. Additionally, it was demonstrated that the existence of methyl or methoxyl groups at position 6 of the benzopyrone scaffold showed no significant influence on the inhibitory potency. Moreover, from the study performed so far, the position of the carbonyl group on both coumarin and chromone scaffolds doesn't seem to be essential on the IMAO-B activity.

Evaluation of drug-like properties. The drug-like properties, like physicochemical descriptors, such as molecular weight (MW), partition coefficient (clogP), topological polar surface area (tPSA in Å^2), number of hydrogen bond acceptors (HBA), number of hydrogen bond donors (HBD), and number of rotatable bonds (n_{rotb}), of the derivatives under study and of known MAO-B inhibitors were calculated. Additionally, the blood (plasma)−brain partitioning (log BB) multiparameter score was calculated according to Clark *et al*.[33] From the data depicted in Table 2 it is concluded that in general all compounds comply with the Lipinski's rule of five.[34] Furthermore, the clogP and tPSA (2.17-3.94 and 59.31-88.77 Å^2 respectively) values are within the ideal parameters for oral bioavailability and blood-brain barrier (BBB) permeability. In fact, the data attained from the prediction of BBB permeability properties, determined in this case by the log BB (the ratio of the steady-state concentrations of the drug in the brain and in the blood), is very encouraging since all coumarin and chromone derivatives displayed log BB > −1. Usually, compounds with log BB below −1 are poorly distributed in the brain and are unlikely to function as effective CNS drugs.[33] The same parameters were calculated for known IMAOs, rasagiline and (R)-(−)-deprenyl and safinamide (Table 2). The data reveal that rasagiline and (R)-(−)-deprenyl have an outlier behaviour for a number of parameters, namely tPSA and log BB. Importantly, it was observed that our compounds have predicted drug-like properties similar to safinamide.

Concerning the multiparameter score LLE,[35] the values displayed for the overall compounds ranged from 3 to 5, with the exception of chromone **15b** (LLE = 5.36) and coumarin **17a** (LLE = 5.08), which showed slightly higher ligand-lipophilicity efficiencies. Similar LLE data was attained for the standard MAO-B inhibitors.

Table 2. Theoretical physico-chemical properties of benzopyrone derivatives and known MAO-B inhibitors.

Compd	MW^a	pIC$_{50}$	cLogP^b	LLE	tPSA (Å^2)^b	HBA^b	HBD^b	n$_{rotb}$^{b}	Log BB
8a / 8b	279.30	7.67 / 7.81	3.06 / 3.26	4.61 / 4.55	59.31	4	1	2	-0.274 / -0.243
9a / 9b	293.32	7.77 / 8.12	3.49 / 3.68	4.55 / 4.44	59.31	4	1	2	-0.208 / -0.179
10a / 10b	313.74	8.38 / 8.29	3.71 / 3.91	4.67 / 4.38	59.31	4	1	2	-0.175 / -0.144
11a / 11b	295.29	7.11 / 7.34	2.56 / 2.75	4.55 / 4.59	79.54	5	2	2	-0.649 / -0.620
12a / 12b	293.32	6.82 / 7.86	3.51 / 3.71	3.31 / 4.15	59.31	4	1	2	-0.205 / -0.175
13a / 13b	313.74	7.34 / 7.96	3.74 / 3.94	3.60 / 4.02	59.31	4	1	2	-0.170 / -0.140
14a / 14b	295.29	6.29 / 6.21	2.58 / 2.78	3.71 / 3.43	79.54	5	2	2	-0.646 / -0.616
15a / 15b	295.29	7.38 / 8.23	2.67 / 2.87	4.71 / 5.36	68.54	5	1	3	-0.470 / -0.439
16a / 16b	309.32	7.66 / 7.33	3.09 / 3.29	4.57 / 4.04	68.54	5	1	3	-0.406 / -0.375
17a / 17b	329.74	8.40 / 8.04	3.32 / 3.52	5.08 / 4.52	68.54	5	1	3	-0.371 / -0.340
18a / 18b	311.29	6.95 / 6.64	2.17 / 2.36	4.78 / 4.28	88.77	6	2	3	-0.845 / -0.816
19a / 19b	309.32	6.68 / 7.71	3.12 / 3.31	3.56 / 4.40	68.54	5	1	3	-0.401 / -0.372
20a / 20b	329.74	7.99 / 7.72	3.35 / 3.54	4.64 / 4.18	68.54	5	1	3	-0.366 / -0.337
21a / 21b	311.29	6.17 / NA	2.19 / 2.39	3.98 / -	88.77	6	2	3	-0.842 / -0.812
R-(-)-Deprenyl	187.29	7.77	2.64	5.13	3.24	1	0	4	0.492
Rasagiline	171.24	7.30	2.10	5.20	12.03	1	1	2	0.280
Safinamide	302.35	7.64	2.91	4.73	64.36	4	3	7	-0.371
CNS+ drugs[34,36–38]	<450		<5	>5	<70	<7	<3	<8	≥-1

^{a}MW, Molecular Weight; ^{b} clog P, calculated logarithm of the octanol−water partition coefficient; tPSA, topological polar surface area; LLE: ligand-lipophilicity efficiency; HBA, number of hydrogen acceptors; HBD, number of hydrogen donors; n$_{rotb}$, number of rotatable bonds; log BB, logarithm of the ratio of the concentration of a drug in the brain and in the blood; Properties calculated using Cheminformatics software [http://www.molinspiration.com]

Evaluation of MAO inhibition mechanism. The MAO-B inhibition mechanism of two promising inhibitors, one from each series (coumarin **10a** and chromone **10b**), has been investigated. Both compounds have a *meta*-chloro substituent on the exoxyclic aromatic ring and a methyl group on the benzopyrone structure.

The initial rates of *p*-tyramine MAO-B-catalyzed oxidation, in the absence or presence of the selected inhibitors, were measured at five different substrate concentrations

(Figure 2). Graphical analysis of the reciprocal Lineweaver-Burk plots allowed the determination of Michaelis−Menten reaction kinetic parameters (Michaelis constant (K_m) and maximum velocity (V_{max})). From the data it was observed that K_m was practically not influenced by different concentrations either of **10a** or **10b**, whereas a decrease of V_{max} was observed. The Lineweaver-Burk plots obtained with different concentrations of **10a** (Figure 3a) showed a series of converging lines on the same point of the x-axis (1/[S]), profiling a non-competitive inhibition mechanism.

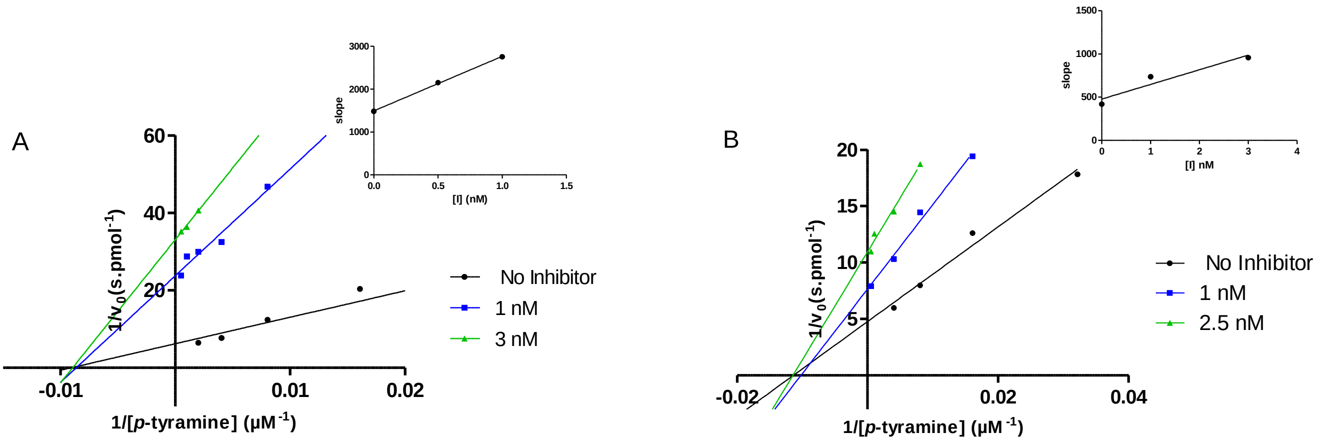

Figure 3. Kinetic studies on the mechanism of *h*MAO-B inhibition by (**A**) coumarin **10a** and (**B**) chromone **10b**. The enzyme inhibition was determined from the double reciprocal plot of 1/rate (1/V) *versus* 1/substrate concentration in presence of various concentrations of the inhibitors. The *Ki* values were calculated by the intersection of the curves obtained by plotting 1/V versus the inhibitor concentration for each substrate concentration (Dixon plots insets on the top right of each graphic).

From the Dixon plots, obtained from the replots of the slopes of the Lineweaver–Burk plots *vs* inhibitor concentrations (upper right corner), the enzyme binding affinities, determined as inhibition constants (*Ki*), were calculated. Coumarin **10a** (Figure 3A) and chromone **10b** (Figure 3B) displayed *Ki* values of 1.17 and 2.69 nM, respectively. Indeed, the estimated *Ki* values correlated well with the compounds experimental IC_{50}

values: coumarin **10a** (IC_{50} = 5.07 nM) and chromone **10b** (IC_{50} = 4.20 nM) displayed IC_{50} and *Ki* values slightly different but within the low nanomolar range.

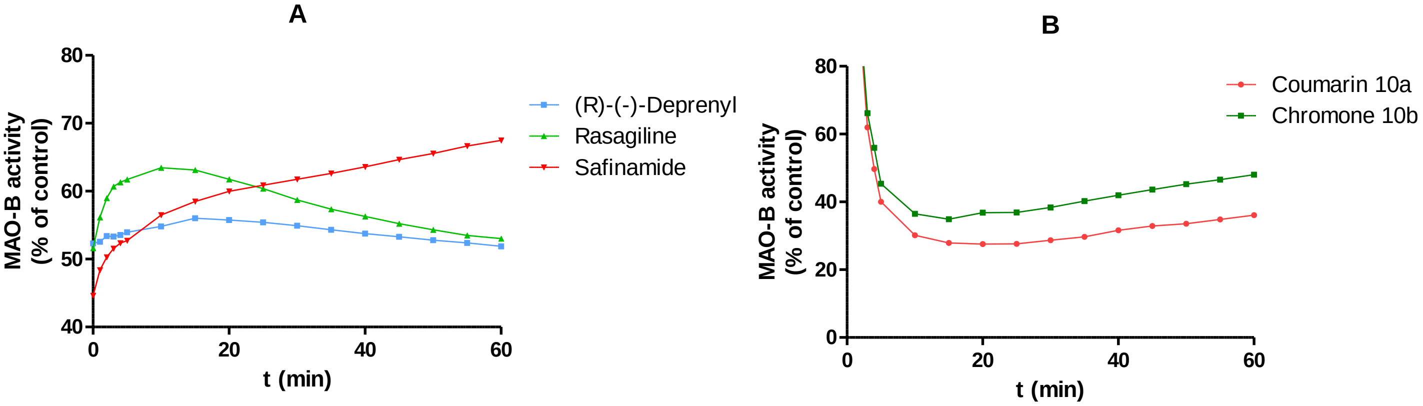

Figure 4. Time-dependent inhibition of recombinant human MAO-B by (**A**) standard compounds (R)-(−)-deprenyl (50 nM), safinamide (40 nM) and rasagiline (200 nM) and (**B**) tested compounds **10a** (12.5 nM), and **10b** (12.5 nM). The remaining activity was expressed as %. Data are the mean ± S.D. of three different experiments.

Additionally, time-dependent inhibition studies, in which MAO-B activity (% of control) was measured along 60 min incubation with compounds **10a** and **10b**, were performed (Figure 4B). To validate the data, the behavior of known irreversible ((*R*)-(−)-deprenyl and rasagiline) and reversible (safinamide) inhibitors was also evaluated under the same experimental conditions (Figure 4A).

The analysis of time-dependent inhibition studies performed with the irreversible inhibitors (Figure 4A) showed that the enzyme residual activity decayed continuously after the first 15 minutes of incubation, which is consistent with irreversible enzymatic inhibition. In case of the reversible inhibitor safinamide (Figure 4A), an enhancement on enzymatic activity was observed across the analysis time. A similar behaviour was observed for the compounds **10a** and **10b** (Figure 4B), as a slow binding to the active site was observed in the first 15 minutes, proceeded by an activity enhancement along the last 60 minutes. The data is in accordance to what is expected for a MAO-B reversible inhibitor.[26]

Modeling studies. Theoretical studies were performed in order to highlight the contribution of coumarin and chromone scaffolds, as well as R1-R2 substituents on the studied compounds *h*MAOs recognition. In order to eliminate the R1-R2 moiety effects on the ligand target binding, two new derivatives, **1a** and **1b**, were theoretically designed by replacing R1 methyl group with and hydrogen atom from **8a** and **8b**, respectively.

The *h*MAO-A and *h*MAO–B active site interaction of coumarin and chromone-based derivatives **8-21** was evaluated by means of docking simulation (Experimental section). The results analysis clearly indicated that **1a** and **1b** could almost equally interact to the targets, but preferring the *h*MAO–B isoform (Supporting information, Table S1). The docking geometries graphical examination showed that **1a** and **1b** preferably recognized the *h*MAO-A active site by positioning the benzopyrone moiety towards the FAD cofactor, whereas the anilide ring was located at the entrance gorge. Regarding MAO-A, benzopyrone and exocyclic aromatic rings seemed to play the main role in complexes stabilization. In fact, the moieties of **1a** and **1b** were involved in stacking to Tyr444 and Phe208 sidechains, respectively. Other productive interactions were basically weak hydrophobic contacts to active site residues. Notably, unfavorable electrostatic repulsion was observed between the Asn181 sidechain and the benzopyrone ring in both **1a** and **1b**. On the other hand, the most stable **1a** and **1b** poses into the *h*MAO-B active site were similar to those previously reported, even if ligands opposite orientations were also observed in higher energy theoretical complexes. In *h*MAO-B a remarkable stabilizing contribution was due to a hydrogen bond (HB) between ligands oxygen atoms and the Cys172 sidechain. In both compounds *h*MAO-B best poses involved the anilide sp2 oxygen whereas in less stable complexes such an interaction occurred by means of benzopyrone ring HB acceptor atoms. Since the other complexes stabilizing contribution were basically equivalent to the *h*MAO-A ones, and taking into account that *h*MAO-B Cys172 is replaced by Asn181 in *h*MAO-A, we could mainly address the experimentally observed *h*MAO-B selectivity to the ligands-Cys172 hydrogen bonding (Figure 5).

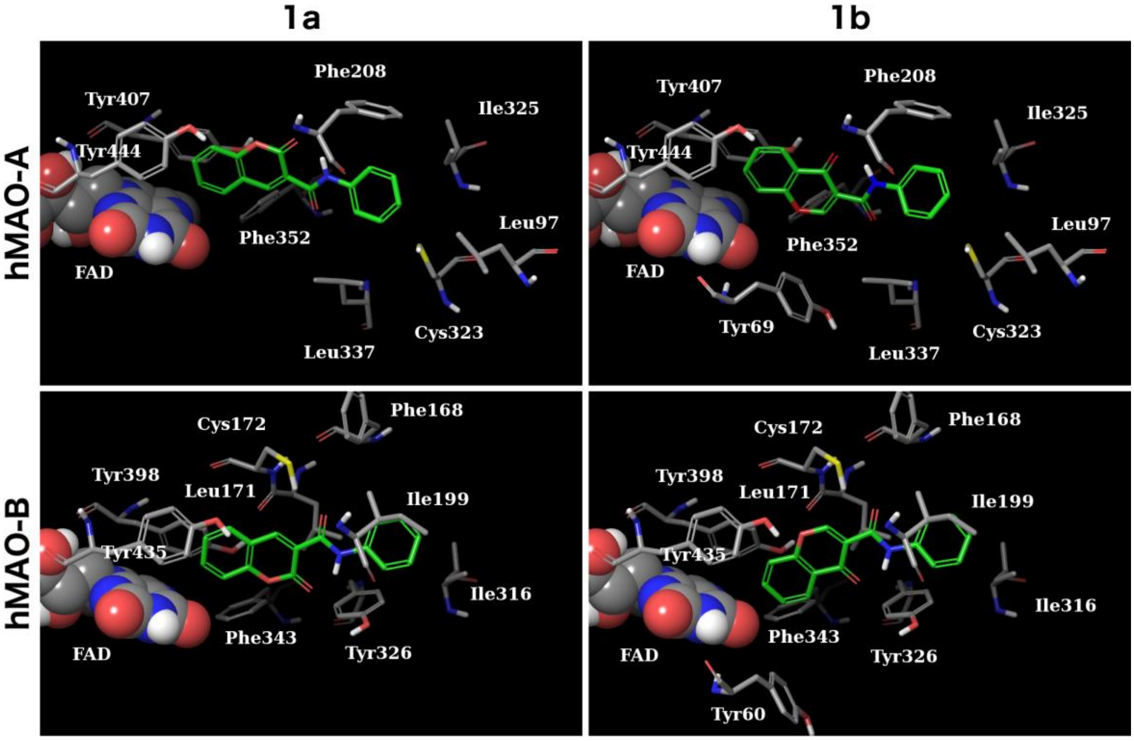
1a
1b
hMAO-A
hMAO-B
Tyr407
Phe208
Ile325
Tyr444
Leu97
Phe352
FAD
Cys323
Leu337
Tyr69
Cys172
Phe168
Tyr398
Leu171
Ile199
Tyr435
Ile316
Phe343
Tyr326
Tyr60

Figure 5. Best docking poses of compounds **1a** and **1b** into the *h*MAOs active sites. Most relevant interacting residues are depicted in polytube CPK colored, FAD cofactor is shown as spacefill and ligands as green carbons polytube.

Additionally, the **1a** and **1b** binding modes analysis confirmed that no relevant differences can be observed between coumarin and chromone scaffolds with respect to the recognition of the same target, this was particularly evident as these structures played a key role in isoform selectivity.

Further molecular docking simulations were carried out to explore targets recognition of other promising studied derivatives. All compounds, excluding **10a** with respect to *h*MAO-A, were able to bind to both MAO isoforms. Even if a linear correlation between docking score and experimental data was not observed (Supporting information, Table S1), the theoretical descriptor GScore clearly indicated that the complexes between the studied molecules and *h*MAO-B are more stable than the corresponding *h*MAO-A ones. Afterwards, the aim of the molecular modeling studies was focused into the role of R1 and R2 substituents.

Regarding *h*MAO-A, the docking most stable poses suggested a modest role of methyl and methoxyl substituents at R1 position, since they didn’t alter significantly the ligand bind modes. All global minimum energy complexes showed almost equivalent configuration to those discussed for **1a** and **1b**: the benzopyrone towards the FAD cofactor and the anilide group located at the active site entrance. Subsequently, the effects of methyl, chlorine and hydroxyl groups at the anilide R2 position were investigated. Methyl and particularly chlorine substituents decreased both the number of docking poses and the ligands-target predicted affinities. Such an observation was mainly addressed to steric clashes between ligands R2 moieties and *h*MAO-A peripheral residues Phe208 and Cys323. In particular, **10a** docking simulation didn’t propose energy favorable binding modes and **17b** was estimated as *h*MAO-A worst affinity binder. Instead, **11a**, **11b** and **18a**, **18b** derivatives, established HB to Tyr197 and Tyr444 by means of the hydroxyl group at *meta* position of the aromatic ring, and stacking interactions between the benzopyrone moiety and Phe208. A deep investigation of R2 positioning role has been performed, comparing the best poses of the couples of compounds differing in such a feature only. Isomeric analogues **9a**, **9b** - **12a**, **12b** and **16a**, **16b** - **19a**, **19b** displayed a similar contribution of the methyl group that is not related to its *meta* or *para* position on the aromatic ring. A different scenario was highlighted when R2 consisted of a chlorine atom. First of all, such a substituent at *meta* position prevented the *h*MAO-A recognition of **10a**, while at *para* position it allowed **13a** to establish stacking interactions to Phe208, Phe352 and Tyr407, although with an a target affinity lower than **1a** and **8a**. When R1 consisted of a methyl group, **10b** - **13b**, the R2 chlorine substituent induced opposite configuration of the inhibitors into the target active site. Differently, any recognition difference was induced by R2 chlorine if R1 was equal to methoxy group (**17a**, **17b** – **20a**, **20b**). The last investigated R2 substituent was the hydroxyl group. Excluding **18a** and **21a**, which showed the same target binding mode, the positioning of R2 hydroxyl group caused a different compounds' orientation. Indeed, **11a**, **11b** directed their anilide moiety towards FAD, whereas **14a**, **14b** interacted to the cofactor by means of the benzopyrone scaffold. Despite such different binding modes, the stacking interactions to Tyr407, Tyr444 and Phe208 were always established, even if by different ligand moieties. Same consideration could be addressed to **18b** and **21b** that bound to *h*MAO-A similarly to **11a**, **11b** and **14a**, **14b**, respectively.

In *h*MAO-B, the best poses of **8a** and **8b** reported a quite similar interaction profile when compared to **1a** and **1b**. The most evident difference was related to the opposite configuration of the global minimum **8a** complex with respect to the **1a** one. Besides, such a change was not observed in higher energy poses. Even the most stable docking models of **15a** matched with the non-substituted compounds. In particular, the positioning of the coumarin scaffold overlapped with **1a**, meanwhile the methoxyl group, accepting one HB by Tyr188, led to a greater complex stabilization, thus resulting in a better theoretical affinity. Such an interaction could be also addressed to **15b**, even if its complex geometry limited the HB energy contribution. The presence of a methoxyl group at R1, allowed **15b** to establish one HB between benzopyrone carbonyl oxygen and target Cys172. The anilide moiety was similarly located when compared to the previously reported **1b**. Then, as well as for *h*MAO-A, it was investigated the role of the different chemical nature of substituents at R2 and their placement. The top poses either of coumarins and chromones showing methyl, hydroxyl or chlorine R2 at *meta* position (**9-11**, **16-18**), reported the benzopyrone moiety towards FAD cofactor, except for **11a** that remarked the same binding mode of **8a**. Theses derivatives were mainly involved in stacking interactions to Tyr398 and in HB to Cys172. Additionally, regarding *h*MAO-B, it was found no differences among higher affinity poses of R2 *para* derivatives with respect to the corresponding *meta* analogues. Since its chlorine substituent was directed toward FAD, **17b** represented the only exception to the previous observation.

CONCLUSION

As coumarin and chromone are structural isomers, a project was developed involving the synthesis of a small library of coumarin (**8a-21a**) and chromone (**8b-21b**) derivatives and its screening towards MAO-A and MAO-B isoforms. From the current study, coumarin **10a** (IC_{50} = 5.07 nM) and chromones **10b** (IC_{50} = 4.2 nM) and **17b** (IC_{50} = 3.94 nM) were found to be the most potent IMAO-B. In both series the presence of a chlorine substituent at *meta*-position is favourable for the enhancement of MAO-B inhibitory activity. Generally, the presence of methyl or methoxyl groups at position 6 of the benzopyrone has not a noteworthy influence on the inhibitory potency. Compounds **10a** and **10b** present drug-like properties and are potent reversible and non-competitive inhibitors. The data of molecular modeling studies, performed to better understand the interactions regarding MAO targets, indicates the existence of a Cys172 hydrogen bonding involving the carboxamide spacer located at position 3 of the pyrone ring. Considering that *h*MAO-B Cys172 is replaced by Asn181 in *h*MAO-A, this feature validates the experimental *h*MAO-B selectivity of compounds **10a** and **10b**. Additionally, it was concluded that the benzopyrone core, and in particular the carbonyl group, is a positive contributor for the ligand–enzyme complex stability.

EXPERIMENTAL SECTION

GENERAL: All starting materials and reagents were obtained from commercial suppliers and were used without further purification (Sigma–Aldrich). Melting points (mp) were determined using a Reichert Kofler thermopan or in capillary tubes on a Büchi 510 apparatus and were not corrected. ^{1}H (400 MHz) and ^{13}C (100 MHz) NMR spectra were recorded on a Bruker AMX spectrometer, using DMSO-d_6 or $CDCl_3$ as solvents. Chemical shifts (δ) and coupling constants (*J*) were expressed in ppm and in Hz, respectively, using TMS as internal standard. The notations used for spin multiplicities were: s (singlet), d (doublet), dd (double doublet), t (triplet), dt (double triplet) and m (multiplet). Mass spectrometry data was acquired with a Hewlett-Packard-5972-MSD spectrometer. Silica gel (Merck 60, 230–400 mesh) was used for flash chromatography (FC). Analytical thin layer chromatography (TLC) was performed on plates precoated with silica gel (Merck 60 F254, 0.25 mm). Organic solutions were dried over anhydrous Na_2SO_4. The solvents were evaporated on a rotary evaporator (Büchi Rotavapor).

CHEMISTRY

A) Synthesis of coumarin derivatives

Synthesis of ethyl 6-methylcoumarin-3-carboxylate (4a) and ethyl 6-methoxycoumarin-3-carboxylate (5a)

A solution of 5-methylsalicylaldehyde (**2a**) or 5-methoxysalicylaldehyde (**3a**) (1 mmol) and diethyl malonate (1 mmol) in ethanol (10 mL) was stirred at room temperature for 5 min. Pirimidine (15µL) was then added and the reaction was mantainedt under reflux overnight. Afterwards, it was allowed to cool at room temperature and the resulting suspension was filtered off. The solid was washed with cold ethanol and diethyl ether and recrystallized from ethanol.

Ethyl 6-methylcoumarin-3-carboxylate (4a) Yield: 89% m.p. 100-101 ºC ^{1}H NMR ($CDCl_3$) δ (ppm), *J* (Hz): 1.39 (t, 3H, CH_2*CH_3*, *J* = 7.1), 2.41 (s, 3H, CH_3), 4.39 (q, 2H, *CH_2*CH_3, *J* = 7.1), 7.21-7.45 (m, 3H, H-5, H-7, H-8), 8.46 (s, 1H, H-4). ^{13}C NMR ($CDCl_3$) δ (ppm): 163.1, 153.2, 148.6, 135.5, 135.4, 134.5, 129.0, 118.0, 117.5, 116.3, 61.8, 20.6, 14.1. MS/EI m/z (%):232 (M, 48), 187 (80), 160 (100), 132 (19), 103 (19), 77 (20).

Ethyl 6-methoxycoumarin-3-carboxylate (5a) Yield: 94% m.p. 138-139 ºC ^{1}H NMR ($CDCl_3$) δ (ppm), *J* (Hz): 1.35 (t, 3H, CH_2*CH_3*, *J* = 7.1), 3.81 (s, 3H, OCH_3), 4.35 (q, 2H, *CH_2*CH_3, *J* = 7.1), 6.95 (d, 1H, H-5, *J* = 1.7), 7.14-7.26 (m, 2H, H-7, H-8), 8.43 (s, 1H, H-4). ^{13}C NMR ($CDCl_3$) δ (ppm): 167.5, 163.1, 156.1, 149.6, 122.5, 118.3, 118.0, 117.7, 110.4, 61.81, 55.8, 14.1. MS/EI m/z (%): 249 (M+, 32), 248 (M, 95), 203 (94), 177 (33), 176 (100), 161 (38), 148 (35), 133 (31), 119 (39), 76 (35).

Synthesis of 6-methylcoumarin-3-carboxylic acid (6a) and 6-methoxycoumarin-3-carboxylic (7a)

To a solution of coumpound **4a** or **5a** (2 mmol) in ethanol (25 mL) was added an aqueous solution of NaOH (0.5%, 5mL). The mixture was kept under reflux for 1h. Afterwards, an aqueous solution of HCl (10%) was added dropwise until pH around 2. The resulting solid was filtered, washed with water and recrystallized from ethanol.

6-Methylcoumarin-3-carboxylic acid (6a) Yield: 93% m.p. 162-163 ºC ^{1}H NMR (DMSO-*d_6*) δ (ppm), *J* (Hz): 2.33 (s, 3H, CH_3), 7.29 (d, 1H, H-8, *J* = 8.5), 7.50 (dd, 1H, H-7, *J* = 2.7, 8.5), 7.63 (d, 1H, H-5, *J* = 2.7), 8.62 (s, 1H, H-4), 13.19 (s, 1H, COOH). ^{13}C NMR (DMSO-d_6) δ (ppm): 164.5, 157.3, 153.0, 148.7, 135.6, 134.6, 130.0, 118.7, 118.3, 116.3, 20.6. MS/EI m/z (%): 204 (M, 91), 160 (100), 132 (64), 131 (63), 104 (31), 105 (35), 77 (43), 63 (15), 51 (30).

6-Methoxycoumarin-3-carboxylic acid (7a) Yield: 88% m.p. 202-203 ºC ^{1}H NMR (DMSO-d_6) δ (ppm), *J* (Hz): 3.77 (s, 3H, OCH_3), 7.27 (dd, 1H, H-7, *J* = 2.8, 9.1), 7.35 (d, 1H, H-8, *J* = 9.1), 7.43 (d, 1H, H-5, *J* = 2.8), 8.65 (s, 1H, H-4), 13.20 (s, 1H, COOH). ^{13}C NMR (DMSO-d_6) δ (ppm): 170.5, 164.3, 155.9, 149.3, 148.5, 122.2, 118.7, 118.5, 117.5, 112.1, 56.1. MS/EI m/z (%): 220 (M, 100), 176 (61), 161 (55), 148 (48), 133 (60), 105 (25), 77 (33).

Synthesis of coumarin derivatives (8a-21a)

To a solution of the appropriate coumarin-3-carboxylic acid (**6a** or **7a**, 1 mmol) in dichloromethane (DCM) (5 mL) 1-ethyl-3-(3-dimethylaminopropyl)carbodiimide (EDC) (1.10 mmol) and 4-dimethylaminopyridine (DMAP) (1.10 mmol) were added. The mixture was kept with a flux of argon at 0 ºC for ten minutes. Shortly after, the aromatic amine (1 mmol) with the intended substitution pattern was added in small portions. The reaction mixture was stirred for 4 h at room temperature. The solid obtained was filtered and purified by column chromatography (hexane/ethyl acetate 9:1) or by recrystallization from ethanol to give the desired products **8a-21a**.

Compounds **9a**, **11a**, **12a** and **14a** have already been described.[32]

***N*-Phenyl-6-methylcoumarin-3-carboxamide (8a)** Yield: 62% m.p. 194-195 ºC ^{1}H NMR ($CDCl_3$) δ (ppm), *J* (Hz): 2.46 (s, 3H, CH_3), 7.16 (ddd, 1H, H-4’, *J* = 1.1, 1.1, 7.4), 7.32-7.40 (m, 3H, H-8, H-3’, H-5’), 7.48-7.52 (m, 2H, H-5, H-7), 7.72-7.76 (m, 2H, H-2’, H-6’), 8.97 (s, 1H, H-4), 10.87 (s, 1H, NH). ^{13}C NMR ($CDCl_3$) δ (ppm): 162.0, 155.5, 152.7, 148.9, 137.7, 135.6, 135.4, 129.5, 129.0, 124.7, 120.6, 118.5, 118.4, 116.4, 20.8. MS/EI m/z (%): 279 (M, 88), 173 (100), 101 (32), 63 (21).

***N*-(3-Chlorophenyl)-6-methylcoumarin-3-carboxamide (10a)** Yield: 61% m.p. 238-239 ºC ^{1}H NMR (DMSO-d_6) δ (ppm), *J* (Hz): 2.36 (s, 1H, CH_3), 7.17 (ddd, 1H, H-4’, *J* = 0.9, 1.8, 8.0), 7.32-7.44 (m, 2H, H-8, H-5’), 7.50-7.60 (m, 2H, H-7, H-6’), 7.75 (d, 1H, H-5, *J* = 1.3), 7.93 (dd, 1H, H-2’, *J* = 1.8, 1.8), 8.79 (s, 1H, H-4), 10.73 (s, 1H, NH). ^{13}C NMR (DMSO-d_6) δ (ppm): 174.7, 166.3, 160.5, 152.2, 149.2, 147.7, 135.5, 134.9, 133.4, 130.8, 129.9, 120.9, 119.6, 118.6, 118.2, 108.6, 20.4. MS/EI m/z (%): 315 (M+2, 60), 313 (M, 93), 188 (77), 187 (100), 115 (70), 103 (63), 89 (16), 77 (53), 63 (19).

***N*-(4-Chlorophenyl)-6-methylcoumarin-3-carboxamide (11a)** Yield: 42% m.p. 216-217 ºC ^{1}H NMR (DMSO-d_6) δ (ppm), *J* (Hz): 2.36 (s, 3H, CH_3), 7.35-7.45 (m, 3H, H-8, H-3’, H-5’), 7.57 (dd, 1H, H-7, *J* = 2.0, 8.6), 7.69-7.79 (m, 3H, H-5, H-2’, H-6’), 8.79 (s, 1H, H-4), 10.70 (s, 1H, NH). ^{13}C NMR (DMSO-d_6) δ (ppm): 165.7, 160.3, 152.2, 147.7, 137.4, 135.53, 134.9, 132.1, 130.0, 122.0, 119.9, 118.6, 116.2, 107.8, 20.5 MS/EI m/z (%): 315 (M+2, 40), 313 (M, 92), 188 (42), 187 (100), 115 (36), 103 (29), 77 (23).

***N*-Phenyl-6-methoxycoumarin-3-carboxamide (15a)** Yield: 75% m.p. 195-197 ºC ^{1}H NMR ($CDCl_3$) δ (ppm), *J* (Hz): 3.89 (s, 1H, OCH_3), 7.11 (d, 1H, H-5, *J* = 2.9), 7.16 (ddd, 1H, H-4, *J* = 0.8, 1.0, 7.4), 7.27 (dd, 1H, H-7, *J* = 2.9, 9.1), 7.34-7.40 (m, 2H, H-3’, H-5’), 7.72-7.78 (m, 3H, H-8, H-2’, H-6’), 8.97 (s, 1H, H-4), 10.89 (s, 1H, NH). ^{13}C NMR ($CDCl_3$) δ (ppm): 161.9, 159.4, 156.8, 148.9, 148.7, 137.7, 135.5,129.0, 124.8, 122.8, 120.6, 117.8, 116.4, 110.7, 56.0. MS/EI m/z (%): 296 (26), 295 (92), 187 (30), 186 (100), 115 (25).

***N*-(3-Methylphenyl)-6-methoxycoumarin-3-carboxamide (16a)** Yield: 73% m.p. 186-187 ºC ^{1}H NMR (CDCl$_3$) δ (ppm), *J* (Hz): 2.34 (s, 3H, CH$_3$), 3.87 (s, 3H, OCH$_3$), 7.07 (d, 1H, H-5, *J* = 2.9), 7.17-7.28 (m, 2H, H-2', H-5'), 7.34 (d, 1H, H-8, *J* = 9.1), 7.47-7.55 (m, 2H, H-7, H-6'), 8.92 (s, 1H, H-4), 10.81 (s, 1H, NH). ^{13}C NMR (CDCl$_3$) δ (ppm): 162.1, 159.2, 158.8, 148.6, 136.0, 135.9, 130.3, 128.8, 126.6, 125.0, 122.8, 121.7, 118.9, 117.7, 115.53, 110.52, 55.8, 18.0. MS/EI m/z (%): 310 (M+, 22), 309 (86), 291 (51), 281 (30), 203 (100), 119 (49), 106 (72), 77 (17).

***N*-(3-Chlorophenyl)-6-methoxycoumarin-3-carboxamide (17a)** Yield: 48% m.p. 222-223 ºC ^{1}H NMR (DMSO-*d$_6$*) δ (ppm), *J* (Hz): 3.80 (s, 3H, OCH$_3$), 7.17 (ddd, 1H, H-4', *J* = 0.7, 1.9, 7.8), 7.30-7-38 (m, 2H, H-5, H-7), 7.47 (d, 1H, H-8, *J* = 9.1), 7.50-7.57 (m, 2H, H-5', H-6'), 7.94 (dd, 1H, H-2', *J* = 1.8, 1.9), 8.83 (s, 1H, H-4), 10.76 (s, 1H, NH). ^{13}C NMR (DMSO-*d$_6$*) δ (ppm): 162.0, 160.5, 156.2, 149.3, 147.6, 139.5, 133.4, 130.8, 128.6, 127.7, 122.5, 119.6, 118.6, 117.6, 112.0, 103.6, 55.9. MS/EI m/z (%): 331 (M+2, 15), 329 (M,45), 295 (54), 294 (99), 204 (37), 203 (100), 119 (60).

***N*-(3-Hydroxyphenyl)-6-methoxycoumarin-3-carboxamide (18a)** Yield: 57% m.p. 232-233 ºC ^{1}H NMR (DMSO-*d$_6$*) δ (ppm), *J* (Hz): 3.80 (s, 3H, CH$_3$), 6.51 (ddd, 1H, H-4', *J* = 1.0, 2.3, 8.0), 7.11 (dd, 1H, H-5', *J* = 8.0, 8.0), 7.26-7.37 (m, 2H, H-7, H-6'), 7.48 (d, 1H, H-8, *J* = 9.1), 7.55 (d, 1H, H-2', *J* = 3.0), 8.83 (s, 1H, H-4), 9.55 (s, 1H, OH), 10.59 (s, 1H, NH). ^{13}C NMR (DMSO-*d$_6$*) δ (ppm): 161.6, 160.0, 157.8, 153.1, 147.4, 130.0, 125.7, 122.5, 120.0, 117.6, 111.7, 110.9, 108.9, 107.0, 106.7, 104.4, 56.6. MS/EI m/z (%): 312 (M+, 32), 311 (100), 204 (62), 203 (96), 119 (60), 80 (18).

***N*-(4-Methylphenyl)-6-methoxycoumarin-3-carboxamide (19a)** Yield: 61% m.p. 186-187 ºC ^{1}H NMR (DMSO-*d$_6$*) δ (ppm), *J* (Hz): 2.24 (s, 3H, CH$_3$), 3.72 (s, 3H, OCH$_3$), 7.10-7.21 (m, 3H, H-5, H-2', H-6'), 7.41 (d, 1H, H-8, *J* = 8.6), 7.52-7.61 (m, 3H, H-7, H-3', H-5'), 8.79 (s, 1H, H-4), 10.56 (s, 1H, NH). ^{13}C NMR (DMSO-*d$_6$*) δ (ppm): 162.1, 159.2, 158.8, 148.6, 136.0, 135.9, 130.3, 128.8, 126.6, 125.0, 122.8, 121.7, 118.9, 117.7, 115.5, 110.5, 55.80, 18.0. MS/EI m/z (%): 309 (M, 86), 291 (51), 281 (29), 203 (100), 119 (49), 106 (72).

***N*-(4-Chlorophenyl)-6-methoxycoumarin-3-carboxamide (20a)** Yield: 49% m.p. 216-217 ºC ^{1}H NMR (DMSO-*d*$_6$) δ (ppm), *J* (Hz): 3.80 (s, 3H, OCH$_3$), 7.28-7.40 (m, 2H, H-3’, H-5’), 7.46 (d, 1H, H-8, *J* = 9.1), 7.53 (d, 1H, H-5, *J* = 2.8), 8.82 (s, 1H, H-4), 10.71 (s, 1H, NH). ^{13}C NMR (DMSO-*d*$_6$) δ (ppm): 162.9, 160.9, 155.8, 149.1, 148.7, 139.5, 131.2, 131.1, 128.0, 126.3, 122.7, 119.1, 118.2, 117.8, 113.7, 100.4, 56.0. MS/EI m/z (%): 329 (M, 41), 295 (56), 294 (97), 204 (30), 203 (100), 119 (66), 76 (25).

***N*-(4-Hydroxyphenyl)-6-methoxycoumarin-3-carboxamide (21b)** Yield: 59% m.p. 242-243 ºC ^{1}H NMR (DMSO-*d*$_6$) δ (ppm), *J* (Hz): 3.80 (s, 3H, OCH$_3$), 7.23-7.60 (m, 5H, H-5, H-7, H-8, H-3’, H-5’), 7.80 (d, 2H, H-2’, H-6’, *J* = 8.4), 8.86 (s, 1H, H-4), 9.01 (s, 1H, OH), 10.76 (s, 1H, NH). ^{13}C NMR (DMSO-*d*$_6$) δ (ppm): 161.2, 159.0, 156.2, 148.6, 148.3, 146.8, 126.6, 124.5, 122.5, 120.1, 119.3, 119.2, 118.9, 117.5, 114.7, 112.0, 56.0. MS/EI m/z (%): 312 (M+, 21), 311 (86), 204 (22), 203 (100), 119 (23).

B) Synthesis of chromone derivatives

Synthesis of 6-methylchromone-3-carbaldehyde (4b) and 6-methoxychromone-3-carbaldehyde (5b)

A solution of 5-methyl-2-hydroxyacetophenone (**2b**), or 5′-methoxy-2′-hydroxyacetophenone (**3b**) (6 mmol), in anhydrous *N,N*-dimethylformamide (12 mL) was stirred at -10 ºC for 30 minutes. Phosphoryl chloride (POCl$_3$) (12 mmol) was added dropwise at a temperature below -10 ºC during 1 hour. The mixture was stirred at room temperature for 15 h and poured into water (40 mL).[29] The product was filtered and washed with ethyl ether.

6-Methylchromone-3-carbaldehyde (4b) Yield: 78% ^{1}H NMR ($CDCl_3$) δ (ppm), *J* (Hz): 1.65 (s, 3H, CH_3),7.43 (d, 1H, H-8, *J* = 8.6), 7.55 (dd, 1H, H-7, *J* = 1.5, 8.6), 8.08 (d, 1H, H-5, *J* = 1.5), 8.52 (s, 1H, H-2), 10.39 (s, 1H, CHO) ^{13}C NMR ($CDCl_3$) δ (ppm): 188.7, 176.0, 160.5, 154.5, 136.9, 135.9, 125.5, 125.0, 120.2, 118.4, 21.0.

6-Methoxychromone-3-carbaldehyde (5b*)* Yield: 72% ^{1}H NMR ($CDCl_3$) δ (ppm), *J* (Hz): 3.93 (s, 3H, OCH3), 7.32 (dd, 1H, H-7, *J* = 3.1, 9.2), 7.47 (d, 1H, H-8, *J* = 9.2), 7.66 (d, 1H, H-5, *J* = 3.1), 8.53 (s, 1H, H-2), 10.41 (s, 1H, CHO). ^{13}C NMR ($CDCl_3$) δ (ppm): 188.8, 175.9, 160.2, 158.0, 151.0, 126.2, 124.5, 120.0, 119.7, 105.5, 56.1.

Synthesis of 6-methylchromone-3-carboxylic acid (6b) and 6-methoxychromone-3-carboxylic (7b)

A solution of sodium chlorite ($NaClO_2$) (80 %, 32 mmol) in water (25 mL) was added dropwise to a mixture of 6-methyl-4-oxo-*4H*-chromene-3-carbaldehyde (**4b**) or 6-methoxy-4-oxo-*4H*-chromene-3-carbaldehyde (**5b**) (8 mmol) in dicloromethane (50 mL) and sulfamic acid (NH_2SO_3H) (40 mmol) in water (50 mL) at 0 ºC. After 15 hours, the reaction was extracted with dicloromethane.[30] The combined organic phases were dried over Na_2SO_4, filtered and evaporated. The product was finally washed with ethyl ether.

6-Methylchromone-3-carboxylic acid (6b) Yield: 78% ^{1}H NMR (DMSO-d_6), δ (ppm), *J* (Hz): 2.47 (s, 3H, CH_3), 7.72-7.78 (m, 2H, H-7, H-8), 7.96 (s, 1H, H-5), 9.10 (s, 1H, H-2). ^{13}C NMR (DMSO-d_6) δ (ppm): 176.8, 164.4, 164.2, 154.6, 137.2, 137.1, 125.0, 123.4, 119.1, 114.4, 20.9.

6-Methoxychromone-3-carboxylic (7b) Yield: 60% ^{1}H NMR (DMSO-d_6), δ (ppm), *J* (Hz): 3.90 (s, 3H, OCH_3), 7.52-7.54 (m, 2H, H-5, H-8), 7.77-7.79 (m, 1H, H-7), 9.11 (s, 1H, H-2). ^{13}C NMR (DMSO-d_6) δ (ppm): 176.5, 164.3, 163.9, 157.9, 151.0, 125.0, 124.5, 120.9, 113.8, 105.6, 56.4.

Synthesis of chromone derivatives (**8b-21b)**

To a solution of the correspondent chromone-3-carboxylic acid (**6b** or **7b**, 2.6 mmol) in DMF (4 mL) $POCl_3$ (2.6 mmol) was added. The mixture was stirred at room temperature for 30 min for the *in situ* formation of the acyl chloride. Then, the aromatic amine with the desired aromatic pattern (for compounds **8b-21b**) was added. After 1-5 hours, the mixture was diluted with dichloromethane (20 mL), washed with H_2O (2 x 10 mL) and with saturated $NaHCO_3$ solution (2 x 10 mL). The organic phases were combined, dried, filtered and concentrated under reduced pressure. The crude product was purified by flash chromatography and/or crystallization.

***N*-Phenyl-6-methylchromone-3-carboxamide (8b**) Yield: 48% ^{1}H NMR (DMSO-d_6) δ (ppm), *J* (Hz): 2.46 (s, 3H, CH_3), 7.11-7.14 (m, 1H, H-4), 7.34-7.36 (m, 2H, H-3’, H-5’), 7.54-7.72 (m, 4H, H-7, H-8, H-2’, H-6’), 8.01 (d, 1H, H-5, *J* = 2.6), 9.00 (s, 1H, H-2), 11.39 (s, 1H, NH). ^{13}C NMR (DMSO-d_6) δ (ppm): 177.3, 162.8, 160.8, 154.5, 138.1, 136.8, 136.4, 129.0, 125.3, 124.4, 123.6, 120.4, 118.4, 115.6, 21.1. MS/EI m/z (%): 280 (M+, 28), 279 (M, 75), 187 (100), 135 (55), 77 (24).

***N*-(3-Methylphenyl)-6-methylchromone-3-carboxamide (9b)** Yield: 45% ^{1}H NMR ($CDCl_3$) δ (ppm), *J* (Hz): 2.37 (s, 3H, CH_3), 2.50 (s, 3H, CH_3), 6.91-6.98 (m, 1H, H-5’), 7.25 (dd, 1H, H-4’, *J* = 4.8, 10.8), 7.47 (dd, 1H, H-8, *J* = 8.6), 7.52-7.62 (m, 3H, H-7, H-2’, H-6’), 8.09 (d, 1H, H-5, *J* = 1.3), 9.03 (s, 1H, H-2), 11.38 (s, 1H, NH). ^{13}C NMR

($CDCl_3$) δ (ppm): 177.4, 162.6, 160.8, 154.5, 138.9, 138.0, 136.7, 136.1, 128.8, 125.5, 125.2, 123.8, 121.2, 118.2, 117.6, 115.9, 21.5, 21.1. MS/EI m/z (%): 293 (M, 60), 187 (100), 135 (36), 77 (22).

***N*-(3-Chlorophenyl)-6-methylchromone-3-carboxamide (10b)** Yield: 47% ^{1}H NMR (DMSO-d_6) δ (ppm), *J* (Hz): 2.51 (s, 3H, CH_3), 7.16 (ddd, 1H, H-4', *J* = 0.9, 2.0, 8.1), 7.38 (dd, 1H, H-5', *J* = 8.1, 8.1), 7.53 (ddd, 1H, H-6', *J* = 8.1, 2.0, 0.9), 7.69 (d, 1H, H-8, *J* = 8.6), 7.74 (dd, 1H, H-7, *J* = 2.0, 8.6), 7.98 (dd, 1H, H-2', *J* = 2.0, 2.0), 8.03 (dd, 1H, H-5, *J* = 2.0), 9.16 (s, 1H, H-2), 11.46 (s, 1H, NH). ^{13}C NMR (DMSO-d_6) δ (ppm): 178.2, 164.7, 162.0, 155.5, 140.8', 137.9, 137.8, 134.8, 131.8, 126.1, 125.2, 120.9, 119.9, 119.7, 116.5, 22.0. MS/EI m/z (%): 313 (M, 32), 187 (100), 135 (39), 77 (17).

***N*-(3-Hydroxyphenyl)-6-methylchromone-3-carboxamide (11b)** Yield: 11% ^{1}H NMR (DMSO-d_6) δ (ppm), *J* (Hz): 2.47 (s, 3H, CH_3), 6.55 (ddd, 1H, H-4', *J* = 0.7, 2.1, 8.2), 7.02 (d, 1H, H-6', *J* = 8.2), 7.16 (dd, 1H, H-5', *J* = 8.2, 8.2), 7.31 (dd, 1H, H-2', *J* = 2.1, 2.1), 7.68-7.77 (m, 2H, H-7, H-8), 8.00 (s, 1H, H-5), 9.12 (s, 1H, H-2), 9.53 (s, 1H, OH), 11.26 (s, 1H, NH). ^{13}C NMR (DMSO-d_6) δ (ppm): 177.1, 163.6, 160.8, 158.3, 154.5, 139.5, 137.0, 136.9, 130.2, 125.2, 123.6, 119.0, 115.9, 111.8, 111.0, 107.4, 21.0. MS/EI m/z (%): 295 (M, 52), 187 (100), 135 (51), 77 (17), 53 (23).

***N*-(4-Methylphenyl)-6-methylchromone-3-carboxamide (12b)** Yield 41% ^{1}H NMR ($CDCl_3$) δ (ppm), *J* (Hz): 2.36 (s, 3H, CH_3), 2.53 (s, 3H, CH_3), 7.19 (d, 2H, H-2', H-6', *J* = 8.2), 7.51 (d, 1H, H-8, *J* = 8.6), 7.61 (dd, 1H, H-7, *J* = 2.5, 8.6), 7.64 (d, 2H, H-3', H-5', *J* = 8.2), 8.13 (d, 1H, H-5, *J* = 2.5), 9.07 (s, 1H, H-2), 11.39 (s, 1H, NH). ^{13}C NMR ($CDCl_3$) δ (ppm): 178.4, 163.5, 161.6, 155.4, 137.6, 137.0, 136.4, 134.9, 130.4, 126.4, 124.7, 121.4, 119.1, 116.8, 22.0, 21.8. MS/EI m/z (%): 293 (M, 54), 187 (100), 135 (39), 77 (26), 53 (27).

***N*-(4-Chlorophenyl)-6-methylchromone-3-carboxamide (13b)** Yield 20% % ^{1}H NMR ($CDCl_3$) δ (ppm), *J* (Hz): 2.49 (s, 3H, CH_3), 7.28 (d, 2H, H-3’, H-5’, *J* = 8.2), 7.64 (d, 2H, H-2’, H-6’, *J* = 8.2), 7.72 (dd, 1H, H-7, *J* = 2.2, 8.5), 7.77 (d, 1H, H-8, *J* = 8.5), 8.24 (d, 1H, H-5, *J* = 2.2), 9.16 (s, 1H, H-2), 11.46 (s, 1H, NH). ^{13}C NMR ($CDCl_3$) δ (ppm): 178.5, 163.4, 161.0 155.9, 138.0, 137.9, 135.6, 134.1, 130.2, 126.1, 124.4, 122.0, 119.8, 116.8, 21.7. MS/EI m/z (%): 314 (M+, 21), 313 (M, 67), 187 (100), 135 (39).

***N*-(4-Hydroxyphenyl)-6-methylchromone-3-carboxamide (14b)** Yield: 18% ^{1}H NMR (DMSO-*d*$_6$) δ (ppm), *J* (Hz): 2.47 (s, 3H, CH_3), 6.78 (d, 2H, H-3’, H-5’, *J* = 8.8), 7.51 (d, 2H, H-2’, H-6’, *J* = 8.8), 7.70 (d, 1H, H-8, *J* = 8.6), 7.74 (dd, 1H, H-7, *J* = 2.0, 8.6), 8.00 (d, 1H, H-5, *J* = 2.0), 9.11(s, 1H, H-2), 11.11 (s, 1H, NH). ^{13}C NMR (DMSO-*d*$_6$) δ (ppm): 177.1, 163.4, 160.3, 154.5, 154.5, 136.9, 136.9, 130.1, 125.2, 123.6, 122.0, 119.0, 115.9, 115.9, 21.0. MS/EI m/z (%): 295 (M, 47), 187 (100), 135 (66), 77 (22), 53 (16).

***N*-Phenyl-6-methoxychromone-3-carboxamide (15b)** Yield: 60% ^{1}H NMR (DMSO-*d*$_6$) δ (ppm), *J* (Hz): 3.96 (s, 3H, OCH_3), 7.15-7.20 (m, 1H, H-4’), 7.37-7.41 (m, 2H, H-3’, H-5’), 7.43 (dd, 1H, H-7, *J* = 3.1, 9.2), 7.59 (d, 1H, H-8, *J* = 9.2), 7.68 (d, 1H, H-5, *J* = 3.1), 7.69-7.73 (m, 2H, H-2’, H-6’), 9.06 (s, 1H, H-2), 11.41 (s, 1H, NH). ^{13}C NMR (DMSO-*d*$_6$) δ (ppm): 179.0, 164.3, 163.0, 159.8, 152.9, 139.3, 130.7, 126.8, 126.5, 126.4, 122.4, 121.7, 116.7, 106.9, 57.6. MS/EI m/z (%): 295 (M, 50), 203 (100), 175 (26), 151 (23), 77 (39).

***N*-(3-Methylphenyl)-6-methoxychromone-3-carboxamide (16b)** Yield 42% ^{1}H NMR ($CDCl_3$) δ (ppm), *J* (Hz): 2.38 (s, 3H, CH_3), 3.94 (s, 3H, OCH_3), 6.94-6.99 (ddd, 1H, H-4’, *J* = 1.0, 2.0, 8.0), 7.26 (dd, 1H, H-5’, *J* = 8.0, 8.0), 7.37 (dd, 1H, H-7, *J* = 3.1, 9.2), 7.54 (m, 2H, H-8, H-6’), 7.59 (s, 1H, H-2’), 7.67 (d, 1H, H-5, *J* = 3.1), 9.06 (s, 1H, H-2), 11.42 (s, 1H, NH). ^{13}C NMR ($CDCl_3$) δ (ppm): 177.2, 162.4, 160.8, 157.9, 151.1, 138.9, 138.0, 128.9, 125.2, 125.0, 124.9, 121.2, 119.9, 117.6, 115.3, 105.2, 56.0, 21.5. MS/EI m/z (%): 309 (M, 62), 203 (100), 151 (40), 79 (14), 77 (14), 53 (18).

***N*-(3-Chlorophenyl)-6-methoxychromone-3-carboxamide (17b)** Yield: 49% ^{1}H NMR ($CDCl_3$) δ (ppm), *J* (Hz): 3.94 (s, 3H, OCH_3), 7.11 (ddd, 1H, H-4’, *J* = 1.0, 2.0, 8.0), 7.29 (dd, 1H, H-5’, *J* = 8.0, 8.0), 7.37 (dd, 1H, H-7, *J* = 2.8, 8.8), 7.51-7.58 (m, 2H, H-8, H-6’), 7.66 (d, 1H, H-5, *J* = 2.8), 7.89 (dd, 1H, H-2’, *J* = 2.0, 2.0), 9.05 (s, 1H, H-2), 11.55 (s, 1H, NH). ^{13}C NMR ($CDCl_3$) δ (ppm): 177.2, 162.6, 161.1, 158.0, 151.1, 139.2, 134.7, 130.0, 125.1, 124.8, 124.4, 120.6, 120.0, 118.4,115.0, 105.2, 56.0. MS/EI m/z (%): 331 (M+2, 18), 329 (M, 50), 203 (100), 173 (21), 151 (33).

***N*-(3-Hydroxyphenyl)-6-methoxychromone-3-carboxamide (18b)** Yield: 21% ^{1}H NMR (DMSO-d_6) δ (ppm), *J* (Hz): 3.96 (s, 3H, OCH_3), 6.65 (ddd, 1H, H-4’, *J* = 0.7, 2.3, 8.0), 7.10 (d, 1H, H-6’, *J* = 8.0), 7.20 (dd, 1H, H-5’, *J* = 8.0, 8.0), 7.33-7.68 (m, 5H, H-5, H-6, H-7, H-8, H-2’), 9.05 (s, 1H, H-2), 11.52 (s, 1H, NH). ^{13}C NMR (DMSO-d_6) δ (ppm): 178.2, 163.5, 162.2, 159.0, 158.4, 152.0, 139.4, 130.6, 125.8, 125.5, 120.9, 115.8, 112.8, 112.7, 108.6, 106.0, 56.6. MS/EI m/z (%): 311 (M, 61), 203 (100), 151 (42), 53 (29).

***N*-(4-Methylphenyl)-6-methoxychromone-3-carboxamide (19b)** Yield: 40% ^{1}H NMR ($CDCl_3$) δ (ppm), *J* (Hz): 2.34 (s, 3H, CH_3), 3.94 (s, 3H, OCH_3), 7.18 (d, 2H, H-2’, H-6’, *J* = 8.1), 7.37 (dd, 1H, H-7, *J* = 3.1, 9.2), 7.53 (d, 1H, H-8, *J* = 9.2), 7.63 (d, 2H, H-3’, H-5’, *J* = 8.5), 7.67 (d, 1H, H-5, *J* = 3.1), 9.06 (s, 1H, H-2), 11.39 (s, 1H, NH). ^{13}C NMR ($CDCl_3$) δ (ppm): 177.2, 162.4, 160.7, 157.9, 151.1, 135.5, 134.0, 129.5, 124.9, 124.9, 120.5, 119.9, 115.4, 105.2, 56.0, 20.9. MS/EI m/z (%): 310 (M+, 20), 309 (M, 78), 203 (100), 151 (25).

***N*-(4-Chlorophenyl)-6-methoxychromone-3-carboxamide (20b)** Yield: 32% ^{1}H NMR (DMSO-d_6) δ (ppm), *J* (Hz): 3.93 (s, 3H, OCH_3), 7.36 (d, 2H, H-3’, H’5’, *J* = 8.0), 7.48 (dd, 1H, H-7, *J* = 3.1, 9.2), 7.63 (d, 1H, H-5, *J* = 3.1), 7.70 (d, 1H, H-8, *J* = 9.2), 7.74 (d, 2H, H-2’, H-6’, *J* = 8.0), 9.14 (s, 1H, H-2), 11.51 (s, 1H, NH). ^{13}C NMR (DMSO-d_6) δ (ppm): 175.1, 161.5, 159.6, 156.2, 149.3, 136.0, 131.4, 127.4, 123.1, 123.0, 120.0, 119.9, 113.2, 104.0, 57.6. MS/EI m/z (%): 331 (M+2, 24), 329 (M, 57), 203 (100), 151 (28).

***N*-(4-Hydroxyphenyl)-6-methoxychromone-3-carboxamide (21b)** Yield: 24% ^{1}H NMR (DMSO-d_6) δ (ppm), *J* (Hz): 3.93 (s, 1H, OCH_3), 6.81 (d, 2H, H-2’, H-6’, *J* = 8.0), 7.44 (dd, 1H, H-7, *J* = 3.1, 9.2), 7.48 (d, 2H, H-3’, H-5’, *J* = 8.0), 7.63 (d, 1H, H-8, *J* = 9.2), 7.68 (d, 1H, H-5, *J* = 3.1), 9.03 (s, 1H, H-2), 11.40 (s, 1H, NH). ^{13}C NMR (DMSO-d_6) δ (ppm): 165.2, 162.4, 161.1, 158.1, 154.3, 151.1, 130.8, 124.7, 124.6, 122.3, 119.9, 115.3, 114.8, 105.1, 55.4. MS/EI m/z (%): 311 (M, 74), 203 (100), 151 (24).

Pharmacology.

Evaluation of monoamine oxidase (hMAOs) inhibitiory activity. The inhibitory activity of the compounds under study on both *h*MAO isoforms was assessed following a previously described method.[26] Briefly, the inhibitory activity on *h*MAOs was evaluated by measuring the effects of the coumarins and chromones derivatives on the production of hydrogen peroxide (H_2O_2) from p-tyramine, using the Amplex Red MAO assay kit (Molecular Probes, Inc., Eugene, OR, U.S.) and microsomal MAO isoforms prepared from insect cells (BTI-TN-5B1-4) infected with recombinant baculovirus containing cDNA inserts for *h*MAO-A or *h*MAO-B (Sigma-Aldrich Química S.A). The test compounds/ standard inhibitors and adequate amounts of recombinant *h*MAO-A or *h*MAO-B were incubated for 15 min at 37˚C in a flat-black-bottom 96-well microplate (BRANDplates, pureGradeTM, BRAND GMBH, Wertheim, Germany) with Amplex Red® reagent, 1 U/mL horseradish peroxidase, and 1 mM *p*-tyramine. The production of H_2O_2 and consequently of resorufin was quantified at 37˚C in a multimode microplate reader (Biotek Synergy HT), based on the fluorescence generated (excitation, 545 nm, emission, 590 nm) over a 15 min period, in which the fluorescence increased linearly. Control experiments were carried out simultaneously by replacing the test drugs (new compounds and standard inhibitors) with appropriate dilutions of the vehicles. The IC_{50} values were determined in triplicate from the dose-response inhibition curves and are expressed as mean ± standard deviation (SD). IC_{50} values are the mean ± S.D. from three experiments.

Evaluation of hMAO-A and hMAO-B kinetics. The steady-state kinetic parameters (K_m, Michaelis constant and V_{max}, maximum rate) of *h*MAO-A and *h*MAO-B the enzymatic activity of both isoforms were evaluated (under the experimental conditions described above) in the presence of different p-tyramine concentrations. Under our experimental conditions, *h*MAO-A displayed a K_m of 449.08 ± 28.42 µM and a V_{max} of 30.03 ± 0.6529 nmol/min whereas *h*MAO-B showed a K_m of 58.76 ± 11.67 µM and a V_{max} of 22.60 ± 1.018 nmol/min (*n*=3).

Evaluation of hMAO-B-inhibitor kinetics. To evaluate the mechanism of *h*MAO-B inhibition of coumarin **10a** and chromone **10b**, substrate-dependent kinetic experiments were performed. The catalytic rates of *h*MAO-B were measured at five different concentrations of p-tyramine substrate (0.031 – 2 mM) in the absence or presence of the selected inhibitors (compounds **10a** and **10b**) and standard inhibitors, at concentrations between 0.5 and 1.0 nM. The results are presented as double reciprocal Lineweaver-Burk plots (1/V vs. 1/[S]) and the kinetic data, namely Michaelis-Menten constant (K_m) and maximum reaction rate (V_{max}), was acquired employing Michaelis-Menten equation. The *Ki* values were estimated using Dixon plots, by replotting the slope of each Lineweaver-Burk plot versus the inhibitor concentration. In the Dixon plots, the *Ki* valued were obtained from the x-axis intercept ($–K_i$). The enzymatic reactions and measurements were performed using the same *h*MAO-B assay conditions as described above (n=3). Linear regression analysis was performed using Prism 5.

Evaluation of hMAO-B-inhibitior type of binding affinity. The analysis of the type of binding of compounds **10a** and **10b** and the standard inhibitors with *h*MAO-B was performed by a time-dependent inhibition assay. The enzyme was incubated for a 60 minute period with the chromone based inhibitors as well as the standard inhibitors at their IC_{80} values. The final well concentrations were: coumarin **10a** (12.5 nM), chromone **10b** (12.5 nM), (R)-(−)-deprenyl (50 nM), safinamide (40 nM) and rasagiline (200 nM) and MAO-B (6.4 µg/mL). Control experiments without inhibitors were run simultaneously. The enzymatic activity was determined as described above (see determination of *h*MAO isoform activity). The percentage of enzyme activity was plotted against the incubation time to determine time-dependent enzyme-inhibition. Data are the mean ± SD of three independent experiments.

Molecular modelling. Schrödinger Suite was adopted for computing all theoretical investigation. The 3D structures of **8-21 (a**, **b)** were built using the Maestro GUI[39] and, with the aim to take into account their most stable protomers at pH 7.4, submitted to LigPrep tool.[40] The Protein Data Bank[41] crystallographic entries 2Z5X[42] and 2V5Z[43] were used for building *h*MAO-A and *h*MAO-B theoretical models, respectively. In order to be suitable for our simulation, original PDB structures were modified by: a) removing ligands and co-crystallized water molecules, b) adding missing hydrogen atoms and c) fixing FAD connectivity. Ligand targets recognition evaluation was carried out by means of Glide software.[44] The binding site of both target models was defined by means of a regular grid box of about 64,000 $Å^3$ centred on the FAD N5 atom. Docking simulations were computed using Glide ligand flexible algorithm at standard precision (SP) level.

Acknowledgments

The authors would like to thank Fundação para a Ciência e Tecnologia (FCT) - QUI/UI0081/2013, POCI-01-0145-FEDER-006980 - for the financial support. Thanks are due to FCT, POPH and FEDER/COMPETE for A. Fonseca (SFRH/BD/80831/2011), J Reis (SFRH/BD/96033/2013) and M. J. Matos (SFRH/BPD/95345/2013) grants. The authors also thank the COST action CA15135 (Multi-Target Paradigm for Innovative Ligand Identification in the Drug Discovery Process, MuTaLig) for support.

References

1. Castellani, R. J.; Rolston, R. K.; Smith, M. a. *Disease-a-Month* **2010**, *56*, 484–546.
2. de Lau, L. M. L.; Breteler, M. M. B. *Lancet. Neurol.* **2006**, *5*, 525–35.
3. Farlow, M. R.; Cummings, J. L. *Am. J. Med.* **2007**, *120*, 388–397.
4. Tipton, K. F. *Cell Biochem. Funct.* **1986**, *4*, 79–87.
5. Johnson, J. P. *Biochem. Pharmacol.* **1968**, *17*, 1285–1297.
6. Ma, J.; Yoshimura, M.; Yamashita, E.; Nakagawa, A.; Ito, A.; Tsukihara, T. *J. Mol. Biol.* **2004**, *338*, 103–114.
7. Youdim, M. B.; Edmondson, D.; Tipton, K. F. *Nat Rev Neurosci* **2006**, *7*, 295–309.
8. Gaspar, A.; Milhazes, N. J. da S. P.; Santana, L.; Uriarte, E.; Borges, F.; Matos, M. J. *Curr. Top. Med. Chem.* **2015**, *15*, 432–445.
9. Rojas, R. J.; Edmondson, D. E.; Almos, T.; Scott, R.; Massari, M. E. *Bioorganic Med. Chem.* **2015**, *23*, 770–778.
10. Riederer, P. *Neurotoxicology* **2004**, *25*, 271–277.
11. Jain, V.; Langham, M. C.; Wehrli, F. W. *J. Cereb. Blood Flow Metab.* **2010**, *30*, 1598–1607.
12. Rouault, T. A. *Nat Rev Neurosci* **2013**, *14*, 551–564.
13. Hepworth, J. D.; Katritzky, A. R.; Rees, C. W. *Comprehensive Heterocyclic Chemistry*; **1984**.
14. Evans, B. E.; Rittle, K. E.; DiPardo, R. M.; Freidinger, R. M.; Whitter, W. L.; Lundell, G. F.; Veber, D. F.; Anderson, P. S.; Chang, R. S. L.; Lotti, V. J.; Cerino, D. J.; Chen, T. B.; Kling, P. J.; Kunkel, K. A.; Springer, J. P.; Hirshfield, J. *J. Med. Chem.* **1988**, *31*, 2235–2246.
15. Lachance, H.; Wetzel, S.; Kumar, K.; Waldmann, H. *J. Med. Chem.* **2012**, *55*, 5989–6001.

16. Polanski, J.; Kurczyk, A.; Bak, A.; Musiol, R. *Curr. Med. Chem.* **2012**, *19*, 1921–1945.

17. Chimenti, F.; Secci, D.; Bolasco, A.; Chimenti, P.; Bizzarri, B.; Granese, A.; Carradori, S.; Yáñez, M.; Orallo, F.; Ortuso, F.; Alcaro, S. *J. Med. Chem.* **2009**, *52*, 1935–1942.

18. Cagide, F.; Silva, T.; Reis, J.; Gaspar, A.; Borges, F.; Gomes, L. R.; Low, J. N. *Chem. Commun.* **2015**, *51*, 2832–2835.

19. Borges, F.; Roleira, F.; Milhazes, N.; Santana, L.; Uriarte, E. *Curr. Med. Chem.* **2005**, *12*, 887–916.

20. Matos, M.; Vazquez-Rodriguez, S.; Santana, L.; Uriarte, E.; Fuentes-Edfuf, C.; Santos, Y.; Munoz-Crego, A. *Med. Chem. (Los. Angeles).* **2012**, *8*, 1140–1145.

21. Srivastava, P.; Vyas, V. K.; Variya, B.; Patel, P.; Qureshi, G.; Ghate, M. *Bioorg. Chem.* **2016**, *accepted*.

22. Gaspar, A.; Matos, M. J.; Garrido, J.; Uriarte, E.; Borges, F. *Chromone: a valid scaffold in medicinal chemistry.*; **2014**; Vol. 114.

23. Cagide, F.; Reis, J.; Gaspar, A.; Chavarria, D.; Kachler, S.; Klotz, K. N.; Gomes, L. R.; Low, J. N.; Vilar, S.; Hripcsak, G.; Borges, F. *RSC Adv.* **2016**, *6*, 46972–46976.

24. Phosrithong, N.; Samee, W.; Nunthanavanit, P.; Ungwitayatorn, J. *Chem. Biol. Drug Des.* **2012**, *79*, 981–9.

25. Park, J. H.; Lee, S. U.; Kim, S. H.; Shin, S. Y.; Lee, J. Y.; Shin, C. G.; Yoo, K. H.; Lee, Y. S. *Arch. Pharm. Res.* **2008**, *31*, 1–5.

26. Reis, J.; Cagide, F.; Chavarria, D.; Silva, T. B.; Fernandes, C.; Gaspar, A.; Uriarte, E.; Remião, F.; Alcaro, S.; Ortuso, F.; Borges, F. M. *J. Med. Chem.* **2016**, *59*, 5879–5893.

27. Chimenti, F.; Bizzarri, B.; Bolasco, A.; Secci, D.; Chimenti, P.; Granese, A.; Carradori, S.; Rivanera, D.; Zicari, A.; Scaltrito, M. M.; Sisto, F. *Bioorganic Med. Chem. Lett.* **2010**, *20*, 4922–4926.

28. Murata, C.; Masuda, T.; Kamochi, Y.; Todoroki, K.; Yoshida, H.; Nohta, H.;

Yamaguchi, M.; Takadate, A. *Chem. Pharm. Bull. (Tokyo).* **2005**, *53*, 750–758.

29. Zhao, P. L.; Li, J.; Yang, G. F. *Bioorganic Med. Chem.* **2007**, *15*, 1888–1895.

30. Ishizuka, N.; Matsumura, K.; Sakai, K.; Fujimoto, M.; Mihara, S.; Yamamori, T. *J. Med. Chem.* **2002**, *45*, 2041–2055.

31. Gaspar, A.; Silva, T.; Yáñez, M.; Vina, D.; Orallo, F.; Ortuso, F.; Uriarte, E.; Alcaro, S.; Borges, F. *J. Med. Chem.* **2011**, *54*, 5165–5173.

32. Fonseca, A.; Matos, M. J.; Reis, J.; Duarte, Y.; Santana, L.; Uriarte, E.; Borges, F. *RSC Adv.* **2016**, *6*, 49764–49768.

33. Clark, D. E. *J. Pharm. Sci.* **1999**, *88*, 815–821.

34. Lipinski, C.; Lombardo, F.; Dominy, B. W.; Feeney, P. J. *Adv. Drug Deliv. Rev.* **2001**, *46*, 3–26.

35. Leeson, P. D.; Springthorpe, B. *Nat. Rev. Drug Discov.* **2007**, *6*, 881–890.

36. Barton, P.; Riley, R. J. *Drug Discov. Today* **2016**, *21*, 72–81.

37. Hitchcock, S. A.; Pennington, L. D. *J. Med. Chem.* **2006**, *49*, 7559–7583.

38. Pajouhesh, H.; Lenz, G. R. *J. Am. Socity Exp. Neurother.* **2005**, *2*, 541–553.

39. **Schrödinger Release 2016-4**: MS Jaguar, Schrödinger, LLC, New York, NY, 2016.

40. **Schrödinger Release 2016-4**: LigPrep, Schrödinger, LLC, New York, NY, 2016.

41. Berman, H. M.; Westbrook, J.; Feng, Z.; Gilliland, G.; Bhat, T. N.; Weissig, H.; Shindyalov, I. N.; Bourne, P. E. *Nucleic Acids Res.* **2000**, *28*, 235–242.

42. Son, S.-Y.; Ma, J.; Kondou, Y.; Yoshimura, M.; Yamashita, E.; Tsukihara, T. *Proc. Natl. Acad. Sci. U. S. A.* **2008**, *105*, 5739–5744.

43. Binda, C.; Wang, J.; Pisani, L.; Caccia, C.; Carotti, A.; Salvati, P.; Edmondson, D. E.; Mattevi, A. *J. Med. Chem.* **2007**, *50*, 5848–5852.

44. **Schrödinger Release 2016-4**: Glide, Schrödinger, LLC, New York, NY, 2016.

Manuscript V

Structural elucidation of a series of 6-methyl-3-carboxamidocoumarins.

Magnetic Resonance in Chemistry, **2016**, published online: DOI 10.1002/mrc.4541

Published online in Wiley Online Library

(wileyonlinelibrary.com) DOI 10.1002/mrc.4541

Structural elucidation of a series of 6-methyl-3-carboxamidocoumarins

Keywords: coumarin; 6-methyl-3-carboxamidocoumarin

Introduction

The original concept of privileged structure introduced by Evans in 1988 has evolved from the original meaning.[1] Nowadays, privileged structures can be defined as molecular frameworks that are able to provide potent and selective ligands for more than one type of biological targets through judicious structural modifications.[2] Benzopyran-based systems, namely chromones and coumarins, are actually recognized as privileged structures[3] and used as templates for the design of new chemical libraries for drug discovery programmes.[4]

Simple coumarins are considered an unparalleled template to perform structural modifications allowing the synthesis of an array of compounds with a remarkable pharmacological profile exhibiting diverse activities such as anticancer, antiviral, anti-inflammatory and antimicrobial.[5] Owing to the synthetic accessibility and substitution variability, this type of heterocyclic compounds play an important role not only in the organic chemistry but also in the medicinal chemistry field.

The application of coumarins in the development of therapeutic solutions for ageing-related diseases is still an emerging field even though the data acquired so far point out their importance in the development of novel drug candidates for targets ascribed to Alzheimer's and Parkinson's diseases. In the past years, our group has screened a large library of benzopyran-based derivatives towards monoaminoxidase isoforms (MAO-A and MAO-B). MAO-B is an important target in Parkinson's disease as it plays a key role in the metabolism of dopamine, a neurotransmitter critical for the maintenance of cognitive function.[6] Within this framework, some coumarin-based MAO-B inhibitors have been discovered.[5] Such knowledge led to an ongoing effort to improve their potency and selectivity, and as a result, a small library of 6-methyl-3-carboxamidocoumarin derivatives (Table 1) was designed and synthesized. Along this framework, a complete structural elucidation by one-dimensional (1D) and two-dimensional (2D) NMR techniques of the heterocyclic compounds is found to be relevant. Therefore, in this work, some coumarins of our library containing different electron donor groups in diverse positions of the exocyclic aromatic ring (Scheme 1, Table 1) were selected for complete structural analysis. Finally, to complete the study, single crystal X-ray crystallographic analysis of compound **3,** *N*-(4′-hydroxyphenyl)-6-methyl-3-carboxamidocoumarin, was carried out.

Experimental

General procedures

^{1}H NMR and ^{13}C NMR were recorded on a Bruker Avance III 400 NMR spectrometer operating at 400.14 and 100.62 MHz, respectively. For the ^{1}H NMR experiments, the relaxation delay was 90° pulse, spectral width of 8012 Hz and 65 K data points. In the case of the ^{13}C NMR experiments, the corresponding parameters were 30° pulse, 24038 Hz and 65 K, respectively, and 2.0 s relaxation delay. For the distortionless enhancement by polarization transfer (DEPT) sequence, the width of the 90° pulse for ^{13}C was 7.7 μs, and the 90° pulse for ^{1}H was 9.8 μs; the delay 2JC, H was set to 2.0 ms. For correlation spectroscopy (COSY) and heteronuclear single quantum coherence (HSQC), the data points were set to 2 K × 256 (t2 × t1) with a relaxation delay D_1 of 1.5 s. The heteronuclear multiple bond connectivity (HMBC) was acquired with data points set to 4 K × 256 (t2 × t1) and relaxation delay D_1 of 1 s. Furthermore, the long-range coupling time for HMBC was set to 71 ms. The data were processed using quadratic sine-bell weighting functions in both dimensions. The spectra were recorded at room temperature in 5 mm outer-diameter tubes. Samples were prepared in deuterated dimethyl sulfoxide (DMSO-d_6) for compounds **1–3** and deuterated chloroform ($CDCl_3$) for compounds **4–6**. Tetramethylsilane was used as internal standard, and chemical shifts (δ) were expressed in parts per million (ppm) and coupling constants (*J*) in Hertz. The ^{1}H and ^{13}C chemical shifts of DMSO-d_6 were 2.5 and 40.0 ppm and of $CDCl_3$ 7.3 and 77.0 ppm.

Electronic impact mass spectroscopy (EI/MS) was carried out on a VG AutoSpec (Fison, Ipswich, UK) instrument, and data were reported as m/z (percentage of relative intensity of the most important fragments).

X-ray diffraction

A crystal of compound **3** (recrystallized from methanol) was used for X-ray crystallographic analysis. Information about crystal data, experimental data collection conditions and refinement as well as the structural geometric parameters are available as an Electronic Supplementary Publication from the Cambridge Crystallographic Data Centre[7] (CCDC-1479922) at https://www.ccdc.cam.ac.uk/structures in CIF format. The compound crystallized in space group P-1 with two molecules in the asymmetric unit as a hemisolvate.

Materials

Starting materials and reagents were obtained from commercial suppliers and were used without further purification (Sigma-Aldrich, Portugal). Melting points (mp) are uncorrected and were determined with a Reichert Kofler thermopan or with a Büchi 510 apparatus. Flash chromatography was performed on silica gel (Merck 60, 230–400 mesh), and thin-layer chromatography (TLC) was performed on pre-coated silica gel plates (Merck 60 F254). The spots were visualized under UV detection (254 and 366 nm). Following the workup, the organic solutions were dried over

Table 1. Structure, names, melting points, yields and mass spectroscopy analysis of compounds **1–6**

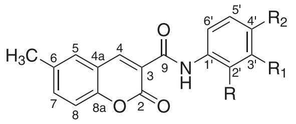

Compound	*R*	*R*$_1$	*R*$_2$	Name	MS/EI (rel. int.)	Melting point/°C	Yield (%)
1	OH	H	H	*N*-(2'-hydroxyphenyl)- 6-methyl-3-carboxamidocoumarin	295 (M, 46), 187 (100), 115 (12)	274–275	56
2	H	OH	H	*N*-(3'-hydroxyphenyl)- 6-methyl-3-carboxamidocoumarin	296 (M$^+$, 40), 295 (M, 99), 187 (100), 115 (64), 103 (51)	217–218	61
3	H	H	OH	*N*-(4'-hydroxyphenyl)- 6-methyl-3-carboxamidocoumarin	296 (M$^+$, 26), 295 (M, 92), 187 (100), 115 (25), 103 (18)	230–231	61
4	OCH_3	H	H	*N*-(2'-methoxyphenyl)- 6-methyl-3-carboxamidocoumarin	310 (M$^+$, 29), 309 (M, 78), 187 (100), 115 (34), 77 (20).	204–205	82
5	H	OCH_3	H	*N*-(3'-methoxyphenyl)- 6-methyl-3-carboxamidocoumarin	310 (M$^+$, 16), 309 (M, 66), 187 (100), 115 (33), 77 (20).	174–175	74
6	H	H	OCH_3	*N*-(4'-methoxyphenyl)- 6-methyl-3-carboxamidocoumarin	310 (M$^+$, 70), 309 (M, 96), 187 (100), 115 (62), 77 (44)	199–200	73

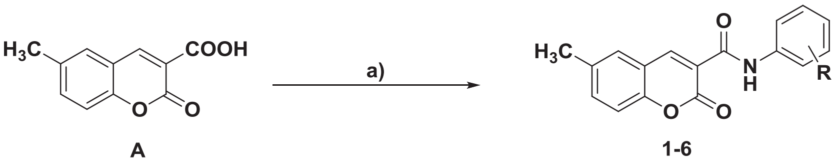

Scheme 1. Reagents and conditions: a) EDC, DMAP, DCM, aromatic amine with the appropriate substituent, 0 °C to r.t., 4 h.

Na_2SO_4. Solvents were evaporated in a Buchi Rotavapor. Organic solutions were dried over anhydrous Na_2SO_4.

Synthesis of coumarin derivatives (1–6)

The starting material 6-methylcoumarin-3-carboxylic acid (**A**) was synthesized in an 89% yield according to a previously described method.[8] The structural data (NMR and MS) were in accordance with the literature.[9]

General synthetic method

Compound **A** (1 mmol) was dissolved in dichloromethane (10 ml), and then 1-ethyl-3-(3-dimethylaminopropyl)carbodiimide (1.1 mmol) and 4-dimethylaminopyridine (1.1 mmol) were added. The mixture was stirred under a positive argon pressure at 0 °C for 5 min.[10] After this period, the aromatic amine with the appropriated substitution pattern was added. The reaction mixture was stirred for 4 h at room temperature. Upon completion, the crude products were filtered and purified by flash chromatography (hexane/ethyl acetate 9 : 1) or recrystallization (ethanol) to give the desired products (**1–6**) in yields ranging from 56% to 82% (Table 1).[11]

Results and discussion

The synthetic strategy briefly described in Scheme 1, was used to efficiently obtain the coumarin derivatives (**1–6**) with an overall yield between 56% and 82%.

All synthesized coumarins (**1–6**) are listed in Table 1. To complete compounds characterization, the melting point and mass spectrometry of all the derivatives were also acquired and the data included in Table 1. The unambiguous assignment of all protons and carbons of coumarin derivatives was achieved by means of 1D and 2D resonance techniques. The NMR data are depicted in Tables 2 and 3.

Firstly, the NMR data of compound **1** were acquired. From ^{1}H and ^{13}C spectra, 13 protons and 17 carbons were observed. In the ^{1}H NMR spectrum (Table 2) the signal at 8.98 ppm was set up as H-4, a characteristic singlet of coumarin nucleus. The protons of the methyl substituent were readily assigned from the spectrum and are found to resonate at 2.41 ppm. Additionally, the protons at 7.83, 7.61 and 7.46 ppm were found to correlate with each other. Taking into account COSY data and proton multiplicity pattern, it was concluded that these protons take part of the coumarin core: A *meta* coupling of 1.5 Hz at 7.83 ppm consistent with H-5, an *ortho* and *meta* coupling of 8.5 and 1.5 Hz at 7.61 ppm and an *ortho* coupling of 8.5 Hz at 7.46 ppm, which are consistent with H-7 and H-8, respectively, were observed. From HSQC data, it was possible to assign the carbons bonded to the protons of the coumarin nucleus. Accordingly, the peaks located at 148.7, 130.4, 135.9 and 116.5 ppm were assigned as C-4, C-5, C-7 and C-8, respectively. As COSY indicates the correlation with coupled protons, it was concluded that the four protons located at 6.83, 6.92, 6.96 and 8.39 ppm correlate to each other. Based on their multiplicity pattern and HMBC data, they were unequivocally assigned to the protons H-5', H-3', H-4' and H-6', respectively. The exocyclic aromatic ring protons have been found to be bonded to the carbons resonating at 119.6, 115.1, 124.8 and 120.4, respectively. By a linear combination of DEPT-135 and proton decoupled ^{13}C spectra, eight quaternary carbons at 118.8, 119.1, 127.0, 135.1, 147.1, 152.7, 159.4 and 161.6 ppm were observed. From 2D spectra analysis, it was concluded that the signals at 7.61 ppm (H-7) and at 7.46 ppm (H-8)

Table 2. ^{1}H NMR chemical shifts, multiplicity and coupling constants of coumarins **1–6**

	Compounds					
Position	**1**[a]	**2**[a]	**3**[a]	**4**[b]	**5**[b]	**6**[b]
4	8.98 (s)	8.82 (s)	8.82 (s)	8.94 (s)	8.96 (s)	8.95 (s)
5	7.83 (d, 1.5)	7.78 (d, 1.5)	7.78 (d, 1.6)	*	**	*
				7.46–7.50 (m)	7.46–7.50 (m)	7.46–7.50 (m)
7	7.61 (dd, 1.5, 8.5)	7.60 (dd, 1.5, 8.5)	7.58 (dd, 1.6, 8.5)	*	**	*
8	7.46 (d, 8.5)	7.45 (d, 8.5)	7.44 (d, 8.5)	7.32 (d, 8.1)	7.34 (d, 9.1)	7.33 (d, 9.1)
2′	—	7.31 (dd, 2.1, 2.1)	7.51 (d, 8.7)	—	**	7.65 (d, 9.0)
3′	6.92 (dd, 1.7, 8.0)	—	6.77 (d, 8.7)	6.94 (dd, 1.6, 8.0)	—	6.91 (d, 9.0)
4′	6.94–6.98 (m)	6.56 (ddd, 1.0, 2.1, 8.1)	—	7.11 (ddd, 1.6, 7.8, 8.0)	6.72 (ddd, 1.4, 2.5, 7.8)	—
5′	6.83 (ddd, 1.7, 6.8, 8.0)	7.16 (dd, 8.1, 8.1)	6.77 (d, 8.7)	7.00 (ddd, 1.6, 7.8, 8.0)	7.27 (dd, 7.8, 8.1)	6.91 (d, 9.0)
6′	8.39 (dd, 1.4, 8.0)	7.01–7.05 (m)	7.51 (d, 8.7)	8.54 (dd, 1.6, 8.0)	7.22 (ddd, 1.4, 1.6, 8.1)	7.65 (d, 9.0)
CH_3	2.41 (s)	2.40 (s)	2.40 (s)	2.45 (s)	2.46 (s)	2.46 (s)
OH	10.22 (s)	9.54 (s)	9.38 (s)	—	—	—
OCH_3	—	—	—	3.97 (s)	3.84 (s)	3.82 (s)
NH	11.12 (s)	10.58 (s)	10.47 (s)	11.31 (s)	10.87 (s)	10.75 (s)

[a] Solvent was DMSO-d_6.
[b] Solvent was $CDCl_3$.
*H-7 is more downshielded than H-5 (from HSQC data).
**The multiplet integrates for three protons. H-2′ is upshielded in relation to H-5 and H-7 (from HSQC data).

Table 3. ^{13}C NMR chemical shifts of compounds **1–6**

	Compounds					
Position	**1**[a]	**2**[a]	**3**[a]	**4**[b]	**5**[b]	**6**[b]
2	161.6	161.2	161.2	161.7	162.0	162.0
3	119.1	120.3	120.2	119.0	118.6	118.6
4	148.7	147.7	147.6	148.5	148.5	148.6
4a	118.8	118.7	118.7	118.5	118.4	118.6
5	130.4	130.2	130.1	129.4	129.5	129.5
6	135.1	135.2	135.1	135.2	135.4	135.4
7	135.9	135.7	135.6	135.3	135.6	135.4
8	116.5	116.5	116.4	116.4	116.4	116.4
8a	152.7	152.5	152.5	152.8	152.7	152.7
9	159.4	160.2	159.6	159.3	159.5	159.2
1′	127.0	139.4	130.0	127.8	138.9	131.0
2′	147.1	107.3	122.0	149.2	106.0	122.1
3′	115.1	158.3	115.3	110.3	160.2	114.2
4′	124.7	111.9	154.6	124.5	111.1	156.7
5′	119.4	130.2	115.3	120.7	129.7	114.2
6′	120.4	111.0	122.0	121.0	112.8	122.1
CH_3	20.7	20.7	20.7	20.8	20.8	20.8
OCH_3	—	—	—	56.0	55.4	55.5

[a] Solvent was DMSO-d_6.
[b] Solvent was $CDCl_3$.

have a long-range correlation with the carbons at 152.7 and 118.8 ppm, respectively. Based on their dissimilar chemical environment the signals were assigned to carbons C-8a and C-4a, respectively. The signals at 161.6 and at 159.4 ppm were assigned to C-2 and C-9, respectively, as they exhibit long-range interactions with H-4 and NH/H-4, respectively (Fig. 1A). Moreover, a long-range interaction was observed between the signal of the proton H-4 and the signal at 119.1 ppm that was assigned as C-3. However, the unequivocal assignment of the quaternary carbons C-1′ and C-2′ was not possible to be performed from analysis of the HMBC spectrum. For that reason, C-1′ was assigned at 127.0 ppm and C-2′ at 147.1 ppm using the increment system to estimate carbon chemical shifts of substituted benzene.[12] Conversely, the long-range couplings that occur between the proton peak at 10.22 ppm and three carbon peaks (C1′, C2′ and C3′) observed in HMBC (Fig. 1B) allowed the unequivocal assignment of the proton of the hydroxyl function. The chemical shifts of OH and NH protons have been strongly affected by the presence of the two intramolecular hydrogen bonds.

As all the compounds herein reported (compounds **1–6**, Table 1) own the same coumarin nucleus substitution pattern (3-carboxamide-6-methylcoumarin) as compound **1**, the unambiguous assignment of the subsubstructure was performed directly from their 1D and 2D NMR spectra (Tables 2 and 3). However, as they have different substitution patterns on the exocyclic aromatic substituent, a thorough spectral analysis was carried out for compound **2**, which has a hydroxyl group in the *meta* position, and compound **3**, which has a hydroxyl group in *para* position. A correlation analysis similar to that performed for compound **1** was tracked.

For compound **2**, H-2′, H-4′, H-5′ and H-6′ protons were assigned taking into account the multiplicity pattern of each signal in the ^{1}H NMR spectrum (Table 2), COSY and HMBC correlation data (Fig. 2). The peak at 7.31 ppm was assigned as H-2′ because it shows a multiplicity pattern of *doublet of doublets* with a constant of 2.1 Hz, owed to the coupling of two *meta* protons. H-4′ was attributed to the signal at 6.56 ppm, while the peaks at 7.16 and 7.03 ppm were identified as H-5′ and H-6′, respectively, based on their multiplicity patterns. The corresponding carbons were ascribed based on the HSQC data. Thus, the carbon directly attached to proton H was assigned as 107.3 ppm, and C-4′ resonate at 111.9 ppm. The quaternary carbons of the exocyclic aromatic ring, namely, C-1′ and C-3′, were assigned taking into account DEPT-135 and HMBC data. The peak at 139.4 ppm was labelled as C-1′ as it has a long-range

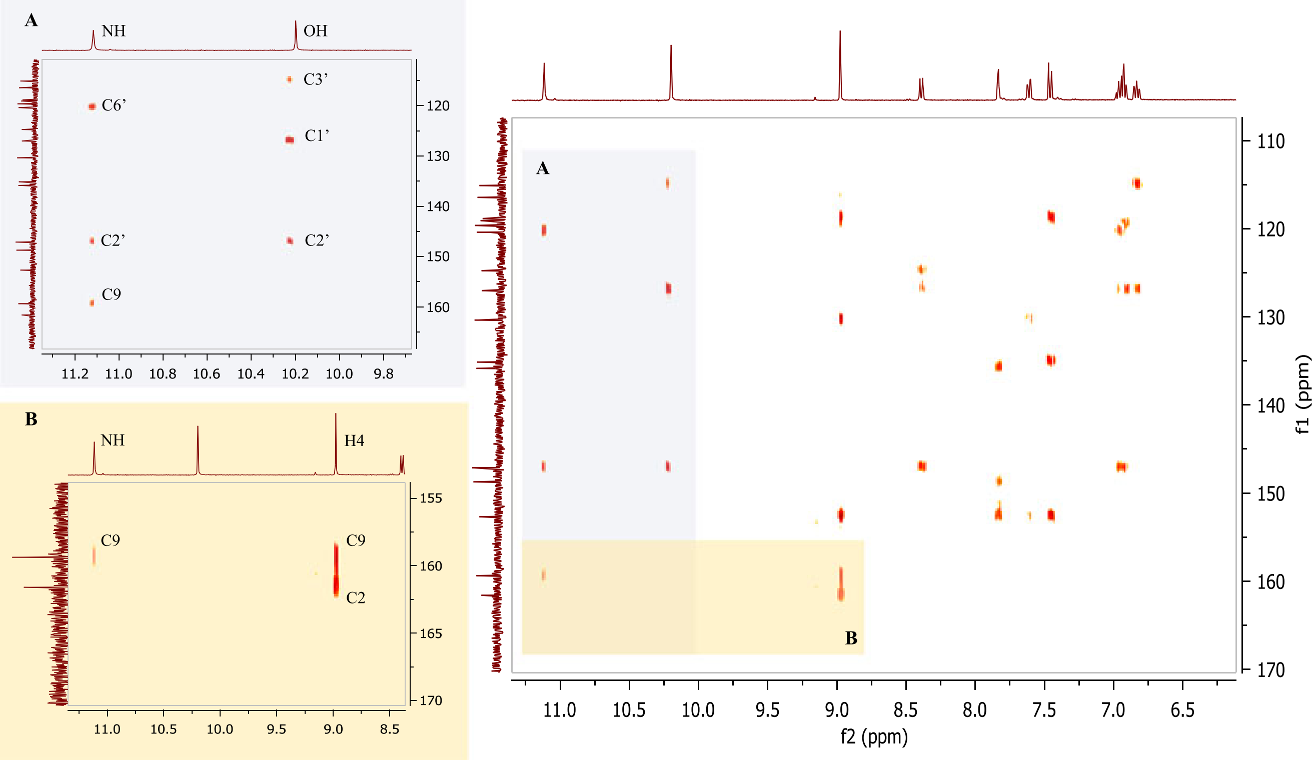

Figure 1. HMBC spectrum of compound **1**. Sections of the long-range couplings of proton peaks (A) at 10.22 ppm (–OH) and 11.12 ppm (NH) and (B) at 8.98 (H4) and at 11.12 ppm (NH) with structural and carbonyl carbons peaks, respectively, are shown.

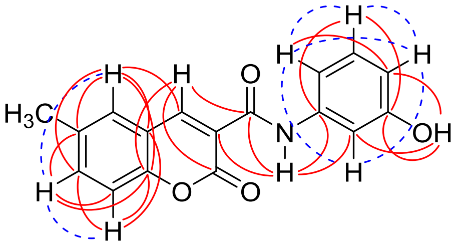

Figure 2. Correlations observed in COSY (dotted lines) and HMBC (solid lines) spectra of compound **2**.

interaction with the proton of the hydroxyl group. The signal at 158.3 ppm was attributed to C-3′.

Regarding compound **3**, the ^{1}H NMR spectrum showed the presence of equivalent protons with the signals at 7.51 and 6.77 ppm. Bearing in mind that the proton of the amide group shows a long-range interaction with two carbons at 122.0 ppm while the proton of the hydroxyl group possess a long-range interaction with other two carbons at 115.3 ppm, C-2′ and C-6′ were then assigned at 122.0 ppm. As a result, C-3′ and C-5′ were found to resonate at 115.3 ppm. From HSQC data, the peak at 7.51 ppm was attributed to both H-2′ and H-6′, whereas H-3′ and H-5′ were assigned with the signal at 6.77 ppm. In both cases, a difference of NH and OH proton shifts was observed, when compared with compound **1**, owing to the absence of one of the intramolecular hydrogen bonds.

The NMR signal assignments of compounds **4**, **5** and **6** were performed by a correlation with the data acquired for compounds **1**, **2** and **3** (Tables 2 and 3). However, owing to solubility constraints, the spectra were recorded using $CDCl_3$ as solvent instead of DMSO-d_6. So, a slight alteration on chemical shift values was observed. The main changes were found in the ^{1}H NMR multiplicity signals of the coumarin nucleus. In the ^{1}H NMR spectra of compounds **4**, **5** and **6,** the H-5 and H-7 appeared as multiplets. In the case of compound **5,** it was found a similar multiplet that was assigned as H-5, H-7 and H-2′, as it integrates for three protons. From the HSQC spectra (compounds **4** and **6**), we can observe that H-7 is more downshielded than H-5. In the case of compound 5, proton H-2′ is upshielded in relation to H-5 and H-7.

X-ray diffraction

Compound **3** provided suitable crystals for X-ray analysis. The thermal ellipsoid plot for compound **3** together with the adopted numbering scheme is shown in Fig. 3. There are two molecules in the asymmetric unit connected by hydrogen bonding via a methanol solvent molecule. The configuration of the molecule is given by the C–N rotamer of the amide that defines the position of the aromatic rings with respect to one another: Both molecules display an *anti* configuration, with respect to carbonyl of the coumarin (Table 1), thus allowing for the establishment of an N–H···O intramolecular H bond (geometric parameters are given in Table 4). In addition, there is a weak hydrogen bond linking the exocyclic aromatic ring, namely, between H-2′ and the carbonyl of the amide group. Both intramolecular bonds form pseudo S6 rings interactions in each molecule. The two molecules, named as A and B, are linked by one molecule of methanol solvent via hydrogen bonding where the methanol acts as a bridge because its oxygen atom acts as acceptor of the 4′-hydroxyl group of one molecule of **3** and as a donor to the amide carbonyl oxygen atom in the other molecule. An inspection of the bond lengths shows that there is a slightly asymmetry of the electronic distribution around the pyrone ring:

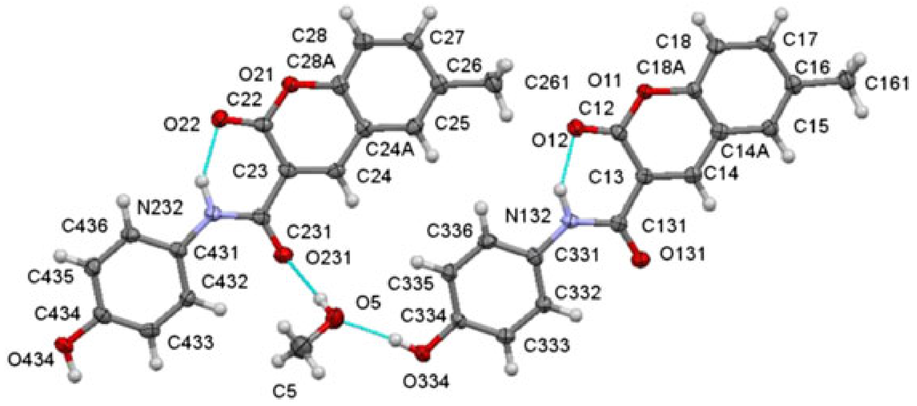

Figure 3. Structure and the adopted numbering scheme of compound **3**.

Table 4. Hydrogen bond geometry (distances in Å and angles in °) for compound **3**

D–H···*A*	*D*–H	H···*A*	*D*···*A*	*D*–H···*A*
O5–H5···O231	0.83	1.89	2.719 (2)	176
O334–H334···O5	0.86	1.80	2.655 (2)	173
N132–H132···O12	0.92 (3)	1.83 (3)	2.655 (2)	148 (2)
C332–H332···O131	0.95	2.38	2.972 (2)	120
N232–H232···O22	0.94 (3)	1.87 (3)	2.675 (2)	143 (2)
C432–H432···O231	0.95	2.34	2.936 (2)	120

Table 5. Selected dihedral angles, ° for compound **3**

Compound	θ_1°	θ_2°	θ_3°
A	3.28 (11)	3.0 (2)	4.4 (2)
B	2.06 (12)	2.2 (3)	1.1 (3)

θ_1 is the dihedral angle between the mean planes of the coumarin and exocyclic benzene ring . θ_2 is the dihedral angle between the mean planes of the coumarin ring and the plane defined by the OCN amide atoms. θ_3 is the dihedral angle between the mean planes of the exocyclic benzene ring and the plane defined by the OCN amide atoms.

The C23–C24 and C13–C14 bonds (Fig. 3), correspondent to the pyrone double bond of each molecule, distances have values of 1.350(3) and 1.352(2) Å, respectively. The shorter distance values, which are lower than that expected for a *Car–Car* bond, indicate the existence of a higher electronic density area in the pyrone ring. The values for distances of C13–C131 and C23–C231 bonds connecting the coumarin to the amide spacer are typical of a C_{sp3}–C_{sp3} bond conferring freedom for the rotation of the phenylamide substituent around it. The dihedral angles between the mean planes of the coumarin, OCN spacer and exocyclic aromatic ring (Table 5) indicate that the molecules are essentially planar.

Conclusions

In the present work, 6-methyl-3-carboxamidocoumarin derivatives (compounds **1–6**), bearing electron-donating substituents in different positions of the exocyclic aromatic ring, were synthesized in good yields and in mild reaction conditions and characterized by homonuclear and heteronuclear NMR techniques. Their unequivocal identification constitutes a valuable database for the accurate identification of the coumarins of our library. In addition, these results can be used as reference for structural elucidation of newer naturally occurring and synthetic coumarins.

Acknowledgements

This project was supported by the Foundation for Science and Technology (FCT) and FEDER/COMPETE2020 (UID/QUI/00081/2015 and POCI-01-0145-FEDER-006980).

The authors thank Fundação para a Ciência e Tecnologia (FCT) for their grants. A. Fonseca (SFRH/BD/80831/2011), A. Gaspar (SFRH/BPD/93331/2013) and M. J. Matos (SFRH/BPD/95345/2013) were supported by grants from the FCT, POPH and QREN. Crystallographic data were collected at the Engineering and Physical Sciences Research Council (EPSRC) X-ray crystallography service UK. Thanks are due to the staff at the National Crystallographic Service, University of Southampton for the data collection, help and advice.[13]

André Fonseca,[a] Alexandra Gaspar,[a] Maria João Matos,[a] Ligia R. Gomes,[b,c] John N. Low,[d] Eugenio Uriarte[e] and Fernanda Borges[a]*

[a]*CIQUP/Department of Chemistry and Biochemistry, Faculty of Sciences, University of Porto, Porto, Portugal*
[b]*FP-ENAS-Faculdade de Ciências de Saúde, Escola Superior de Saúde da UFP, Universidade Fernando Pessoa, Rua Carlos da Maia, Porto, Portugal*
[c]*REQUIMTE, Department of Chemistry and Biochemistry, Faculty of Sciences, University of Porto, Porto, Portugal*
[d]*Department of Chemistry, University of Aberdeen, Old Aberdeen, Scotland*
[e]*Department of Organic Chemistry, Faculty of Pharmacy, University of Santiago de Compostela, Santiago de Compostela, Spain*

**Correspondence to: Fernanda Borges, CIQUP/Department of Chemistry and Biochemistry, Faculty of Sciences, University of Porto, Porto, Portugal.*
E-mail: fborges@fc.up.pt

Received: 13 June 2016 Revised: 5 October 2016 Accepted: 8 October 2016

References

[1] B. E. Evans, K. E. Rittle, M. G. Bock, R. M. DiPardo, R. M. Freidinger, W. L. Whitter, G. F. Lundell, D. F. Veber, P. S. Anderson. *J. Med. Chem.* **1988**, *31*, 2235–2246.

[2] M. E. Welsch, S. A. Snyder, B. R. Stockwell. *Curr. Opin. Chem. Biol.* **2010**, *14*, 347–361.

[3] (a) R. W. DeSimone, K. S. Currie, S. A. Mitchell, J. W. Darrow, D. A. Pippin. *Comb. Chem. High Throughput Screen.* **2004**, *7*, 473–494; (b) J. Klekota, F. P. Roth. *Bioinformatics* **2008**, *24*, 2518–2525; (c) H. Lachance, S. Wetzel, K. Kumar, H. Waldmann. *J. Med. Chem.* **2012**, *55*, 5989–6001; (d) J. Polanski, A. Kurczyk, A. Bak, R. Musiol. *Curr. Med. Chem.* **2012**, *19*, 1921–1945; (e) V. R. Solomon, H. Lee. *Curr. Med. Chem.* **2011**, *18*, 1488–1508.

[4] A. Gaspar, N. Milhazes, L. Santana, E. Uriarte, F. Borges, M. J. Matos. *Curr. Top. Med. Chem.* **2015**, *15*, 432–455.

[5] (a) C. Kontogiorgis, D. J. Hadjipavlou-Litina. *Enzyme Inhib. Med. Chem.* **2003**, *18*, 63–69; (b) F. Borges, F. Roleira, N. Milhazes, L. Santana, E. Uriarte. *Curr. Med. Chem.* **2005**, *12*, 887–916; (c) F. Borges, F. M. F. Roleira, N. Milhazes, E. Uriarte, L. Santana. *Front. Med. Chem.* **2009**, *4*, 23–85; (d) M. Riveiro, N. De Kimpe, A. Moglioni, R. Vazquez, F. Monczor, C. Shayo, C. Davio. *Curr. Med. Chem.* **2010**, *17*, 1325–1338; (e) S. Vazquez-Rodriguez, M. J. Matos, L. Santana, E. Uriarte, F. Borges, S. Kachler, K. N. Klotz. *J. Pharm. Pharmacol.* **2013**, *65*, 697–703; (f) I. Kostova, S. Bhatia, P. Grigorov, S. Balkansky, V. S. Parmar, A. K. Prasad, L. Saso. *Curr. Med. Chem.* **2011**, *18*, 3929–3951; (g) M. J. Matos, S. Vazquez-Rodriguez, L. Santana, E. Uriarte, C. Fuentes-Edfuf, Y. Santos, A. Muñoz-Crego. *Molecules* **2013**, *18*, 1394–1404.

[6] (a) M. J. Matos, D. Viña, P. Janeiro, F. Borges, L. Santana, E. Uriarte. *Bioorg. Med. Chem. Lett.* **2010**, *20*, 5157–5160; (b) M. J. Matos, D. Viña, E. Quezada, C. Picciau, G. Delogu, F. Orallo, L. Santana, E. Uriarte. *Bioorg. Med. Chem. Lett.* **2009**, *19*, 3268–3270.

[7] S. J. Coles, P. A. Gale. *Chem. Sci.* **2012**, *3*, 683–689.

[8] F. Chimenti, B. Bizzarri, A. Bolasco, D. Secci, P. Chimenti, A. Granese, S. Carradori, D. Rivanera, A. Zicari, M. Scaltrito, F. Sisto. *Bioorg. Med. Chem. Lett.* **2010**, *20*, 4922–4926.

[9] S. Robert, C. Bertolla, B. Masereel, J. Dogné, L. Pochet. *J. Med. Chem.* **2008**, *51*, 3077–3080.

[10] C. Murata, T. Masuda, Y. Kamochi, K. Todoroki, H. Yoshida, H. Nohta, M. Yamaguchi, A. Takadate. *Chem. Pharm. Bull. (Tokyo)* **2005**, *53*, 750–758.

[11] A. Fonseca, M. J. Matos, J. Reis, Y. Duarte, M. Gutierrez, L. Santana, E. Uriarte, F. Borges. *RSC Adv.* **2016**, *6*, 49764–49768.

[12] D. E. Ewing. *Org. Magn. Reson.* **1979**, *12*, 499–524.

[13] S. J. Coles, P. A. Gale. *Chem. Sci.* **2012**, *3*, 683–689.

Manuscript VI

Crystal structures of three 6-substituted coumarin-3-carboxamide derivatives.

Acta Crystallographica Section E: Structure Reports Online, Volume 72, **2016**, Pages 926-932

Acta Cryst E
CRYSTALLOGRAPHIC COMMUNICATIONS

ISSN 2056-9890

Crystal structures of three 6-substituted coumarin-3-carboxamide derivatives

Lígia R. Gomes,[a,b] John Nicolson Low,[c]* André Fonseca,[d] Maria João Matos[d] and Fernanda Borges[d]

[a]REQUIMTE, Departamento de Química e Bioquímica, Faculdade de Ciências da Universidade do Porto, Rua do Campo Alegre, 687, P-4169-007, Porto, Portugal, [b]FP-ENAS-Faculdade de Ciências de Saúde, Escola Superior de Saúde da UFP, Universidade Fernando Pessoa, Rua Carlos da Maia, 296, P-4200-150 Porto, Portugal, [c]Department of Chemistry, University of Aberdeen, Meston Walk, Old Aberdeen AB24 3UE, Scotland, and [d]CIQUP/Departamento de Química e Bioquímica, Faculdade de Ciências, Universidade do Porto, 4169-007 Porto, Portugal. *Correspondence e-mail: jnlow111@gmail.com

Received 24 May 2016
Accepted 29 May 2016

Edited by W. T. A. Harrison, University of Aberdeen, Scotland

Keywords: crystal structure; coumarin; carboxamide.

CCDC references: 1482450; 1482449; 1482448

Supporting information: this article has supporting information at journals.iucr.org/e

Three coumarin derivatives, *viz*. 6-methyl-*N*-(3-methylphenyl)-2-oxo-2*H*-chromene-3-carboxamide, $C_{18}H_{15}NO_3$ (**1**), *N*-(3-methoxyphenyl)-6-methyl-2-oxo-2*H*-chromene-3-carboxamide, $C_{18}H_{15}NO_4$ (**2**), and 6-methoxy-*N*-(3-methoxyphenyl)-2-oxo-2*H*-chromene-3-carboxamide, $C_{18}H_{15}NO_5$ (**3**), were synthesized and structurally characterized. The molecules display intramolecular N—H$\cdots$O and weak C—H$\cdots$O hydrogen bonds, which probably contribute to the approximate planarity of the molecules. The supramolecular structures feature C—H$\cdots$O hydrogen bonds and π–π interactions, as confirmed by Hirshfeld surface analyses.

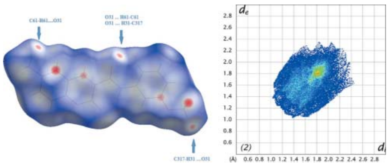

OPEN ACCESS

1. Chemical context

Benzopyrones are oxygen-containing heterocycles recognised as privileged structures for drug-discovery programs (Klekota & Roth, 2008; Lachance *et al.*, 2012). Within this class of compounds, coumarin has emerged as an interesting building block due to its synthetic accessibility and substitution variability. Furthermore, coumarins display anticancer, antiviral, anti-inflammatory and anti-oxidant biological properties (Matos *et al.*, 2009, 2014; Vazquez-Rodriguez *et al.*, 2013).

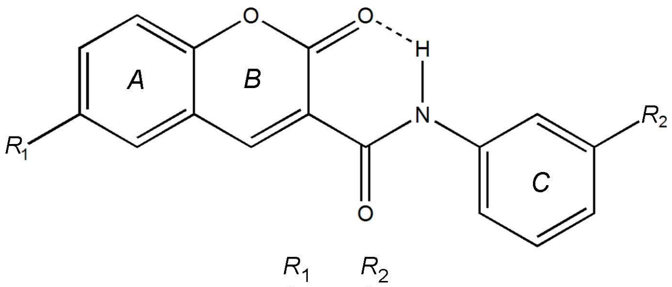

	R_1	R_2
1	CH_3	CH_3
2	CH_3	OCH_3
3	OCH_3	OCH_3

Previous work reported by our research group has shown that coumarin is a valid scaffold for the development of monoamino oxidase B inhibitors (Matos *et al.*, 2009). As part of our ongoing studies of these compounds, we now describe the syntheses and crystal structures of three coumarin derivatives: 6-methyl-*N*-(3-methylphenyl)-2-oxo-2*H*-chromene-3-carboxamide (**1**), *N*-(3-methoxyphenyl)-6-methyl-2-oxo-2*H*-

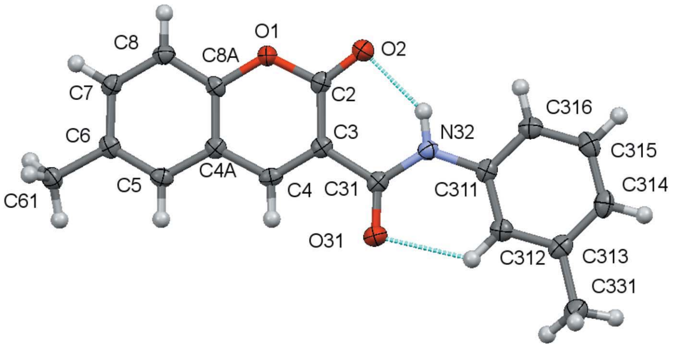

Figure 1
A view of the asymmetric unit of **1** with the atom-numbering scheme. Displacement ellipsoids are drawn at the 70% probability level.

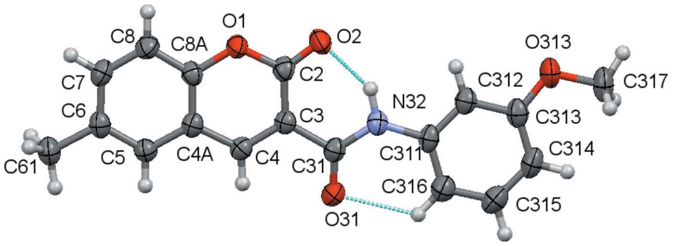

Figure 2
A view of the asymmetric unit of **2** with the atom-numbering scheme. Displacement ellipsoids are drawn at the 70% probability level.

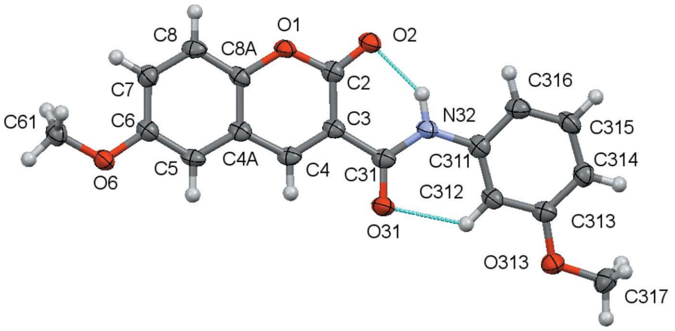

Figure 3
A view of the asymmetric unit of **3** with the atom-numbering scheme. Displacement ellipsoids are drawn at the 70% probability level.

chromene-3-carboxamide (**2**) and 6-methoxy-*N*-(3-methoxyphenyl)-2-oxo-2*H*-chromene-3-carboxamide (**3**).

2. Structural commentary

The structural analyses revealed that the molecules are coumarin derivatives with a phenylamide substituent at position 3 of the coumarin ring, as seen in the chemical scheme. The coumarin component rings are identified by the letters *A* and *B* while the exocyclic benzene ring is denoted *C*. Figs. 1–3 show the molecular structures of compounds **1**–**3**, respectively: they differ in the type of substituents at the 6-position of the coumarin ring system and at the 3-position of the pendant benzene ring.

Table 1
Selected dihedral angles (°).

θ_1 is the dihedral angle between the mean planes of the coumarin ring system and exocyclic phenyl ring. θ_2 is the dihedral angles between the mean plane of the coumarin ring system and the plane defined by the atoms O31/C31/N32. θ_3 is the dihedral angle between the mean planes of the exocyclic phenyl ring and the plane defined by atoms O31/C31/N32.

Compound	θ_1	θ_2	θ_3
1	4.69 (6)	4.8 (2)	0.21 (23)
2	4.28 (3)	4.46 (13)	8.60 (12)
3	8.17 (13)	2.9 (4)	10.2 (4)
BONKAS	4.70 (6)	3.2 (2)	7.8 (2)
DISXUA	10.29 (7)	3.9 (2)	6.42)
DISYAH	0.04 (6)	2.70 (17)’	2.76 (17)
DISYEL	3.07 (8)	3.4 (2)	1.0 (3)
DISYIP	12.75 (6)	1.21 (17)	12.73 (17)
WOJXOK	1.9 (4)	4.6 (9)	2.7 (9)

If the mean planes for the combined coumarin ring system and exocyclic phenyl rings are considered, then the maximum deviations of atoms within these rings from this plane are −0,1024 (12) Å or C6 in **1**, −0.0754 (15) Å in **2** and 0.0699 (14) Å in **3**. Considering all non-hydrogen atoms, the maximum deviations from this plane are 0.1783 (10) Å for O31 in **1**, −0.1809 (12) Å for O31 in **2** and −0.2181 (15) Å for O313 in **3**.

An inspection of the bond lengths shows that there is a slight asymmetry of the electronic distribution around the coumarin ring: the mean C3—C4 bond length [1.3517 (3) Å] and the mean value for the C3—C2 bond length [1.461 (6) Å)] are shorter and longer, respectively, that those expected for an C_{ar}—C_{ar} bond, suggesting that there is an increased electronic density located in the C3—C4 bond at the pyrone ring.

The values for the distances of the C3—C31 bonds [mean value 1.508 (4) Å] connecting the coumarin system to the amide spacer are of the same order as a Csp^3—Csp^3 bond. This confers freedom of rotation of the phenylamide substituent around it. Despite that, the molecules are approximately planar, as can be inferred by the set of values of the dihedral angles in Table 1, which refer to the combination of the dihedral angles between the best planes formed by all non-H atoms of the 2*H*-chromen-2-one ring, the O31/C31/N32 atoms of the amide residue and the phenyl substituent, which are all less than 11°. This may be correlated with the conformation assumed by the amide group around the C—N rotamer which displays an *—anti* orientation with respect to the *oxo* oxygen atom of the coumarin, thus allowing the establishment, in all three structures, of an intramolecular N—H···O hydrogen bond between the amino group of the carboxamide and the *oxo* group at the O2 position of the coumarin and a weak C—H···O intramolecular hydrogen bond between an *ortho*-CH group on the exocyclic phenyl ring and the O atom of the carboxamide. Thus these two interactions, which both form *S*(6) rings, probably contribute to the overall approximate planarity of the molecules since they may prevent the molecules from adopting some other possible conformations by restraining their geometry.

3. Supramolecular features

As mentioned above, the NH group is involved in an intramolecular hydrogen bond. It is not involved in any intermolecular interactions thus only carbon atoms may act as donors for the carbonyl and methoxy-type acceptors. Details

Table 2
Hydrogen-bond geometry (Å, °) for **1**.

D—H$\cdots A$	D—H	H$\cdots A$	$D\cdots A$	D—H$\cdots A$
N32—H32$\cdots$O2	0.893 (18)	1.957 (18)	2.7149 (14)	141.7 (16)
C312—H312$\cdots$O31	0.95	2.26	2.8838 (16)	122
C5—H5$\cdots$O1^{i}	0.95	2.98	3.7304 (15)	137

Symmetry code: (i) $x - 1, y, z$.

Table 3
Hydrogen-bond geometry (Å, °) for **2**.

D—H$\cdots A$	D—H	H$\cdots A$	$D\cdots A$	D—H$\cdots A$
N32—H32$\cdots$O2	0.96 (2)	1.85 (2)	2.6952 (16)	145.7 (17)
C8—H8$\cdots$O1^{i}	0.95	2.52	3.3676 (18)	149
C61—H61$B\cdots$O31^{ii}	0.98	2.57	3.4044 (19)	143
C317—H31$A\cdots$O31^{iii}	0.98	2.57	3.2769 (19)	129

Symmetry codes: (i) $-x + 1, -y + 1, -z$; (ii) $-x + 2, -y, -z + 1$; (iii) $x, y + 1, z$.

Table 4
Hydrogen-bond geometry (Å, °) for **3**.

D—H$\cdots A$	D—H	H$\cdots A$	$D\cdots A$	D—H$\cdots A$
N32—H32$\cdots$O2	0.92 (3)	1.91 (3)	2.699 (2)	143 (2)
C4—H4$\cdots$O2^{i}	0.95	2.43	3.319 (3)	155
C5—H5$\cdots$O1^{i}	0.95	2.47	3.391 (3)	164
C8—H8$\cdots$O6^{ii}	0.95	2.46	3.364 (3)	160
C312—H312$\cdots$O31	0.95	2.26	2.868 (3)	121
C315—H315$\cdots$O313^{ii}	0.95	2.59	3.536 (4)	171

Symmetry codes: (i) $x - 1, y, z$; (ii) $x + 1, y, z$.

of the hydrogen bonding for compounds **1**, **2** and **3** are given in Tables 2, 3 and 4, respectively.

In **1**, the molecules are linked by the C5—H5$\cdots$O1($x - 1, y, z$) weak hydrogen bond to form a $C(6)$ chain, which runs parallel to the a axis, Fig. 4. In **2**, the molecules are linked by the C8—H8$\cdots$O1($-x + 1, -y + 1, -z$) weak hydrogen bond to form an $R_2^2(8)$ centrosymmetric dimer centred on (1/2, 1/2, 0), Fig. 5. There is also a short C317—H31$A\cdots$O31($x, y + 1, z$) contact involving a methyl hydrogen atom. In **3**, the molecules are linked by the C4—H4$\cdots$O2($x - 1, y, z$), C5—H5$\cdots$O1($x - 1, y, z$) and C8—H8$\cdots$O6($x + 1, y, z$) bonds to form a chain of $R_2^2(8)$ rings, which runs parallel to the a axis, Fig. 6. This chain is supplemented by the action of the C315—H315$\cdots$O313($x + 1, y, z$) weak hydrogen bond.

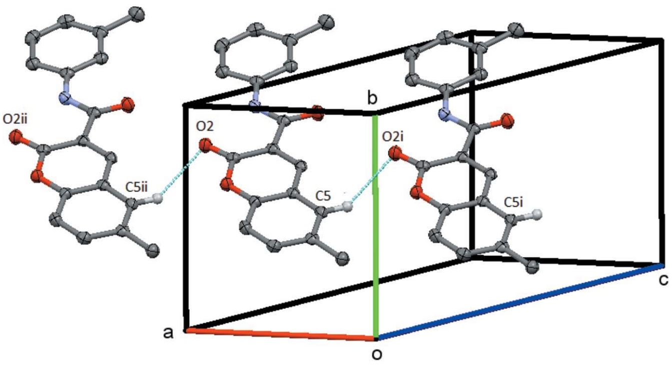

Figure 4
Compound **1**, the simple chain formed by the C5—H5$\cdots$O1 weak hydrogen bond. This chain extends by unit translation along the a axis. Symmetry codes: (i) $x - 1, y, z$; (ii) $x + 1, y, z$. H atoms not involved in the hydrogen bonding are omitted.

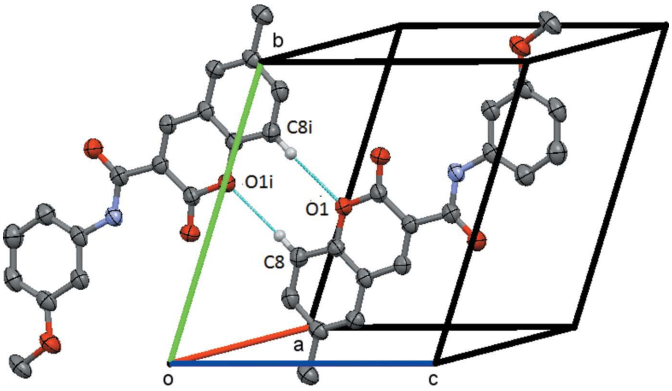

Figure 5
Compound **2**, view of the C8—H8$\cdots$O1 centrosymmetric $R_2^2(8)$ ring structure centred on $(\frac{1}{2}, \frac{1}{2}, 0)$. Symmetry code: (i) $-x + 1, -y + 1, z$. H atoms not involved in the hydrogen bonding are omitted.

4. Hirshfeld surfaces

The Hirshfeld surfaces and two-dimensional fingerprint (FP) plots (Rohl *et al.*, 2008) were generated using *Crystal Explorer 3.1* (Wolff *et al.*, 2012). The surfaces, mapped over $d_{\rm norm}$ and

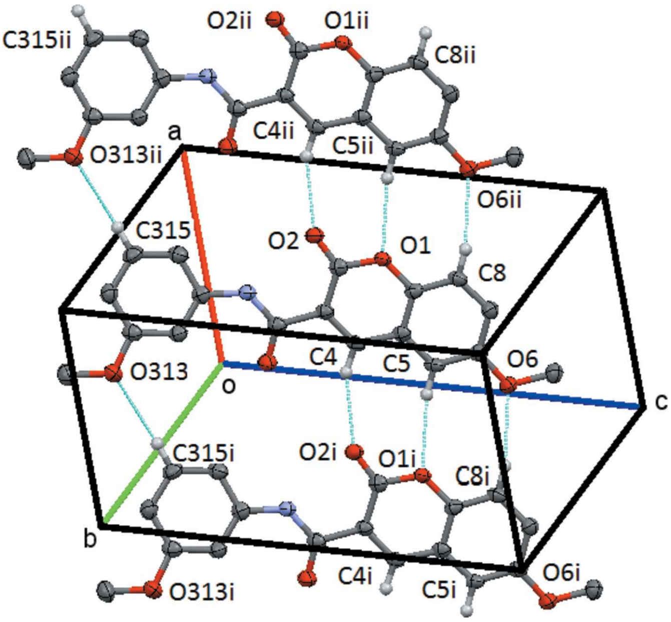

Figure 6
Compound **3**, view of the chain of the linked $R_2^2(8)$, $R_2^2(8)$ and $R_2^2(16)$ structures formed by the interaction of the C8—H8$\cdots$O6, C5—H5$\cdots$O1, C4—H4$\cdots$O1 and C315—H315$\cdots$O313 hydrogen bonds. This chain extends by unit translation along the a axis. Symmetry codes: (i) $x - 1, y, z$; (ii) $-x + 1, y, z$. H atoms not involved in the hydrogen bonding are omitted.

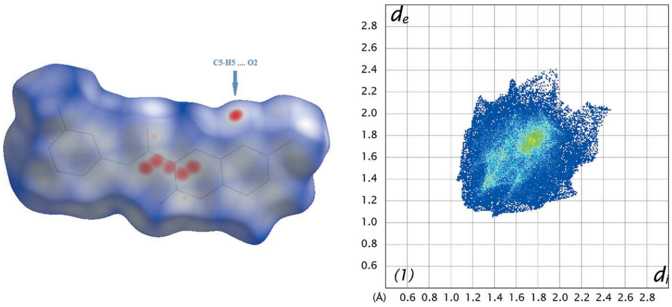

Figure 7
A view of the Hirshfeld surface mapped over $d_{\rm norm}$ (left) and fingerprint plot (right) for **1**. The highlighted red spots on the top face of the surfaces indicate contact points with the atoms participating in the C—H···O intermolecular interactions whereas those on the middle of the surface correspond to C···C contacts consequent of the π–π stacking. The C···C contacts contribute to higher the frequency of the pixels at $d_{\rm e} \simeq d_{\rm i} \simeq$ 1.8 Å on the FP plots (yellow spot).

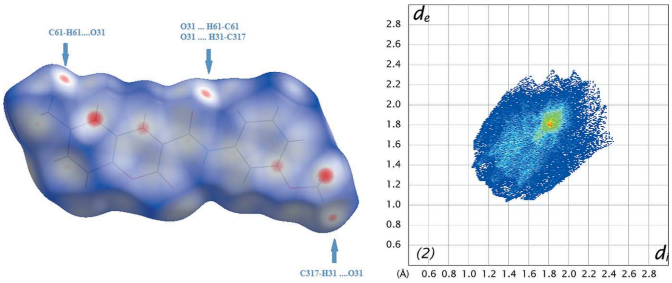

Figure 8
A view of the Hirshfeld surface mapped over $d_{\rm norm}$ (left) and fingerprint plot (right) for **2**. The highlighted red spots on the top face of the surfaces indicate contact points with the atoms participating in the C–H···O intermolecular interactions whereas those on the middle of the surface correspond to C···C contacts consequent of the π–π stacking. The C···C contacts contribute to higher the frequency of the pixels at $d_{\rm e} \simeq d_{\rm i} \simeq$ 1.8 Å on the FP plots.

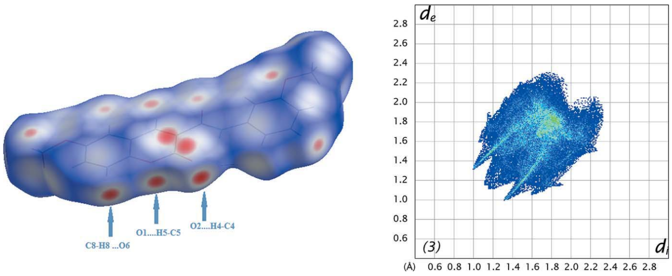

Figure 9
A view of the Hirshfeld surface mapped over $d_{\rm norm}$ (left) and fingerprint plot (right) for **3**. The highlighted red spots on the bottom face of the surfaces indicate contact points with the atoms participating in the C—H···O intermolecular interactions whereas those on the middle of the surface correspond to C···C and C···H contacts. The FP plot displays two couple of spikes (external ends corresponding to C···H contacts and middle spikes corresponding to O···H contacts).

the FP plots are presented in Figs. 7 to 9 for **1**, **2** and **3**, respectively. They provide complementary information concerning the intermolecular interactions discussed above.

Table 5
Percentages of atom–atom contacts.

Contact	**1**	**2**	**3**
H···H	47.1	42.9	38.3
H···O/O···H	19.9	26.9	27.4
H···C/C···H	14.5	12.9	20.7
H···N/N···H	1.5	0.2	1.6
C···C	12.1	12.6	5.4

The contributions from various contacts, listed in Table 5, were selected by the partial analysis of the FP plots.

Forgetting the prevalence of the H···H contacts on the surface, inherent to organic molecules, the most significant contacts are the H···O/O···H ones. Those appear as highlighted red spots on the top face of the surfaces (Fig. 7 to 9) that indicate contact points with the atoms participating in the C—H···O intermolecular interactions. Those contacts correspond to weak hydrogen bonds, as seen in the FP plots where the pair of sharp spikes that would be characteristic of hydrogen bond are masked by the H···H interactions appearing near $d_{\rm e} \simeq d_{\rm i}$ = 1.20 Å. Compound **1** has the smallest percentage for H···O/O···H contacts since it has no methoxy substituents. The most representative of these corresponds to the C5—H5···O2 contact that links the molecules in the C6 chain. In the surface of **2**, two red spots appear perpendicular to the C8—H8 bond and near O1 indicating the C8—H8···O1 contact that links the molecules into dimers. The red spots near O31 indicate that this atom establishes two weak contacts (C61—H61*B*···O31 and C317—H31*A*···O31). In **3**, there are several contacts, three of those involving the oxygen atoms of the coumarin system and those directly connected to it that are acceptors for H atoms of the coumarin residue of another molecule. These multiple contacts result in chains of hydrogen-bonded rings, as described in the previous section, and seem to operate a co-operative effect since the hydrogen bonds in **3** are stronger than in **1** and **2** (see the well-defined sharp spikes in the FP plot of **3**).

The values for the remaining contacts listed in Table 5 suggest that the supramolecular structure is built by H···C/C···H and C···C contacts. In **3**, the percentage for H···C/C···H contacts is higher than that for the other compounds. The FP plots also reveal a cluster at $d_{\rm e}/d_{\rm i} \simeq$ 1.8 Å and $d_{\rm i}/d_{\rm e} \simeq$ 1.2 Å characteristic of C—H···π contacts that seem to assume higher importance in the supramolecular structure in **3**. On the other hand, the C···C contacts prevail in **1** and **2**. In fact, the packing in **1** is built up by several π–π interactions (Table 6). Also, when the surface is mapped with shape index, several complementary triangular red hollows and blue bumps appear that are characteristic of the six-ring stacking (Figs. 10 and 11). In **1**, ring *A* stacks with ring *C* by a twofold rotation, and ring *B* with ring *A* when the molecule is placed above another centrosymmetrically related molecule. This gives rise to close C···C contacts in the middle of the surface identified as red spots. Molecule **2** also displays a significant percentage of C···C contacts on the Hirshfeld surface, resulting from the continuous π–π stacking where ring *C* stacks with rings *A* and *B* (up and down) of centrosymmetrically related molecules.

Table 6
Selected π–π contacts (Å).

$CgI(J)$ = plane number $I(J)$; $Cg\cdots Cg$ = distance between ring centroids; CgI_{perp} = perpendicular distance of $Cg(I)$ on ring J; CgJ_{perp} = perpendicular distance of $Cg(J)$ on ring I; Slippage = distance between Cg(I) and perpendicular projection of $Cg(J)$ on ring I.

Compound	CgI	CgJ(aru)	Cg···Cg	CgI$_{perp}$	CgJ$_{perp}$	Slippage
1	Cg1	Cg1($-x + 1, -y + 1, -z$)	3.7630 (7)	−3.3400 (5)	−3.3400 (5)	1.733
1	Cg1	Cg2($-x + 1, -y + 1, -z$)	3.4853 (7)	−3.3281 (5)	−3.3171 (5)	1.069
1	Cg2	Cg1($-x + 1, -y + 1, -z$)	3.4853 (7)	−3.3172 (5)	−3.3281 (5)	1.035
1	Cg2	Cg3($-x + 1, -y + 2, -z$)	3.6253 (7)	3.3547 (5)	3.4673 (5)	1.058
1	Cg3	Cg2($-x + 1, -y + 1, -z$)	3.6253 (7)	3.4673 (5)	3.3548 (5)	1.374
2	Cg1	Cg3($-x + 1, -y + 1, -z + 1$)	3.5379 (9)	−3.4691 (6)	−3.4872 (6)	0.597
2	Cg3	Cg1($-x + 1, -y + 1, -z + 1$)	3.5378 (9)	−3.4872 (6)	−3.4691 (6)	0.694
2	Cg1	Cg3($-x + 2, -y + 1, -z + 1$)	3.5974 (9)	3.4237 (6)	3.4068 (6)	1.156
2	Cg3	Cg1($-x + 2, -y + 1, -z + 1$)	3.5975 (9)	3.4069 (6)	3.4237 (6)	1.105
2	Cg2	Cg3($-x + 1, -y + 1, -z + 1$)	3.9325 (9)	−3.5309 (6)	−3.4844 (6)	1.823
2	Cg3	Cg2($-x + 1, -y + 1, -z + 1$)	3.9324 (9)	−3.4844 (6)	−3.5309 (6)	1.731
3	Cg1	Cg2($-x + 1, -y, -z + 1$)	3.5978 (13)	−3.3575 (9)	−3.3307 (9)	1.360
3	Cg2	Cg1($-x + 1, -y, -z + 1$)	3.5978 (13)	−3.3307 (9)	−3.3575 (9)	1.293

Plane 1 is the plane of the pyran ring with $Cg1$ as centroid, ring B. Plane 2 is the plane of the coumarin phenyl ring with $Cg2$ as centroid, ring A. Plane 3 is the plane of the exocyclic phenyl ring with $Cg3$ as centroid, ring C. Some planes are repeated since they are inclined to each other and as a result give slightly different slippages.

5. Database survey

A search made in the Cambridge Structural Database (Groom *et al.*, 2016) revealed the existence of 35 deposited compounds (42 molecules) containing the coumarin carboxamide unit, all of which contained the same intramolecular N—H···O hydrogen bond as seen here. The hydrogen atoms in these structures were riding with ideally fixed positions or refined positions. The range of values for N—H were 0.78 to 1.02 Å with a median value of 0.88 Å, the range of values for H···O were 1.87 to 2.04 Å with a median value of 2.00 Å, the range of values for N···O were 2.639 to 2.801 Å with a median value of 2.722 Å and the range of values for the N—H···O angle was 125 to 146° with a median value of 138°.

Six of these compounds, with CSD codes: BONKAS (Julien *et al.*, 2014); DISXUA, DISYAH, DISYEL and DISYIP (Maldonado-Domínguez *et al.*, 2014); WOJXOK (Pan *et al.*, 2014), have a phenyl group attached to the carboxamide N atom and these molecules have similar conformations to the present compounds, Table 1. These compounds also had a short intramolecular contact between the *ortho*-C hydrogen atom of the exocyclic benzene ring and the carboxamide O atom as in the present compounds. Details of the searches can be found in the supporting information.

6. Synthesis and crystallization

The coumarin derivatives **1–3** were synthesized by a two-step process. In the first step, 5-methylsalicylaldehyde (1 mmol) and diethyl malonate (1 mmol) and catalytic amounts of piperidine were dissolved in ethanol (10 ml) and refluxed for 4 h. After cooling to room temperature, the suspension was filtered off and ethyl 6-methylcoumarin-3-carboxylate was obtained. This compound was then dissolved in 20 ml of an ethanolic solution with 0.5% NaOH (aq.) and hydrolyzed under reflux for 1h. After reaction, 10% HCl (aq.) was added and the desired carboxylic acid was then filtered and washed with water (Chimenti *et al.*, 2010).

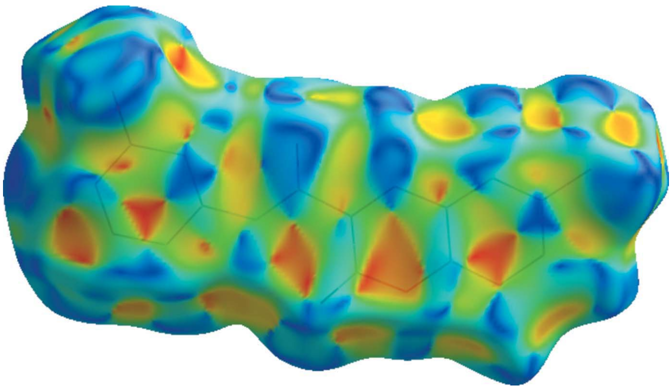

Figure 10
Surface of **1** mapped with shape index showing the complementary triangular red hollows and blue bumps that are characteristic of six-ring stacking.

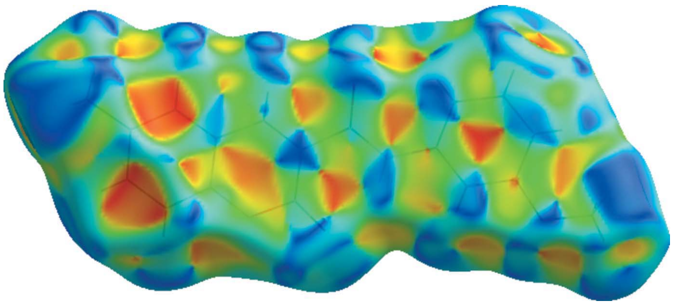

Figure 11
Surface of **2** mapped with shape index showing the complementary triangular red hollows and blue bumps that are characteristic of six-ring stacking.

Table 7
Experimental details.

	1	**2**	**3**
Crystal data			
Chemical formula	$C_{18}H_{15}NO_3$	$C_{18}H_{15}NO_4$	$C_{18}H_{15}NO_5$
M_r	293.31	309.31	325.31
Crystal system, space group	Monoclinic, $P2_1/c$	Triclinic, $P\bar{1}$	Triclinic, $P\bar{1}$
Temperature (K)	100	100	100
a, b, c (Å)	7.2117 (3), 8.0491 (3), 23.6242 (9)	7.1028 (4), 10.1367 (4), 10.8171 (5)	6.7722 (5), 8.3098 (7), 14.4202 (13)
α, β, γ (°)	90, 94.388 (4), 90	75.827 (4), 88.318 (4), 71.271 (4)	91.874 (7), 100.009 (7), 113.042 (7)
V (Å^3)	1367.31 (9)	714.10 (6)	730.84 (11)
Z	4	2	2
Radiation type	Mo $K\alpha$	Mo $K\alpha$	Mo $K\alpha$
μ (mm^{-1})	0.10	0.10	0.11
Crystal size (mm)	0.42 × 0.03 × 0.02	0.20 × 0.04 × 0.02	0.17 × 0.11 × 0.02
Data collection			
Diffractometer	Rigaku AFC12 (Right)	Rigaku AFC12 (Right)	Rigaku AFC12 (Right)
Absorption correction	Multi-scan (*CrysAlis PRO*; Rigaku Oxford Diffraction, 2015)	Multi-scan (*CrysAlis PRO*; Rigaku Oxford Diffraction, 2015)	Multi-scan (*CrysAlis PRO*; Rigaku Oxford Diffraction, 2015)
T_{min}, T_{max}	0.895, 1.000	0.893, 1.000	0.792, 1.000
No. of measured, independent and observed [$I > 2\sigma(I)$] reflections	12045, 3135, 2593	15638, 3262, 2704	8745, 3302, 2666
R_{int}	0.023	0.025	0.033
$(\sin \theta/\lambda)_{max}$ (Å^{-1})	0.649	0.649	0.649
Refinement			
$R[F^2 > 2\sigma(F^2)]$, $wR(F^2)$, S	0.041, 0.120, 1.03	0.047, 0.139, 1.02	0.071, 0.152, 1.16
No. of reflections	3134	3261	3302
No. of parameters	205	214	223
H-atom treatment	H atoms treated by a mixture of independent and constrained refinement	H atoms treated by a mixture of independent and constrained refinement	H atoms treated by a mixture of independent and constrained refinement
$\Delta\rho_{max}$, $\Delta\rho_{min}$ (e Å^{-3})	0.35, −0.26	0.37, −0.21	0.25, −0.26

Computer programs: *CrysAlis PRO* (Rigaku Oxford Diffraction, 2015), *OSCAIL* (McArdle *et al.*, 2004), *SHELXT* (Sheldrick, 2015*a*), *ShelXle* (Hübschle *et al.*, 2011), *SHELXL2014* (Sheldrick, 2015*b*), *Mercury* (Macrae *et al.*, 2006) and *PLATON* (Spek, 2009).

Then, to a solution of 6-methylcoumarin-3-carboxylic acid (1 mmol) in dichloromethane, 1-ethyl-3-(3-dimethylaminopropyl)carbodiimide (EDC) (1.10 mmol) and 4-dimethylaminopyridine (DMAP) (1.10 mmol) were added. The mixture was kept under a flux of argon gas at 273 K for five minutes. Shortly after, the aromatic amine (1 mmol) with the intended substitution pattern was added. The reaction mixture was stirred for 4 h at room temperature. The crude product was filtered and purified by column chromatography (hexane/ethyl acetate 9:1) or by recrystallization with ethanol to give the desired product, (Murata *et al.*, 2005). 6-Methyl-*N*-(3′-methylphenyl)coumarin-3-carboxamide (**1**) (yield: 79%; m.p. 467–468 K; crystallization solvent: methanol); 6-methyl-*N*-(3′-methoxyphenyl)coumarin-3-carboxamide (**2**) (yield: 74%; m.p. 447–448 K; crystallization solvent: methanol); 6-methoxy-*N*-(3′-methoxyphenyl)coumarin-3-carboxamide (**3**) (yield: 50.7%; m.p. 440–441 K; crystallization solvent: ethyl acetate).

7. Refinement

Crystal data, data collection and structure refinement details are summarized in Table 7. H atoms were treated as riding atoms with C—H(aromatic) = 0.95 Å and $U_{iso} = 1.2U_{eq}(C)$, C—H(methyl) 0.98 Å and $U_{iso} = 1.5U_{eq}(C)$ The amino H atoms were refined.

Acknowledgements

The authors thank the staff at the National Crystallographic Service, University of Southampton (Coles & Gale, 2012), for the data collection, help and advice and the Foundation for Science and Technology (FCT) and FEDER/COMPETE2020 (UID/QUι00081/2015 and POCI-01–0145-FEDER-006980). AF (SFRH/BD/80831/2011) and MJM (SFRH/BPD/95345/2013) were supported by grants from FCT, POPH and QREN.

References

Chimenti, F., Bizzarri, B., Bolasco, A., Secci, D., Chimenti, P., Granese, A., Carradori, S., Rivanera, D., Zicari, A., Scaltrito, M. M. & Sisto, F. (2010). *Bioorg. Med. Chem. Lett.* **20**, 4922–4926.
Coles, S. J. & Gale, P. A. (2012). *Chem. Sci.* **3**, 683–689.
Groom, C. R., Bruno, I. J., Lightfoot, M. P. & Ward, S. C. (2016). *Acta Cryst.* B**72**, 171–179.
Hübschle, C. B., Sheldrick, G. M. & Dittrich, B. (2011). *J. Appl. Cryst.* **44**, 1281–1284.
Julien, O., Kampmann, M., Bassik, M. C., Zorn, J. A., Venditto, V. J., Shimbo, K., Agard, N. J., Shimada, K., Rheingold, A. L., Stockwell, B. R., Weissman, J. S. & Wells, J. A. (2014). *Nat. Chem. Biol.* **10**, 969–976.
Klekota, J. & Roth, F. P. (2008). *Bioinformatics*, **24**, 2518–2525.
Lachance, H., Wetzel, S., Kumar, K. & Waldmann, H. (2012). *J. Med. Chem.* **55**, 5989–6001.

Macrae, C. F., Edgington, P. R., McCabe, P., Pidcock, E., Shields, G. P., Taylor, R., Towler, M. & van de Streek, J. (2006). *J. Appl. Cryst.* **39**, 453–457.

Maldonado-Domínguez, M., Arcos-Ramos, R., Romero, M., Flores-Pérez, B., Farfán, N., Santillan, R., Lacroix, P. G. & Malfant, I. (2014). *New J. Chem.* **38**, 260–268.

Matos, M. J., Janeiro, P., González Franco, R. M., Vilar, S., Tatonetti, N. P., Santana, L., Uriarte, E., Borges, F., Fontenla, J. A. & Viña, D. (2014). *Future Med. Chem.* **6**, 371–383.

Matos, M. J., Viña, D., Quezada, E., Picciau, C., Delogu, G., Orallo, F., Santana, L. & Uriarte, E. (2009). *Bioorg. Med. Chem. Lett.* **19**, 3268–3270.

McArdle, P., Gilligan, K., Cunningham, D., Dark, R. & Mahon, M. (2004). *CrystEngComm*, **6**, 303–309.

Murata, C., Masuda, T., Kamochi, Y., Todoroki, K., Yoshida, H., Nohta, H., Yamaguchi, M. & Takadate, A. (2005). *Chem. Pharm. Bull.* **53**, 750–758.

Pan, Z.-Y., He, X., Chen, Y.-Y., Tang, W.-J., Shi, J.-B., Tang, Y.-L., Song, B.-A., Li, J. & Liu, X. H. (2014). *Eur. J. Med. Chem.* **80**, 278–284.

Rigaku Oxford Diffraction (2015). *CrysAlis PRO*, Rigaku Corporation, Tokyo, Japan.

Rohl, A. L., Moret, M., Kaminsky, W., Claborn, K., McKinnon, J. J. & Kahr, B. (2008). *Cryst. Growth Des.* **8**, 4517–4525.

Sheldrick, G. M. (2015*a*). *Acta Cryst.* A**71**, 3–8.

Sheldrick, G. M. (2015*b*). *Acta Cryst.* C**71**, 3–8.

Spek, A. L. (2009). *Acta Cryst.* D**65**, 148–155.

Vazquez-Rodriguez, S., Matos, M. J., Santana, L., Uriarte, E., Borges, F., Kachler, S. & Klotz, K. N. (2013). *J. Pharm. Pharmacol.* **65**, 697–703.

Wolff, S. K., Grimwood, D. J., McKinnon, J. J., Turner, M. J., Jayatilaka, D. & Spackman, M. A. (2012). *Crystal Explorer*. The University of Western Australia.

supporting information

Acta Cryst. (2016). E**72**, 926-932   [doi:10.1107/S2056989016008665]

Crystal structures of three 6-substituted coumarin-3-carboxamide derivatives

Lígia R. Gomes, John Nicolson Low, André Fonseca, Maria João Matos and Fernanda Borges

Computing details

For all compounds, data collection: *CrysAlis PRO* (Rigaku Oxford Diffraction, 2015); cell refinement: *CrysAlis PRO* (Rigaku Oxford Diffraction, 2015); data reduction: *CrysAlis PRO* (Rigaku Oxford Diffraction, 2015); program(s) used to solve structure: *OSCAIL* (McArdle *et al.*, 2004) and SHELXT (Sheldrick, 2015a). Program(s) used to refine structure: *OSCAIL* (McArdle *et al.*, 2004), *ShelXle* (Hübschle *et al.*, 2011) and *SHELXL2014*/7 (Sheldrick, 2015b) for (1), (2); *OSCAIL* (McArdle *et al.*, 2004), *ShelXle* (Hübschle *et al.*, 2011) and *SHELXL2014*/6 (Sheldrick, 2015b) for (3). For all compounds, molecular graphics: *Mercury* (Macrae *et al.*, 2006); software used to prepare material for publication: *OSCAIL* (McArdle *et al.*, 2004), *SHELXL2014* (Sheldrick, 2015b) and *PLATON* (Spek, 2009).

(1) 6-Methyl-*N*-(3-methylphenyl)-2-oxo-2*H*-chromene-3-carboxamide

Crystal data

$C_{18}H_{15}NO_3$
M_r = 293.31
Monoclinic, $P2_1/c$
a = 7.2117 (3) Å
b = 8.0491 (3) Å
c = 23.6242 (9) Å
β = 94.388 (4)°
V = 1367.31 (9) Å^3
Z = 4
$F(000)$ = 616
D_x = 1.425 Mg m^{-3}
Mo $K\alpha$ radiation, λ = 0.71075 Å
Cell parameters from 5809 reflections
θ = 2.7–27.6°
μ = 0.10 mm^{-1}
T = 100 K
Needle, yellow
0.42 × 0.03 × 0.02 mm

Data collection

Rigaku AFC12 (Right) diffractometer
Radiation source: Rotating Anode
Detector resolution: 28.5714 pixels mm^{-1}
profile data from ω–scans
Absorption correction: multi-scan (*CrysAlis PRO*; Rigaku Oxford Diffraction, 2015)
T_{min} = 0.895, T_{max} = 1.000
12045 measured reflections
3135 independent reflections
2593 reflections with $I > 2\sigma(I)$
R_{int} = 0.023
θ_{max} = 27.5°, θ_{min} = 1.7°
$h = -9 \rightarrow 8$
$k = -10 \rightarrow 7$
$l = -30 \rightarrow 29$

Refinement

Refinement on F^2
Least-squares matrix: full
$R[F^2 > 2\sigma(F^2)]$ = 0.041
$wR(F^2)$ = 0.120
S = 1.03
3134 reflections
205 parameters
0 restraints
Hydrogen site location: mixed
H atoms treated by a mixture of independent and constrained refinement

$w = 1/[\sigma^2(F_o^2) + (0.0741P)^2 + 0.3348P]$
where $P = (F_o^2 + 2F_c^2)/3$
$(\Delta/\sigma)_{max} = 0.001$

$\Delta\rho_{max} = 0.35$ e Å^{-3}
$\Delta\rho_{min} = -0.26$ e Å^{-3}

Special details

Experimental. CrysAlisPro 1.171.38.41 (Rigaku Oxford Diffraction, 2015) Empirical absorption correction using spherical harmonics, implemented in SCALE3 ABSPACK scaling algorithm.

Geometry. All esds (except the esd in the dihedral angle between two l.s. planes) are estimated using the full covariance matrix. The cell esds are taken into account individually in the estimation of esds in distances, angles and torsion angles; correlations between esds in cell parameters are only used when they are defined by crystal symmetry. An approximate (isotropic) treatment of cell esds is used for estimating esds involving l.s. planes.

Fractional atomic coordinates and isotropic or equivalent isotropic displacement parameters (Å^2)

	x	y	z	U_{iso}*/U_{eq}
O1	0.69397 (12)	0.68051 (12)	−0.05947 (3)	0.0158 (2)
O2	0.88820 (13)	0.82921 (12)	−0.00415 (4)	0.0191 (2)
O31	0.45616 (13)	0.95381 (12)	0.10022 (4)	0.0199 (2)
N32	0.76928 (15)	0.97441 (14)	0.09028 (4)	0.0153 (2)
H32	0.855 (2)	0.949 (2)	0.0664 (7)	0.033 (5)*
C2	0.72934 (18)	0.77998 (16)	−0.01268 (5)	0.0147 (3)
C3	0.57335 (17)	0.81575 (16)	0.02182 (5)	0.0137 (3)
C4	0.40358 (17)	0.75122 (16)	0.00695 (5)	0.0144 (3)
H4	0.3034	0.7759	0.0294	0.017*
C4A	0.37082 (17)	0.64663 (15)	−0.04177 (5)	0.0140 (3)
C5	0.19774 (18)	0.57410 (16)	−0.05816 (5)	0.0152 (3)
H5	0.0946	0.5956	−0.0365	0.018*
C6	0.17503 (18)	0.47192 (16)	−0.10530 (5)	0.0148 (3)
C7	0.32959 (18)	0.44378 (16)	−0.13696 (5)	0.0159 (3)
H7	0.3155	0.3739	−0.1694	0.019*
C8	0.50106 (18)	0.51447 (16)	−0.12233 (5)	0.0160 (3)
H8	0.6034	0.4950	−0.1445	0.019*
C8A	0.52020 (17)	0.61462 (16)	−0.07444 (5)	0.0139 (3)
C31	0.59396 (18)	0.92182 (16)	0.07469 (5)	0.0144 (3)
C61	−0.01018 (18)	0.39458 (17)	−0.12285 (5)	0.0178 (3)
H61A	0.0066	0.2759	−0.1302	0.027*
H61B	−0.0642	0.4489	−0.1574	0.027*
H61C	−0.0937	0.4085	−0.0924	0.027*
C311	0.83193 (18)	1.06916 (16)	0.13848 (5)	0.0150 (3)
C312	0.71473 (18)	1.12797 (16)	0.17828 (5)	0.0163 (3)
H312	0.5861	1.1013	0.1745	0.020*
C313	0.78614 (19)	1.22628 (17)	0.22372 (5)	0.0175 (3)
C314	0.97525 (19)	1.26281 (17)	0.22921 (5)	0.0194 (3)
H314	1.0244	1.3307	0.2597	0.023*
C315	1.09272 (19)	1.20017 (17)	0.19020 (5)	0.0197 (3)
H315	1.2221	1.2236	0.1947	0.024*
C316	1.02253 (18)	1.10408 (17)	0.14486 (5)	0.0175 (3)
H316	1.1032	1.0622	0.1183	0.021*
C317	0.6556 (2)	1.29639 (18)	0.26456 (5)	0.0220 (3)

H31A	0.7234	1.3144	0.3016	0.033*
H31B	0.5535	1.2180	0.2687	0.033*
H31C	0.6050	1.4023	0.2499	0.033*

Atomic displacement parameters (Å²)

	U^{11}	U^{22}	U^{33}	U^{12}	U^{13}	U^{23}
O1	0.0138 (5)	0.0177 (5)	0.0158 (4)	−0.0013 (4)	0.0014 (3)	−0.0033 (4)
O2	0.0158 (5)	0.0214 (5)	0.0204 (5)	−0.0018 (4)	0.0029 (3)	−0.0037 (4)
O31	0.0178 (5)	0.0229 (5)	0.0195 (5)	0.0001 (4)	0.0044 (4)	−0.0047 (4)
N32	0.0157 (6)	0.0153 (6)	0.0150 (5)	0.0015 (4)	0.0017 (4)	−0.0020 (4)
C2	0.0174 (7)	0.0116 (6)	0.0148 (6)	0.0008 (5)	0.0000 (5)	0.0004 (5)
C3	0.0166 (6)	0.0111 (6)	0.0136 (6)	0.0019 (5)	0.0013 (4)	0.0019 (5)
C4	0.0163 (6)	0.0122 (6)	0.0149 (6)	0.0036 (5)	0.0035 (5)	0.0021 (5)
C4A	0.0156 (6)	0.0115 (6)	0.0147 (6)	0.0021 (5)	0.0003 (5)	0.0020 (5)
C5	0.0143 (6)	0.0137 (6)	0.0179 (6)	0.0021 (5)	0.0027 (5)	0.0018 (5)
C6	0.0150 (6)	0.0126 (6)	0.0164 (6)	0.0022 (5)	−0.0016 (4)	0.0037 (5)
C7	0.0178 (7)	0.0157 (7)	0.0140 (6)	0.0013 (5)	−0.0006 (5)	−0.0010 (5)
C8	0.0153 (6)	0.0176 (7)	0.0154 (6)	0.0031 (5)	0.0025 (5)	0.0003 (5)
C8A	0.0127 (6)	0.0127 (6)	0.0161 (6)	0.0006 (5)	−0.0007 (5)	0.0021 (5)
C31	0.0179 (7)	0.0115 (6)	0.0138 (6)	0.0010 (5)	0.0012 (5)	0.0016 (5)
C61	0.0147 (6)	0.0175 (7)	0.0210 (6)	−0.0002 (5)	−0.0004 (5)	−0.0007 (5)
C311	0.0188 (7)	0.0116 (6)	0.0142 (6)	0.0011 (5)	−0.0005 (5)	0.0019 (5)
C312	0.0171 (6)	0.0152 (6)	0.0166 (6)	0.0016 (5)	0.0010 (5)	0.0025 (5)
C313	0.0237 (7)	0.0143 (7)	0.0147 (6)	0.0017 (5)	0.0020 (5)	0.0027 (5)
C314	0.0243 (7)	0.0168 (7)	0.0163 (6)	−0.0022 (5)	−0.0034 (5)	0.0010 (5)
C315	0.0180 (7)	0.0195 (7)	0.0210 (6)	−0.0025 (5)	−0.0020 (5)	0.0039 (5)
C316	0.0187 (7)	0.0172 (7)	0.0168 (6)	0.0014 (5)	0.0027 (5)	0.0032 (5)
C317	0.0247 (7)	0.0229 (7)	0.0183 (6)	0.0008 (6)	0.0018 (5)	−0.0026 (5)

Geometric parameters (Å, º)

O1—C2	1.3730 (15)	C8—C8A	1.3874 (17)
O1—C8A	1.3817 (15)	C8—H8	0.9500
O2—C2	1.2144 (15)	C61—H61A	0.9800
O31—C31	1.2287 (15)	C61—H61B	0.9800
N32—C31	1.3573 (16)	C61—H61C	0.9800
N32—C311	1.4154 (16)	C311—C312	1.3943 (17)
N32—H32	0.893 (18)	C311—C316	1.3998 (18)
C2—C3	1.4672 (17)	C312—C313	1.3997 (18)
C3—C4	1.3514 (18)	C312—H312	0.9500
C3—C31	1.5109 (16)	C313—C314	1.3914 (19)
C4—C4A	1.4309 (17)	C313—C317	1.5082 (18)
C4—H4	0.9500	C314—C315	1.3931 (19)
C4A—C8A	1.3964 (17)	C314—H314	0.9500
C4A—C5	1.4053 (17)	C315—C316	1.3851 (18)
C5—C6	1.3841 (18)	C315—H315	0.9500
C5—H5	0.9500	C316—H316	0.9500

C6—C7	1.4074 (18)	C317—H31A	0.9800
C6—C61	1.5029 (17)	C317—H31B	0.9800
C7—C8	1.3810 (18)	C317—H31C	0.9800
C7—H7	0.9500		

C2—O1—C8A	122.61 (10)	O31—C31—C3	119.49 (11)
C31—N32—C311	128.30 (11)	N32—C31—C3	115.55 (11)
C31—N32—H32	115.8 (11)	C6—C61—H61A	109.5
C311—N32—H32	115.8 (12)	C6—C61—H61B	109.5
O2—C2—O1	116.01 (11)	H61A—C61—H61B	109.5
O2—C2—C3	126.69 (11)	C6—C61—H61C	109.5
O1—C2—C3	117.29 (11)	H61A—C61—H61C	109.5
C4—C3—C2	119.88 (11)	H61B—C61—H61C	109.5
C4—C3—C31	117.51 (11)	C312—C311—C316	120.00 (12)
C2—C3—C31	122.61 (11)	C312—C311—N32	123.55 (12)
C3—C4—C4A	121.71 (12)	C316—C311—N32	116.44 (11)
C3—C4—H4	119.1	C311—C312—C313	120.18 (12)
C4A—C4—H4	119.1	C311—C312—H312	119.9
C8A—C4A—C5	118.53 (11)	C313—C312—H312	119.9
C8A—C4A—C4	117.80 (12)	C314—C313—C312	119.43 (12)
C5—C4A—C4	123.68 (11)	C314—C313—C317	121.11 (12)
C6—C5—C4A	121.09 (12)	C312—C313—C317	119.41 (12)
C6—C5—H5	119.5	C313—C314—C315	120.21 (12)
C4A—C5—H5	119.5	C313—C314—H314	119.9
C5—C6—C7	118.26 (11)	C315—C314—H314	119.9
C5—C6—C61	121.07 (12)	C316—C315—C314	120.59 (13)
C7—C6—C61	120.66 (11)	C316—C315—H315	119.7
C8—C7—C6	122.08 (12)	C314—C315—H315	119.7
C8—C7—H7	119.0	C315—C316—C311	119.55 (12)
C6—C7—H7	119.0	C315—C316—H316	120.2
C7—C8—C8A	118.34 (12)	C311—C316—H316	120.2
C7—C8—H8	120.8	C313—C317—H31A	109.5
C8A—C8—H8	120.8	C313—C317—H31B	109.5
O1—C8A—C8	117.61 (11)	H31A—C317—H31B	109.5
O1—C8A—C4A	120.71 (11)	C313—C317—H31C	109.5
C8—C8A—C4A	121.68 (12)	H31A—C317—H31C	109.5
O31—C31—N32	124.96 (12)	H31B—C317—H31C	109.5

C8A—O1—C2—O2	179.71 (11)	C4—C4A—C8A—O1	0.84 (17)
C8A—O1—C2—C3	−0.18 (17)	C5—C4A—C8A—C8	0.31 (18)
O2—C2—C3—C4	−179.80 (12)	C4—C4A—C8A—C8	179.93 (11)
O1—C2—C3—C4	0.07 (18)	C311—N32—C31—O31	2.3 (2)
O2—C2—C3—C31	−0.5 (2)	C311—N32—C31—C3	−177.45 (11)
O1—C2—C3—C31	179.32 (10)	C4—C3—C31—O31	−4.22 (18)
C2—C3—C4—C4A	0.50 (19)	C2—C3—C31—O31	176.51 (12)
C31—C3—C4—C4A	−178.79 (11)	C4—C3—C31—N32	175.55 (11)
C3—C4—C4A—C8A	−0.95 (18)	C2—C3—C31—N32	−3.72 (17)
C3—C4—C4A—C5	178.65 (12)	C31—N32—C311—C312	−1.5 (2)

C8A—C4A—C5—C6	0.54 (18)	C31—N32—C311—C316	178.94 (12)
C4—C4A—C5—C6	−179.05 (11)	C316—C311—C312—C313	1.97 (19)
C4A—C5—C6—C7	−0.72 (18)	N32—C311—C312—C313	−177.58 (12)
C4A—C5—C6—C61	−179.92 (11)	C311—C312—C313—C314	−0.86 (19)
C5—C6—C7—C8	0.06 (19)	C311—C312—C313—C317	176.73 (12)
C61—C6—C7—C8	179.26 (12)	C312—C313—C314—C315	−0.84 (19)
C6—C7—C8—C8A	0.75 (19)	C317—C313—C314—C315	−178.39 (12)
C2—O1—C8A—C8	−179.42 (11)	C313—C314—C315—C316	1.4 (2)
C2—O1—C8A—C4A	−0.29 (18)	C314—C315—C316—C311	−0.3 (2)
C7—C8—C8A—O1	178.18 (11)	C312—C311—C316—C315	−1.37 (19)
C7—C8—C8A—C4A	−0.94 (19)	N32—C311—C316—C315	178.21 (11)
C5—C4A—C8A—O1	−178.78 (11)		

Hydrogen-bond geometry (Å, º)

D—H···*A*	*D*—H	H···*A*	*D*···*A*	*D*—H···*A*
N32—H32···O2	0.893 (18)	1.957 (18)	2.7149 (14)	141.7 (16)
C312—H312···O31	0.95	2.26	2.8838 (16)	122
C5—H5···O1^{i}	0.95	2.98	3.7304 (15)	137

Symmetry code: (i) $x-1, y, z$.

(2) *N*-(3-Methoxyphenyl)-6-methyl-2-oxo-2*H*-chromene-3-carboxamide

Crystal data

$C_{18}H_{15}NO_4$
M_r = 309.31
Triclinic, $P\overline{1}$
a = 7.1028 (4) Å
b = 10.1367 (4) Å
c = 10.8171 (5) Å
α = 75.827 (4)°
β = 88.318 (4)°
γ = 71.271 (4)°
V = 714.10 (6) Å^3

Z = 2
$F(000)$ = 324
D_x = 1.439 Mg m^{-3}
Mo $K\alpha$ radiation, λ = 0.71075 Å
Cell parameters from 9156 reflections
θ = 2.0–27.5°
μ = 0.10 mm^{-1}
T = 100 K
Needle, colourless
0.20 × 0.04 × 0.02 mm

Data collection

Rigaku AFC12 (Right) diffractometer
Radiation source: Rotating Anode
Confocal mirrors, HF Varimax monochromator
Detector resolution: 28.5714 pixels mm^{-1}
profile data from ω–scans
Absorption correction: multi-scan (*CrysAlis PRO*; Rigaku Oxford Diffraction, 2015)

T_{min} = 0.893, T_{max} = 1.000
15638 measured reflections
3262 independent reflections
2704 reflections with $I > 2\sigma(I)$
R_{int} = 0.025
θ_{max} = 27.5°, θ_{min} = 2.0°
$h = -9 \rightarrow 9$
$k = -13 \rightarrow 13$
$l = -14 \rightarrow 14$

Refinement

Refinement on F^2
Least-squares matrix: full
$R[F^2 > 2\sigma(F^2)]$ = 0.047
$wR(F^2)$ = 0.139
S = 1.02

3261 reflections
214 parameters
0 restraints
Hydrogen site location: mixed

H atoms treated by a mixture of independent and constrained refinement
$w = 1/[\sigma^2(F_o^2) + (0.0823P)^2 + 0.2203P]$ where $P = (F_o^2 + 2F_c^2)/3$
$(\Delta/\sigma)_{max} = 0.001$
$\Delta\rho_{max} = 0.37$ e Å^{-3}
$\Delta\rho_{min} = -0.21$ e Å^{-3}

Special details

Experimental. CrysAlisPro 1.171.38.41 (Rigaku Oxford Diffraction, 2015) Empirical absorption correction using spherical harmonics, implemented in SCALE3 ABSPACK scaling algorithm.

Geometry. All esds (except the esd in the dihedral angle between two l.s. planes) are estimated using the full covariance matrix. The cell esds are taken into account individually in the estimation of esds in distances, angles and torsion angles; correlations between esds in cell parameters are only used when they are defined by crystal symmetry. An approximate (isotropic) treatment of cell esds is used for estimating esds involving l.s. planes.

Fractional atomic coordinates and isotropic or equivalent isotropic displacement parameters (Å^2)

	x	*y*	*z*	U_{iso}*/U_{eq}
O1	0.65788 (15)	0.44209 (11)	0.15778 (9)	0.0286 (3)
O2	0.62079 (16)	0.61257 (11)	0.25621 (10)	0.0336 (3)
O31	0.86393 (17)	0.30291 (11)	0.59953 (9)	0.0342 (3)
N32	0.73898 (17)	0.54313 (13)	0.50493 (12)	0.0254 (3)
H32	0.687 (3)	0.604 (2)	0.423 (2)	0.050 (6)*
O313	0.68878 (17)	0.96846 (12)	0.62447 (11)	0.0367 (3)
C8A	0.6993 (2)	0.30000 (15)	0.15628 (13)	0.0245 (3)
C2	0.6741 (2)	0.48376 (15)	0.26677 (14)	0.0263 (3)
C3	0.75233 (19)	0.37076 (14)	0.38259 (12)	0.0227 (3)
C4	0.79282 (19)	0.23155 (15)	0.38073 (13)	0.0241 (3)
H4	0.8409	0.1587	0.4573	0.029*
C4A	0.76523 (19)	0.19084 (15)	0.26675 (13)	0.0232 (3)
C5	0.8052 (2)	0.04818 (15)	0.25954 (13)	0.0249 (3)
H5	0.8508	−0.0279	0.3343	0.030*
C6	0.7792 (2)	0.01685 (15)	0.14495 (14)	0.0258 (3)
C7	0.7102 (2)	0.13159 (16)	0.03699 (14)	0.0281 (3)
H7	0.6904	0.1114	−0.0420	0.034*
C8	0.6702 (2)	0.27245 (16)	0.04094 (14)	0.0293 (3)
H8	0.6238	0.3486	−0.0336	0.035*
C31	0.7903 (2)	0.40253 (15)	0.50651 (13)	0.0250 (3)
C61	0.8246 (2)	−0.13560 (16)	0.13511 (15)	0.0325 (3)
H61A	0.7066	−0.1464	0.0995	0.049*
H61B	0.8615	−0.2012	0.2202	0.049*
H61C	0.9351	−0.1586	0.0792	0.049*
C311	0.75735 (19)	0.60513 (16)	0.60585 (13)	0.0252 (3)
C312	0.7157 (2)	0.75307 (16)	0.57413 (14)	0.0268 (3)
H312	0.6788	0.8065	0.4882	0.032*
C313	0.7276 (2)	0.82377 (16)	0.66755 (14)	0.0289 (3)
C314	0.7787 (2)	0.74642 (17)	0.79326 (14)	0.0321 (3)
H314	0.7861	0.7937	0.8578	0.039*
C315	0.8186 (2)	0.59968 (18)	0.82285 (15)	0.0356 (4)
H315	0.8534	0.5465	0.9090	0.043*
C316	0.8099 (2)	0.52680 (17)	0.73131 (14)	0.0318 (3)

H316	0.8392	0.4254	0.7540	0.038*
C317	0.6726 (2)	1.04748 (18)	0.71900 (16)	0.0368 (4)
H31A	0.6357	1.1504	0.6774	0.055*
H31B	0.8008	1.0162	0.7670	0.055*
H31C	0.5703	1.0302	0.7775	0.055*

Atomic displacement parameters (Å²)

	U^{11}	U^{22}	U^{33}	U^{12}	U^{13}	U^{23}
O1	0.0367 (6)	0.0231 (5)	0.0253 (5)	−0.0075 (4)	−0.0064 (4)	−0.0066 (4)
O2	0.0443 (6)	0.0214 (5)	0.0336 (6)	−0.0075 (4)	−0.0094 (5)	−0.0070 (4)
O31	0.0488 (7)	0.0300 (6)	0.0241 (5)	−0.0119 (5)	−0.0046 (4)	−0.0073 (4)
N32	0.0263 (6)	0.0262 (6)	0.0261 (6)	−0.0088 (5)	0.0001 (5)	−0.0103 (5)
O313	0.0481 (7)	0.0317 (6)	0.0376 (6)	−0.0158 (5)	0.0010 (5)	−0.0181 (5)
C8A	0.0228 (6)	0.0233 (7)	0.0285 (7)	−0.0071 (5)	−0.0009 (5)	−0.0083 (5)
C2	0.0260 (7)	0.0274 (7)	0.0274 (7)	−0.0093 (6)	−0.0027 (5)	−0.0092 (6)
C3	0.0203 (6)	0.0251 (7)	0.0242 (7)	−0.0083 (5)	0.0010 (5)	−0.0073 (5)
C4	0.0222 (6)	0.0266 (7)	0.0238 (7)	−0.0082 (5)	0.0005 (5)	−0.0066 (5)
C4A	0.0194 (6)	0.0280 (7)	0.0248 (7)	−0.0091 (5)	0.0023 (5)	−0.0099 (5)
C5	0.0245 (7)	0.0250 (7)	0.0261 (7)	−0.0086 (5)	0.0025 (5)	−0.0072 (5)
C6	0.0226 (6)	0.0277 (7)	0.0314 (7)	−0.0098 (5)	0.0047 (5)	−0.0132 (6)
C7	0.0276 (7)	0.0338 (8)	0.0256 (7)	−0.0098 (6)	0.0002 (5)	−0.0122 (6)
C8	0.0320 (7)	0.0295 (7)	0.0251 (7)	−0.0077 (6)	−0.0033 (6)	−0.0071 (6)
C31	0.0241 (7)	0.0278 (7)	0.0255 (7)	−0.0096 (5)	0.0016 (5)	−0.0094 (5)
C61	0.0359 (8)	0.0300 (8)	0.0363 (8)	−0.0114 (6)	0.0040 (6)	−0.0156 (6)
C311	0.0199 (6)	0.0322 (7)	0.0293 (7)	−0.0106 (5)	0.0035 (5)	−0.0154 (6)
C312	0.0247 (7)	0.0308 (7)	0.0284 (7)	−0.0101 (6)	0.0012 (5)	−0.0119 (6)
C313	0.0241 (7)	0.0323 (8)	0.0367 (8)	−0.0126 (6)	0.0051 (6)	−0.0161 (6)
C314	0.0304 (8)	0.0440 (9)	0.0309 (8)	−0.0156 (7)	0.0060 (6)	−0.0211 (7)
C315	0.0390 (8)	0.0434 (9)	0.0264 (7)	−0.0136 (7)	0.0031 (6)	−0.0118 (6)
C316	0.0339 (8)	0.0339 (8)	0.0293 (8)	−0.0113 (6)	0.0025 (6)	−0.0109 (6)
C317	0.0360 (8)	0.0392 (9)	0.0471 (9)	−0.0166 (7)	0.0072 (7)	−0.0273 (7)

Geometric parameters (Å, º)

O1—C2	1.3656 (16)	C6—C61	1.5040 (19)
O1—C8A	1.3785 (16)	C7—C8	1.375 (2)
O2—C2	1.2137 (17)	C7—H7	0.9500
O31—C31	1.2247 (17)	C8—H8	0.9500
N32—C31	1.3488 (18)	C61—H61A	0.9800
N32—C311	1.4145 (17)	C61—H61B	0.9800
N32—H32	0.96 (2)	C61—H61C	0.9800
O313—C313	1.3629 (18)	C311—C312	1.387 (2)
O313—C317	1.4267 (17)	C311—C316	1.387 (2)
C8A—C8	1.3785 (19)	C312—C313	1.3931 (19)
C8A—C4A	1.3871 (19)	C312—H312	0.9500
C2—C3	1.4560 (19)	C313—C314	1.386 (2)
C3—C4	1.3518 (19)	C314—C315	1.377 (2)

C3—C31	1.5038 (18)	C314—H314	0.9500
C4—C4A	1.4297 (18)	C315—C316	1.386 (2)
C4—H4	0.9500	C315—H315	0.9500
C4A—C5	1.4028 (19)	C316—H316	0.9500
C5—C6	1.3841 (19)	C317—H31A	0.9800
C5—H5	0.9500	C317—H31B	0.9800
C6—C7	1.400 (2)	C317—H31C	0.9800

C2—O1—C8A	122.60 (11)	O31—C31—C3	119.53 (12)
C31—N32—C311	128.29 (13)	N32—C31—C3	115.57 (12)
C31—N32—H32	112.4 (12)	C6—C61—H61A	109.5
C311—N32—H32	119.3 (12)	C6—C61—H61B	109.5
C313—O313—C317	116.71 (12)	H61A—C61—H61B	109.5
O1—C8A—C8	116.95 (12)	C6—C61—H61C	109.5
O1—C8A—C4A	120.97 (12)	H61A—C61—H61C	109.5
C8—C8A—C4A	122.07 (13)	H61B—C61—H61C	109.5
O2—C2—O1	115.82 (12)	C312—C311—C316	120.02 (13)
O2—C2—C3	126.86 (13)	C312—C311—N32	116.32 (13)
O1—C2—C3	117.32 (12)	C316—C311—N32	123.65 (14)
C4—C3—C2	119.74 (12)	C311—C312—C313	120.38 (14)
C4—C3—C31	117.86 (12)	C311—C312—H312	119.8
C2—C3—C31	122.40 (12)	C313—C312—H312	119.8
C3—C4—C4A	121.83 (13)	O313—C313—C314	124.95 (13)
C3—C4—H4	119.1	O313—C313—C312	115.09 (13)
C4A—C4—H4	119.1	C314—C313—C312	119.96 (14)
C8A—C4A—C5	118.50 (12)	C315—C314—C313	118.75 (13)
C8A—C4A—C4	117.36 (12)	C315—C314—H314	120.6
C5—C4A—C4	124.12 (13)	C313—C314—H314	120.6
C6—C5—C4A	120.84 (13)	C314—C315—C316	122.32 (15)
C6—C5—H5	119.6	C314—C315—H315	118.8
C4A—C5—H5	119.6	C316—C315—H315	118.8
C5—C6—C7	118.07 (13)	C315—C316—C311	118.57 (15)
C5—C6—C61	121.52 (13)	C315—C316—H316	120.7
C7—C6—C61	120.41 (13)	C311—C316—H316	120.7
C8—C7—C6	122.46 (13)	O313—C317—H31A	109.5
C8—C7—H7	118.8	O313—C317—H31B	109.5
C6—C7—H7	118.8	H31A—C317—H31B	109.5
C7—C8—C8A	118.06 (13)	O313—C317—H31C	109.5
C7—C8—H8	121.0	H31A—C317—H31C	109.5
C8A—C8—H8	121.0	H31B—C317—H31C	109.5
O31—C31—N32	124.90 (13)		

C2—O1—C8A—C8	177.70 (12)	O1—C8A—C8—C7	−179.94 (12)
C2—O1—C8A—C4A	−1.7 (2)	C4A—C8A—C8—C7	−0.6 (2)
C8A—O1—C2—O2	−175.39 (12)	C311—N32—C31—O31	−0.1 (2)
C8A—O1—C2—C3	4.54 (19)	C311—N32—C31—C3	−179.84 (12)
O2—C2—C3—C4	175.53 (13)	C4—C3—C31—O31	3.1 (2)
O1—C2—C3—C4	−4.39 (19)	C2—C3—C31—O31	−177.02 (13)

O2—C2—C3—C31	−4.3 (2)	C4—C3—C31—N32	−177.06 (11)
O1—C2—C3—C31	175.77 (11)	C2—C3—C31—N32	2.78 (19)
C2—C3—C4—C4A	1.4 (2)	C31—N32—C311—C312	172.29 (12)
C31—C3—C4—C4A	−178.73 (11)	C31—N32—C311—C316	−9.0 (2)
O1—C8A—C4A—C5	−179.94 (11)	C316—C311—C312—C313	0.5 (2)
C8—C8A—C4A—C5	0.7 (2)	N32—C311—C312—C313	179.28 (12)
O1—C8A—C4A—C4	−1.47 (19)	C317—O313—C313—C314	−9.2 (2)
C8—C8A—C4A—C4	179.19 (12)	C317—O313—C313—C312	171.67 (12)
C3—C4—C4A—C8A	1.5 (2)	C311—C312—C313—O313	178.26 (12)
C3—C4—C4A—C5	179.88 (12)	C311—C312—C313—C314	−0.9 (2)
C8A—C4A—C5—C6	−0.1 (2)	O313—C313—C314—C315	−178.48 (13)
C4—C4A—C5—C6	−178.51 (12)	C312—C313—C314—C315	0.6 (2)
C4A—C5—C6—C7	−0.5 (2)	C313—C314—C315—C316	0.1 (2)
C4A—C5—C6—C61	178.98 (12)	C314—C315—C316—C311	−0.6 (2)
C5—C6—C7—C8	0.7 (2)	C312—C311—C316—C315	0.2 (2)
C61—C6—C7—C8	−178.82 (13)	N32—C311—C316—C315	−178.48 (13)
C6—C7—C8—C8A	−0.1 (2)		

Hydrogen-bond geometry (Å, º)

D—H···*A*	*D*—H	H···*A*	*D*···*A*	*D*—H···*A*
N32—H32···O2	0.96 (2)	1.85 (2)	2.6952 (16)	145.7 (17)
C8—H8···O1^{i}	0.95	2.52	3.3676 (18)	149
C61—H61*B*···O31^{ii}	0.98	2.57	3.4044 (19)	143
C317—H31*A*···O31^{iii}	0.98	2.57	3.2769 (19)	129

Symmetry codes: (i) −*x*+1, −*y*+1, −*z*; (ii) −*x*+2, −*y*, −*z*+1; (iii) *x*, *y*+1, *z*.

(3) 6-Methoxy-*N*-(3-methoxyphenyl)-2-oxo-2*H*-chromene-3-carboxamide

Crystal data

$C_{18}H_{15}NO_5$
$M_r = 325.31$
Triclinic, $P\bar{1}$
$a = 6.7722\ (5)$ Å
$b = 8.3098\ (7)$ Å
$c = 14.4202\ (13)$ Å
$\alpha = 91.874\ (7)°$
$\beta = 100.009\ (7)°$
$\gamma = 113.042\ (7)°$
$V = 730.84\ (11)$ Å^3

$Z = 2$
$F(000) = 340$
$D_x = 1.483$ Mg m^{-3}
Mo *Kα* radiation, $\lambda = 0.71073$ Å
Cell parameters from 3630 reflections
$\theta = 2.7–27.4°$
$\mu = 0.11$ mm^{-1}
$T = 100$ K
Plate, yellow
0.17 × 0.11 × 0.02 mm

Data collection

Rigaku AFC12 (Right) diffractometer
Radiation source: Rotating Anode, Rotating Anode
Confocal mirrors, HF Varimax monochromator
Detector resolution: 28.5714 pixels mm^{-1}
profile data from ω–scans

Absorption correction: multi-scan (*CrysAlis PRO*; Rigaku Oxford Diffraction, 2015)
$T_{min} = 0.792$, $T_{max} = 1.000$
8745 measured reflections
3302 independent reflections
2666 reflections with $I > 2\sigma(I)$
$R_{int} = 0.033$

$\theta_{max} = 27.5°$, $\theta_{min} = 2.7°$
$h = -7 \rightarrow 8$
$k = -10 \rightarrow 9$
$l = -18 \rightarrow 18$

Refinement

Refinement on F^2
Least-squares matrix: full
$R[F^2 > 2\sigma(F^2)] = 0.071$
$wR(F^2) = 0.152$
$S = 1.16$
3302 reflections
223 parameters
0 restraints
Hydrogen site location: mixed
H atoms treated by a mixture of independent and constrained refinement
$w = 1/[\sigma^2(F_o^2) + (0.0606P)^2 + 0.3539P]$ where $P = (F_o^2 + 2F_c^2)/3$
$(\Delta/\sigma)_{max} < 0.001$
$\Delta\rho_{max} = 0.25$ e Å^{-3}
$\Delta\rho_{min} = -0.26$ e Å^{-3}

Special details

Experimental. CrysAlisPro 1.171.38.41 (Rigaku Oxford Diffraction, 2015) Empirical absorption correction using spherical harmonics, implemented in SCALE3 ABSPACK scaling algorithm.

Geometry. All esds (except the esd in the dihedral angle between two l.s. planes) are estimated using the full covariance matrix. The cell esds are taken into account individually in the estimation of esds in distances, angles and torsion angles; correlations between esds in cell parameters are only used when they are defined by crystal symmetry. An approximate (isotropic) treatment of cell esds is used for estimating esds involving l.s. planes.

Fractional atomic coordinates and isotropic or equivalent isotropic displacement parameters (Å^2)

	x	y	z	U_{iso}*/U_{eq}
O1	0.7758 (2)	0.24765 (19)	0.52564 (10)	0.0207 (3)
O2	0.9491 (2)	0.3631 (2)	0.41317 (11)	0.0227 (4)
O6	0.0500 (2)	0.0132 (2)	0.68826 (11)	0.0244 (4)
O31	0.4048 (2)	0.4552 (2)	0.27644 (11)	0.0249 (4)
O313	0.5339 (3)	0.7656 (2)	0.01169 (11)	0.0272 (4)
N32	0.7594 (3)	0.4985 (2)	0.27488 (13)	0.0212 (4)
H32	0.872 (4)	0.476 (3)	0.3080 (18)	0.032 (7)*
C2	0.7823 (3)	0.3270 (3)	0.44407 (15)	0.0195 (5)
C3	0.5890 (3)	0.3567 (3)	0.40191 (15)	0.0183 (4)
C4	0.4121 (3)	0.3038 (3)	0.44288 (15)	0.0193 (5)
H4	0.2872	0.3236	0.4147	0.023*
C4A	0.4085 (3)	0.2184 (3)	0.52792 (15)	0.0188 (5)
C5	0.2277 (3)	0.1573 (3)	0.57142 (16)	0.0200 (5)
H5	0.0987	0.1733	0.5454	0.024*
C6	0.2368 (3)	0.0732 (3)	0.65245 (15)	0.0203 (5)
C7	0.4289 (4)	0.0548 (3)	0.69251 (16)	0.0214 (5)
H7	0.4362	0.0012	0.7495	0.026*
C8	0.6098 (4)	0.1144 (3)	0.64972 (15)	0.0213 (5)
H8	0.7399	0.1004	0.6763	0.026*
C8A	0.5963 (3)	0.1941 (3)	0.56802 (15)	0.0190 (5)
C31	0.5759 (3)	0.4431 (3)	0.31191 (15)	0.0203 (5)
C61	0.0465 (4)	−0.0852 (3)	0.76813 (16)	0.0252 (5)
H61A	−0.0977	−0.1238	0.7851	0.038*
H61B	0.1593	−0.0108	0.8219	0.038*
H61C	0.0755	−0.1882	0.7520	0.038*
C311	0.7911 (3)	0.5766 (3)	0.19019 (15)	0.0203 (5)

C312	0.6436 (3)	0.6337 (3)	0.13821 (15)	0.0210 (5)
H312	0.5130	0.6212	0.1588	0.025*
C313	0.6884 (3)	0.7093 (3)	0.05573 (16)	0.0216 (5)
C314	0.8761 (4)	0.7263 (3)	0.02325 (16)	0.0239 (5)
H314	0.9040	0.7762	−0.0339	0.029*
C315	1.0229 (4)	0.6682 (3)	0.07684 (17)	0.0256 (5)
H315	1.1530	0.6802	0.0559	0.031*
C316	0.9831 (4)	0.5942 (3)	0.15912 (16)	0.0239 (5)
H316	1.0846	0.5553	0.1947	0.029*
C317	0.5672 (4)	0.8430 (3)	−0.07431 (17)	0.0296 (5)
H31A	0.4426	0.8715	−0.1002	0.044*
H31B	0.5798	0.7598	−0.1203	0.044*
H31C	0.7020	0.9508	−0.0615	0.044*

Atomic displacement parameters (Å²)

	U^{11}	U^{22}	U^{33}	U^{12}	U^{13}	U^{23}
O1	0.0169 (8)	0.0216 (8)	0.0281 (8)	0.0112 (6)	0.0064 (6)	0.0086 (6)
O2	0.0189 (8)	0.0229 (8)	0.0302 (9)	0.0109 (7)	0.0078 (6)	0.0075 (6)
O6	0.0193 (8)	0.0271 (9)	0.0313 (9)	0.0115 (7)	0.0101 (6)	0.0116 (7)
O31	0.0169 (8)	0.0281 (9)	0.0315 (9)	0.0101 (7)	0.0058 (6)	0.0106 (7)
O313	0.0262 (9)	0.0306 (9)	0.0318 (9)	0.0168 (7)	0.0091 (7)	0.0130 (7)
N32	0.0176 (10)	0.0238 (10)	0.0267 (10)	0.0116 (8)	0.0068 (8)	0.0081 (8)
C2	0.0186 (11)	0.0131 (10)	0.0254 (11)	0.0051 (8)	0.0044 (8)	0.0014 (8)
C3	0.0172 (10)	0.0133 (10)	0.0252 (11)	0.0069 (8)	0.0047 (8)	0.0025 (8)
C4	0.0182 (11)	0.0133 (10)	0.0268 (12)	0.0076 (8)	0.0022 (8)	0.0027 (8)
C4A	0.0199 (11)	0.0126 (10)	0.0250 (11)	0.0078 (8)	0.0048 (8)	0.0010 (8)
C5	0.0153 (10)	0.0172 (11)	0.0288 (12)	0.0088 (8)	0.0023 (8)	0.0016 (9)
C6	0.0185 (11)	0.0162 (11)	0.0267 (12)	0.0068 (9)	0.0063 (9)	0.0021 (8)
C7	0.0230 (12)	0.0187 (11)	0.0243 (11)	0.0091 (9)	0.0068 (9)	0.0052 (9)
C8	0.0185 (11)	0.0175 (11)	0.0294 (12)	0.0095 (9)	0.0026 (9)	0.0041 (9)
C8A	0.0157 (10)	0.0143 (10)	0.0274 (12)	0.0054 (8)	0.0069 (8)	0.0020 (8)
C31	0.0181 (11)	0.0160 (11)	0.0267 (12)	0.0072 (9)	0.0035 (9)	0.0022 (9)
C61	0.0258 (12)	0.0226 (12)	0.0290 (12)	0.0092 (10)	0.0106 (9)	0.0083 (9)
C311	0.0206 (11)	0.0135 (10)	0.0254 (11)	0.0051 (9)	0.0055 (8)	0.0014 (8)
C312	0.0190 (11)	0.0167 (11)	0.0293 (12)	0.0077 (9)	0.0084 (9)	0.0049 (9)
C313	0.0190 (11)	0.0171 (11)	0.0283 (12)	0.0073 (9)	0.0036 (9)	0.0018 (9)
C314	0.0256 (12)	0.0210 (12)	0.0262 (12)	0.0088 (9)	0.0088 (9)	0.0070 (9)
C315	0.0182 (11)	0.0252 (12)	0.0346 (13)	0.0076 (9)	0.0110 (9)	0.0060 (10)
C316	0.0201 (11)	0.0216 (12)	0.0308 (13)	0.0099 (9)	0.0036 (9)	0.0044 (9)
C317	0.0308 (13)	0.0296 (13)	0.0301 (13)	0.0129 (11)	0.0069 (10)	0.0129 (10)

Geometric parameters (Å, º)

O1—C2	1.366 (2)	C7—C8	1.391 (3)
O1—C8A	1.379 (2)	C7—H7	0.9500
O2—C2	1.218 (2)	C8—C8A	1.377 (3)
O6—C6	1.366 (3)	C8—H8	0.9500

O6—C61	1.432 (3)	C61—H61A	0.9800
O31—C31	1.226 (3)	C61—H61B	0.9800
O313—C313	1.374 (3)	C61—H61C	0.9800
O313—C317	1.428 (3)	C311—C312	1.385 (3)
N32—C31	1.356 (3)	C311—C316	1.404 (3)
N32—C311	1.412 (3)	C312—C313	1.388 (3)
N32—H32	0.92 (3)	C312—H312	0.9500
C2—C3	1.459 (3)	C313—C314	1.388 (3)
C3—C4	1.352 (3)	C314—C315	1.397 (3)
C3—C31	1.509 (3)	C314—H314	0.9500
C4—C4A	1.436 (3)	C315—C316	1.374 (3)
C4—H4	0.9500	C315—H315	0.9500
C4A—C8A	1.394 (3)	C316—H316	0.9500
C4A—C5	1.397 (3)	C317—H31A	0.9800
C5—C6	1.385 (3)	C317—H31B	0.9800
C5—H5	0.9500	C317—H31C	0.9800
C6—C7	1.397 (3)		

C2—O1—C8A	123.06 (16)	O31—C31—N32	124.7 (2)
C6—O6—C61	117.74 (17)	O31—C31—C3	119.63 (19)
C313—O313—C317	117.52 (18)	N32—C31—C3	115.61 (18)
C31—N32—C311	127.96 (19)	O6—C61—H61A	109.5
C31—N32—H32	114.6 (16)	O6—C61—H61B	109.5
C311—N32—H32	117.4 (16)	H61A—C61—H61B	109.5
O2—C2—O1	116.03 (18)	O6—C61—H61C	109.5
O2—C2—C3	126.7 (2)	H61A—C61—H61C	109.5
O1—C2—C3	117.27 (18)	H61B—C61—H61C	109.5
C4—C3—C2	119.95 (19)	C312—C311—C316	120.1 (2)
C4—C3—C31	117.69 (18)	C312—C311—N32	123.3 (2)
C2—C3—C31	122.35 (18)	C316—C311—N32	116.59 (19)
C3—C4—C4A	121.62 (19)	C311—C312—C313	119.3 (2)
C3—C4—H4	119.2	C311—C312—H312	120.3
C4A—C4—H4	119.2	C313—C312—H312	120.3
C8A—C4A—C5	118.77 (19)	O313—C313—C314	124.3 (2)
C8A—C4A—C4	117.53 (19)	O313—C313—C312	114.19 (19)
C5—C4A—C4	123.69 (19)	C314—C313—C312	121.5 (2)
C6—C5—C4A	119.93 (19)	C313—C314—C315	118.3 (2)
C6—C5—H5	120.0	C313—C314—H314	120.9
C4A—C5—H5	120.0	C315—C314—H314	120.9
O6—C6—C5	115.76 (19)	C316—C315—C314	121.4 (2)
O6—C6—C7	124.16 (19)	C316—C315—H315	119.3
C5—C6—C7	120.1 (2)	C314—C315—H315	119.3
C8—C7—C6	120.5 (2)	C315—C316—C311	119.4 (2)
C8—C7—H7	119.7	C315—C316—H316	120.3
C6—C7—H7	119.7	C311—C316—H316	120.3
C8A—C8—C7	118.6 (2)	O313—C317—H31A	109.5
C8A—C8—H8	120.7	O313—C317—H31B	109.5
C7—C8—H8	120.7	H31A—C317—H31B	109.5

C8—C8A—O1	117.40 (18)	O313—C317—H31C	109.5
C8—C8A—C4A	122.04 (19)	H31A—C317—H31C	109.5
O1—C8A—C4A	120.55 (19)	H31B—C317—H31C	109.5

C8A—O1—C2—O2	−178.07 (17)	C4—C4A—C8A—C8	179.69 (19)
C8A—O1—C2—C3	0.7 (3)	C5—C4A—C8A—O1	178.01 (18)
O2—C2—C3—C4	177.7 (2)	C4—C4A—C8A—O1	−1.3 (3)
O1—C2—C3—C4	−1.0 (3)	C311—N32—C31—O31	−1.1 (4)
O2—C2—C3—C31	−1.4 (3)	C311—N32—C31—C3	177.28 (19)
O1—C2—C3—C31	−179.99 (18)	C4—C3—C31—O31	−3.4 (3)
C2—C3—C4—C4A	0.1 (3)	C2—C3—C31—O31	175.63 (19)
C31—C3—C4—C4A	179.18 (18)	C4—C3—C31—N32	178.15 (18)
C3—C4—C4A—C8A	1.0 (3)	C2—C3—C31—N32	−2.8 (3)
C3—C4—C4A—C5	−178.2 (2)	C31—N32—C311—C312	10.4 (3)
C8A—C4A—C5—C6	−0.5 (3)	C31—N32—C311—C316	−169.2 (2)
C4—C4A—C5—C6	178.8 (2)	C316—C311—C312—C313	−0.5 (3)
C61—O6—C6—C5	175.76 (18)	N32—C311—C312—C313	179.91 (19)
C61—O6—C6—C7	−4.4 (3)	C317—O313—C313—C314	1.5 (3)
C4A—C5—C6—O6	−178.04 (18)	C317—O313—C313—C312	−179.27 (19)
C4A—C5—C6—C7	2.2 (3)	C311—C312—C313—O313	−178.17 (19)
O6—C6—C7—C8	177.8 (2)	C311—C312—C313—C314	1.1 (3)
C5—C6—C7—C8	−2.4 (3)	O313—C313—C314—C315	178.0 (2)
C6—C7—C8—C8A	1.0 (3)	C312—C313—C314—C315	−1.2 (3)
C7—C8—C8A—O1	−178.30 (18)	C313—C314—C315—C316	0.7 (3)
C7—C8—C8A—C4A	0.8 (3)	C314—C315—C316—C311	−0.1 (3)
C2—O1—C8A—C8	179.51 (19)	C312—C311—C316—C315	0.0 (3)
C2—O1—C8A—C4A	0.4 (3)	N32—C311—C316—C315	179.6 (2)
C5—C4A—C8A—C8	−1.0 (3)		

Hydrogen-bond geometry (Å, º)

D—H···*A*	*D*—H	H···*A*	*D*···*A*	*D*—H···*A*
N32—H32···O2	0.92 (3)	1.91 (3)	2.699 (2)	143 (2)
C4—H4···O2$^{\text{i}}$	0.95	2.43	3.319 (3)	155
C5—H5···O1$^{\text{i}}$	0.95	2.47	3.391 (3)	164
C8—H8···O6$^{\text{ii}}$	0.95	2.46	3.364 (3)	160
C312—H312···O31	0.95	2.26	2.868 (3)	121
C315—H315···O313$^{\text{ii}}$	0.95	2.59	3.536 (4)	171

Symmetry codes: (i) $x-1, y, z$; (ii) $x+1, y, z$.

Manuscript VII

6-methyl-2-oxo-*N*-(quinolin-6-yl)-2H-chromene-3-carboxamide: crystal structure and Hirshfeld surface analysis.

Acta Crystallographica Section E: Structure Reports Online, Volume 72, **2016**, Pages 1121-1125

research communications

Acta Cryst E
CRYSTALLOGRAPHIC COMMUNICATIONS

ISSN 2056-9890

6-Methyl-2-oxo-*N*-(quinolin-6-yl)-2*H*-chromene-3-carboxamide: crystal structure and Hirshfeld surface analysis

Lígia R. Gomes,[a,b] John Nicolson Low,[c]* André Fonseca,[d] Maria João Matos[d] and Fernanda Borges[d]

[a]FP–ENAS–Faculdade de Ciências de Saúde, Escola Superior de Saúde da UFP, Universidade Fernando Pessoa, Rua Carlos da Maia, 296, P-4200-150 Porto, Portugal, [b]REQUIMTE, Departamento de Química e Bioquímica, Faculdade de Ciências da Universidade do Porto, Rua do Campo Alegre, 687, P-4169-007 Porto, Portugal, [c]Department of Chemistry, University of Aberdeen, Meston Walk, Old Aberdeen AB24 3UE, Scotland, and [d]CIQUP/Departamento de Química e Bioquímica, Faculdade de Ciências, Universidade do Porto, 4169-007 Porto, Portugal. *Correspondence e-mail: jnlow111@gmail.com

Received 1 July 2016
Accepted 7 July 2016

Edited by W. T. A. Harrison, University of Aberdeen, Scotland

Keywords: crystal structure; coumarin; carboxamide; Hirshfeld surface analysis.

CCDC reference: 1491340

Supporting information: this article has supporting information at journals.iucr.org/e

The title coumarin derivative, $C_{20}H_{14}N_2O_3$, displays intramolecular N—H···O and weak C—H···O hydrogen bonds, which probably contribute to the approximate planarity of the molecule [dihedral angle between the coumarin and quinoline ring systems = 6.08 (6)°]. The supramolecular structures feature C—H···O hydrogen bonds and π–π interactions, as confirmed by Hirshfeld surface analyses.

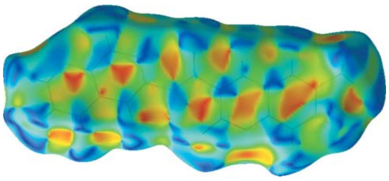

OPEN ACCESS

1. Chemical context

Coumarin and its derivatives are widely recognized by their unique biological properties (Matos *et al.*, 2014; Vazquez-Rodriguez *et al.*, 2013; Chimenti *et al.*, 2010). Our work in this area has shown that coumarin is a valid scaffold for the development of new drugs for aging related diseases, specifically within the class of monoamino oxidase B inhibitors (Matos *et al.*, 2009). On the other hand, quinoline is a nitrogen heterocycle also often used in drug-discovery programs due to its remarkable biological properties, some of them related to neurodegenerative diseases (Sridharan *et al.*, 2011), for instance, as γ-secretase and acetylcholinesterase inhibitors (Camps *et al.*, 2009). As part of our ongoing studies in this area (Gomes *et al.*, 2016), we describe the synthesis and crystal structure of the title coumarin–quinoline hybrid, 6-methyl-2-oxo-*N*-(quinolin-6-yl)-2*H*-chromene-3-carboxamide, (1) (see Scheme).

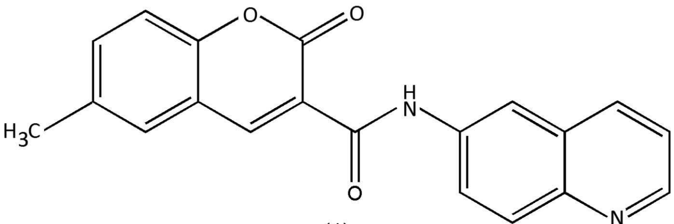

(1)

2. Structural commentary

Fig. 1 shows an ellipsoid plot of the molecular structure of (1). An inspection of the bond lengths shows that there is a slight

Table 1
Hydrogen-bond geometry (Å, °).

D—H···*A*	*D*—H	H···*A*	*D*···*A*	*D*—H···*A*
C314—H314···O31^{i}	0.95	2.50	3.278 (2)	139
C8—H8···N311^{ii}	0.95	2.68	3.394 (3)	133
C317—H317···O31	0.95	2.29	2.903 (2)	122
N32—H32···O2	0.907 (18)	1.879 (18)	2.686 (2)	147.3 (15)

Symmetry codes: (i) $x + 1, y, z$; (ii) $x - \frac{1}{2}, -y + \frac{1}{2}, z - \frac{1}{2}$; (iii) $x - 1, y, z$.

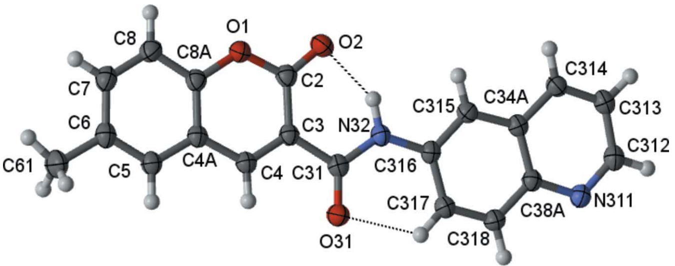

Figure 1
A view of the asymmetric unit of (1), showing the atom-numbering scheme. Displacement ellipsoids are drawn at the 70% probability level.

asymmetry of the electronic distribution around the coumarin ring: the C3—C4 [1.3609 (15) Å] and C3—C2 [1.4600 (18) Å)] bond lengths are shorter and longer, respectively, than those expected for a C_{ar}—C_{ar} bond, suggesting that the electronic density is rather located near the C3—C4 bond at the pyrone ring, as occurs in other coumarin-3-carboxamide derivatives (Gomes *et al.*, 2016). Also, the C3—C31 bond length [1.5075 (18) Å] is similar to the mean value displayed by other coumarin-3-carboxamide derivatives previously characterized (Gomes *et al.*, 2016) and is of the same order as a Csp^3—Csp^3 bond.

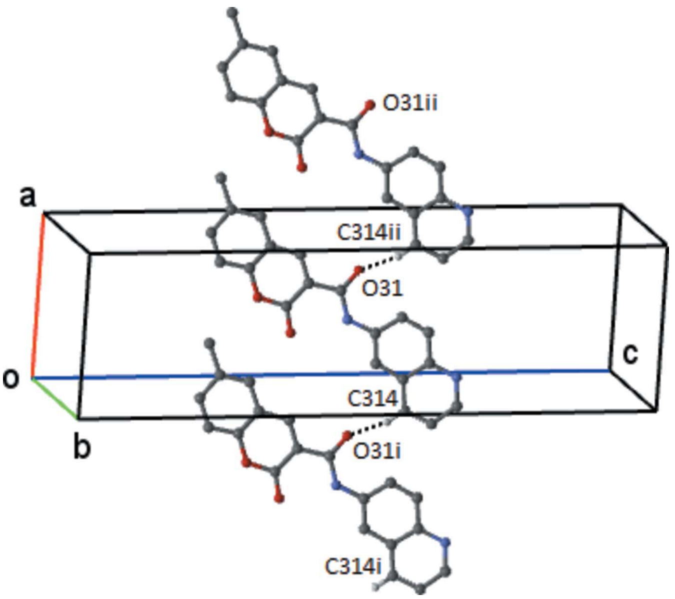

Figure 2
The simple *C*4 chain in compound (1) formed by the weak C314—H314···O3^{i} hydrogen bond. This chain extends by unit translation along the *a* axis. H atoms not involved in the hydrogen bonding have been omitted. [Symmetry codes: (i) $x - 1, y, z$; (ii) $x + 1, y, z$.]

Table 2
Selected dihedral angles (°).

Compound	θ_1 (°)	θ_2 (°)	θ_3 (°)
(1)	6.08 (6)	5.0 (12)	1.73 (11)

Notes: θ_1 is the dihedral angle between the mean planes of the coumarin and quinoline rings; θ_2 is the dihedral angle between the mean plane of the coumarin ring and the plane defined by atoms O31/C31/N32; θ_3 is the dihedral angle between the mean plane of the quinoline ring and the plane defined by atoms O31/C31/N32.

The C—N rotamer of the amide group governs the conformation of the molecule: the —*anti* orientation where the N atom is —*cis* positioned with respect to the oxo O atom of the coumarin system allows the establishment of an intramolecular N32—H32···O2 hydrogen bond between the amino group of the carboxamide and the oxo group of the coumarin system, and of a weak intramolecular C317—H317···O31 hydrogen bond that connects the quinoline ring with the O atom of the carboxamide group (Table 1). Both these interactions form *S*(6) rings and connect the spacer carboxamide group with the heteroaromatic rings, probably constraining the rotation/bending of those rings with respect to the plane formed by the amide atoms. In fact, the molecule is roughly planar, as may be evaluated by the set of values for the dihedral angles which are less than 7° (Table 2).

3. Supramolecular features

In the crystal of (1), molecules are linked by a weak C314—H314···O31^{i} hydrogen bond to form a *C*(8) chain, which runs parallel to the *a* axis (Fig. 2 and Table 1). There are several π–π contacts that will be described below.

4. Hirshfeld surface analyses

The Hirshfeld surfaces and two-dimensional fingerprint (FP) plots (Rohl *et al.*, 2008) were generated using *Crystal Explorer* (Wolff *et al.*, 2012). Compound (1) has three O atoms and an N atom that can potentially act as acceptors for hydrogen bonds, but one of the lone pairs of the oxo O atoms of the coumarin nucleus and of the amide moiety are involved in the establishment of intramolecular hydrogen bonds, as discussed above. As such, they contribute to the electronic density of the pro-molecule in the calculation of the Hirshfeld surface, leaving only the remaining pairs available for participation in the supramolecular structure formation. The surface mapped over d_{norm} displays several red spots that correspond to areas of close contacts between the surface and the neighbouring environment, and the FP plot is presented in Fig. 3.

The contributions from various contacts, listed in Table 3, were selected by partial analysis of the FP plot. Taking out the H···H contacts on the surface that are inherent to organic molecules, the most significant contacts can be divided in three groups: (i) H···O/O···H together with H···N/N···H that correspond to weak C—H···O/N intermolecular interactions (24.5%); (ii) C···C and N···C/C···N contacts that are related

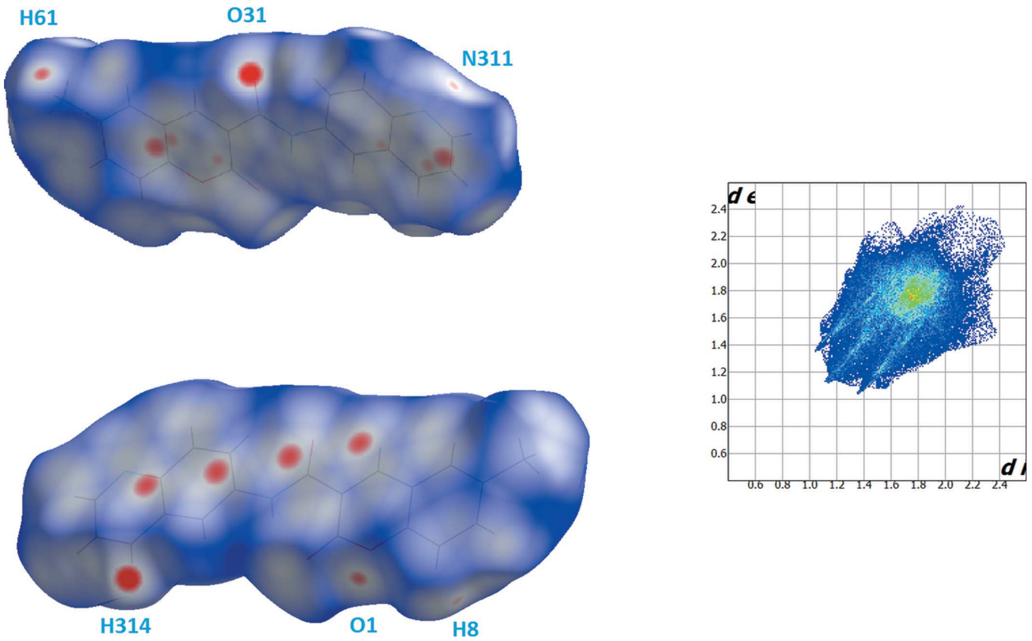

Figure 3
Views of the Hirshfeld surface mapped over $d_{\rm norm}$ (left) and fingerprint plot (right, FP) for (1). The highlighted red spots on the top face of the surfaces indicate contact points with the atoms participating in the intermolecular C—H$\cdots$O interactions, whereas those on the middle of the surface corresponds to C$\cdots$C contacts consequent of the π–π stacking. The C$\cdots$C contacts contribute to the higher frequency of the pixels at d_e/d_i at 1.8° on the FP plot (yellow spot). The FP plot displays two light-blue spikes (external ends corresponding to C$\cdots$ H contacts).

with π–π stacking (17.9%): (iii) H$\cdots$C/C$\cdots$H contacts (14.3%).

Table 3
Percentages of atom–atom contacts for (1) (%).

Contact	H$\cdots$H	H$\cdots$O/ O$\cdots$H	H$\cdots$N/ N$\cdots$H	C$\cdots$C	N$\cdots$C/ C$\cdots$N	H$\cdots$C/ C$\cdots$H
(%)	40.6	21.2	3.3	13.2	4.7	14.3

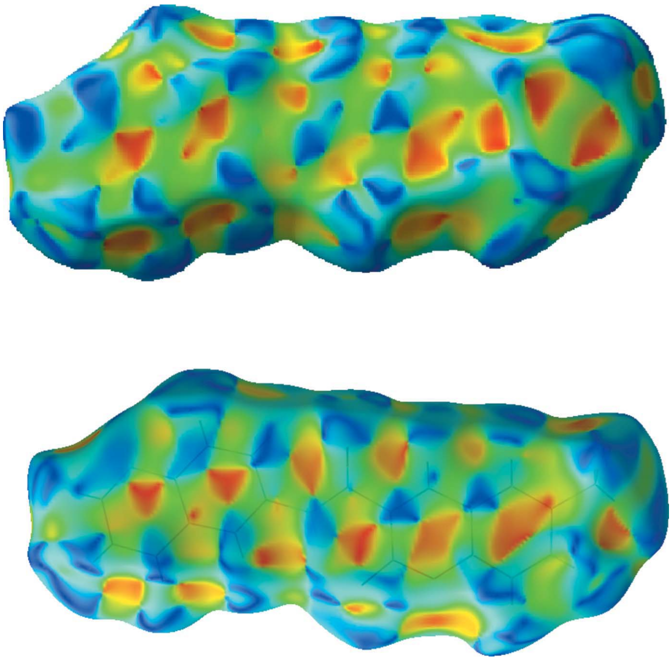

Figure 4
Shape index plots showing the interactions arising from π–π stacking. The upper corresponds to the stacking across $(\frac{1}{2}, 1, \frac{1}{2})$, while the lower corresponds to the stacking across $(\frac{1}{2}, \frac{1}{2}, \frac{1}{2})$.

The H$\cdots$N/O contacts appear as three highlighted red spots on the top and bottom edges of the surface which form pairs of spots of comlementary size, indicating the contact points of the labelled atoms participating in the C–H$\cdots$N/O interactions (Fig. 3). The strongest spots correspond to oxo atom O31 of the carboxamide acceptor and donor atom H314, which forms the C314—H314$\cdots$O31$^{\rm i}$ hydrogen bond (Table 1), and the other spots correspond to very weak hydrogen-bond contacts, one involving pyrone atom O1 and a H atom of the methyl group (C61—H61$B\cdots$O1$^{\rm ii}$; Table 1), and the other appearing perpendicular to the quinoline N atom indicating a very weak C8—H8$\cdots$N311$^{\rm ii}$ contact (Table 1). In spite of the weakness of these contacts, their relative strength is reflected in the FP plots where the pair of sharp spikes pointing to south-west is highlighted in light blue.

In this structure, C/N$\cdots$C contacts prevail over the C—H$\cdots$C ones. In fact, the packing in (1) is built up by several π–π interactions (Table 4). The red spots in the frontal zone of the surface correspond to these close contacts. Furthermore, the FP plot also reveals an intense cluster at d_e/d_i at 1.8 Å characteristic of C$\cdots$C contacts. Also, when the surface is mapped with shape index, several complementary triangular red hollows and blue bumps appear that are characteristic of the six-ring stacking (Fig. 4). The molecules stack in a column in a head-to-tail fashion along the b axis (Fig. 5). The molecules in these stacks lie across centres of symmetry at $(\frac{1}{2}, 1, \frac{1}{2})$,

Table 4
Selected π–π contacts.

Compound	*CgI*	*CgJ*(aru)	*Cg*–*Cg* (Å)	*CgI*_Perp (Å)	*CgJ*_Perp (Å)	Slippage (Å)
1	*Cg*1	*Cg*2($-x + 1, -y, -z - 1$)	3.548 (2)	3.1477 (4)	3.3051 (4)	1.290
1	*Cg*1	*Cg*2($-x + 1, -y + 1, -z - 1$)	3.911 (3)	−3.3848 (4)	−3.3352 (4)	2.043
1	*Cg*1	*Cg*4($-x + 1, -y + 1, -z - 1$)	3.525 (2)	−3.3851 (4)	−3.2952 (4)	1.252
1	*Cg*2	*Cg*1($-x + 1, -y, -z - 1$)	3.548 (2)	3.3050 (4)	3.1476 (4)	1.637
1	*Cg*2	*Cg*1($-x + 1, -y + 1, -z - 1$)	3.911 (3)	−3.3352 (4)	−3.3849 (4)	1.960
1	*Cg*2	*Cg*3($-x + 1, -y + 1, -z - 1$)	3.797 (3)	−3.3389 (4)	−3.5276 (5)	1.406
1	*Cg*3	*Cg*2($-x + 1, -y + 1, -z - 1$)	3.798 (3)	−3.5277 (5)	−3.3388 (4)	1.809
1	*Cg*4	*Cg*1($-x + 1, -y + 1, -z - 1$)	3.525 (2)	−3.2951 (4)	−3.3852 (4)	0.983

Notes: *CgI*(*J*) = Plane number *I*(*J*); *Cg*–*Cg* = distance between ring centroids; *CgI*_Perp = perpendicular distance of *CgI* on ring *J*; *CgJ*_Perp = perpendicular distance of *CgJ* on ring *I*; Slippage = distance between *CgI* and perpendicular projection of *CgJ* on ring *I*.Plane 1 is the plane of the coumarin pyran ring with *Cg*1 as centroid; Plane 2 is the plane of the quinoline pyridine ring with *Cg*2 as centroid; Plane 3 is the plane of the coumarin phenyl ring with *Cg*3 as centroid; Plane 4 is the plane of the quinoline phenyl ring with *Cg*4 as centroid.Some planes are repeated since they are inclined to each other and as a result give slightly different slippages

Table 5
Experimental details.

Crystal data	
Chemical formula	$C_{20}H_{14}N_2O_3$
M_r	330.33
Crystal system, space group	Monoclinic, $P2_1/n$
Temperature (K)	100
a, b, c (Å)	7.799 (3), 7.014 (3), 27.640 (18)
β (°)	90.18 (6)
V (Å^3)	1512.0 (13)
Z	4
Radiation type	Synchrotron, λ = 0.68891 Å
μ (mm^{-1})	0.09
Crystal size (mm)	0.18 × 0.01 × 0.004
Data collection	
Diffractometer	Three-circle diffractometer
Absorption correction	Empirical (using intensity measurements) (aimless *CCP4*; Evans, 2006)
No. of measured, independent and observed [$I > 2\sigma(I)$] reflections	18408, 4587, 3717
$R_{\rm int}$	0.060
$(\sin \theta/\lambda)_{\max}$ (Å^{-1})	0.714
Refinement	
$R[F^2 > 2\sigma(F^2)]$, $wR(F^2)$, S	0.051, 0.156, 1.13
No. of reflections	4587
No. of parameters	231
H-atom treatment	H atoms treated by a mixture of independent and constrained refinement
$\Delta\rho_{\max}$, $\Delta\rho_{\min}$ (e Å^{-3})	0.54, −0.25

Computer programs: GDA http://www.opengda.org/OpenGDA.html, XIA2 0.4.0.370-g47f3bc3 (Winter, 2010), *SHELXT* (Sheldrick, 2015*a*), ShelXle (Hübschle *et al.*, 2011), *SHELXL2014* (Sheldrick, 2015*b*), *Mercury* (Macrae *et al.*, 2006) and *PLATON* (Spek, 2009).

a centrosymetrically related contact between the pyran and pyridine rings, and across the centre at ($\frac{1}{2}, \frac{1}{2}, \frac{1}{2}$), which involves three short centrosymmetrically related contacts: (i) between the pyran and pyridine rings, (ii) between the pyran ring and the quinoline phenyl ring and (iii) between the coumarin phenyl ring and the pyridine ring.

5. Database survey

As reported by Gomes *et al.* (2016), a search made in the Cambridge Structural Database (CSD, Version 35.7; Groom *et al.*, 2016) revealed the existence of 35 deposited compounds (42 molecules) containing the coumarin carboxamide unit, all of which contained the same intramolecular hydrogen bonds. The present compound also contains these bonds, as described above.

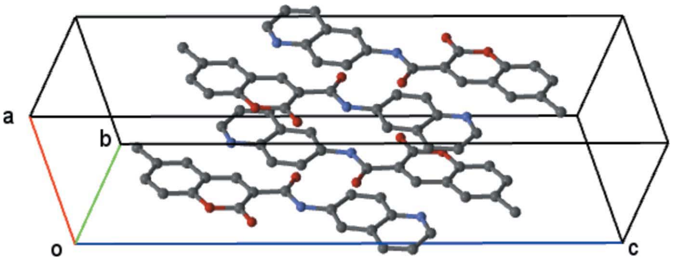

Figure 5
View of the π–π stacking along the *b* axis.

6. Synthesis and crystallization

6-Methylcoumarin-3-carboxylic acid (Murata *et al.*., 2005) (1 mmol) was dissolved in dichloromethane and 3-[3-(dimethylamino)propyl]-1-ethylcarbodiimide (1.10 mmol) and 4-dimethylaminopyridine (1.10 mmol) were added. The mixture was kept under a flux of argon at 273 K for 5 min. 6-Aminoquinoline (1 mmol) was then added in small portions. The reaction mixture was stirred for 4 h at room temperature. The obtained precipitate was filtered off and recrystallized from methanol to give colourless needles of (1). Overall yield: 53%; m.p. 545–546 K.

7. Refinement

H atoms were treated as riding atoms, with aromatic C—H = 0.95 Å, with $U_{\rm iso}$(H) = 1.2$U_{\rm eq}$(C), and methyl C—H = 0.98 Å, with $U_{\rm iso}$(H) = 1.5$U_{\rm eq}$(C). The amino H atoms were freely refined. Crystal data, data collection and structure refinement details are summarized in Table 5.

Acknowledgements

The authors thank the staff at the National Crystallographic Service, University of Southampton, for the data collection, help and advice (Coles & Gale, 2012), and the Foundation for Science and Technology (FCT) and FEDER/COMPETE2020 (UID/QUι00081/2015 and POCI-01–0145-FEDER-006980). AF (SFRH/BD/80831/2011) and MJM (SFRH/BPD/95345/2013) were supported by grants from FCT, POPH and QREN.

References

Camps, P., Formosa, X., Galdeano, C., Muñoz-Torrero, D., Ramírez, L., Gómez, E., Isambert, N., Lavilla, R., Badia, A., Clos, M. V., Bartolini, M., Mancini, F., Andrisano, V., Arce, M. P., Rodríguez-Franco, M. I., Huertas, O., Dafni, T. & Luque, F. J. (2009). *J. Med. Chem.* **52**, 5365–5379.

Chimenti, F., Bizzarri, B., Bolasco, A., Secci, D., Chimenti, P., Granese, A., Carradori, S., Rivanera, D., Zicari, A., Scaltrito, M. M. & Sisto, F. (2010). *Bioorg. Med. Chem. Lett.* **20**, 4922–4926.

Coles, S. J. & Gale, P. A. (2012). *Chem. Sci.* **3**, 683–689.

Evans, P. (2006). *Acta Cryst.* D**62**, 72–82.

Gomes, L. R., Low, J. N., Fonseca, A., Matos, M. J. & Borges, F. (2016). *Acta Cryst.* E**72**, 926–932.

Groom, C. R., Bruno, I. J., Lightfoot, M. P. & Ward, S. C. (2016). *Acta Cryst.* B**72**, 171–179.

Hübschle, C. B., Sheldrick, G. M. & Dittrich, B. (2011). *J. Appl. Cryst.* **44**, 1281–1284.

Macrae, C. F., Edgington, P. R., McCabe, P., Pidcock, E., Shields, G. P., Taylor, R., Towler, M. & van de Streek, J. (2006). *J. Appl. Cryst.* **39**, 453–457.

Matos, M. J., Janeiro, P., Gonz\'alez Franco, R. M., Vilar, S., Tatonetti, N. P., Santana, L., Uriarte, E., Borges, F., Fontenla, J. A. & Viña, D. (2014). *Future Med. Chem.* **6**, 371–383.

Matos, M. J., Viña, D., Quezada, E., Picciau, C., Delogu, G., Orallo, F., Santana, L. & Uriarte, E. (2009). *Bioorg. Med. Chem. Lett.* **19**, 3268–3270.

Murata, C., Masuda, T., Kamochi, Y., Todoroki, K., Yoshida, H., Nohta, H., Yamaguchi, M. & Takadate, A. (2005). *Chem. Pharm. Bull. (Tokyo)*, **53**, 750–758.

Rohl, A. L., Moret, M., Kaminsky, W., Claborn, K., McKinnon, J. J. & Kahr, B. (2008). *Cryst. Growth Des.* **8**, 451–4525.

Sheldrick, G. M. (2015*a*). *Acta Cryst.* A**71**, 3–8.

Sheldrick, G. M. (2015*b*). *Acta Cryst.* C**71**, 3–8.

Spek, A. L. (2009). *Acta Cryst.* D**65**, 148–155.

Sridharan, V., Suryavanshi, P. & Menéndez, J. C. (2011). *Chem. Rev.* **111**, 7157–7259.

Vazquez-Rodriguez, S., Matos, M. J., Santana, L., Uriarte, E., Borges, F., Kachler, S. & Klotz, K. N. (2013). *J. Pharm. Pharmacol.* **65**, 607–703.

Winter, G. (2010). *J. Appl. Cryst.* **43**, 186–190.

Wolff, S. K., Grimwood, D. J., McKinnon, J. J., Turner, M. J., Jayatilaka, D. & Spackman, M. A. (2012). *Crystal Explorer*. The University of Western Australia.

supporting information

Acta Cryst. (2016). E**72**, 1121-1125 [doi:10.1107/S2056989016011026]

6-Methyl-2-oxo-*N*-(quinolin-6-yl)-2*H*-chromene-3-carboxamide: crystal structure and Hirshfeld surface analysis

Lígia R. Gomes, John Nicolson Low, André Fonseca, Maria João Matos and Fernanda Borges

Computing details

Data collection: GDA http://www.opengda.org/OpenGDA.html; cell refinement: XIA2 0.4.0.370-g47f3bc3, (Winter, 2010; data reduction: XIA2 0.4.0.370-g47f3bc3 (Winter, 2010; program(s) used to solve structure: SHELXT (Sheldrick, 2015a); program(s) used to refine structure: ShelXle (Hübschle *et al.*, 2011) *SHELXL2014*/7 (Sheldrick, 2015b); molecular graphics: *Mercury* (Macrae *et al.*, 2006); software used to prepare material for publication: *SHELXL2014*/17 (Sheldrick, 2015b) *PLATON* (Spek, 2009).

(I)

Crystal data

$C_{20}H_{14}N_2O_3$	$F(000) = 688$
$M_r = 330.33$	$D_x = 1.451$ Mg m^{-3}
Monoclinic, $P2_1/n$	Synchrotron′ radiation, $\lambda = 0.68891$ Å
$a = 7.799$ (3) Å	Cell parameters from 3773 reflections
$b = 7.014$ (3) Å	$\theta = 2.6$–$33.9°$
$c = 27.640$ (18) Å	$\mu = 0.09$ mm^{-1}
$\beta = 90.18$ (6)°	$T = 100$ K
$V = 1512.0$ (13) Å^3	Needle, colourless
$Z = 4$	0.18 × 0.01 × 0.004 mm

Data collection

Three-circle diffractometer	18408 measured reflections
Radiation source: synchrotron, DLS beamline I19, undulator	4587 independent reflections
	3717 reflections with $I > 2\sigma(I)$
Si 111, double crystal monochromator	$R_{\text{int}} = 0.060$
Detector resolution: 5.81 pixels mm^{-1}	$\theta_{\text{max}} = 29.5°$, $\theta_{\text{min}} = 2.9°$
profile data from ω–scans	$h = -11 \rightarrow 11$
Absorption correction: empirical (using intensity measurements) aimless ccp4 (Evans, 2006)	$k = -10 \rightarrow 10$
	$l = -39 \rightarrow 39$

Refinement

Refinement on F^2	231 parameters
Least-squares matrix: full	0 restraints
$R[F^2 > 2\sigma(F^2)] = 0.051$	Hydrogen site location: mixed
$wR(F^2) = 0.156$	H atoms treated by a mixture of independent and constrained refinement
$S = 1.13$	
4587 reflections	

$w = 1/[\sigma^2(F_o^2) + (0.0954P)^2]$
where $P = (F_o^2 + 2F_c^2)/3$
$(\Delta/\sigma)_{max} = 0.001$

$\Delta\rho_{max} = 0.54$ e Å^{-3}
$\Delta\rho_{min} = -0.25$ e Å^{-3}

Special details

Geometry. All esds (except the esd in the dihedral angle between two l.s. planes) are estimated using the full covariance matrix. The cell esds are taken into account individually in the estimation of esds in distances, angles and torsion angles; correlations between esds in cell parameters are only used when they are defined by crystal symmetry. An approximate (isotropic) treatment of cell esds is used for estimating esds involving l.s. planes.

Fractional atomic coordinates and isotropic or equivalent isotropic displacement parameters (Å^2)

	x	y	z	U_{iso}*/U_{eq}
O1	0.61633 (10)	0.57511 (12)	0.33247 (3)	0.02193 (19)
O2	0.42390 (10)	0.67655 (12)	0.38475 (3)	0.0244 (2)
O31	0.79011 (10)	0.65810 (12)	0.49728 (3)	0.0240 (2)
N32	0.50968 (12)	0.71842 (13)	0.47835 (3)	0.0186 (2)
N311	0.21868 (12)	0.98576 (13)	0.65151 (3)	0.0204 (2)
C2	0.57274 (14)	0.62613 (16)	0.37867 (4)	0.0196 (2)
C3	0.70619 (13)	0.61438 (15)	0.41571 (4)	0.0177 (2)
C4	0.86585 (13)	0.55411 (15)	0.40316 (4)	0.0180 (2)
H4	0.9519	0.5451	0.4275	0.022*
C5	1.07250 (14)	0.44450 (15)	0.33910 (4)	0.0200 (2)
H5	1.1628	0.4362	0.3622	0.024*
C4A	0.90818 (14)	0.50369 (15)	0.35425 (4)	0.0182 (2)
C6	1.10480 (15)	0.39806 (16)	0.29103 (4)	0.0222 (2)
C7	0.97020 (15)	0.41362 (17)	0.25763 (4)	0.0238 (2)
H7	0.9904	0.3821	0.2247	0.029*
C8	0.80789 (15)	0.47398 (17)	0.27134 (4)	0.0230 (2)
H8	0.7184	0.4858	0.2482	0.028*
C8A	0.77937 (14)	0.51669 (16)	0.31972 (4)	0.0195 (2)
C31	0.67345 (13)	0.66578 (15)	0.46783 (4)	0.0185 (2)
C34A	0.18814 (13)	0.89163 (15)	0.56639 (4)	0.0176 (2)
C38A	0.28705 (13)	0.91692 (15)	0.60890 (4)	0.0178 (2)
C61	1.27981 (16)	0.3329 (2)	0.27477 (5)	0.0312 (3)
H61A	1.3103	0.2147	0.2916	0.047*
H61B	1.3647	0.4316	0.2824	0.047*
H61C	1.2781	0.3101	0.2398	0.047*
C312	0.05500 (14)	1.03063 (16)	0.65149 (4)	0.0219 (2)
H312	0.0075	1.0795	0.6806	0.026*
C313	−0.05445 (14)	1.01098 (16)	0.61122 (4)	0.0219 (2)
H313	−0.1717	1.0466	0.6133	0.026*
C314	0.01123 (13)	0.93934 (16)	0.56876 (4)	0.0199 (2)
H314	−0.0609	0.9220	0.5413	0.024*
C315	0.26757 (13)	0.82186 (15)	0.52375 (4)	0.0183 (2)
H315	0.2006	0.8037	0.4954	0.022*
C316	0.44016 (14)	0.78004 (15)	0.52286 (4)	0.0178 (2)
C317	0.53856 (14)	0.80040 (16)	0.56555 (4)	0.0197 (2)
H317	0.6569	0.7683	0.5655	0.024*

C318	0.46224 (14)	0.86712 (16)	0.60735 (4)	0.0198 (2)
H318	0.5297	0.8798	0.6358	0.024*
H32	0.440 (2)	0.709 (3)	0.4521 (6)	0.042 (5)*

Atomic displacement parameters (Å²)

	U^{11}	U^{22}	U^{33}	U^{12}	U^{13}	U^{23}
O1	0.0188 (4)	0.0271 (4)	0.0199 (4)	−0.0001 (3)	0.0003 (3)	−0.0025 (3)
O2	0.0186 (4)	0.0295 (5)	0.0250 (4)	0.0018 (3)	−0.0007 (3)	−0.0027 (3)
O31	0.0209 (4)	0.0295 (5)	0.0216 (4)	0.0024 (3)	−0.0005 (3)	−0.0043 (3)
N32	0.0184 (4)	0.0194 (5)	0.0180 (4)	0.0012 (3)	0.0018 (3)	−0.0009 (3)
N311	0.0226 (4)	0.0201 (5)	0.0186 (5)	−0.0011 (3)	0.0019 (3)	−0.0011 (3)
C2	0.0200 (5)	0.0186 (5)	0.0203 (5)	−0.0020 (4)	0.0014 (4)	−0.0007 (4)
C3	0.0185 (5)	0.0164 (5)	0.0183 (5)	−0.0012 (4)	0.0012 (4)	−0.0004 (4)
C4	0.0192 (5)	0.0155 (5)	0.0193 (5)	−0.0012 (4)	0.0008 (4)	0.0000 (4)
C5	0.0208 (5)	0.0178 (5)	0.0214 (5)	−0.0001 (4)	0.0019 (4)	−0.0001 (4)
C4A	0.0199 (5)	0.0154 (5)	0.0194 (5)	−0.0022 (4)	0.0021 (4)	−0.0006 (4)
C6	0.0242 (5)	0.0197 (5)	0.0227 (5)	−0.0012 (4)	0.0046 (4)	−0.0018 (4)
C7	0.0273 (5)	0.0240 (6)	0.0202 (5)	−0.0030 (4)	0.0042 (4)	−0.0024 (4)
C8	0.0248 (5)	0.0258 (6)	0.0185 (5)	−0.0030 (4)	−0.0011 (4)	−0.0013 (4)
C8A	0.0188 (5)	0.0193 (5)	0.0202 (5)	−0.0024 (4)	0.0021 (4)	−0.0007 (4)
C31	0.0194 (5)	0.0151 (5)	0.0212 (5)	−0.0009 (4)	0.0025 (4)	−0.0005 (4)
C34A	0.0178 (5)	0.0144 (5)	0.0205 (5)	−0.0002 (3)	0.0016 (4)	0.0011 (4)
C38A	0.0194 (5)	0.0158 (5)	0.0181 (5)	−0.0013 (4)	0.0016 (4)	0.0003 (4)
C61	0.0253 (6)	0.0408 (8)	0.0274 (6)	0.0069 (5)	0.0052 (5)	−0.0060 (5)
C312	0.0238 (5)	0.0204 (5)	0.0214 (5)	−0.0012 (4)	0.0057 (4)	−0.0012 (4)
C313	0.0188 (5)	0.0216 (5)	0.0251 (6)	0.0002 (4)	0.0032 (4)	0.0006 (4)
C314	0.0180 (5)	0.0202 (5)	0.0215 (5)	−0.0006 (4)	−0.0001 (4)	0.0015 (4)
C315	0.0195 (5)	0.0167 (5)	0.0188 (5)	0.0004 (4)	−0.0001 (4)	0.0003 (4)
C316	0.0201 (5)	0.0148 (5)	0.0185 (5)	−0.0001 (4)	0.0029 (4)	0.0006 (4)
C317	0.0183 (5)	0.0203 (5)	0.0206 (5)	0.0010 (4)	0.0016 (4)	0.0002 (4)
C318	0.0204 (5)	0.0207 (5)	0.0185 (5)	−0.0005 (4)	−0.0011 (4)	−0.0002 (4)

Geometric parameters (Å, º)

O1—C2	1.3701 (16)	C7—H7	0.9500
O1—C8A	1.3827 (14)	C8—C8A	1.3887 (18)
O2—C2	1.2255 (14)	C8—H8	0.9500
O31—C31	1.2201 (16)	C34A—C38A	1.4149 (18)
N32—C31	1.3618 (14)	C34A—C315	1.4200 (17)
N32—C316	1.4136 (16)	C34A—C314	1.4214 (15)
N32—H32	0.907 (18)	C38A—C318	1.4111 (16)
N311—C312	1.3147 (15)	C61—H61A	0.9800
N311—C38A	1.3814 (16)	C61—H61B	0.9800
C2—C3	1.4600 (18)	C61—H61C	0.9800
C3—C4	1.3609 (15)	C312—C313	1.4075 (19)
C3—C31	1.5075 (18)	C312—H312	0.9500
C4—C4A	1.4368 (17)	C313—C314	1.3769 (17)

C4—H4	0.9500	C313—H313	0.9500
C5—C6	1.3918 (18)	C314—H314	0.9500
C5—C4A	1.4119 (16)	C315—C316	1.3779 (15)
C5—H5	0.9500	C315—H315	0.9500
C4A—C8A	1.3866 (18)	C316—C317	1.4128 (18)
C6—C7	1.4000 (19)	C317—C318	1.3830 (17)
C6—C61	1.5092 (17)	C317—H317	0.9500
C7—C8	1.3886 (17)	C318—H318	0.9500

C2—O1—C8A	123.10 (10)	N32—C31—C3	115.51 (11)
C31—N32—C316	129.15 (11)	C38A—C34A—C315	119.63 (10)
C31—N32—H32	111.5 (11)	C38A—C34A—C314	117.32 (10)
C316—N32—H32	119.3 (11)	C315—C34A—C314	123.05 (11)
C312—N311—C38A	117.43 (11)	N311—C38A—C318	119.26 (11)
O2—C2—O1	116.17 (11)	N311—C38A—C34A	122.75 (10)
O2—C2—C3	126.42 (11)	C318—C38A—C34A	117.98 (10)
O1—C2—C3	117.42 (10)	C6—C61—H61A	109.5
C4—C3—C2	119.32 (11)	C6—C61—H61B	109.5
C4—C3—C31	118.40 (11)	H61A—C61—H61B	109.5
C2—C3—C31	122.28 (10)	C6—C61—H61C	109.5
C3—C4—C4A	121.96 (11)	H61A—C61—H61C	109.5
C3—C4—H4	119.0	H61B—C61—H61C	109.5
C4A—C4—H4	119.0	N311—C312—C313	124.28 (11)
C6—C5—C4A	121.27 (12)	N311—C312—H312	117.9
C6—C5—H5	119.4	C313—C312—H312	117.9
C4A—C5—H5	119.4	C314—C313—C312	118.92 (10)
C8A—C4A—C5	118.13 (11)	C314—C313—H313	120.5
C8A—C4A—C4	117.61 (11)	C312—C313—H313	120.5
C5—C4A—C4	124.25 (11)	C313—C314—C34A	119.27 (11)
C5—C6—C7	118.28 (11)	C313—C314—H314	120.4
C5—C6—C61	121.45 (12)	C34A—C314—H314	120.4
C7—C6—C61	120.28 (11)	C316—C315—C34A	121.13 (11)
C8—C7—C6	121.73 (11)	C316—C315—H315	119.4
C8—C7—H7	119.1	C34A—C315—H315	119.4
C6—C7—H7	119.1	C315—C316—C317	119.45 (11)
C7—C8—C8A	118.52 (12)	C315—C316—N32	117.26 (11)
C7—C8—H8	120.7	C317—C316—N32	123.29 (10)
C8A—C8—H8	120.7	C318—C317—C316	119.86 (10)
O1—C8A—C4A	120.59 (10)	C318—C317—H317	120.1
O1—C8A—C8	117.36 (11)	C316—C317—H317	120.1
C4A—C8A—C8	122.06 (11)	C317—C318—C38A	121.90 (11)
O31—C31—N32	124.57 (11)	C317—C318—H318	119.0
O31—C31—C3	119.91 (10)	C38A—C318—H318	119.0

C8A—O1—C2—O2	179.41 (9)	C4—C3—C31—O31	2.12 (16)
C8A—O1—C2—C3	−0.94 (15)	C2—C3—C31—O31	−178.23 (10)
O2—C2—C3—C4	179.54 (11)	C4—C3—C31—N32	−177.74 (9)
O1—C2—C3—C4	−0.06 (15)	C2—C3—C31—N32	1.91 (15)

O2—C2—C3—C31	−0.09 (18)	C312—N311—C38A—C318	179.98 (10)
O1—C2—C3—C31	−179.70 (9)	C312—N311—C38A—C34A	−0.77 (16)
C2—C3—C4—C4A	0.81 (16)	C315—C34A—C38A—N311	179.40 (10)
C31—C3—C4—C4A	−179.54 (9)	C314—C34A—C38A—N311	−0.32 (16)
C6—C5—C4A—C8A	−0.76 (16)	C315—C34A—C38A—C318	−1.34 (15)
C6—C5—C4A—C4	−179.86 (10)	C314—C34A—C38A—C318	178.94 (10)
C3—C4—C4A—C8A	−0.58 (16)	C38A—N311—C312—C313	0.74 (17)
C3—C4—C4A—C5	178.52 (10)	N311—C312—C313—C314	0.39 (18)
C4A—C5—C6—C7	0.76 (17)	C312—C313—C314—C34A	−1.51 (16)
C4A—C5—C6—C61	−179.40 (11)	C38A—C34A—C314—C313	1.45 (15)
C5—C6—C7—C8	0.15 (18)	C315—C34A—C314—C313	−178.25 (10)
C61—C6—C7—C8	−179.69 (11)	C38A—C34A—C315—C316	−0.68 (16)
C6—C7—C8—C8A	−1.03 (18)	C314—C34A—C315—C316	179.02 (10)
C2—O1—C8A—C4A	1.19 (16)	C34A—C315—C316—C317	2.29 (16)
C2—O1—C8A—C8	−178.25 (10)	C34A—C315—C316—N32	−177.58 (9)
C5—C4A—C8A—O1	−179.57 (9)	C31—N32—C316—C315	−178.87 (10)
C4—C4A—C8A—O1	−0.41 (15)	C31—N32—C316—C317	1.27 (18)
C5—C4A—C8A—C8	−0.15 (17)	C315—C316—C317—C318	−1.86 (16)
C4—C4A—C8A—C8	179.00 (10)	N32—C316—C317—C318	178.01 (10)
C7—C8—C8A—O1	−179.54 (10)	C316—C317—C318—C38A	−0.20 (17)
C7—C8—C8A—C4A	1.03 (18)	N311—C38A—C318—C317	−178.93 (10)
C316—N32—C31—O31	2.43 (19)	C34A—C38A—C318—C317	1.78 (16)
C316—N32—C31—C3	−177.72 (10)		

Hydrogen-bond geometry (Å, º)

D—H···*A*	*D*—H	H···*A*	*D*···*A*	*D*—H···*A*
C314—H314···O31^{i}	0.95	2.50	3.278 (2)	139
C8—H8···N311^{ii}	0.95	2.68	3.394 (3)	133
C317—H317···O31	0.95	2.29	2.903 (2)	122
N32—H32···O2	0.907 (18)	1.879 (18)	2.686 (2)	147.3 (15)

Symmetry codes: (i) *x*−1, *y*, *z*; (ii) *x*+1/2, −*y*+3/2, *z*−1/2.

Manuscript VIII

Coumarins and adenosine receptors: new perceptions in structure-affinity relationships.

To be submitted to Chemical Biology & Drug Design

Coumarins and adenosine receptors: new perceptions in structure-affinity relationships

André Fonseca[a, b], Maria João Matos[a], Santiago Vilar[a,b], Sonja Kachler[c], Karl-Norbert Klotz[c], Eugenio Uriarte[b] and Fernanda Borges[a]

[a]CIQUP/Department of Chemistry and Biochemistry, Faculty of Sciences, University of Porto, 4169-007, Porto, Portugal
[b]Organic Chemistry Department, Faculty of Pharmacy, University of Santiago de Compostela, 15782, Santiago de Compostela, Spain
[c]Pharmacology and Toxicology Institute, University of Würzburg, 97078, Würzburg, Germany

*Corresponding Author: Fernanda Borges, CIQUP/Department of Chemistry and Biochemistry, Faculty of Sciences, University of Porto, 4169-007, Porto, Portugal. E-mail: fborges@fc.up.pt

Keywords: Coumarins; Adenosine Receptors; carboxamidocoumarin;

Abstract

Adenosine receptors (ARs) subtypes are involved in several physiological and pharmacological processes. Ligands able to selectively modulate one receptor subtype can delay or slow down the progression of diverse diseases. In this context, our research group focused its investigation into the discovery and development of novel, potent and selective ARs ligands based on coumarin scaffold. Therefore, a series 3-phenylcarboxamidocoumarins were synthesised and their affinity for the human ARs subtypes was screened by radioligand binding assays for A_1, A_{2A} and A_3 receptors and for A_{2B} by adenylyl cyclase assay. Compound **26** was found to be the most remarkable, with a hA_1/hA_3 and hA_{2A}/hA_3 selectivity of 42, for the A_3 AR (K_i = 2.4 μM). Receptor-driven molecular modelling studies have provided valuable information on the binding/selectivity data of compound **26** and for the following optimization process. Moreover, compound **26** present drug-like properties according to the general guidelines linked to the concept.

Introduction

Adenosine is an endogenous purine nucleoside with an important role in a diversity of biochemical processes, namely in energy transfer (adenosine triphosphate or ATP) and in cellular signalling (cyclic AMP). In the 1920's it was demonstrated for the first time adenosine biologic action in the cardiovascular system.[1] In addition to its clinical role as anti-arrhythmic agent, adenosine has been implicated in diverse areas of medicine and throughout the years adenosine signaling pathways have often been used in drug design and development projects, with adenosine itself or its derivatives being used clinically since the 1940s.[2]

Generally, extracellular adenosine is a signaling molecule that can activate adenosine receptors (ARs).[2] To this date four distinct and widely expressed human AR subtypes – A_1, A_{2A}, A_{2B} and A_3 – have been discovered, each one implicated in a number of physiological and pathological processes. The structure, function, and basis for classification of ARs and their genes has been extensively reviewed.[3] In particular, activation of ARs can induce inhibition (A_1AR and A_3AR) or activation (A_{2A}AR and A_{2B}AR) of adenylyl cyclase an enzyme that catalyses the conversion of ATP into cyclic adenosine monophosphate (cAMP). Activation or blockade of ARs is responsible for a wide range of effects in numerous organ systems and therefore the regulation of ARs can have many potential therapeutic applications.[4] Pharmacological modulation of AR pathways open a new window for drug treatment of a variety of pathologies, such as asthma, neurodegenerative disorders, cancer, inflammatory and ischaemic related diseases.[5–9]

Coumarins are naturally occurring heterocyclic compounds with an in-depth history in Medicinal Chemistry,[10] as they have been exploited in quite a lot of projects aiming to find, for instance, anti-cancer, antioxidant, anti-inflammatory, antimicrobial and antiviral agents.[11] Although benzopyran is considered a privileged structure, few studies have been addressed towards its application in the discovery of new ARs ligands. In this context, a number of coumarin based derivatives have been reported by our group as inspiring ligands (**Figure 1**), in particular 3-arylcoumarins. [12–15]

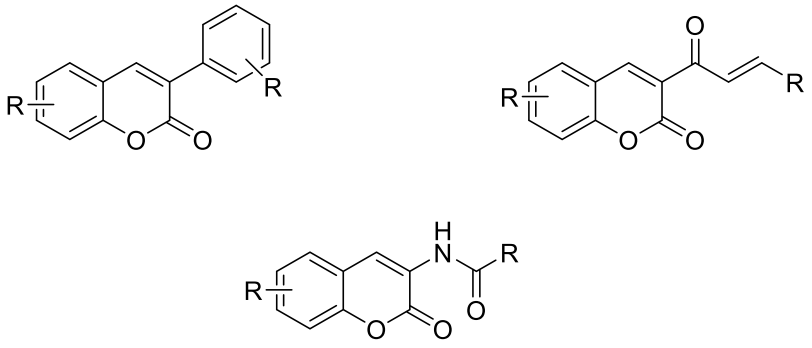

Figure 1. General structure of coumarin based derivatives described as AR ligands.[12–15]

Preliminary structure-activity relationship studies indicated that the nature of the substituents located in the coumarin ring, the presence or absence of a spacer between the pyrone ring and an aryl or alkyl side chain can modulate their affinity and selectivity, in particular towards A_3AR. To gain insight over the structural requirements needed for the attainment of a potent and selective AR coumarin-based ligand a series of 6-substituted coumarin derivatives was synthesised, characterised and pharmacologically evaluated. In addition, as amide group has also been proposed as operative either in coumarins or chromones this type of spacer was chosen.[16] The research was accomplished by receptor-driven molecular modelling studies.

Methods and materials

Materials and instruments

All starting materials and reagents were obtained from commercial suppliers and were used without further purification. Melting points (mp) were determined using a Reichert Kofler thermopan or a Büchi 510 apparatus and were not corrected. ^{1}H (250 MHz) and ^{13}C (63 MHz) NMR spectra were recorded on a Bruker AMX spectrometer, using DMSO-d_6 or $CDCl_3$ as solvents. Chemical shifts (δ) and coupling constants (*J)* were expressed in ppm and in Hz, respectively. TMS was used as internal standard. The notations for multiplicity patterns were: *s* (singlet), *d* (doublet), *dd* (double doublet), *t* (triplet), *dt* (double triplet) and *m* (multiplet). Mass spectrometry data was acquired with a Hewlett-Packard-5972-MSD spectrometer. Silica gel (Merck 60, 230–400 mesh) was used for flash chromatography (FC). Analytical thin layer chromatography (TLC) was performed on plates precoated with silica gel (Merck 60 F254, 0.25 mm). Organic solutions were dried over anhydrous Na_2SO_4. The solvents were evaporated on a rotary evaporator (Büchi Rotavapor).

Synthesis

General procedure for the synthesis of coumarin 3-phenylcarboxamides (**8-19**):

To a solution of coumarin-3-carboxylic acid (**5**, **6** or **7**, 1.0 mmol) in dichloromethane (DCM, 5 mL) 1-ethyl-3-(3-dimethylaminopropyl)carbodiimide (EDC, 1.1 mmol) and 4-dimethylaminopyridine (DMAP, 1.1 mmol) were added. The mixture was kept in an argon flux at 0 ºC for five minutes. Shortly after, the aromatic amine (1.0 mmol) with the pretended substitution pattern was added in small portions. The reaction mixture was stirred at room temperature for 4 hours. The obtained precipitate was filtered and purified by column chromatography (hexane/ethyl acetate 9:1) or by recrystallization with ethanol to give the desired compounds.

The synthesis of the precursors (**3-7**) and compounds (**9**, **12**, **15**, **21**, **24**, **27**, **30**, **36**, **39**, **42**, **45** and **51**) has been previously described.[17]

N-(2'-Hydroxyphenyl)coumarin-3-carboxamide (**8**) Yield: 54%; mp: 269-270 ºC. ^{1}H NMR (DMSO-d_6) δ (ppm), *J* (Hz): 6.82-6-92 (m, 3H, H-8, H-4', H-5'), 7.46-7.57 (m, 2H, H-6, H-7), 7.76 (d, 1H, H-5, *J*=7.4), 8.04 (d, 1H, H-3', *J*=7.1), 8.39 (d, 1H, H-6', *J*=7.1), 9.05 (s, 1H, H-4), 10.23 (s, 1H, OH), 11.11 (s, 1H, NH). ^{13}C NMR (DMSO-d_6) δ (ppm): 161.2, 154.1, 148.5, 146.8, 134.6, 130.6, 126.7, 125.4, 124.4, 120.0, 119.3, 118.8, 116.4, 114.7, 101.4, 98.2. MS m/z (%): 281 (M+, 81), 174 (38), 173 (100), 101 (40), 89 (34).

N-(2'-Hydroxyphenyl)-6-methoxycoumarin-3-carboxamide (**10**) Yield: 47%; mp: 232-233 ºC. ^{1}H NMR (DMSO-d_6) δ (ppm), *J* (Hz): 3.80 (s, 3H, OCH_3), 6.75-6.82 (m, 1H, H-4'), 6.86-6.95 (m, 2H, H-3', H-5'), 7.33 (dd, 1H, H-7, *J*=2.9, 9.1), 7.46 (d, 1H, H-8, *J*=9.1), 7.58 (d, 1H, H-5, *J*=2.9), 8.36 (dd, 1H, H-6', *J*=1.3, 7.8), 8.96 (s, 1H, H-4), 10.17 (s, 1H, OH), 11.10 (s, 1H, NH). ^{13}C NMR (DMSO-d_6) δ (ppm): 161.2, 158.9, 156.1, 148.6, 148.3, 146.7, 126.6, 124.4, 122.4, 120.0, 119.3, 119.7, 118.8, 117.4, 114.7, 111.9, 55.9. MS m/z (%): 312 (M+, 32), 311 (100), 204 (62), 203 (96), 119 (60), 65 (18).

N-(2'-Methylphenyl)coumarin-3-carboxamide (**11**) Yield: 56%; mp: 212-213 ºC. ^{1}H NMR ($CDCl_3$) δ (ppm), *J* (Hz): 2.42 (s, 3H, CH_3), 7.10 (td, 1H, H-4', *J*=1.2, 7.4), 7.22-7.29 (m, 2H, H-7, H-8), 7.38-7.47 (m, 2H, H-6, H-5'), 7.67-7.77 (m, 2H, H-5, H-3'), 8.25 (d, 1H, H-6', *J*=8.2), 9.04 (s, 1H, H-4), 10.79 (s, 1H, NH). ^{13}C NMR ($CDCl_3$) δ (ppm): 164.3, 158.2, 148.8, 148.8, 134.2, 130.3, 129.8, 128.4, 126.6, 125.3, 124.8, 121.7, 118.6, 116.6, 116.5, 99.9, 18.0. MS m/z (%): 279 (M+, 71), 261 (29), 173 (100), 106 (70), 101, (37), 89 (35), 77 (10), 63 (11).

N-(2'-Methylphenyl)-6-methoxycoumarin-3-carboxamide (**13**) Yield: 71%; mp: 186-187 ºC. ^{1}H NMR (CDCl$_3$) δ (ppm), *J* (Hz): 2.39 (s, 3H, CH$_3$), 3.86 (s, 3H, OCH$_3$), 7.02- 7.12 (m, 2H, H-4', H-5'), 7.18- 7.25 (m, 2H, H-3', H-7), 7.27 (d, 1H, H-5, *J*=2.9), 7.36 (d, 1H, H-8, *J*=9.1), 8.22 (d, 1H, H-6', *J*=8.1), 8.96 (s, 1H, H-4), 10.82 (s, 1H, NH). ^{13}C NMR (CDCl$_3$) δ (ppm): 162.1, 159.2, 158.8, 148.9, 136.0, 135.9, 130.3, 128.7, 126.5, 125.0, 122.7, 121.7, 118.9, 117.6, 115.5, 110.5, 55.8, 17.9. MS m/z (%): 309 (M+, 86), 291 (51), 281 (29), 203 (100), 119 (49), 106 (72), 77 (18), 65 (15).

N-(2'-Methoxyphenyl)coumarin-3-carboxamide (**14**) Yield: 64%; mp: 239-240 ºC. ^{1}H NMR (CDCl$_3$) δ (ppm), J (Hz): 3.97 (s, 3H, OCH$_3$), 6.92-7.14 (m, 3H, H-8, H-3', H-6'), 7.41 (m, 2H, H-6, H-4'), 7.71 (m, 2H, H-7, H-5'), 8.54 (d, 1H, H-5, *J*=7.6), 9.00 (s, 1H, H-4), 11.28 (s, 1H, NH). ^{13}C NMR (CDCl$_3$) δ (ppm): 172.1, 150.2, 148.4, 144.5, 140.9, 134.0, 129.7, 127.4, 125.2, 124.4, 120.8, 120.5, 118.3, 116.6, 111.0, 110.1, 55.9. MS m/z (%): 295 (M+, 79), 264 (27), 187 (10), 173 (100), 122 (17), 101 (30), 89 (23).

N-(2'-Methoxyphenyl)-6-methoxycoumarin-3-carboxamide (**16**) Yield: 78%; mp: 193-194 ºC. ^{1}H NMR (CDCl$_3$) δ (ppm), *J* (Hz): 3.85 (s, 3H, OCH$_3$), 3.94 (s, 3H, OCH$_3$'), 6.91 (td, 1H, H-4', *J*=1.4, 8.0), 6.99 (dd, 1H, H-3', *J*=1.5, 7.8), 7.03- 7.12 (m, 2H, H-5, H-5'), 7.22 (dd, 1H, H-7, *J*=3.0, 9.1), 7.33 (d, 1H, H-8, *J*=9.1), 8.51 (dd, 1H, H-6', *J*=1.7, 7.9), 8.91 (s, 1H, H-4), 11.32 (s, 1H, NH). ^{13}C NMR (CDCl$_3$) δ (ppm): 156.5, 149.0, 148.2, 134.5, 131.9, 127.5, 124.39, 122.5, 120.7, 120.4, 119.0, 118.9, 117.6, 110.5, 110.0, 106.8, 63.4, 55.8. MS (%): 326(M+, 30), 325 (82), 294 (28), 204 (30), 203 (100), 119 (53), 65 (18).

N-(2'-Chlorophenyl)coumarin-3-carboxamide (**17**) Yield: 68%; mp: 220-221 ºC. ^{1}H NMR (CDCl$_3$) δ (ppm), *J* (Hz): 7.10 (dt, 1H, H-7, *J*=1.5, 7.7), 7.26-7.47 (m, 4H, H-6, H-4', H-5', H-6'), 7.67-7.76 (m, 2H, H-8, H-3'), 8.56 (dd, 1H, H-5, *J*=1.5, 8.7), 9.02 (s, 1H, H-4), 11.34 (s, 1H, NH). ^{13}C NMR (CDCl$_3$) δ (ppm): 159.4, 154.4, 150.7, 149.0, 134.3, 129.8, 129.2, 127.3, 125.3, 125.1, 122.1, 118.4, 117.7, 116.6, 114.9, 99.9. MS m/z (%): 299 (M+, 37), 264 (100), 173 (99), 145 (9), 101 (51), 89 (47), 75 (13), 63 (22).

N-(2’-Chlorophenyl)-6-methylcoumarin-3-carboxamide (**18**) Yield: 61%; mp: 203-204 ºC. ^{1}H NMR (DMSO-d_6) δ (ppm), *J* (Hz): 2.35 (s, 3H, CH_3), 7.14 (td, 1H, H-4’, *J*=1.6, 6.2), 7.32-7.45 (m, 2H, H-8, H-5’), 7.50-7.60 (m, 2H, H-6, H-3’), 7.79 (s, 1H, H-5), 8.48 (dd, 1H, H-6’, *J*=1.4, 6.8), 8.95 (s, 1H, H-4), 11.24 (s, 1H, NH). ^{13}C NMR (DMSO-d_6) δ (ppm): 171.4, 168.9, 159.7, 152.5, 149.2, 136.3, 134.9, 130.2, 129.5, 128.0, 125.5, 121.8, 118.5, 118.0, 116.8, 115.6, 20.6. MS m/z (%): 313 (M+, 22), 279 (32), 278 (93), 187 (100), 115 (25), 103 (20), 77 (15).

N-(2’-Chlorophenyl)-6-methoxycoumarin-3-carboxamide (**19**) Yield: 73%; mp: 200-201 ºC. ^{1}H NMR (DMSO-d_6) δ (ppm), *J* (Hz): 3.80 (s, 3H, OCH_3), 7.15 (td, 1H, H-4’, *J*=1.4, 7.7), 7.31-7.42 (m, 2H, H-7, H-5’), 7.48 (d, 1H, H-8, *J*=9.0), 7.54 (dd, 1H, H-3’, *J*=1.3, 8.0), 7.61 (d, 1H, H-5, *J*=3.0), 8.49 (dd, 1H, H-6’, *J*=1.4, 8.4), 9.01 (s, 1H, H-4), 11.29 (s, 1H, NH). ^{13}C NMR (DMSO-d_6) δ (ppm): 166.6, 159.8, 156.2, 154.9, 149.0, 148.7, 138.0, 134.8, 129.6, 128.3, 128.1, 122.9, 121.5, 118.4, 117.8, 112.1, 56.0. MS m/z (%): 329 (M+, 45), 295 (54), 294 (99), 204 (37), 205 (100), 119 (60).

N-(2’-Bromophenyl)coumarin-3-carboxamide (**20**) Yield: 32%; mp: 218-219 ºC. ^{1}H NMR ($CDCl_3$) δ (ppm), *J* (Hz): 7.04 (t, 1H, H-4’, *J*=7.6), 7.33-7.47 (m, 3H, H-6, H-8, H-5’), 7.60-7.76 (m, 3H, H-5, H-7, H-3’), 8.51 (d, 1H, H-6’, *J*=8.0), 9.01 (s, 1H, H-4), 11.21 (s, 1H, NH). ^{13}C NMR ($CDCl_3$) δ (ppm): 160.9, 160.0, 154.4, 149.1, 136.1, 134.4, 132.6, 129.8, 128.0, 125.6, 125.3, 122.7, 118.5, 118.4, 116.7, 114.4. MS m/z (%): 346 (M+2, 25), 343 (24), 265 (58), 264 (99), 173 (100), 101 (59), 89 (66), 63 (33)

N-(2’-Bromophenyl)-6-methoxycoumarin-3-carboxamide (**22**) Yield: 36%; mp: 203-204 ºC. ^{1}H NMR (DMSO-d_6) δ (ppm), *J* (Hz): 3.80 (s, 3H, -OCH_3), 7.09 (td, 1H, H-4’, *J*=1.6, 8.0), 7.33-7.45 (m, 2H, H-7, H-5’), 7.49 (d, 1H, H-8, *J*=9.1), 7.61 (d, 1H, H-5, *J*= 2.9), 7.69 (dd, 1H, H-3’, *J*=1.4, 8.0), 8.43 (dd, 1H, H-6’, *J*= 1.5, 8.3), 9.02 (s, 1H, H-4), 11.16 (s, 1H, NH). ^{13}C NMR (DMSO-d_6) δ (ppm): 171.9, 170.1, 166.9, 156.3, 149.1, 148.7, 148.0, 142.8, 136.6, 128.5, 124.4, 122.9, 122.6, 122.4, 117.6, 112.3, 56.0. MS m/z (%): 375 (M+, 16), 295 (44), 294 (98), 204 (23), 203 (100), 187 (55), 119 (24).

N-(3’-Hydroxyphenyl)coumarin-3-carboxamide (**23**) Yield: 51%; mp: 283-284 ºC. ^{1}H NMR (DMSO-d_6) δ (ppm), *J* (Hz): 6.53 (dd, 1H, H-4’, *J*=2.0, 8.1), 6.97-7.19 (m, 2H, H-8, H-5’), 7.31 (dd, 1H, H-2’, *J*=1.8, 2.0), 7.41-7.58 (m, 2H, H-6, H-7), 7.72-7.80 (m, 1H, H-5), 8.00 (dd, 1H, H-6’, *J*=2.0, 7.8), 8.88 (s, 1H, H-4), 9.55 (s, 1H, OH), 10.57 (s, 1H, NH). ^{13}C NMR (DMSO-*d*$_6$) δ (ppm): 161.3, 160.8, 156.7, 149.1, 147.0, 134.9, 129.9, 126.9, 125.1, 122.6, 119.8, 119.7, 119.0, 117.2, 114.1, 100.4. MS m/z (%): 281 (M+, 60), 253 (21), 173 (100), 101 (30), 89 (24).

N-(3’-Hydroxyphenyl)-6-methoxycoumarin-3-carboxamide (**25**) Yield: 57%; mp: 232-233 ºC ^{1}H NMR (DMSO-*d*$_6$) δ (ppm), *J* (Hz): 3.80 (s, 3H, CH_3), 6.51 (ddd, 1H, H-4’, *J*=1.0, 2.3, 8.0), 7.11 (dd, 1H, H-5’, *J*=8.0, 8.0), 7.26-7.37 (m, 2H, H-7, H-6’), 7.48 (d, 1H, H-8, *J*=9.1), 7.55 (d, 1H, H-2’, *J*=3.0), 8.83 (s, 1H, H-4), 9.55 (s, 1H, OH), 10.59 (s, 1H, NH). ^{13}C NMR (DMSO-*d*$_6$) δ (ppm): 161.6, 160.0, 157.8, 153.1, 147.4, 130.0, 125.7, 122.5, 120.0, 117.6, 111.7, 110.9, 108.9, 107.0, 106.7, 104.4, 56.6. MS/EI m/z (%): 312 (M+, 32), 311 (100), 204 (62), 203 (96), 119 (60), 80 (18).

N-(3’-Methylphenyl)coumarin-3-carboxamide (**26**) Yield: 34%; mp: 206-207 ºC. ^{1}H NMR ($CDCl_3$) δ (ppm), J (Hz): 2.38 (s, 3H, CH_3), 6.98 (d, 1H, H-4’, *J*=7.4), 7.24 (dd, 1H, H-5, *J*=1.3, 7.4), 7.38-7.46 (m, 2H, H-6, H-7), 7.50-7.59 (m, 2H, H-8, H-6’), 7.66-7.75 (m, 2H, H-5, H-2’), 9.02 (s, 1H, H-4), 10.79 (s, 1H, NH). ^{13}C NMR ($CDCl_3$) δ (ppm): 161.1, 159.1, 154.3, 148.8, 138.8, 134.2, 129.8, 128.8, 125.5, 125.4, 121.4, 117.5, 116.6, 103.6, 101.6, 98.4, 21.4. MS m/z (%): 279 (M, 75), 173 (100), 101 (29), 89 (24).

N-(3’-Methylphenyl)-6-methoxycoumarin-3-carboxamide (**28**) Yield: 73%; mp: 186-187 ºC ^{1}H NMR ($CDCl_3$) δ (ppm), *J* (Hz): 2.34 (s, 3H, CH_3), 3.87 (s, 3H, OCH_3), 7.07 (d, 1H, H-5, *J*=2.9), 7.17-7.28 (m, 2H, H-2’, H-5’), 7.34 (d, 1H, H-8, *J*=9.1), 7.47-7.55 (m, 2H, H-7, H-6’), 8.92 (s, 1H, H-4), 10.81 (s, 1H, NH). ^{13}C NMR ($CDCl_3$) δ (ppm): 162.1, 159.2, 158.8, 148.6, 136.0, 135.9, 130.3, 128.8, 126.6, 125.0, 122.8, 121.7, 118.9, 117.7, 115.53, 110.52, 55.8, 18.0. MS m/z (%): 310 (M+, 22), 309 (86), 291 (51), 281 (30), 203 (100), 119 (49), 106 (72), 77 (17).

N-(3’-Methoxyphenyl)coumarin-3-carboxamide (**29**) Yield: 47%; mp: 189-190 ºC. ^{1}H NMR ($CDCl_3$) δ (ppm), J (Hz): 3.85 (s, 3H, OCH_3), 6.70-6.76 (m, 1H, H-4’), 7.21-7.32 (m, 2H, H-8, H-2’), 7.38-7.52 (m, 3H, H-6, H-7, H-5’), 7.67-7.77 (m, 2H, H-5, H-6’), 9.02 (s, 1H, H-4), 10.85 (s, 1H, NH). ^{13}C NMR ($CDCl_3$) δ (ppm): 161.6, 160.0, 159.1, 154.3, 148.8, 138.7, 134.2, 129.8, 129.6, 125.4, 118.6, 118.5, 116.6, 112.7, 110.8, 109.8, 55.2. MS m/z (%): 295 (M, 68), 267 (35), 187 (10), 173 (100), 101 (32), 89 (21).

N-(3’-Methoxyphenyl)-6-methoxycoumarin-3-carboxamide (**31**) Yield: 67%; mp: 193-194 ºC. ^{1}H NMR (CDCl$_3$) δ (ppm), J (Hz): 3.81 (s, 3H, OCH$_3$’), 3.85 (s, 3H, OCH$_3$), 6.68 (ddd, 1H, H-4’, *J*=2.2, 2.2, 7.0), 7.06 (d, 1H, H-5, *J*=2.8), 7.18-7.28 (m, 3H, H-7, H-2’, H-5’), 7.34 (d, 1H, H-8, *J*=9.1), 7.44 (d, 1H, H-6’, *J*=2.2), 8.92 (s, 1H, H-4), 10.87 (s, 1H, NH). ^{13}C NMR (CDCl$_3$) δ (ppm): 161.8, 160.0, 159.2, 156.6, 149.0, 148.6, 138.7, 129.6, 122.8, 118.9, 118.5, 117.7, 112.7, 110.7, 110.5, 105.8, 55.8, 55.2. MS m/z (%): 325 (M, 53), 204 (100), 173 (94), 122 (30).

N-(3’-Chlorophenyl)coumarin-3-carboxamide (**32**) Yield: 60%; mp: 217-218 ºC. ^{1}H NMR (DMSO-*d*$_6$) δ (ppm), *J* (Hz): 7.10 (ddd, 1H, H-4’, *J*=1.2, 1.5, 7.8), 7.37-7.49 (m, 2H, H-6, H-8), 7.53-7.59 (m, 2H, H-7, H-5’), 7.78 (dd, 1H, H-2’, *J*=1.2, 1.5), 7.96 (s, 1H, H-5), 8.01 (dd, 1H, H-6’, *J*=1.5, 7.8), 8.89 (s, 1H, H-4), 10.74 (s, 1H, NH). ^{13}C NMR (DMSO-*d*$_6$) δ (ppm): 164.4, 160.9, 159.4, 147.7, 133.4, 132.7, 130.8, 130.5, 128.4, 125.5, 120.0, 119.6, 118.6, 116.4, 113.4, 101.0. MS m/z (%): 299 (M, 67), 173 (100), 101 (36), 89 (30), 63 (13).

N-(3’-Chlorophenyl)-6-methylcoumarin-3-carboxamide (**33**) Yield: 61%; mp: 238-239 ºC ^{1}H NMR (DMSO-*d*$_6$) δ (ppm), *J* (Hz): 2.36 (s, 1H, CH$_3$), 7.17 (ddd, 1H, H-4’, *J*=0.9, 1.8, 8.0), 7.32-7.44 (m, 2H, H-8, H-5’), 7.50-7.60 (m, 2H, H-7, H-6’), 7.75 (d, 1H, H-5, *J*=1.3), 7.93 (dd, 1H, H-2’, *J*=1.8, 1.8), 8.79 (s, 1H, H-4), 10.73 (s, 1H, NH). ^{13}C NMR (DMSO-*d*$_6$) δ (ppm): 174.7, 166.3, 160.5, 152.2, 149.2, 147.7, 135.5, 134.9, 133.4, 130.8, 129.9, 120.9, 119.6, 118.6, 118.2, 108.6, 20.4. MS/EI m/z (%): 315 (M+2, 60), 313 (M, 93), 188 (77), 187 (100), 115 (70), 103 (63), 89 (16), 77 (53), 63 (19).

N-(3’-Chlorophenyl)-6-methoxycoumarin-3-carboxamide (**34**) Yield: 48%; mp: 222-223 ºC ^{1}H NMR (DMSO-*d*$_6$) δ (ppm), *J* (Hz): 3.80 (s, 3H, OCH$_3$), 7.17 (ddd, 1H, H-4’, *J* = 0.7, 1.9, 7.8), 7.30-7-38 (m, 2H, H-5, H-7), 7.47 (d, 1H, H-8, *J*=9.1), 7.50-7.57 (m, 2H, H-5’, H-6’), 7.94 (dd, 1H, H-2’, *J*=1.8, 1.9), 8.83 (s, 1H, H-4), 10.76 (s, 1H, NH). ^{13}C NMR (DMSO-*d*$_6$) δ (ppm): 162.0, 160.5, 156.2, 149.3, 147.6, 139.5, 133.4, 130.8, 128.6, 127.7, 122.5, 119.6, 118.6, 117.6, 112.0, 103.6, 55.9. MS/EI m/z (%): 331 (M+2, 15), 329 (M,45), 295 (54), 294 (99), 204 (37), 203 (100), 119 (60).

N-(3’-Bromophenyl)coumarin-3-carboxamide (**35**) Yield: 33%; mp: 232-233 ºC. ^{1}H NMR ($CDCl_3$) δ (ppm), *J* (Hz): 7.21 (d, 1H, H-8, *J*=7.8), 7.26-7.31 (m, 1H, H-7), 7.40-7.47 (m, 2H, H-6, H-5’), 7.62 (ddd, 1H, H-6’, *J*=1.7, 1.8, 7.7), 7.68-7.76 (m, 2H, H-4’, H-5), 8.03 (d, 1H, H-2’, *J*=1.8), 9.02 (s, 1H, H-4), 10.88 (s, 1H, NH). ^{13}C NMR ($CDCl_3$) δ (ppm): 161.6, 160.9, 156.2, 154.4, 145.4, 144.0, 143.6, 141.2, 139.5, 138.8, 132.6, 129.9, 125.7, 125.5, 118.9, 106.1. MS m/z (%): 345 (M+2, 58), 343 (58), 174 (36), 173 (100), 101 (46), 90 (17), 89 (51), 63 (30).

N-(3’-Bromophenyl)-6-methoxycoumarin-3-carboxamide (**37**) Yield: 53%; mp: 234-235 ºC. ^{1}H NMR (DMSO-d_6) δ (ppm), *J* (Hz): 3.81 (s, 3H, OCH3), 7.28-7.33 (m, 2H, H-5’, H-7), 7.36 (d, 1H, H-5, *J*=3.0), 7.47 (d, 1H, H-8, *J*=9.0), 7.54- 7.63 (m, 2H, H-4’, H-6’), 8.07 (s, 1H, H-2’), 8.82 (s, 1H, H-4), 10.74 (s, 1H, NH). ^{13}C NMR (DMSO-d_6) δ (ppm): 161.5, 160.6, 159.1, 155.0, 145.9, 145.2, 143.6, 141.2, 138.8, 132.6, 129.9, 125.7, 125.5, 120.7, 118.9, 101.4, 56.0. MS m/z (%): 375 (M+, 23), 374 (61), 203 (100), 187 (42), 119 (33).

N-(4’-Hydroxyphenyl)coumarin-3-carboxamide (**38**) Yield: 42%; mp: 261-262 ºC. ^{1}H NMR (DMSO-d_6) δ (ppm), *J* (Hz): 6.75 (d, 2H, H-3’, H-5’, *J*=7.5), 7.41- 7.58 (m, 4H, H-7, H-8, H-2’, H-6’), 7.76 (dd, 1H, H-6, *J*= 6.8, 6.8), 8.01 (d, 1H, H-5, *J*=6.8), 8.89 (s, 1H, H-4), 9.37 (s, 1H, OH), 10.44 (s, 1H, NH). ^{13}C NMR (DMSO-d_6) δ (ppm): 164.0, 161.0, 159.1, 152.0, 151.5, 144.2, 139.0, 135.1, 130.1, 126.4, 121.1, 120.3, 107.4. MS m/z (%): 281 (M+, 59), 173 (100), 101 (17), 89 (20)

N-(4’-Hydroxyphenyl)-6-methoxycoumarin-3-carboxamide (**40**) Yield: 59%; mp: 242-243 ºC ^{1}H NMR (DMSO-d_6) δ (ppm), *J* (Hz): 3.80 (s, 3H, OCH_3), 7.23-7.60 (m, 5H, H-5, H-7, H-8, H-3’, H-5’), 7.80 (d, 2H, H-2’, H-6’, *J*=8.4), 8.86 (s, 1H, H-4), 9.01 (s, 1H, OH), 10.76 (s, 1H, NH). ^{13}C NMR (DMSO-d_6) δ (ppm): 161.2, 159.0, 156.2, 148.6, 148.3, 146.8, 126.6, 124.5, 122.5, 120.1, 119.3, 119.2, 118.9, 117.5, 114.7, 112.0, 56.0. MS/EI m/z (%): 312 (M+, 21), 311 (86), 204 (22), 203 (100), 119 (23).

N-(4’-Methylphenyl)coumarin-3-carboxamide (**41**) Yield: 88%; mp: 236-237 ºC ^{1}H NMR ($CDCl_3$) δ (ppm), *J* (Hz): 2.27 (s, 3H, CH_3), 7.17 (d, 2H, H-3’, H-5’, *J*=8.4), 7.45 (m, 1H, H-6), 7.53 (d, 1H, H-8, *J*= 8.3), 7.59 (d, 2H, H-2’, H-6’, *J*=8.4), 7.75 (m, 1H, H-7), 7.99 (dd, 1H, H-5, *J*=1.7, 8.0), 8.89 (s, 1H, H-4), 10.57 (s, 1H, NH). ^{13}C NMR ($CDCl_3$)

δ (ppm): 160.4, 160.2, 159.8, 157.2, 147.5, 135.6, 134.4, 133.5, 130.4, 129.6, 122.5, 120.0, 118.7, 116.4, 20.6. MS m/z (%): 279 (M+, 54), 173 (100), 137 (53), 101 (19), 84 (21), 66 (22).

N-(4’-Methylphenyl)-6-methoxycoumarin-3-carboxamide (**43**) Yield: 61%; mp: 186-187 ºC ^{1}H NMR (CDCl$_3$) δ (ppm), *J* (Hz): 2.24 (s, 3H, CH$_3$), 3.72 (s, 3H, OCH$_3$), 7.10-7.21 (m, 3H, H-5, H-2’, H-6’), 7.41 (d, 1H, H-8, *J*=8.6), 7.52-7.61 (m, 3H, H-7, H-3’, H-5’), 8.79 (s, 1H, H-4), 10.56 (s, 1H, NH). ^{13}C NMR (CDCl$_3$) δ (ppm): 162.1, 159.2, 158.8, 148.6, 136.0, 135.9, 130.3, 128.8, 126.6, 125.0, 122.8, 121.7, 118.9, 117.7, 115.5, 110.5, 55.80, 18.0. MS m/z (%): 309 (M+, 86), 291 (51), 281 (29), 203 (100), 119 (49), 106 (72).

N-(4’-Methoxyphenyl)coumarin-3-carboxamide (**44**) Yield: 74%; mp: 219-220 ºC ^{1}H NMR (CDCl$_3$) δ (ppm), *J* (Hz): 3.96 (s, 3H, OCH$_3$), 6.96 (d, 2H, H-3’, H-5’, *J*=8.3), 7.32-7.43 (m, 2H, H-6, H-8), 7.59-7.66 (m, 3H, H-7, H-2’, H-6’), 7.89 (m, 1H, H-5), 8.76 (s, 1H, H-4), 10.88 (s, 1H, NH). ^{13}C NMR (CDCl$_3$) δ (ppm): 163.7, 160.5, 159.9, 158.3, 146.1, 134.2, 134.0, 133.0, 131.4, 129.9, 120.5, 120.1, 118.7, 109.8, 55.9. MS m/z (%): 295 (M+, 66), 187 (22), 173 (100), 101 (43), 89 (18).

N-(4’-Methoxyphenyl)-6-methoxycoumarin-3-carboxamide (**46**) Yield: 59%; mp: 201-202 ºC ^{1}H NMR (CDCl$_3$) δ (ppm), *J* (Hz): 3.80 (s, 3H, OCH$_3$’), 3.85 (s, 3H, OCH$_3$), 6.87-6.95 (m, 3H, H-5, H-3’, H-5’), 7.29 (d, 1H, H-8, *J*=9.0), 7.44-7.58 (m, 3H, H-8, H-2’, H-6’), 8.34 (s, 1H, H-4), 10.46 (s, 1H, NH). ^{13}C NMR (CDCl$_3$) δ (ppm): 162.9, 159.8, 159.3, 153.0, 148.6, 148.4, 130.1, 128.7, 120.0, 119.2, 118.4, 114.4, 112.4, 110.0, 105.1, 102.1, 55.8, 55.3. MS m/z (%): 325 (M+, 61), 203 (100), 173 (90), 108 (21).

N-(4’-Chlorophenyl)coumarin-3-carboxamide (**47**) Yield: 41%; mp: 264-265 ºC ^{1}H NMR (DMSO-*d*$_6$) δ (ppm), *J* (Hz): 7.46 (d, 2H, H-3’, H-5’, *J*=7.5), 7.52-7.58 (m, 2H, H-6, H-8), 7.76 (d, 2H, H-2’, H-6’, *J*=7.5), 7.80-7.83 (m, 1H, H-7), 7.97 (d, 1H, H-5, *J*=8.3), 8.90 (s, 1H, H-4), 10.72 (s, 1H, NH). ^{13}C NMR (DMSO-*d*$_6$) δ (ppm): 163.1, 160.8, 159.2, 140.7, 139.7, 136.7, 132.7, 130.0, 129.4, 120.3, 119.7, 111.5, 110.9, 110.3, 102.0, 101.9. MS m/z (%): 301 (M+2, 28), 299 (M, 59), 173 (100), 101 (33), 89 (29), 63 (15).

N-(4’-Chlorophenyl)-6-methylcoumarin-3-carboxamide (**48**) Yield: 42%; mp: 216-217 ºC ^{1}H NMR (DMSO-*d*$_6$) δ (ppm), *J* (Hz): 2.36 (s, 3H, CH$_3$), 7.35-7.45 (m, 3H, H-8, H-3’, H-5’), 7.57 (dd, 1H, H-7, *J*=2.0, 8.6), 7.69-7.79 (m, 3H, H-5, H-2’, H-6’), 8.79 (s, 1H, H-4), 10.70 (s, 1H, NH). ^{13}C NMR (DMSO-d_6) δ (ppm): 165.7, 160.3, 152.2, 147.7, 137.4, 135.53, 134.9, 132.1, 130.0, 122.0, 119.9, 118.6, 116.2, 107.8, 20.5 MS/EI m/z (%): 315 (M+2, 40), 313 (M, 92), 188 (42), 187 (100), 115 (36), 103 (29), 77 (23).

N-(4’-Chlorophenyl)-6-methoxycoumarin-3-carboxamide (**49**) Yield: 49%; mp: 216-217 ºC ^{1}H NMR (DMSO-d_6) δ (ppm), *J* (Hz): 3.80 (s, 3H, OCH$_3$), 7.28-7.40 (m, 2H, H-3’, H-5’), 7.46 (d, 1H, H-8, *J*=9.1), 7.53 (d, 1H, H-5, *J*=2.8), 8.82 (s, 1H, H-4), 10.71 (s, 1H, NH). ^{13}C NMR (DMSO-d_6) δ (ppm): 162.9, 160.9, 155.8, 149.1, 148.7, 139.5, 131.2, 131.1, 128.0, 126.3, 122.7, 119.1, 118.2, 117.8, 113.7, 100.4, 56.0. MS m/z (%): 329 (M+, 41), 295 (56), 294 (97), 204 (30), 203 (100), 119 (66), 76 (25).

N-(4’-Bromophenyl)coumarin-3-carboxamide (**50**) Yield: 34%; mp: 247-248 ºC ^{1}H NMR (DMSO-d_6) δ (ppm), *J* (Hz): 7.44-7.49 (m, 1H, H-6), 7.52-7.57 (m, 3H, H-8, H-3’, H-5’), 7.72 (d, 2H, H-2’, H-6’, *J*=8.6), 7.71-7.77 (m, 1H, H-7), 8.00 (dd, 1H, H-5, *J*=1.5, 7.9), 8.89 (s, 1H, H-4), 10.70 (s, 1H, NH). ^{13}C NMR (DMSO-d_6) δ (ppm): 168.6, 167.3, 148.0, 147.2, 145.4, 139.7, 136.2, 132.0, 129.7, 128.7, 117.4, 117.0, 111.1, 101.4. MS m/z (%): 345 (M+, 25), 343 (25), 173 (100), 101 (15), 89 (15).

N-(4’-Bromophenyl)-6-methoxycoumarin-3-carboxamide (**52**) Yield: 42%; mp: 269-270 ºC ^{1}H NMR (DMSO-d_6) δ (ppm), *J* (Hz): 7.56-7.69 (m, 4H, H-7, H-8, H-3’, H-5’), 7.72 (d, 2H, H-2’, H-6’, *J*=8.4), 7.78 (d, 1H, H-5, *J*=1.2), 8.64 (s, 1H, H-4), 10.49 (s, 1H, NH). ^{13}C NMR (DMSO-d_6) δ (ppm): 163.4, 161.2, 158.9, 148.8, 144.4, 140.0, 136.6, 130.1, 129.7, 129.5, 128.4, 117.8, 100.6, 99.6. MS m/z (%): 376 (M+2, 27), 374 (69), 173 (100), 101 (22).

Pharmacology

The affinity of compounds **8**–**52** for the human AR subtypes *h*A$_1$, *h*A$_2$A, *h*A$_3$, was determined with radioligand competition experiments in Chinese hamster ovary (CHO) cells that were stably transfected with the individual receptor subtypes. The radioligands used were 1.0 nM (2R,3R,4S,5R)-2-(2-chloro-6-cyclopentylamino-purin-9-yl)-5-hydroxymethyl-tetrahydro-3,4-diol([^{3}H]CCPA) for *h*A$_1$, 10.0 nM (1-(6-amino-9H-purin-9-yl)-1-deoxy-N-ethyl-b-D-ribofuronamide) ([^{3}H]NECA) for *h*A$_2$A, and 1.0 nM 2-(1-

hexynyl)-N^6-methyladenosine [^{3}H] ([^{3}H]HEMADO) for *h*A$_3$ receptors. The results were expressed as K_i values (dissociation constants), which were calculated with the program GraphPad. Due to the lack of a suitable radioligand for *h*A$_2$B receptors, the potency of antagonists at the *h*A$_2$B receptor (expressed on CHO cells) was determined by inhibition of NECA-stimulated adenylyl cyclase activity. The 50% inhibitory concentration (IC$_{50}$) for inhibition of cAMP (cyclic adenosine monophosphate) production was determined and converted to a K_i value using the Cheng and Prusoff equation. The K_i values (Table 1) are reported as geometric means of three independent experiments, with each tested concentration measured in duplicate. As an interval estimate for the dissociation constants, 95% confidence intervals are given in parentheses. Details for pharmacological experiments are described in a previous work.[14]

Adenosine receptor homology models

Homology models of the *h*A$_3$ were previously developed by our group.[15,16] Briefly, MOE software[18] was used for the construction of the models and the *h*A$_3$ sequence was aligned to our template, the crystallized *h*A$_{2A}$ AR (PDB code: 3EML).[19] The alignment was based on previous studies related to adenosine homology modeling carried out by Katritch *et al.*.[20] The geometry of the *h*A$_3$ model was assessed with the Protein Geometry module.[18] Ability to discriminate ligands from decoys was also evaluated through ROC curves (area greater than 0.80).[15,16,20] A more detailed description of the published homology models can be found in our previous studies.[15,16,21]

Molecular docking

Molecular docking simulations in the *h*A$_{2A}$ and the *h*A$_3$ were performed with Glide from the Schrödinger software.[22] For the *h*A$_3$ docking the homology model previously described was used, whereas the crystal structure 3EML (PDB code)[19] was used for the docking in the *h*A$_{2A}$. Protein structures were pre-processed with the Protein Preparation Wizard workflow included in Schrödinger.[22] This process includes the assignation of bond orders, addition of cap termini, optimization of protonation states of the residues, and optimization of the hydrogen-bond protein network, among others. Ligands were prepared with the LigPrep module. No water molecules were included in the simulations. The compounds were docked to the proteins with Glide SP scoring function (standard precision).[22] Binding modes described for graphical purposes were selected using parameters such as Emodel as well as number of similar poses generated through the calculations.

Theoretical evaluation of drug-like properties

The drug-like properties of the compounds under study were calculated using the Molinspiration property program. In this program, cLogP and topological polar surface area (TPSA) were calculated as a sum of fragment-based contributions and correction factors. The calculation of molecule volume has been performed by fitting the sum of fragment contributions to 'real' three dimensional (3D) volume for a training set of about 12 000 compounds, mostly drug-like molecules.[23]

Results and discussion

Chemistry

Coumarin carboxamides **8-52** were efficiently synthesised following the strategy shown in Scheme 1. Generally, the compounds were obtained by an amidation reaction occurring between a coumarin-3-carboxylic acid (**5**, **6** and **7**) and the appropriate substituted amines using EDC as coupling reagent. Compounds **8**-**52** were obtained in moderate to high yields (32% to 88%). As only coumarin-3-carboxylic acid (**5**) was commercially available, 6-methylcoumarin-3-carboxylic (**6**) and 6-methoxycoumarin-3-carboxylic (**7**) acids were prepared by a Knoevenagel condensation of 5-methylsalicylaldehyde (**1**) and 5-methoxysalicylaldehyde (**2**), respectively, with diethyl malonate in ethanol using piperidine as catalyst and subsequent basic hydrolysis of the corresponding ester derivatives (compounds **3** and **4**, respectively). The overall reaction yield was 89% for the methyl substituted compound and 86% for its methoxy counterpart.

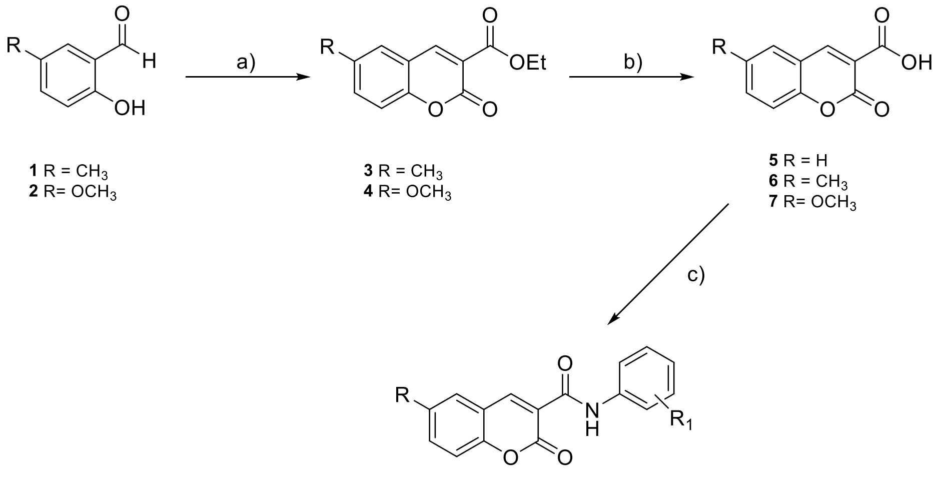

1 R = CH_3
2 R= OCH_3

3 R = CH_3
4 R= OCH_3

5 R = H
6 R = CH_3
7 R= OCH_3

8 R = H; R_1 = 2-OH
9 R = CH_3; R_1 = 2-OH
10 R = OCH_3; R_1 = 2-OH

11 R = H; R_1 = 2-CH_3
12 R = CH_3; R_1 = 2-CH_3
13 R = OCH_3; R_1 = 2-CH_3

14 R = H; R_1 = 2-OCH_3
15 R = CH_3; R_1 = 2-OCH_3
16 R = OCH_3; R_1 = 2-OCH_3

17 R = H; R_1 = 2-Cl
18 R = CH_3; R_1 = 2-Cl
19 R = OCH_3; R_1 = 2-Cl

20 R = H; R_1 = 2-Br
21 R = CH_3; R_1 = 2-Br
22 R = OCH_3; R_1 = 2-Br

23 R = H; R_1 = 3-OH
24 R = CH_3; R_1 = 3-OH
25 R = OCH_3; R_1 = 3-OH

26 R = H; R_1 = 3-CH_3
27 R = CH_3; R_1 = 3-CH_3
28 R = OCH_3; R_1 = 3-CH_3

29 R = H; R_1 = 3-OCH_3
30 R = CH_3; R_1 = 3-OCH_3
31 R = OCH_3; R_1 = 3-OCH_3

32 R = H; R_1 = 3-Cl
33 R = CH_3; R_1 = 3-Cl
34 R = OCH_3; R_1 = 3-Cl

35 R = H; R_1 = 3-Br
36 R = CH_3; R_1 = 3-Br
37 R = OCH_3; R_1 = 3-Br

38 R = H; R_1 = 4-OH
39 R = CH_3; R_1 = 4-OH
40 R = OCH_3; R_1 = 4-OH

41 R = H; R_1 = 4-CH_3
42 R = CH_3; R_1 = 4-CH_3
43 R = OCH_3; R_1 = 4-CH_3

44 R = H; R_1 = 4-OCH_3
45 R = CH_3; R_1 = 4-OCH_3
46 R = OCH_3; R_1 = 4-OCH_3

47 R = H; R_1 = 4-Cl
48 R = CH_3; R_1 = 4-Cl
49 R = OCH_3; R_1 = 4-Cl

50 R = H; R_1 = 4-Br
51 R = CH_3; R_1 = 4-Br
52 R = OCH_3; R_1 = 4-Br

Scheme 1. Synthetic strategy followed for the preparation of coumarin 3-phenylcarboxamides. Reagents and conditions: a) diethyl malonate, EtOH, piperidine, reflux, overnight. b) NaOH (0.5% aq./EtOH), reflux, 2 h. c) EDC, DMAP, DCM, corresponding amine, 0 ºC to r.t., 4 h.

Pharmacology

The affinity of the coumarin carboxamides (compounds **8-52**) for the human AR subtypes *h*A_1, *h*A_{2A}, *h*A_3, which were expressed in Chinese hamster ovary (CHO) cells, was determined in radioligand competition experiments. In these assays, the competition with the following agonist radioligands: (i) [^{3}H]CCPA at *h*A_1AR, (ii) [3H]NECA at *h*A_{2A} and [^{3}H]HEMADO at *h*A_3 receptors was measured. The resulting binding affinity data expressed as K_i (dissociation constant) is reported in **Table 1**. The data regarding A_{2B} AR was not included as none of the tested compounds revealed a measurable affinity (K_i > 30 µM).

Table 1. Binding affinity (*Ki* in µM and 95% confidence intervals in parentheses) of coumarins **8-19** in radioligand binding assays at human A_1, A_{2A}, A_3 AR subtypes.

Compound	***h*A₁** K_i (µM)	***h*A₂A** K_i (µM)	***h*A₃** K_i (µM)	**Selectivity**	
				hA_1/hA_3	hA_{2A}/hA_3
8	> 100	> 30	31.5 (2.39 – 4.16)	3.17	0.95
9	> 100	> 100	> 30	_	_.
10	39.5 (34.3 – 45.4)	38.0 (34.5 -41.9)	32.7 (27.6 – 38.8)	1.21	1.16
11	> 100	> 100	> 100	_	_
12	> 100	> 100	> 100	_	_
13	> 100	> 100	45.4 (38.7 – 53.3)	2.20	2.20
14	> 100	> 100	> 100	_	_
15	> 100	> 100	> 100	_	_
16	> 100	> 100	> 100	_	_
17	> 100	> 100	> 100	_	_
18	> 100	> 100	> 100	_	_
19	> 100	> 100	> 100	_	_
20	> 100	> 100	> 100	_	_
21	> 100	> 100	> 100	_	_
22	> 100	> 100	> 100	_	_
23	> 100	> 100	> 100	_	_
24	> 100	> 100	> 100	_	_
25	41.0 (29.0 – 58.1)	> 100	22.0 (15.3 – 31.7)	1.86	4.54
26	> 100	> 100	2.4 (1.81 – 3.19)	41.67	41.67
27	> 100	> 100	> 100	_	_
28	> 100	> 100	> 100	_	_
29	> 100	> 100	> 100	_	_
30	> 100	> 100	> 100	_	_
31	> 100	> 100	> 100	_	_
32	> 30	> 30	> 30	_	_
33	> 30	> 30	> 30	_	_
34	> 100	> 100	> 100	_	_
35	> 30	> 30	> 100	_	_
36	> 10	> 10	> 10	_	_
37	> 100	> 100	> 100	_	_
38	> 30	> 30	> 30	_	_
39	> 100	> 100	> 100	_	_
40	22.3 (21.5 – 23.2)	28.3 (25.2 – 31.8)	24.2 (22.2 – 26.4)	0.79	1.17
41	> 100	> 100	> 100	_	_
42	> 100	> 100	> 100	_	_
43	> 100	> 100	> 100	_	_
44	> 100	> 100	> 100	_	_
45	> 100	> 100	> 100	_	_
46	> 100	> 100	> 100	_	_
47	> 100	> 100	> 100	_	_
48	> 100	> 100	> 100	_	_
49	> 100	> 100	> 100	_	_
50	> 30	> 30	> 30	_	_
51	> 100	> 100	> 100	_	_
52	> 100	> 100	> 100	_	_
theophylline[26]	6.77 (4.07 -11.30)	-	86.40 (73.60 – 101.30)	0.08	1.2

Structure-affinity relationship studies

In an effort for validate coumarin as a privileged structure for the design of AR ligands our research group acquired so far relevant data about scaffold recognized decorations (Figure 1). However, at the present step it was found important to perform a systematic study to attain reliable structure-activity-relationship (SAR) studies. Herein we present the first studies on coumarin decoration using carboxamide as a spacer and different substituents at position 6 of aromatic coumarin ring and at the exocyclic aromatic ring (**Figure 2**). The significance of the presence of a substituent at position 6 of the coumarin core was studied by the introduction of methyl or methoxy groups, as this position was denoted as relevant in some previous publications of our research group[14,15] In addition, the effect of electron-donating and electron-withdrawing groups located at *ortho, meta* and *para* positions of the exocyclic aryl ring was studied.

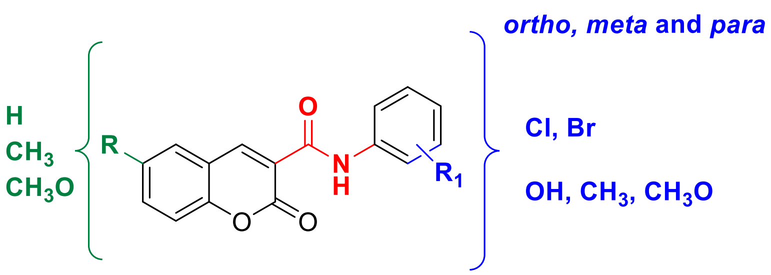

Figure 2. Rational design followed in the present study.

Generally, no relevant affinity data in any of ARs subtypes (K_i > 100 µM) was attained for the majority of the coumarin derivatives under study. However, it must be stressed that this non expected results are of the utmost importance to improve our understanding on the effect of spacers and substituents on coumarin scaffold towards ARs subtypes. Accordingly, it can be concluded that the presence of electron-withdrawing substituents in the exocyclic aromatic ring (**17-22**, **32-37**, **47-52, Table 1**) have a negative outcome either in the absence or presence of substituents at the position 6 of coumarin ring.

In spite of these results, some interesting data was attained with electron-donating substituents allowing to draw some insights in the significance of 3-carboxamidocoumarin scaffold for the design of AR ligands. Although the introduction of a methoxy group in aromatic ring located on the side chain (**14-16**, **29-31**, **44-46**, **Table 1**), even in the presence or absence of substituents at the position 6 of coumarin ring substituents, was not beneficial relevant data was attained by its replacement by methyl substituent (**11-13**, **26-38**, **41-43**, **Table 1**). In fact, compound **26** (hA_3 K_i = 2.4 µM) in which the group is located in *meta* position, display a noticeable activity and selectivity towards hA_3, which is weakened if the group is moved for *ortho* (compound **13**, hA_3 K_i = 45.4 µM) or *para* position (compound **43**, hA_3 K_i >100 µM). However, the affinity is dramatically reduced when methoxy or methyl substituents at the position 6 are present. For coumarins with a hydroxyl function in the exocyclic aromatic ring the data attained was not so ruled. Compound **8**, without any substituent in the coumarin core and a hydroxyl group located in *ortho* position, behave as a selective A_3AR ligand (hA_3 K_i = 31.5 µM) Interestingly, it was noticed that the introduction of a methyl group at position 6 of the coumarin led to a loss of activity (compound **9**) whereas a methoxy group lead to a 30-fold decrease of the selectivity towards A_3AR (compound **10**, hA_1/hA_3 K_i = 1.21). In the case of compounds **25** and **40**, with a hydroxyl group in the *meta* and *para* position and a methoxy at the position 6 of coumarin, respectively, a loss of selectivity was observed. Compound **25** has an A_1 AR binding affinity of 41 µM and a A_3 AR K_i of 22 µM, while compound **40** has poor selectivity (hA_1 K_i = 22.3 µM, hA_{2A} K_i = 28.3 µM and hA_3 K_i = 24.2 µM). The same tendency was observed for compounds **10** (hA_1 K_i = 39.5 µM, hA_{2A} K_i = 38.0 µM and hA_3 K_i = 32.7 µM) and **38** (hA_1 K_i > 30 µM, hA_{2A} K_i > 30 µM and hA_3 K_i > 30 µM).

Theoretical drug-like properties

To have a prediction of the drug-like properties of the best compounds some physicochemical parameters were calculated using the tool Molinspiration (**Table 2**).[23] These parameters include molecular weight (MW), number of heavy atoms (*N*), partition coefficient (clogP), topological polar surface area (tPSA in $Å^2$), number of hydrogen bond acceptors (HBA), number of hydrogen bond donors (HBD), and number of rotatable bonds (n_{rotb}) and volume ($Å^3$) (**Table 2**). For the coumarins under study no violation of Lipinski's rule of five (MW, log P, number of hydrogen donors and acceptors) were found. Moreover, the TPSA values, described as a predictive indicator of the drug capacity of membrane penetration, are encouraging for pursuing a drug-like lead. Consequently, the data represented in Table 2 provides a preliminary indication that these type of compounds have drug-like properties.

Table 2. Drug-like properties of the most promising coumarins.

Compd	MW	*N*	clogP	tPSA (Å^2)	HBA	HBD	n_{rotb}	Vol (Å^3)
8	281.27	21	2.56	79.54	5	2	3	239.4
9	295.29	22	2.99	79.54	5	2	3	256.0
10	311.29	23	2.60	88.77	6	2	4	264.9
13	295.29	22	2.84	68.54	5	1	4	256.9
25	311.29	23	2.36	88.77	6	2	3	264.94
26	279.30	21	3.26	59.31	4	1	2	247.94
40	311.29	23	2.39	88.77	6	2	3	264.94

Molecular docking simulations

Molecular docking simulations in the hA_{2A} and the hA_3 were carried out to study adenosine selectivity and provide some insights in the relationship between the molecular structure and the protein affinity. The crystal structure 3EML for the hA_{2A} and a homology model for the hA_3 were used in the simulations. Ligands were docked with Glide SP.[20] In previous studies[15] our docking protocol was validated and a root mean square deviation (RMSD) of 0.69 and 1.92 between the co-crystallized and docking conformations for the ligands ZM241385 and T4E inside the hA_{2A} pocket was obtained.[19,24]

Our studies have been initially focused on compound **26** as a significant selective binding affinity against the hA_3 (K_i = 2.4 µM, **Table 1**) has been attained. Molecular docking in the hA_3 yielded a pose for compound **26** in which the coumarin ring is oriented towards the bottom of the pocket whereas the 3'-methylphenyl group is located towards the extracellular area (see **Figure 3a**). The oxygen in the pyrone ring establishes a hydrogen bond with the amide group of the residue Asn250. Interactions with this residue have been already described in the literature for the different adenosine receptors.[15,16,25] Moreover, the benzene ring in the coumarin nucleus of compound **26** establishes π-π stacking interactions with the residue Trp243. In addition, the contributions of the different residues to the binding of the ligand were also measured (see **Figure 3b**). The residue contribution score was calculated as the addition of *van der Waals* and Coulomb energies. The key contribution of some residues in the recognition of the ligand, such as Phe168, Leu246, Met177, Ile268, Trp243, Asn250 and Ala69 are shown in Figure 3b. However, other type of interactions, such as hydrophobic interactions, could also be important to explain the different affinity between the compound and the protein. In fact, compound **26** placed the coumarin ring in a deep hydrophobic area and the 3’-methylphenyl is inserted also in a hydrophobic region (see **Figure 3a** with the hydrophobic/hydrophilic surface calculated in the *h*A3 pocket).

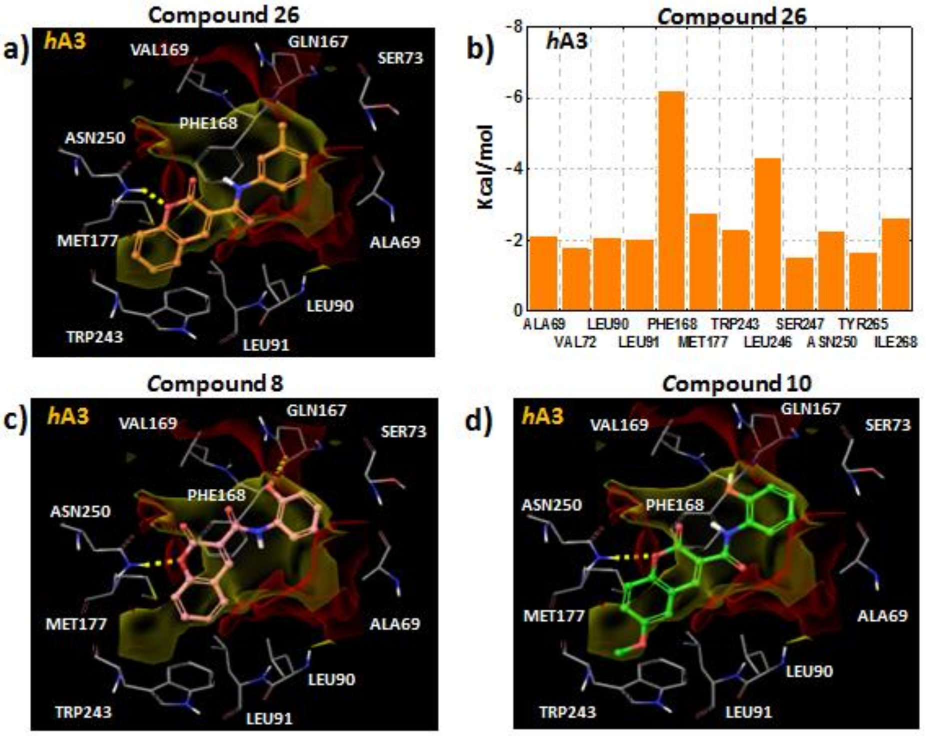
a)
Compound 26
hA3
VAL169
GLN167
SER73
PHE168
ASN250
MET177
ALA69
LEU90
TRP243
LEU91
b)
Compound 26
hA3
Kcal/mol
-8
-6
-4
-2
0
ALA69
VAL72
LEU90
LEU91
PHE168
MET177
TRP243
LEU246
SER247
ASN250
TYR265
ILE268
c)
Compound 8
hA3
VAL169
GLN167
SER73
PHE168
ASN250
MET177
ALA69
LEU90
TRP243
LEU91
d)
Compound 10
hA3
VAL169
GLN167
SER73
ASN250
PHE168
MET177
ALA69
LEU90
TRP243
LEU91

Figure 3. a) Hypothetical binding mode extracted from molecular docking for compound **26** in the *h*A3. Hydrogen bond with the residue Asn250 is shown in yellow dashes. Hydrophobic areas in the pocket are represented in yellow and hydrophilic regions in red color. b) Residue contributions to the binding between *h*A3 and compound **26** (sum of *van der Waals* and Coulomb energies). c) Pose extracted for compound **8** in the *h*A3. Hydrogen bonds with the residues Asn250 and Gln167 are shown in yellow dashes. d) Hypothetical binding mode calculated for compound **10** in the *h*A3 (hydrophobic surface in yellow and hydrophilic in red color).

The introduction of a hydroxyl group at ortho position of the phenyl group (compound **8**) lead to a dramatic decrease of the *h*A3 binding affinity (K_i = 31.5 µM, Table 1), compared to compound **26**. The docking pose for compound **8** yielded a hydrogen bond with the residue Asn250 and π-π stacking interactions with the Phe168. A second hydrogen bond was detected between the 2’-hydroxyl group in the phenyl exoxyclic ring and the residue Gln167 of the second extracellular loop (see **Figure 3c**). This fact could be a key factor to explain the *h*A3 selectivity shown by compound **8**, since the other adenosine receptors do not present a glutamine residue (Gln) at the same position. However, the coumarin ring is placed in the *h*A_3 in a shallower hydrophobic region compared to compound **26** that could be responsible for the decrease of *h*A_3 activity. Docking studies have also been accomplished for compound **10** and from the pose extracted it was verified that the compound can establish a hydrogen bond with the residue Asn250 and π-π stacking interactions with the Phe168. Yet, the binding mode did not yield a hydrogen bond with the residue Gln167. However, the hydrophobic/hydrophilic surface of the receptor can accommodate the methoxy substituent in the hydrophobic area at the bottom of the cavity (see **Figure 3d**).

As compound **10** also exhibited a moderate affinity against *h*A_1 and *h*A_{2A} additional computational studies were performed. Since the crystal structure of *h*A_{2A} is available docking simulations were carried out to explain the increment in the affinity for *h*A_{2A} compared to the other compounds in the series. The simulations showed that compound **10** has a similar binding mode inside the *h*A_{2A} (see **Figure 4a**).

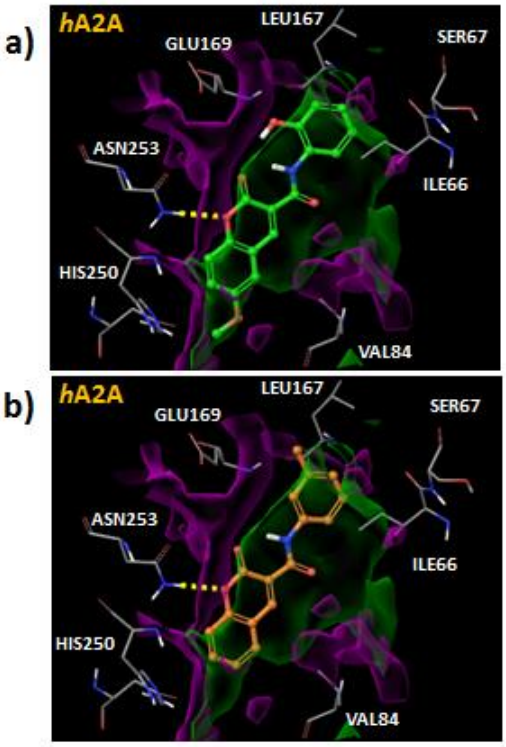

Figure 4. a) Hypothetical binding mode calculated with molecular docking for compound **10** in the *h*A_{2A}. Hydrogen bonds are represented in yellow dashes, hydrophobic surface in green color and hydrophilic surface in magenta. b) Pose calculated with docking for the compound **26** in the *h*A_{2A}.

The ligand establishes a hydrogen bond with the residue Asn253. Moreover, π-π stacking interactions have been detected between the benzene ring in the coumarin nucleus and the imidazole of the residue His250. The 6-methoxy substituent was found to be well accommodated in a hydrophobic region, a pose that could be accountable for the observed increase on the hA_{2A} affinity compared to compounds **8** and **9**. Moreover, the 2'-hydroxyl substituent in the phenyl ring is oriented towards a hydrophilic area. The replacement in that position of a hydroxyl group by hydrophobic substituents, such as methyl or methoxy groups in compounds **13** and **16**, is not suitable for the interaction with the hA_{2A} with the consequent loss of affinity. Compound **26** showed a similar pose as compound **10**. However, the lack of the 6-methoxy substituent in the deep hydrophobic region along with the position of the 3'-methyl group of the phenyl ring in an area not well defined as hydrophobic could be the reason for the decreased hA_{2A} affinity (see **Figure 4b**) of compounds **13** and **16**, is not be suitable for the interaction with the hA_{2A} with the consequent loss of affinity.

Conclusions

In this study, further evidences for the validation of 3-phenylcarboxamidocoumarin as a scaffold for the development of AR ligands have been acquired. Due to coumarin synthetic accessibility and decoration capability a small library has been successfully attained and a concise SAR study performed. Although the majority of the compounds were not active for any of AR subtypes the data can be useful for validate the ligand requirements for AR. In general, a loss of activity/selectivity was found for coumarins substituted in 6-position and with electron- withdrawing substituents in the aryl exocyclic ring. From the study interesting remarks must be highlighted: compound **26** displayed a relevant affinity and selectivity for hA_3 (K_i = 2.4 μM), turning it in the most stimulating compound of the series. Its hA_3 selectivity was elucidated by docking experiments that indicate that the coumarin ring is oriented towards the bottom of the pocket whereas the 3'-methylphenyl group is located towards the extracellular area and that the oxygen in the pyrone ring establishes a hydrogen bond with the amide group of the residue Asn250. Taking into account that A_1 and A_3 AR ligands are beneficial for the treatment of disorders of the nervous system, such as chronic pain, neurodegeneration and brain injury, compound **26** can be considered an interesting starting point for further studies aiming the development of effective and selective coumarin-based AR ligands.

In summary, the data suggests that for this type of compounds the presence of substituents at position 6 can be detrimental for the AR affinity constituting per *se* an important tool for building upon the coumarin hits.

Acknowledgments

The authors would like to thank Fundação para a Ciência e Tecnologia (FCT) – QUI/UI0081/2013, POCI-01-0145-FEDER-006980 for the financial support. Thanks are due to FCT, POPH and QREN for A. Fonseca (SFRH/BD/80831/2011) and M. J. Matos (SFRH/BPD/95345/2013) doctoral and post-doctoral grants. S. Vilar also thanks "Angeles Alvariño program, Plan Galego de Investigación, Innovación e Crecemento 2011-2015 (I2C)" and "European Social Fund (ESF)".

References

1. Drury, N.; Szent-Györgyi, *J. Physiol.* **1929**, *68*, 213–237.
2. Chen, J.-F.; Eltzschig, H. K.; Fredholm, B. B. *Nat. Rev. Drug Discov.* **2013**, *12*, 265–286.
3. Fredholm, B. B.; IJzerman, A. P.; Jacobson, K. A.; Klotz, K.-N.; Linden, J. *Pharmacol. Rev.* **2001**, *53*, 527–552.
4. Bours, M. J. L.; Swennen, E. L. R.; Di Virgilio, F.; Cronstein, B. N.; Dagnelie, P. C. *Pharmacol. Ther.* **2006**, *112*, 358–404.
5. Fredholm, B. B. *Exp. Cell Res.* **2010**, *316*, 1284–1288.
6. Gessi, S.; Cattabriga, E.; Avitabile, A.; Gafa, R.; Lanza, G.; Cavazzini, L.; Bianchi, N.; Gambari, R.; Feo, C.; Liboni, A.; Gullini, S.; Leung, E.; Mac-Lennan, S.; Borea, P. A. *Clin Cancer Res* **2004**, *10*, 5895–5901.
7. Jacobson, K. A.; Gao, Z. *Nat. Rev. Drug Discov.* **2006**, *5*, 247–264.
8. Fonslow, B. R.; Stein, B. D.; Webb, K. J.; Xu, T.; Choi, J.; Kyu, S.; Iii, J. R. Y. **2013**, *10*, 54–56.
9. Press, N. J.; Fozard, J. R. *Expert Opin. Ther. Pat.* **2010**, *20*, 987–1005.
10. Borges, F.; Roleira, F.; Milhazes, N.; Santana, L.; Uriarte, E. *Curr. Med. Chem.* **2005**, *12*, 887–916.
11. Borges, F.; Roleira, F. M. F.; Milhazes, N. J. da S. P.; Uriarte, E.; Santana, L. *Front. Med. Chem.* **2009**, *4*, 23–85.
12. Matos, M. J.; Vilar, S.; Kachler, S.; Celeiro, M.; Vazquez-Rodriguez, S.; Santana, L.; Uriarte, E.; Hripcsak, G.; Borges, F.; Klotz, K.-N. *Bioorg. Chem.* **2015**, *61*, 1–

6.

13. Vazquez-Rodriguez, S.; Matos, M. J.; Santana, L.; Uriarte, E.; Borges, F.; Kachler, S.; Klotz, K.-N. *J. Pharm. Pharmacol.* **2013**, *65*, 697–703.
14. Matos, M. J.; Hogger, V.; Gaspar, A.; Kachler, S.; Borges, F.; Uriarte, E.; Santana, L.; Klotz, K.-N. *J. Pharm. Pharmacol.* **2013**, *65*, 1590–1597.
15. Matos, M. J.; Vilar, S.; Kachler, S.; Fonseca, A.; Santana, L.; Uriarte, E.; Borges, F.; Tatonetti, N. P.; Klotz, K.-N. *ChemMedChem* **2014**, *9*, 2245–2253.
16. Cagide, F.; Gaspar, A.; Reis, J.; Chavarria, D.; Vilar, S.; Hripcsak, G.; Uriarte, E.; Kachler, S.; Klotz, K. N.; Borges, F. *RSC Adv.* **2015**, *5*, 78572–78585.
17. Fonseca, A.; Matos, M. J.; Reis, J.; Duarte, Y.; Santana, L.; Uriarte, E.; Borges, F. *RSC Adv.* **2016**, *6*, 49764–49768.
18. MOE, version 2011.10; Chemical Computing Group, Inc.: Available at: http://www.chemcomp.com. (Accessed: Jan 2012).
19. Veli-Pekka, J.; Mark, G.; Michael, H.; Vadim, C.; Ellen, Y. T. C.; J. Robert, L.; Adriaan, P. I.; Raymond, C. S. *Science (80-.).* **2008**, *322*, 1211–1217.
20. Katritch, V.; Kufareva, I.; Abagyan, R. *Neuropharmacology* **2011**, *60*, 108–115.
21. Matos, M. J.; Vilar, S.; Kachler, S.; Vazquez-Rodriguez, S.; Varela, C.; Delogu, G.; Hripcsak, G.; Santana, L.; Uriarte, E.; Klotz, K.-N.; Borges, F. *Med. Chem. Commun.* **2016**, *7*, 845–852.
22. Schrödinger suite 2016-3, Schrödinger, LLC, New York, USA, 2016. Available at: http://www.schrodinger.com/ (Accessed: August 2016).
23. Lipinski, C. a.; Lombardo, F.; Dominy, B. W.; Feeney, P. J. *Adv. Drug Deliv. Rev.* **2012**, *64*, 4–17.
24. Congreve, M.; Andrews, S. P.; Doré, A. S.; Hollenstein, K.; Hurrell, E.; Langmead, C. J.; Mason, J. S.; Ng, I. W.; Tehan, B.; Zhukov, A.; Weir, M.; Marshall, F. H. *J. Med. Chem.* **2012**, *55*, 1898–1903.
25. Kolb, P.; Phan, K.; Gao, Z. G.; Marko, A. C.; Sali, A.; Jacobson, K. A. *PLoS One* **2012**, *7*, e49910.
26. Klotz, K.-N.; Hessling, J.; Hegler, J.; Owman, C.; Kull, B.; Fredholm, B. B.; Lohse, M. J. *Naunyn. Schmiedebergs. Arch. Pharmacol.* **1997**, *357*, 1–9.

CHAPTER 3

3.1. Discussion

Over the years the need for new drugs to treat ND has increased exponentially. Although multifactorial processes are linked to neurodegeneration, some important targets which contribute to cause and/or accelerate ND have been validated. Accordingly, the work presented in this thesis represents a continued effort for the development of NCE based on the benzopyrone scaffold as MAO-B and AChE inhibitors, and also as AR ligands. The process behind the rational design of this thesis comprises the development of concise benzopyrone libraries suitable for SAR studies and the discovery of hits and, ultimately, lead optimization. This type of chemical libraries must have a common functionalized scaffold suitable to attain derivatives by diverse approaches, for instance combinatorial chemistry. In the pharmaceutical industry, combinatorial chemistry is often used to obtain a large number of derivatives in a short amount of time, that subsequently undergo high throughput screening (HTS) for an array of pharmacological targets.[324]

3.1.1. Design and development of benzopyrone-based libraries

The libraries developed along the thesis embedded the privileged benzopyrone motif, and were designed to achieve a broad set of derivatives. Within this framework four small benzopyrone-based libraries (compounds **1-129**, Fig. 48) were synthesized and screened towards different ND targets.

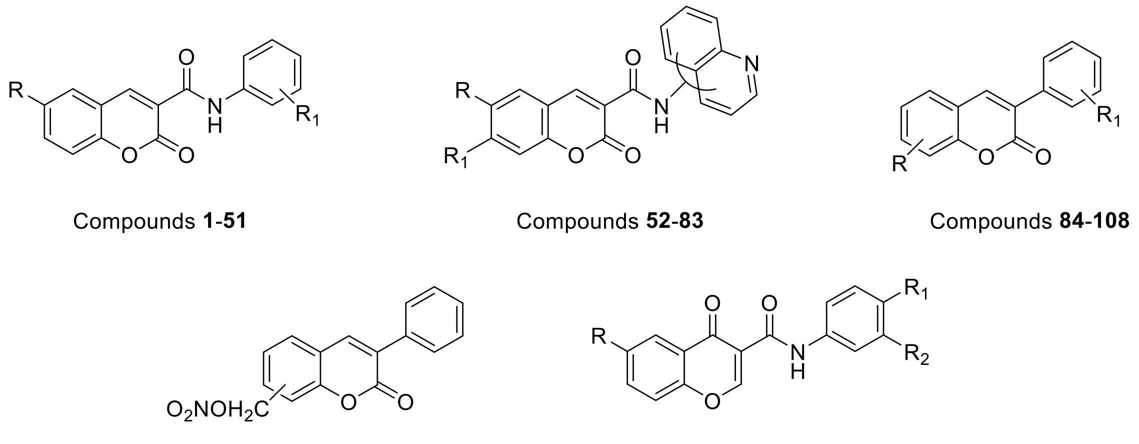

Compounds **1-51**

Compounds **52-83**

Compounds **84-108**

Compounds **109-113**

Compounds **116-129**

Figure 48 – Benzopyrone-based libraries developed in the thesis.

The synthetic methodologies were selected foreseeing the possibility of scale-up processes, using cost effective materials and, whenever possible, one-pot synthetic strategies. Finally, efforts have been made to keep products' purification, isolation and work-ups simple, straightforward and environmental-friendly. An overview of the type of compounds and synthetic methodologies will be presented in the ensuing subsections.

3.1.1.1. Synthesis of 3-carboxamidocoumarin library

One of the libraries developed along this thesis focused on the introduction of aromatic type substituents, with diverse substitution patterns, on position 3 of the coumarin scaffold using an amide function as a spacer (Fig. 48). Moreover, to generate chemical diversity other positions of the benzopyrone were functionalized with diverse substituents, including methyl, methoxy, halogens and amines (Tables 1 and 2).

The 3-carboxamidocoumarin-based derivatives (compounds **1**-**83**, Tables 1 and 2) were obtained by a classic amidation reaction (Fig. 49) using coumarin carboxylic acids and the appropriate aromatic amines as starting materials, 1-ethyl-3-(3-dimethylaminopropyl)carbodiimide (EDC) as a coupling reagent and 4-dimethylaminopyridine (DMAP) as a catalyst (Fig. 49).

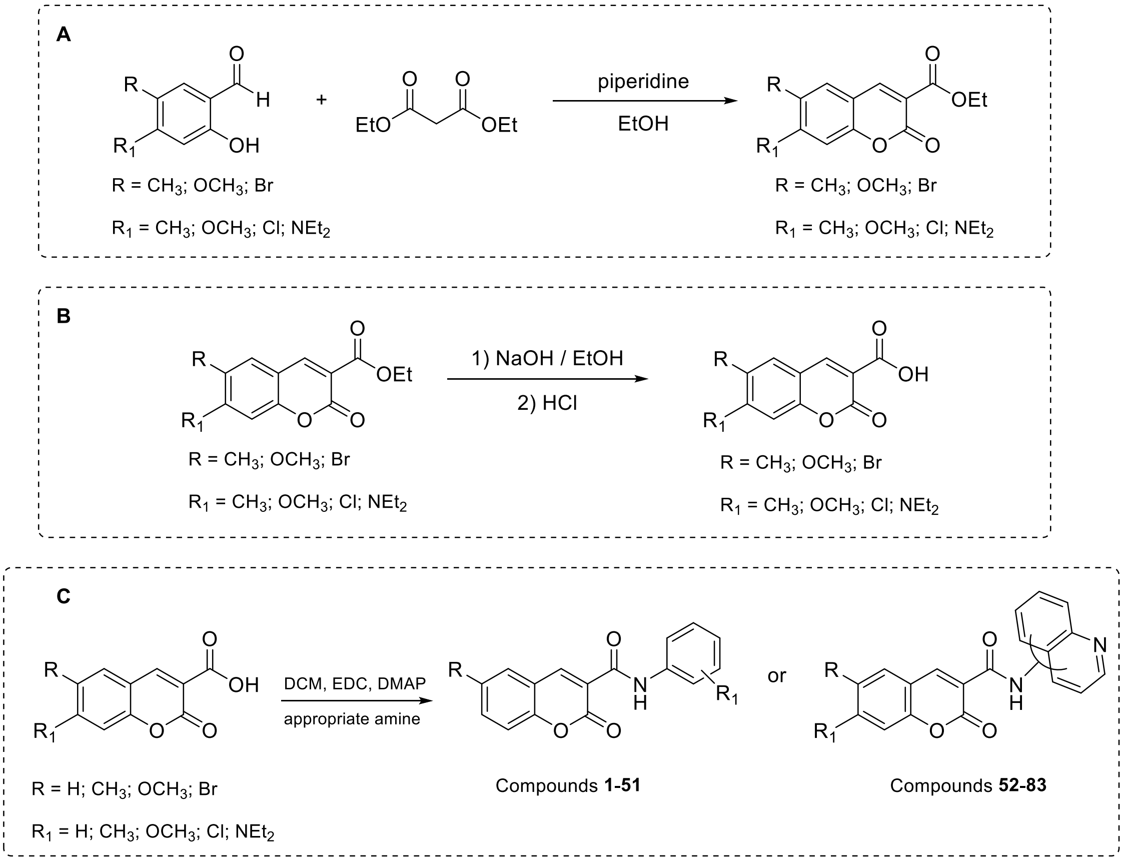
A
R
R1
O
H
OH
+
O
O
EtO
OEt
piperidine
EtOH
OEt
R = CH3; OCH3; Br
R1 = CH3; OCH3; Cl; NEt2
B
1) NaOH / EtOH
2) HCl
OH
C
DCM, EDC, DMAP
appropriate amine
N
H
or
Compounds 1-51
Compounds 52-83
R = H; CH3; OCH3; Br
R1 = H; CH3; OCH3; Cl; NEt2

Figure 49 – Methodologies followed for the synthesis of 3-carboxamidocoumarin-based libraries.

The starting materials needed for the synthesis of unsubstituted coumarins (compounds **1**-**17**, **52**-**55**, Tables 1 and 2) were commercially available. However, for the synthesis of derivatives with substituents in the benzopyrone ring, it was mandatory to synthesize the required starting materials. Accordingly, they were obtained by a Knoevenagel condensation reaction using the appropriate salicylaldehyde derivatives and diethyl malonate, in presence of catalytic amounts of piperidine (Fig. 49A). The versatility of this reaction enabled the synthesis of coumarin carboxylic esters in good yields, regardless of the nature of the starting materials (Manuscripts I and II).

As in the Knoevenagel reaction ester intermediates were formed, a subsequent reaction was necessary to obtain the required starting materials. As such, a basic hydrolysis reaction was performed using an aqueous sodium hydroxide in ethanol (Fig. 49B). The starting materials needed for compounds' **18**-**51** and **56**-**83** synthesis were obtained in moderate-to-high yields. (Manuscripts I and II)

Table 1 – Benzopyrone library based on aryl-3-carboxamidocoumarins.

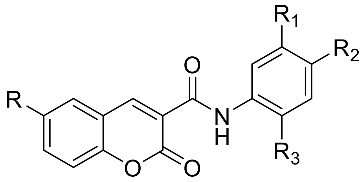

Compound	R	R_1	R_2	R_3	Yield	Manuscript
1	H	H	H	H	89%	VIII
2	H	H	H	Br	32%	VIII
3	H	H	H	Cl	68%	VIII
4	H	H	H	OCH_3	64%	VIII
5	H	H	H	OH	54%	VIII
6	H	H	H	CH_3	56%	VIII
7	H	Br	H	H	33%	VIII
8	H	Cl	H	H	60%	VIII
9	H	OCH_3	H	H	47%	VIII
10	H	OH	H	H	51%	VIII
11	H	CH_3	H	H	34%	VIII
12	H	H	Br	H	34%	VIII
13	H	H	Cl	H	41%	VIII
14	H	H	OCH_3	H	74%	VIII
15	H	H	OH	H	42%	VIII

16	H	H	CH_3	H	88%	VIII
17	H	NO_2	H	OH	52%	
18	CH_3	H	H	H	62%	I, VIII
19	CH_3	H	H	Br	52%	I, VIII
20	CH_3	H	H	Cl	46%	I, VIII
21	CH_3	H	H	OCH_3	82%	I, V, VIII
22	CH_3	H	H	OH	56%	I, V,VIII
23	CH_3	H	H	CH_3	83%	I, VIII
24	CH_3	H	Br	H	68%	I, IV, VIII
25	CH_3	H	Cl	H	61%	I, IV, VIII
26	CH_3	H	OCH_3	H	74%	I, IV, V, VIII
27	CH_3	H	OH	H	61%	I, IV, V, VIII
28	CH_3	H	CH_3	H	79%	I, IV, VIII
29	CH_3	Br	H	H	63%	I, IV, VIII
30	CH_3	Cl	H	H	42%	I, IV, VIII
31	CH_3	OCH_3	H	H	73%	I, IV, V, VIII
32	CH_3	OH	H	H	61%	I, IV, V, VIII
33	CH_3	CH_3	H	H	69%	I, IV, VI, VIII
34	CH_3	NO_2	H	OH	44%	
35	OCH_3	H	H	H	75%	IV, VIII
36	OCH_3	H	H	Br	26%	VIII
37	OCH_3	H	H	Cl	29%	VIII
38	OCH_3	H	H	OCH_3	21%	VIII
39	OCH_3	H	H	OH	41%	VIII
40	OCH_3	H	H	CH_3	28%	VIII
41	OCH_3	Br	H	H	32%	IV, VIII
42	OCH_3	Cl	H	H	48%	IV, VIII
43	OCH_3	OCH_3	H	H	46%	IV, VI, VIII
44	OCH_3	OH	H	H	57%	IV, VIII
45	OCH_3	CH_3	H	H	73%	IV, VIII
46	OCH_3	H	Br	H	34%	IV, VIII
47	OCH_3	H	Cl	H	49%	IV, VIII
48	OCH_3	H	OCH_3	H	33%	IV, VIII
49	OCH_3	H	OH	H	59%	IV, VIII
50	OCH_3	H	CH_3	H	61%	IV, VIII
51	OCH_3	NO_2	H	OH	40%	

Table 2 - Benzopyrone library based on quinolinyl-3-carboxamidocoumarins.

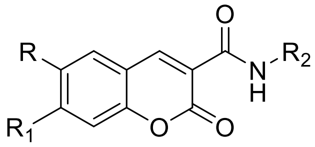

Compound	R	R_1	R_2	Yield	Manuscript
52	H	H	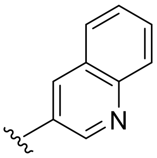	81%	II
53	H	H	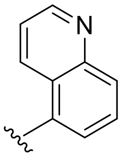	76%	II
54	H	H	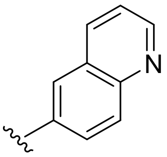	68%	II
55	H	H	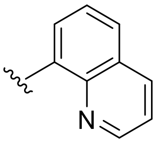	68%	II
56	CH_3	H	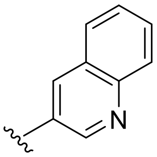	51%	
57	CH_3	H	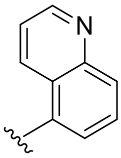	66%	
58	CH_3	H	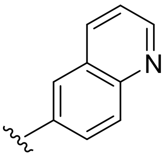	53%	VII
59	CH_3	H	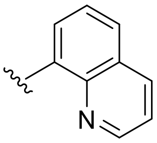	72%	
60	OCH_3	H	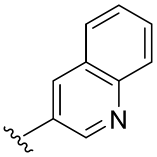	68%	

61	OCH_3	H	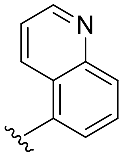	55%	
62	OCH_3	H	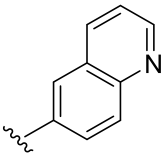	59%	
63	OCH_3	H	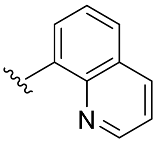	50%	
64	Br	H	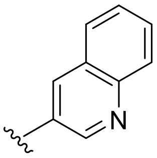	49%	
65	Br	H	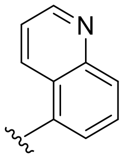	42%	
66	Br	H	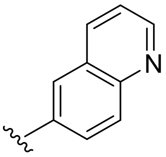	57%	
67	Br	H	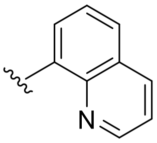	53%	
68	H	CH_3	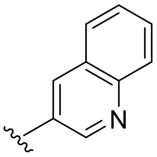	74%	II
69	H	CH_3	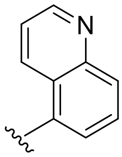	67%	II
70	H	CH_3	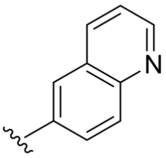	53%	II
71	H	CH_3	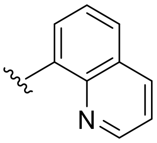	61%	II

72	H	OCH_3	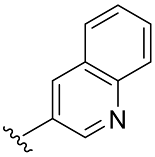	58%	II
73	H	OCH_3	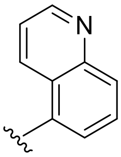	67%	II
74	H	OCH_3	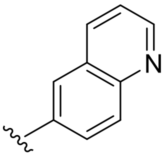	57%	II
75	H	OCH_3	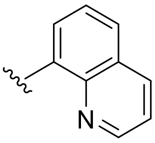	61%	II
76	H	Cl	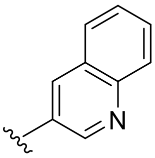	73%	II
77	H	Cl	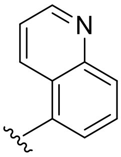	69%	II
78	H	Cl	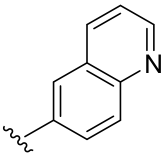	53%	II
79	H	Cl	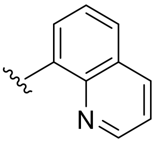	62%	II
80	H	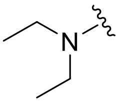	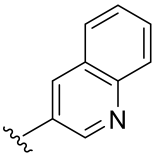	68%	II
81	H	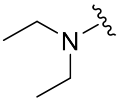	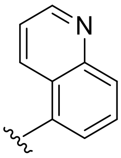	64%	II
82	H	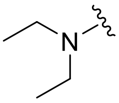	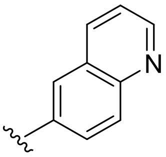	71%	II

83	H	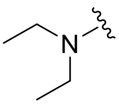	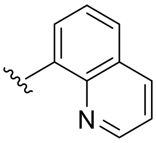	59%	II

3.1.1.2. Synthesis of 3-arylcoumarin based library

The synthesis of 3-arylcoumarins (Table 3) was performed by Perkin reaction using diverse salicylaldehydes and arylacetic acids. The reaction was carried out in the presence of DCC, a dehydrating agent, and dimethyl sulfoxide (DMSO) at reflux temperatures (Fig. 50).[325]

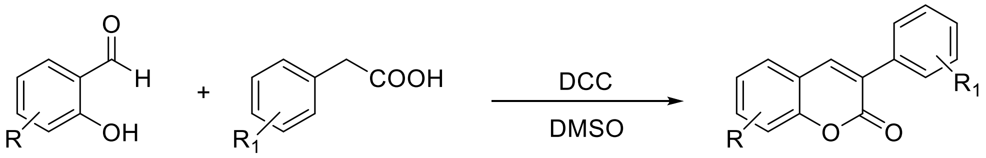
O
H
R
OH
+
COOH
R1
DCC
DMSO
R
O
O
R1

Figure 50 – Methodology followed for the synthesis of 3-arylcoumarin-based library.

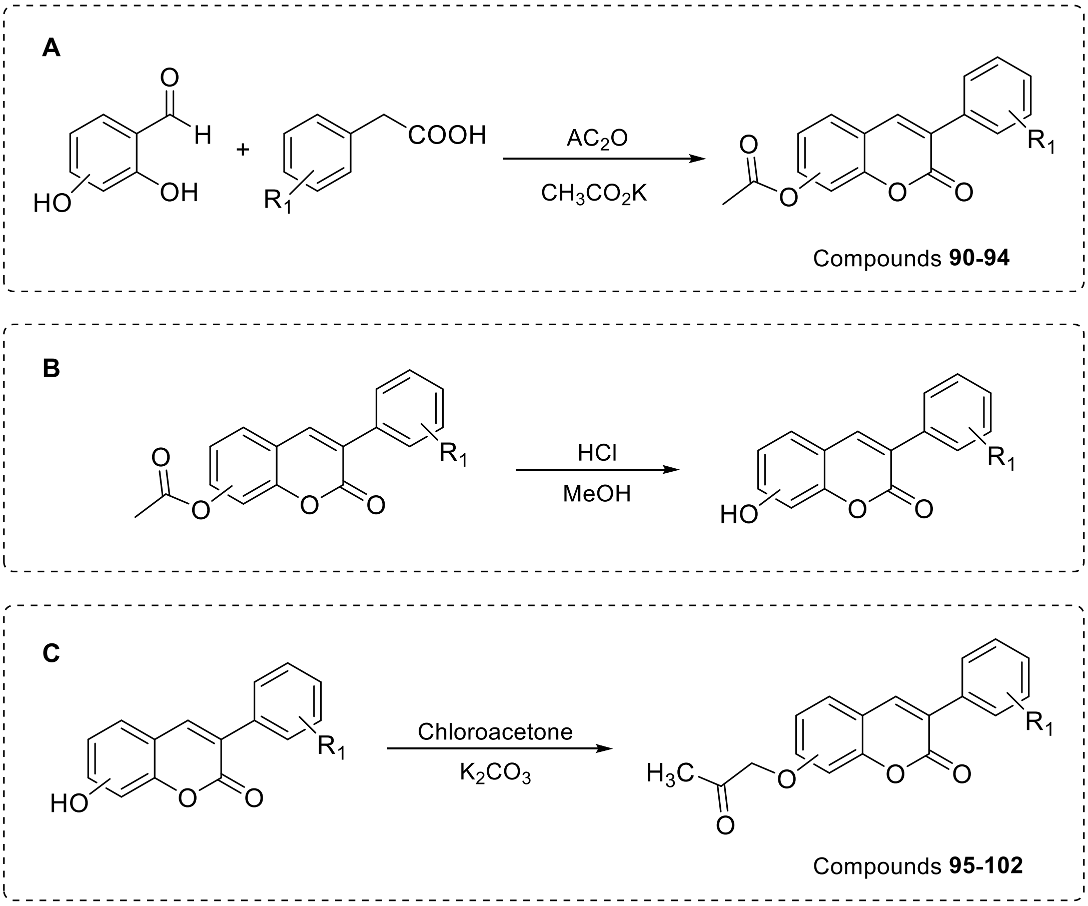
A
O
H
HO
OH
+
COOH
R1
AC2O
CH3CO2K
O
O
O
O
R1
Compounds 90-94
B
O
O
O
O
R1
HCl
MeOH
HO
O
O
R1
C
HO
O
O
R1
Chloroacetone
K2CO3
H3C
O
O
O
O
R1
Compounds 95-102

Figure 51 – Methodology followed for the synthesis of compounds **90**-**102**.

The reaction operated well for the synthesis of methyl derivatives (compounds **84**-**89**). However, it was found that the same reaction conditions were not suitable for the synthesis of compounds **90**-**102**, due to the use of hydroxylated salicylaldehydes as starting materials. As such, the Perkin-Oglialoro modification was introduced.[249] In this adjustment, acetic anhydride and potassium acetate were used, allowing the *in situ* acetylation of the hydroxyl groups and the synthesis of compounds **90**-**94** (Fig. 51A).

Subsequently, the acetylated derivatives (Fig. 51A) were hydrolyzed using aqueous HCl solution and MeOH, under reflux, to yield hydroxylated coumarins (Fig. 51B).[326] Finally, compounds **95**-**99** and **100**-**102** were synthesized by means of a Williamson reaction using 3-aryl-6-hydroxycoumarins or 3-aryl-8-hydroxycoumarins as starting materials, respectively, and choloroacetone, in the presence of potassium carbonate as the base (Fig. 51C). (Manuscript III)

Table 3 - Benzopyrone library based on 3-arylcoumarins derivatives.

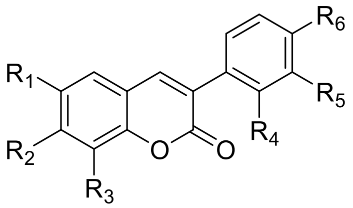

Cmpd	R1	R2	R3	R4	R5	R6	Yield	Manuscript
84	CH_3	H	H	H	H	H	21%	
85	H	CH_3	H	H	H	H	18%	
86	H	H	CH_3	H	H	H	20%	
87	H	H	H	CH_3	H	H	11%	
88	H	H	H	H	CH_3	H	13%	
89	H	H	H	H	H	CH_3	31%	
90	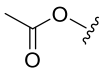	H	H	H	H	CH_3	61%	III
91	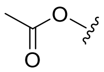	H	H	H	CH_3	H	75%	III
92	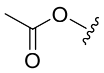	H	H	H	H	Br	82%	III
93	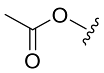	H	H	H	H	NH_2	69%	III
94	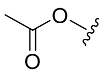	H	H	H	Br	H	84%	III

95	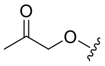	H	H	H	H	CH_3	74%	III
96	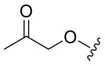	H	H	H	CH_3	H	79%	III
97	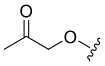	H	H	H	H	Br	81%	III
98	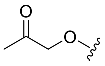	H	H	H	H	NH_2	90%	III
99	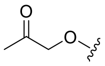	H	H	H	Br	H	83%	III
100	H	H	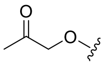	H	H	H	76%	III
101	H	H	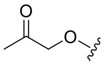	H	H	CH_3	80%	III
102	H	H	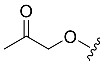	H	H	Br	78%	III
103	CH_2Br	H	H	H	H	H	39%	
104	H	CH_2Br	H	H	H	H	46%	
105	H	H	CH_2Br	H	H	H	41%	
106	H	H	H	CH_2Br	H	H	34%	
107	H	H	H	H	CH_2Br	H	39%	
108	H	H	H	H	H	CH_2Br	43%	

Bromomethyl derivatives (compounds **103**-**108**, Table 3), were synthesized from their methyl analogues (compounds **84**-**89**, Table 3) using *N*-bromosuccinimide (NBS) as a bromide radical source and azobisisobutyronitrile (AIBN) in carbon tetrachloride (Fig. 52). To minimize the formation of multibromide derivatives one equivalent of NBS is used. The reaction was kept under reflux for 24h and the products are easily separated by column chromatography.

Although several bromination agents can be used to obtain this type of bromine derivatives such as tetrabutylammonium tribromide,[327] hexamethylenetetramine tribromide,[328] NBS[329] is often the primary agent choice for radical bromination reactions,[330] either in solid phase or in classic homogenous reactions.[331] The advantages of using this reagent are related to its availability and relative handle safety. Additionally, due to the easy removal of the reaction byproduct (succinimide), reaction yields are usually high.

The compounds **103**-**108** were synthesized as they were needed as starting material for compounds **109-111**.

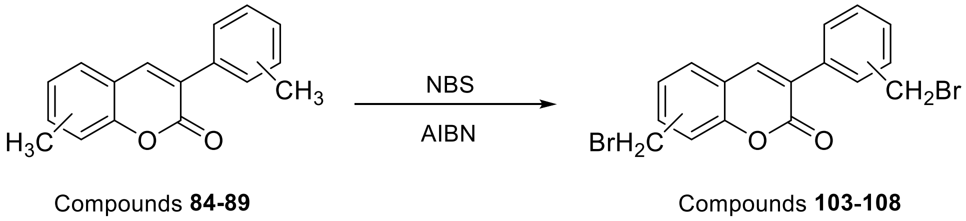
NBS
AIBN
Compounds **84-89**
Compounds **103-108**

Figure 52 – Methodology followed for the synthesis of compounds **103**-**108**.

3.1.1.3. Synthesis of nitrooxy-coumarin based library

Nitric oxide donor coumarin-based derivatives (compounds **109**-**115**, Table 4) were synthesized as an effort to obtain potent MAO-B inhibition while improving the blood intake to the brain by the means of vasorelaxant activity. Compounds **109**-**111** were synthesized from the bromomethylcoumarin derivatives **103**-**108** (Fig. 53A), while compounds **112**-**115**, Table 4 were synthesized using other type of starting materials previously prepared by our group (Fig. 53B).

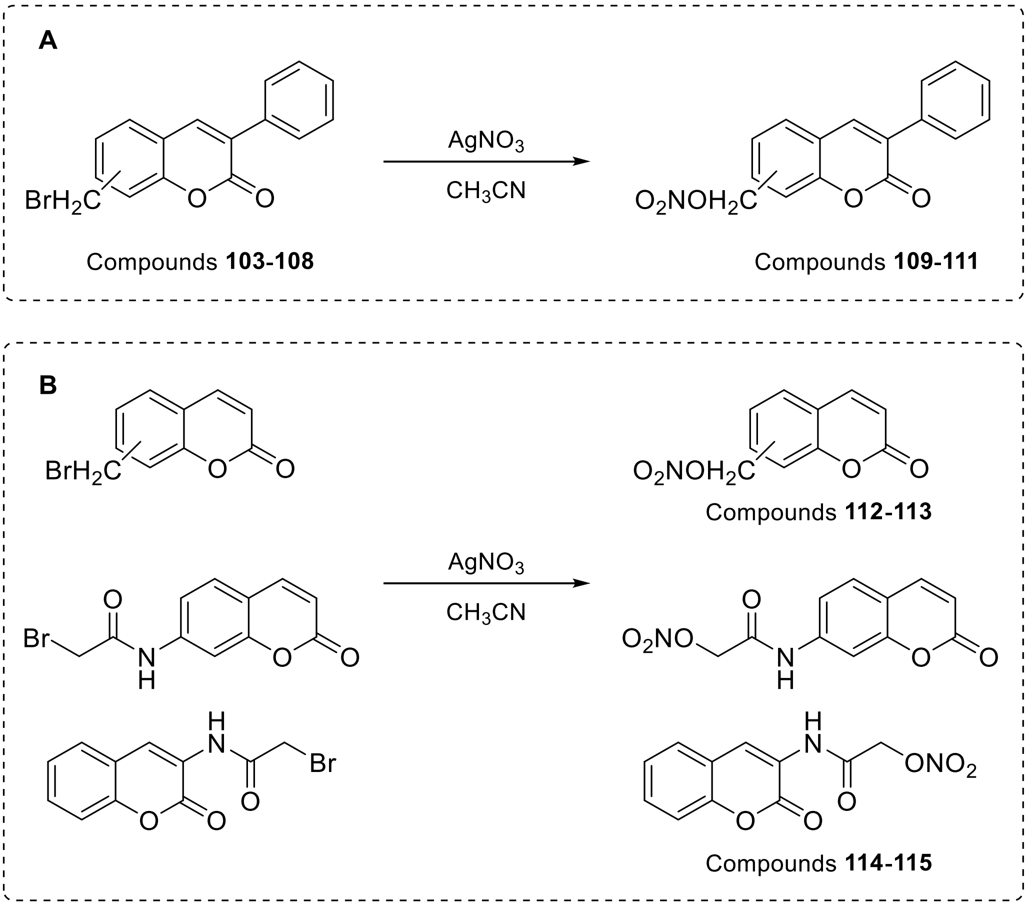
A
AgNO3
CH3CN
Compounds **103-108**
Compounds **109-111**
B
AgNO3
CH3CN
Compounds **112-113**
Compounds **114-115**

Figure 53 – Methodology followed for the synthesis of compounds **109**-**115**.

The synthesis of these derivatives was straightforward and in high yields, using silver nitrate in acetonitrile under reflux as reaction conditions (Fig. 53B). Due to time and technical restrictions, preliminary data from MAO-B inhibition and vasorelaxant activity screenings for these series of compounds has not yet been attained.

Table 4 - Benzopyrone library based on nitrooxy coumarin derivatives.

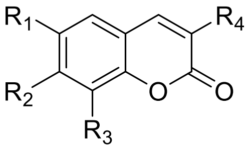

Compound	R₁	R₂	R₃	R₄	Yield
109	CH_2ONO_2	H	H	Ph	84%
110	H	CH_2ONO_2	H	Ph	80%
111	H	H	CH_2ONO_2	Ph	85%
112	CH_2ONO_2	H	H	H	94%
113	H	CH_2ONO_2	H	H	92%
114	H	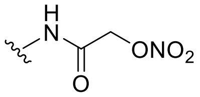	H	H	94%
115	H	H	H	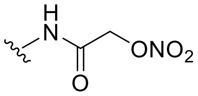	88%

3.1.1.4. Synthesis of 3-carboxamidochromone-based library

A library of benzopyrone derivatives, focused on the introduction of aromatic type substituents, with diverse patterns, on position 3 of chromone scaffold using as a spacer an amide function was developed (Table 5). Moreover, in analogy with the 3-carboxamidcoumarin-based library developed previously, the benzopyrone moiety was functionalized with methyl and methoxy groups at C-6 position.

The 3-carboxamidochromone derivatives (Table 5) were synthesized using chromone-3-carboxylic acids, DMF and phosphoryl chloride (Fig. 54). The synthetic methodology encompasses the *in situ* acylation of the carboxylic acid and subsequent addition of the appropriate amine (Fig. C).

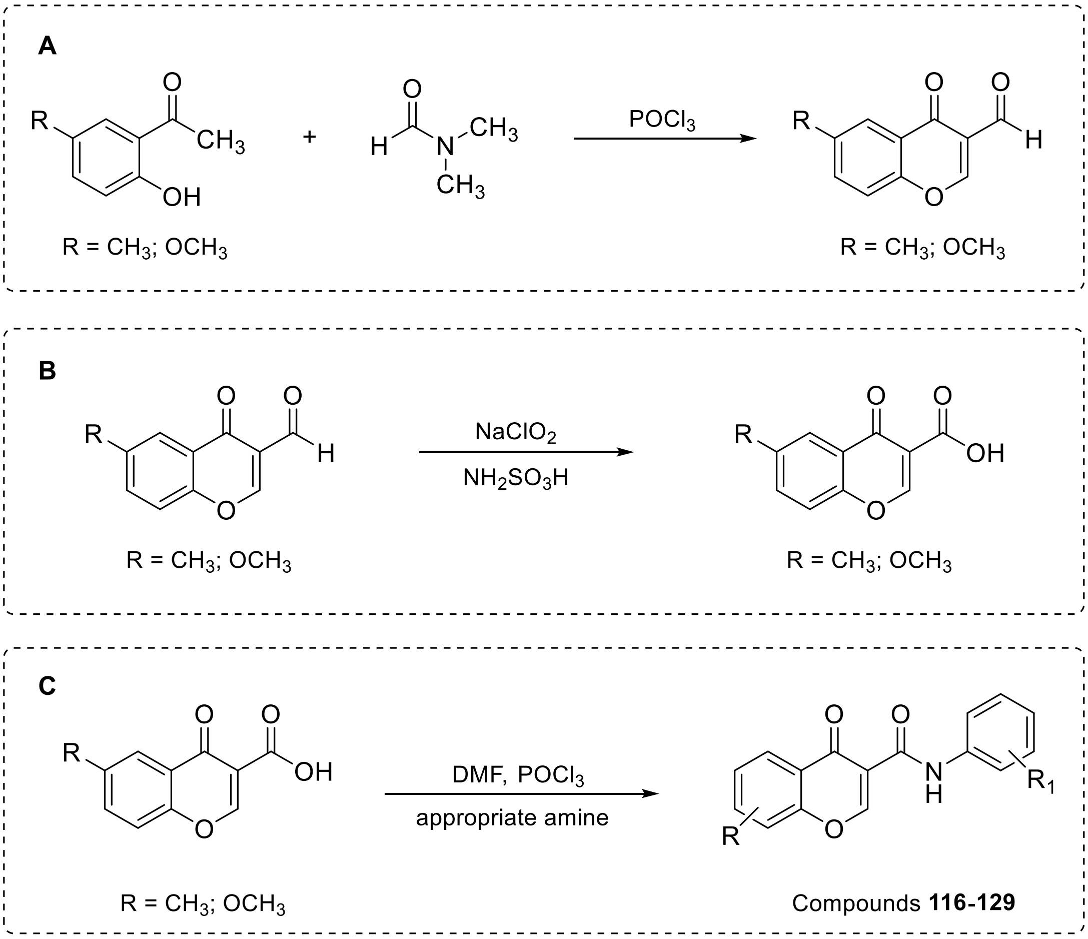
A
R = CH3; OCH3
POCl3
R = CH3; OCH3
B
R = CH3; OCH3
NaClO2
NH2SO3H
R = CH3; OCH3
C
R = CH3; OCH3
DMF, POCl3
appropriate amine
Compounds 116-129

Figure 54 – Methodologies followed for the synthesis of 3-carboxamidochromone-based library.

The chromone carboxylic acids were obtained from chromone-3-aldehydes synthesized *via* Vilsmeier-Haack reaction between the appropriate acetophenone and DMF (Fig. 54A), and a subsequent oxidation reaction performed with sodium chlorite and sulphamic acid (Fig. 54B). The reaction yields were generally high and not dependent of acetophenone’s substitution pattern. Also, this methodology allowed a rapid reaction work-up, with few byproducts. (Manuscript IV)

Table 5 - Benzopyrone library based on 3-carboxamidochromone.

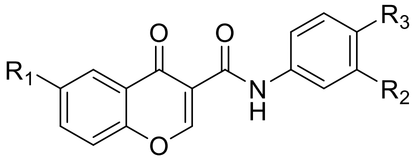

Compound	R_1	R_2	R_3	Yield	Manuscript
116	CH_3	H	H	48%	IV
117	CH_3	CH_3	H	45%	IV
118	CH_3	Cl	H	47%	IV
119	CH_3	OH	H	11%	IV
120	CH_3	H	CH_3	41%	IV
121	CH_3	H	Cl	20%	IV
122	CH_3	H	OH	18%	IV
123	OCH_3	H	H	60%	IV
124	OCH_3	CH_3	H	42%	IV
125	OCH_3	Cl	H	49%	IV
126	OCH_3	OH	H	21%	IV
127	OCH_3	H	CH_3	40%	IV
128	OCH_3	H	Cl	32%	IV
129	OCH_3	H	OH	24%	IV

3.1.2.Structural characterization of the benzopyrone derivatives

All the synthesized compounds (Tables 1-5) were fully characterized by one-dimensional (1D) NMR (1H, 13C and DEPT) techniques and electron impact mass spectrometry (EI/MS). Additionally, two-dimensional (2D) NMR (COSY, HSQC and HMBC) studies were also performed. Structural elucidation of compounds not yet published can be found in Annex I.

Along this thesis a complete structural elucidation of a series of 6-methyl-3-carboxamidocoumarin derivatives, bearing electron-donating substituents in different positions of the exocyclic ring, using 1D and 2D NMR techniques and X-ray diffraction was performed. (Manuscript V) From this study one can highlight the unequivocal assignment of the signals at 161.6 and at 159.4 ppm to C-2 and C-9 respectively, as they exhibit long range interaction with H-4 and NH/H-4 (Fig. 55). In the figure are represented sections of the long-range couplings of proton peaks at 10.22 ppm (OH) and

11.12 ppm (NH) (Fig. 55A) and at 8.98 (H-4) and at 11.12 ppm (NH) (Fig. 55B) with carbons peaks, for compound **22**.

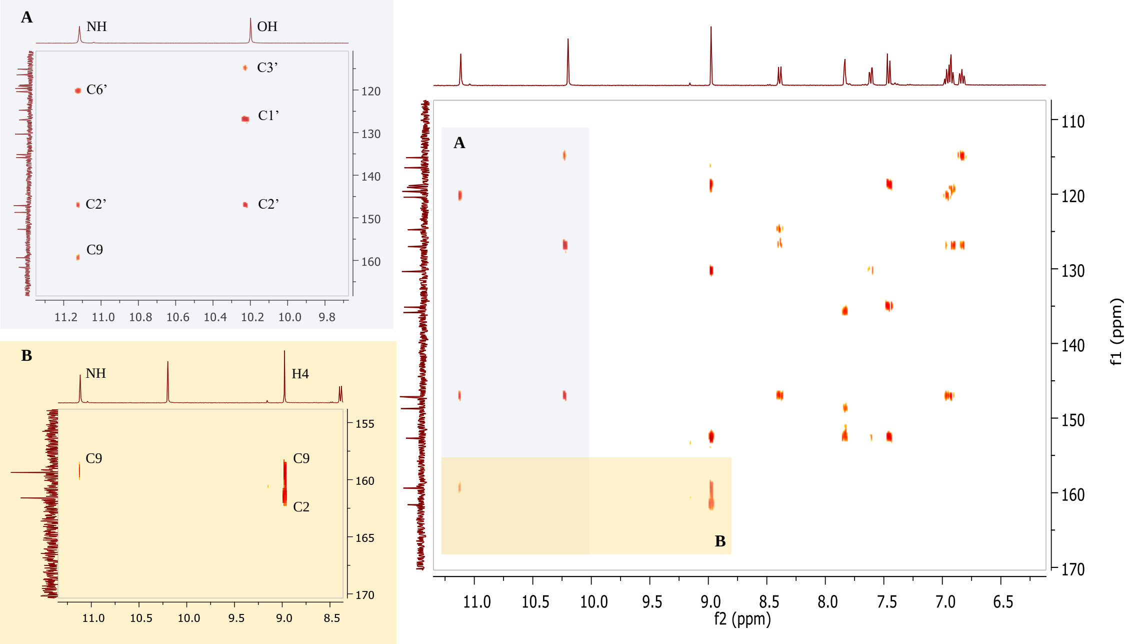

Figure 55 – HMBC spectrum of compound **22**.

Their unequivocal identification constitutes *per se* a valuable database for the accurate identification of the coumarins of our library. In addition, these results can be used as reference for structural elucidation of newer naturally occurring and synthetic coumarins.

On the other hand, as tridimensional shape or configuration and the formation of intramolecular hydrogen bonds have a very pronounced effect on molecular structure and its properties,[332] X-ray studies have been performed. (Manuscripts VI)

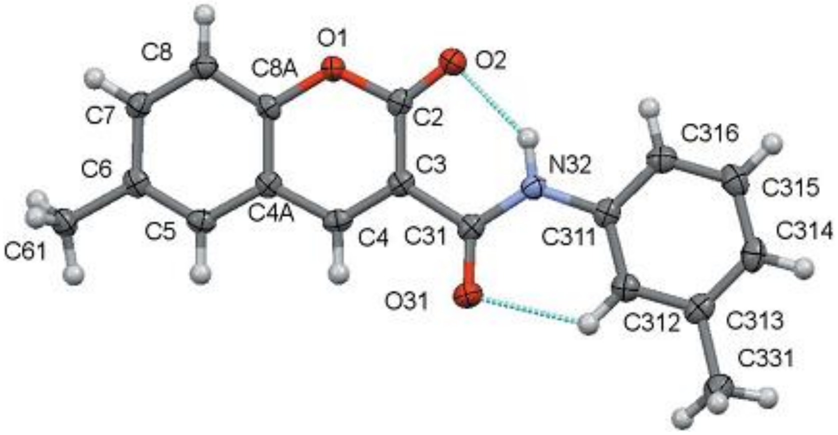

Figure 56 – X-ray structure of compound **33**.

From the data gathered, it was observed that compounds **1**-**51**, Table 1 are roughly planar probably due to the presence of intramolecular hydrogen bonds between the oxygen of the C-2 carbonyl and the hydrogen of the amide linker, forming form pseudo hexagonal rings that may restrain their geometry (Fig. 56). (Manuscript VI)

Additionally, through the X-ray data it was observed that compounds **52**-**83**, Table 2 have intramolecular hydrogen bonds between the carbonyl group of the amide linker and a hydrogen of the heteroaromatic exocyclic ring, constraining the rotation and bending of both rings (Fig. 57). Consequently, these molecules are roughly planar, being this data important when considering ligand-enzyme/receptor interactions. (Manuscript VII)

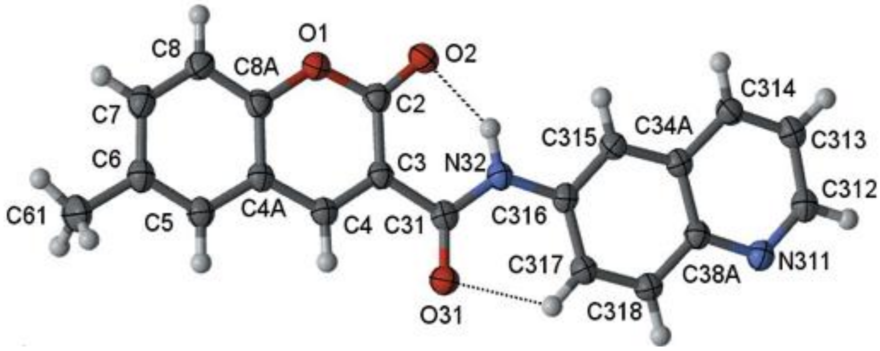
O1
C8
O2
C8A
C7
C2
C314
C34A
C315
C313
C6
C3
N32
C312
C61
C5
C4A
C4
C31
C316
N311
C317
C38A
O31
C318

Figure 57 – X-ray structure of compound **58**.

Moreover, additional data was acquired about the crystallization of compounds with a hydroxyl group. It was found that compound **27** (Fig. 58) can crystallize asymmetrically through solvent mediation. (Manuscript V)

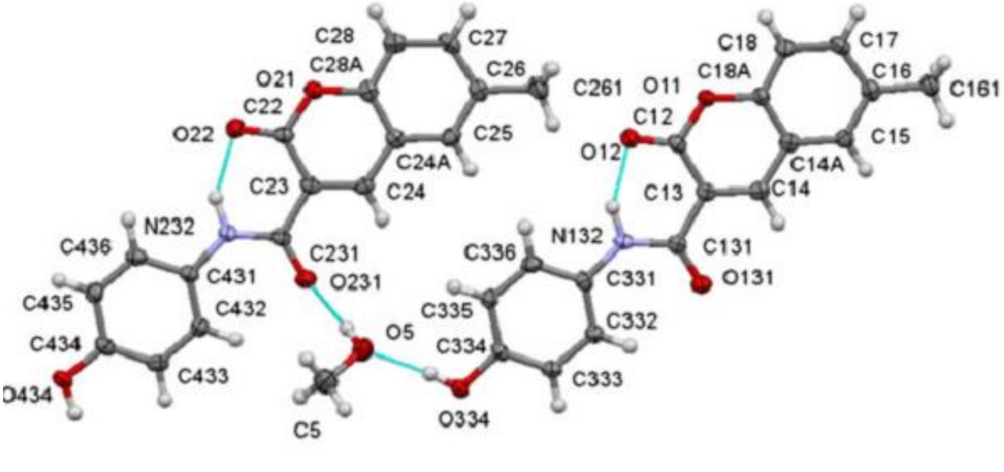
C28
C27
C28A
C26
O21
C261
O11
C18
C17
C18A
C16
C161
C22
C12
O22
C25
C15
C24A
O12
C14A
C23
C24
C13
C14
N232
C436
C431
C231
C336
N132
C131
C331
O131
O231
C435
C432
C335
C332
C434
O5
C334
C433
D434
C333
C5
O334

Figure 58 – X-ray structure of compound **27**.

3.1.3. Looking for target directed drugs for neurodegenerative diseases based on the benzopyrone scaffold

Drug discovery is continuously advancing as new fundamental knowledge, methods, technologies, and strategies are introduced. Every new technology result in changes in the drug discovery process. For example: a) Screening for lead structures changed from direct testing in living systems to *in vitro* HTS and computational virtual screening, b) Initial leads for optimization changed from natural products and natural ligands to compounds from large synthetic libraries of diverse structures that cover a wide chemical space, c) Information from SAR studies is now complemented by x-ray crystallography, nuclear magnetic resonance binding studies, and computational modeling, and d) Lead optimization chemistry changed from one-at-a-time synthesis to parallel synthesis of multiple analogs.[333]

Another shift of drug discovery paradigms is related with the rational design of agents for multifactorial diseases, such as cancer and ND. The drugs currently used in ND therapy allow a better quality of life of the patients, relieving their symptoms, however they are unable to halt neurodegeneration and modify disease progression. In the specific case of AD and PD, the current therapy is based on single target drugs, pinpointing one specific target involved in cognitive decline and/or neurodegeneration in general.[334,335] Indeed, ND have a multifactorial etiology, which does not fit with the currently available "one drug, one target" therapeutic strategy. Under this hypothesis, single-target drugs do not offer the best strategy towards the development of disease-modifying drugs.[336] Contrarily, using a single drug that aims at multiple ND-associated targets may lead to drugs with a more favorable clinical outcome. Furthermore, this multi target approach is advantageous over combination therapy with multiple drugs, since it can reduce the potential risk of drug interactions and side-effects thereof, but also provides more predictable pharmacokinetics and pharmacodynamics.[166,337,338] However, as discussed by Merino et al.,[339] it is important to emphasize that there are different levels of polypharmacology (or promiscuity) that could lead to positive or negative effects, some of them largely dependent on the dose of the drug. In this scenario, non-specific binding to antitargets may be a potential source of adverse effects of multi-target drugs.[339]

The multi-target approach indeed opened a door for new therapeutic strategies for the treatment of cognitive impairment, motor dysfunction, depression and neurodegeneration.[168,340] This approach has fueled extensive research concerning the design and development of multi target drugs, and several scaffolds have since been identified as privileged structures for this purpose, including benzopyrones (Fig. 22A). In fact, benzopyrones have been widely used as scaffolds in drug discovery programs, including for ND.[191] Enclosed in this thesis, we present a review that reinforces the most relevant advances in the development of coumarins and chromones as potential drug candidates for ND in the last 5 years, focusing on their effects in the enzymatic systems involved in ND (Annex II).

3.1.3.1. Evaluation of drug-like properties

The later stages of drug development impose very stringent and strict drug-like requirements on potential drug candidates, which is often a source of attrition and discontinuation. Thus, it is necessary to anticipate these requirements along the development process, and only advance with compounds with the appropriate properties, which have higher chances of success.[333] As such, the prediction drug-like properties is a priority and needs to be encompassed in early-stage drug discovery programs. Accordingly, these properties were calculated using Molinspiration[341] software.

Table 6 – Drug-like properties of several compounds of the benzopyrone library.

Compound	MW	cLogP	TPSA (Å^2)	HBA	HBD	*N*rotb	Log BB
28	293.3	3.71	59.31	4	1	2	-0.205
44	311.3	2.17	88.77	6	2	3	-0.845
72	346.3	3.02	81.44	6	1	3	-0.607
101	308.3	3.74	56.52	4	0	4	-0.129
110	297.3	4.31	85.27	6	0	4	-0.468
120	293.3	3.71	59.31	4	1	2	-0.175
127	309.3	3.31	68.54	5	1	3	-0.372
CNS+ drugs[342–345]	<450	<5	<90	<7	<3	<8	≥-1

For the majority of derivatives developed in this thesis, no violations of Lipinski's rule[343] [molecular weight (MW), log P, number of hydrogen bond donors (HBD) and acceptors (HBA)] were found. Furthermore, the calculated log P and topological polar surface area (TPSA) values pointed towards oral bioavailability and BBB permeability, an essential pharmacokinetic requirement for CNS drug candidates. In fact, the blood (plasma)−brain partitioning multiparameter score (log BB), calculated according to Clark *et al.*,[346] allows the prediction that these compounds would be able to effectively function as CNS drugs.

In table 6 are represented the drug-like properties of several synthesized derivatives as well as the parameters observed in BBB permeable compounds (CNS+ drugs).

3.1.3.2. Benzopyrones as monoamine oxidase B inhibitors

Inhibitors of MAO-B were the earliest drugs undergoing trials in PD.[347] As discussed in item 1.4.2., MAO-B inhibitors block the metabolism of biogenic amine neurotransmitters, particularly DA, increasing their concentrations in the synaptic cleft and post synaptic receptors sites. Commonly used as co-adjuvant drugs alongside L-DOPA, MAO-B inhibitors effectively contribute to enhance cerebral DA levels.[347] Nevertheless, with the exception of recently introduced safinamide (Fig. 8), the MAO-B inhibitors currently in therapy are irreversible inhibitors. As such, the development of selective and reversible MAO-B inhibitors is still a goal of numerous medicinal chemistry programs.

Previous reports highlighted 6-methyl-3-arylcoumarins as potent MAO-B inhibitors,[348] as well as the potential role of an amide linker in the modulation of MAO-B inhibitory potency.[236,349] In this context, a rational design strategy based on the benzopyrone scaffold was planned and focused on the study of: a) the effect of different substituents on the benzopyrone ring (methyl and methoxy), b) the effect of electron-donating and withdrawing groups (halogen, methyl, methoxy and hydroxyl) in the exocyclic ring and c) the influence on MAO-B inhibitory activity of the position of the carbonyl group on the benzopyrone isomeric structures, coumarins and chromones.

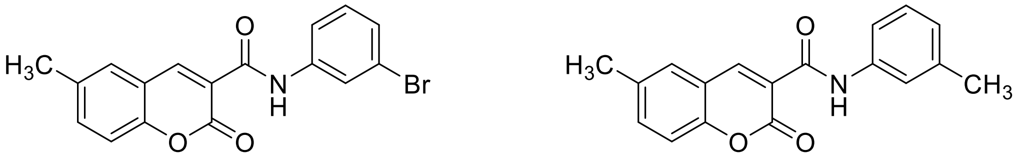

Compound **29**

IC_{50} MAO-B = 4.66 nM

IC_{50} MAO-A > 10 μM

Compound **33**

IC_{50} MAO-B = 7.52 nM

IC_{50} MAO-A > 10 μM

Figure 59 – MAO-B activity of compounds **29** and **33**.

Accordingly, a series of 6-methyl-3-carboxamidocoumarins was developed and screened for MAO-B inhibition (compounds **18**-**34**, Table 1). Overall, these compounds displayed remarkable selectivity towards MAO-B (IC_{50} MAO-B ≤ 0.621 μM, IC_{50} MAO-A ≥ 10 μM, SI ≥ 16.1) (Manuscript I). The bromine (compounds **19**, **24** and **29**, Table 1) and methyl derivatives (compounds **23**, **28** and **33**, Table 1) exhibited MAO-B activity in the low nanomolar range, with negligible MAO-A inhibitory activity (Manuscript I). In particular, compounds **29** and **33** were the most potent of the present series (Fig. 59).

These promising results lead to further research into the mechanism of MAO-B inhibition of compound **29** (Fig. 60). Analyzing the initial reaction rate at different *p*-tyramine concentrations (0-500 µM), in the absence or presence of inhibitor (0-5 nM), we were able to study kinetic parameters of enzyme inhibition (Manuscript I). The results obtained in the Lineweaver-Burk plots showed a non-competitive inhibition mechanism for compound **29** (Fig. 60). The reversibility of compound **29** was then studied by time-dependent inhibition experiments, which were also run for standard irreversible (R-(-)-deprenyl) and reversible (safinamide) inhibitors. The time-dependent inhibition profile obtained for compound **29** showed that, after an initial steep decrease, the enzymatic activity gradually increased (Fig. 60). The progressive increase on MAO-B activity was similar to that of reversible inhibitor safinamide, indicating that compound **29** is a reversible enzymatic inhibitor (Fig. 60, Manuscript I).

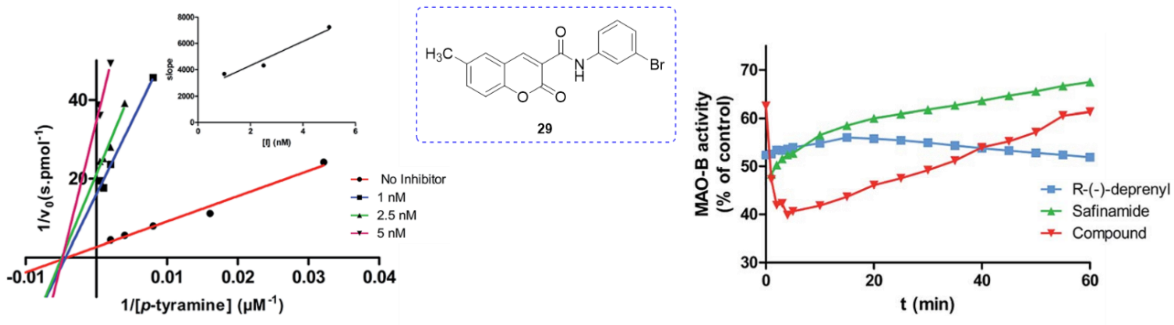

Figure 60 – Kinetic and reversibility profiles of compound **29**.

Based on the gathered data, two series of coumarins (compounds **18**-**51**, Table 1) and chromones (compounds **116**-**129**, Table 5) were then synthesized and evaluated for their potential as MAO-B inhibitors. (Manuscript IV) The main goal was to understand the influence of the position of the benzopyrone carbonyl on MAO-B inhibition. The results showed that the majority of the compounds were potent and selective MAO-B inhibitors. Interestingly, 6-methylcoumarins were slightly more potent than the corresponding chromones (Fig. 61A), while the reverse outcome was observed for 6-methoxy derivatives (Fig. 61B). (Manuscript IV)

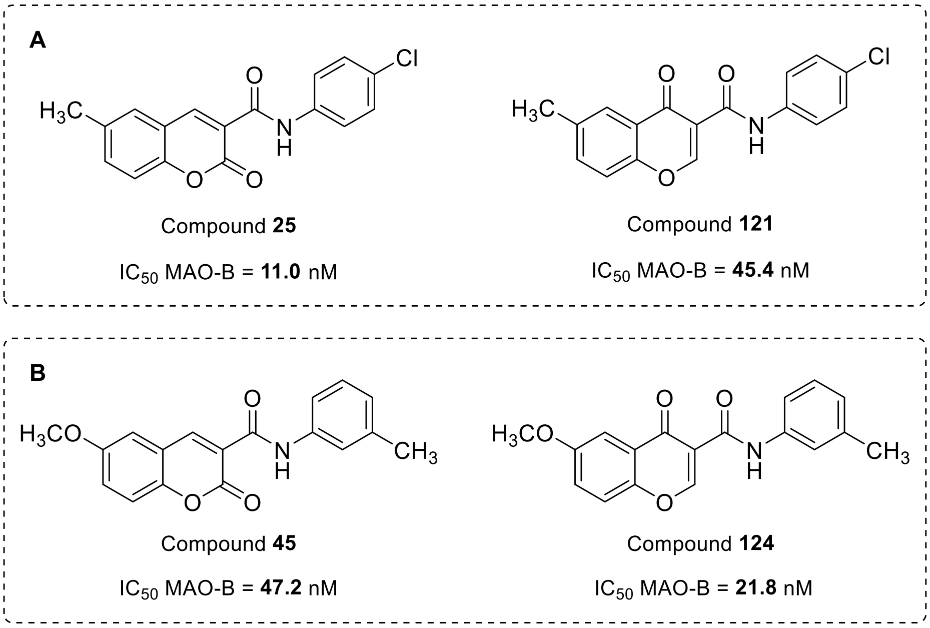

Compound **25**

IC_{50} MAO-B = **11.0** nM

Compound **121**

IC_{50} MAO-B = **45.4** nM

Compound **45**

IC_{50} MAO-B = **47.2** nM

Compound **124**

IC_{50} MAO-B = **21.8** nM

Figure 61 – MAO-B activity of coumarin and chromone derivatives.

Moreover, the reversibility and kinetic profile were assessed for compounds **30** (Table 1) and **118** (Table 5) and no variations were found between the two scaffolds (Fig. 62). Both coumarin and chromone derivatives were reversible and non-competitive inhibitors. (Manuscript IV) This information is in accordance with the findings for compound **29** (Fig. 60), and corroborates the hypothesis that these scaffolds are indeed similar in potency, reversibility and kinetic profiles. (Manuscripts I and IV)

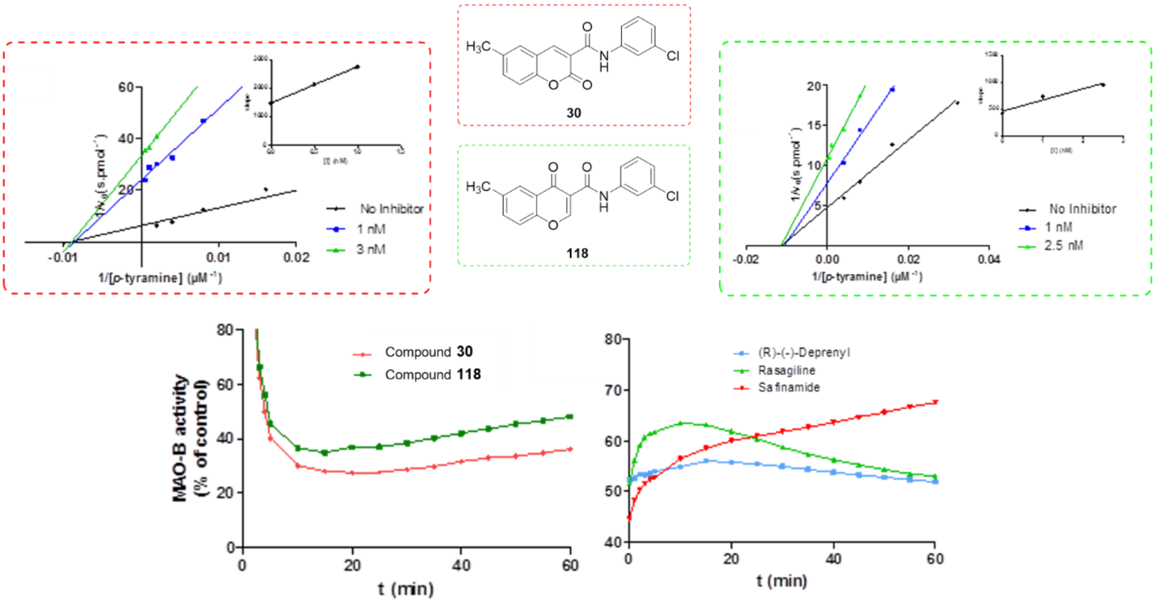

Figure 62 - Kinetic and reversibility profiles of compounds **30** and **118**.

Overall, all the compounds were selective towards MAO-B and the position of the benzopyrone carbonyl did not exert a significant influence on inhibitory potency. As such, both scaffolds appear to be equivalent regarding MAO-B inhibition, which can be important for further lead optimization steps. (Manuscript IV)

Nevertheless, a conformational difference between coumarins and chromones was observed in molecular modeling and docking studies. Coumarins adopt a planar conformation and interact with the enzyme's pocket in two equally valid binding poses: one where the coumarin is oriented towards the FAD co-factor, and another where it is facing away from it (Fig. 63A). Regardless of the binding poses adopted, the establishment of a hydrogen bond with Cys172 seems to be relevant to MAO-B inhibition. Interestingly, the plasticity presented in coumarin derivatives did not apply to their chromone analogues, without compromising inhibitory activity. This behavior can be attributed to the fact that chromone derivatives establish an extra hydrogen bond with Cys172, since both carbonyl groups are facing the same direction (Fig. 63B).

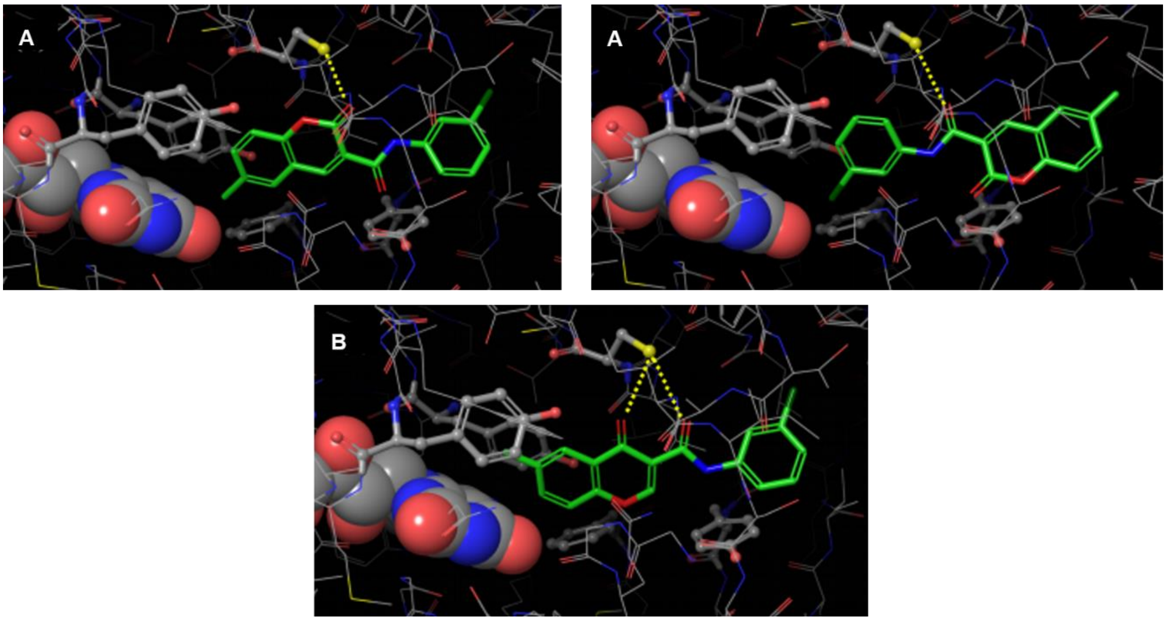

Figure 63 – MAO-B docking poses of compounds **30** and **118**.

3.1.3.3. Benzopyrones as adenosine receptors ligands

The multi target approach for the development of new PD therapies has been progressively gathering attention. Indeed, several AR subtypes, namely A$_1$, A$_{2A}$ and A$_3$, have been validated as putative PD targets. In fact, A$_{2A}$AR and A$_1$AR antagonists with modest MAO-B activity have been recently reported.[350,351] As such, it was relevant to screen the synthesized coumarin-based libraries towards AR.

Previous studies performed by our group have already established the potential of coumarins as AR ligands, particularly when derivatized at the C-3 position.[229,352,353] Accordingly, a series of 3-arylcoumarins (compounds **90**-**102**, Table 3) was developed and screened towards AR in order to obtain a preliminary SAR (Manuscript III). The results demonstrated that almost all compounds in this series had affinity towards A_3AR, with compound **101** reaching the nanomolar range (Fig. 64). Additionally, it was found that the affinity/selectivity is strongly dependent on the position and type of substituents, since other derivatives (compounds **96** and **100**) showed low selectivity and presented A_1AR and A_{2A}AR affinity (Fig. 64). For instance, the presence of a methyl group in the exocyclic ring seems to be relevant for A_3AR affinity and selectivity.

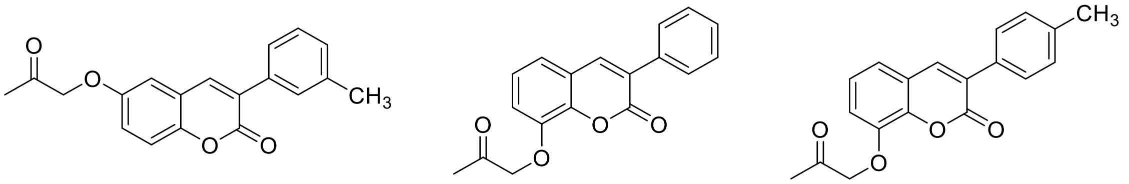

Compound **96**

K_i A_1AR = 15.4 µM
K_i A_{2A}AR > 30 µM
K_i A_3AR = 25.5 µM

Compound **100**

K_i A_1AR = 10.4 µM
K_i A_{2A}AR = 16.1 µM
K_i A_3AR = 7.1 µM

Compound **101**

K_i A_1AR > 100 µM
K_i A_{2A}AR > 100 µM
K_i A_3AR = 630 nM

Figure 64 – AR affinity of compounds **96**, **100** and **101**.

In order to scope the potential for dual target AR ligands/MAO-B inhibitors, we then screened the set of MAO-B active C-3 carboxamide derivatives (compounds **1-51**, Table 1, manuscript VIII) for its activity on AR. Interestingly, the introduction of a 6-methyl group led to a complete loss of activity towards all AR. (Manuscript VII). In fact, the manipulation of the C-6 position was responsible for the loss of selectivity showed by compound **39** (Fig. 65).

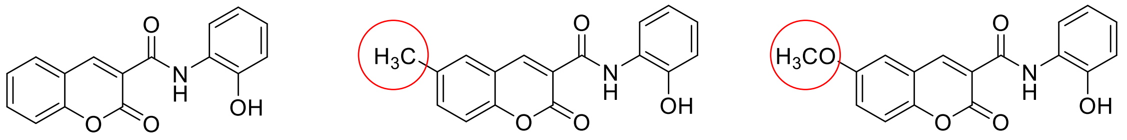

Compound **5**

A_3AR selective
K_i A_1AR > 100 µM
K_i A_{2A}AR > 30 µM
K_i A_3AR = 31.5 µM

Compound **22**

Inactive
K_i A_1AR > 100 µM
K_i A_{2A}AR > 100µM
K_i A_3AR > 30 µM

Compound **39**

Non-selective AR ligand
K_i A_1AR = 39.5 µM
K_i A_{2A}AR = 38.0 µM
K_i A_3AR = 32.7 µM

Figure 65 – AR selectivity and affinity of ocmpounds **5**, **22** and **39**.

When searching for a dual target hit, potency is often overlooked in order to achieve moderate affinity for both targets.[165] Although showing a slight loss of AR selectivity and affinity, compound **44** retained nanomolar MAO-B inhibition (Manuscript IV), and can be considered a good hit for further development (Fig. 66). Although less active towards MAO-B (unpublished results), compound **11** was the most potent A_3AR ligand of the series, and could also be considered for future hit-to-lead optimization. (Fig. 66)

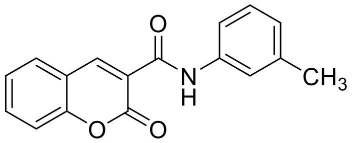

Compound **11**

K_i A_1AR > 100 μM
K_i A_{2A}AR > 100 μM
K_i A_3AR = 2.4 μM
IC_{50} MAO-B = 600 nM

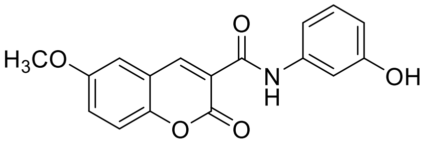
H3CO
O
N
H
OH
O
O

Compound **44**

K_i A_1AR = 41.0 μM
K_i A_{2A}AR > 100 μM
K_i A_3AR = 22.0 μM
IC_{50} MAO-B = 228.6 nM

Figure 66 – AR affinity and MAO-B activity of compounds **11** and **44**.

Docking studies on AR ligands were subsequently performed to support the results obtained from the *in vitro* assays. To this end, several derivatives encompassing different AR potencies and affinities (compound **5**, **11** and **39**) were selected.

The docking pose for compound **5** in A_3AR yielded a hydrogen bond with the residue Asn250 and π-π stacking interactions with the Phe168. A second hydrogen bond was also detected between the *o*-hydroxyl group in the phenyl exoxyclic ring and the residue Gln167 of the second extracellular loop (Fig. 67).

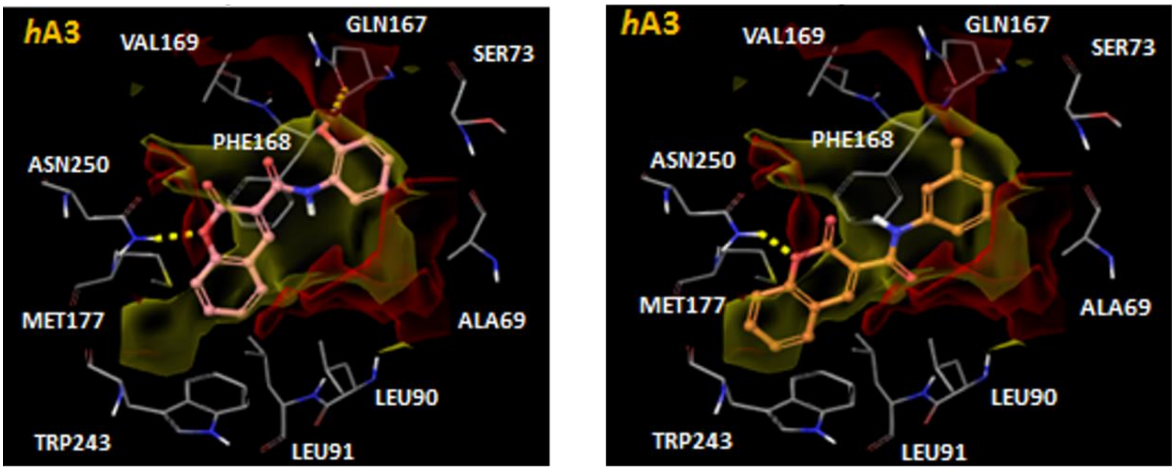
hA3
VAL169
GLN167
SER73
PHE168
ASN250
MET177
ALA69
LEU90
TRP243
LEU91
hA3
VAL169
GLN167
SER73
PHE168
ASN250
MET177
ALA69
LEU90
TRP243
LEU91

Compound **5**

Compound **11**

Figure 67 - A_3AR docking poses of compounds **5** and **11**.

This feature could be a key factor to explain the A_3AR selectivity shown by compound **5**, since other adenosine receptors do not present a Gln residue at the same position. Similarly, compound **11** establishes a hydrogen bond with the residue Asn250 but has no interaction with the specific A_3AR Gln residue. However, the benzopyrone ring is placed deeper in the A_3AR hydrophobic region compared to compound **5**, which can account for its greater affinity (Fig. 67).

The pose extracted for compound **39** showed that it can establish a hydrogen bond with the residue Asn250 and π-π stacking interactions with Phe168 (Fig. 68A). Nevertheless, the binding mode did not yield a hydrogen bond with Gln167, which may account for its decreased A_3AR affinity. However, the receptor's surface can still accommodate the 6-methoxy substituent in the hydrophobic area at the bottom of the cavity, which can ensure A_3AR binding. Additionally, the binding mode of compound **39** with A_{2A}AR was assessed in order to explain the increased affinity over compounds **5** and **11**. The 6-methoxy substituent was well accommodated in a hydrophobic region of the receptor and was ultimately responsible for the observed increase on A_{2A}AR affinity (Fig. 68B). (Manuscript VIII)

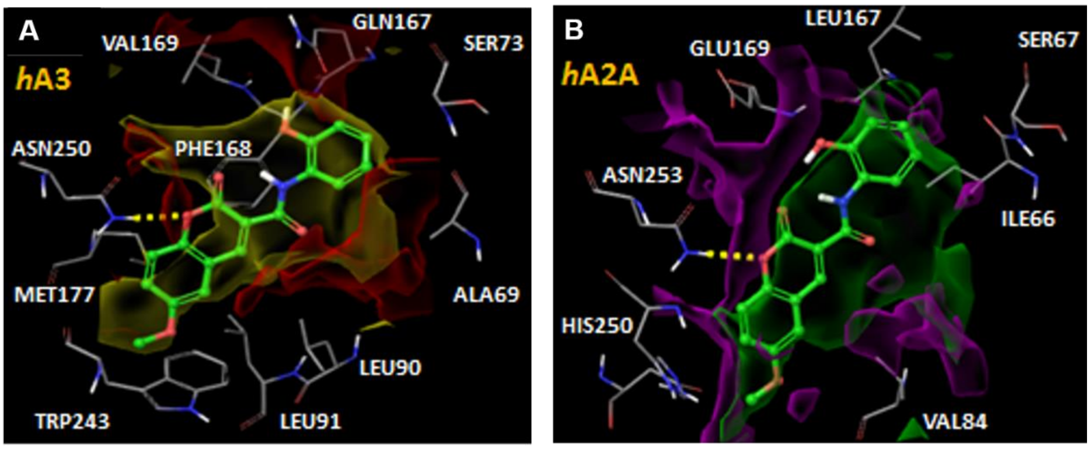

Figure 68 - A_3AR and A_{2A}AR docking poses of compound **39**.

3.1.3.4. Benzopyrones as AChE inhibitors

Following the results regarding the MAO-B and AR activity screenings, we focused our efforts on AChE. Thus, we screened compounds **1**-**51** (Table 1) for *in vitro* AChE inhibition according to a previously validated protocol.[354] The preliminary results obtained in this screening for unsubstituted 3-carboxamidocoumarins were not promising (IC_{50} ≥ 186 µM). The compounds were active only in high micromolar concentrations and the most potent were compounds **12** and **14** (Fig. 69). Similarly, 6-methyl-3-

carboxamidocoumarins inhibited AChE rather modestly, within the same magnitude order of compounds **12** and **14**. However, 6-methyl-3-carboxamidocoumarins already demonstrated potent nanomolar activity towards MAO-B, and could thus be potential hits for the development of dual target MAO-B/AChE inhibitors (Fig. 69).

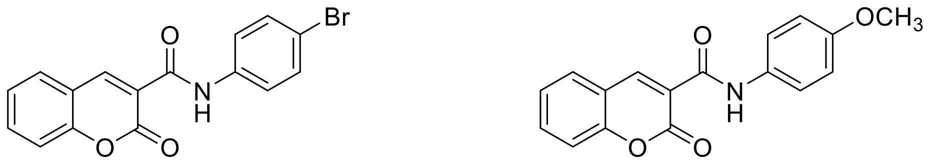

Compound **12**

IC$_{50}$ AChE = 193 μM

IC$_{50}$ MAO-B = 411 nM

Compound **14**

IC$_{50}$ AChE = 186 μM

IC$_{50}$ MAO-B = 680 nM

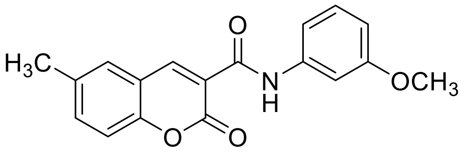

Compound **31**

IC$_{50}$ AChE = 470 μM

IC$_{50}$ MAO-B = 10.1 nM

Figure 69 – Structures and AChE and MAO-B inhibitory activities of compounds **12**, **14** and **24**.

In order to improve AChE inhibitory activity, we followed a molecular hybridization approach and developed a set of coumarin derivatives bearing the quinolone moiety of tacrine (Fig. 70). The amide linker at C-3 was maintained for the coumarin-quinoline hybrids, as it enabled straightforward one step synthesis. This rationale led to compounds **68**-**83** (Table 2), which were then screened for AChE inhibition following the same protocol. (Manuscript II)

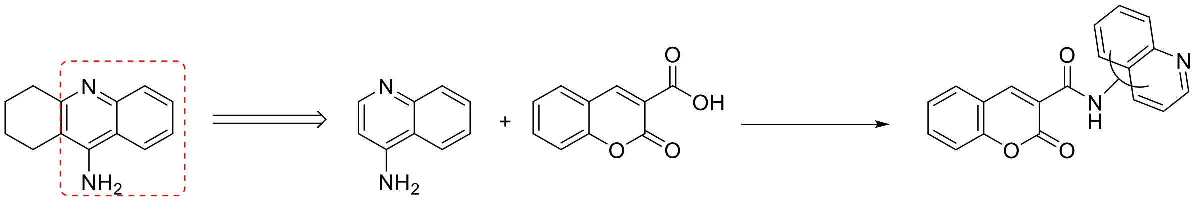

Tacrine

Quinoline

Compounds **52**-**83**

Figure 70 – Rational design of coumarin-quinoline hybrids.

Overall, *in vitro* results showed that AChE inhibition did not improve when compared to the previous preliminary screenings of compounds **1**-**51** (Table 1). Docking studies were then performed as an attempt to understand the coumarin-quinoline hybrids' interaction with AChE. Interestingly, 5-quinoline derivatives (compounds **69**, **73**, **77** and **81**, Table 2) adopted an unfavorable orientation within the enzyme's active pocket, and were thus inactive (Fig. 71, in yellow). For the remaining derivatives (Table 2), the coumarin moiety was stacked against the PAS and the quinoline ring was oriented towards the anionic site. Notwithstanding, these favorable results were not in accordance with the previous data from *in vitro* assays (IC_{50} > 159 µM). (Manuscript II)

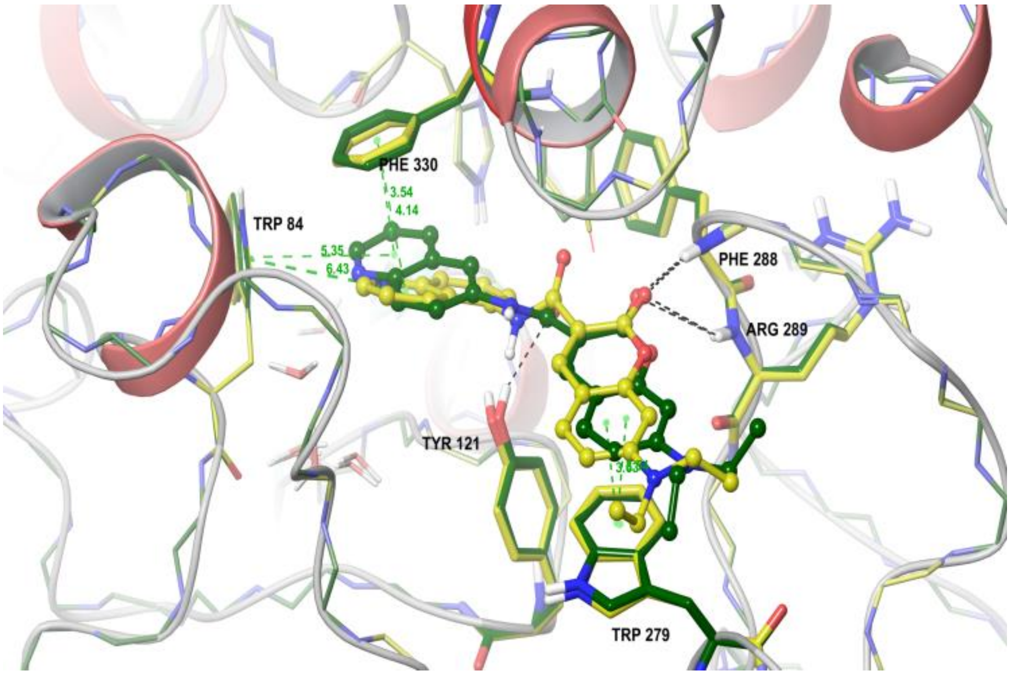

Figure 71 – Docking pose of compound **81**, in yellow, in AChE active site.

A similar series of C-6 substituted coumarin hybrids (compounds **52**-**67**, Table 2) was also designed and synthesized. However, these derivatives were not soluble in a vast array of solvents and no biological assays could be performed. Nevertheless, relevant structural information was gathered, namely crystal structures and Hirshfeld surface analysis. In fact, compound **58** (Fig. 57) was described in detail in manuscript VII.

3.2. Conclusions and future perspectives

The work developed and subsequent experimental results led to the following conclusions:

- Several benzopyrone-based libraries were successfully synthesized. Using straightforward synthetic methodologies and cost effective materials led to overall satisfactory yields.
- The majority of the synthesized compounds displayed no violations of Lipinski's rules. Compounds' drug-likeness properties were calculated and all the theoretical parameters pointed towards oral bioavailability and BBB permeability.
- A valuable database for the accurate identification of coumarin-based libraries was set. Complete structural elucidation by 1D and 2D NMR techniques and X-ray diffraction were carried out for several derivatives in Table 1 and 2. It was found that all these compounds were roughly planar due the establishment of intramolecular hydrogen bonds.
- Compounds **1**-**51** were potent and selective MAO-B inhibitors. Specifically, 6-methyl-3-carboxamidocoumarins selectively inhibited MAO-B within the low nanomolar range. Methyl, bromine and chlorine groups, when introduced to the exocyclic ring, appear to have a positive effect on bioactivity.
- The carbonyl group of the benzopyrone scaffold was a positive contributor for the ligand–MAO-B complex stability. Molecular modeling studies validated the *in vitro* MAO-B selectivity and inhibition.
- *In vitro* assays comparing selected coumarins and chromones did not yield significant variations on MAO-B inhibition between the two scaffolds. The position of the benzopyrone carbonyl was not a key determinant of MAO-B inhibitory activity.
- All the tested derivatives were non-competitive and reversible MAO-B inhibitors. Coumarins and chromones shared the same mechanism, reversibility and kinetics of MAO-B inhibition.
- The introduction of an amide spacer in coumarin C-3 position led to the loss of AR affinity. 3-arylcoumarins had an overall better affinity towards AR, especially for the A3 subtype.
- The C-6 position of the coumarin scaffold might modulate selectivity and affinity towards AR. Although extremely beneficial in modulating MAO-B inhibitory activity, the introduction of 6-methyl groups did not improve AR binding affinity.

On the other hand, 6-methoxy derivatives decreased selectivity while maintaining affinity.

- Interesting dual target MAO-B/AChE hits were found. Overall further development is still required regarding AChE inhibition.
- The introduction of a quinoline moiety led to an overall decrease in compound solubility.
- The quinoline ring nitrogen might modulate AChE activity. Molecular modeling studies showed that 5-quinoline substituents had unfavorable binding poses comparing to its 3-, 6- and 8-quinoline counterparts.

In this work, the benzopyrone scaffold was further validated as a relevant framework for ND. The data gathered from the previously discussed pharmacologic screening assays provided a solid understanding of the bioactivity of the developed benzopyrone libraries. Additionally, it also provided a base for further exploration of this scaffold towards other ND-related targets.

Due to their remarkable MAO-B selective and reversible inhibition, 6-substituted-3-carboxamidocoumarins and chromones, are a good starting point for single-target, single-drug approaches to ND. Compound **29** and compound **125** can be considered leads due to their potent MAO-B inhibition (Fig. 72).

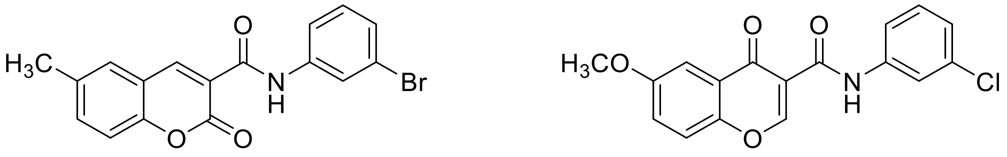

Compound **29**
IC$_{50}$ MAO-B = 4.66 nM

Compound **125**
IC$_{50}$ MAO-B = 3.94 nM

Figure 72 – Lead compounds for MAO-B inhibitors.

However, the complex pathophysiology of ND demands new approaches and the development of multi target drugs directed at ND-relevant targets is still an unmet demand. With this work, we tried to mitigate that fact by also targeting AChE and AR. To that effect, some compounds were identified as dual-target hits, namely compound **24** as a MAO-B/AChE inhibitor and compound **44** as a MAO-B inhibitor/AR ligand (Fig. 73).

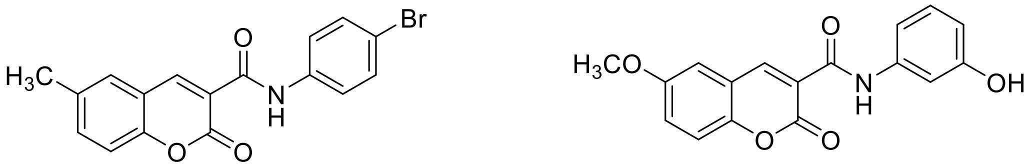

Compound **24**

IC$_{50}$ MAO-B = 11.4 nM

IC$_{50}$ AChE = 359 μM

Compound **44**

K_i A$_1$AR = 41.0 μM

K_i A$_{2A}$AR > 100 μM

K_i A$_3$AR = 22.0 μM

IC$_{50}$ MAO-B = 228.6 nM

Figure 73 – Multi target hits: compound **24** and **44**.

In a near future, these derivatives could function as a first step in order to reach compounds with enhanced bioactivity. One of the main goals of future research will focus on improving AChE inhibition while maintaining potent MAO-B inhibition. Moreover, modulation of AR selectivity and the development of more potent AR ligands, mainly A$_{2A}$AR, will also be a focus in future works. In terms of AR selectivity, the work developed in this thesis led only to selective A$_3$AR ligands, such as compounds **11** (Fig. 65) and **101** (Fig. 63). This unexpected result can lead to further SAR studies and screenings to establish the role of benzopyrones in this field.

Finally, the MAO-B leads encountered in this thesis will undergo safety and toxicological screenings.

CHAPTER 4

4.1. References

1. Chang, R. *Chemistry*; 6th ed.; McGraw Hill: New York, **1998**.
2. Silverman, R. B. *The Organic Chemistry of Drug Design and Drug Action*; 2nd ed.; Elsevier Academic Press: London, **2004**.
3. Raviña, E. *The Evolution of Drug Discovery*; 1st ed.; John Wiley & Sons, Ltd.: Weinheim, **2011**.
4. Dobson, C. M. *Rend. Lincei* **2015**, *26*, 251–262.
5. Prince, M.; Wimo, A.; Guerchet, M.; Gemma-Claire, A.; Wu, Y.-T.; Prina, M. *Alzheimer's Dis. Int.* **2015**, 1–84.
6. de Lau, L. M. L.; Breteler, M. M. B. *Lancet. Neurol.* **2006**, *5*, 525–535.
7. Dorsey, E. R.; Constantinescu, R.; Thompson, J. P.; Biglan, K. M.; Holloway, R. G.; Kieburtz, K.; Marshall, F. J.; Ravina, B. M.; Schifitto, G.; Siderowf, A.; Tanner, C. M. *Neurology* **2007**, *68*, 384–386.
8. Gustavsson, A.; Svensson, M.; Jacobi, F.; Allgulander, C.; Alonso, J.; Beghi, E.; Dodel, R.; Ekman, M.; Faravelli, C.; Fratiglioni, L.; Gannon, B.; Jones, D. H.; Jennum, P.; Jordanova, A.; Jonsson, L.; Karampampa, K.; Knapp, M.; Kobelt, G.; Kurth, T.; Lieb, R.; Linde, M.; Ljungcrantz, C.; Maercker, A.; Melin, B.; Moscarelli, M.; Musayev, A.; Norwood, F.; Preisig, M.; Pugliatti, M.; Rehm, J.; Salvador-Carulla, L.; Schlehofer, B.; Simon, R.; Steinhausen, H. C.; Stovner, L. J.; Vallat, J. M.; den Bergh, P. Van; van Os, J.; Vos, P.; Xu, W.; Wittchen, H. U.; Jonsson, B.; Olesen, J. *Eur. Neuropsychopharmacol.* **2011**, *21*, 718–779.
9. Matos, M. J.; Vazquez-Rodriguez, S.; Uriarte, E.; Santana, L. *Expert Opin. Ther. Pat.* **2015**, *25*, 351–366.
10. Samadi, A.; Valderas, C.; de los Ríos, C.; Bastida, A.; Chioua, M.; González-Lafuente, L.; Colmena, I.; Gandía, L.; Romero, A.; Del Barrio, L.; Martín-de-Saavedra, M. D.; López, M. G.; Villarroya, M.; Marco-Contelles, J. *Bioorg. Med. Chem.* **2011**, *19*, 122–133.
11. Dias, K. S. T.; Viegas, C.; Jr *Curr. Neuropharmacol.* **2014**, *12*, 239–255.
12. Parkinson, J. *J. Neuropsychiatry Clin. Neurosci.* **2002**, *14*, 223–236.
13. Nelson, A. B.; Kreitzer, A. C. *Annu. Rev. Neurosci.* **2014**, *37*, 117–135.
14. Rodriguez-Oroz, M. C.; Jahanshahi, M.; Krack, P.; Litvan, I.; Macias, R.; Bezard, E.; Obeso, J. A. *Lancet Neurol.* **2009**, *8*, 1128–1139.
15. Dauer, W.; Przedborski, S. *Neuron* **2003**, *39*, 889–909.
16. McNaught, K. S. P.; Olanow, C. W. *Neurobiol. Aging* **2006**, *27*, 530–545.
17. Emerit, J.; Edeas, M.; Bricaire, F. *Biomed. Pharmacother.* **2004**, *58*, 39–46.
18. Uttara, B.; Singh, A. V; Zamboni, P.; Mahajan, R. T. *Curr. Neuropharmacol.* **2009**, *7*, 65–74.
19. Bras, J. M.; Singleton, A. *Biochim. Biophys. Acta - Mol. Basis Dis.* **2009**, *1792*, 597–603.
20. Freire, C.; Koifman, S. *Neurotoxicology* **2012**, *33*, 947–971.

21. Caudle, W. M.; Guillot, T. S.; Lazo, C. R.; Miller, G. W. *Neurotoxicology* **2012**, *33*, 178–188.

22. Galvan, A.; Wichmann, T. *Clin. Neurophysiol.* **2008**, *119*, 1459–1474.

23. Lees, A. J.; Tolosa, E.; Olanow, C. W. *Mov. Disord.* **2015**, *30*, 19–36.

24. Nagatsu, T.; Sawada, M. *Parkinsonism Relat. Disord.* **2009**, *15*, S3–S8.

25. Jankovic, J.; Aguilar, L. G. *Neuropsychiatr. Dis. Treat.* **2008**, *4*, 743–757.

26. Nutt, J. G.; Holford, N. H. G. *Ann. Neurol.* **1996**, *39*, 561–573.

27. Lees, A. J. *J. Neurol. Neurosurg. Psychiatry* **1989**, *January*, 29–37.

28. Mercuri, N. B.; Bernardi, G. *Trends Pharmacol. Sci.* **2005**, *26*, 341–344.

29. Radad, K.; Gille, G.; Rausch, W. D. *Pharmacol. Reports* **2005**, *57*, 701–712.

30. Bonuccelli, U.; Del Dotto, P.; Rascol, O. *Parkinsonism Relat. Disord.* **2009**, *15*, S44–S53.

31. Rascol, A.; Guiraud, B.; Montastruc, J. L. *J. Neurol. Neurosurg. Psychiatry* **1979**, *42*, 143–150.

32. Dong, J.; Cui, Y.; Li, S.; Le, W. *Curr. Neuropharmacol.* **2016**, *14*, 339–355.

33. VanKampen, J. M.; Hagg, T.; Robertson, H. a; Van Kampen, J. M. *Neuroscience* **2004**, *19*, 2377–87.

34. Connolly, B. S.; Lang, A. E. *J. Am. Med. Assoc.* **2014**, *311*, 1670–1683.

35. Axelrod, J. *Science (80-.).* **1957**, *126*, 400–401.

36. Mannisto, P. T.; Kaakkola, S. *Pharmacol. Rev.* **1999**, *51*, 593–628.

37. Calne, D. *N. Engl. J. Med.* **1993**, *329*, 1021–1027.

38. Endres, C. J.; DeJesus, O. T.; Uno, H.; Doudet, D. J.; Nickles, J.; Holden, J. E. *Front. Biosci.* **2004**, *9*, 505–512.

39. Rod, F.; Humphrey, P. R.; Maureen, M. D.; Ritter, J. M. *Rang & Dale's pharmacology*; 7th ed.; Churchill Livingstone: Edinburgh, **2007**.

40. Guldberg, H. C.; Marsden, C. A. *Pharmacol. Rev.* **1975**, *27*, 135–206.

41. Buddhala, C.; Loftin, S. K.; Kuley, B. M.; Cairns, N. J.; Campbell, M. C.; Perlmutter, J. S.; Kotzbauer, P. T. *Ann. Clin. Transl. Neurol.* **2015**, *2*, 949–959.

42. Assal, F.; Spahr, L.; Hadengue, A.; Rubbici-Brandt, L.; Burkhard, P. R. *Lancet* **1988**, *352*, 958.

43. Spahr, L.; Rubbia-Brandt, L.; Burkhard, P. R.; Assal, F.; Hadengue, A. *Dig. Dis. Sci.* **2000**, *45*, 1881–1884.

44. Parashos, S. A.; Wielinski, C. L.; Kern, J. A. *Clin. Neuropharmacol.* **2004**, *27*, 119–123.

45. Ferreira, J. J.; Lees, A.; Rocha, J. F.; Poewe, W.; Rascol, O.; Soares-da-Silva, P. *Lancet Neurol.* **2016**, *15*, 154–165.

46. Scott, L. J. *Drugs* **2016**, *76*, 1293–1300.

47. Carradori, S.; Silvestri, R. *J. Med. Chem.* **2015**, *58*, 6717–6732.

48. Youdim, M. B.; Edmondson, D.; Tipton, K. F. *Nat Rev Neurosci* **2006**, *7*, 295–309.

49. Kehrer, J. P. *Toxicology* **2000**, *149*, 43–50.

50. Kanti, T.; Wati, M.; Fatima-Shad, K. *Arch. Neurosci.* **2014**, *2*, 1–8.

51. Caslake, R.; Macleod, A.; Ives, N.; Stowe, R.; Counsell, C. *Cochrane Database Syst. Rev.* **2009**, *4*, 1–26.

52. Magyar, K.; Pálfi, M.; Jenei, V.; Szöko, E. *J. Neural Transm. Suppl.* **2006**, 143–156.

53. Lecht, S.; Haroutiunian, S.; Hoffman, A.; Lazarovici, P. *Ther. Clin. Risk Manag.* **2007**, *3*, 467–474.

54. Rascol, O.; Brooks, D. J.; Melamed, E.; Oertel, W.; Poewe, W.; Stocchi, F.; Tolosa, E. *Lancet* **2005**, *365*, 947–954.

55. Youdim, M. B. H.; Maruyama, W.; Naoi, M. *Drugs of Today* **2005**, *41*, 369–391.

56. Blair, H. A.; Dhillon, S. *CNS Drugs* **2017**.

57. Riederer P, M. T. *Expert Opin Drug Metab Toxicol* **2017**, Epub ahead of print.

58. Schapira, A. H. V; Fox, S. H.; Hauser, R. A.; Jankovic, J.; Jost, W. H.; Kenney, C.; Kulisevsky, J.; Pahwa, R.; Poewe, W.; Anand, R. *JAMA Neurol.* **2016**, Epub ahead of print.

59. Poirier, A.-A.; Aubé, B.; Côté, M.; Morin, N.; Di Paolo, T.; Soulet, D. *Parkinsons. Dis.* **2016**, *2016*, 1–23.

60. Sperlágh, B.; Vizi, E. S. *Curr. Top. Med. Chem.* **2011**, *11*, 1034–1046.

61. St. Hilaire, C.; Carroll, S. H.; Chen, H.; Ravid, K. *J. Cell. Physiol.* **2009**, *218*, 35–44.

62. Chen, J.-F.; Eltzschig, H. K.; Fredholm, B. B. *Nat. Rev. Drug Discov.* **2013**, *12*, 265–286.

63. Gessi, S.; Merighi, S.; Fazzi, D.; Stefanelli, A.; Varani, K.; Borea, P. A. *Expert Opin. Investig. Drugs* **2011**, *20*, 1591–1609.

64. Hickey, P.; Stacy, M. *Curr. Neurol. Neurosci. Rep.* **2012**, *12*, 376–385.

65. Schiffmann, S. N.; Fisone, G.; Moresco, R.; Cunha, R. A.; Ferré, S. *Prog. Neurobiol.* **2007**, *83*, 277–292.

66. Diniz, C.; Borges, F.; Santana, L.; Uriarte, E.; Oliveira, J. M.; Gonçalves, J.; Fresco, P. *Curr. Pharm. Des.* **2008**, *14*, 1698–1722.

67. Sheth, S.; Brito, R.; Mukherjea, D.; Rybak, L. P.; Ramkumar, V. *Int. J. Mol. Sci.* **2014**, *15*, 2024–2052.

68. Ricci, A.; Collier, W. L.; Rossodivita, I.; Amenta, F. *J Aut. Pharmacol* **1991**, *11*, 121–127.

69. Xu, K.; Bastia, E.; Schwarzschild, M. *Pharmacol. Ther.* **2005**, *105*, 267–310.

70. Stocchi, F. *Neurotherapeutics* **2014**, *11*, 24–33.

71. Grondin, R.; Bedard, P. J.; Hadj Tahar, A.; Gregoire, L.; Mori, A.; Kase, H. *Neurology* **1999**, *52*, 1673–1677.

72. Cieślak, M.; Komoszyński, M.; Wojtczak, A. *Purinergic Signal.* **2008**, *4*, 305–312.

73. Nash, J. E.; Nash, J. E.; Brotchie, J. M.; Brotchie, J. M. *J. Neurosci.* **2000**, *20*, 7782–7789.

74. Dungo, R.; Deeks, E. D. *Drugs* **2013**, *73*, 875–882.

75. LeWitt, P. A.; Guttman, M.; Tetrud, J. W.; Tuite, P. J.; Mori, A.; Chaikin, P.; Sussman, N. M. *Ann. Neurol.* **2008**, *63*, 295–302.

76. Hauser, R. A.; Cantillon, M.; Pourcher, E.; Micheli, F.; Mok, V.; Onofrj, M.; Huyck, S.; Wolski, K. *Lancet Neurol.* **2011**, *10*, 221–229.

77. Hodgson, R.; Bertorelli, R.; Varty, G. B.; Lachowicz, J. E.; Forlani, A.; Fredduzzi, S.; Cohen-williams, M. E.; Higgins, G.; Impagnatiello, F.; Nicolussi, E.; Parra, L. E.; Foster, C.; Zhai, Y.; Neustadt, B. R.; Stamford, A. W.; Parker, E. M.; Reggiani, A.; Hunter, J. C. *J. Pharmacol. Exp. Ther.* **2009**, *330*, 294–303.

78. Kakkar, A. K.; Dahiya, N. *Eur. J. Pharmacol.* **2015**, *750*, 74–81.

79. Brooks, D. J.; Papapetropoulos, S.; Vandenhende, F.; Tomic, D.; He, P.; Coppell, A.; O'Neill, G. *Clin. Neuropharmacol.* **2010**, *33*, 55–60.

80. Pinna, A. *CNS Drugs* **2014**, *28*, 455–474.

81. Santos, A.; Chand, K.; Chaves, S. *Future Med. Chem.* **2016**.

82. Förstl, H.; Kurz, A. *Eur. Arch. Psychiatry Clin. Neurosci.* **1999**, *249*, 288–290.

83. Teri, L.; Larson, E. B.; Reifler, B. V *J. Am. Geriatr. Soc.* **1988**, *36*, 1–6.

84. Wragg, R.; Jeste, D. *Am. J. Psychiatry* **1989**, *146*, 577–587.

85. Scarmeas, N.; Brandt, J.; Albert, M.; Hadjigeorgiou, G.; Papadimitriou, A.; Dubois, B.; Sarazin, M.; Devanand, D.; Honig, L.; Marder, K.; Bell, K.; Wegesin, D.; Blacker, D.; Stern, Y. *Arch. Neurol.* **2005**, *62*, 1601–1608.

86. Monczor, M. *Curr. Med. Chem.* **2005**, *5*, 5–13.

87. Silva, T.; Reis, J.; Teixeira, J.; Borges, F. *Ageing Res. Rev.* **2014**, *15*, 116–145.

88. Wollmer, M. A. *Biochim. Biophys. Acta - Mol. Cell Biol. Lipids* **2010**, *1801*, 762–773.

89. Silva, T.; Teixeira, J.; Remião, F.; Borges, F. *Angew. Chemie - Int. Ed.* **2013**, *52*, 1110–1121.

90. Kerr, M. L.; Small, D. H. *J. Neurosci. Res.* **2005**, *80*, 151–159.

91. Gamblin, T. C.; Chen, F.; Zambrano, A.; Abraha, A.; Lagalwar, S.; Guillozet, A. L.; Lu, M.; Fu, Y.; Garcia-Sierra, F.; LaPointe, N.; Miller, R.; Berry, R. W.; Binder, L. I.; Cryns, V. L. *Proc. Natl. Acad. Sci. U. S. A.* **2003**, *100*, 10032–10037.

92. Mosconi, L.; Murray, J.; Tsui, W. H.; Li, Y.; Davies, M.; Williams, S.; Pirraglia, E.; Spector, N.; Osorio, R. S.; Glodzik, L.; McHugh, P.; de Leon, M. J. *J. Prev. Alzheimer's Dis.* **2014**, *1*, 23–32.

93. Mufson, E. J.; Counts, S. E.; Perez, S. E.; Ginsberg, S. D. *Expert Rev. Neurother.* **2009**, *8*, 1703–1718.

94. McKhann, G.; Drachman, D.; Folstein, M.; Katzman, R. *Neurology* **1984**, *34*, 939–944.

95. McKhann, G. M.; Knopman, D. S.; Chertkow, H.; Hyman, B. T.; Jack, C. R.; Kawas, C. H.; Klunk, W. E.; Koroshetz, W. J.; Manly, J. J.; Mayeux, R.; Mohs, R. C.; Morris, J. C.; Rossor, M. N.; Scheltens, P.; Carrillo, M. C.; Thies, B.; Weintraub, S.; Phelps, C. H. *Alzheimer's Dement.* **2011**, *7*, 263–269.

96. Craig, L. A.; Hong, N. S.; McDonald, R. J. *Neurosci. Biobehav. Rev.* **2011**, *35*, 1397–1409.

97. Terry, A. V.; Buccafusco, J. J. *J. Pharmacol. Exp. Ther.* **2003**, *306*, 821–827.

98. Schaeffer, E. L.; Gattaz, W. F. *Psychopharmacology (Berl).* **2008**, *198*, 1–27.

99. Goedert, M.; Spillantini, M. G. *Science (80-.).* **2006**, *314*, 777–781.

100. Sadqi, M.; Hernández, F.; Pan, U.; Pérez, M.; Schaeberle, M. D.; Ávila, J.; Muñoz, V. *Biochemistry* **2002**, *41*, 7150–7155.

101. Flirski, M.; Sobow, T. *Curr. Alzheimer Res.* **2005**, *2*, 47–64.

102. Hynd, M. R.; Scott, H. L.; Dodd, P. R. *Neurochem. Int.* **2004**, *45*, 583–595.

103. Bezprozvanny, I.; Mattson, M. P. *Trends Neurosci.* **2008**, *31*, 454–463.

104. Marcus, D. L.; Thomas, C.; Rodriguez, C.; Simberkoff, K.; Tsai, J. S.; Strafaci, J. A.; Freedman, M. L. *Exp. Neurol.* **1998**, *150*, 40–44.

105. Praticò, D. *Trends Pharmacol. Sci.* **2008**, *29*, 609–615.

106. Smith, M. A.; Rottkamp, C. A.; Nunomura, A.; Raina, A. K.; Perry, G. *Biochim. Biophys. Acta - Mol. Basis Dis.* **2000**, *1502*, 139–144.

107. Bush, A. I.; Tanzi, R. E. *Neurotherapeutics* **2008**, *5*, 421–432.

108. Hung, Y. H.; Bush, A. I.; Cherny, R. A. *JBIC J. Biol. Inorg. Chem.* **2010**, *15*, 61–76.

109. Bonda, D. J.; Lee, H.; Blair, J. A.; Zhu, X.; Perry, G.; Smith, M. A. *Metallomics* **2011**, *3*, 267–270.

110. Khandelwal, P. J.; Herman, A. M.; Moussa, C. E.-H. *J. Neuroimmunol.* **2011**, *238*, 1–11.

111. Trepanier, C. H.; Milgram, N. W. *J. Alzheimer's Dis.* **2010**, *21*, 1089–1099.

112. Yiannopoulou, K. G.; Papageorgiou, S. G. *Ther. Adv. Neurol. Disord.* **2013**, *6*, 19–33.

113. Purves, D.; Augustine, G. J.; Fitzpatrick, D. *Neuroscience*; 5th ed.; Sinauer Associates: Sunderland, **2012**.

114. Siegal, A.; Sapru, H. N. *Essential Neuroscience*; Third Edit.; Lippincott, Williams & Wilkins: Philadelphia, **2014**.

115. García-Ayllón, M.-S.; Small, D. H.; Avila, J.; Sáez-Valero, J. *Front. Mol. Neurosci.* **2011**, *4*, 1–9.

116. Cummings, J. L.; Back, C. *Am. J. Geriatr. Psychiatry* **1998**, *6*, 64–78.

117. Sussman, J. L.; Harel, M.; Frolow, F.; Oefner, C.; Goldmant, A.; Toker, L.; Silman, I. *Science (80-.).* **1991**, *253*, 872–879.

118. Anand, P.; Singh, B. *Arch. Pharm. Res.* **2013**, *36*, 375–399.

119. Inestrosa, N. C.; Alvarez, A.; Calderon, F. *Mol. Psychiatry* **1996**, *1*, 359–361.

120. Alfirevic, A.; Mills, T.; Carr, D.; Barratt, B. J.; Jawaid, A.; Sherwood, J.; Smith, J. C.; Tugwood, J.; Hartkoorn, R.; Owen, A.; Park, K. B.; Pirmohamed, M. *Pharmacogenet. Genomics* **2007**, *17*, 1091–1100.

121. Colovic, M. B.; Krstic, D. Z.; Lazarevic-Pasti, T. D.; Bondzic, A. M.; Vasic, V. M. *Curr. Neuropharmacol.* **2013**, *11*, 315–335.

122. Birks, J. *Cholinesterase inhibitors for Alzheimer ' s disease (Review)*; John Wiley & Sons, Ltd.: Oxford, **2012**.

123. Farlow, M. *Int. psychogeriatrics* **2002**, *14*, 93–126.

124. Cummings, J.; Jones, R.; Wilkinson, D.; Lopez, O.; Gauthier, S.; Waldemar, G.; Zhang, R.; Xu, Y.; Sun, Y.; Richardson, S.; Mackell, J. *J. Alzheimer's Dis.* **2010**, *21*, 843–851.

125. Gill, S. S.; Anderson, G. M.; Fischer, H. D.; Bell, C. M.; Li, P.; Normand, S.-L. T.; Rochon, P. *Arch. Intern. Med.* **2009**, *169*, 867–873.

126. Mohamed, T.; Rao, P. P. N. *Eur. J. Med. Chem.* **2016**, *126*, 823–843.

127. Okubo, Y.; Sekiya, H.; Namiki, S.; Sakamoto, H.; Iinuma, S.; Yamasaki, M.; Watanabe, M.; Hirose, K.; Iino, M. *Proc. Natl. Acad. Sci. U. S. A.* **2010**, *107*, 6526–6531.

128. Lau, A.; Tymianski, M. *Pflügers Arch. - Eur. J. Physiol.* **2010**, *460*, 525–542.

129. Coyle, J. T.; Puttfarcken, P. *Science (80-.).* **1993**, *262*, 689–695.

130. Meldrum, B. S. *J. Nutr.* **2000**, *130*, 1007–1015.

131. Reisberg, B.; Doody, R.; Stöffler, A.; Schmitt, F.; Ferris, S.; Möbius, H. J. *N. Engl. J. Med.* **2003**, *348*, 1333–1341.

132. Farber, N. B.; Newcomer, J. W.; Olney, J. W. *Prog. Brain Res.* **1988**, *116*, 421–437.

133. Mcshane, R.; Areosa Sastre, A.; Minakaran, N. *Memantine for dementia (Review)*; John Wiley: Oxford, **2009**.

134. Maidment, I. D.; Fox, C. G.; Boustani, M.; Rodriguez, J.; Brown, R. C.; Katona, C. L. *Ann. Pharmacother.* **2008**, *42*, 32–38.

135. Alva, G.; Cummings, J. L. *Psychiatry (Edgmont)* **2008**, *5*, 27–36.

136. Howard, R.; McShane, R.; RLindesay, J.; Ritchie, C.; Dening, T.; Findlay, D.; Holmes, C.; Hughes, A.; Jacoby, R.; Jones, R.; McKeith, I. *N. Engl. J. Med.* **2012**, *366*, 893–903.

137. Feldman, H. H.; Schmitt, F. a; Olin, J. T. *Alzheimer Dis. Assoc. Disord.* **2006**, *20*, 263–268.

138. Tariot, P. N.; Farlow, M. R.; Grossberg, G. T.; Graham, S. M.; McDonald, S.; Gergel, I. *Jama* **2004**, *291*, 317–324.

139. Farlow, M. R.; Alva, G.; Meng, X.; Olin, J. T. *Curr. Med. Res. Opin.* **2010**, *26*, 263–269.

140. Fonseca, A.; Matos, M. J.; Reis, J.; Duarte, Y.; Santana, L.; Uriarte, E.; Borges, F. *RSC Adv.* **2016**, *6*, 49764–49768.

141. Krishna, R.; Ali, M.; Moustafa, A. A. *Front. Aging Neurosci.* **2014**, *6*, 1–9.

142. Riederer, P. *Neurotoxicology* **2004**, *25*, 271–277.

143. Jain, V.; Langham, M. C.; Wehrli, F. W. *J. Cereb. Blood Flow Metab.* **2010**, *30*, 1598–1607.

144. Rouault, T. A. *Nat Rev Neurosci* **2013**, *14*, 551–564.

145. Strooper, B. De *Nat. Rev. Neurol.* **2010**, *6*, 99–107.

146. Sinha, S.; Anderson, J. P.; Barbour, R.; Basi, G. S.; Caccavello, R.; Davis, D.; Doan, M.; Dovey, H. F.; Frigon, N.; Hong, J.; Jacobson-Croak, K.; Jewett, N.; Keim, P.; Knops, J.; Lieberburg, I.; Power, M.; Tan, H.; Tatsuno, G.; Tung, J.; Schenk, D.; Seubert, P.; Suomensaari, S. M.; Wang, S.; Walker, D.; Zhao, J.; McConlogue, L.; John, V. *Nature* **1999**, *402*, 537–540.

147. Silvestri, R. *Med. Res. Rev.* **2009**, *29*, 295–338.

148. Hernández-Rodríguez, M.; Correa-Basurto, J.; Martínez-Ramos, F.; Padilla-Martínez, I. I.; Benítez-Cardoza, C. G.; Mera-Jiménez, E.; Rosales-Hernández, M. C. *J. Alzheimer's Dis.* **2014**, *41*, 1073–1085.

149. Vassar, R. *Alzheimers. Res. Ther.* **2014**, *6*, 89–104.

150. McIlwain, D. R.; Berger, T.; Mak, T. W. *Cold Spring Harb. Perspect. Biol.* **2013**, *5*, 1–28.

151. Rohn, T. T. *Apoptosis* **2010**, *15*, 1403–1409.

152. Yuan, J.; Shaham, S.; Ledoux, S.; Ellis, H. M.; Horvitz, H. R. *Cell* **1993**, *75*, 641–652.

153. Ekert, P. G.; Silke, J.; Vaux, D. L. *Cell Death Differ* **1999**, *6*, 1081–1086.

154. MacKenzie, S. H.; Schipper, J. L.; Clark, A. C. *Curr. Opin. Drug Discov. Devel.* **2010**, *13*, 568–576.

155. Rissman, R. A.; Poon, W. W.; Blurton-Jones, M.; Oddo, S.; Torp, R.; Vitek, M. P.; LaFerla, F. M.; Rohn, T. T.; Cotman, C. W. *J. Clin. Invest.* **2004**, *114*, 121–130.

156. Meduri, G.; Guillemeau, K.; Dounane, O.; Sazdovitch, V.; Duyckaerts, C.; Chambraud, B.; Baulieu, E. E.; Giustiniani, J. *Neurobiol. Aging* **2016**, *46*, 124–137.

157. Zhao, X.; Kotilinek, L. A.; Smith, B.; Hlynialuk, C.; Zahs, K.; Ramsden, M.; Cleary, J.; Ashe, K. H. *Nat. Med.* **2016**, 1–12.

158. Ross, J.; Brough, D.; Gibson, R. M.; Loddick, S. A.; Rothwell, N. J. *Neuropharmacology* **2007**, *53*, 638–642.

159. Zhang, Y.; Zheng, Y. *Clin. Exp. Rheumatol.* **2016**, *34*, 111–118.

160. Brumatti, G.; Ma, C.; Lalaoui, N.; Nguyen, N.-Y.; Navarro, M.; Tanzer, M. C.; Richmond, J.; Ghisi, M.; Salmon, J. M.; Silke, N.; Pomilio, G.; Glaser, S. P.; de Valle, E.; Gugasyan, R.; Gurthridge, M. A.; Condon, S. M.; Johnstone, R. W.; Lock, R.; Salvesen, G.; Wei, A.; Vaux, D. L.; Ekert, P. G.; Silke, J. *Sci. Transl. Med.* **2016**, *8*, 339–369.

161. Fiorucci, S.; Antonelli, E.; Tocchetti, P.; Morelli, A. *Cardiovasc. Drug Rev.* **2004**, *22*, 135–146.

162. Schwartz, R. S. *N. Engl. J. Med.* **2004**, *350*, 1079–1080.

163. Hartman, J. L.; Garvik, B.; Hartwell, L. *Science* **2001**, *291*, 1001–1004.

164. Paolini, G. V; Shapland, R. H.; van Hoorn, W. P.; Mason, J. S.; Hopkins, A. L. *Nat. Biotechnol.* **2006**, *24*, 805–815.

165. Talevi, A. *Front. Pharmacol.* **2015**, *6*, 1–7.

166. Anighoro, A.; Bajorath, J.; Rastelli, G. *J Med Chem* **2014**, *57*, 7874–7887.

167. Hu, Y.; Bajorath, J. *J. Chem. Inf. Model.* **2010**, *50*, 2112–2118.

168. Cavalli, A.; Bolognesi, M. L.; Mìnarini, A.; Rosini, M.; Tumiatti, V.; Recanatini, M.; Melchiorre, C. *J. Med. Chem.* **2008**, *51*, 347–372.

169. Weinreb, O.; Amit, T.; Bar-Am, O.; Youdim, M. B. H. *Int. Rev. Neurobiol.* **2011**, *100*, 191–215.

170. Moradov, D.; Finkin-Groner, E.; Bejar, C.; Sunita, P.; Schorer-Apelbaum, D.; Barasch, D.; Nemirovski, A.; Cohen, M.; Weinstock, M. *Biochem. Pharmacol.* **2015**, *94*, 164–172.

171. Bar-Am, O.; Amit, T.; Youdim, M. B.; Weinreb, O. *J. Neural Transm.* **2016**, *123*, 125–135.

172. Zheng, H.; Gal, S.; Weiner, L. M.; Bar-Am, O.; Warshawsky, A.; Fridkin, M.; Youdim, M. B. H. *J. Neurochem.* **2005**, *95*, 68–78.

173. Gal, S.; Zheng, H.; Fridkin, M.; Youdim, M. B. H. *J. Neurochem.* **2005**, *95*, 79–88.

174. Petzer, J. P.; Steyn, S.; Castagnoli, K. P.; Chen, J.-F.; Schwarzschild, M. A.; Van der Schyf, C. J.; Castagnoli, N. *Bioorg. Med. Chem.* **2003**, *11*, 1299–1310.

175. Pretorius, J.; Malan, S. F.; Castagnoli, N.; Bergh, J. J.; Petzer, J. P. *Bioorganic Med. Chem.* **2008**, *16*, 8676–8684.

176. Leon, R.; Garcia, A.; Marco-Contelles, J. *Med. Res. Rev.* **2013**, *33*, 139–189.

177. Kryger, G.; Silman, I.; Sussman, J. L. *Structure* **1999**, *7*, 297–307.

178. Tumiatti, V.; Milelli, A.; Minarini, A.; Rosini, M.; Bolognesi, M. L.; Micco, M.; Andrisano, V.; Bartolini, M.; Mancini, F.; Recanatini, M.; Cavalli, A.; Melchiorre, C. *J. Med. Chem.* **2008**, *51*, 7308–7312.

179. Bolognesi, M. L.; Cavalli, A.; Melchiorre, C. *Neurotherapeutics* **2009**, *6*, 152–162.

180. Capurro, V.; Busquet, P.; Lopes, J. P.; Bertorelli, R.; Tarozzo, G.; Bolognesi, M. L.; Piomelli, D.; Reggiani, A.; Cavalli, A. *PLoS One* **2013**, *8*, e56870.

181. Rosini, M.; Andrisano, V.; Bartolini, M.; Bolognesi, M. L.; Hrelia, P.; Minarini, A.; Tarozzi, A.; Melchiorre, C. *J. Med. Chem.* **2005**, *48*, 360–363.

182. Lipton, S. A. *Nat Rev Drug Discov* **2006**, *5*, 160–170.

183. Rosini, M.; Simoni, E.; Bartolini, M.; Cavalli, A.; Ceccarini, L.; Pascu, N.; McClymont, D. W.; Tarozzi, A.; Bolognesi, M. L.; Minarini, A.; Tumiatti, V.; Andrisano, V.; Mellor, I. R.; Melchiorre, C. *J. Med. Chem.* **2008**, *51*, 4381–4384.

184. Joule, J. A.; Mills, K. *Heterocyclic Chemistry*; 5th ed.; John Wiley & Sons, Ltd.: London, **2010**.

185. Evans, B. E.; Rittle, K. E.; DiPardo, R. M.; Freidinger, R. M.; Whitter, W. L.;

Lundell, G. F.; Veber, D. F.; Anderson, P. S.; Chang, R. S. L.; Lotti, V. J.; Cerino, D. J.; Chen, T. B.; Kling, P. J.; Kunkel, K. A.; Springer, J. P.; Hirshfield, J. *J. Med. Chem.* **1988**, *31*, 2235–2246.

186. Welsch, M. E.; Snyder, S. A.; Stockwell, B. R. *Curr. Opin. Chem. Biol.* **2010**, *14*, 347–361.

187. Sravanthi, T. V.; Manju, S. L. *Eur. J. Pharm. Sci.* **2016**, *91*, 1–10.

188. Oliveri, V.; Vecchio, G. *Eur. J. Med. Chem.* **2016**, *120*, 252–274.

189. Lachance, H.; Wetzel, S.; Kumar, K.; Waldmann, H. *J. Med. Chem.* **2012**, *55*, 5989–6001.

190. Jameel, E.; Umar, T.; Kumar, J.; Hoda, N. *Chem. Biol. Drug Des.* **2015**, *87*, 21–38.

191. Gaspar, A.; Matos, M. J.; Garrido, J.; Uriarte, E.; Borges, F. *Chem. Rev.* **2014**, *114*, 4960–4992.

192. Borges, F.; Roleira, F.; Milhazes, N.; Santana, L.; Uriarte, E. *Curr. Med. Chem.* **2005**, *12*, 887–916.

193. Vogel, A. *Ann. der Phys. und der Phys. Chemie* **1820**, *64*, 161–166.

194. Hussain, H.; Hussain, J.; Al-Harrasi, A.; Krohn, K. *Tetrahedron* **2012**, *68*, 2553–2578.

195. Bourgaud, F.; Hehn, A.; Larbat, R.; Doerper, S.; Gontier, E.; Kellner, S.; Matern, U. *Phytochem. Rev.* **2006**, *5*, 293–308.

196. Matos, M. J.; Santana, L.; Uriarte, E.; Abreu, O. A.; Molina, E.; Guardado, E. In *Phytochemicals - isolation , characterization and role in human health*; Intech, **2015**; pp. 113–140.

197. Borges, F.; Roleira, F. M. F.; Milhazes, N. J. da S. P.; Uriarte, E.; Santana, L. *Front. Med. Chem.* **2009**, *4*, 23–85.

198. Frederick, R.; Robert, S.; Charlier, C.; De Ruyck, J.; Wouters, J.; Pirotte, B.; Masereel, B.; Pochet, L. *J. Med. Chem.* **2005**, *48*, 7592–7603.

199. Wardrop, D.; Keeling, D. *Br. J. Haematol.* **2008**, *141*, 757–763.

200. Verhoef, T. I.; Redekop, W. K.; Daly, A. K.; van Schie, R. M. F.; de Boer, A.; Maitland-van der Zee, A.-H. *Br. J. Clin. Pharmacol.* **2014**, *77*, 626–641.

201. Campos-Toimil, M.; Orallo, F.; Santana, L.; Uriarte, E. *Bioorganic Med. Chem. Lett.* **2002**, *12*, 783–786.

202. Kawase, M.; Varu, B.; Shah, A.; Motohashi, N.; Tani, S.; Saito, S.; Debnath, S.; Mahapatra, S.; Dastidar, S. G.; Chakrabarty, N. *Arzneimittelforschung.* **2001**, *51*, 67–71.

203. Walsh, T. J.; Standiford, H. C.; Reboli, A. E. C.; John, J. F.; Mulligan, M. E.; Ribner, B. S.; Montgomerie, J. Z.; Goetz, M. B.; Mayhall, C. G.; Rimland, D.; Stevens, D. A.; Hansen, S. L.; Gerard, G. C.; Ragual, R. J. *Antimicrob. Agents Chemother.* **1993**, *37*, 1334–1342.

204. Donnelly, A. C.; Zhao, H.; Kusuma, B. R.; Blagg, B. S. *Medchemcomm* **2010**, *1*, 165–170.

205. Heide, L. In *Methods in Enzymology*; Elsevier Inc., **2009**; Vol. 459, pp. 437–455.

206. Vazquez-Rodriguez, S.; Figueroa, R.; Matos, M. J.; Olea-Azar, C.; Maya, J. D.; Uriarte, E.; Santana, L.; Borges, F. *Med. Chem. (Los. Angeles).* **2015**, *5*, 173–177.

207. Sardari, S.; Mori, Y.; Horita, K.; Micetich, R. G.; Nishibe, S.; Daneshtalab, M. *Bioorganic Med. Chem.* **1999**, *7*, 1933–1940.

208. De Alcantara, F. C.; Lozano, V. F.; Vale Velosa, A. S.; Dos Santos, M. R. M.; Pereira, R. M. S. *Polyhedron* **2015**, *101*, 165–170.

209. Matos, M.; Vazquez-Rodriguez, S.; Santana, L.; Uriarte, E.; Fuentes-Edfuf, C.; Santos, Y.; Munoz-Crego, A. *Med. Chem. (Los. Angeles).* **2012**, *8*, 1140–1145.

210. Lee, T. T. Y.; Kashiwada, Y.; Huang, L.; Snider, J.; Cosentino, M.; Lee, K. H. *Bioorganic Med. Chem.* **1994**, *2*, 1051–1056.

211. Xie, L.; Takeuchi, Y.; Cosentino, L. M.; Lee, K. *J. Med. Chem.* **1999**, *42*, 2662–2672.

212. Lahey, F. N.; Macleod, J. K. *Aust. J. Chem.* **1967**, *20*, 1943–1955.

213. Viola, G.; Vedaldi, D.; Dall'Acqua, F.; Basso, G.; Disarò, S.; Spinelli, M.; Cosimelli, B.; Boccalini, M.; Chimichi, S. *Chem. Biodivers.* **2004**, *1*, 1265–1280.

214. Valenti, P.; Rampa, A.; Recanatini, M.; Bisi, A.; Belluti, F.; Da Re, P.; Carrara, M.; Cima, L. *Anticancer Drug Des.* **1997**, *12*, 443–451.

215. Zhao, H.; Donnelly, A. C.; Kusuma, B. R.; Brandt, G. E. L.; Brown, D.; Rajewski, R. A.; Vielhauer, G.; Holzbeierlein, J.; Cohen, M. S.; Blagg, B. S. J. *J. Med. Chem.* **2011**, *54*, 3839–3853.

216. Bansal, Y.; Sethi, P.; Bansal, G. *Med. Chem. Res.* **2013**, *22*, 3049–3060.

217. Lv, H. N.; Wang, S.; Zeng, K. W.; Li, J.; Guo, X. Y.; Ferreira, D.; Zjawiony, J. K.; Tu, P. F.; Jiang, Y. *J. Nat. Prod.* **2015**, *78*, 279–285.

218. Kostova, I.; Bhatia, S.; Grigorov, P.; Balkansky, S.; Parmar, V. S.; Prasad, A. K.; Saso, L. Coumarins as antioxidants. *Curr. Med. Chem.* **2011**, *18*, 3929–3951.

219. Bubols, G. B.; Vianna, R.; Medina-Remon, A.; von Poser, G.; Lamuela-Raventos, R. M.; Eifler-Lima, V. L.; Garcia, S. C. *Mini Rev. Med. Chem.* **2013**, *13*, 318–334.

220. Witaicenis, A.; Seito, L. N.; Da Silveira Chagas, A.; De Almeida, L. D.; Luchini, A. C.; Rodrigues-Orsi, P.; Cestari, S. H.; Di Stasi, L. C. *Phytomedicine* **2014**, *21*, 240–246.

221. Fylaktakidou, K. C.; Hadjipavlou-Litina, D. J.; Litinas, K. E.; Nicolaides, D. N. *Curr. Pharm. Des.* **2004**, *10*, 3813–3833.

222. Antonella Fais; Corda, M.; Era, B.; Fadda, M. B.; Matos, M. J.; Quezada, E.; Santana, L.; Picciau, C.; Podda, G.; Delogu, G. *Molecules* **2009**, *14*, 2514–2520.

223. Matos, M. J.; Santana, L.; Uriarte, E.; Serra, S.; Corda, M.; Fadda, M. B.; Era, B.; Fais, A. *J. Pharm. Pharmacol.* **2012**, *64*, 742–746.

224. Borges, F.; Roleira, F.; Milhazes, N.; Santana, L.; Uriarte, E. *Curr. Med. Chem.* **2005**, *12*, 887–916.

225. Anand, P.; Singh, B.; Singh, N. *Bioorg. Med. Chem.* **2012**, *20*, 1175–1180.

226. de Souza, L. G.; Rennã, M. N.; Figueroa-Villar, J. D. *Chem. Biol. Interact.* **2016**,

254, 11–23.

227. Nam, S. O.; Park, D. H.; Lee, Y. H.; Ryu, J. H.; Lee, Y. S. *Bioorganic Med. Chem.* **2014**, *22*, 1262–1267.

228. Razavi, S. F.; Khoobi, M.; Nadri, H.; Sakhteman, A.; Moradi, A.; Emami, S.; Foroumadi, A.; Shafiee, A. *Eur. J. Med. Chem.* **2013**, *64*, 252–259.

229. Matos, M. J.; Gaspar, A.; Kachler, S.; Klotz, K. N.; Borges, F.; Santana, L.; Uriarte, E. *J. Pharm. Pharmacol.* **2013**, *65*, 30–34.

230. Sun, Q.; Peng, D. Y.; Yang, S. G.; Zhu, X. L.; Yang, W. C.; Yang, G. F. *Bioorganic Med. Chem.* **2014**, *22*, 4784–4791.

231. Fernández-Bachiller, M. I.; Horatscheck, A.; Lisurek, M.; Rademann, J. *ChemMedChem* **2013**, *8*, 1041–1056.

232. Marumoto, S.; Miyazawa, M. *Bioorganic Med. Chem.* **2012**, *20*, 784–788.

233. Matos, M. J.; Viña, D.; Quezada, E.; Picciau, C.; Delogu, G.; Orallo, F.; Santana, L.; Uriarte, E. *Bioorg. Med. Chem. Lett.* **2009**, *19*, 3268–3270.

234. Viña, D.; Matos, M. J.; Ferino, G.; Cadoni, E.; Laguna, R.; Borges, F.; Uriarte, E.; Santana, L. *ChemMedChem* **2012**, *7*, 464–70.

235. Matos, M. J.; Vazquez-Rodriguez, S.; Uriarte, E.; Santana, L.; Viña, D. *Bioorg. Med. Chem. Lett.* **2011**, *21*, 4224–4227.

236. Viña, D.; Matos, M. J.; Yáñez, M.; Santana, L.; Uriarte, E. *Medchemcomm* **2012**, *3*, 213.

237. Xie, S.-S.; Lan, J.-S.; Wang, X.; Wang, Z.-M.; Jiang, N.; Li, F.; Wu, J.-J.; Wang, J.; Kong, L.-Y. *Bioorg. Med. Chem.* **2016**, *24*, 1528–1539.

238. Xie, S. S.; Wang, X.; Jiang, N.; Yu, W.; Wang, K. D. G.; Lan, J. S.; Li, Z. R.; Kong, L. Y. *Eur. J. Med. Chem.* **2015**, *95*, 153–165.

239. Pisani, L.; Farina, R.; Catto, M.; Iacobazzi, R. M.; Nicolotti, O.; Cellamare, S.; Mangiatordi, G. F.; Denora, N.; Soto-Otero, R.; Siragusa, L.; Altomare, C. D.; Carotti, A. *J. Med. Chem.* **2016**, *59*, 6791–6806.

240. Piazzi, L.; Cavalli, A.; Colizzi, F.; Belluti, F.; Bartolini, M.; Mancini, F.; Recanatini, M.; Andrisano, V.; Rampa, A. *Bioorganic Med. Chem. Lett.* **2008**, *18*, 423–426.

241. Rozhkov, R. V; Larock, R. C. *J. Org. Chem.* **2003**, *68*, 6314–6320.

242. Woods, L.; Sapp, J. *J. Org. Chem.* **1962**, *11*, 7–9.

243. Perkin, W. . *J. Chem. Soc.* **1868**, *21*, 53–63.

244. Li, J. J. In *Name Reactions*; Springer Berlin Heidelberg, **2003**; pp. 305–306.

245. Janeiro, P.; Matos, M. J.; Santana, L.; Uriarte, E.; Oliveira-Brett, A. M. *J. Electroanal. Chem.* **2013**, *689*, 243–251.

246. Mahal, H. S.; Venkataraman, K. *J. Chem. Soc.* **1933**, *1*, 616–617.

247. Murray, R. D. H. *Nat. Prod. Reports* **1995**, *12*, 477–505.

248. Woods, L. L.; Shamma, S. M. *J. Chem. Eng. Data* **1970**, *15*, 355–356.

249. Crawford, M.; Moore, G. W. *J. Chem. Soc.* **1955**, *1955*, 3445–3448.

250. Pechmann, H. v. *Eur. J. Inorg. Chem.* **1884**, *17*, 929–936.

251. Singh, P. R.; Singh, D. U.; Samant, S. D. *Synlett* **2004**, 1909–1912.

252. Potdar, M. K.; Mohile, S. S.; Salunkhe, M. M. *Tetrahedron Lett.* **2001**, *42*, 9285–9287.

253. De, S. K.; Gibbs, R. A. *Synthesis (Stuttg).* **2005**, 1231–1233.

254. Daru, J.; Stirling, A. *J. Org. Chem.* **2011**, *76*, 8749–8755.

255. Pillai, S. P.; Menon, S. R.; Mitscher, L. A.; Pillai, C. A.; Shankel, D. M. *J. Nat. Prod.* **1999**, *62*, 1358–1362.

256. March, J. *Advanced Organic Chemistry: Reactions, Mechanisms, and Structure*; 3rd ed.; John Wiley & Sons, Ltd.: New York, **1985**.

257. Aldabalde, V.; Risso, M.; Derrudi, M. L.; Geymonat, F.; Seoane, G.; Gamenara, D.; Saenz-Mendez, P. *Open J. Phys. Chem.* **2011**, *1*, 85–93.

258. Doebner, O. *Eur. J. Inorg. Chem.* **1902**, *35*, 1136–1147.

259. Vahabi, V.; Hatamjafari, F. *Molecules* **2014**, *19*, 13093–13103.

260. Kumbar, M. N.; Kamble, R. R.; Kamble, A. A.; Salian, S. R.; Kumari, S.; Nair, R.; Kalthur, G.; Adiga, S. K.; Prasad, D. J. *Int. J. Med. Chem.* **2016**, *2016*, 1–16.

261. Das, S.; Majee, A.; Hajra, A. *Green Chem. Lett. Rev.* **2011**, *4*, 349–353.

262. Potdar, M. K.; Rasalkar, M. S.; Mohile, S. S.; Salunkhe, M. M. *J. Mol. Catal. A Chem.* **2005**, *235*, 249–252.

263. Bloch, M.; Kostanecki, S. *Eur. J. Inorg. Chem.* **1900**, *33*, 471–476.

264. Ruhemann, S.; Stapleton, H. E. *J. Chem. Soc.* **1900**, *77*, 1179–1185.

265. Miyahisa, I.; Funa, N.; Ohnishi, Y.; Martens, S.; Moriguchi, T.; Horinouchi, S. *Appl. Microbiol. Biotechnol.* **2006**, *71*, 53–58.

266. Falcone Ferreyra, M. L.; Rius, S. P.; Casati, P. *Front. Plant Sci.* **2012**, *3*, 1–15.

267. Park, S. R.; Paik, J. H.; Ahn, M. S.; Park, J. W.; Yoon, Y. J. *J. Microbiol. Biotechnol.* **2010**, *20*, 1295–1299.

268. Svendsen, A. B.; Scheffer, J. J. C. *Pharm. Weekbl. Sci. Ed.* **1982**, *4*, 93–103.

269. Barnes, P. J. *Br. J. Pharmacol.* **2009**, *147*, 297–303.

270. Cohen, B. E.; Elbuluk, N.; Mu, E. W.; Orlow, S. J. *Am. J. Clin. Dermatol.* **2015**, *16*, 463–474.

271. Sina, A.; Schonberg, A. *J. Am. Chem. Soc.* **1950**, *72*, 3396–3399.

272. Cox, J. J. G.; Beach, J. E.; Blair, A. M. J. N.; Clarke, A. J.; King, J.; Lee, T. B.; Loveday, D. E. E.; Moss, G. F.; Orr, T. S. C.; Richie, J. T.; Sheard, P. *Advances in Drug Research*; Harper, N. J.; Simmonds, A. B., Eds.; 5th ed.; Academic Press: London, **1970**.

273. Smith, D. A.; Brown, K.; Neale, M. G. *Drug Metab. Rev.* **1985**, *16*, 365–388.

274. Netzer, N. C.; Küpper, T.; Voss, H. W.; Eliasson, A. H. *Sleep Breath.* **2012**, *16*, 1027–1032.

275. Inaba, T.; Tanaka, K.; Takeno, R.; Nagaki, H.; Yoshida, C.; Takano, S. *Chem. Pharm. Bull. (Tokyo).* **2000**, *48*, 131–139.

276. Nakade, S.; Ueda, S.; Ohno, T.; Nakayama, K.; Miyata, Y.; Yukawa, E.; Higuchi, S. *Drug Metab. Pharmacokinet.* **2006**, *21*, 133–139.

277. Hutter, J. A.; Salman, M.; Stavinoha, W. B.; Satsangi, N.; Williams, R. F.; Streeper, R. T.; Weintraub, S. T. *J. Nat. Prod.* **1996**, *59*, 541–543.

278. Chen, H. J.; Chung, C. P.; Chiang, W.; Lin, Y. L. *Food Chem.* **2011**, *126*, 1741–1748.

279. Coussens, L. M.; Werb, Z. *Nature* **2002**, *420*, 860–867.

280. Glass, C. K.; Saijo, K.; Winner, B.; Marchetto, M. C.; Gage, H. *Cell* **2010**, *140*, 918–934.

281. Chen, W. W.; Zhang, X.; Huang, W. J. *Mol. Med. Rep.* **2016**, *13*, 3391–3396.

282. Shaveta; Singh, A.; Kaur, M.; Sharma, S.; Bhatti, R.; Singh, P. *Eur. J. Med. Chem.* **2014**, *77*, 185–192.

283. Dyrager, C.; Möllers, L. N.; Kjäll, L. K.; Alao, J. P.; Dinér, P.; Wallner, F. K.; Sunnerhagen, P.; Grøtil, M. *J. Med. Chem.* **2011**, *54*, 7427–7431.

284. Saeed, A.; Ashraf, Z.; Rafique, H. *J. Asian Nat. Prod. Res.* **2011**, *13*, 97–104.

285. Gautam, R.; Jachak, S. M.; Kumar, V.; Mohan, C. G. *Bioorganic Med. Chem. Lett.* **2011**, *21*, 1612–1616.

286. Chohan, Z. H.; Shaikh, A. U.; Rauf, A.; Supuran, C. T. *J. Enzyme Inhib. Med. Chem.* **2006**, *21*, 741–748.

287. Said, M. A.; Perl, T. M.; Sears, C. L. *Clin. Infect. Dis.* **2008**, *47*, 1202–1208.

288. Rocha-Pereira, J.; Cunha, R.; Pinto, D. C. G. A.; Silva, A. M. S.; Nascimento, M. S. J. *Bioorganic Med. Chem.* **2010**, *18*, 4195–4201.

289. Park, H. R.; Park, K. S.; Chong, Y. *Bioorganic Med. Chem. Lett.* **2011**, *21*, 3202–3205.

290. Kaye, P. T.; Musa, M. A.; Nchinda, A. T.; Nocanda, X. W. *Synth. Commun.* **2004**, *34*, 2575–2589.

291. Yu, D.; Chen, C.; Brossi, A.; Lee, K. *Synthesis (Stuttg).* **2004**, *47*, 4072–4082.

292. Chen, Yi.; Ming, C.; Liu, F.; Xia, P.; Qian, K.; Yu, D.; Xia, Y.; Yang, Z.-Y.; Chen, C.-H.; Morris-Natschke, S.; Lee, K.-H. *Eur. J. Med. Chem.* **2011**, *46*, 4924–4936.

293. Jung, J.-C.; Min, J.-P.; Park, O.-S. *Synth. Commun.* **2001**, *31*, 1837–1845.

294. Raj, T.; Bhatia, R. K.; kapur, A.; Sharma, M.; Saxena, A. K.; Ishar, M. P. S. *Eur. J. Med. Chem.* **2010**, *45*, 790–794.

295. Khan, K. M.; Ambreen, N.; Hussain, S.; Perveen, S.; Iqbal Choudhary, M. *Bioorganic Med. Chem.* **2009**, *17*, 2983–2988.

296. Forghieri, M.; Laggner, C.; Paoli, P.; Langer, T.; Manao, G.; Camici, G.; Bondioli, L.; Prati, F.; Costantino, L. *Bioorg. Med. Chem.* **2009**, *17*, 2658–2672.

297. Recanatini, M.; Hartmann, R. W.; Bisi, A.; Cavalli, A.; Belluti, F.; Gobbi, S.; Rampa, A.; Valenti, P.; Palzer, M.; Palusczak, A. *J. Med. Chem.* **2001**, *44*, 672–680.

298. Walker, E. H.; Pacold, M. E.; Perisic, O.; Stephens, L.; Hawkins, P. T.; Wymann, M. P.; Williams, R. L. *Mol. Cell* **2000**, *6*, 909–919.

299. Gunn, R. M.; Hailes, H. C. *J Chem Biol* **2008**, *1*, 49–62.

300. Frazzetto, M.; Suphioglu, C.; Zhu, J.; Schmidt-Kittler, O.; Jennings, I. G.; Cranmer, S. L.; Jackson, S. P.; Kinzler, K. W.; Vogelstein, B.; Thompson, P. E. *Biochem. J.* **2008**, *414*, 383–390.

301. Gaspar, A.; Reis, J.; Fonseca, A.; Milhazes, N.; Viña, D.; Uriarte, E.; Borges, F. *Bioorganic Med. Chem. Lett.* **2011**, *21*, 707–709.

302. Gaspar, A.; Silva, T.; Yáñez, M.; Vina, D.; Orallo, F.; Ortuso, F.; Uriarte, E.; Alcaro, S.; Borges, F. *J. Med. Chem.* **2011**, *54*, 5165–5173.

303. Reis, J.; Cagide, F.; Chavarria, D.; Silva, T. B.; Fernandes, C.; Gaspar, A.; Uriarte, E.; Remião, F.; Alcaro, S.; Ortuso, F.; Borges, F. M. *J. Med. Chem.* **2016**, *59*, 5879–5893.

304. Parveen, M.; Malla, A. M.; Yaseen, Z.; Ali, A.; Alam, M. *J. Photochem. Photobiol. B Biol.* **2014**, *130*, 179–187.

305. Sang, Z.; Qiang, X.; Li, Y.; Yuan, W.; Liu, Q.; Shi, Y.; Ang, W.; Luo, Y.; Tan, Z.; Deng, Y. *Eur. J. Med. Chem.* **2015**, *94*, 348–366.

306. Razzaghi-Asl, N.; Aggarwal, N.; Srivastava, S.; Parmar, V. S.; Prasad, A. K.; Miri, R.; Saso, L.; Firuzi, O. *Med. Chem. Res.* **2015**, *24*, 3230–3241.

307. Zhao, L.; Wang, J.-L.; Liu, R.; Li, X.-X.; Li, J.-F.; Zhang, L. *Molecules* **2013**, *18*, 9949–9965.

308. Descamps, O.; Spilman, P.; Zhang, Q.; Libeu, C. P.; Poksay, K.; Gorostiza, O.; Campagna, J.; Jagodzinska, B.; Bredesen, D. E.; John, V. *J. Alzheimers. Dis.* **2013**, *37*, 343–355.

309. Jung, H. A.; Karki, S.; Kim, J. H.; Choi, J. S. *Arch. Pharm. Res.* **2015**, *38*, 1178–1187.

310. Cagide, F.; Reis, J.; Gaspar, A.; Chavarria, D.; Kachler, S.; Klotz, K. N.; Gomes, L. R.; Low, J. N.; Vilar, S.; Hripcsak, G.; Borges, F. *RSC Adv.* **2016**, *6*, 46972–46976.

311. Cagide, F.; Gaspar, A.; Reis, J.; Chavarria, D.; Vilar, S.; Hripcsak, G.; Uriarte, E.; Kachler, S.; Klotz, K. N.; Borges, F. *RSC Adv.* **2015**, *5*, 78572–78585.

312. Obrecht, D. *Helv. Chim. Acta* **1989**, *72*, 447–456.

313. Fillion, E.; Dumas, A. M.; Kuropatwa, B. A.; Malhotra, N. R.; Sitler, T. C. *J. Org. Chem.* **2006**, *71*, 409–412.

314. Kumar, P.; Bodas, M. S. *Org. Lett.* **2000**, *2*, 3821–3823.

315. Porter, W. R.; Trager, W. F. *J. Heterocycl. Chem.* **1982**, *19*, 475–480.

316. Clerk-Bory, M.; Pacheco, H.; Mentzer, C. *Bull. soc. chim Fr.* **1955**, *1*, 1083.

317. Becket, G. J. P.; Ellis, G. P. *Tetrahedron Lett.* **1976**, *17*, 719–720.

318. Zanwar, M. R.; Raihan, M. J.; Gawande, S. D.; Kavala, V.; Janreddy, D.; Kuo, C. W.; Ambre, R.; Yao, C. F. *J. Org. Chem.* **2012**, *77*, 6495–6504.

319. Kaye, P. T.; Nchinda, A. T.; Gray, C. A. *J. Chem. Res.* **2002**, *2002*, 321–325.

320. Ellis, G. P.; Lockart, I. M.; Meeder-Nycz, D.; Schweizer, E. E. *Heterocyclic Compounds: Chromenes, chromanones and chromones*; Ellis, G. P., Ed.; 1st ed.; John Wiley & Sons, Ltd.: New York, **1977**.

321. Königs, P.; Neumann, O.; Kataeva, O.; Schnakenburg, G.; Waldvogel, S. R. *Eur J. Org. Chem.* **2010**, 6417–6422.

322. Baker, W. *J. Chem. Soc.* **1933**, 1381–1389.

323. Zhu, W. F.; Tu, Y. B.; Xu, S.; Tu, Q. D.; Wang, W. H.; Wang, M.; Lei, F.; Xia, H.; Zheng, P. W. *Adv. Mater. Res.* **2014**, *1081*, 16–19.

324. Khanna, I. *Drug Discov. Today* **2012**, *17*, 1088–1102.

325. Wang, Z. In *Comprehensive Organic Name Reactins and Reagents*; John Wiley & Sons, Ltd., **2010**; pp. 2160–2163.

326. Kabeya, L. M.; de Marchi, A. A.; Kanashiro, A.; Lopes, N. P.; da Silva, C. H. T. P.; Pupo, M. T.; Lucisano-Valim, Y. M. *Bioorg. Med. Chem.* **2007**, *15*, 1516–1524.

327. Bora, U.; Bose, G.; Chaudhuri, M. K.; Dhar, S. S.; Gopinath, R.; Khan, A. T.; Patel, B. K. *Org. Lett.* **2000**, *2*, 247–249.

328. Moghaddam, F. M.; Zargarani, D. *Synth. Commun.* **2009**, *39*, 4212–4220.

329. Abhyankar, S. B.; Strickland, D. W. *J. Chem. Educ.* **1991**, *68*, 253.

330. Du, B.; Jiang, X.; Sun, P. *J. Org. Chem.* **2013**, *78*, 2786–2791.

331. Matos, M. J.; Delogu, G.; Podda, G.; Santana, L.; Uriarte, E. *Synthesis (Stuttg).* **2010**, 2763–2766.

332. Kuhn, B.; Mohr, P.; Stahl, M. *J. Med. Chem.* **2010**, *53*, 2601–2611.

333. Di, L.; Kerns, E. H. *Drug-Like Properties. Concepts, Structure, Design, and Methods from ADME to Toxicity Optimization.*; 2nd ed.; Elsevier Academic Press: London, **2008**.

334. Zheng, H.; Fridkin, M.; Youdim, M. *Pharmaceuticals* **2014**, *7*, 113–135.

335. Katselou, M. G.; Matralis, A. N.; Kourounakis, A. P. *Curr. Med. Chem.* **2014**, *21*, 2743–2787.

336. Van der Schyf, C. J. *Expert Rev. Clin. Pharmacol.* **2011**, *4*, 293–298.

337. Smid, P.; Coolen, H. K. a C.; Keizer, H. G.; van Hes, R.; de Moes, J.-P.; den Hartog, A. P.; Stork, B.; Plekkenpol, R. H.; Niemann, L. C.; Stroomer, C. N. J.; Tulp, M. T. M.; van Stuivenberg, H. H.; McCreary, A. C.; Hesselink, M. B.; Herremans, A. H. J.; Kruse, C. G. *J. Med. Chem.* **2005**, *48*, 6855–6869.

338. Holmes, H. M.; Sachs, G. A.; Shega, J. W.; Hougham, G. W.; Cox Hayley, D.; Dale, W. *J. Am. Geriatr. Soc.* **2008**, *56*, 1306–1311.

339. Merino, A.; Bronowska, A. K.; Jackson, D. B.; Cahill, D. J. *Drug Discov. Today* **2010**, *15*, 749–756.

340. Youdim, M. B. H.; Buccafusco, J. J. *Trends Pharmacol. Sci.* **2005**, *26*, 27–35.

341. http://www.molinspiration.com/.

342. Barton, P.; Riley, R. J. *Drug Discov. Today* **2016**, *21*, 72–81.

343. Lipinski, C.; Lombardo, F.; Dominy, B. W.; Feeney, P. J. *Adv. Drug Deliv. Rev.* **2001**, *46*, 3–26.

344. Hitchcock, S. A.; Pennington, L. D. *J. Med. Chem.* **2006**, *49*, 7559–7583.

345. Pajouhesh, H.; Lenz, G. R. *J. Am. Socity Exp. Neurother.* **2005**, *2*, 541–553.

346. Clark, D. E. *J. Pharm. Sci.* **1999**, *88*, 815–821.

347. Riederer, P.; Laux, G. *Exp. Neurobiol.* **2011**, *20*, 1–17.

348. Matos, M. J.; Terán, C.; Pérez-Castillo, Y.; Uriarte, E.; Santana, L.; Viña, D. *J. Med. Chem.* **2011**, *54*, 7127–7137.

349. Chimenti, F.; Secci, D.; Bolasco, A.; Chimenti, P.; Bizzarri, B.; Granese, A.; Carradori, S.; Yáñez, M.; Orallo, F.; Ortuso, F.; Alcaro, S. *J. Med. Chem.* **2009**, *52*, 1935–1942.

350. Brunschweiger, A.; Koch, P.; Schlenk, M.; Rafehi, M.; Radjainia, H.; K??ppers, P.; Hinz, S.; Pineda, F.; Wiese, M.; Hockemeyer, J.; Heer, J.; Denonne, F.; Muller, C. E. *Bioorganic Med. Chem.* **2016**, *24*, 5462–5480.

351. Van Der Walt, M. M.; Terre'Blanche, G.; Petzer, A.; Petzer, J. P. *Bioorg. Chem.* **2015**, *59*, 117–123.

352. Vazquez-Rodriguez, S.; Matos, M. J.; Santana, L.; Uriarte, E.; Borges, F.; Kachler, S.; Klotz, K.-N. *J. Pharm. Pharmacol.* **2013**, *65*, 697–703.

353. Matos, M. J.; Hogger, V.; Gaspar, A.; Kachler, S.; Borges, F.; Uriarte, E.; Santana, L.; Klotz, K.-N. *J. Pharm. Pharmacol.* **2013**, *65*, 1590–1597.

354. Torre, P.; Saavedra, L.; Caballero, J.; Quiroga, J.; Alzate-Morales, J.; Cabrera, M.; Trilleras, J. *Molecules* **2012**, *17*, 12072–12085.

ANNEXES

Annex I

Structural elucidation of the unpublished compounds.

Compounds **17**, **34** and **51**.

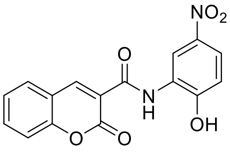 **17**	**^{1}H RMN** (DMSO) δ (ppm), *J* (Hz): 7.01 (d, 1H, H-3', J=8.27), 7.46-7.55 (m, 4H, H-6, H-7, H-8, H-6'), 8.01 (d, 2H, H-5, H-4', J=7.92), 9.04 (s, 1H, H-4), 9.30 (s, 1H, OH), 11.29 (s, 1H, NH). **MS** *m/z* (%): 326 (M, 27), 308 (54), 174 (23), 173 (100), 123 (22), 101 (25), 84 (43)
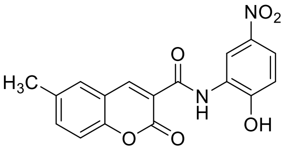 **34**	**^{1}H NMR** ($CDCl_3$) δ (ppm), J (Hz): 2.36 (s, 3H, CH3), 7.00 (d, 1H, H-3', J=8.2), 7.41 (d, 1H, H-8, J=9.0), 7.58 (dd, 1H, H-7, J= 2.2, 9.0), 7.80 (s, 1H, H- 6'), 7.88-7.93 (m, 2H, H-5, H-4'), 8.96 (s, 1H, H-4), 9.29 (s, 1H, OH), 11.30 (s, 1H, NH). **^{13}C RMN** ($CDCl_3$) δ (ppm): 20.4, 110.1, 11.2, 119.2, 119.3, 132.9, 133.8, 134.0, 135.2, 142.8, 148.1, 152.4, 158.3, 159.4, 161.0, 162.6. **MS** *m/z* (%):340 (M, 95), 188 (84), 187 (100), 115 (70), 103 (49), 77 (31)
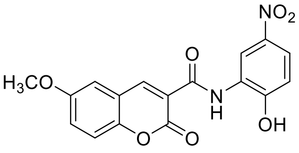 **51**	**^{1}H NMR** ($CDCl_3$) δ (ppm), *J* (Hz): 3.72 (s, 3H, OCH3), 6.88 (d, 1H, H-3', J=8.1), 7.34 (d, 1H, H-8, J=8.9), 7.54-7.63 (m, 2H, H-5, H-7), 7.88-7.93 (m, 2H, H-4', H-6'), 8.90 (s, 1H, H-4), 9.21 (s, 1H, OH), 10.71 (s, 1H, NH) **MS** *m/z* (%):356 (M, 77), 338 (30), 204 (62), 203 (100), 193(44), 119 (42), 105 (25), 91 (25) 77 (30).

Compounds **56**, **57** and **59**-**67**

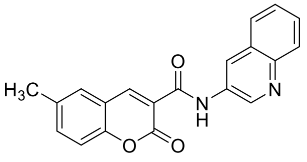 **56**	**^{1}H NMR** (DMSO) δ (ppm), J (Hz): 2.44 (s, 3H, CH_3), 7.33 (d, 1H, H-8, *J*= 9.1), 7.49- 7.65 (m, 4H, H-5, H-7, H-5’, H-6’), 7.83 (d, 1H, H-7’, *J*= 8.0), 8.04 (d, 1H, H-4’, *J*= 8.3), 8.86 (d, 1H, H-8’, *J*= 2.3), 8.94 (s, 1H, H-4), 8.96 (d, 1H, H-2’, *J*= 2.4), 11.17 (s, 1H, NH) **^{13}C NMR** (DMSO) δ (ppm): 20.6, 116.4, 124.3, 127.1, 128.0, 128.3, 129.0, 129.5, 135.5, 135.8, 144.5, 145.4, 149.2, 166.0.
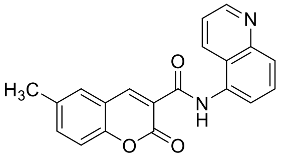 **57**	**^{1}H NMR** (DMSO) δ (ppm), J (Hz): 2.43 (s, 3H, CH_3), 7.32 (d, 1H, H-8, *J*= 9.0), 7.43- 7.54 (m, 3H, H-7, H-6’. H-7’), 7.68-7.76 (m, 1H, H-3’), 7.92 (d, 1H, H-5, *J*= 8.3), 8.40 (d, 1H, H-2’, *J*= 7.6), 8.47 (d, 1H, H-8’, *J*= 8.3), 8.93 (d, 1H, H-4’, *J*= 3.5), 8.99 (s, 1H, H-4), 11.52 (s, 1H, NH). **^{13}C NMR** (DMSO) δ (ppm): 20.7, 116.4, 118.0, 118.6, 121.1, 121.4, 126.5, 129.3, 132.6, 135.5, 135.7, 148.4, 149.3, 149.6, 150.2, 152.6, 160.0, 162.5
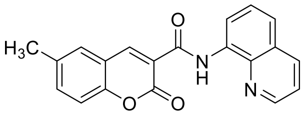 **59**	**^{1}H NMR** (DMSO) δ (ppm), J (Hz): 2.42 (s, 3H, CH_3), 7.31 (d, 1H, H-8, *J*= 8.1), 7.43- 7.48 (m, 3H, H-5, H-7, H-7’), 7.52-7.60 (m, 2H, H-4’, H-6’), 8.14 (dd, 1H, H-5’, *J*= 1.7, 8.3), 8.93-8.97 (m, 3H, H-4, H-3’, H-8’), 12.78 (s, 1H, NH). **^{13}C NMR** (DMSO) δ (ppm): 20.6, 115.2, 116.3, 117.4, 118.4, 119.2, 122.4, 127.0, 128.1, 129.3, 134.9, 135.9, 139.5, 148.9, 148.8, 148.9, 152.9, 157.7, 160.0
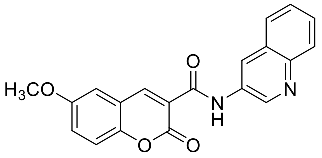 **60**	**^{1}H NMR** (DMSO) δ (ppm), J (Hz): 3.90 (s, 3H, OCH_3), 7.05 (d, 1H, H-8, *J*= 9.1), 7.31- 7.49 (m, 4H, H-5, H-7, H-5’, H-6’), 7.62 (d, 1H, H-7’, *J*= 8.0), 8.00 (d, 1H, H-4’, *J*= 8.1), 8.71 (d, 1H, H-8’, *J*= 2.5), 9.05 (s, 1H, H-4), 8.96 (d, 1H, H-2’, *J*= 2.5), 11.17 (s, 1H, NH) **^{13}C NMR** (DMSO) δ (ppm): 56.0, 116.2, 117.3, 118.8, 119.2, 120.0, 122.0, 128.1, 128.5, 129.2, 135.7, 135.9, 140.4, 148.0, 150.1, 150.2, 152.9, 159.0, 162.1.
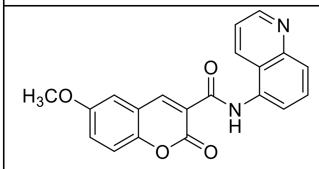 **61**	**^{1}H NMR** (DMSO) δ (ppm), J (Hz): 3.88 (s, 3H, OCH_3), 7.12 (d, 1H, H-8, *J*= 9.1), 7.55- 7.66(m, 3H, H-7, H-6’. H-7’), 7.73-7.79 (m, 1H, H-3’), 7.99 (d, 1H, H-5, *J*= 8.0), 8.31 (d, 1H, H-2’, *J*= 7.8), 8.51 (d, 1H, H-8’, *J*= 8.2), 8.90 (d, 1H, H-4’, *J*= 2.9), 9.01 (s, 1H, H-4), 11.52 (s, 1H, NH). **^{13}C NMR** (DMSO) δ (ppm): 56.0, 110.0, 115.5, 118.6, 121.5, 121.9, 125.8,

	129.0, 131.1, 134.4, 135.8, 148.4, 148.6, 150.0, 150.2, 153.7, 160.2, 162.9
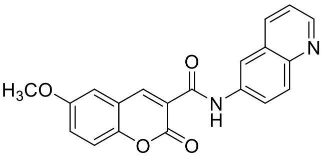 **62**	**^{1}H NMR** (DMSO) δ (ppm), J (Hz): 3.86 (s, 3H, OCH$_3$), 7.08-7.27 (m, 2H, H-8, H-6’), 7.33- 7.37 (m, 2H, H-7, H-7’), 7.78 (d, 1H, H-2’, *J*= 8.0), 8.04- 8.15 (m, 2H, H-5, H-3’), 8.48 (s, 1H, H-8’), 8.79- 8.82 (m, 1H, H-5’), 8.95 (s, 1H, H-4), 11.14 (s, 1H, NH). **^{13}C NMR** (DMSO) δ (ppm): 55.8, 110.6, 116.8, 117.8, 18.3, 118.8, 121.5, 123.1, 123.2, 123.8, 128.7, 130.2, 135.8, 145.6, 145.8, 148.8, 149.5, 159.7, 161.2, 162.8.
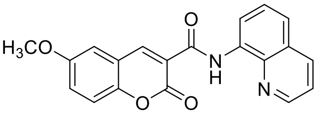 **63**	**^{1}H NMR** (DMSO) δ (ppm), J (Hz): 3.82 (s, 3H, OCH$_3$), 7.09 (d, 1H, H-5, *J*= 2.9), 7.23 (dd, 1H, H-7, *J*= 2.9, 9.1), 7.35 (d, 1H, H-8, *J*= 9.1), 7.42- 7.48 (m, 1H, H-7), 7.54- 7.57 (m, 2H, H-4’, H-6’), 8.14 (dd, 1H, H-5’, *J*= 1.7, 8.3), 8.92- 8.98 (m, 3H, H-4, H-3’, H-8’), 12.80 (s, 1H, NH). **^{13}C NMR** (DMSO) δ (ppm): 55.9, 114.0, 115.3, 120.1, 121.7, 122.2, 122.4, 125.6, 127.1, 129.3, 135.0, 135.8, 139.0, 143.2, 148.8, 149.0, 153.0, 158.7, 161.4.
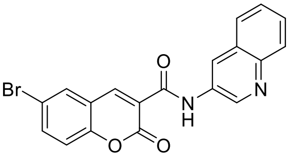 **64**	**^{1}H NMR** (DMSO) δ (ppm), J (Hz): 7.50 (d, 1H, H-8, *J*= 8.8), 7.55- 7.70 (m, 2H, H-5’, H-6’), 7.87- 8.00 (m, 2H, H-7, H-7’), 8.04- 8.12 (m, 1H, H-4’), 8.25 (d, 1H, H-5, *J*= 2.2), 8.78 (d, 1H, H-8’, *J*= 2.4), 8.86 (s, 1H, H-4), 9.04 (d, 1H, H-2’, *J*= 2.5), 10.91 (s, 1H, NH). **^{13}C NMR** (DMSO) δ (ppm): 97.2, 98.3. 100.5, 104.5, 109.4, 119.0, 119.4, 126.1, 130.5, 131.9, 132.2, 135.8, 139.5, 143.9, 146.5, 153.2, 158.9, 160.1, 166.0
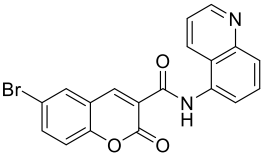 **65**	**^{1}H NMR** (DMSO) δ (ppm), J (Hz): 7.36 (d, 1H, H-8, *J*= 8.9), 7.47- 7.53 (m, 1H, H-7’), 7.74- 7.78 (m, 2H, H-7, H-6’), 7.88 (d, 1H, H-5, *J*= 1.5), 7.96 (d, 1H, H-3’, *J*= 8.0), 8.40 (d, 1H, H-2’, *J*= 7.7), 8.47 (d, 1H, H-8’, *J*= 8.6), 8.94 (d, 1H, H-4’, *J*= 3.5), 8.99 (s, 1H, H-4), 11.39 (s, 1H, NH). **^{13}C NMR** (DMSO) δ (ppm): 117.0, 118.7, 119.9, 121.7, 126.5, 129.5, 130.0, 132.4, 132.5, 139.6, 141.0, 146.7, 150.9, 160.1, 160.2, 160.3, 160.8, 163.6, 165.0,
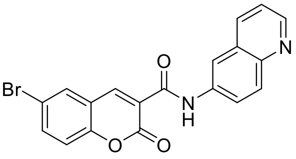 **66**	**^{1}H NMR** (DMSO) δ (ppm), J (Hz): 7.45- 7.51 (m, 2H, H-8, H-6’), 7.86- 8.01 (m, 3H, H-7, H-7’, H-2’), 8.24 (d, 1H, H-5, *J*= 2.1), 8.31 (d, 1H, H-3’, *J*= 8.0), 8.43 (s, 1H, H-8’), 8.79 (dd, 1H, H-5’, *J*= 1.5, 4.1), 8.84 (s, 1H, H-4), 10.86 (s, 1H, NH).. **^{13}C NMR** (DMSO) δ (ppm):, , , , , , , , , , , , 99.2, 100.2, 114.4,

	118.5, 122.3, 124.0, 128.4, 129.4, 130.1, 136.0, 136.7, 141.0, 146.3, 149.6, 151.7, 153.1, 160.9, 164.8, 171.0
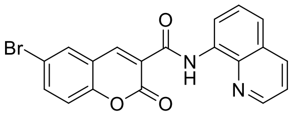 **67**	**^{1}H NMR** (DMSO) δ (ppm), J (Hz): 7.49 (d, 1H, H-8, *J*= 8.8), 7.60- 7.65 (m, 2H, H-4', H-6'), 7.69- 7.74 (m, 1H, H-7'), 7.88 (dd, 1H, H-7, *J*= 2.4, 8.8), 8.30 (d, 1H, H-5, *J*= 2.4), 8.40 (dd, 1H, H-5', *J*= 1.6, 8.3), 8.86 (dd, 1H, H-8', *J*= 1.3, 7.6), 8.95 (dd, 1H, H-3', *J*= 1.7, 4.2), 9.03 (s, 1H, H-4), 12.50 (s, 1H, NH). **^{13}C NMR** (DMSO) δ (ppm): 117.3, 118.6, 120.1, 120.7, 122.5, 122.9, 127.2, 127.8, 128.0, 132.5, 134.6, 136.7, 147.5, 147.8, 149.5, 153.2, 159.4, 160.4, 165.2

Compounds **84-89**

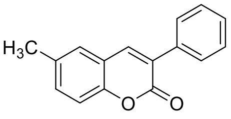 **84**	^{1}**H RMN** ($CDCl_3$) δ (ppm), *J* (Hz): 2.42 (s, 3H, CH_3), 7.27 (m, 1H, H-7), 7.34 (m, 2H, H-5, H-8), 7.43 (m, 3H, H-3', H-4', H-5'), 7.70 (dd, 2H, H-2', H-6', *J* = 6.3, *J* = 1.9), 7.77 (s, 1H, H-4)**.** ^{13}**C RMN** ($CDCl_3$) δ (ppm): 21.2, 116.6, 119.5, 128.1, 128.7, 128.9, 129.0, 129.2, 132.9, 134.6, 135.3, 140.3, 152.1, 161.3. **MS** *m/z* (%): 236 (M+, 100), 208 (50), 51 (69).
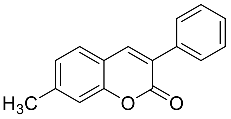 **85**	^{1}**H NMR** ($CDCl_3$) δ (ppm), J (Hz): 2.45 (s, 3H, CH_3), 7.09 (dd, 1H, H-6, *J* = 7.9, *J* = 1.5), 7.15 (s, 1H, H-8), 7.40 (m, 4H, H-5, H-3', H-4', H-5'), 7.67 (m, 2H, H-2', H-6'), 7.76 (s, 1H, H4). ^{13}**C RMN** ($CDCl_3$) δ (ppm): 21.0, 115.9, 119.0, 128.1, 128.2, 128.7, 129.0, 129.8, 133.3, 134.0, 135.1, 142.7, 153.9, 160.9. **MS** *m/z* (%): 236 (M+, 100), 208 (61), 178 (44), 51 (77).
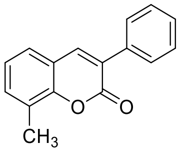 **86**	^{1}**H NMR** ($CDCl_3$) δ (ppm), *J* (Hz): 2.50 (s, 3H, CH_3), 7.21 (m, 2H, H-6, H-7), 7.42 (m, 4H, H-3', H-4', H-5', H-5), 7.71 (m, 2H, H-2', H-6'), 7.80 (s, 1H, H-4). ^{13}**C NMR** ($CDCl_3$) δ (ppm): 15.4, 119.3, 124.5, 125.6, 125.9, 127.9, 128.4, 128.7, 132.7, 134.8, 140.2, 140.3, 151.8, 160.1. **MS** *m/z* (%): 236 (M+, 94), 209 (20), 208 (77), 207 (38), 179 (22), 178 (36), 165 (35), 86 (76), 84 (91), 51 (59), 49 (80)
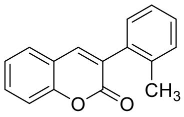 **87**	^{1}**H NMR** ($CDCl_3$) δ (ppm), J (Hz): 2.28 (s, 3H, CH_3), 7.30 (m, 6H, H-2', H-3', H-4', H-6', H-6, H-8), 7.52 (m, 2H, H-5, H-7), 7.63 (s, 1H, H-4); ^{13}**C RMN** ($CDCl_3$) δ (ppm): 19.8, 116.5, 119.1, 124.3, 125.8, 127.7, 128.7, 129.6, 130.2, 131.3, 134.5, 136.8, 141.5, 148.38, 153.7, 160.2. **MS** *m/z* (%): 236 (M+, 100)
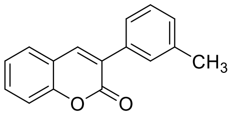 **88**	^{1}**H NMR** ($CDCl_3$) δ (ppm), J (Hz): 2.39 (s, 3H, CH_3), 7.20 (d, 1H, H-3', *J* = 7.2), 7.32 (m, 3H, H-4', H-6, H-8), 7.48 (m, 4H, H-5, H-7, H-2', H-5'), 7.77 (s, 1H, H-4); ^{13}**C RMN** ($CDCl_3$) δ (ppm): 21.4, 116.3, 119.6, 124.3, 125.5, 127.7, 128.2, 129.0, 129.5, 131.2, 134.5, 137.9, 139.6, 153.5. **MS** *m/z* (%):236 (M+, 88), 208 (77), 178 (44), 165 (35), 86 (61)
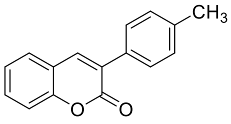 **89**	^{1}**H RMN** (CDCl3) δ (ppm), *J* (Hz): 2.40 (s, 3H, CH_3), 7.31 (m, 4H, H-2', H-3', H-5', H-6'), 7.57 (m, 4H, H-5, H-6, H-7, H-8), 7.79 (s, 1H, H-4); ^{13}**C RMN** ($CDCl_3$) δ (ppm): 21.2, 116.6, 119.5, 128.1, 128.7, 128.9, 129.0, 129.2, 132.9, 134.6, 135.3, 140.3, 152.1, 161.3. **MS** *m/z* (%): 236 (M+, 100), 210 (21), 178 (14), 134 (19), 112 (32).

Compounds **103**-**108**

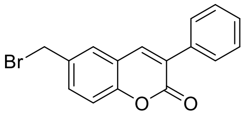 **103**	**^{1}H RMN** ($CDCl_3$) δ (ppm), *J* (Hz): 4.56 (s, 2H, CH_2), 7.35 (d, 2H, H-7, H-8, *J* = 8,2), 7.43 (m, 2H, H-5, H-4’), 7.51 (dd, 2H, H-3’, H-5’, *J* = 8.2, *J* = 2.1), 7.65 (m, 2H, H-2’, H-6’), 7.79 (s, 1H, H-4); **^{13}C RMN** ($CDCl_3$) δ (ppm): 32.1, 116.9, 119.7, 128.1, 128.4, 128.8, 129.0, 132.0, 134.2, 134.3, 139.1, 153.1, 160.2. **MS** *m/z* (%): 316 (M+, 41), 314 (10), 235 (100), 207 (70), 178 (28), 103 (15)
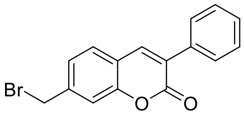 **104**	**^{1}H NMR** ($CDCl_3$) δ (ppm), J (Hz): 4.50 (s, 2H, CH_2), 7.3 (dd, 1H, H-6, *J* = 8.0, 1.6), 7.42 (m, 4H, H-8, H-3’, H-4’, H-5’), 7.50 (d, 1H, H-5, *J* = 8.0), 7.67 (m, 2H, H-2’, H-6’), 7.77 (s, 1H, H-4). **^{13}C RMN** ($CDCl_3$) δ (ppm): 31.9, 115.8, 121.3, 128.0, 128.4, 129.0, 129.1, 133.6, 134.8, 135.3, 138.0, 153.0, 160.1. **MS** *m/z* (%): 316 (M+2, 10), 235 (100), 207 (66)
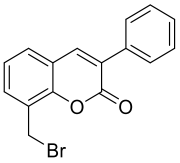 **105**	**^{1}H NMR** ($CDCl_3$) δ (ppm), J (Hz): 4.74 (s, 2H, CH_2), 7.25 (t, 1H, H-6, *J*=7.7), 7.45 (m, 4H, H-7, H-3’, H-4’, H-5’), 7.58 (dd, 1H, H-5, *J*=7.5, 1.5), 7.68 (m, 2H, H-2’, H-6’), 7.77 (s, 1H, H-4). **^{13}C RMN** ($CDCl_3$) δ (ppm): 29.7, 122.5, 124.7, 125.6, 127.9, 128.1, 129.0, 129.2, 135.2, 135.6, 140.1, 150.4, 160.8. **MS** *m/z* (%): 316 (M+2, 14), 314 (42), 235 (100), 207 (51), 178 (32)
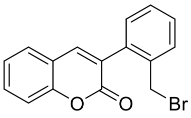 **106**	**^{1}H NMR** ($CDCl_3$) δ (ppm), J (Hz): 4.66 (s, 2H, CH_2), 7.33 (m, 5H, H-6, H-7, H-3’, H-4’, H-5’), 7.69 (dd, 1H, H-5, *J* = 7.5, 1.5), 7.81 (m, 2H, H-8, H-6’), 8.12 (s, 1H, H-4). **^{13}C RMN** ($CDCl_3$) δ (ppm): 30.1, 122.9, 125.0, 125.5, 127.7, 128.3, 128.8, 129.1, 135.2, 135.7, 142.0, 151.2, 160.9.
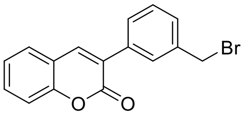 **107**	**^{1}H NMR** ($CDCl_3$) δ (ppm), J (Hz): 4.58 (s, 2H, CH_2), 7.40 (m, 5H, H-5, H-6, H-7, H-4’, H-5’), 7.68 (m, 2H, H-2’, H-6’), 7.79 (s, 1H, H-4). **^{13}C RMN** ($CDCl_3$) δ (ppm): 29.9, 122.0, 121.1, 125.0, 126.6, 127.2, 128.5, 130.3, 134.4, 135.8, 138.9, 151.2, 160.7.
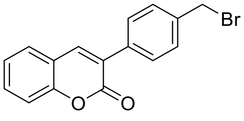 **108**	**^{1}H NMR** ($CDCl_3$) δ (ppm), J (Hz): 4.61 (s, 2H, CH_2), 7.36 (m, 4H, H-5, H-6, H-7, H-8), 7.54 (m, 2H, H-3’, H-5’), 7.72 (m, 2H, H-2’, H-6’), 7.70 (s, 1H, H-4). **^{13}C RMN** ($CDCl_3$) δ (ppm): 29.8, 119.1, 125.4, 125.5, 126.2, 127.3, 129.4, 131.7, 135.0, 135.1, 143.7, 149.2, 160.9.

Compounds **109**-**115**

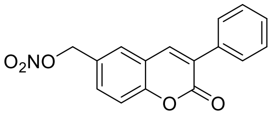 **109**	**^{1}H NMR** (DMSO) δ (ppm), J (Hz): 5.63 (s, 2H, CH_2), 7.46 (m, 4H, H-8, H-3’, H-4’, H-5’), 7.68 (m, 3H, H-7, H-2’, H-6’), 7.86 (s, 1H, H-5), 8.25 (s, 1H, H-4); **^{13}C NMR** (DMSO) δ (ppm): 74.3, 116.5, 119.7, 127.6, 128.4, 128.7, 128.9, 129.7, 132.8, 134.6, 140.3, 153.4, 159.7, 170.5.
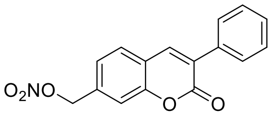 **110**	**^{1}H NMR** (DMSO) δ (ppm), J (Hz): 5.66 (s, 2H, CH_2), 7.42 (m, 4H, H-6, H-2’, H-4’, H-6’), 7.53 (s, 1H, H-8), 7.70 (m, 2H, H-3’, H-5’), 7.79 (d, 1H, H-5, *J* = 8.0), 8.24 (s, 1H, H-4); **^{13}C NMR** (DMSO) δ (ppm): 74.2, 116.4, 120.1, 125.1, 125.9, 128.4, 128.7, 128.9, 129.1, 134.7, 135.1, 136.3, 140.2, 152.9, 159.6, 161.1 .
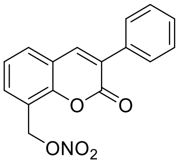 **111**	**^{1}H NMR** (DMSO) δ (ppm), J (Hz): 5.69 (s, 2H, CH_2), 7.26 (m, 5H, H-6, H-7, H-2’, H-4’, H-6’), 7.39 (m, 2H, H-3’, H-5’), 7.83 (m, 1H, H-5), 8.10 (s, 1H, H-4); **^{13}C NMR** (DMSO) δ (ppm): 74.0, 122.4, 124.2, 125.6, 126.8, 127.9, 128.3, 128.6, 128.9, 134.4, 141.1, 144.9, 148.5, 160.6 .
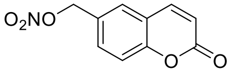 **112**	**^{1}H NMR** (DMSO) δ (ppm), J (Hz): 5.61 (s, 2H, CH_2), 6.51 (d, 1H, H-3, *J* = 9.6), 7.43 (d, 1H, H-8, *J* = 8.6), 7.69 (dd, 1H, H-7, *J* = 8.6, 1.9), 7.81 (d, 1H, H-1 , *J* = 1.8), 8.07 (d, 1H, H-4, *J* = 9.6); **^{13}C NMR** (DMSO) δ (ppm): 74.3, 116.9, 118.9, 128.8, 129.6, 133.1, 135.5, 144.1, 154.0, 159.8
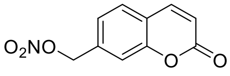 **113**	**^{1}H NMR** (DMSO) δ (ppm), J (Hz): 5.25 (s, 2H, CH_2), 6.50 (d, 1H, H-3, *J* = 9.5), 7.40 (dd, 1 H, H-6, *J*=7.9, 1.5), 7.48 (d, 1H, H-8, *J* = 7.8), 7.73 (d, 1H, H-5, *J* = 7.8) 8.09 (d, 1H, H-4, *J* = 9.5); **^{13}C NMR** (DMSO) δ (ppm): 74.0, 116.8, 117.1, 119.3, 125.0, 129.0, 136.7, 143.9, 153.5, 159.9.
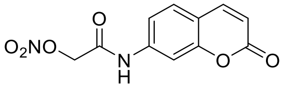 **114**	**^{1}H NMR** (DMSO) δ (ppm), J (Hz): 5.25 (s, 2H, CH_2), 6.91 (s, 1H, H-3), 7.50 (dd, 1H, H-6, *J* = 8.9, 1.5), 7.68 (d, 1H, H-5, *J* = 8.9), 7.79 (d, 1H, H-8, *J* = 1.5), 8.02 (s, 1H, H-4), 10.97 (s, 1H, NH); **^{13}C NMR** (DMSO) δ (ppm): 69.6,106.7, 107.3, 109.0, 116.3, 142.2, 154.7, 155.9, 156.2, 158.8, 165.0
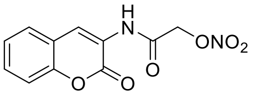 **115**	**^{1}H NMR** (DMSO) δ (ppm), J (Hz): 5.32 (s, 2H, CH_2), 7.34 (m, 2H, H-6, H-8), 7.49 (m, 1H, H-7), 7.70 (dd, 1H, H-5, *J* = 7.7, 1.5), 8.59 (s, 1H, H-4), 10.42 (s, 1H, NH); **^{13}C NMR** (DMSO) δ (ppm): 69.8, 116.0, 119.5, 124.0, 124.8, 125.2, 128.2, 130.2, 150.0, 157.4, 165.7.

Annex II

Benzopyrone scaffolds and their role in enzymatic systems involved in neurodegenerative diseases: Coumarins and chromones (from 2010 – 2015).

Benzopyrone scaffolds and their role in enzymatic systems involved in neurodegenerative diseases: Coumarins and chromones (from 2010 – 2015).

Saleta Vazquez-Rodriguez*[a], Maria João Matos[a], Andre Fonseca[a,b], Fernanda Borges,[b] Eugenio Uriarte[a] , Lourdes Santana[a]

[a]*Departmento de Química Orgánica, Faculdade de Farmacia, Universidade de Santiago de Compostela, 15782 Santiago de Compostela, Spain*

[b]*CIQ/Departmento de Química e Bioquímica, Faculdade de Ciências, Universidade do Porto 4169-007, Portugal*

Abstract: Neurodegenerative diseases are a heterogeneous group of disorders characterized by the progressive degeneration of the structure and function of the central nervous system or peripheral nervous system. The complex etiology of these diseases has encouraged an active research in the development of new drugs targeting one or various key enzymes involved in these pathologies. In this intense search for new drug candidates, many coumarin and chromone derivatives have shown promising inhibitory activity against different enzymes related to neurodegenerative disorders. The purpose of this review is to summarize the findings reported in this area in the last 5 years, reinforcing the important recent advances in the development of coumarins and chromones as potential drug candidates for the treatment of neurodegenerative diseases focused on their role in enzymatic systems involved in these pathologies.

Keywords: Coumarins, Chromones, neurodegenerative diseases, enzymatic inhibition, ChE, MAO, BACE-1

1. INTRODUCTION

Neurodegenerative diseases (NDs) are defined as hereditary and sporadic conditions, which are characterized by progressive nervous system dysfunction. These disorders are often associated with atrophy of the affected central or peripheral structures of the nervous system. Among these disorders are diseases such as Alzheimer's Disease (AD) and other dementias, brain cancer, degenerative nerve diseases, encephalitis, epilepsy, genetic brain disorders, head and brain malformations, hydrocephalus, stroke, Parkinson's disease (PD), multiple sclerosis (MS), amyotrophic lateral sclerosis (ALS or Lou Gehrig's disease), Huntington's disease and prion diseases [1,2]. These progressive, age-related multifactorial diseases have an increasing prevalence and no cure or lasting symptomatic therapy, affecting almost 30 million individuals leading to disability and death. With an increasingly ageing population, it is predicted that the prevalence of NDs will almost double worldwide by 2030 with a very substantial burden on the healthcare and social services [3].

Despite the differences in clinical manifestations and neuronal vulnerability, the pathological processes appear similar, suggesting common neurodegenerative pathways. The major basic processes involved are multifactorial in nature, caused by genetic, environmental, and endogenous factors. However, the main causes of neurodegeneration in these diseases, besides normal brain aging, are several cellular and molecular events such as oxidative stress and free radical formation, impaired mitochondrial function, deposition of aggregated proteins, neuroinflammation, and activation of apoptotic factors [2,4,5].

People who suffer from NDs such as PD or AD are usually treated with drugs developed to act on a single molecular target. However, there is a new therapeutic approach that comprises drug candidates designed specifically to act on multiple neural and biochemical targets for the treatment of cognition impairment, motor dysfunction, depression and neurodegeneration [6,7].

Heterocycles play an important role in the design and discovery of new physiological/pharmacologically active compounds [8]. Privileged structures such as benzopyrones, are currently considered as helpful approaches for the development of new scaffolds in drug discovery. Compounds such as coumarin and chromones are benzopyrone-family compounds that constitute the core skeleton of many flavonoid compounds and that have been widely used as scaffolds in drug discovery programs [9,10,11].

In view of these facts, this review reinforces the important recent advances in the development of coumarins and chromones as potential drug candidates for the treatment of NDs in the last 5 years focused on their role in enzymatic systems involved in these pathologies.

2. BENZOPYRANE SCAFFOLDS: COUMARIN AND CHROMONES

Among other different heterocyclic compounds, coumarins (Figure 1) are a large and well-known family of natural and synthetic origin compounds existing in remarkable amounts in nature with great structural variety [12,13,14]. Representative compounds occur for instance in the vegetable kingdom, either in free or combined state [15,16]. Coumarins show a wide range of pharmacological activities, but recent studies pay special attention to their anti-inflammatory [17,18], antioxidant [19,20,21], cardioprotective [22], antitumor [23], antimicrobial [24,25,26] and enzymatic inhibition [27,28] properties. First isolated in 1820 by Vogel [29], coumarin has a 2*H*-1-benzopyran-2-one system (benzo-α-pyrone) as main core and its systematic name was established by the IUPAC [30]. Its biosynthesis starts with L-phenylalanine as precursor in plants such as *Melilotus alba* also known as yellow sweet clove.

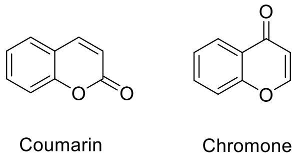

Figure 1. Coumarin and chromone scaffolds

There are a great number of coumarins discovered by isolation from hundreds of species of plants and other organisms. For many years, naturally occurring coumarins were the only ones known, and it was not until the synthetic methods of Perkin and Pechmann in the latter part of the 19th century combined to produce virtually any synthetic coumarin desired. Therefore, thanks to the advances in synthetic chemistry, there are nowadays many coumarin derivatives of synthetic origin, which significantly increases the number of coumarin structures known till today.

As well as coumarins, chromones (Figure 1) are pyrone-containing compounds presenting a benzoannelated γ-pyrone ring. In nature, chromone (4*H*-chromen-4-one, 4*H*-1-benzopyran-4-one) is the main core of several flavonoids, such as flavones and isoflavone the parent compound.

As coumarins, chromones are widely spread in nature and they constitute one of the most abundant groups of naturally occurring heterocyclic compounds [31]. Chromones therefore constitute an important class of compounds in the natural and synthetic realm not only for their structural features but also for the numerous pharmacological activities that these compounds present. Among them, anti-inflammatory, antiplatelet, anticancer, and antimicrobial activities, including those related with central nervous system and obesity have been extensively described [11].

But it has been also found in the literature some chromones with antioxidant activity [32,33], as antidiabetics and cardiovascular agents [34], as anti-HIV agents [35] or with enzymatic inhibition properties [36].

In this review we have tried to concentrate all the advances made in coumarin and chromones presenting pharmacological activities in enzymatic systems involved in NDs from 2010 to the end of 2015. For this reason this review is classified based on the targeted enzymes.

3. COUMARIN AND CHROMONES IN NDs

3.1. Aβ aggregation inhibitors

AD is a common neurodegenerative disorder characterized by the excessive deposition of amyloids plaques in the brain. The pathological features mainly include the extracellular amyloid plaques and intracellular neurofibrillary tangles, which are the production of amyloid precursor protein (APP) processed by the α-, β- and γ-secretases. Therefore the development of amyloid-β agents and secretase inhibitors against AD that are able to prevent aggregation of amyloid-β (Aβ) peptide allowing to decrease the Aβ levels has been a hot topic for the treatment of this pathology. Numerous small molecules have been reported to interfere with the process of Aβ aggregation [37,38,39]. However, only a few examples of coumarin and chromone containing compounds have been developed as Aβ inhibitors.

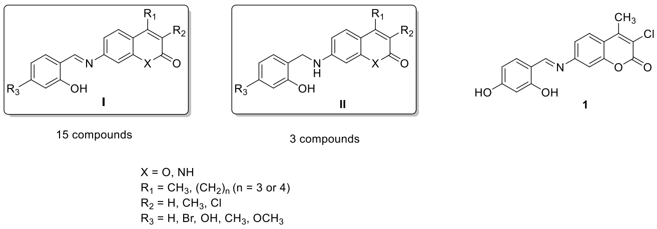

Figure 2. Coumarin derivatives synthesized by Huang and collaborators as Aβ aggregation inhibitors.

Huang and collaborators [40] prepared different coumarin and coumarin-like derivatives as both monoamine oxidase (MAO) and Aβ aggregation inhibitors (Figure 2). Their results showed that from the synthesized series with general structures I and II (Figure 2), only some compounds with general structure I presented Aβ aggregation inhibition percentages up to 50%, being compound **1** the one with higher Aβ aggregation inhibition percentage at 20µM ($A\beta_{1-42}$ aggregation inhibition % = 60.2).

Some hybrid compounds such as series of tacrine-coumarin and tacrine-chromones were studied as Aβ aggregation inhibitors. Coumarin-tacrine hybrids were synthesized and evaluated by Xie [41] and by Sun [42] and collaborators as Aβ aggregation inhibitors. This series of compounds not only exhibit Aβ aggregation inhibition but also exhibit acetylcholinesterase (AChE) and butyrylcholinesterase (BuChE) inhibition, and therefore those compounds can be considered as multifunctional agents for AD treatment. In the series of hybrid compounds (Figure 3) with general structure III, compounds **2** and **3** presented the best activity as Aβ aggregation inhibitors, with inhibition percentages of 67.8 and 67.5 at 20µM respectively. On the other hand, in the series of hybrid compounds with general structure IV, compounds **4**-**7** showed moderate IC_{50} values at 100 µM against Aβ aggregation ranging between 5-24.2 µM.

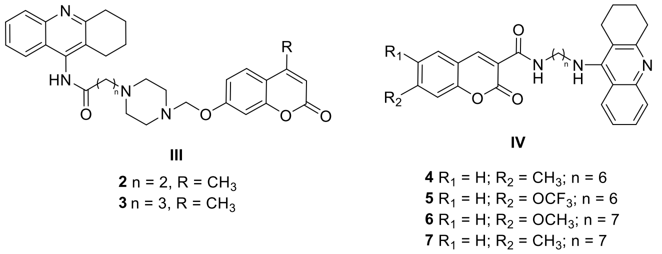
N
HN
O
n
N
N
O
R
O
O
III
2 n = 2, R = CH3
3 n = 3, R = CH3
R1
R2
O
N
H
n
N
H
N
IV
4 R1 = H; R2 = CH3; n = 6
5 R1 = H; R2 = OCF3; n = 6
6 R1 = H; R2 = OCH3; n = 7
7 R1 = H; R2 = CH3; n = 7

Figure 3. Tacrine-coumarin hybrids as Aβ aggregation inhibitors.

Chromone-tacrine hybrid compounds were synthesized and studied by Liao and collaborators [43]. In this study, significant inhibitory potencies of self-induced Aβ aggregation were obtained for the synthesized compounds. In particular, compound **11** (Figure 4) had the strongest inhibition of self-induced $A_{\beta 1-42}$ aggregation with inhibition ratio of 35.5% at 25 µM.

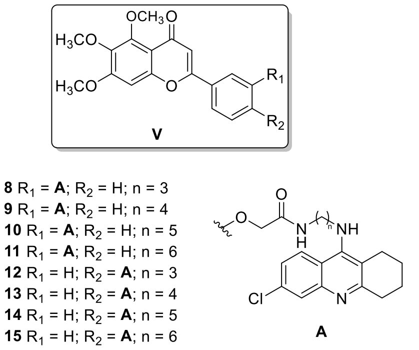
OCH3O
H3CO
H3CO
O
R1
R2
V
8 R1 = A; R2 = H; n = 3
9 R1 = A; R2 = H; n = 4
10 R1 = A; R2 = H; n = 5
11 R1 = A; R2 = H; n = 6
12 R1 = H; R2 = A; n = 3
13 R1 = H; R2 = A; n = 4
14 R1 = H; R2 = A; n = 5
15 R1 = H; R2 = A; n = 6
O
N
H
NH
n
Cl
N
A

Figure 4. Tacrine-chromone hybrids as Aβ self-assembly inhibitors.

In 2013 Bag et al synthesized coumarin derivatives with general structure VI (Figure 5) with the ability to inhibit Aβ self-assembly [44]. As fibrillar and oligomeric aggregates of Aβ are neurotoxic, the activity of this series of compounds was determined against the formation of these species. In the oligomer assembly assay the coumarin derivatives (**15**-2**1**, Figure 5) showed excellent results as inhibitors of the Aβ self-assembly (inhibition >65%). For this series of compounds, the IC_{50} was calculated, and the concentration dependence studies revealed that IC_{50} values at 50 µM ranged between 14 and 36 µM, with exception of compound **19**, with an IC_{50} of 1 µM.

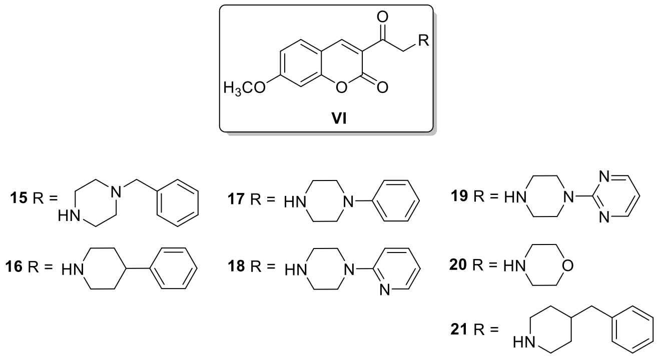
O
R
H3CO
O
O
VI
15 R =
HN
N
16 R =
HN
17 R =
HN
N
18 R =
HN
N
N
19 R =
HN
N
N
N
20 R =
HN
O
21 R =
HN

Figure 5. 3-Substituted coumarins as Aβ self-assembly inhibitors.

Luo [45] and Li [46] and their collaborators synthesized some flavone derivatives in 2013. These compounds with general structure VII (Figure 6) showed potent self-induced Aβ aggregation inhibitory activity at 20 µM with percentage from 20% to 48%. The most potent compounds of those series were compounds **22-32**, outlined in Figure 6, with percentages of inhibition greater than 40%. Despite the inhibitory potency of each derivative did not depend on the chain length of the connecting linker, further studies need to be done for an accurate structure-activity relationship.

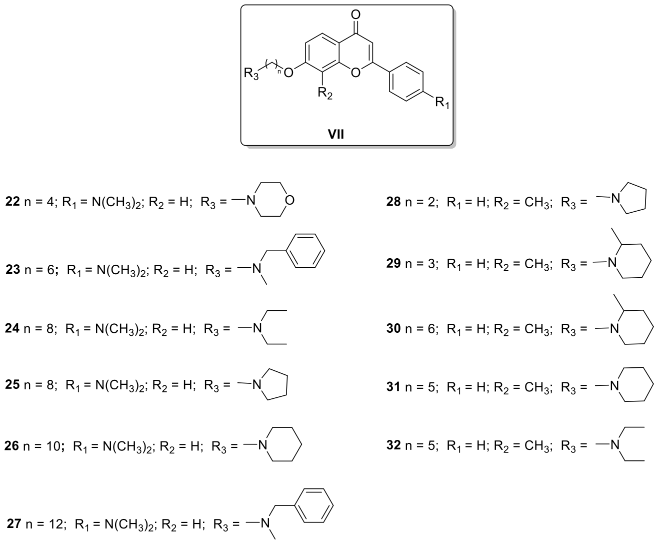
O
R3
n
O
O
R2
R1
VII
22 n = 4; R1 = N(CH3)2; R2 = H; R3 = —N O
23 n = 6; R1 = N(CH3)2; R2 = H; R3 = —N
24 n = 8; R1 = N(CH3)2; R2 = H; R3 = —N
25 n = 8; R1 = N(CH3)2; R2 = H; R3 = —N
26 n = 10; R1 = N(CH3)2; R2 = H; R3 = —N
27 n = 12; R1 = N(CH3)2; R2 = H; R3 = —N
28 n = 2; R1 = H; R2 = CH3; R3 = —N
29 n = 3; R1 = H; R2 = CH3; R3 = —N
30 n = 6; R1 = H; R2 = CH3; R3 = —N
31 n = 5; R1 = H; R2 = CH3; R3 = —N
32 n = 5; R1 = H; R2 = CH3; R3 = —N

Figure 6. Flavone derivatives with potent self-induced Aβ aggregation inhibitory activity.

3.2. γ-secretase inhibitors

Although the amount of γ-secretase activity does not appear to increase in AD, alterations in γ-secretase activity leading to the production of longer forms of Aβ are the major genetic cause of early onset, familial AD [47,48], an effect that can be mimicked with a variety of allosteric γ-secretase modulating agents [49].

In the last 5 years, only some dicoumarin derivatives have been developed as γ-secretase inhibitors for treating or preventing neurodegenerative diseases such as AD [50]. The most potent compounds of the series with general structure VII are represented in Figure 7.

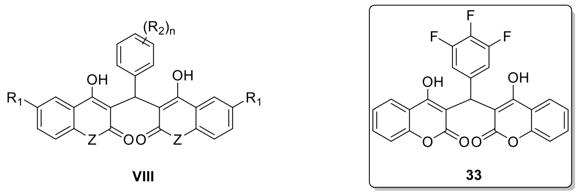

Z = O, NH, S
R_1 = H, CH_3
R_2 = X, OH, C_1-C_8 alkoxy, CN, NH_2 or C_2-C_8 alkyl
n = 2 to 5

Figure 7. Dicoumarin derivatives as γ-secretase inhibitors.

The most promising molecule of the tested compounds was compound **33** (Figure 7) with an IC_{50} = 0.6 μM and 0.2 μM against γ-secretase Aβ40 and Aβ42 respectively. These compounds are selective and non-competitive γ-secretase inhibitors.

3.3. β-secretase (BACE-1) inhibitors

BACE, known as β-site amyloid precursor protein (APP) cleaving enzyme [51] is a membrane anchored aspartyl protease required for the generation of Aβ [52,53]. In brains of patients with AD, abnormally accumulated Aβ peptides tends to oligomerize, aggregate and induce synaptic dysfunction and memory loss [54,55,56]. For this reason, the inhibition of BACE-1 has been seen as a therapeutic target to treat patients suffering from AD because BACE-1 is the sole β-secretase that generates Aβ peptide.

Some previously mentioned coumarin-tacrine derivatives (Figure 3, general structure IV) not only presented activity as Aβ aggregation inhibitors, but also as BACE-1 inhibitors [42]. The most promising compound of the series was compound **34** (Figure 8), presenting an IC_{50} = 17.2 μM at 100 μM.

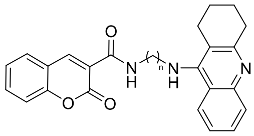

n = 6
34

Figure 8. Coumarin-tacrine compound as BACE-1 inhibior.

In 2013, Fernandez-Bachiller and collaborators identified 3-(aminophenyl)coumarin fragments as a starting point for developing entirely nonpeptidic drug-like BACE-1 inhibitors in the low-micromolar range [57] with general structure IX displayed in Figure 9.

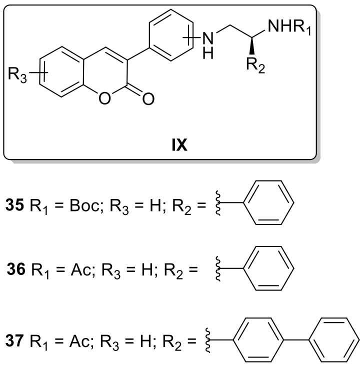

35 R_1 = Boc; R_3 = H; R_2 =
36 R_1 = Ac; R_3 = H; R_2 =
37 R_1 = Ac; R_3 = H; R_2 =

Figure 9. 3-(Aminophenyl)coumarin derivatives as BACE-1 inhibitors.

In this series, compounds **35**-**37** (Figure 9) showed the most potent activity with IC_{50} and K_i values ranging between 15.1-10.7 and 5.3-3.7 μM respectively.

Marumoto and collaborators studied some naturally occurring coumarins as BACE-1 inhibitors [58]. The naturally occurring coumarins studied were simple coumarins, furanocoumarins, and pyranocoumarins, but only the furanocoumarins showed significant activity. Furanocoumarins **38**-**41** showed the best BACE-1 activity ranging between 9.9 and 32.2 μM at the concentration 500 μM of the compounds.

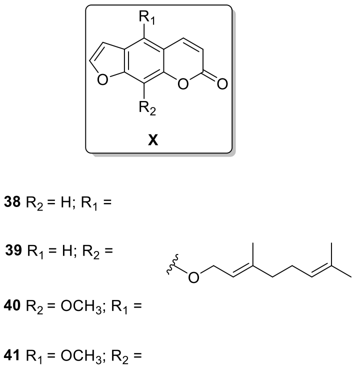

Figure 10. Natural furanocoumarins as BACE-1 inhibitors.

In the case of chromones, all the compounds containing the chromone core presenting BACE-1 activity were flavone derivatives isolated from natural sources.

Some natural flavones reported by Jung [59], Descamps [60] and Zhao [61] and collaborators showed significant BACE-1 inhibitory activity. The most active bioflavones (Figure 11) were vitexin (**42**) and quercetin 3-*O*-glucoside (**43**), showing IC_{50} values of 19.25 ad 41.23 μM respectively against BACE-1. Apigenin (**44**, Figure 11) showed effects affecting APP processing and preventing Aβ burden due to the down-regulation of BACE-1 and β-CTF levels, the relief of Aβ deposition, and the decrease of insoluble Aβ levels and galagin (**45**) has the ability to bind AβPP and inhibit the BACE cleavage of AβPP and APLP2, thus suggesting that it may be AβPP/APLP2-selective BACE inhibitor.

Other natural flavones isolated from the stem bark of *Morus lhou* showed β-secretase inhibitory activity range between 3.4 and 146.1 μM [62]. The most active compound isolated from the natural source were prenylated flavones **46** and **47** (Figure 12) presenting IC_{50} of 3.4 and 5.3 μM, respectively. The stronger activity was related to the resorcinol moiety on the chromone core and to the isoprenyl functionality at C-3.

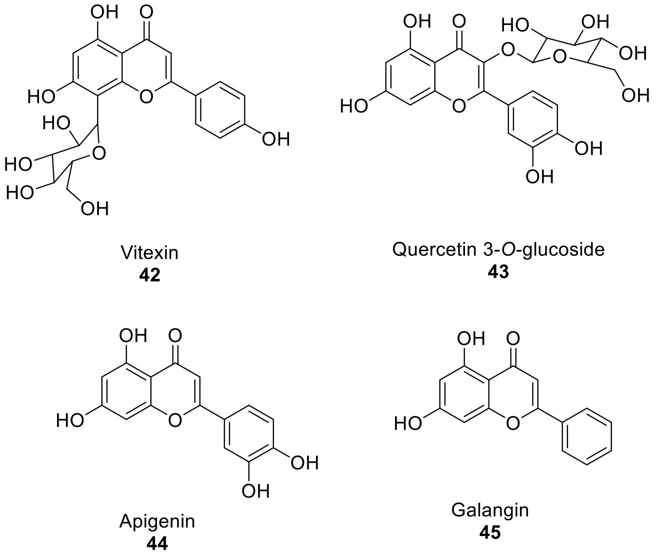
Vitexin
42
Quercetin 3-*O*-glucoside
43
Apigenin
44
Galangin
45

Figure 11. Natural flavones as BACE-1 inhibitors.

Biflavonoids are well known constituents of gymnospermous plants. They are flavonoid dimers connected by C–C or C–O–C bonds. Some biflavonoids reported by Sasaki and collaborators in 2010 [63] showed significant BACE-1 inhibitory activity.

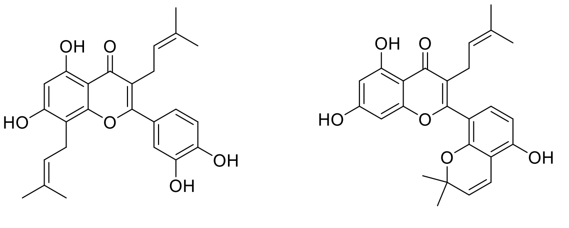
46 **47**

Figure 12. Natural prenylated flavones isolated from the stem bark of *Morus lhou* with β-secretase inhibitory activity.

These compounds, with general structure X (Figure 13), showed IC_{50} values ranging from 0.99 to 6.25 μM. However, two 2,3- dihydro analogue of this series (Figure 13, compounds **48** and **49**) were the most active compounds tested, with IC_{50} of 0.75 and 0.35 μM respectively.

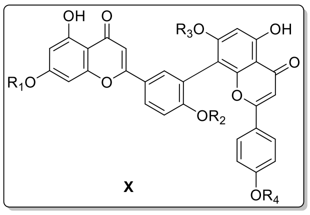

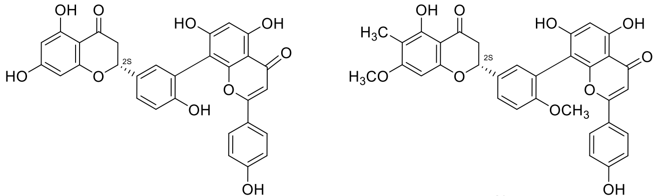
48

49

Figure 13. Natural biflavonoids with BACE-1 inhibitory activity.

3.4. Cholinesterase inhibitors (ChEI)

Cholinesterases (ChE) are a type of esterase enzymes that lyses choline-based esters, several of which serve as neurotransmitters. There are two types of ChE, AChE and BuChE, and the difference between the two types has to do with their respective preferences for substrates. These reactions are necessary to allow a cholinergic neuron to return to its resting state after activation.

ChE inhibitors (ChEIs) are currently considered as one of the most efficacious treatments of AD. In AD, a significant reduction in cholinergic neurotransmission is thought to be responsible for many cognitive and behavioral symptoms of the disease [64,65,66]. Several studies have proved that inhibition of either AChE or BuChE is capable of increasing the levels of acetylcholine in the brain [67,68]. For this reason, many ChEIs have been used to raise the level of acetylcholine in the AD brain and have demonstrated effectiveness in treating AD symptoms [69].

Many coumarins and chromones reported in the literature present ChE inhibitory activities. The first reported ChE inhibitory action of coumarins date from the early 1950s stating that 4-hydroxycoumarins inhibited human serum ChE [70]. Since then, many coumarin and chromone derivatives have been reported as good ChEIs. In this section of the review we will report the advances in this type of compounds as ChEIs.

Based on the natural coumarin scopoletin, Nam and collaborators synthesized some aminoalkyl substituted coumarins showing the potential activity of this series as AchEIs [71]. This series of compounds (**50**-**55**, Figure 14), with general structure XI, showed IC_{50} ranging from 2.87 to 30.53 µM at 100 µM of the tested compounds, being compounds **51** and **54** the most active of the series with AChE inhibition IC_{50} of 6.85 and 2.87 µM respectively.

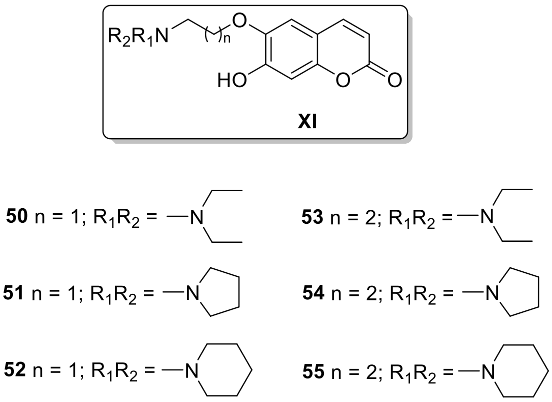

Figure 14. Scopoletin-inspired derivatives as AChEIs.

When Vanzolini and collaborators where trying to validate the use of immobilized capillary enzyme reactors (ICERs) for online ligand screening [72], the find out that two new 3-substituted coumarins (compounds **56** and **57**, Figure 15), out of a library of 17 coumarin derivatives, were identified as AChEIs, showing IC_{50} and *Ki* values of 0.356 and 0.031 µM for compound **56** and 12.6 and 13.8 µM for compound **57**, respectively.

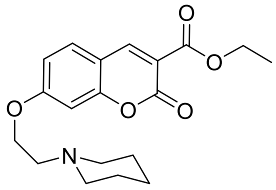

56

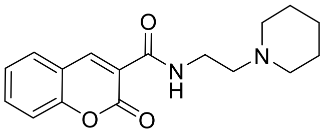

57

Figure 15. Coumarin derivatives as AChEIs validated by ICERs.

Some other 3-substituted coumarins such as 3-aryl or 3-amidocoumarins were studied as AChEI.[73] From these series of compounds with general structures XII and XIII (Figure 16), only the 3-amidocoumarins (XIII) presented moderated AChE inhibitory activity. The best compounds of the series (compounds **58**-**63**) showed IC_{50} ranging from 12.89 to 69.47 μM.

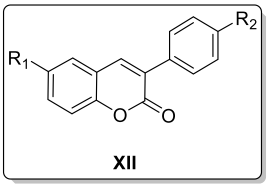

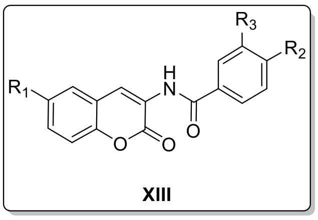

58 $R_1 = CH_3$; $R_2 = CH_3$; $R_3 = H$
59 $R_1 = H$; $R_2 = CH_3$; $R_3 = H$
60 $R_1 = H$; $R_2 = OCH_3$; $R_3 = H$
61 $R_1 = H$; $R_2 = Cl$; $R_3 = H$
62 $R_1 = H$; $R_2 = NO_2$; $R_3 = H$
63 $R_1 = H$; $R_2 = R_3 = Cl$

Figure 16. 3-Substituted coumarins as AChEIs.

Substitution at position 4 of the coumarin core also gave new coumarin derivatives with AChE inhibitory activity. The 4-hydroxycoumarin derivatives with general structure XIV (Figure 17), were synthesized by Razavi and collaborators [74]. Compounds **64-69** (Figure 16) were the most promising compounds of the series showing IC_{50} values inferior to 3.5 μM for the inhibition against AChE. Compound **68** was the most potent compound of the studied series, with an IC_{50} value of 1.2 μM.

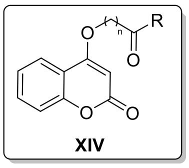

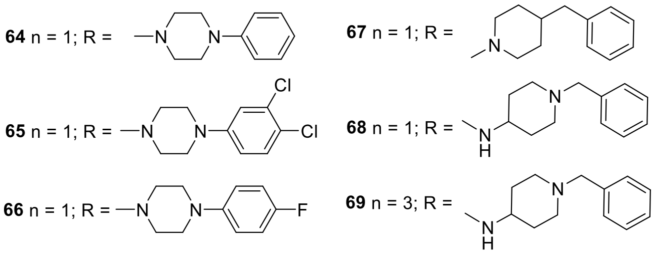

Figure 17. 4-Hydroxycoumarin derivatives as AChEIs.

On the other hand, some 4-phenylcoumarins isolated from the plant *Mesua elegans* (general structure XV, Figure 18) showed significant AChE inhibitory activity, with mesuagein A (compound **70**) and mesuagenin B (compound **71**) being the most potent compounds with IC_{50} 1.06 and 0.70 μM respectively [75].

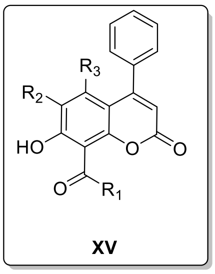

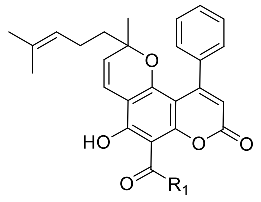

70 Mesuagenin A: $R_1 = CH_2CH(CH_3)_2$
71 Mesuagenin B: $R_1 = CH(CH_3)CH_2CH_3$

Figure 18. Natural 4-phenyl coumarins from *Mesua elegans*.

It was found in the literature some coumarin derivatives containing *N*-benzylpyrimidinium [76,77] with general structures XVI, XVII and XVIII (Figure 19) or *N*-benzylpiperidine [78] (general structure XIX) with significant AChE or BuChE inhibitory activity. Compounds with general structures XVIII and XIX in Figure 19, showed AChE inhibitory activity in de low nanomolar range (0.11 and 0.30 nM for the best compounds of each series respectively). However, the four series of compounds (general structures XVI-XIX, Figure 19) showed BuChE inhibitory activity in the same micromolar range.

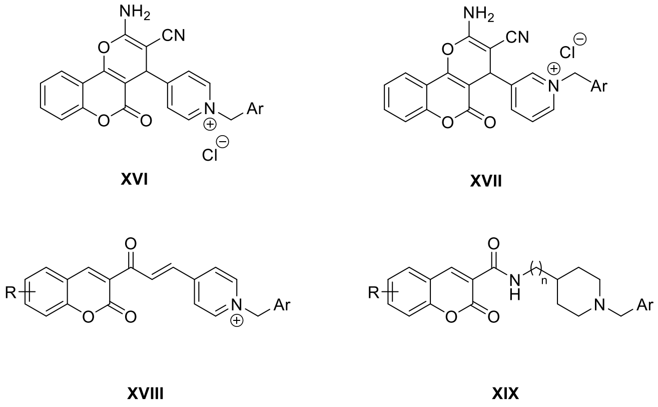

Figure 19. *N*-benzylpirimidinium and *N*-benzylpiperidine coumarin derivatives as ChEI.

Some substituted coumarins linked through different spacers to 3-hydroxy-*N*,*N*-dimethylanilino (general structure XX, Figure 20) or 3-hydroxy-*N*,*N*,*N*-trialkylbenzaminium (general structure XXI, Figure 20) moieties were synthesized and evaluated as AChE and BuChE inhibitors [79]. Compound **72** showed the highest AChE inhibitory potency for the 3-hydroxy-*N*,*N*-dimethylanilino series with an IC_{50} value of 0.236 nm and an excellent AChE/BChE selectivity (SI>300000). The same scaffold (compound **73**) was the most active against AChE for the series of the 3-hydroxy-*N*,*N*,*N*-trialkylbenzaminium salts displaying an affinity in picomolar range (IC_{50} = 0.0120 nM) and also an excellent AChE/BChE selectivity (SI = 138333).

Other coumarin derivatives using different spacers to link the coumarin moiety to protonable benzylamino groups were synthesized by Catto and collaborators [80]. This series of compounds were designed based on the structural features of donepezil (Figure 21), a palliative treatment for AD. The 6,7-dimethoxy substitution and the alkylamines were selected based on the structural features of the commercial drug.

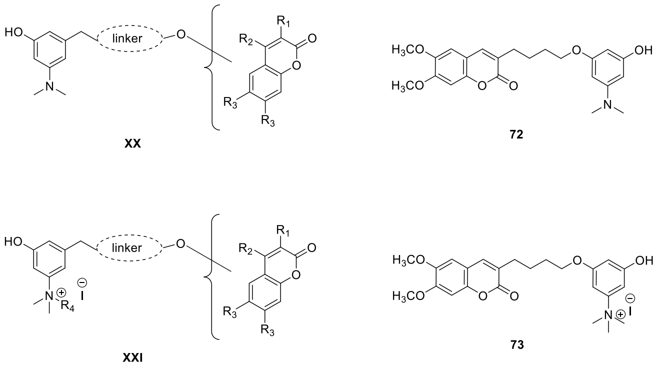

Figure 20. 3-Hydroxy-*N*,*N*-dimethylanilino and 3-hydroxy-*N*,*N*,*N*-trialkylbenzaminium salt derivatives and the corresponding most active compounds of the series as excellent AChEIs.

The AChE and BuChE inhibitory activity were tested, and as a result, the series of compounds showed activity in the micromolar range, with exception of compound **74** (Figure 21), which showed an IC_{50} value in the nanomolar range (IC_{50} = 7.6 nM), confirming its binding at both the catalytic and peripheral binding sites of AChE.

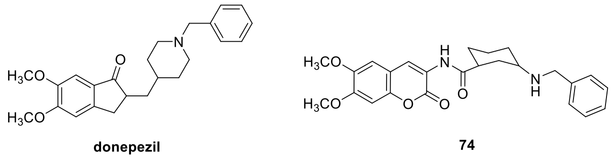

Figure 21. Coumarin derivative **74** as AChEI based o the drug donepezil.

Gulcan and collaborators have also developed some coumarin derivatives based on donepezil drug [81]. For the design of these scaffolds, their starting point was to consider urlithin derivatives, human metabolites of dietary ellagic acids, which have negligible inhibitory potential to inhibit cholinesterase enzymes, and generate hybrid-type molecules such as rivastigmine-like and donepezil-like analogues (general structures XII and XIII in Figure 22, respectively). The synthesized molecules tested within the two groups exerted similarity in terms of potential to inhibit AChE and BuChE, regarding the activity potentials of donepezil and rivastigmine, showing also similar activity not only *in vitro*, but also in the *in vivo* studies.

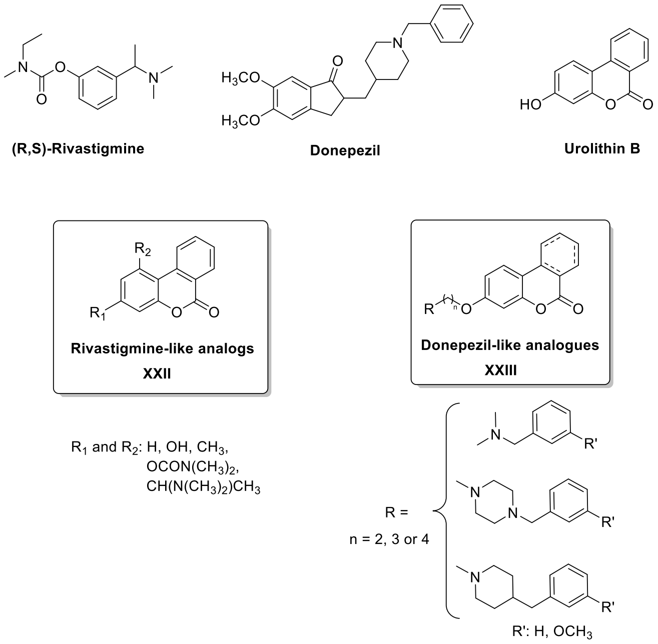

Figure 22. Rational design of rivastigmine-like and donepezil-like coumarin analogs as ChEIs.

Following the same strategy that Razavi and collaborators employed to synthesized 4-hydroxycoumarin derivative compounds **64-69** (Figure 17), in which an *N*-phenylpiperazine or *N*-benzylpiperidine moiety was connected with an alkoxy amide spacer to the coumarin scaffold, the same group developed 7-substituted coumarins in which the side chain was displaced from position 4 to position 7 of the coumarin core. Thus, compounds with general structure XXIV (Figure 23) were synthesized and their AChE and BuChE inhibitory activity was tested. The most potent compounds of the series presented IC_{50} values lower than 10 μM (compounds **75-81**, Figure 22) showing moderate AChE inhibitory activity but good selectivity comparing to BuChE. The most active compound of the studied series was compound **81** (Figure 22) showing an IC_{50} value of 1.6 μM. These findings revealed that *N*-(1-benzylpiperidin-4-yl) substituent is a favorable scaffold to attach to the 4- or 7-hydroxycoumarin scaffold *via* an acetamido linker.

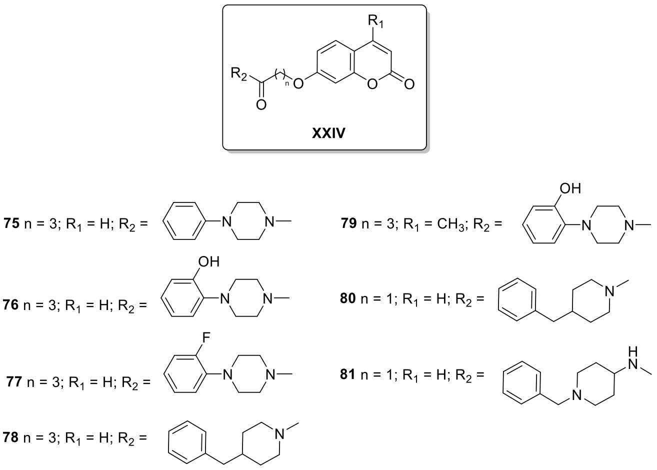

Figure 23. 7-Hydroxycoumarin derivatives as selective AChEIs with moderate activity in the micromolar range.

Hybrid coumarin-tacrine compounds as ChEIs are one of the most studied coumarin derivatives found in the literature. Some of those hybrid molecules (general structures III and IV in Figure 3) have been previously described in this review also as Aβ aggregation or β-secretase inhibitors [41,42]. From the series with general structure III (Figure 3), most of these compounds could effectively inhibit ChEs in the sub-micromolar range *in vitro*. The most potent compound of this series as AChEI, was compound **2** (Figure 3 and Figure 24), which also showed moderate BuChE inhibition with IC_{50} value of 0.234 μM and good Aβ aggregation inhibition.

From the series with general structure IV (Figure 3), all the hybrids exhibited *Ki* values in the nanomolar range and some of them were more potent than tacrine. In particular, compound **82** (Figure 24) was identified as the most potent dual-site AChE inhibitor with a *Ki* value of 16.7 nM.

New series of coumarin-tacrine derivatives with general structures XXV and XVI (Figure 24) were also studied as ChEIs. Hybrid compounds with general structure XXV were studied by Hamulakova and collaborators [82] and their studies revealed that the most potent inhibitor of *h*AChE was compound **83** (Figure 24) which showed IC_{50} value of 15.4

nM. This compound also demonstrated high efficiency against *h*BuChE with a IC_{50} value of 0.228 μM. Hybrid compounds with general structure XXVI were studied by Xie and collaborators [83] not only as ChEIs, but also as MAO inhibitors (MAOI). These studies revealed that most of the studied compounds showed potent inhibitory activity toward AChE and BuChE and clearly selective inhibition for MAO-B. Among these hybrids, compound **84** (Figure 24) was the most potent compound against AChE, with an IC_{50} value of 17.70 nM.

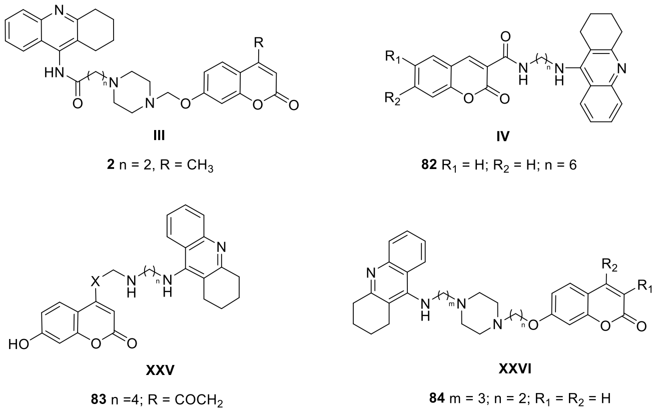
III
2 n = 2, R = CH$_3$
IV
82 R$_1$ = H; R$_2$ = H; n = 6
XXV
83 n =4; R = COCH$_2$
XXVI
84 m = 3; n = 2; R$_1$ = R$_2$ = H

Figure 24. Most active coumarin-tacrine hybrid compounds as AChEIs.

The chromone derivatives have also emerged as interesting scaffolds for the development of new ChEIs. Most of the studies related to chromone derivatives as ChEIs include studies on their ability as Aβ aggregation or β-secretase inhibitors [11]. Some of those compounds have already been described in previous sections highlighting their properties as Aβ aggregation or β-secretase inhibitors, but in this section we will described their properties as ChEIs. For example, flavone derivatives described by Luo [45] and Li [46] with general structure VII (Figure 6) not only presented self-induced Aβ aggregation inhibitory activity but also showed moderate ChE inhibitory activity in the mocromolar range. Also, natural flavones reported by Jung [59], vitexin and quercetin 3-*O*-glucoside (Figure 11, compounds **42** and **43** respectively) isolated from *Nelumbo nucifera* embryos, exerted significant BACE1 and ChEs inhibitory effects in the micromolar range.

As well as for coumarins, flavone-tacrine derivatives have been widely studied for their inhibitory effects in Aβ aggregation, β-secretase and in ChEs. The two first inhibitory activities have already been mentioned in previous sections for some of those flavone-tacrine derivatives. For example, flavone-tacrine hybrids with general structure V (Figure 4) described by Liao [43] presented good inhibition of self-induced $A_{\beta1\text{-}42}$ aggregation. In addition, from this series of compounds, molecules **10** and **14** (Figure 4) also showed the best AchE inhibitory activity with IC_{50} values of 17.3 and 6.9 nM.

Some other flavone-tacrine derivatives with general structures XXVII and XXVIII (Figure 25) also showed excellent AChE inhibitory activity in the nanomolar range. From the series studied by Li [84] with general structure XXVII, compounds **85**-**87** resulted in the most potent derivatives studied, with IC_{50} values for AChE ranging from 8.4 to 15.4 nM. From the series designed and synthesized by Fernandez-Bachiller [85] with general structure XXVIII (Figue 25), results showed that these compounds were potent inhibitors of both human AChE and BuChE, with IC_{50} values in the nano- and picomolar ranges, being in general more potent than the parent inhibitor tacrine. Compounds **88** and **89** (Figure 25) were the most active toward *h*BuChE showing IC_{50} values of 80 and 38 pM, whereas compounds **90**-**92** were the best *h*AChE inhibitors with IC_{50} values of 35, 65 and 90 pM respectively. In general, these tacrine−flavonoid hybrids did not show a clear selectivity toward human ChEs, although some outstanding exceptions were found such as compound **92**, which was 1056-fold more potent toward *h*AChE than toward *h*BuChE.

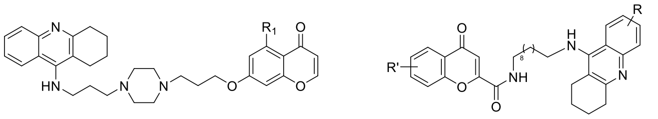

XXVII

85 R_1 = OH
86 R_1 = OCH_3
87 R_1 = H

XXXVIII

88 R = 6-Cl; R' = H
89 R = H; R' = 6-OCH_3
90 R = 6-Cl; R' = 5-OH, 7-OCH_3
91 R = H; R' = 5,7-diOH
92 R = H; R' = 6,7-diOH

Figure 25. Flavone-tacrine derivatives as potent ChEIs.

Some other flavone and chromone derivatives were studied as ChEIs but the results on those scaffolds were not as promising as for the flavone-tacrine derivatives. Flavone derivatives with general structure XIX and chromone derivatives with general structure XXX (Figure 26) were prepared by Sang [86] and Liu [87] respectively, but only showed ChE inhibitory activity in the micromolar range with exception of the chromone-2-carboxamido-alkylbenzylamine **93** (Figure 26), which showed an IC_{50} value of 70 nM against rat AChE.

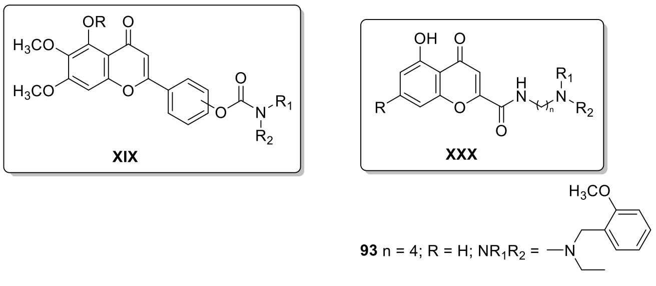

93 n = 4; R = H; NR_1R_2 =

Figure 26. Flavone and chromone derivatives as ChEIs.

3.5. Inducible nitric oxide synthase (iNOS)

Nitric oxide (NO) is an important signaling molecule that is widely used in the nervous system and it is an enzymatic product of nitric oxide synthase (NOS). NO is therefore an endogenous free radical involved in a wide range of physiological functions, as well as pathophysiological states [88]. NO is generated from L-arginine by a family of NOS including major of isozymes, endothelial NOS (eNOS), neuronal NOS (nNOS), and inducible NOS (iNOS) [89,90]. Both eNOS and nNOS are constitutively expressed and produce NO at a low level. However, iNOS is often expressed at high levels and is essentially unregulated once expressed. NO has significant physiological functions and an increasing body of evidence suggests that NO pathways are implicated in a number of neurological disorders, including AD and other neurodegenerative dementias. Therefore, as drug development targets, inhibitors of NO overproduction and over expression of iNOS might be beneficial for treatment of diseases affecting the central nervous system.

Despite the possible implications of iNOS in neurodegenerative disorders, as far as our knowledge, there are not many examples of coumarin or chromones with inhibitory effects on NO production or iNOS inhibitory activity in the last 5 years.

Based on the coumarin scaffolds, some natural coumarins isolated from *Mammea siamensis* (*Calophyllaceae*) were found to inhibit nitric oxide (NO) production in lipopolysaccharide-activated RAW264.7 cells [91]. Among the isolated coumarins (Figure 27), mammeasins and surangins (general structure XXXI, compounds **94-98**), kayeassamins (general structure XXXII, compounds **99-101**), and mammea A/AD (compound **102**) showed NO production inhibitory activity with IC_{50} ranging from 0.8 to 6.8 µM. In addition, compounds 94, 101 and 102 were found to inhibit induction of iNOS.

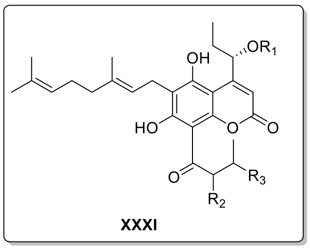

XXXI

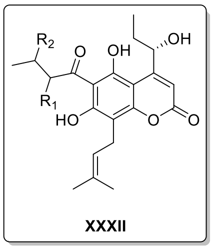

XXXII

94 Mammeasin A: R_1 = Ac; R_2 = H; R_3 = H
95 Mammeasin B: R_1 = Ac; R_2 = H; R_3 = CH_3
96 Surangin B: R_1 = Ac; R_2 = CH_3; R_3 = H
97 Surangin C: R_1 = H; R_2 = CH_3; R_3 = H
98 Surangin D: R_1 = H; R_2 = H; R_3 = CH_3

99 Kayeassamin E: R_1 = H; R_2 = H;
100 Kayeassamin F: R_1 = CH_3; R_2 = H;
101 Kayeassamin G: R_1 = H; R_2 = CH_3;

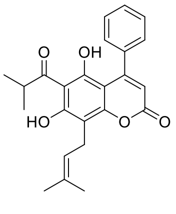

102 Mammea A/AD

Figure 27. Natural coumarins isolated from *Mammea siamensis* with NO production and iNOS inhibitory activity.

Among chromones, compounds with general structures XXXIII and XXXIV (Figure 28), were the most relevant examples of chromones showing inhibitory activity on NO production. Among the series with general structure XXXIII studied by Liu and collaborators [92], compounds **103-107** (Figure 28) showed quite potent inhibitory activities on NO production with IC_{50} values ranging from 0.35 to 3.48 µM. In addition, further studies indicate that compounds **105-107** inhibited NO production by suppressing the expression of iNOS mRNA in a dose dependent manner.

For the series with general structure XXXIV (Figure 28), studies carried out by Pham and collaborators on the inhibitory activities against iNOS-mediated NO production from lipopolysaccharide (LPS)-stimulated BV2 cells [93] showed that the flavone derivatives **108-111** exhibited strong inhibitory activities with IC_{50} values ranging from 4.73 to 11.42 µM, being compound **108** the most active of the series.

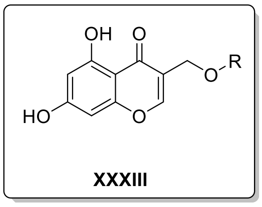

XXXIII

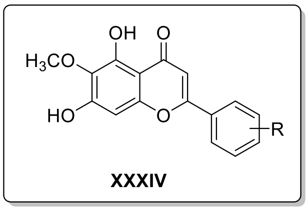

XXXIV

103 R = Ac
104 R = 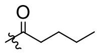
105 R = benzoyl
106 R = 4'-methoxybenzoyl
107 R = 2'-methylbenzoyl

108 R = 4-NO_2
109 R = 4-F
110 R = 3-F
111 R = 4-Br

Figure 28. Chromone and flavone derivatives with inhibitory activity on NO production.

3.6. Monoamine oxidase inhibitors

MAO is an iron containing flavoenzyme (FAD-depending enzyme) generally found in the outer surface of the mitochondria's outer membrane of glial cells and neurons [94,95]. MAO enzymes are involved in the degradation of biogenic amines [96]. MAO is present abundantly in noradrenergic nerve terminals. MAO-A and MAO-B, MAO known isoenzymes, oxidize xenobiotic amines and neurotransmitters via oxidative deamination, which is important for maintaining the normal mental state [97]. Large affinity of MAO-B towards benzyl amine and phenylethylamine marks their importance in monoamine destruction resulting in neurotransmitter activation [98]. Thus, primarily MAO-B regulation is responsible for the rooted interest of MAO drugs in the field of neurodegenerative diseases specially Parkinson's disease [99,100].

The emergence of coumarin moiety as potential MAO inhibitors (Figure 29) for neurodegenerative diseases has promoted studies on a significant number of new compounds derived by incorporating different structures with more potent and less toxic MAO-B inhibitory activity [28,101,102].

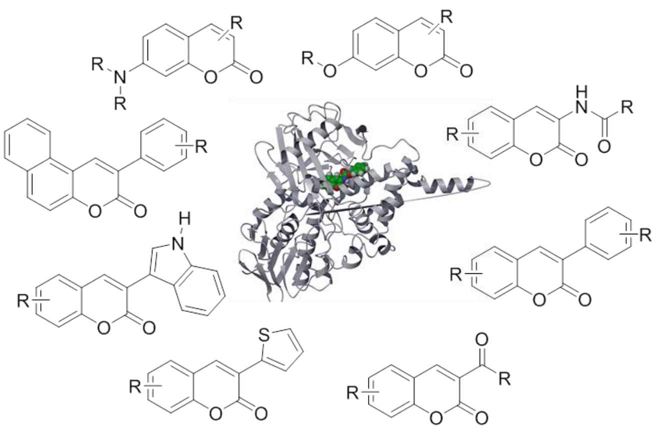

Figure 29. Differently substituted coumarins as selective MAO-B inhibitors.

Basic coumarin moiety has been ascertained as a potent MAOI [103]. It was in 1981 that the interest of the coumarin moiety against MAOs was described for the first time. At this time, an organophosphate group was attached to the umbelliferone ring and this new derivative was studied [104]. But it was only in the 1990's when the coumarin nucleus emerged as a promising scaffold for MAOI [105]. In particular, some coumarins isolated from *Psoralea corylifolia*, *Peucedanum japonicum* or *Monascus anka* have been described as potential MAOI [106,107,108]. Since there are many recent reviews on the area, in this manuscript only the most relevant examples are going to be described and presented.

Although natural coumarins generally show low MAO inhibitory potency, properly modified coumarins have been characterized as potent and selective MAOI. For example, the desmethyl congener of geiparvarin, a natural 7-substitued coumarin from the leaves of *Geijera parviflora*, exhibits potent and selective MAO-B inhibition [109]. This was the first step for the development of several 7-substituted coumarins as MAOI. In the last five years, this substitution is still one of the most explored [40,110,111].

Several modifications in coumarin scaffold have been performed to obtain 3-acyl/carboxy derivatives that were found to be potent and selective MAOI-B [112]. Furthermore, variations in position 7 of the coumarins were also explored (general structure XXXV Figure 30) suggesting that the introduction of aryl/alkyloxy substituents at this position can affect the MAO-B potency and selectivity. It was also reported that some compounds with acyl or benzyloxy substituted groups linked to C-3 or C-7 positions of coumarin possess the ability to improve inhibitory activity and selectivity towards MAO-B with IC_{50} values in the low nanomolar range, such as compounds **112** and **113** with IC_{50} values of 3 and 0.14 nM.

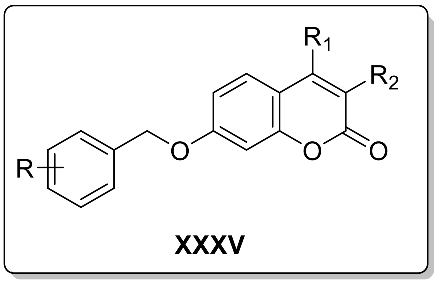

112 R = 3-Cl ; R_1 = CH_2NHCH_3 ; R_2 = H
113 R = 3,4-F ; R_1 = R_2 =CH_3

Figure 30. Examples of 7-benzyloxycoumarin derivatives with MAO-B activity.

In relation to this research, 3-arylaminocoumarins showed MAO-A and B inhibitory property or selectively MAO-B inhibition with substitution at position-7 [113]. Displacing the substituent at position-7 to position-6 and the 3,4-condensed benzene ring to third position (3-arylcoumarin scaffold) it showed MAO-B more potent and selective inhibitory activity [114,115,116]. Matos and collaborators have described large series of compounds with activities in the low nano- or picomolar ranges [27,115,116,117, 118,119,120].

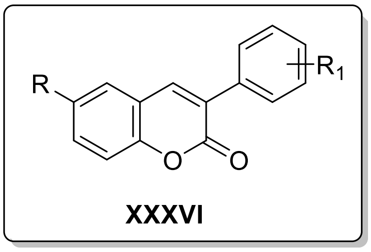

XXXVI

114 $R = CH_3$; R_1 = 4-CH_3
115 $R = CH_3$; R_1 = 3-OCH_3
116 $R = CH_3$; R_1 = 4-OCH_3
117 $R = CH_3$; R_1 = 3-Br, 4-OCH_3
118 $R = CH_3$; R_1 = 3-Br
119 $R = CH_3$; R_1 = 4-Br
120 $R = OCH_3$; R_1 = 3-Br

Figure 31. Examples of 3-arylcoumarin derivatives with MAO-B activity.

In particular, 3-arylcoumarins with general structure XXXVI (compounds **114-120**, Figure 31) showed very potent and selective activity towards *h*MAO-B, 3 with IC_{50} values ranging from 134 to 800 pM. SAR studies revealed that 3-Arylcoumarins with a methyl group at position 6 and different positions of the bromine atom linked in the 3-aryl ring proved to be the best candidates. Compounds presenting the same 3-aryl ring substitution pattern and present a methoxy group at position 6 slightly lose their activity. Additionally, prediction of blood–brain partitioning through a QSPR model showed the great potential of this type of compound to cross the blood brain barrier (BBB) and display their activity in the central nervous system.

3-Aryl condensed benzo[*f*]coumarin derivatives also proved to be very interesting MAOI-B [121]. In this series of compounds with general structure XXXVII (Figure 32) the substitutions in the phenyl ring at position 3 presented the same profile as for the uncondensed derivatives. In general, the introduction of a second methoxy substituent on the phenyl at position 3 leads to a decrease of the inhibitory activity against MAO-B. The most potent compounds of this series, compounds **121-123** (Figure 32) showed IC_{50} values against hMAO-B ranging from 2.4 to 48.8 nM.

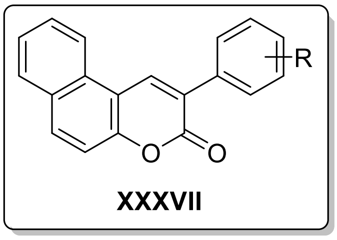

XXXVII

121 R = 3-OCH_3
122 R = 2-OCH_3
123 R = 3,4-OCH_3

Figure 32. Examples of condensed benzo[*f*]-3-aryl coumarin derivatives with MAO-B activity.

In a series of 3-aryl-4-hydroxycoumarin derivatives described by Serra and collaborators [119], substitution of methoxy group in the *para* position of the 3-phenyl ring resulted an effective compound against MAO-B. Introduction of chlorine atom at the *meta* position of the methoxy 3-phenyl ring, in compounds, increased MAO inhibition, and similarly substitution of the chlorine atom at the sixth position of the same compounds significantly improved MAO-B inhibitory activity.

More recently, 3-amidocoumarins with general structure XXXVIII (Figure 33) also described by Matos and collaborators [122] have been proved to be potential multifunctional agents against neurodegenerative diseases. In this work, variously substituted 3-amidocoumarins were identified as selective and reversible inhibitors of the MAO-B isoform. In addition, these compounds exert neuroprotection *in vitro* against hydrogen peroxide in rat cortical neurons, as well as antioxidant activity in a DPPH radical scavenging assay.

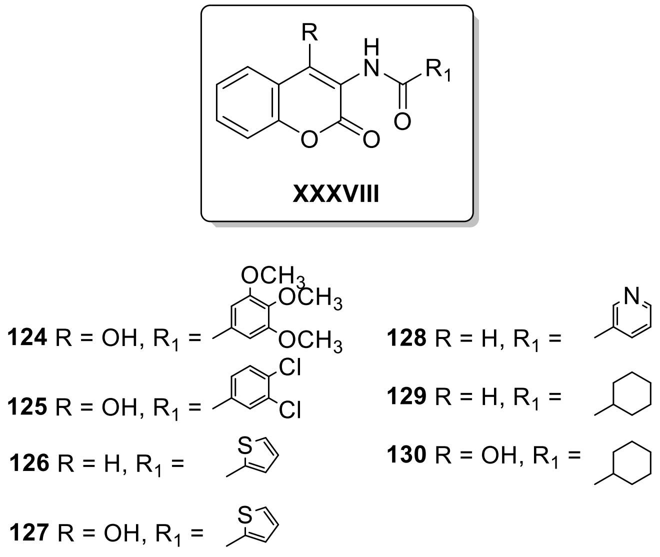

Figure 33. 3-amidocoumarins with MAO-B activity and neuroprotective effects.

Interestingly, in the case of the 3-benzamidocoumarins (compounds **124** and **125**, Figure 33), substitution at position 4 with a hydroxy group abolishes MAO-B activity, but the compounds remain active in the neuroprotection model. Further evaluation of 3-heteroarylamide or 3-cyclohexyl derivatives (compounds **126**-**128** and **129**-**130**, respectively) indicated that it is the nature of the heterocycle that determines the neuroprotective effects. The heterocyclic rings at the 3 position of the coumarin nucleus, attached to the amido groups, showed an improved inhibitory potency compared to aryl groups such as nitro, methyl, chloro and methoxy substituted rings. The IC_{50} values of this series of compounds range from 2.3 to 50 μM. Evaluation in several assays highlighted the need to further improve the BBB permeability, suggesting that this novel scaffolds have desirable properties for the development of potential drug candidates.

Finally, theoretical studies still play a key role in the design of new potent an selective MAOI [123,124]. The number of papers dealing with the structure-based drug design is continuously growing, which demonstrates the importance of such tools in medicinal chemistry. The published literature concerning Ferino and collaborators recently reviewed the use of the ligand-protein docking methodologies in the study of the MAO enzymes [125]. From these studies, it seems that through this computational approach, more selective and potent molecules can be proposed as inhibitors by applying precise modifications on the basic scaffold [126].

As well as for coumarins, in recent years an intensive search for the discovery of novel MAOI-B was carry out and in line chromones have been recognized as an important scaffold for the development of novel MAOI.

From the studied chromone derivatives in the last 5 years, two main chromone cores showed MAO-B inhibitory activity in the nanomolar range. These scaffolds are represented in general structures XXXIX and XL in Figure 34. From this previous SAR studies it was concluded that chromone derivatives showing substituents in position-3 of γ-pyrone nucleus (compounds with general structure XXXIX, Figure 34) act preferably as MAOI-B, with IC_{50} values in the nanomolar to micromolar range [127,128,129]. Compounds **131-135** showed the most potent MAO-B inhibitory activities with IC_{50} ranging from 63 to 76 nM.

Compounds with general structure XL (Figure 34), bearing C-6 or C-7 benzyloxy substituents, also showed MAO-B inhibitory activities in the nanomolar range [130,131]. The most potent compounds of these series were compounds **136-142**, which showed excellent IC_{50} values ranging from 2-8.4 nM and good selectivity index comparing to MAO-A.

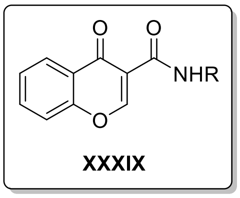

XXXIX

131 R = 4'-OH-Ph
132 R = 3'-OH,4'-OCH$_3$-Ph
133 R = 4'-Cl-Ph
134 R = 4'-I-Ph
135 R = 4'-CH$_3$-Ph

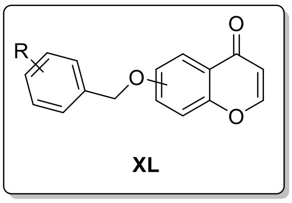

XL

136 C-6, R = 3'Cl
137 C-6 R = 4'-Cl
138 C-6 R = 3'-Br
139 C-6 R = 4'-Br
140 C-6 R = 4'-F
141 C-6 R = 4'-CH$_3$
142 C-6 R = 4'-CF$_3$

Figure 34. Chromone scaffolds with potent and selective MAO-B inhibitory activity.

CONCLUSION

The development of new drugs for the treatment of neurodegenerative related diseases remains as one of the most encouraging topics in the Medicinal Chemistry field. It has been proved that both coumarin and chromone cores are excellent scaffolds to target different enzymes involved in these pathologies. Particularly, ChE and MAO resulted the most studied targets for these compounds, showing in some cases inhibitory activities in the nano- or picomolar ranges. In addition, remarkable activities of coumarin and chromone derivatives as amyloid β-agents and secretase inhibitors have been found. Different SAR studies on the corresponding targets for each case have allowed to establish the key features for these type of scaffolds and therefore opening a window for future development of new drug candidates.

CONFLICT OF INTEREST

The authors confirm that this article content has no conflict of interest.

ACKNOWLEDGEMENTS

S.V.R. and M.J.M. thank Xunta de Galicia for the postdoctoral grant (ED481B 2014/027-0 and ED481B 2014/086-0, respectively). A.F. thanks Fundação para a Ciência e Tecnologia, POPH and QREN for the postdoctoral predoctoral grant (SFRH/BD/80831/2011).

REFERENCES

[1] Amor, S.; Puentes, F.; Baker, D.; van der Valk, P. Inflammation in neurodegenerative diseases. *Immunology*, **2010**, *129*, 154–169.
[2] Jellinger, K.A. Cell death mechanisms in neurodegeneration. *J. Cell. Mol. Med.*, **2001**, *5*, 1–17.
[3] Tofaris, G.K.; Schapira, A.H.V. Neurodegenerative diseases in the era of targeted therapeutics: how to handle a tangled issue. *Mol. Cell. Neurosci.*, **2015**, *66*, 1–2.
[4] Jellinger, K.A. General aspects of neurodegeneration. *J Neural Transm Suppl.* **2003**, *65*, 101–144.
[5] Gaspar, A.; Milhazes, N.; Santana, L.; Uriarte, E.; Borges, F.; Matos, M.J. Oxidative Stress and Neurodegenerative Diseases: Looking for a Therapeutic Solution Inspired on Benzopyran Chemistry. *Curr.Top. Med. Chem*,. **2015**, *15*, 432–445.
[6] Youdim, M.B.H.; Buccafusco, J.J. Multi-functional drugs for various CNS targets in the treatment of neurodegenerative disorders. *Trends Pharmacol. Sci.*, **2005**, *26*, 27–35.
[7] Cavalli, A.; Bolognesi, M.L.; Minarini, A.; Rosini, M.; Tumiatti, V.; Recanatini, M.; Melchiorre, C. (). Multi-target-directed ligands to combat neurodegenerative diseases. *J. Med. Chem.*, **2008**, *51*, 347–372.
[8] Hepworth, J.D., C*omprehensive Heterocyclic Chemistry*. Katritzky, A. R.; Rees, C. W., Eds.; Pergamon Press: Oxford, **1984** pp. 835–840.
[9] Kontogiorgis, C.; Detsi, A.; Hadjipavlou-Litina, D. Coumarin-based drugs: a patent review (2008 – present). *Expert Opin. Ther. Pat.*, **2012**, *22*, 437–454.
[10] Keri, R.S.; Budagumpi, S.; Pai, R.K.; Balakrishna, R.G. Chromones as a privileged scaffold in drug discovery: A review. *Eur. J. Med. Chem.*, **2014**, *78*, 340–374.
[11] Gaspar, A.; Matos, M.J.; Garrido, J.; Uriarte, E.; Borges, F. Chromone: a valid scaffold in medicinal chemistry. *Chem. Rev.*, **2014**, *114*, 4960–4992.
[12] Murray, R.D.H.; Mendez, J.; Brown, S.A. *The natural coumarins occurrence*. *Chemistry and Biochemistry*; John Wiley and Sons: Chichester, **1982**.
[13] Murray, R.D.H. Naturally occurring plant coumarins. *Prog. Chem. Org. Nat. Prod.*, **2002**, *83*, 1–673.
[14] Vazquez-Rodriguez, S.; Matos, M.J.; Borges, F.; Uriarte, E. Bioactive coumarins from marine sources: origin, structural features and pharmacological properties. *Curr. Top. Med. Chem.*, **2015**, *15*, 1755–1766.
[15] Borges, F.; Roleira, F.; Milhazes, N.; Santana, L.; Uriarte, E. Simple coumarins and analogues in medicinal chemistry: occurrence, synthesis and biological activity. *Curr. Med. Chem.*, **2005**, *12*, 887–916.

[16] Borges, F.; Roleira, F.; Milhazes, N.; Uriarte, E.; Santana, L. Simple Coumarins: Privileged Scaffolds in Medicinal Chemistry. *Front. Med. Chem.*, **2009**, *4*, 23–85.

[17] Melagraki, G.; Afantitis, A.; Igglessi-Markopoulou, O.; Detsi, A.; Koufaki, M.; Kontogiorgis, C.; Hadjipavlou-Litina, D.J. Synthesis and evaluation of the antioxidant and anti-inflammatory activity of novel coumarin-3-aminoamides and their alphalipoic acid adducts. *Eur. J. Med. Chem.*, **2009**, *44*, 3020–3026.

[18] Symeonidis, T.; Fylaktakidou, K.C.; Hadjipavlou-Litina, D.J.; Litinas, K.E. Synthesis and anti-inflammatory evaluation of novel angularly or linearly fused coumarins. *Eur. J. Med. Chem.*, **2009**, *44*, 5012–5017.

[19] Kostova, I.; Bhatia, S.; Grigorov, P.; Balkansky, S.; Parmar, V.S.; Prasad, A.K.; Saso, L. Coumarins as antioxidants. *Curr. Med. Chem.*, **2011**, *18*, 3929–3951.

[20] Pérez-Cruz, F.; Vazquez-Rodriguez, S.; Matos, M.J.; Herrera- Morales, A.; Villamena, F.A.; Das, A.; Gopalakrishnan, B.; Olea- Azar, C.; Santana, L.; Uriarte, E. Synthesis and electrochemical and biological studies of novel coumarin-chalcone hybrid compounds. *J. Med. Chem.*, **2013**, *56*, 6136–6145.

[21] Vazquez-Rodriguez, S.; Figueroa-Guíñez, R.; Matos, M.J.;Santana, L.; Uriarte, E.; Lapier, M.; Maya, J.D.; Olea-Azar, C. Synthesis of coumarin–chalcone hybrids and evaluation of their antioxidant and trypanocidal properties. *Med. Chem. Commun.*, **2013**, *4*, 993–1000.

[22] Vilar, S.; Quezada, E.; Santana, L.; Uriarte, E.; Yanez, M.; Fraiz, N.; Alcaide, C.; Cano, E.; Orallo, F. Design, synthesis, and vasorelaxant and platelet antiaggregatory activities of coumarin-resveratrol hybrids. *Bioorg. Med. Chem. Lett.*, **2006**, *16*, 257–261.

[23] Belluti, F.; Fontana, G.; Bo, L.; Carenini, N.; Giommarelli, C.; Zunino, F. Design, synthesis and anticancer activities of stilbene-coumarin hybrid compounds: Identification of novel proapoptotic agents. *Bioorg. Med. Chem.*, **2010**, *18*, 3543–3550.

[24] Matos, M.J.; Vazquez-Rodriguez, S.; Santana, L.; Uriarte, E.; Fuentes-Edfuf, C.; Santos, Y.; Munoz-Crego, A. Looking for new targets: simple coumarins as antibacterial agents. *Med. Chem.*, **2012**, *8*, 1140–1145.

[25] Matos, M.J.; Vazquez-Rodriguez, S.; Santana, L.; Uriarte, E.; Fuentes-Edfuf, C.; Santos, Y.; Muñoz-Crego, A. Synthesis and structure-activity relationships of novel amino/nitro substituted 3-arylcoumarins as antibacterial agents. *Molecules*, **2013**, 18, 1394–1404.

[26] Vazquez-Rodriguez, S.; López, R.L.; Matos, M.J.; Armesto-Quintas, G.; Serra, S.; Uriarte, E.; Santana, L.; Borges, F.; Muñoz-Crego, A.; Santos, Y. Design, synthesis and antibacterial study of new potent and selective coumarin-chalcone derivatives for the treatment of tenacibaculosis. *Bioorg. Med. Chem.*, **2015**, *23*, 7045-7052.

[27] Matos, M.J.; Vazquez-Rodriguez, S.; Uriarte, E.; Santana, L.; Viña, D. MAO inhibitory activity modulation: 3-Phenylcoumarins versus 3-benzoylcoumarins. *Bioorg. Med. Chem. Lett.*, **2011**, *21*, 4224–4227.

[28] Matos, M.J.; Viña, D.; Vazquez-Rodriguez, S.; Uriarte, E.; Santana, L. Focusing on new monoamine oxidase inhibitors: differently substituted coumarins as an interesting scaffold. *Curr. Top. Med. Chem.*, **2012**, *12*, 2210–2239.

[29] Vogel, A. Darstellung von Benzoesäure aus der Tonka-Bohne und aus den Meliloten oder Steinklee–Blumen. *Annalen der Physik*, **1820**, *64*, 161–166.

[30] IUPAC, *Nomenclature of Organic Chemistry*, Pergamon Press **1979**.

[31] G.P. Ellis (Ed.), *The Chemistry of Heterocyclic Compounds*, *Chromenes*, *Chromanones and Chromones*, , J. Wiley & Sons, New York, **2007**, vol. 31.

[32] Phosrithong, N.; Samee, W.; Nunthanavanit, P.; Ungwitayatorn, J. In Vitro Antioxidant Activity Study of Novel Chromone Derivatives, *Chem. Biol. Drug Des*., **2012**, *79*, 981–989.

[33] Kuroda, M.; Uchida, S.; Watanabe, K.; Mimaki, K. Chromones from the tubers of Eranthis cilicica and their antioxidant activity, *Phytochemistry*, **2009**, *70*, 288–293.

[34] Ceylan-Ünlüsoy, M.; Verspohl, E.J.; Ertan, R. Synthesis and antidiabetic activity of some new chromonyl-2,4-thiazolidinediones. *J. Enzyme Inhib. Med. Chem.*, **2010**, *25*, 784–789.

[35] Zhou, T.; Shi, Q.; Lee, K.H. Efficient microwave-assisted one-pot preparation of angular 2,2-dimethyl-2H-chromone containing compounds. *Tetrahedron Lett.*, **2010**, *51*, 4382–4386.

[36] Shaw, A.Y.; Chang, C.Y.; Liau, H.H.; Lu, P.J.; Chen, H. L.; Yang, C.N.; Li, H.Y. Synthesis of 2-styrylchromones as a novel class of antiproliferative agents targeting carcinoma cells. *Eur. J. Med. Chem.*, **2009**, *44*, 2552–2562.

[37] Stains, C.I.; Mondal, K.; Ghosh, I. Molecules that target beta-amyloid. *ChemMedChem*, **2007**, *2*, 1674–1692.

[38] LeVine, H. Small molecule inhibitors of Abeta assembly. *Amyloid*, **2007**, *14*, 185–187.

[39] Török, B.; Dasgupta, S.; Török, M. Chemistry of small molecule inhibitors of Alzheimer's amyloid-beta fibrillogenesis. *Curr. Bioact. Compd.* **2008**, *4*, 159–174.

[40] Huang, M.; Xie, S.-S.; Jiang, N.; Lan, J.-S.; Kong, L.-Y.; Wang, X.-B. Multifunctional coumarin derivatives: Monoamine oxidase B (MAO-B) inhibition, anti-β-amyloid (Aβ) aggregation and metal chelation properties against Alzheimer's disease. *Bioorg. Med. Chem. Lett.*, **2015**, *25*, 508–513.

[41] Xie, S.S.; Wang, X.B.; Li, J.Y.; Yang, L.; Kong, L.Y. Design, synthesis and evaluation of novel tacrine-coumarin hybrids as multifunctional cholinesterase inhibitors against Alzheimer's disease. *Eur. J. Med. Chem.*, **2013**, *64*, 540–553.

[42] Sun, Q.; Peng, D.Y.; Yang, S.G.; Zhu, X.L.; Yang, W.C.; Yang, G.F. Syntheses of coumarin-tacrine hybrids as dual-site acetylcholinesterase inhibitors and their activity against butylcholinesterase, Aβ aggregation, and β-secretase. *Bioorg. Med. Chem.*, **2014**, *22*, 4784–4791.

[43] Liao, S.; Deng, H.; Huang, S.; Yang, J.; Wang, S.; Yin, B.; Zheng, T.; Zhang, D.; Liu, J.; Gao, G.; Ma, J.; Deng, Z.

Design, synthesis and evaluation of novel 5,6,7-trimethoxyflavone-6-chlorotacrine hybrids as potential multifunctional agents for the treatment of Alzheimer's disease. *Bioorg. Med. Chem. Lett.*, **2015**, *25*, 1541–1545.

[44] Bag, S.; Ghosh, S.; Tulsan, R.; Sood, A.; Zhou, W.; Schifone, C.; Foster, M.; LeVine, H.; Török, B.; Török, M. Design, synthesis and biological activity of multifunctional α,β-unsaturated carbonyl scaffolds for Alzheimer's disease. *Bioorg. Med. Chem. Lett.*, **2013**, *23*, 2614–2618.

[45] Luo, W.; Su, Y.B.; Hong, C.; Tian, R.G.; Su, L.P.; Wang, Y.Q.; Li, Y.; Yue, J.J.; Wang, C.J. Design, synthesis and evaluation of novel 4-dimethylamine flavonoid derivatives as potential multi-functional anti-Alzheimer agents. *Bioorg.c Med. Chem.*, **2013**, *21*, 7275–7282.

[46] Li, R.-S.; Wang, X.-B.; Hu, X.-J.; Kong, L.-Y. Design, synthesis and evaluation of flavonoid derivatives as potential multifunctional acetylcholinesterase inhibitors against Alzheimer's disease. *Bioorg. Med. Chem. Lett.*, **2013**, *23*, 2636–2641.

[47] Scheuner, D.; Eckman, C.; Jensen, M.; Song, X.; Citron, M.; Suzuki, N.; Bird, T.D.; Hardy, J.; Hutton, M.; Kukull, W.; Larson, E.; Levy-Lahad, E.; Viitanen, M.; Peskind, E.; Poorkaj, P.; Schellenberg, G.; Tanzi, R.; Wasco, W.; Lannfelt, L.; Selkoe, D.; Younkin, S. Secreted amyloid beta-protein similar to that in the senile plaques of Alzheimer's disease is increased in vivo by the presenilin 1 and 2 and APP mutations linked to familial Alzheimer's disease. *Nat. Med.*, **1996**, *2*, 864–870.

[48] Suzuki, N.; Cheung, T.T.; Cai, X.-D.; Odaka, A.; Otvos, L.; Eckman, C.; Golde, T.E.; Younkin, S.G. An increased percentage of long amyloid β protein is secreted by familial amyloid β protein precursor (βAPP717) mutants. *Science.* **1994**, *264*, 1336–1340.

[49] Kukar, T.; Murphy, M.P.; Eriksen, J.L.; Sagi, S.A.; Weggen, S.; Smith, T.E.; Ladd, T.; Khan, M.A.; Kache, R.; Beard, J.; Dodson, M.; Merit, S.; Ozols, V.V.; Anastasiadis, P.Z.; Das, P.; Fauq, A.; Koo, E.H.; Golde, T.E. Diverse compounds mimic Alzheimer disease-causing mutations by augmenting Aβ42 production. *Nat. Med.*, **2005**, *11*, 545–550.

[50] Sloan-Kettering Institute For Cancer Research. Preparation of coumarin-based compounds for the treatment of neurodegenerative diseases and cancer. WO 2010075280

[51] Yan, R.; Vassar, R. Targeting the beta secretase BACE1 for Alzheimer's disease therapy. *Lancet Neurol.*, **2014**, *13*, 319–329.

[52] Hussain, I.; Powell, D.; Howlett, D.R.; Tew, D.G.; Meek, T.D.; Chapman, C.; Gloger, I.S.; Murphy, K.E.; Southan, C.D.; Ryan, D.M.; Smith, T.S.; Simmons, D.L.; Walsh, F.S.; Dingwall, C.; Christie, G. Identification of a novel aspartic protease (Asp 2) as beta-secretase. *Mol. Cell Neurosci.*, **1999**, *14*, 419–427.

[53] Vassar, R.; Bennett, B.D.; Babu-Khan, S.; Kahn, S.; Mendiaz, E.A.; Denis, P.; Teplow, D.B.; Ross, S.; Amarante, P.; Loeloff, R.; Luo, Y.; Fisher, S.; Fuller, J.; Edenson, S.; Lile, J.; Jarosinski, M.A.; Biere, A.L.; Curran, E.; Burgess, T.; Louis, J.C.; Collins, F.; Treanor, J.; Rogers, G.; Citron, M. Betasecretase cleavage of Alzheimer's amyloid precursor protein by the transmembrane aspartic protease BACE. *Science*, **1999**, *286*, 735– 741.

[54] Haass, C.; Selkoe, D.J. Soluble protein oligomers in neurodegeneration: lessons from the Alzheimer's amyloid betapeptide. *Nat. Rev. Mol. Cell Biol.* **2007**, *8*, 101–112.

[55] Walsh, D.M.; Klyubin, I.; Fadeeva, J.V.; Rowan, M.J.; Selkoe, D.J. Amyloid-beta oligomers: their production, toxicity and therapeutic inhibition. *Biochem. Soc. Trans.*, **2002**, *30*, 552–557.

[56] Tu, S.; Okamoto, S.; Lipton, S.A.; Xu, H. Oligomeric Abetainduced synaptic dysfunction in Alzheimer's disease. *Mol. Neurodegener.*, **2014**, *9*, 48.

[57] Fernández-Bachiller, M.I.; Horatscheck, A.; Lisurek, M.; Rademann, J. Alzheimer's disease: Identification and development of β-secretase (BACE-1) binding fragments and inhibitors by dynamic ligation screening (DLS). *ChemMedChem*, **2013**, 8, 1041–1056.

[58] Marumoto, S.; Miyazawa, M. Structure–activity relationships for naturally occurring coumarins as β-secretase inhibitor. *Bioorg. Med. Chem.*, **2012**, *20*, 784–788.

[59] Jung, H.A.; Karki, S.; Kim, J.H.; Choi, J.S. BACE1 and cholinesterase inhibitory activities of Nelumbo nucifera embryos. *Arch. Pharm. Res.*, **2015**, *38*, 1178–1187.

[60] Descamps, O.; Spilman, P.; Zhang, Q.; Libeu, C.P.; Poksay, K.; Gorostiza, O.; Campagna, J; Jagodzinska, B.; Bredesen, D.E.; John, V. AβPP-selective BACE inhibitors (ASBI): novel class of therapeutic agents for Alzheimer's. disease. *J. Alzheimers Dis.*, **2013**, *37*, 343–55.

[61] Zhao, L.; Wang, J.-L.; Liu, R.; Li, X.-X.; Li, J.-F.; Zhang, L. Neuroprotective, Anti-amyloidogenic and neurotrophic effects of apigenin in an Alzheimer's disease mouse model. *Molecules*, **2013**, *18*, 9949–9965.

[62] Cho, J.K.; Ryu, Y.B.; Curtis-Long, M.J.; Kim, J.Y.; Kim, D.; Lee, S.; Lee, W.S.; Park, K.H. Inhibition and structural reliability of prenylated flavones from the stem bark of Morus lhou on β-secretase (BACE-1). *Bioorg. Med. Chem. Lett.*, **2011**, *21*, 2945–2948.

[63] Sasaki, H.; Miki, K.; Kinoshita, K.; Koyama, K.; Juliawaty, L.D.; Achmad, S.; Hakim, E.H.; Kaneda, M.; Takahashi, K. Beta-Secretase (BACE-1) inhibitory effect of biflavonoids. *Bioorg. Med. Chem. Lett.*, **2010**, *20*, 4558–4560.

[64] Davies, P; Maloney, A.J. Selective loss of central cholinergic neurons in Alzheimer's disease. *Lancet*, **1976**, *308*, pp1403.

[65] Bartus, R.T.; Dean, R.L.; Beer, B.; Lippa, A.S. The cholinergic hypothesis of geriatric memory dysfunction. *Science*, **1982**, *217*, 408–414.

[66] Coyle, J.T.; Price, D.L.; DeLong, M.R. Alzheimer's disease: A disorder of cortical cholinergic innervation. *Science*, **1983**, *219*, 1184–1190.

[67] Cerbai, F.; Giovannini, M.G.; Melani, C.; Enz, A.; Pepeu, G. N1phenethyl-norcymserine, a selective butyrylcholinesterase inhibitor, increases acetylcholine

release in rat cerebral cortex: A comparison with donepezil and rivastigmine. *Eur. J. Pharmacol.*, **2007**, *572*, 142–150.

[68] Greig, N.H.; Utsuki, T.; Ingram, D.K.; Wang, Y.; Pepeu, G.; Scali, C.; Yu, Q.S.; Mamczarz, J.; Holloway, H.W.; Giordano, T.; Chen, D.; Furukawa, K.; Sambamurti, K.; Brossi, A., D.K. Selective butyrylcholinesterase inhibition elevates brain acetylcholine, augments learning and lowers Alzheimer beta-amyloid peptide in rodent. *Proc. Natl. Acad. Sci. USA*, **2005**, *102*, 17213–17218.

[69] Birks, J. Cholinesterase inhibitors for Alzheimer's disease. *Cochrane Database Syst. Rev*., **2006**, CD005593.

[70] Grossmann, V.; Hais, I.M.; Kasalicky, B. Inhibition of human serum cholinesterase by some 4-hydroxy-coumarin derivatives. *Nature*, **1950**, *165*, 276.

[71] Nam, S.O.; Park, D.H.; Lee, Y.H.; Ryu, J.H.; Lee, Y.S.; Synthesis of aminoalkyl-substituted coumarin derivatives as acetylcholinesterase inhibitors. *Bioorg. Med. Chem.*, **2014**, *22*, 1262–1267.

[72] Vanzolini, K.L.; Vieira, L.C.C.; Correîa, A.G.; Cardoso, C.L.; Cass, Q.B. Acetylcholinesterase immobilized capillary reactors-tandem mass spectrometry: An on-flow tool for ligand screening. *J. Med. Chem.*, **2013**, *56*, 2038–2044.

[73] Viña, D.; Matos, M.J.; Yáñez, M.; Santana, L.; Uriarte, E. 3-Substituted coumarins as dual inhibitors of AChE and MAO for the treatment of Alzheimer's disease. *Med. Chem. Commun*, **2012**, *3*, 213–218.

[74] Razavi, S.F.; Khoobi, M.; Nadri, H.; Sakhteman, A.; Moradi, A.; Emami, S.; Foroumadi, A.; Shafiee, A. Synthesis and evaluation of 4-substituted coumarins as novel acetylcholinesterase inhibitors. *Eur. J. Med. Chem.*, **2013**, *64*, 252–259.

[75] Awang, K.; Chan, G.; Litaudon, M.; Ismail, N.H.; Martin, M.T.; Gueritte, F. 4-Phenylcoumarins from *Mesua elegans* with acetylcholinesterase inhibitory activity. *Bioorg. Med. Chem.*, **2010**, *18*, 7873–7877.

[76] Khoobi, M.; Alipour, M.; Sakhteman, A.; Nadri, H.; Moradi, A.; Ghandi, M.; Emami, S.; Foroumadi, A.; Shafiee, A. Design, synthesis, biological evaluation and docking study of 5-oxo-4,5-dihydropyrano[3,2-*c*]chromene derivatives as acetylcholinesterase and butyrylcholinesterase inhibitors. *Eur. J. Med. Chem.*, **2013**, *68*, 260–269.

[77] Alipour, M.; Khoobi, M.; Foroumadi, A.; Nadri, H.; Moradi, A.; Sakhteman, A.; Ghandi, M.; Shafiee, A. Novel coumarin derivatives bearing N-benzyl pyridinium moiety: Potent and dual binding site acetylcholinesterase inhibitors. *Bioorg. Med. Chem.*, **2012**, *20*, 7214–7222.

[78] Asadipour, A.; Alipour, M.; Jafari, M.; Khoobi, M.; Emami, S.; Nadri, H.; Sakhteman, A.; Moradi, A.; Sheibani, V.; Homayouni Moghadam, F.; Shafiee, A.; Foroumadi, A. Novel coumarin-3-carboxamides bearing *N*-benzylpiperidine moiety as potent acetylcholinesterase inhibitors. *Eur. J. of Med. Chem.*, **2013**, *70*, 623–630.

[79] Pisani, L.; Catto, M.; Giangreco, I.; Leonetti, F.; Nicolotti, O.; Stefanachi, A.; Cellamare, S.; Carotti, A. Design, synthesis, and biological evaluation of coumarin derivatives tethered to an edrophonium-like fragment as highly potent and selective dual binding site acetylcholinesterase inhibitors. *ChemMedChem*, **2010**, *5*, 1616–1630.

[80] Catto, M.; Pisani, L.; Leonetti, F.; Nicolotti, O.; Pesce, P.; Stefanachi, A.; Cellamare, S.; Carotti, A. Design, synthesis and biological evaluation of coumarin alkylamines as potent and selective dual binding site inhibitors of acetylcholinesterase. *Bioorg. Med. Chem.*, **2013**, *21*, 146–152.

[81] Gulcan, H.O.; Unlu, S.; Esiringu, I.; Ercetin, T.; Sahin Y.; Oz, D.; Sahin, M.F. Design, synthesis and biological evaluation of novel 6H-benzo[c]chromen-6-one, and 7,8,9,10-tetrahydro-benzo[c]chromen-6-one derivatives as potential cholinesterase inhibitors. *Bioorg. Med. Chem.*, **2014**, *22*, 5141–5154.

[82] Hamulakova, S.; Janovec, L.; Hrabinova, M.; Spilovska, K.; Korabecny, J.; Kristian, P.; Kuca, K.; Imrich, J. Synthesis and Biological Evaluation of Novel Tacrine Derivatives and Tacrine-Coumarin Hybrids as Cholinesterase Inhibitors. *J. Med. Chem.*, **2014**, *57*, 7073−7084.

[83] Xie, S.-S.; Wang, X.; Jiang, N.; Yu, W.; Wang, K.D.G.; Lan, J.-S.; Li, Z.R.; Kong, L.Y. Multi-target tacrine-coumarin hybrids: Cholinesterase and monoamine oxidase B inhibition properties against Alzheimer's disease. *Eur. J. Med. Chem.*, **2015**, *95*, 153–165.

[84] Li, S.Y.; Wang, X.B.; Xie, S.S.; Jiang, N.; Wang, K.D.G.; Yao, H.Q.; Sun, H,B.; Kong, L.Y. Multifunctional tacrine-flavonoid hybrids with cholinergic, β-amyloid-reducing, and metal chelating properties for the treatment of Alzheimer's disease. *Eur. J. Med. Chem.*, **2013**, *69*, 632–646.

[85] Fernández-Bachiller, M.I.; Pérez, C.; Monjas, L.; Rademann, J.; Rodríguez-Franco, M.I. New tacrine-4-oxo-4H-chromene hybrids as multifunctional agents for the treatment of Alzheimer's disease, with cholinergic, antioxidant, and β-amyloid-reducing properties. *J. Med. Chem.*, **2012**, *55*, 1303–1317.

[86] Sang, Z.; Li, Y.; Qiang, X.; Xiao, G.; Liu, Q.; Tan, Z.; Deng, Y. Multifunctional scutellarin–rivastigmine hybrids with cholinergic, antioxidant, biometal chelating and neuroprotective properties for the treatment of Alzheimer's disease. *Bioorg. Med. Chem.*, **2015**, *23*, 668–680.

[87] Liu, Q.; Qiang, X.; Li, Y.; Sang, Z.; Li, Y.; Tan, Z.; Deng, Y. Design, synthesis and evaluation of chromone-2-carboxamido-alkylbenzylamines as multifunctional agents for the treatment of Alzheimer's disease. *Bioorg. Med. Chem.*, **2015**, *23*, 911–923.

[88] Uzbay, I.T.; Oglesby, M.W. Nitric oxide and substance dependence. *Neurosci. Biobehav. Rev.* **2001**, *25*, 43–52.

[89] Leone, A.M.; Palmer, R.M.J.; Knowles, R.G.; Francis, P.L.; Ashton, D.S.; Moncada, S.J. Constitutive and inducible nitric oxide synthases incorporate molecular oxygen into both nitric oxide and citrulline. *Biol. Chem.*, **1991**, *266*, 23790–23795.

[90] Palmer, R.M.J.; Ashton, D.S.; Moncada, S. Vascular endothelial cells synthesize nitric oxide from L-arginine. *Nature,* **1988**, *333*, 664–666.

[91] Morikawa, T.; Sueyoshi, M.; Chaipech, S.; Matsuda, H.; Nomura, Y.; Yabe, M.; Matsumoto, T.; Ninomiya, K.; Yoshikawa, M.; Pongpiriyadacha, Y.; Hayakawa, T.; Muraoka, O. Suppressive effects of coumarins from Mammea siamensis on inducible nitric oxide synthase expression in RAW264.7 cells. *Bioorg. Med. Chem.*, **2012**, *20*, 4968–4977.

[92] Liu, G.-B.B.; Xu, J.-L.L.; Geng, M.; Xu, R.; Hui, R.-R.R.; Zhao, J.-W. W.; Xu, Q.; Xu, H.X.; Li, J.X. Synthesis of a novel series of diphenolic chromone derivatives as inhibitors of NO production in LPS-activated RAW264.7 macrophages. *Bioorg. Med. Chem.*, **2010**, *18*, 2864–2871.

[93] Pham, T.A.N.; Che, H.; Phan, P.T.T.; Lee, J.W.; Kim, S.S.; Park, H. Oroxylin A analogs exhibited strong inhibitory activities against iNOS-mediated nitric oxide (NO) production. *Bioorg. Med. Chem. Lett.*, **2012**, *22*, 2534–2535.

[94] Binda C.; Wang J.; Pisani L.; Caccia C.; Carotti A.; Salvati P.; Edmondson D.E.; Mattevi A. Structures of human monoamine oxidases A and B complexes with selective noncovalent inhibitors: safinamide and coumarin analogs. *J. Med. Chem.* **2007**, *50*, 5848–5852.

[95] Tipton, K.F. Enzymology of monoamine oxidase. *Cell. Biochem. Funct.*, **1986**, *4*:79–87.

[96] Novaroli L.; Daina A.; Favre E.; Bravo J.; Carotti A.; Leonetti F.; Catto M.; Carrupt P.; Reist, M. Impact of species-dependent differences on screening, design, and development of MAO B inhibitors. *J. Med. Chem.,* **2006**, *49*, 6264–6272.

[97] Chen, K.; Holschneider, D.P.; Wu, W.; Rebrin, I.; Shih, J.C. A spontaneous point mutation produces monoamine oxidase A/B knock-out mice with greatly elevated monoamines and anxiety-like behaviour. *J. Biol. Chem.*, **2004**, *279*, 39645–39652.

[98] Ma, J.; Yoshimura, M.; Yamashita, E.; Nakagawa, A.; Ito, A.; Tsukihara, T. Structure of rat monoamine oxidase A and its specific recognitions for substrates and inhibitors. *J. Mol. Biol.*, **2004**, *338*, 103–114.

[99] Riederer, P.; Danielczyk, W.; Grunblatt, E. Monoamine oxidase-B inhibition in Alzheimer’s disease. *Neurotoxicology*, **2004**, *25*, 271–277.

[100] Guay, D.R. Rasgiline (TVP-1012): a new selective monoamine oxidase inhibitor for Parkinson’s disease. *Am. J. Geriatr. Pharmacother.*, **2006**, *4*, 330–346.

[101] Rendenbach, B.; Weifenbach, H.; Teschendorf, H.J. Preparation of 7-(arylalkoxy)coumarins as central nervous system agents. **1990**, DE 3834861 A1.

[102] Chimenti, F.; Secci, D.; Bolasco, A.; Chimenti, P.; Granese, A.; Carradori, S.; Yanez, M.; Orallo, F.; Sanna, M.L.; Gallinella, B.; Cirilli, R. Synthesis, stereochemical separation, and biological evaluation of selective inhibitors of human MAO-B: 1-(4-arylthiazol-2-yl)-2-(3-methylcyclohexylidene) hydrazines. *J. Med. Chem.*, **2010**, *53*, 6516–6520.

[103] Jameel, E.; Umar, T.; Kumar, J.; Hoda, N. Coumarin: A Privileged Scaffold for the Design and Development of Antineurodegenerative Agents. *Chem. Biol. Drug. Des.*, **2016**, *87*, 21-38.

[104] Kadir, H.A.; Knowles, C.O. Inhibition of rat brain monoamine oxidase by insecticides, acaricides and related compounds. *Gen. Pharmacol.*, **1981**, *12*, 239–247

[105] Rendenbach, B.; Weifenbach, H.; Teschendorf, H.J. Preparation of 7-(arylalkoxy)coumarins as central nervous system agents. Ger. Offen. **1990**, DE 3834861 A1 19900419

[106] Kong, L.D.; Tan, R.X.; Woo, A.Y.; Cheng, C.H. Inhibition of rat brain monoamine oxidase activities by psoralen and isopsoralen: implications for the treatment of affective disorders. *Pharmacol. Toxicol.,* **2001**, *88*, 75–80.

[107] Huong, D.T.; Choi, H.C.; Rho, T.C.; Lee, H.S.; Lee, M.K., Kim, Y.H. Inhibitory activity of monoamine oxidase by coumarins from Peucedanum japonicum. *Arch. Pharm. Res.*, **1999**, *22*, 324-326.

[108] Hossain, C.F.; Okuyama, E.; Yamazaki, M. A new series of coumarin derivatives having monoamine oxidase inhibitory activity from Monascus anka. *Chem. Pharm. Bull.*, **1996**, *44*, 1535–1539.

[109] Carotti, A.; Carrieri, A.; Chimichi, S.; Boccalini, M.; Cosimelli, B.; Gnerre, C.; Carotti, A.; Carrupt, P.-A.; Testa, B. Natural and synthetic Geiparavins are strong and selective MAO-B inhibitors. Synthesis and SAR studies. *Bioorg. Med. Chem. Lett.*, **2002**, *12*, 3551–3555.

[110] Xie, S.-S.; Wang, X.; Jiang, N.; Yu, W.; Wang, K.D.G.; Lan, J.-S.; Li, Z.-R.; Kong, L.-Y. Multi-target tacrine-coumarin hybrids: Cholinesterase and monoamine oxidase B inhibition properties against Alzheimer's disease. *Eur. J. Med. Chem.*, **2015**, *95*, 153–165.

[111] Alipour, M.; Khoobi, M.; Moradi, A.; Nadri, H.; Homayouni Moghadam, F.; Emami, S.; Hasanpour, Z.; Foroumadi, A.; Shafiee, A. Synthesis and anti-cholinesterase activity of new 7-hydroxycoumarin derivatives. *Eur. J. Med. Chem.*, **2014**, *82*, 536–544.

[112] Secci, D.; Carradori, S.; Bolasco, A.; Chimenti, P.; Yañez, M.; Ortuso, F.; Alcaro, S. Synthesis and selective human monoamine oxidase inhibition of 3-carbonyl, 3-acyl, and 3-carboxyhydrazido coumarin derivatives. *Eur. J. Med. Chem.*, **2011**, *46*, 4846–4852.

[113] Santana L.; González-Díaz H.; Quezada E.; Uriarte E.; Yáñez M.; Viña D.; Orallo F. Quantitative structure-activity relationship and complex network approach to monoamine oxidase A and B inhibitors. *J. Med. Chem.,* **2008**, *51*, 6740–6751.

[114] Matos, M.J.; Viña, D.; Quezada, E.; Picciau, C.; Delogu, G.; Orallo, F.; Santana, L.; Uriarte, E. A new series of 3-phenylcoumarins as potent and selective MAO-B inhibitors. *Bioorg. Med. Chem. Lett.*, **2009**, *19*, 3268–3270.

[115] Matos, M.J.; Terán, C.; Pérez-Castillo, Y.; Uriarte, E.; Santana, L.; Viña, D. Synthesis and study of a series of 3-arylcoumarins as potent and selective monoamine oxidase B inhibitors. *J. Med. Chem.*, **2011**, *54*, 7127–7137.

[116] Matos, M.J.; Vilar, S.; García-Morales, V.; Tatonetti, N.P.; Uriarte. E.; Santana, L.; Viña, D. Insight into the functional and structural properties of 3-arylcoumarin as an interesting scaffold in monoamine oxidase B inhibition. *ChemMedChem*, **2014**, *9*, 1488–1500.

[117] Matos, M.J.; Viña, D.; Picciau, C.; Orallo, F.; Santana, L.; Uriarte, E. Synthesis and evaluation of 6-methyl-3-phenylcoumarins as potent and selective MAO-B inhibitors. *Bioorg. Med. Chem. Lett.*, **2009**, *19*, 5053–5055.

[118] Matos, M,J.; Viña, D.; Janeiro, P.; Borges, F.; Santana, L.; Uriarte, E. New halogenated 3-phenylcoumarins as potent and selective MAO-B inhibitors. *Bioorg. Med. Chem. Lett.*, **2010**, *20*, 5157–5160.

[119] Serra, S.; Ferino, G.; Matos, M.J.; Vazquez-Rodriguez, S.; Delogu, G.; Viña, D.; Cadoni, E.; Santana, L.; Uriarte, E. Hydroxycoumarins as selective MAO-B inhibitors. *Bioor. Med. Chem. Lett.*, **2012**, *22*, 258–261.

[120] Matos, M.J.; Rodríguez-Enríquez, F.; Vilar, S.; Santana, L.; Uriarte, E.; Hripcsak, G.; Estrada, M.; Rodríguez-Franco, M.I.; Viña, D. Potent and selective MAO-B inhibitory activity: Amino- versus nitro-3-arylcoumarin derivatives. *Bioorg. Med. Chem. Lett.*, **2015**, *25*, 642–648.

[121] Matos, M.J.; Janeiro, P.; González Franco, R.M.; Vilar, S.; Tatonetti, N.P.; Santana, L.; Uriarte, E.; Borges, F.; Fontenla, J.A.; Viña, D. Synthesis, pharmacological study and docking calculations of new benzo[*f*]coumarin derivatives as dual inhibitors of enzymatic systems involved in neurodegenerative diseases. *Future Med. Chem.*, **2014**, *6*, 371–383.

[122] Matos, M.J.; Rodríguez-Enríquez, F.; Borges, F.; Santana, L.; Uriarte, E.; Estrada, M.; Rodríguez-Franco, M.I.; Laguna, R.; Viña, D. 3-Amidocoumarins as potential multifunctional agents against neurodegenerative diseases. *ChemMedChem*, **2015**, *10*, 2071–2079

[123] Pisani, L.; Farina, R.; Nicolotti, O.; Gadaleta, D.; Soto-Otero, R.; Catto, M.; Di Braccio, M.; Mendez-Alvarez, E.; Carotti, A. In silico design of novel 2H-chromen-2-one derivatives as potent and selective MAO B inhibitors. *Eur. J. Med. Chem.*, **2015**, *89*, 98–105.

[124] Farina, R.; Pisani, L.; Catto, M.; Nicolotti, O.; Gadaleta, D.; Denora, N.; Soto-Otero, R.; Mendez-Alvarez, E.; Passos, C.S.; Muncipinto, G.; Altomare, C.D.; Nurisso, A.; Carrupt, P.A.; Carotti, A. Structure-Based Design and Optimization of Multitarget-Directed 2H-Chromen-2-one Derivatives as Potent Inhibitors of Monoamine Oxidase B and Cholinesterases. *J. Med. Chem.*, **2015**, *58*, 5561–5578.

[125] Ferino, G.; Vilar, S.; Matos, M.J.; Uriarte, E.; Cadoni, E. Monoamine oxidase inhibitors: ten years of docking studies. *Curr. Top. Med. Chem.*, **2012**, *12*, 2145–2162

[126] Ruan, B.F.; Cheng, H.J.; Ren, J.; Li, H.L.; Guo, L.L.; Zhang, X.X.; Liao, C. Novel 2H-chromen-2-one derivatives of resveratrol: Design, synthesis, modeling and use as human monoamine oxidase inhibitors. *Eur. J. Med. Chem.*, **2015**, *103*, 185–190.

[127] Gaspar, A.; Teixeira, F.; Uriarte, E.; Milhazes, N.; Melo, A.; Cordeiro, M.N.; Ortuso, F.; Alcaro, S.; Borges, F. Towards the Discovery of a Novel Class of Monoamine Oxidase Inhibitors: Structure-Property-Activity and Docking Studies on Chromone Amides. *ChemMedChem*, **2011**, *6*, 628–632.

[128] Gaspar, A.; Reis, J.; Fonseca, A.; Milhazes, N.; Viña, D.; Uriarte, E.; Borges, F. Chromone 3-phenylcarboxamides as potent and selective MAO-B inhibitors. *Bioorg. Med. Chem. Lett.*, **2011**, *21*, 707–709.

[129] Gaspar, A.; Silva, T.; Yáñez, M.; Vina, D.; Orallo, F.; Ortuso, F.; Uriarte, E.; Alcaro, S.; Borges, F. Chromone, a privileged scaffold for the development of monoamine oxidase inhibitors. *J. Med. Chem.*, **2011**, *54*, 5165–5173.

[130] Legoabe, L.J.; Petzer, A.; Petzer, J.P. Selected chromone derivatives as inhibitors of monoamine oxidase. *Bioorg. Med. Chem. Lett.*, **2012**, *22*, 5480–5484.

[131] Legoabe, L.J.; Petzer, A.; Petzer, J.P. Inhibition of monoamine oxidase by selected C6-substituted chromone derivatives. *Eur. J. Med. Chem.*, **2012**, *49*, 343–353.

Received: March 20, 2015 Revised: April 16, 2015 Accepted: April 20, 2015